

NAM

Groningen Earthquakes – Structural Upgrading

URM Modelling and Analysis Cross- Validation

ARUP, EUCENTRE, TUDelft

Datum Juni 2015

Editors Jan van Elk & Dirk Doornhof

General Introduction

The structural strength of the buildings in the Groningen area is an important issue for the assessment of risk resulting from induced earthquakes. As the building stock in the Groningen region is quite different from that in other seismically active areas, detailed studies into the structural strength response to earthquakes of the buildings typical for the Groningen area are required.

Especially modelling of the unreinforced masonry (URM) buildings typical for the Groningen area is challenging. Prior to modelling the seismic response of these buildings, NAM therefore set up a URM Modelling and Analysis Cross-Validation study. The expertise of EUCENTRE in modeling the seismic response of URM buildings could be shared and later combined with the knowledge of local building practices in Groningen held by ARUP and TU Delft.

A number of benchmark studies and experiments were chosen for this URM Modelling and Analysis Cross-Validation study and modelled by all three parties. The results were compared. Identified differences, in particular those regarding modeling assumptions, will be addressed and resolved in a future updated version of this report. It is the intention that other groups that will later be engaged in modelling of URM houses will also perform this calibration modelling. Following this study, models of index buildings will be assembled for the different URM building typologies encountered in the Groningen area for input into the fragility models for the different building typologies.

In support of the modelling, measurements of the properties of building materials and building elements are carried out. Building elements are subjected to accelerograms typical for Groningen earthquakes and their response measured. As a calibration, a typical Groningen terraced house will be built on a shake table in the laboratory of EUCENTRE in Pavia, Italy, and subjected to representative accelerograms.

In each of the participating organisations, teams of modelers are involved in the modelling of URM buildings and the determination of their strength. These teams are led and supervised by the following experts:

External Expert	Affiliation	Role	Main Expertise Area
Damian Grant	ARUP	Collaborator	Structural Modeling
Guido Magenes	EUCENTRE Pavia	Collaborator	Modeling and Testing of Masonry structures
Jan Rots	Technical University Delft	Collaborator	Structural Modeling

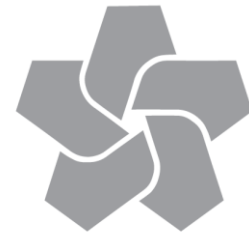
This study has been coordinated by ARUP, who also compiled the report from the individual contributions from the three participants.

As mentioned above, the results of these URM structural modelling activities are then fed into the fragility functions development work stream, which is coordinated by the following experts:

External Expert	Affiliation	Role	Main Expertise Area
Helen Crowley	Independent Consultant, Pavia	Collaborator	Building Fragility and Risk
Rui Pinho	University of Pavia	Collaborator	Structural Modeling and Fragility

Assurance for this study is primarily based on cross-validation between parties involved. The studies into the fragility of buildings will be reviewed by a panel of independent experts. The following experts have been invited:

External Expert	Affiliation	Role	Main Expertise Area
Jack Baker	Stanford University, US	Independent Reviewer	Building Fragility and Risk
Paolo Franchin	University of Rome "La Sapienza"	Independent Reviewer	Building Fragility and Risk
Michael Griffith	University of Adelaide, Australia	Independent Reviewer	Modeling and Testing of Masonry structures
Curt Haselton	California State University, US	Independent Reviewer	Structural Modeling and Fragility
Jason Ingham	University of Auckland	Independent Reviewer	Modeling and Testing of Masonry structures
Nico Luco	United States Geological Survey	Independent Reviewer	Building Fragility and Risk
Dimitrios Vamvatsikos	NTUA, Greece	Independent Reviewer	Building Fragility and Risk



NAM

Title	Groningen Earthquakes – Structural Upgrading URM Modelling and Analysis Cross-Validation		Date	June 2015
			Initiator	NAM
Autor(s)	Damian Grant, Guido Magenes and Jan Rots	Editors	Jan van Elk Dirk Doornhof	
Organisation	ARUP, EUCENTRE, TUDelft	Organisation	NAM	
Place in the Study and Data Acquisition Plan	<p><u>Study Theme:</u> Building Structural Strength</p> <p><u>Comment:</u> The structural strength of the buildings in the Groningen region is an important issue for the assessment of risk resulting from induced earthquakes. As the building stock in the Groningen area is quite different from that in other seismically active areas, detailed studies into the structural strength response to earthquakes of the buildings typical for the Groningen area is required.</p> <p>Especially modelling of the unreinforced masonry (URM) buildings typical for the Groningen area is challenging. Prior to modelling the seismic response of these buildings NAM therefore set up a URM Modelling and Analysis Cross-Validation study. The expertise of EUCENTRE in modeling the seismic response of URM buildings could be shared and later combined with the knowledge of local building practices in Groningen held by ARUP and TU Delft.</p>			
Directly linked research	<ol style="list-style-type: none"> (1) Measurements of the properties of building materials and building elements are carried out. (2) Subjection of building elements to accelerograms typical for Groningen earthquakes and their response measured. (3) Shake table test of a typical Groningen terraced house built in the laboratory of EUCENTRE in Pavia, Italy. (4) Preparation of fragility curves for URM building typologies. 			
Used data				
Associated organisation	ARUP, EUCENTRE, TUDelft			
Assurance	<p>Cross-validation between parties involved supplemented by review consisting of independent experts.</p> <p>Review by a panel of independent experts.</p>			

Client: Nederlandse Aardolie
Maatschappij

**Arup Project Title: Groningen
Earthquakes – Structural
Upgrading**

Modelling and Analysis Cross-
Validation – Arup, EUCENTRE, TU
Delft

229746_032.0_REP127

Rev A.01 | 7 July 2015

This report was prepared by Arup in July 2015 on the basis of a scope of services agreed with our client. It is not intended for and should not be relied upon by any third party and no responsibility or liability is undertaken to any third party.

Job number 229746

This document is part of scientific work and is based on information available at the time of writing. Work is still in progress and the contents may be revised during this process, or to take account of further information or changing needs. This report is in the public domain only for the purpose of allowing thorough scientific discussions and further scientific review. The findings are only estimated outcomes based upon the available information and certain assumptions. We cannot accept any responsibility for actual outcomes, as events and circumstances frequently do not occur as expected.

Arup bv
Naritaweg 118
1043 CA Amsterdam
PO box 57145
1040 BA Amsterdam
The Netherlands
www.arup.com

ARUP

Contents

	Page	
1	Background and Introduction	2
2	Modelling Approaches	3
2.1	Arup – LS-DYNA	3
2.2	EUCENTRE – TREMURI	3
2.3	TU Delft – TNO DIANA	4
3	Comparison with Experimental Benchmarks	5
3.1	The benchmark tests	5
3.2	Ispra In-Plane Panel Tests (Anthoine et al., 1995)	6
3.3	Pavia Full Building Tests (Magenes et al., 1994)	11
3.4	ESECMaSE Calcium Silicate In-Plane Panel Tests (Magenes et al., 2008)	21
3.5	ESECMaSE Calcium Silicate Full-Scale Half-Building Tests (Anthoine et al., 2007)	25
3.6	One-Way Spanning Wall Out-of-Plane Tests (Griffith et al., 2004)	36
3.7	Two-Way Spanning Wall Out-of-Plane Tests (Griffith et al., 2007)	39
4	Index Buildings Cross-Validation	44
4.1	Terraced House (T1*)	44
4.2	Detached Villa, Timber Floors (T3a)	56
5	Conclusions and Recommendations	66
5.1	Experimental benchmark tests	66
5.2	Predictions for index buildings	66
5.3	Comparison of modelling approaches	66

References

Appendices

Appendix A

Modelling Comparison – Arup

Appendix B

Modelling Comparison – EUCENTRE

Appendix C

Modelling Comparison – TU Delft

Executive Summary

Currently, very limited data is available on the seismic response of construction typologies specific to Dutch practice. Therefore, benchmarking and cross-validation against existing and newly planned experimental data are needed to study material characteristics and the response of components and full buildings, to validate and update the guidance.

This report compares the performance of four different modelling approaches used by Arup, EUCENTRE and TU Delft against their ability to model the behaviour of published experimental tests on masonry components and building specimens assumed as benchmark, and their predictions for the performance of two masonry buildings representative of the building stock in the Groningen area.

The results of the analysis models and the benchmark tests were broadly in agreement, although ‘curve-fitting’ was used to different degrees in order to provide the predicted response.

The agreement between the teams for the performance of the index buildings was low. With the lessons learned from the benchmarking and cross-validation exercise, it is recommended that ‘blind’ modelling followed by newly planned experimental testing be carried out so that the most accurate and robust modelling and analysis method can be determined.

1 Background and Introduction

There are a number of different modelling and analysis procedures available for assessment of the seismic performance of unreinforced masonry (URM) residential buildings. Different procedures can give significantly different assessments of expected seismic performance, due to the different simplifying assumptions made. The Arup report “Modelling and Analysis Methods for Unreinforced Masonry Buildings in Groningen Area” [3] provides guidance to the modelling and analysis procedures specifically for typical building stock in the Groningen area.

Currently, very limited data is available on the seismic response of construction typologies specific to Dutch practice. Therefore, benchmarking and cross-validation against existing and newly planned experimental data are needed to study material characteristics and the response of components and full buildings, to validate and update the guidance given in [3].

Arup, in collaboration with modelling teams from the European Centre for Training and Research in Earthquake Engineering (EUCENTRE) and TU Delft, have selected a number of experimental benchmarks to calibrate and validate the various modelling approaches and analysis methods. The comparison of these experimental benchmarks is covered in Section 3. These experimental benchmarks were chosen to provide a consistent set of standard experiments for assessing model performance. Each of the three modelling teams used different software and modelling approaches, as set out in Section 2 and described in more details in the individual reporting done by the modelling teams in Appendix A (Arup), Appendix B (EUCENTRE), and Appendix C (TU Delft).

Following on from the results of the benchmarking exercises, cross-validation comparisons were conducted between various methods from the three modelling teams for assessing the seismic performance of two index buildings with typical geometries representative of the Groningen housing stock used in previous Arup studies, under fixed base assumptions. The two index buildings are T3a, a solid clay-brick detached house with timber floors; and T1*, a single bay of a modern terraced house building, with calcium silicate cavity walls and precast concrete plank floors. These comparisons are covered in Section 4.

Section 5 draws conclusions and recommendations about the current state of the benchmarking and cross-validation of the different modelling and analysis methodologies, and future work and development needed to improve the accuracy and robustness of these methods for use in support of fragility functions development for the Groningen Earthquakes – Structural Upgrading project.



Figure 1 Collaboration partners of Arup

2 Modelling Approaches

2.1 Arup – LS-DYNA

Arup used LS-DYNA for the modelling and analysis of URM buildings and building components. The modelling was performed using 3D brick elements. During the course of the work, Arup developed a shell model that was specifically implemented in a development version of LS-DYNA.

For nonlinear pushover and response history analysis, an explicit time integration scheme was used. For eigenvalue analysis, the Block Shift and Invert Lanczos eigensolver was used. URM was modelled using two different approaches:

1. Using 3D solid elements (brick-by-brick) with tiebreak contact between bricks to model the mortar. Shell elements, beam elements, and discrete (spring) elements were used to model other components of the benchmark and cross-validation tests. Material properties and tiebreak contact parameters were defined based on the available test data for masonry – both brick and mortar – characterisation tests, using a consistent methodology across all benchmarks and index buildings models. Details on the Arup modelling and analysis methodologies can be found in Appendix A of this document and Volume 1 Appendix B in [3].
2. Using 2D shell elements where damage is smeared across each element and crack plane directions are pre-defined to model mortar bonds. Shell elements, beam elements, and discrete (spring) elements were used to model other components of the benchmark tests. Material properties and bond parameters were defined using the same methodology as the one used for the solid model. The Arup LS-DYNA modelling and analysis methodologies for the shell models (as of December 2014) can be found in Volume 1 Appendix C in [3], although significant further enhancement of the masonry shell material model has now been undertaken (as of June 2015). The 2D shell approach was only used to model the benchmark tests and will be extended to the cross-validation tests in future.

2.2 EUCENTRE – TREMURI

EUCENTRE adopted an equivalent-frame modelling strategy which is implemented in the TREMURI computer program [6] and based on a nonlinear macro-element modelling approach. The macro-element model represents the cyclic nonlinear behaviour associated with the two main in-plane masonry failure modes – bending-rocking and shear mechanisms – with eight degrees of freedom and a limited number of internal variables which describe the evolution of masonry damage [13]. The two-node macro-elements – for modelling piers and spandrel beams – are subdivided into three parts: a central body where only shear deformation can occur and two interfaces where the external degrees of freedom are placed, which can have relative axial displacements and rotations with respect to those of the extremities of the central body. In the two interfaces that are infinitely rigid in shear, the axial deformations are due to a distributed system of zero-length springs with no-tension and limited compression behaviour. Floor and roof diaphragms are modelled by means of linear three-node and four-node

orthotropic membrane elements. Guidance for the definition of model parameters – e.g. effective elastic modulus (E') – is explained in more detail in Appendix B.

2.3 TU Delft – TNO DIANA

For the analyses at TU Delft the TNO DIANA implicit solver was used. The unreinforced masonry (URM) modelling approach adopted in DIANA is the total strain based smeared crack model – with or without nonlinearity in compression [4][14]. Numerous validation studies using this approach on masonry structures are available in literature [11][12]. Quadratic plane stress elements were used for in-plane cases and 2D configurations. For combined in-plane/out-of-plane cases and 3D configurations, quadratic shell elements were used. More details about the TU Delft modelling and analysis approach can be found in Appendix C.

3 Comparison with Experimental Benchmarks

3.1 The benchmark tests

The experimental benchmark tests are a series of published physical tests conducted both in the Netherlands and around the world. They were chosen collectively by Arup, EUCENTRE and TU Delft to calibrate and compare numerical modelling techniques. Their selection was such that the masonry modelling techniques could be calibrated for different materials, load cases, and both in-plane and out-of-plane behaviour. The benchmark tests are summarised in Table 1. More details about these experimental benchmarks can be found in Volume 3 of [3].

Table 1 List of experimental benchmark tests

Benchmark test	Report section	Laboratory; Authors	Behaviour investigated
Ispra wall panel	3.2	Joint Research Centre, Ispra Anthoine A., Magonette G., Magenes G.	In-plane behaviour of one-way spanning unreinforced clay brick masonry wall panels under quasi-static cyclic loading.
Pavia full building	3.3	University of Pavia Magenes G., Calvi GM, Kingsley G.	In-plane behaviour of full-scale two-storey building under quasi-static cyclic loading.
ESECMaSE in-plane cyclic calcium silicate panel	3.4	University of Pavia (EUCENTRE Lab) Magenes G, Morandi P, Penna A	In-plane behaviour of single-leaf unreinforced calcium silicate brick masonry wall panels under quasi-static cyclic loading.
ESECMaSE full-scale calcium silicate half-building	3.5	Joint Research Centre, Ispra Anthoine A, Claperan P	Behaviour of full-scale calcium silicate brick half-building under pseudo-dynamic loading.
Australia out-of-plane one-way spanning wall	3.6	University of Adelaide Doherty KT, Griffith MC	Out-of-plane behaviour of one-way spanning, single-leaf, unreinforced clay brick masonry wall panels under quasi-static and dynamic loading.
Australia out-of-plane two-way spanning wall	3.7	University of Adelaide Vaculik J, Griffith MC	Out-of-plane behaviour of two-way spanning, single leaf, unreinforced clay brick masonry wall panels under quasi-static loading.

The following sections compare the analytical predictions of the behaviour of benchmark tests specimens made by the three analysis teams.

3.2 Ispra In-Plane Panel Tests (Anthoine et al., 1995)

3.2.1 LOWSTA test comparison

The peak forces predicted by each model are compared in Table 2, the crack patterns in figure 2 and the cyclic hysteresis loops in figure 3.

Table 2 LOWSTA ultimate load values

	Experiment	LS-DYNA Solid	LS-DYNA Shell	TREMURI	DIANA
Ultimate Load (kN)	84	86	86	86	70

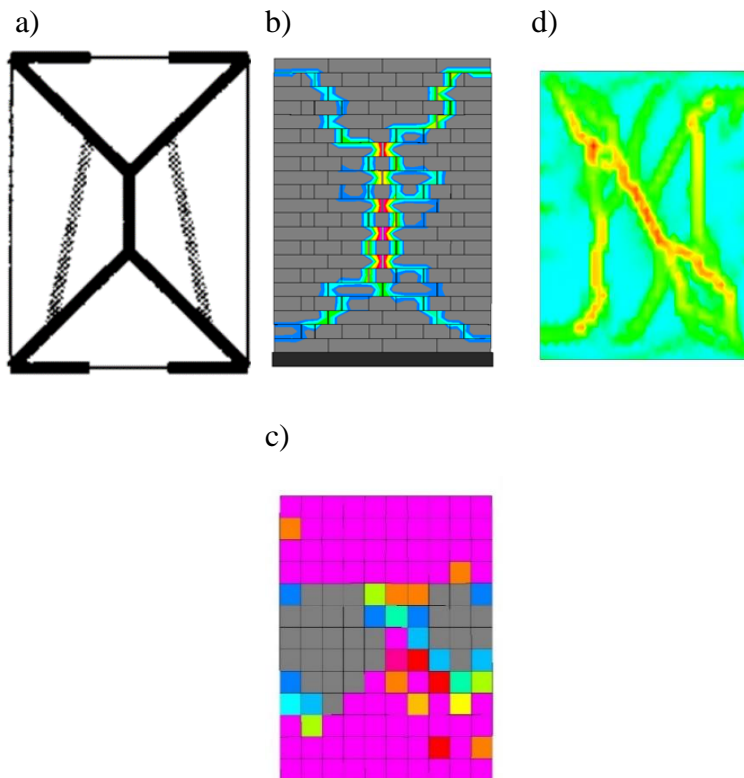


Figure 2 Final crack pattern for LOWSTA – comparison between a) laboratory test, b) LS-DYNA solid element model, c) LS-DYNA shell element model and d) DIANA

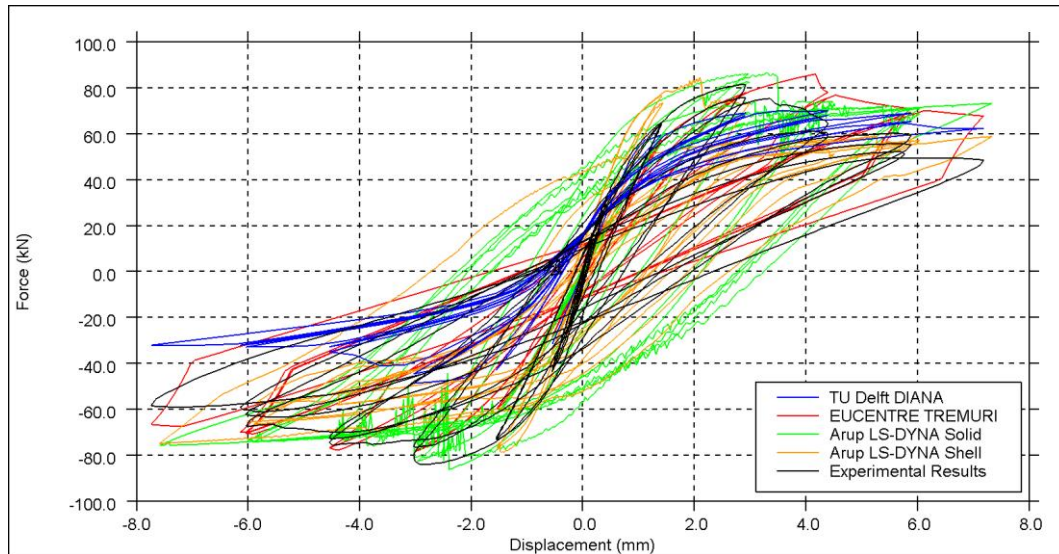


Figure 3 Shear force-displacement comparison plot for LOWSTA

3.2.1.1 DIANA

In the DIANA model of the LOWSTA sample, a diagonal tension crack appears in one direction, whilst in the other direction a set of vertical cracks was observed (Figure 2). The overall crack pattern is quite consistent with the experimental one, although being less symmetrical but the model predicted a lower shear capacity with respect to the experiment, providing an ultimate load of around 70 kN.

3.2.1.2 LS-DYNA Solid model

The crack pattern predicted by the LS-DYNA solid model is very close to the experimental results (Figure 2) where it shows a diagonal tension sliding brittle failure mode, similar to the laboratory observations.

The analysis force-displacement output of the LS-DYNA solid element model shows an ultimate load of 86 kN, which is very close to the laboratory value of 84 kN, at a drift of 2%. The test showed both modest strength degradation and reduction of stiffness during the larger cycles, i.e. above 2.5 mm amplitude. The analysis predicted some strength degradation as the amplitude exceeds 3 mm, but no further degradation for higher amplitudes up to 7 mm. However, the energy dissipation predicted in the LS-DYNA solid element analysis is more than that recorded during the experiment.

3.2.1.3 LS-DYNA Shell model

The LS-DYNA shell model predicted an ultimate load of 86 kN, and the strength degradation and reduction of stiffness in the model was close to that of the experimental results. Diagonal cracking similar to that observed experimentally was reproduced although the crack pattern was slightly less symmetrical than the experimental results.

3.2.1.4 TREMURI

The ultimate load predicted by agrees well with the test result. TREMURI also reproduced the shear force-displacement curves well; however this was achieved through some calibration of the macro-element model parameters governing nonlinear deformability and softening branch (shear behaviour) as described in Appendix B.

3.2.2 HIGSTA1 test comparison

The peak forces predicted by each model are compared in Table 3, the crack patterns in figure 4 and the cyclic hysteresis loops in figure 5.

In the experiment, the deflection mode was predominantly rocking, associated with tensile bed joint failures at the top and bottom. In general, the hysteresis loops on the experiment are somewhat ‘fatter’ than those predicted by the analyses, indicating rather higher energy dissipation.

Table 3 HIGSTA1 ultimate load values

	Experiment	LS-DYNA Solid	LS-DYNA Shell	TREMURI	DIANA
Ultimate Load (kN)	72	68	71	66	52

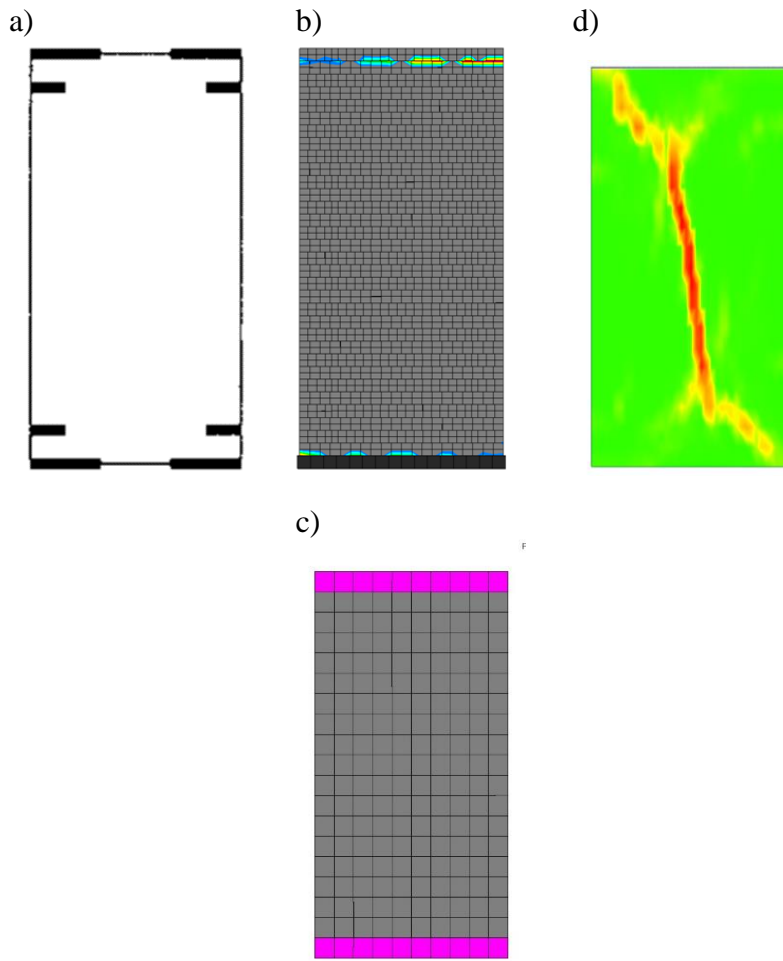


Figure 4 Final crack pattern for HIGSTA1 – comparison between a) laboratory test, b) LS-DYNA solid element model, c) LS-DYNA shell element model and d) DIANA

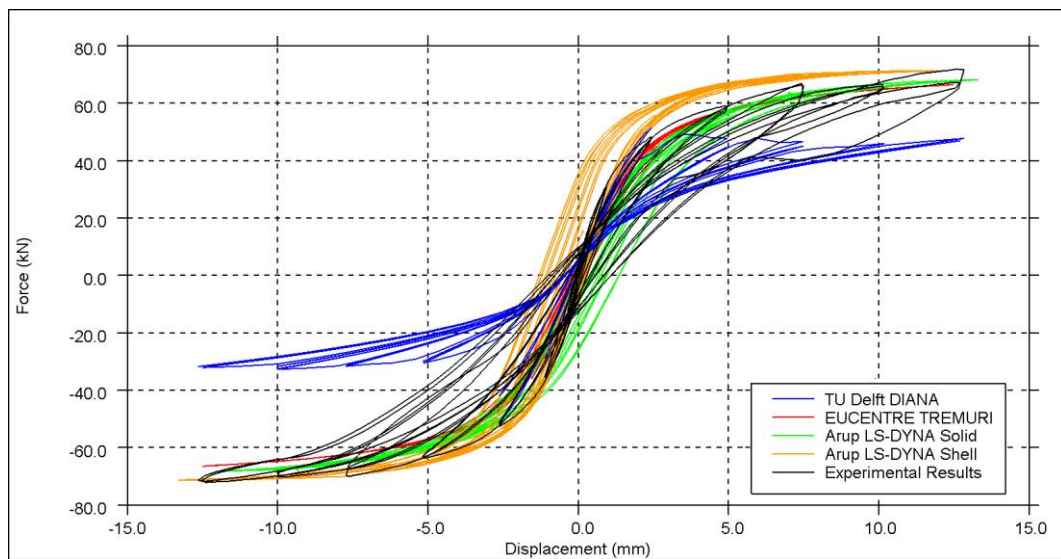


Figure 5 Shear force-displacement comparison plot for HIGSTA1

3.2.2.1 DIANA

In the DIANA model rocking behaviour was initially observed but diagonal cracking occurred at higher drift levels, which were not observed experimentally. The predicted ultimate resistance of 52kN is lower than the experimental value of 72kN.

3.2.2.2 LS_DYNA Solid model

The LS-DYNA solid model predicted ultimate load, crack pattern and rocking behaviour very similar to the experimental results.

3.2.2.3 LS-DYNA shell model

The LS-DYNA shell model predicted ultimate load, crack pattern and rocking behaviour very similar to the experimental results.

3.2.2.4 TREMURI

The TREMURI model predicted ultimate load, crack pattern and rocking behaviour very similar to the experimental results.

3.2.3 Notes and Discussion

The TU Delft team observed a high sensitivity of DIANA results, in terms of predicted shear capacity, amplitude of the hysteresis loops and type of failure, to strength parameters (for detailed results of sensitivity analyses see Section 2.1.1 of Appendix C). In general, TU Delft observed that a higher tensile strength value led to rocking failure in the analysis, with higher global capacity and more compact hysteretic loops. Reducing the strength led to shear failure, characterised by a diagonal crack, with an increase in energy dissipation in the hysteretic loops.

For the elastic modulus of the macro-element in TREMURI, it was assumed that $E' = 3E$, which – according to the EUCENTRE methodology detailed in Appendix B – means that the panel was modelled as fixed-fixed. However, the panel was allowed to rock to some extent in the laboratory tests. With appropriate calibration, the TREMURI model was able to simulate quite accurately the hysteretic response of the LOWSTA models, including the strength deterioration and stiffness degradation associated with shear damage.

For the HIGSTA experiment all the models – DIANA, LS-DYNA solid element, LS-DYNA shell and TREMURI predicted very compact hysteresis loops with less energy dissipation than the experimental results.

3.3 Pavia Full Building Tests (Magenes et al., 1994)

3.3.1 Results comparison

The crack patterns predicted by the analytical approaches were plotted at the end of each run and are presented and compared with experimental tests in Figure 6 to Figure 12. The force-deflection hysteresis behaviours are compared to the experimental results in Figure 13 and Figure 14.

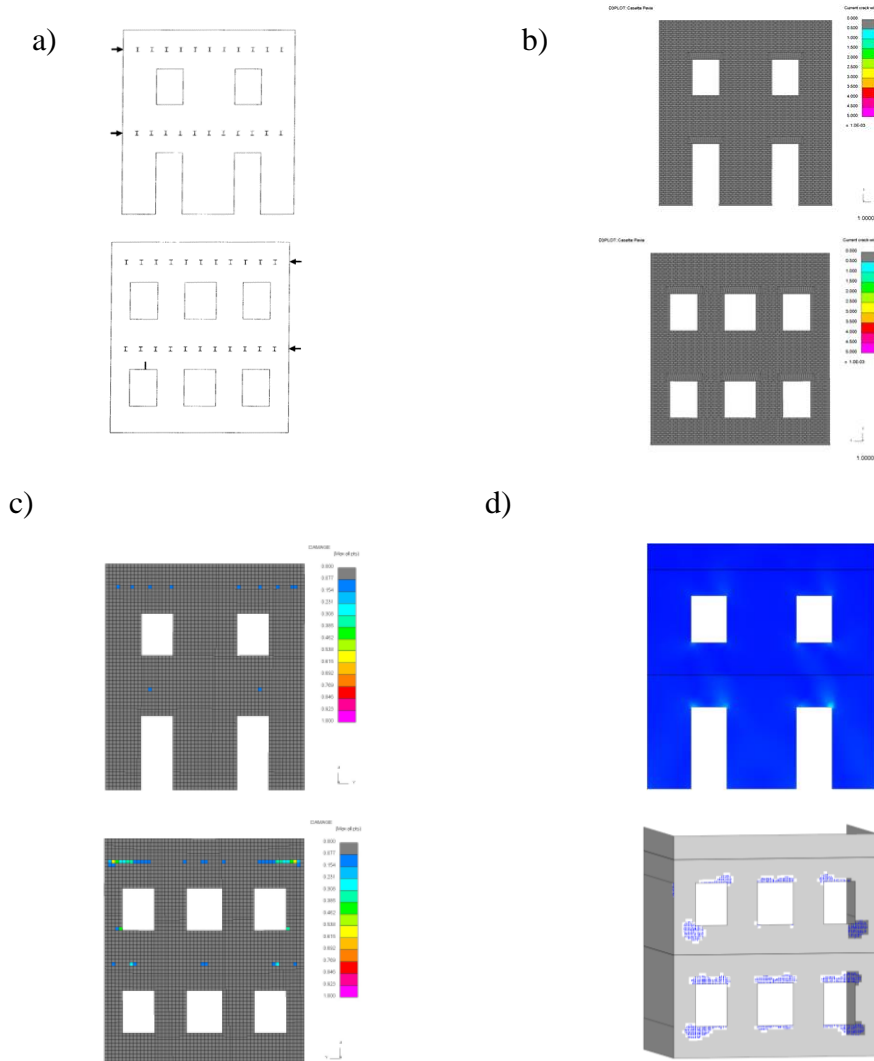


Figure 6 Crack pattern after Run 1. From left to right, top to bottom: a) Laboratory test results; b) LS-DYNA solid element analysis; c) LS-DYNA shell element analysis; d) DIANA analysis in two loading directions. (Top row: Door wall; bottom row: Window wall.)

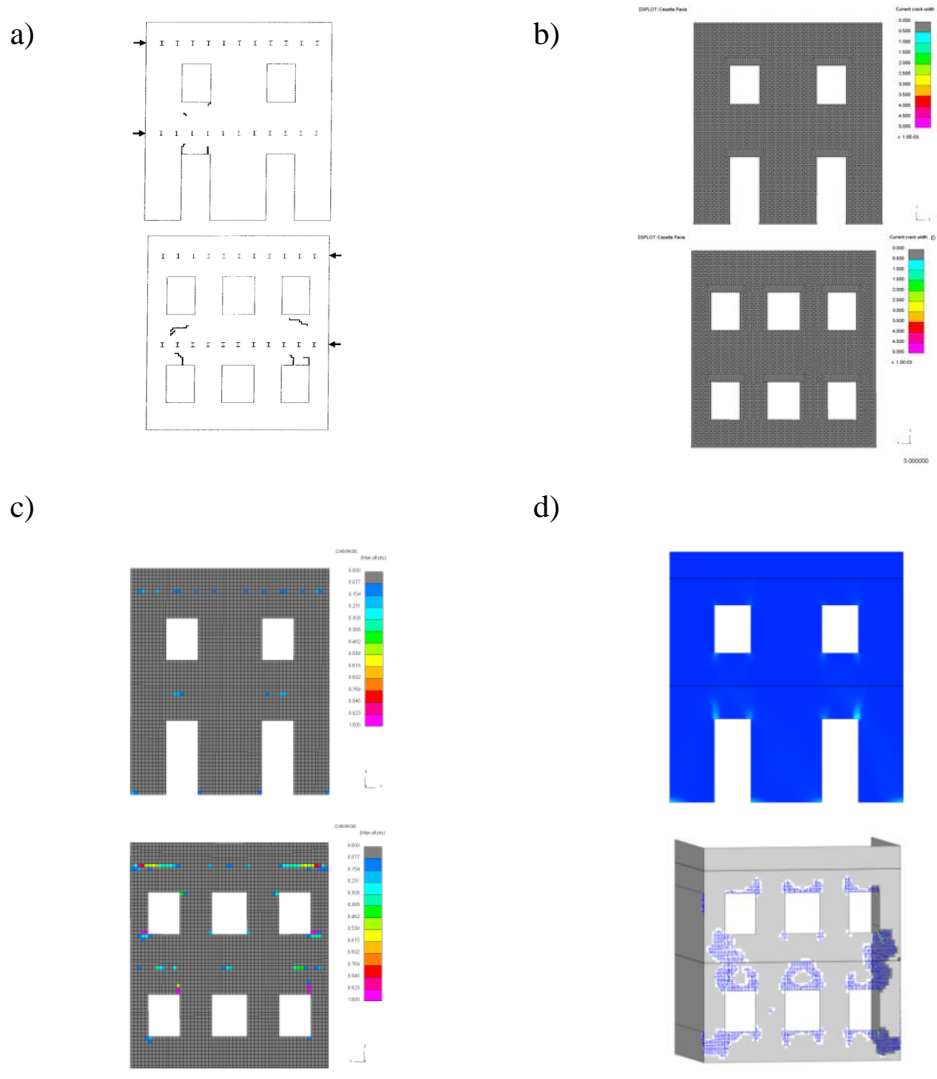


Figure 7 Crack pattern after Run 2. From left to right, top to bottom: a) Laboratory test results; b) LS-DYNA solid element analysis; c) LS-DYNA shell element analysis; d) DIANA analysis in two loading directions. (Top row: Door wall; bottom row: Window wall.)

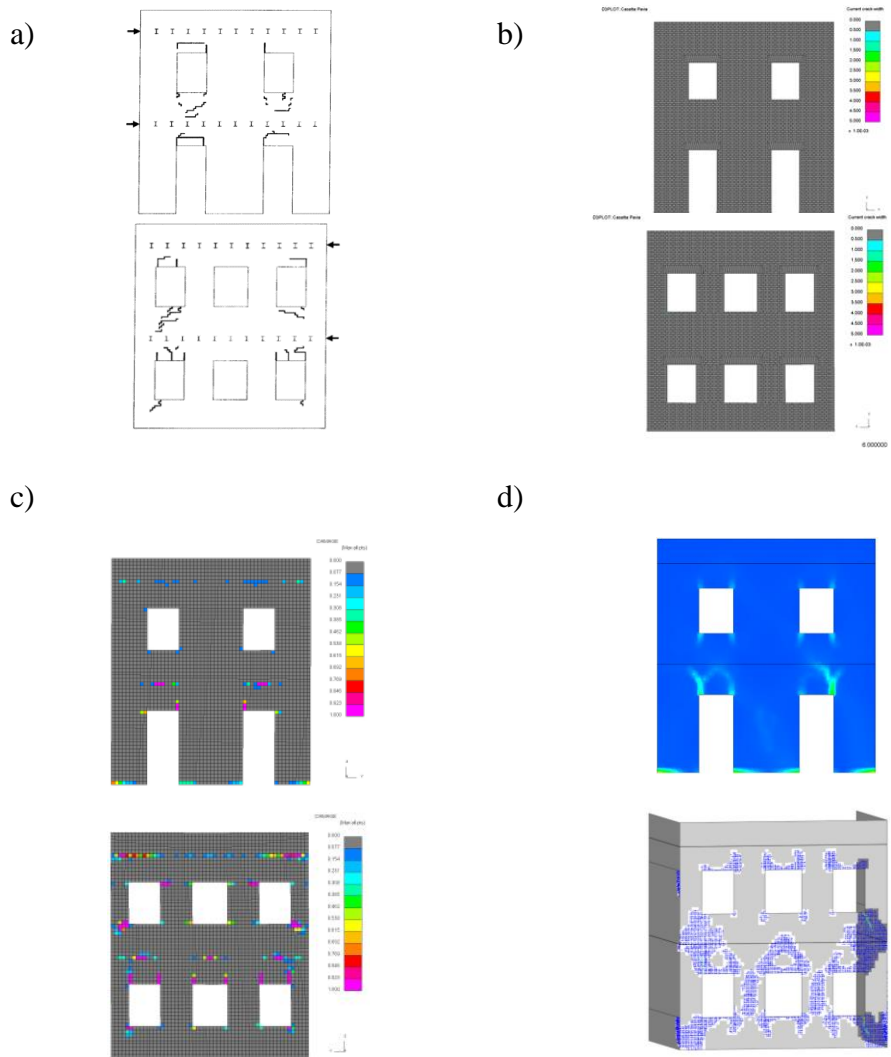


Figure 8 Crack pattern after Run 3. From left to right, top to bottom: a) Laboratory test results; b) LS-DYNA solid element analysis; c) LS-DYNA shell element analysis; d) DIANA analysis in two loading directions. (Top row: Door wall; bottom row: Window wall.)

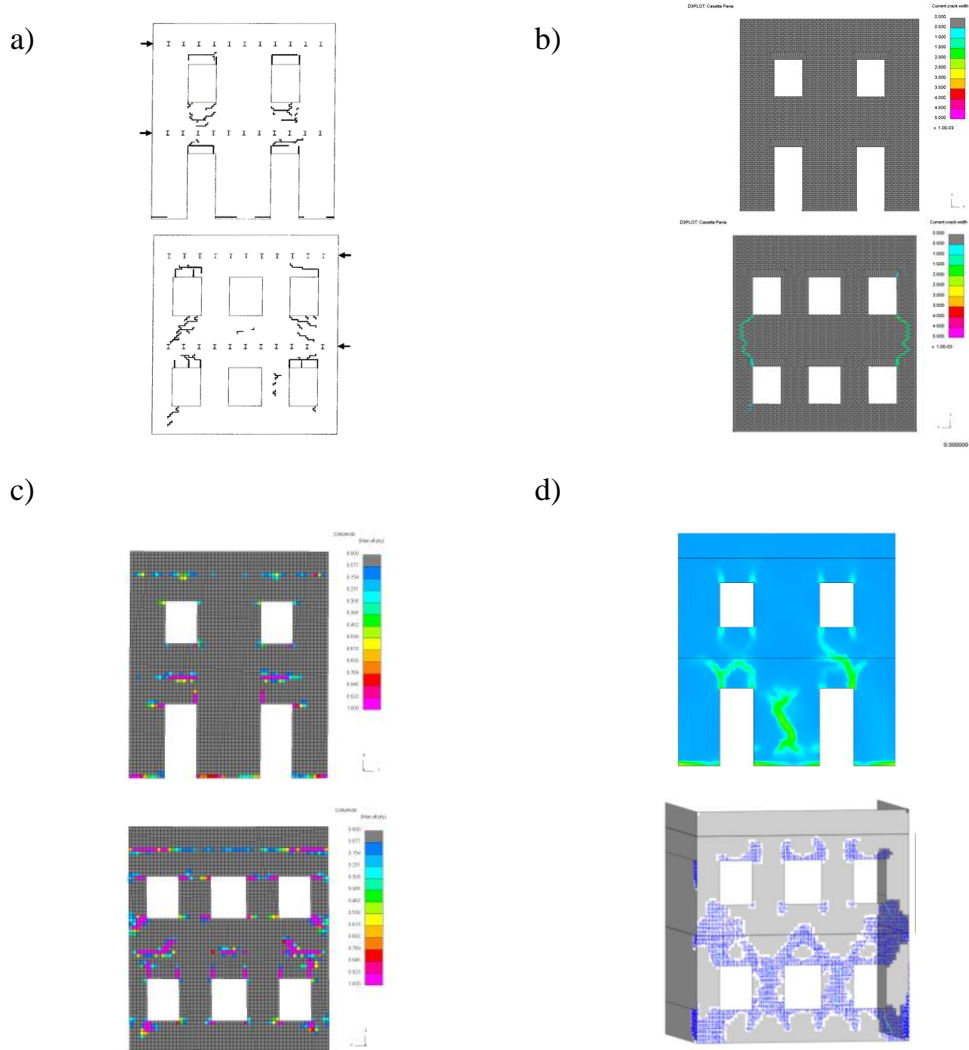


Figure 9 Crack pattern after Run 4. From left to right, top to bottom: a) Laboratory test results; b) LS-DYNA solid element analysis; c) LS-DYNA shell element analysis; d) DIANA analysis in two loading directions. (Top row: Door wall; bottom row: Window wall.)

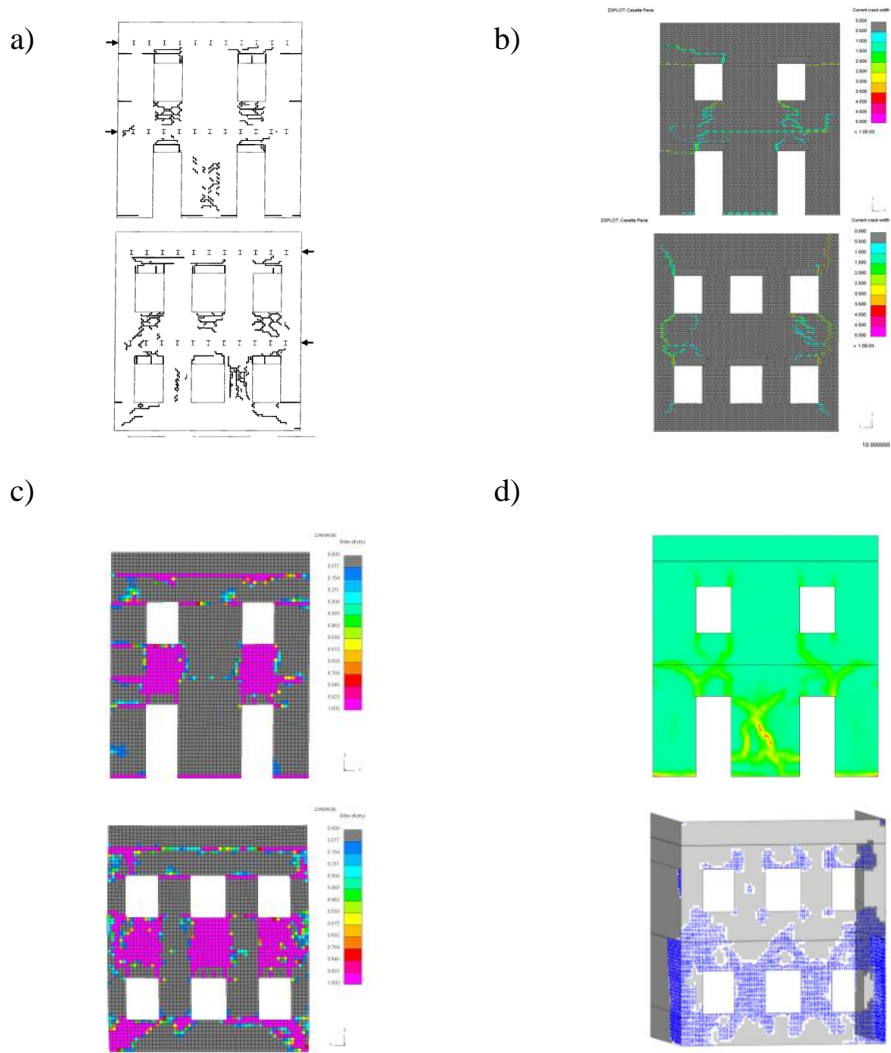


Figure 10 Crack pattern after Run 5. From left to right, top to bottom: a) Laboratory test results; b) LS-DYNA solid element analysis; c) LS-DYNA shell element analysis; d) DIANA analysis in two loading directions. (Top row: Door wall; bottom row: Window wall.)

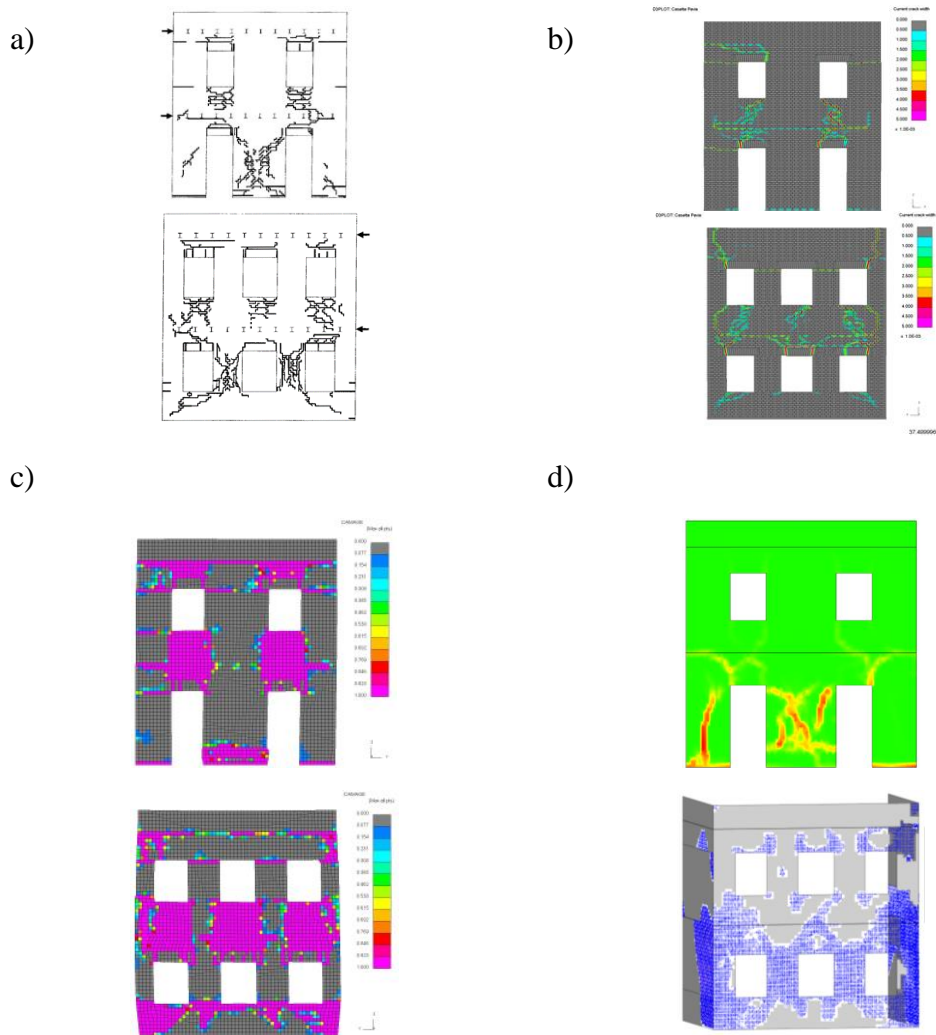


Figure 11 Crack pattern after Run 6. From left to right, top to bottom: a) Laboratory test results; b) LS-DYNA solid element analysis; c) LS-DYNA shell element analysis; d) DIANA analysis in two loading directions. (Top row: Door wall; bottom row: Window wall.)

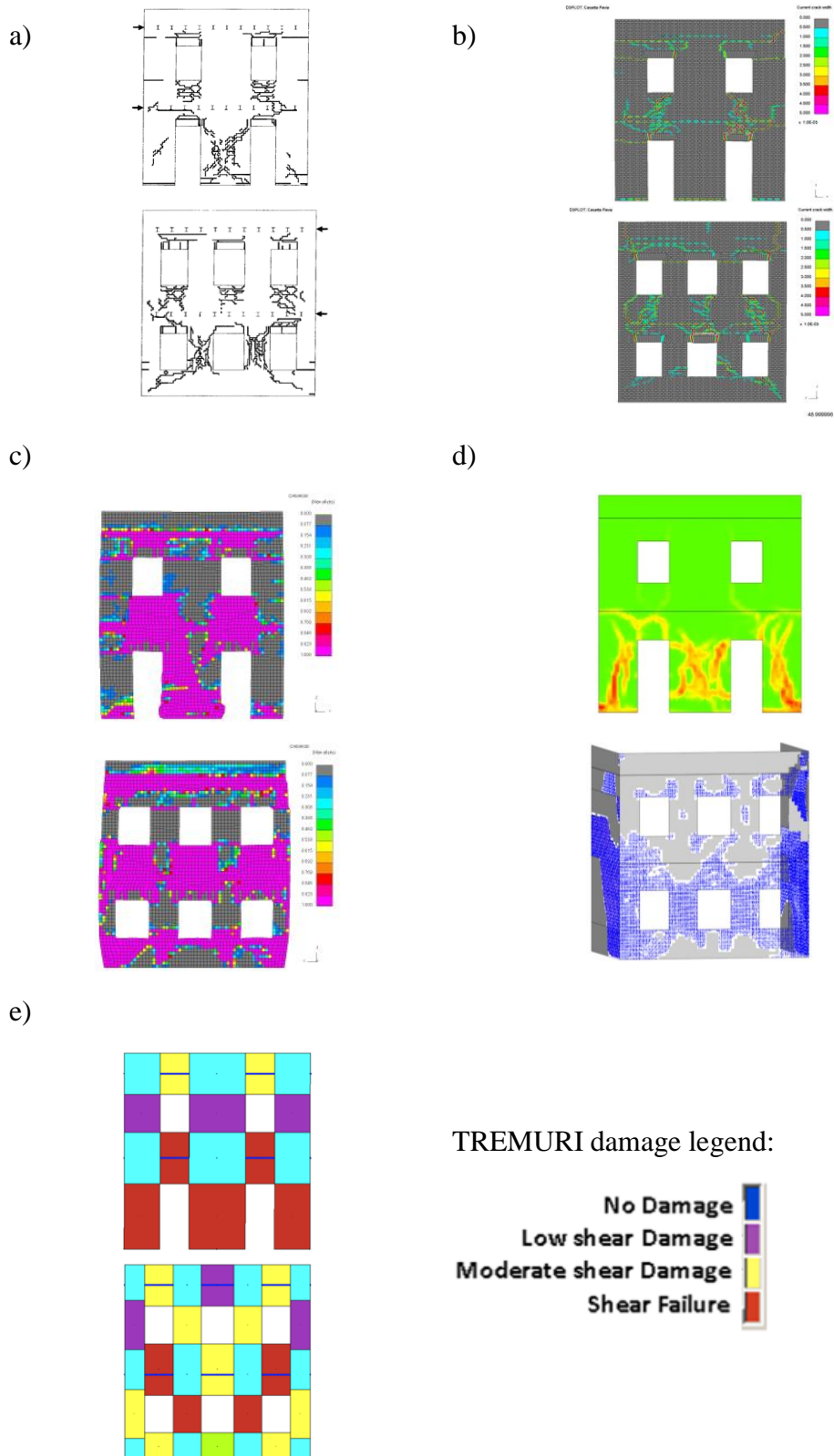


Figure 12 Crack pattern after Run 7 (end of the test). From left to right, top to bottom: a) Laboratory test results; b) LS-DYNA solid element analysis; c) LS-DYNA shell element analysis; d) DIANA analysis in two loading directions; e) TREMURI. (Top row: Door wall; bottom row: Window wall.)

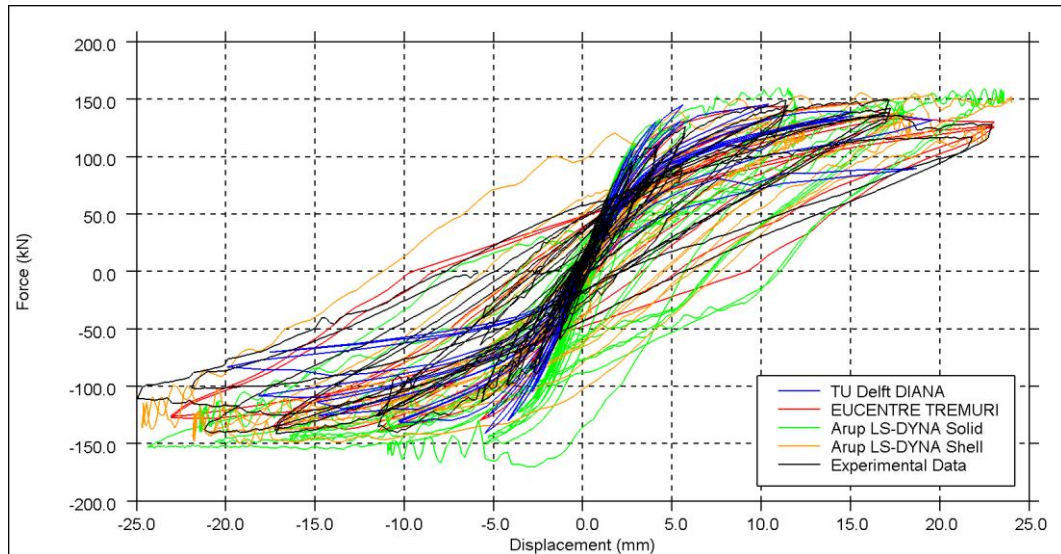


Figure 13 Total base shear force vs. second floor displacement (Door Wall)

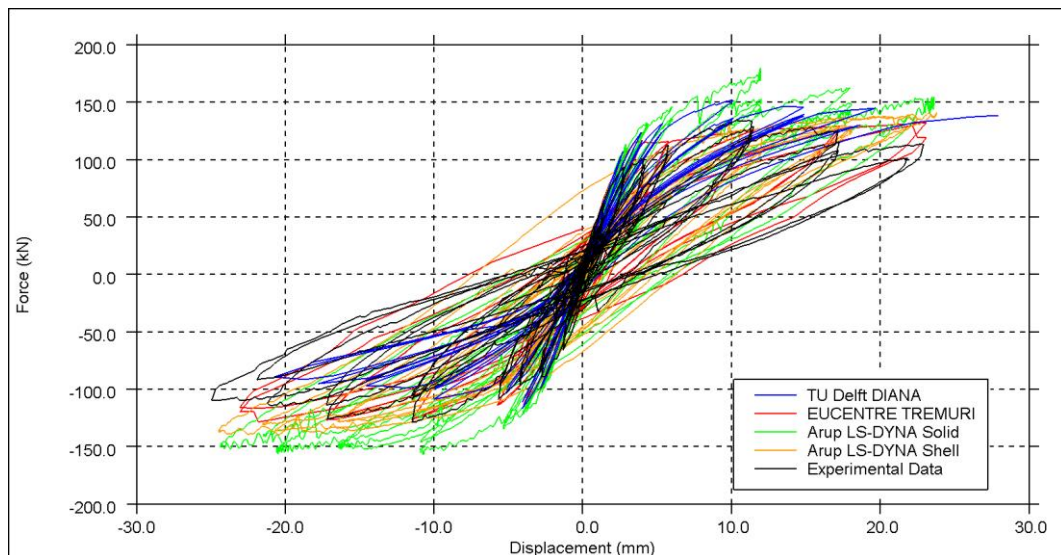


Figure 14 Total base shear force vs. second floor displacement (Window Wall)

3.3.1.1 DIANA

The overall ultimate capacity, energy dissipation and the shear degradation in both door and window walls were reasonably well estimated by the DIANA model. However, the crack patterns do not seem to correspond very well with the experimental observations. Cracks are noticed in the outer piers of the door wall from Run 5; this was not observed in the experiments. In general, in the DIANA shell models most of the damage was observed in the first floor whilst in the experiment there was also extensive damage in the spandrels. The predicted drift of the first level appears reasonable, but the drift of the second is underestimated one, leading the damage to be mainly focused on the first level.

A 2D model of window wall was implemented in DIANA to investigate the impact of the orthogonal walls in the 3D models. The TU Delft modelling team

reported that the 2D model predicted a similar response as the 3D model (see Figure 2.2.24 in Appendix C).

3.3.1.2 LS-DYNA Solid model

The LS-DYNA solid element analysis predicts higher capacities for the door wall in the $-X$ direction and window wall in both directions. The stiffness and strength of the LS-DYNA solid element model is also higher than the experimental results for the window wall, although the energy dissipation is comparable.

In the door wall, the damage patterns in the spandrels closely replicates those observed in the experiment, but the ground floor piers were observed to rock instead of fail in diagonal tension. In the window wall, there was more damage in the spandrels than observed experimentally, and the ground floor piers did not exhibit diagonal cracking. However the behaviour on the first floor followed that of the experiment.

3.3.1.3 LS-DYNA Shell model

The strength and degree of degradation predicted by the LS-DYNA shell model reasonably matches the experiment.

In the door wall, the predicted cracking in the first floor spandrel and the ground floor central pier closely matches that of the experiment; the damage is mostly in diagonal tension. However a horizontal sliding failure is predicted at the level of the second floor diaphragm and there is shear failure across the top of the first floor pier, which was not observed in the experiment.

In the window wall, diagonal tension failures in the spandrels below the extreme left and right first floor windows are consistent with the experiment, as are the diagonal tension failures in the two central piers on the first floor and the cracking in the ground floor spandrels. However there is more degradation in the spandrel below the central window on the first floor than was observed in the experiment and there is again sliding failure at the second floor level which was not observed during the experiment.

3.3.1.4 TREMURI

In the TREMURI model, an equivalent (increased) height of the external piers was adopted by the EUCENTRE modelling team to obtain a good fit to the experimental cyclic curve (see Section 2.2.1 of Appendix B). With this calibration to the results, the initial stiffness, the peak shear force and strength degradation were well captured by the TREMURI models. The TREMURI final damage patterns of both the models (Figure 12e) are consistent to the experimental test results.

3.3.2 Notes and Discussion

The hysteresis comparisons show that the initial stiffness of both the walls was well captured by all the models and there is reasonable agreement with respect to ultimate strength – although the LS-DYNA solid model tended to over-predict strength slightly.

Many detailed comments could be made by looking at the different predicted damage patterns – which are clearly not identical. In particular, the failure of piers in rocking often caused damage to be concentrated in other parts of the structure, which eventually produced global results with an excess in strength in the LS-DYNA and DIANA models. These differences can be used by the analysis teams (and the software developers) to assess where further refinements and improvements could be made.

Good results were obtained from TREMURI for the Window Wall model when an appropriate equivalent pier height was derived in sensitivity studies, as described in Section 2.2.1 of Appendix B. With this calibrated model the TREMURI final damage patterns of both the models are very close to the experimental observations.

3.4 ESECMaSE Calcium Silicate In-Plane Panel Tests (Magenes et al., 2008)

3.4.1 CS03 test comparison

The crack pattern in the laboratory tests was characterised by the opening of the unfilled head joints, which became evident at a top displacement of ± 10 mm. The head and bed joint cracks formed a pattern of stepped diagonal cracks along the height of the wall. These cracks closed during unloading. When the top displacement increased, the cracks became very wide and no further increase of shear capacity was possible. When the top displacement exceeded 15 mm, cracks developed in the units at the centre of the panel, producing significant strength degradation and failure of the wall [10].

The predicted hysteresis loops for wall CS03 are compared to the experimental results in Figure 15 and the final crack patterns are compared in Figure 16.

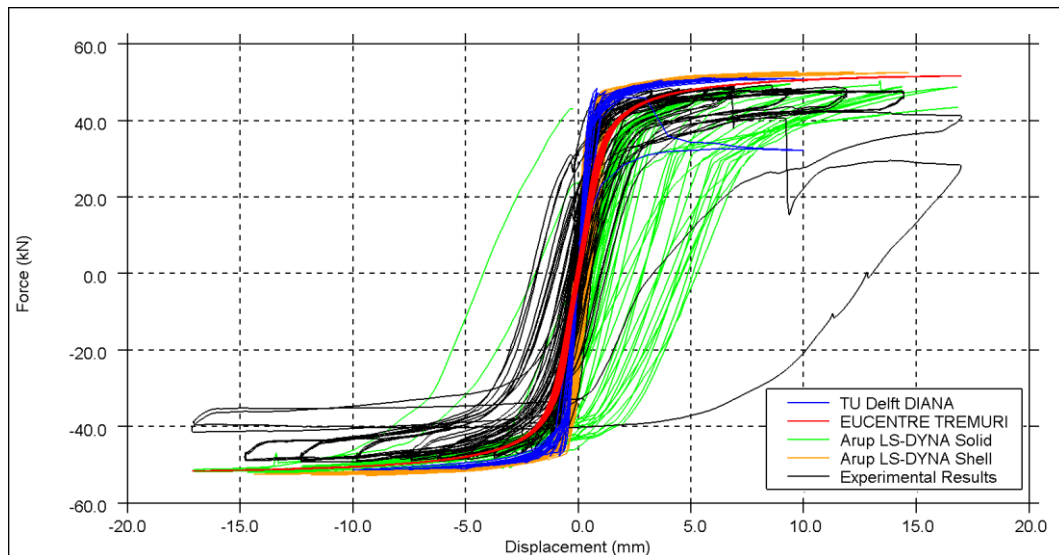


Figure 15 Shear force-displacement comparison plot for CS03

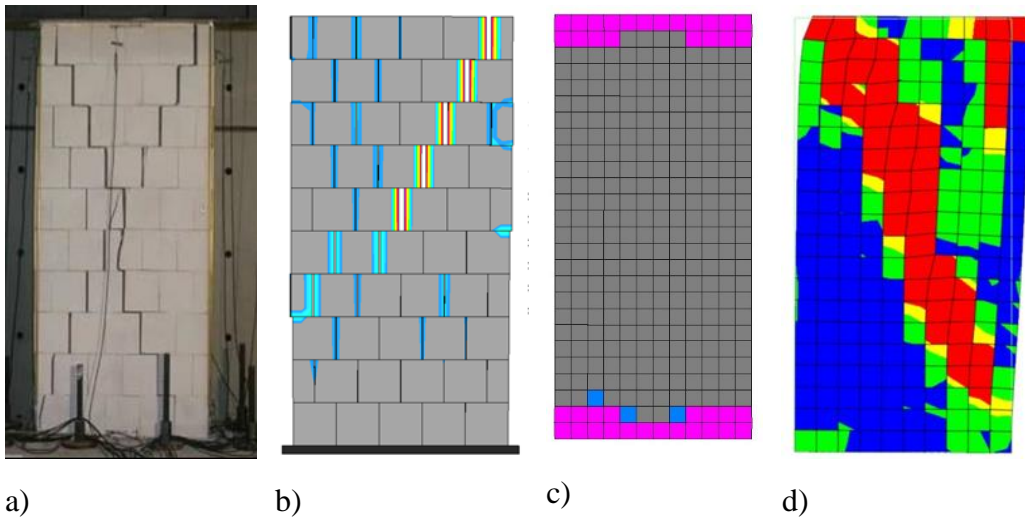


Figure 16 Final crack pattern for CS03 – a) experimental test, b) LS-DYNA solid, c) LS-DYNA shell and d) DIANA

3.4.1.1 DIANA

The DIANA simulation predicted the ultimate strength well and failure by diagonal cracking. The hysteresis loops do not dissipate as much energy as the test results.

3.4.1.2 LS-DYNA solid model

The LS-DYNA solid model predicted the ultimate strength and the step-wise diagonal crack observed. This model predicts significantly higher energy dissipation than the experiment.

3.4.1.3 LS-DYNA shell model

The backbone curve obtained with the LS-DYNA shell model is close to the experimental result in terms of initial stiffness and ultimate strength, but the cyclic displacement mode comprised rocking only, and the observed diagonal cracking failure mode was not predicted.

3.4.1.4 TREMURI

The backbone curve obtained with the TREMURI is close to the experimental result in terms of initial stiffness and ultimate strength, but the macro-element model did not capture the experimental energy dissipation or the diagonal cracking failure mode.

3.4.2 CS05 test comparison

Wall CS05 in the experiments remained undamaged, with the exception of some tension cracks in the bed-joints, up to a horizontal top displacement of 35 mm. When this displacement level was exceeded, the wall failed suddenly in shear with the development of a diagonal crack in the mortar bed joint and in the brick units.

Before this damage the force-displacement curve presented S-shaped cycles with low energy dissipation, similar to a typical rocking behaviour [10].

The predicted hysteresis loops for wall CS05 are compared to the experimental results in figure 17 and the final crack patterns are compared in figure 18.

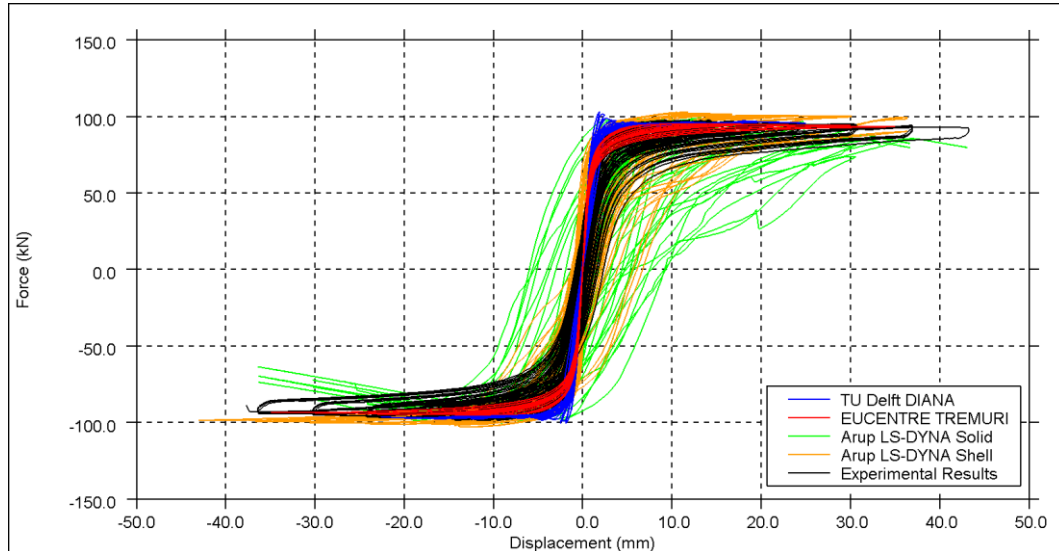


Figure 17 Shear force-displacement comparison plot for CS05

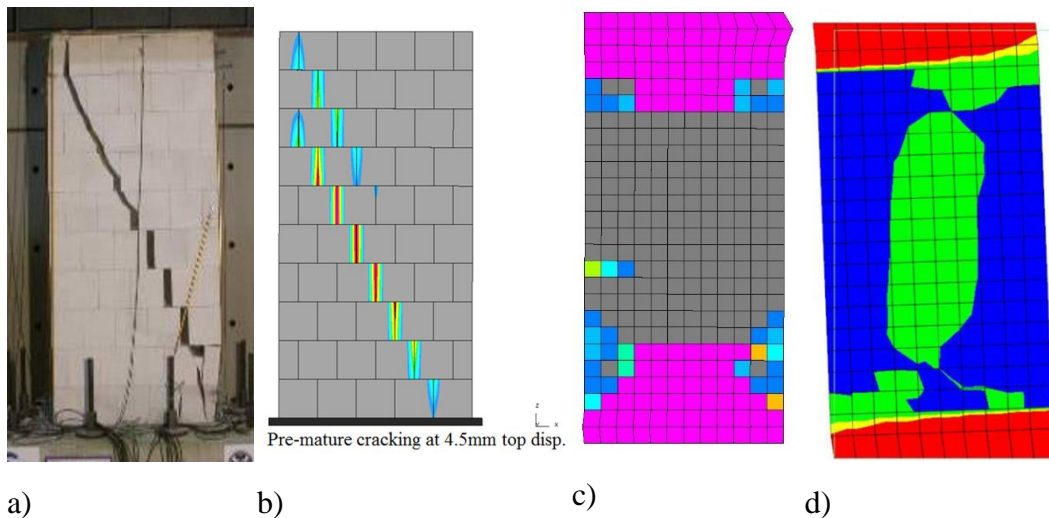


Figure 18 Crack pattern for CS05 – a) experimental test, b) LS-DYNA solid, c) LS-DYNA shell and d) DIANA

3.4.2.1 DIANA

Although the ultimate load was well predicted, the DIANA analysis could not run up to the full displacement range in the experiment, due to convergence issues. TU Delft reported that the DIANA analytical model was not able to reproduce the hysteresis loops of the experiments, mentioning as a possible cause the adoption of secant unloading in the material model.

3.4.2.2 LS-DYNA solid model

The LS-DYNA solid model predicted the ultimate load well, but results show premature mortar cracking and significantly larger cyclic energy dissipation than the experiment.

3.4.2.3 LS-DYNA shell model

The LS-DYNA shell model predicted the ultimate load and overall hysteresis well, though there was slightly more energy dissipation than the experiment during the last few cycles. This occurred as the analytical model began to experience damage spread further into the wall, releasing more energy than would a wall undergoing pure rocking.

3.4.2.4 TREMURI

TREMURI predicted the ultimate load and overall hysteresis well, though there was less energy dissipation than the experiment consistent with a model representing pure rocking behaviour.

3.4.3 Notes and Discussion

For both wall panels, all the models predicted similar peak shear forces compared to the experiments (albeit with different degrees of “curve-fitting” of input parameters), but did not necessarily capture the correct levels of energy dissipation observed in experimental data or the correct ultimate failure modes.

In the DIANA models, similar to their Ispra panel models (Section 3.2), the TU Delft modelling team noted the “*need for the increase of tensile fracture energy (especially for higher vertical loads, i.e. for CS05) to account for the energy consumption in the stepwise diagonal crack associated to friction due to horizontal sliding of the blocks*” (see Section 2.3.1 in Appendix C). It is mentioned in their work that the total strain based crack models can possibly be improved with strength and fracture energy values that are a function of the inclination of the crack with respect to the bedjoint, though this will require more development and validation from the TU Delft modelling team.

The LS-DYNA solid model over-predicted the energy dissipation significantly because of the premature cracking in the model and local sliding with friction in the solid model. In sensitivity analyses (see Section 2.3.1 in Appendix A), a very small change in mortar strength in the CS03 analysis (0.03 MPa) caused 2 mm difference in the top deflection at which these joints opened, showing that the predicted opening is very sensitive to mortar strength. It is possible that analysis with a small further credible increase in assumed mortar strength would predict head joint opening at a similar displacement level to the test.

The LS-DYNA shell model, although predicting backbone behaviour reasonably well, did not predict the ultimate failure modes (by diagonal cracking). The need to improve this aspect of the model was recognized and improved algorithms are now in final testing (June 2015).

TREMURI also predicts the backbone behaviour reasonably well, but does not predict the observed ultimate failure modes.

3.5 ESECMaSE Calcium Silicate Full-Scale Half-Building Tests (Anthoine et al., 2007)

3.5.1 Pushover analyses comparison

The pushover analysis predictions of using DIANA and TREMURI are compared in Figure 28 with the envelope of max-shear and max-displacement reported in the experimental results.

It can be seen that the DIANA monotonic pushover analysis predicts higher capacity than observed in the experiments. A hardening effect is observed in the DIANA output. TU Delft interprets this as due to the fully clamped connection through the orthogonal walls. The TREMURI results are in good agreement with the experimental results in terms of both initial stiffness and ultimate strength capacity.

Pushover analysis was not performed in LS-DYNA, as the experiments were completed using a pseudo-dynamic methodology.

3.5.2 Pseudo-dynamic performance comparison

The predicted hysteresis behaviours of the various predictions are compared to the experimental observations in Figure 19 to 27. The predicted crack patterns are compared to the ESECMaSE laboratory test observations in Figure 29 and 30.

The first significant damage appeared during the 0.12g PGA test. Large stepwise cracks formed in the West slender wall of the ground floor; and in both long transversal walls, horizontal cracks opened at mid-height of the first level – on the East side next to the main shear wall and on the West side next to the slender wall. Threadlike stepwise cracks were also detected in the main shear wall of the ground floor. The final test at 0.20g PGA was characterised by severe cracking (also through the brick units) of the North-West top corner of the specimen, including the slender wall as well as the neighbouring portion of the transversal wall [2].

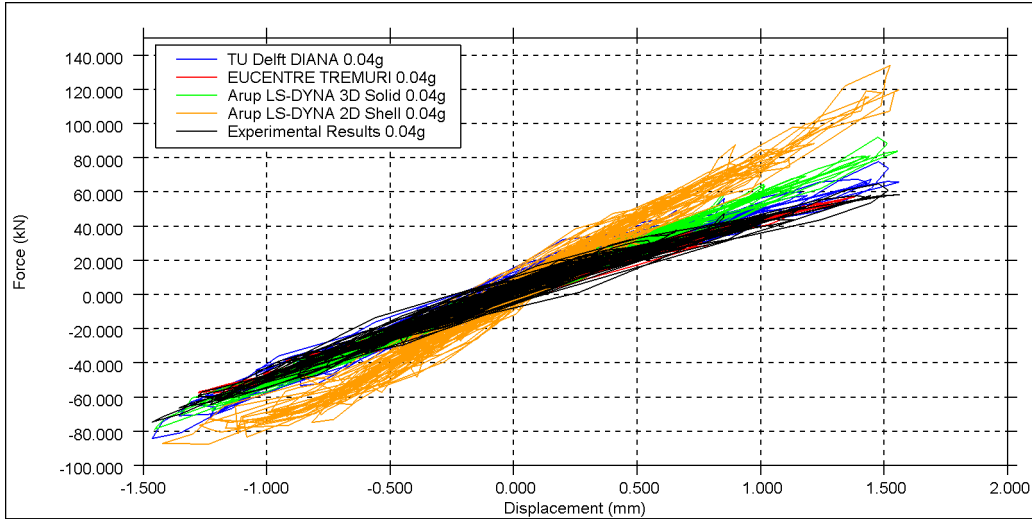


Figure 19 Base shear force vs. top displacement hysteresis plot during 0.04g PGA

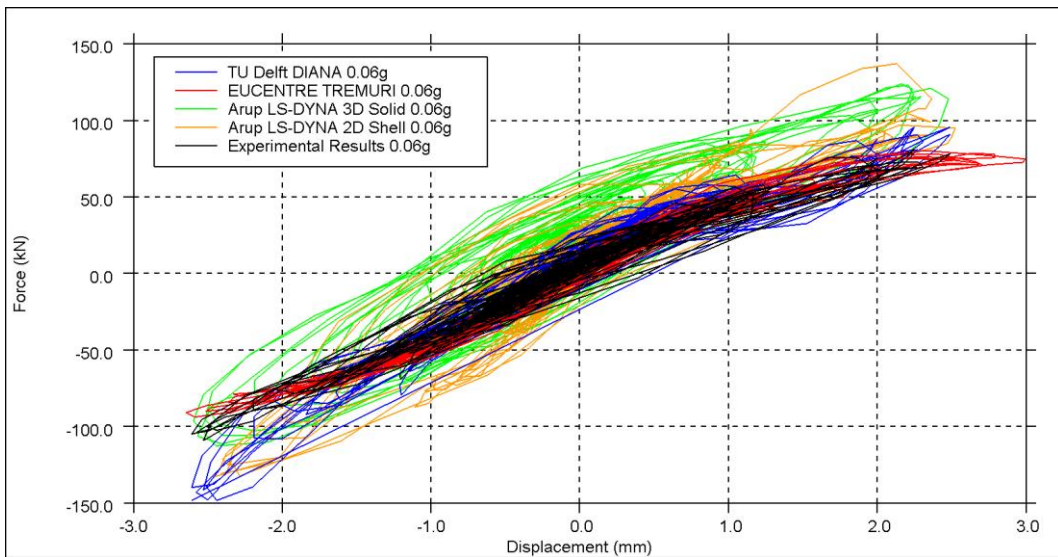


Figure 20 Base shear force vs. top displacement hysteresis plot during 0.06g PGA

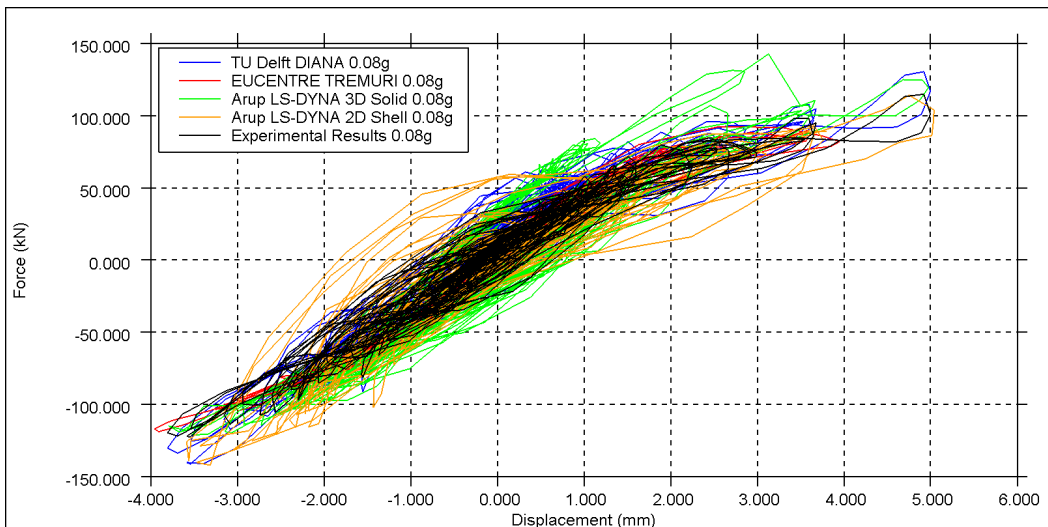


Figure 21 Base shear force vs. top displacement hysteresis plot during 0.08g PGA

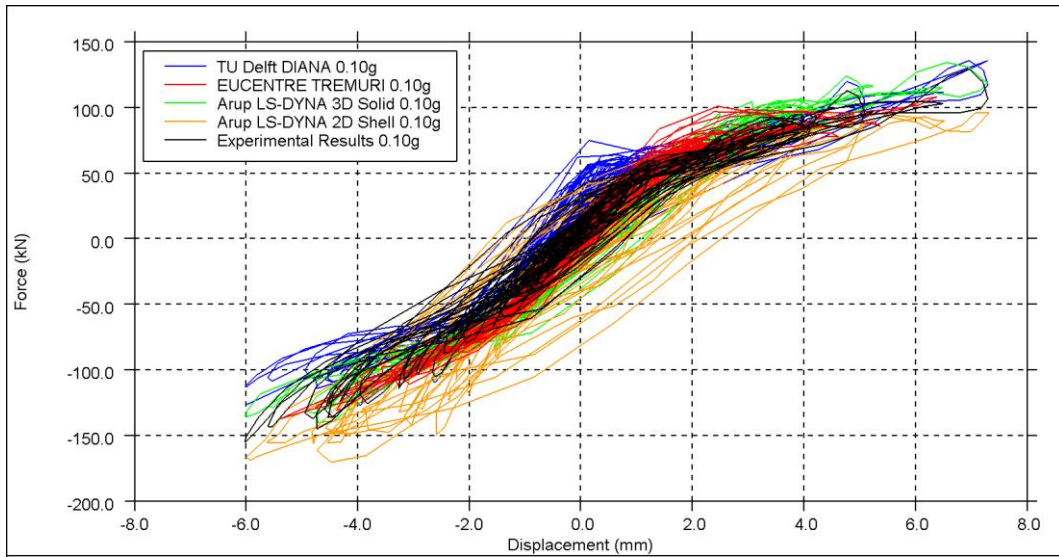


Figure 22 Base shear force vs. top displacement hysteresis plot during 0.10g PGA

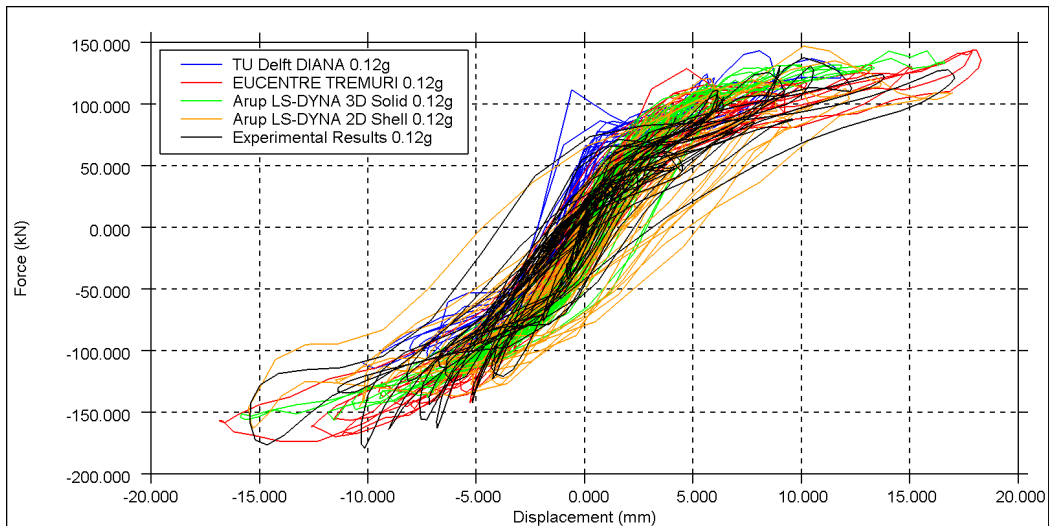


Figure 23 Base shear force vs. top displacement hysteresis plot during 0.12g PGA

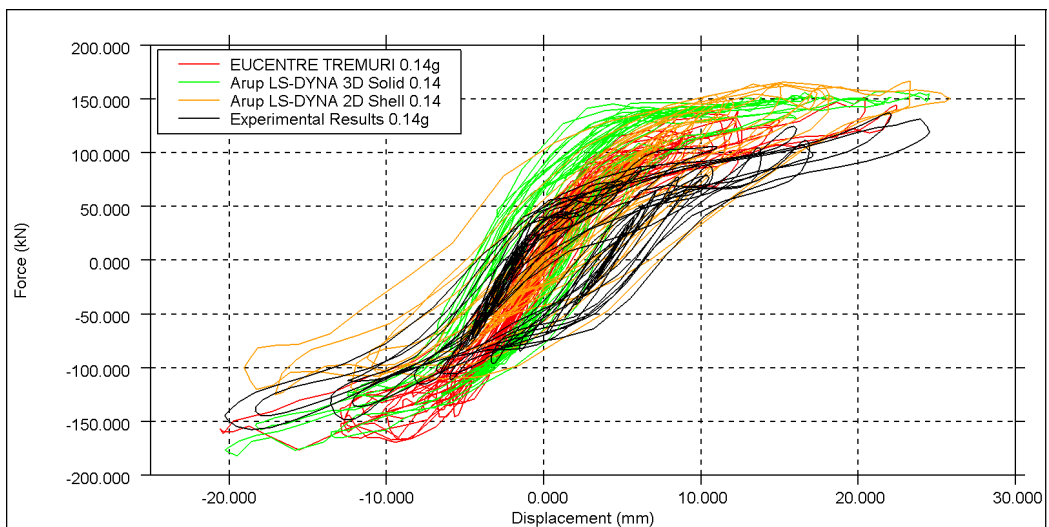


Figure 24 Base shear force vs. top displacement hysteresis plot during 0.14g PGA

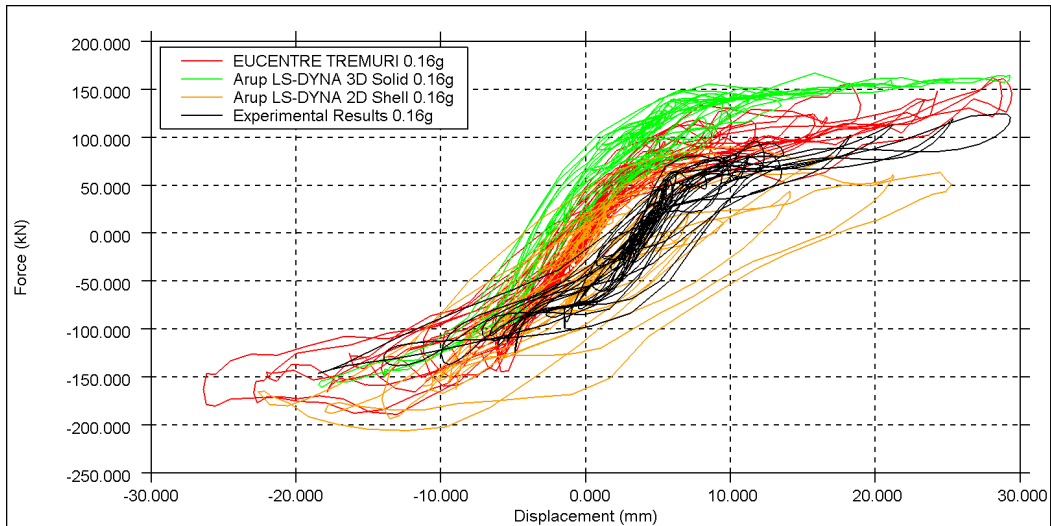


Figure 25 Base shear force vs. top displacement hysteresis plot during 0.16g PGA

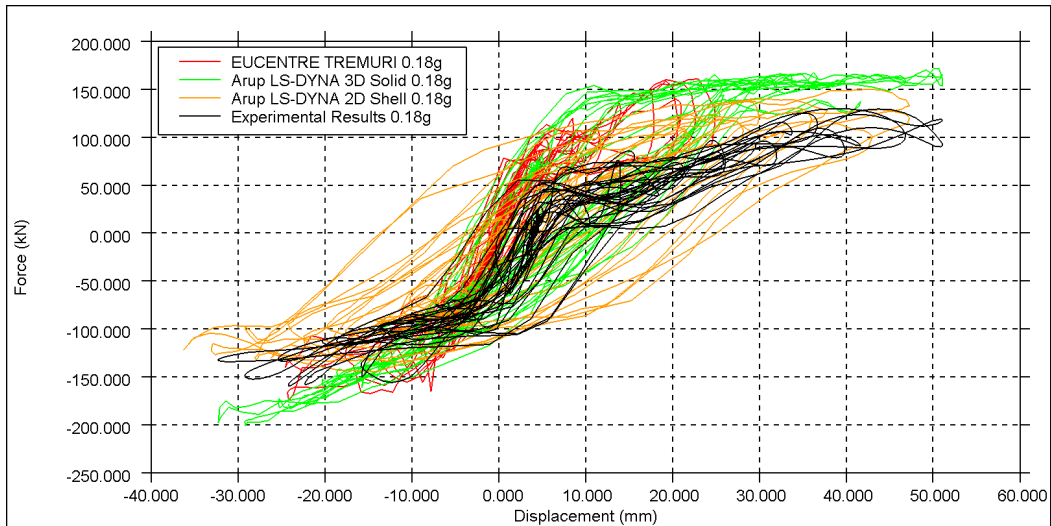


Figure 26 Base shear force vs. top displacement hysteresis plot during 0.18g PGA

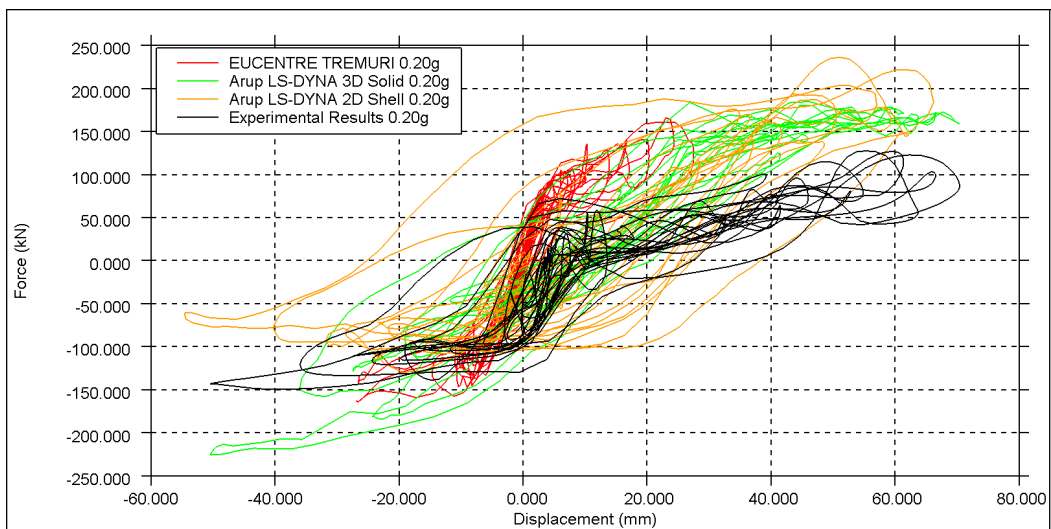


Figure 27 Base shear force vs. top displacement hysteresis plot during 0.20g PGA

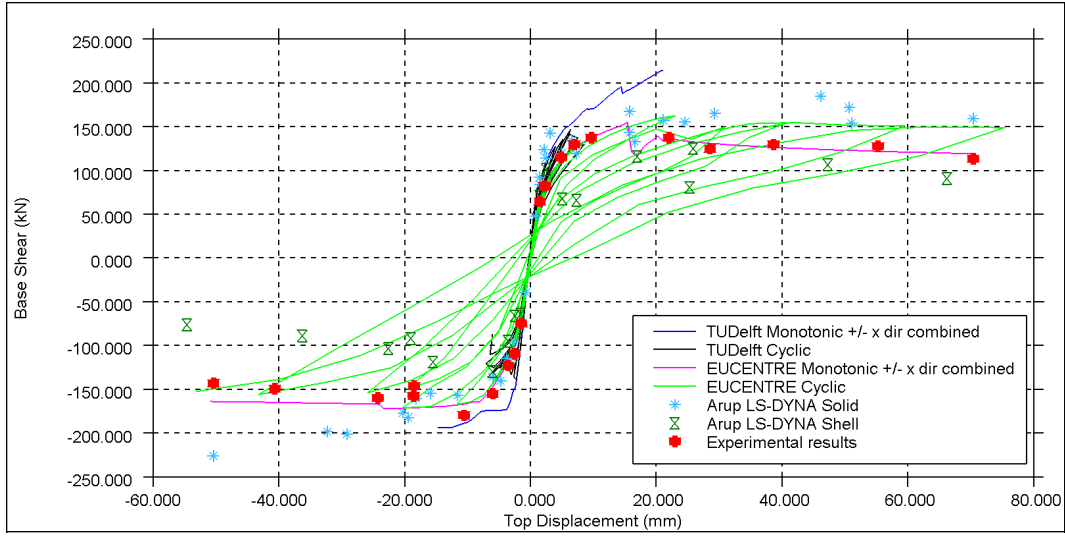


Figure 28 Envelope of max base shear force vs. max top displacement (0.02g to 0.20g PGA)

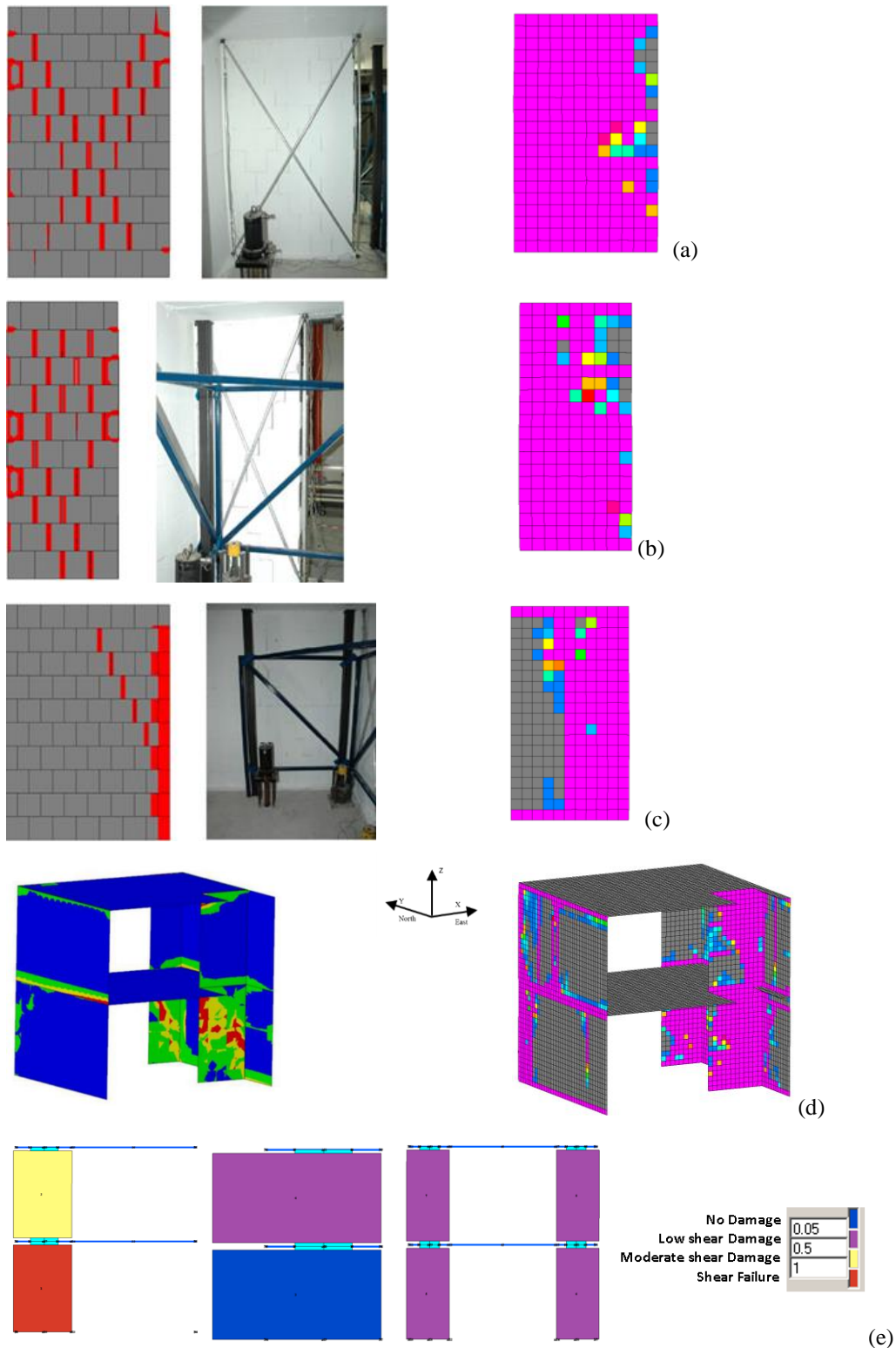


Figure 29 Crack pattern comparison at the end of the analysis with 0.12g PGA. a) Ground floor North cut view of main shear wall; b) Ground floor South cut view of Western slender wall; c) Ground floor East cut view of Western transverse wall; with left-to-right: LS-DYNA solids, test photo, LS-DYNA shells. At the bottom, d) 3D view of the DIANA analysis (left) and LS-DYNA shells analysis (right); e) Main shear wall, transverse wall and slender wall of the TREMURI model.

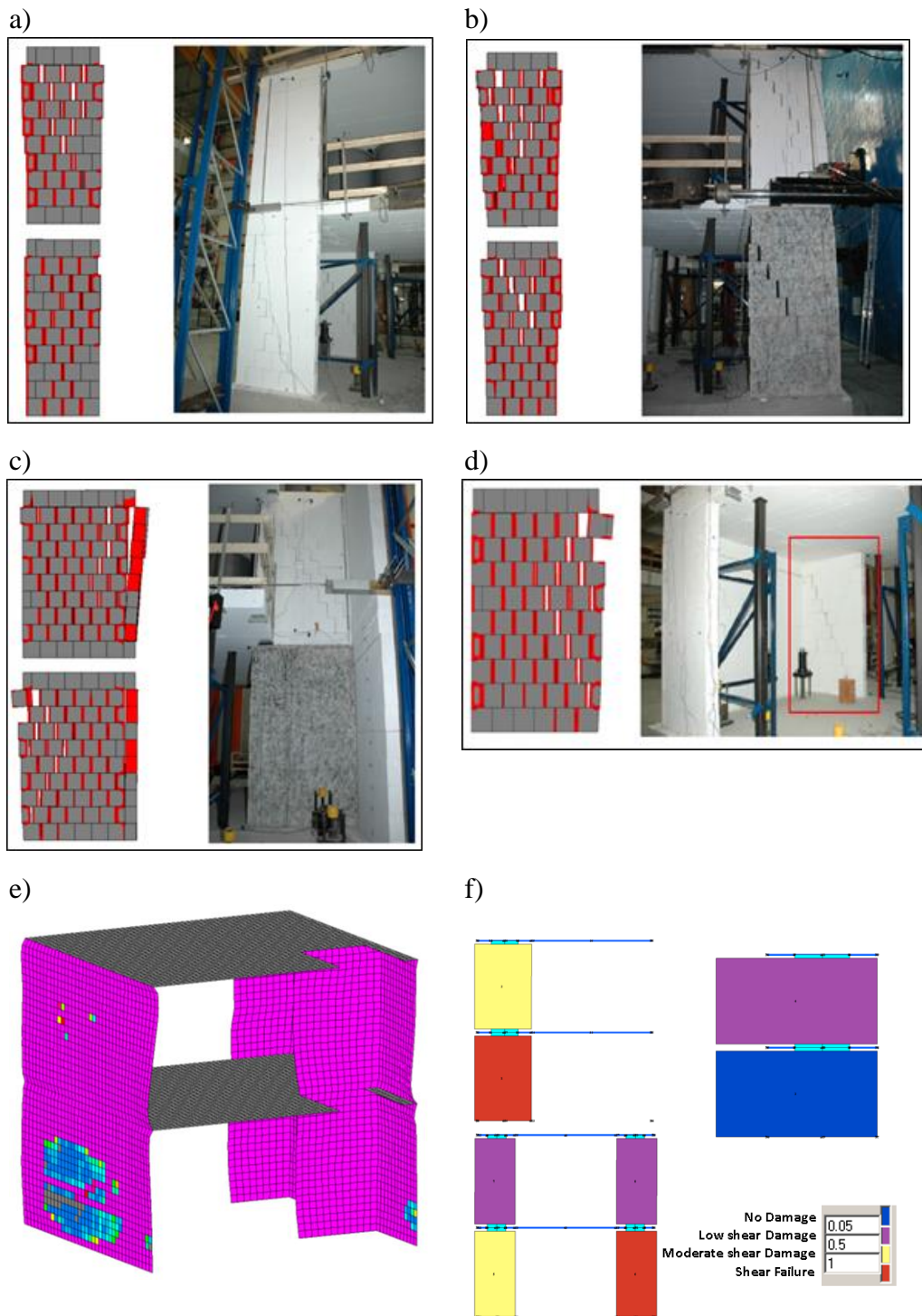


Figure 30 Comparison of the crack patterns at the end of the test with 0.20g PGA. The crack patterns of the LS-DYNA solid element analysis for each wall is compared individually with the experimental tests. a) Ground and First floor view of Eastern slender wall. b) Ground and First floor view of Western slender wall. c) Ground and First floor view of main shear wall. d) Ground floor view of main shear wall. Shown in e) is a 3D view of the LS-DYNA shell model output, and f) main shear wall, transverse wall and slender wall of the TREMURI model.

3.5.2.1 DIANA

The predictions of the DIANA model are in good agreement with the experimental results at 0.08g PGA (Figure 21). However, at 0.12g PGA the ultimate displacement is much lower than the experimental results (Figure 23). The TU Delft modelling team reported that “*divergence of the numerical procedure has been detected*” in the DIANA model at 0.12g PGA (see Section 2.4.1 in Appendix C).

A diagonal crack in the Western transverse wall at ground floor was predicted (Figure 29), which is in agreement with the experimental tests. Shear cracks were predicted in the East slender wall and main shear walls. The cracks in the West slender wall were not visible. The Western transverse wall of the first floor showed a rocking behaviour. Overall, most of the damage observed is in the first level.

DIANA analysis could therefore not be continued beyond the end of the test with 0.12g PGA due to convergence issues. Further calibration of the parameters was recommended in the TU Delft report (Appendix C) to investigate the behaviour for PGA values higher than 0.12g.

3.5.2.2 LS-DYNA solid model

The LS-DYNA solid model shows hysteresis loops that are quite close to the experimental test; however it should be noted that the LS-DYNA analysis was a pseudo-dynamic replication, with the experimentally measured displacements applied at both diaphragm levels. A higher shear capacity is predicated by the LS-DYNA solid model during the last four tests at 0.14–0.20g PGAs (Figure 24 to Figure 27), indicating a divergence from experimental data, which was likely amplified by the nature of the accumulated damage in successive tests of increasing PGAs.

At the end of the record with 0.12g PGA (Figure 29), a diagonal crack similar to the experimental test was predicted in the middle of the main shear wall, although the location of the crack is slightly different. This could be due to the tied contact surface defined between the top row of the wall bricks and the L1 diaphragm in the LS-DYNA solid element model. This can result in a connection stiffer in reality. For the transverse wall, the diagonal crack pattern in the vicinity of the flanged area is generally in agreement with the experimental observations, although an extra diagonal crack observed in experiment was not present in the model output.

For the slender walls and main shear wall, significantly more cracks were predicted than observed in the test at the end of the test with 0.20g PGA (Figure 30). This appears to be due to the micro inertia of each individual brick present in the LS-DYNA solid element analysis, due to the much higher loading rate used in the simulation (required to limit computation time for ‘explicit’ solution analysis) than in the quasi static test.

3.5.2.3 LS-DYNA Shell model

With the material properties specified, the LS-DYNA shell model exhibited a higher initial stiffness than experiment (Figure 19), but the strength and stiffness

degradation at higher PGA phases lead to a good match to the experimental values up through 0.14g PGA. The shell model showed much higher energy dissipation than the experimental results, particularly from 0.16g PGA upwards. This is due to the higher levels of predicted damage to the in-plane wall panels than observed in the experiment (Figure 29).

The predicted crack patterns at the end of the 0.12g PGA phase bear some resemblance to the experimental patterns, however the predicted degree of damage is much higher. At the final PGA, the shell model displays significant cracking in almost every in-plane and out-of-plane wall (Figure 30).

3.5.2.4 TREMURI

TREMURI hysteresis loops show good agreement with the experimental results up to PGA 0.12 g (especially in terms of initial stiffness and strength capacity). However, it should be noted that the assumed Young's modulus value had to be calibrated and reduced between successive tests of increasing PGAs and additional viscous damping (2%) was also needed for only the first stages of the pseudo-dynamic tests in order to obtain this good match.

For higher PGAs, it is possible to observe a general over-estimation of the experimental stiffness and force capacity, while the ultimate displacement demand is under-estimated in the positive direction from 0.18–0.20 g. The EUCENTRE modelling team noted that a possible reason for this last aspect is the material property of the calcium-silicate walls: the blocks are very heavy and assembled without mortar in the head joints. In this arrangement scenario each block, after a certain level of cyclic lateral deformation, could develop a sort of microscopic “relative rocking behaviour”, which is very difficult to capture in the current TREMURI model idealisations.

The levels of damage have been defined according to the value of a damage variable α , which is used to describe the shear behaviour in the friction sliding range. As explained in Penna et al. [2014], the value of α is zero until no damage occurs to the panel and it can only increase, reaching $\alpha = 1$ at the peak shear strength of the panel and $\alpha > 1$ in the post-peak softening branch.

It is possible to observe a fair correspondence between the experimental observations and the predicted damage pattern in the macro-elements.

3.5.3 Modal analysis comparison

A comparison of the first three natural modes of the analysis models is given in Table 4.

The DIANA and LS-DYNA model results are similar in terms of the fundamental modal frequency and the participating mass, although the third mode for the LS-DYNA shell model is a torsional mode instead of a flexural one. The TREMURI model does not develop flexural mode in Y direction because, in order to reproduce the symmetry of the real structure along the Y-axis, displacement constraints in Y direction have been imposed in some crucial nodes of the macro-element model.

Table 4 Modal analysis results comparison

Mode	Analysis package	Period (s)	Frequency (Hz)	Description of mode	Mass participation %	
					X dir.	Y dir.
1	DIANA	0.148	6.75	1 st flexural mode in X	75.3	0.053
	TREMURI	0.166	6.02	1 st flexural mode in X	80.20	
	LS-DYNA Solid	0.140	7.10	1 st flexural mode in X	72.9	
	LS-DYNA Shell	0.128	7.79	1 st flexural mode in X	77.0	0.04
2	DIANA	0.054	18.67	1 st flexural mode in Y	0.30	55.16
	TREMURI			Suppressed by symmetry constraints.		
	LS-DYNA Solid	0.059	16.90	1 st flexural mode in Y		64.7
	LS-DYNA Shell	0.052	19.31	1 st flexural mode in Y	0.02	65.5
3	DIANA	0.037	27.26	2 nd flexural mode in X	12.44	1.06
	TREMURI	0.057	17.65	2 nd flexural mode in X	10.51	
	LS-DYNA Solid	0.050	20.20	2 nd flexural mode in X	7.7	
	LS-DYNA Shell	0.039	25.36	1 st torsional mode	0.18	0.26

3.5.4 Notes and Discussion

In the LS-DYNA solid element model, micro-inertia/dynamics of individual brick units under relatively fast loading rate in analysis – limited by numerical computation costs – lead to some differences in behaviour compared to pseudo-dynamic tests conducted in laboratory at a very slow loading rate. These differences were progressively magnified with successive tests of increasing PGA from 0.02g to 0.20g due to the cumulative nature of the damage and degradation.

With data currently available it is difficult to quantify and model the effects of the unfilled head joint interfaces between calcium silicate brick units with slightly interlocking grooves, in terms of the frictional behaviour both along the groove axes and out-of-plane with respect to the groove axes. Assumptions made may have led to the significantly higher energy dissipation observed in the LS-DYNA shell model.

The DIANA model could only be analysed part way through the 0.12g PGA test, due to difficulties in numerical convergence.

In the TREMURI model, the Young's modulus value was reduced and re-calibrated between successive tests of increasing PGAs. Additional viscous damping (2%) was also needed for the first stages of the pseudo-dynamic tests. This is described in more detail in Section 2.4.1 of Appendix B. With these adjustments incorporated the comparisons both in terms of pushover and dynamic analyses are satisfactory, with the exception of the dynamic tests performed for

PGA levels higher than 0.16g. The EUCENTRE team suggests that a possible reason for these discrepancies could be found in the behaviour of the calcium-silicate walls: the blocks are heavy and assembled without mortar in the head joints. In this arrangement each block, after a certain level of cyclic lateral deformation, could develop a sort of microscopic “relative rocking behaviour” that is very difficult to capture with the current TREMURI model idealisations.

3.6 One-Way Spanning Wall Out-of-Plane Tests (Griffith et al., 2004)

3.6.1 Specimen 8

The predicted lateral response of the wall (assumed initially un-cracked) is compared to the test results in Figure 31. Both DIANA and LS-DYNA analyses show a peak in the response around 1 mm displacement. This peak was not observed in the experiment. A possible explanation is that the wall was in fact cracked prior to the lateral test.

3.6.1.1 DIANA

In the DIANA model the overburden force was applied using a top spring. The spring is connected to the interface element which ensures the eccentricity of the overburden force at significant rotations. The vertical degree of freedom of the top of the interface was “tied”, meaning that it cannot bend.

Average material properties were used in DIANA analysis. This likely resulted in stiffness and strength overestimation in DIANA models. Poisson’s ratio was taken as $\nu = 0$ (TU Delft noted that this is to avoid unrealistic splitting cracks near the top and bottom boundaries).

3.6.1.2 LS-DYNA solid model

In the LS-DYNA analysis, test-specific material properties were used. The sensitivity of the prediction to the action of the restraint system at the top of the wall was examined.

3.6.1.3 LS-DYNA shell model

As seen in figure 31 the LS-DYNA shell model predicts the peak post-cracking more accurately than the other models. This is attributed to the shell having more integration points (and a better distribution) through the thickness of the wall than the solid element model.

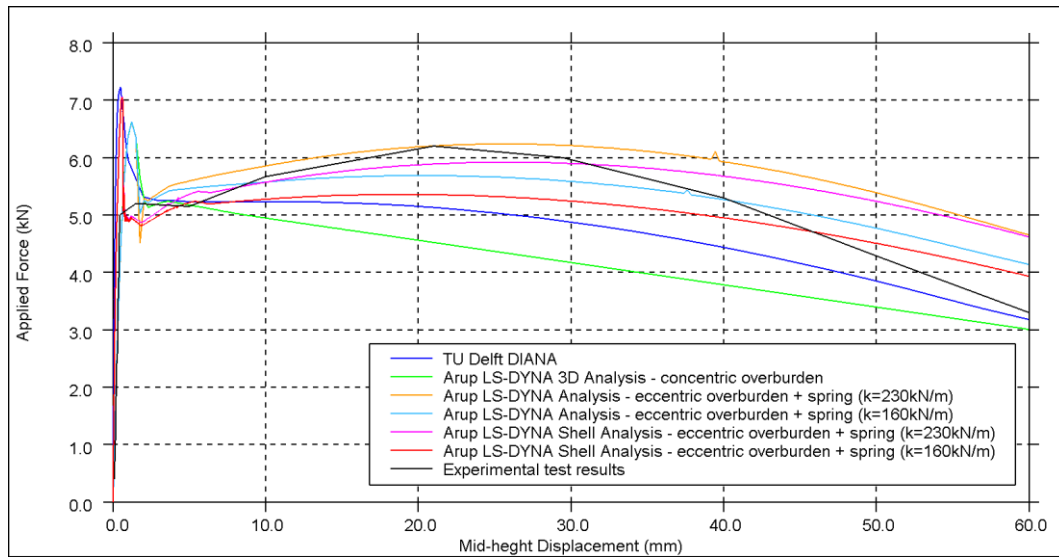


Figure 31 Total applied load vs. mid height displacement for Specimen 8 (uncracked)

EUCENTRE reported the results only for Specimen 8 “cracked” (see Section 2.5 in Appendix B), whereas the other two teams only considered the “uncracked” case, and therefore a direct comparison of the three teams is not available.

3.6.2 Specimen 12

For Specimen 12, Arup noticed significant discrepancies in the Nahani (NH) laboratory test results. The accelerations at the base of the table and the top of the frame were not compatible with the reported displacements. There was a large baseline shift when integrating the accelerations. The El Centro 66% (EL) time history analysis was performed on a ‘cracked’ wall specimen, however LS-DYNA model results showed elastic behaviour throughout the duration of the run and thus the wall did not rock.

The TU Delft modelling team performed NH100% transient analysis on the ‘uncracked’ specimen. In Appendix C, TU Delft show the high influence of the assumed out-of-plane thickness of the interface on the transient results. The reduced out-of-plane thickness is thought to represent initial cracking and crushing of the interface over the thickness of the wall and geometric imperfections.

EUCENTRE reported NH100%, NH200% and EL66% time history results. Rocking of the wall was predicted during the analysis, as shown in Appendix B Section 2.5. It should be noted that TREMURI was not used for these analyses.

3.6.3 Discussions and conclusions

The LS-DYNA models of the static tests showed a good degree of correlation with the experiment results. The predicted crack pattern matched laboratory test results. The ultimate out-of-plane strength capacity of the walls showed a reasonable match with both laboratory test results and mathematical predictions.

The main limitations in modelling these specimens were:

- Lack of clarity of testing regimes used in the laboratory.
- Insufficient information provided by the researcher, such as spring rotational stiffness.
- Errors/inconsistencies in laboratory test data presented.

It was noted that the ultimate post-cracking resistance was better predicted by the shell formulation due to better distribution of integration points through the wall thickness. At large lateral displacements the predicted reduction in lateral resistance was not as great as measured. This is attributed to the potential for mortar to degrade at the rocking compression edge under successive cycles which was not represented.

The DIANA model gives similar results for the static test to the LS-DYNA solid model.

TU Delft questioned the clarity of the dynamic tests. A sensitivity study, in which an effective (and reduced) out-of-plane thickness of the mortar was used, showed that the dynamic test could be replicated reasonably well when reducing the out-of-plane thickness by approximately 20%.

The TREMURI results showed fair agreement for the Specimen 8 ‘cracked’ sample, but are not directly comparable with the Specimen 8 results from the other two teams (‘uncracked’ sample). For the dynamic tests, the EUCENTRE modelling team noted that *“as the dynamic model implemented in Tremuri is still under development, an alternative trilinear model was developed for the dynamic simulation. The trilinear envelope is calibrated against the Tremuri pushover analysis curves”*. The trilinear model is a phenomenological single-degree-of-freedom hysteretic model calibrated specifically for out-of-plane experiments, separate from the TREMURI modelling used in other models and analyses. This means that it is not currently possible for the EUCENTRE modelling team to capture the interaction of in-plane and out-of-plane behaviours.

3.7 Two-Way Spanning Wall Out-of-Plane Tests (Griffith et al., 2007)

Two-way spanning wall panels cannot be analysed using TREMURI, hence only Arup and TU Delft analysis results are presented below.

3.7.1 Wall 1

The force-displacement comparisons are presented in Figure 32. The initial stiffness of the Arup LS-DYNA solid element and TU Delft predictions match the test results well, but over-predict the ultimate strength. The difference in flexural stiffness of the wall may be caused by differences in modelling methods and the support conditions implemented.

The LS-DYNA shell model prediction matches the initial stiffness and the ultimate resistance of the panel extremely well.

As expected, the cracking pattern shows trapezoidal yield lines in all three sets of output (Figure 33).

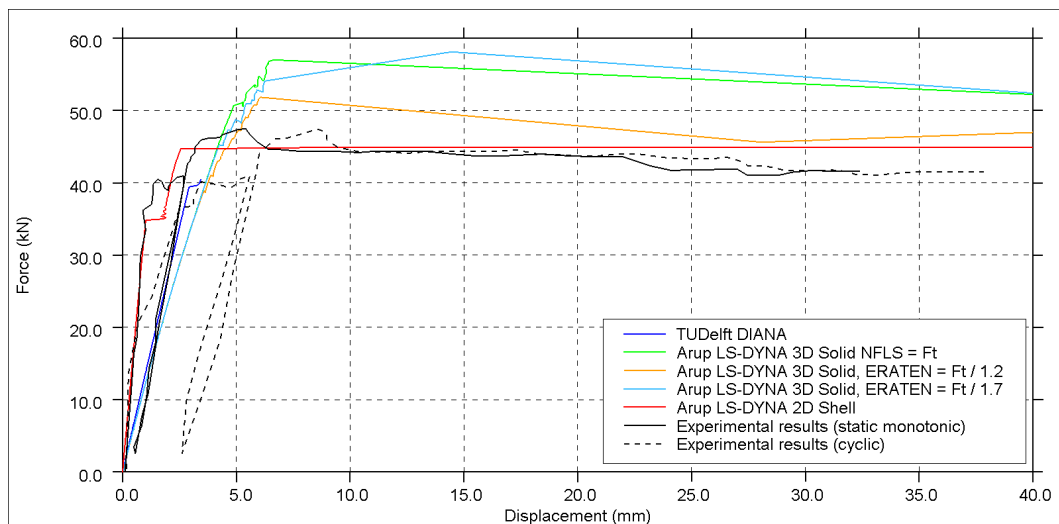


Figure 32 Load-displacement response plot (Wall 1)

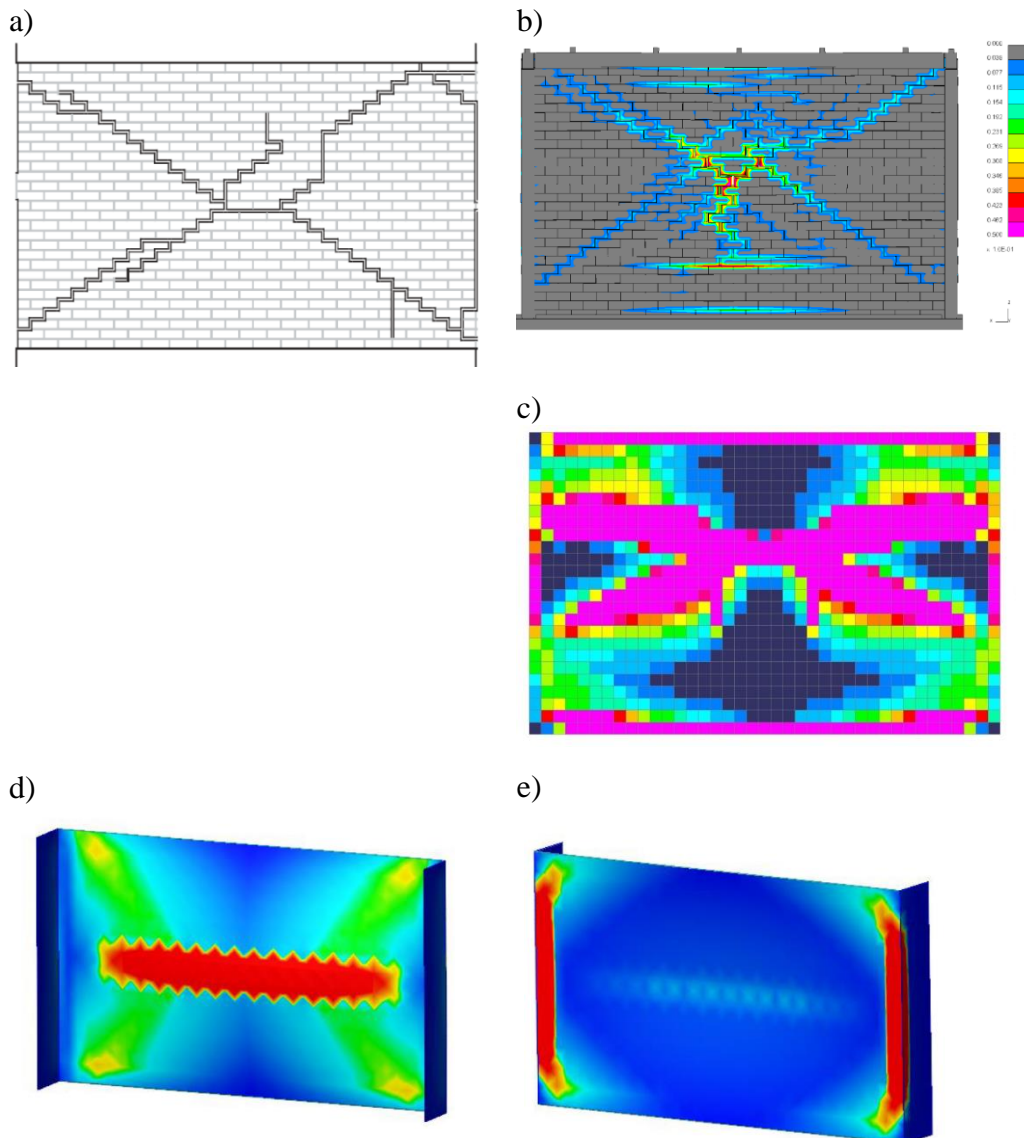


Figure 33 Final crack pattern for Wall 1. a) Experimental result; b) LS-DYNA solid analysis result; c) LS-DYNA shell analysis result; d) DIANA analysis results at inside-face at displacement 5 mm and e) outside-face at displacement 5 mm.

3.7.2 Wall 2

TU Delft presented the elastic and post-crack response of the wall (up to 10 mm displacement), which is very similar to the Arup LS-DYNA solid element results (Figure 34) when the bond wrench test results were used for direct tensile strength between two bricks. The Arup LS-DYNA shell model panel is slightly stiffer than the experimental one but the ultimate strength again was a close match.

Similar to Wall 1, the cracking pattern of Wall 2 follows the trapezoidal yield lines in all three models (Figure 35).

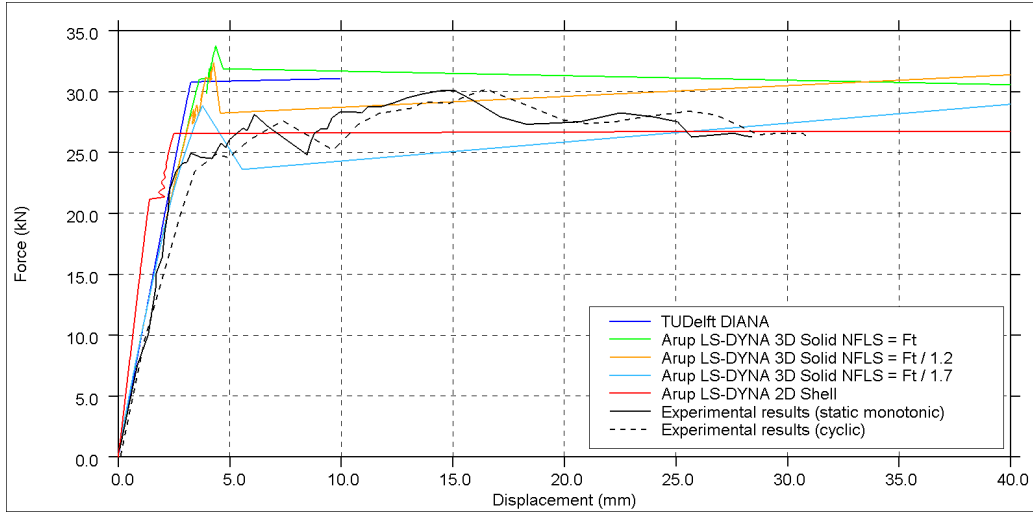


Figure 34 Load-displacement response plot (Wall 2)

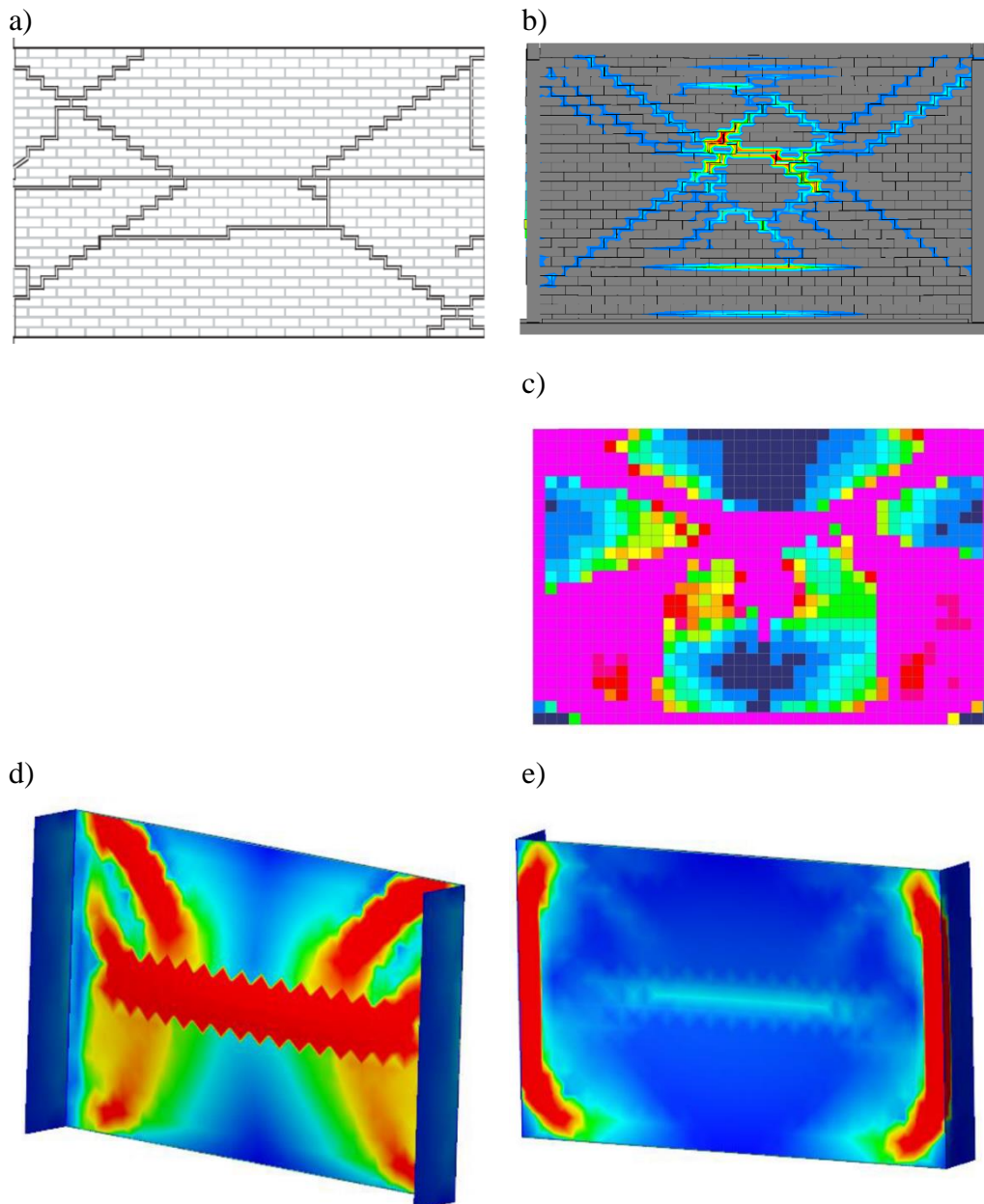


Figure 35 Final crack pattern for Wall 2. a) Experimental result; b) LS-DYNA solid analysis result; c) LS-DYNA shell analysis result; d) DIANA analysis results at the inside-face at displacement 9 mm and e) the outside-face at displacement 9 mm.

3.7.3 Notes and Discussion

Overall, both the LS-DYNA solids models and DIANA models, give reasonable predictions but over-estimate the ultimate strength. The DIANA analyses were only completed up to lower displacement values. The TU Delft modelling team noted that they were *“unable to reproduce the ductility as observed in the experimental results despite the numerous ways of the application on the load – such as load control and indirect displacement control”*.

The LS-DYNA shell models showed very good correlations on initial stiffness and peak strength, which is encouraging. This is likely because the shell model

incorporates a larger number of integration points through the thickness of the wall, hence increasing accuracy.

Two-way spanning wall panels under out-of-plane action cannot be analysed using TREMURI.

4 Index Buildings Cross-Validation

This Section describes the cross-validation comparisons that were completed by the three modelling teams for assessing the seismic performance of two index buildings with typical geometries representative of the Groningen housing stock used in previous Arup studies, under fixed base assumptions.

More details about the two index buildings – T1* (Section 4.1) and T3a (Section 4.2) – can be found in [3] Volume 4.

The Arup models for these Cross-Validation studies adopted the LS-DYNA solid element modelling technique, not the shell model.

4.1 Terraced House (T1*)

4.1.1 Modal analysis comparison

Modal analysis using DIANA and TREMURI were performed assuming un-cracked masonry. The LS-DYNA solid element analysis was initially carried out assuming cracked masonry but later re-analysed assuming un-cracked properties, to allow comparison to the other software.

The first mode periods in the X and Y directions predicted by modal analyses in DIANA and TREMURI are comparable; the LS-DYNA X mode (un-cracked) has a period 40% shorter, corresponding to a much higher stiffness in the X direction. This is attributable to the inclusion of the out-of plane resistance of the cross-walls in the LS-DYNA model. The mass participation was very similar for all models.

In the Y mode, the period for all models is in good agreement (un-cracked), but with different mass participations.

Table 5 Modal analysis comparison of T1*

Fundamental Mode	Analysis package	Period (s)	Frequency (HZ)	Mass participation %	
				X dir.	Y dir.
1 st lateral sway in X direction	DIANA uncracked	0.64	1.6	80.7	0
	TREMURI uncracked	0.66	1.5	82.0	0
	LS-DYNA cracked (50% E _{masonry})	0.54	1.9	76.5	0
	LS-DYNA uncracked	0.41	2.5	76.2	0
1 st lateral sway in Y direction	DIANA uncracked	0.080	12.4	0	29.2
	TREMURI uncracked	0.082	12.1	0	83.9
	LS-DYNA cracked (50% E _{masonry})	0.11	9.1	0	63.7
	LS-DYNA uncracked	0.08	12.5	0	43.9

4.1.2 Pushover analysis comparison

The monotonic pushover analysis comparisons show that in the X direction **Error! Reference source not found.**the predicted capacity of the DIANA model

is around 35kN, while the TREMURI results of monotonic pushover show a maximum shear capacity of 57kN, and the LS-DYNA model around 47kN.

Figure 36 also shows cyclic pushover predictions with TREMURI and LS-DYNA.

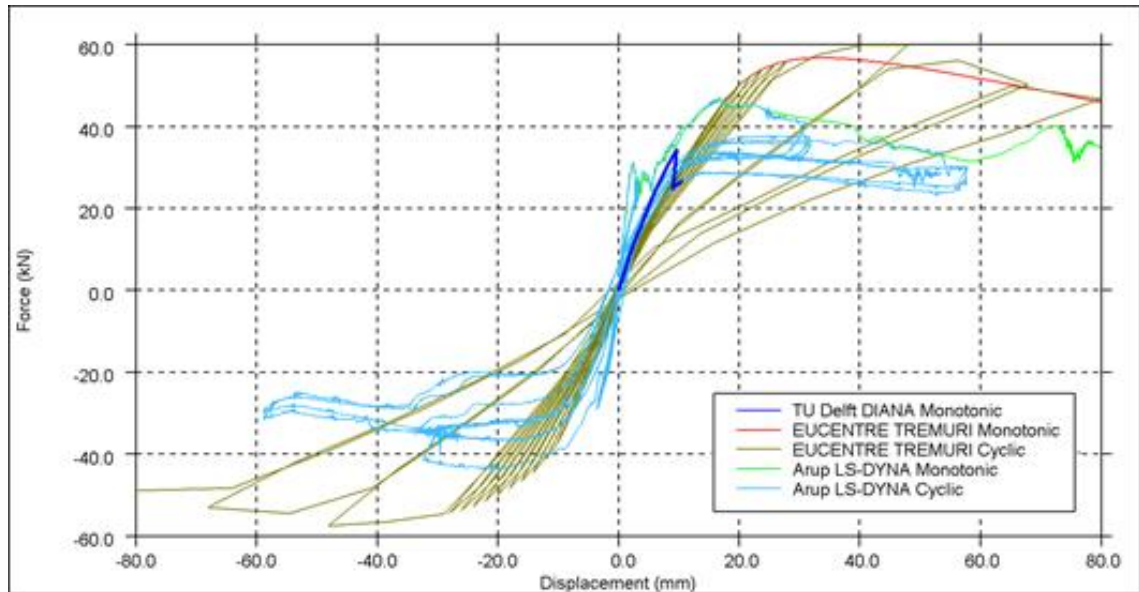


Figure 36 X-direction base shear versus average reference height displacement

Figure 37 shows comparisons for Y direction monotonic and cyclic pushover.

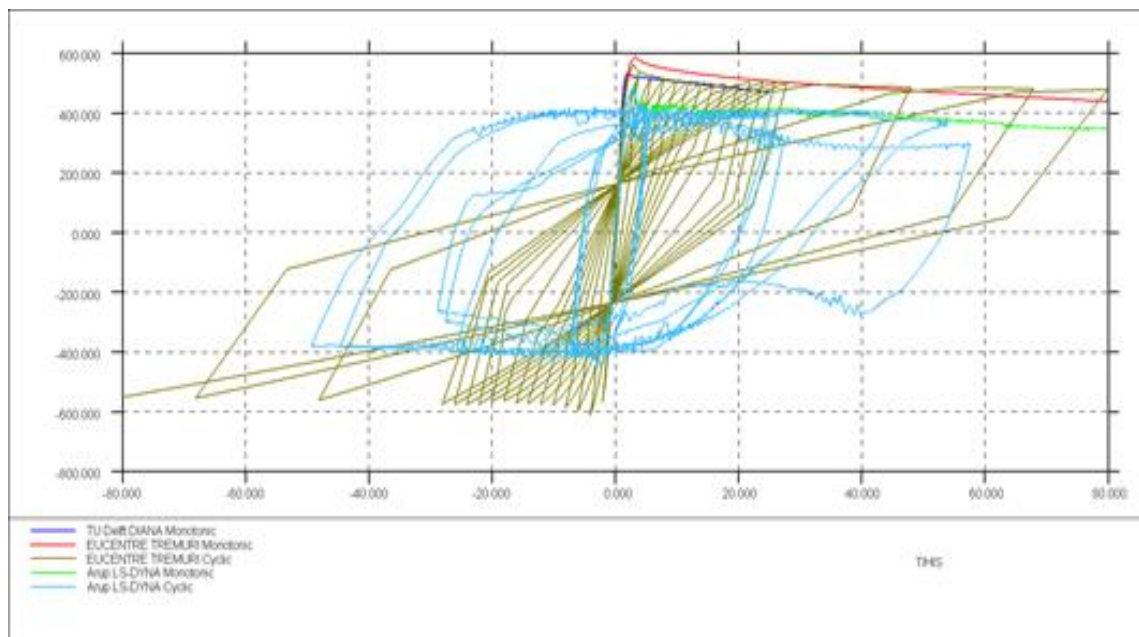


Figure 37 Y-direction base shear versus average reference height displacement

4.1.2.1 DIANA

In the DIANA analysis monotonic pushover was conducted until maximum top displacements of around 11 and 25 mm in the X and Y directions respectively. TU Delft noted that it was not possible for the analysis to continue up to higher displacement levels due to computational convergence issues. The curve in X-

direction presents a drop in the capacity related to the complete detachment of the vertical joints between the slender piers and the long orthogonal walls. Along the Y-direction a peak capacity of around 530 kN and a following descending branch was observed.

4.1.2.2 LS-DYNA

The LS-DYNA model predicts lower capacity in the X and Y directions compared to the other two models. LS-DYNA predicts degradation and also reduced ultimate displacement capacity under cyclic loading.

4.1.2.3 TREMURI

TREMURI predicts the highest monotonic force resistances in both directions. It also predicts no significant degradation between the cyclic (envelope) and monotonic results - even showing a slightly higher backbone response in the cyclic analysis in one direction.

4.1.3 Basis of differences

4.1.3.1 Gravity load distribution

Some differences were noted between the analysis models. The axial pier forces of the models under gravity loading varied somewhat.

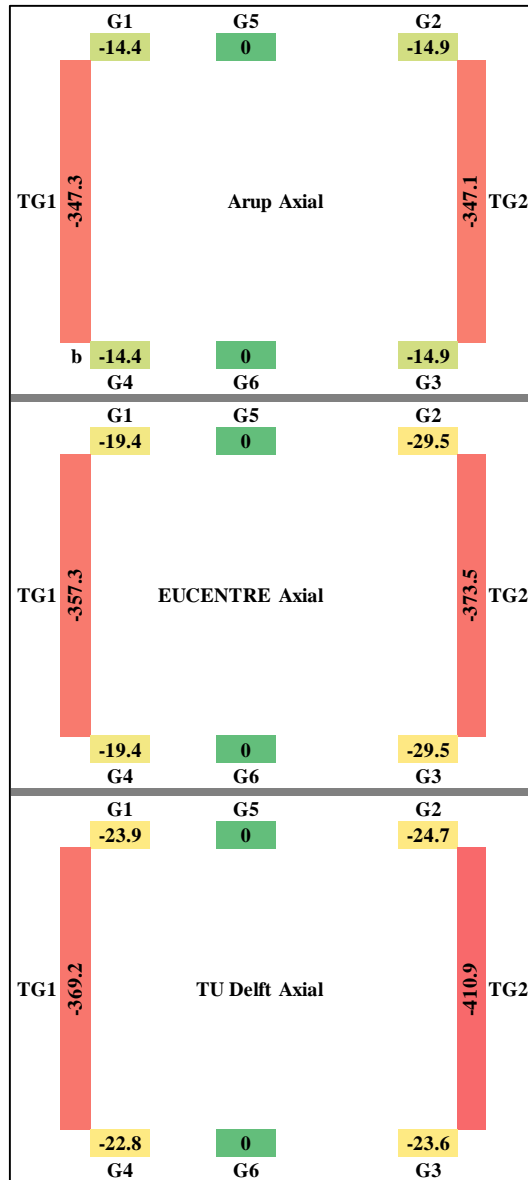


Figure 38 Plan view of the cut-section axial distributions after application of gravity loading for each of the three models. The colour gradient indicates the magnitude of the force distribution – red being the highest magnitude, and green being the lowest.

4.1.3.2 Lateral stiffness

The initial lateral stiffness predictions in the X direction differed significantly, as summarised in Table 6:

Table 6 Pushover elastic analysis comparison of T1* - initial stiffness

Analysis package	Initial Stiffness X direction (N/mm)
DIANA	5470
TREMURI	8890
LS-DYNA	26600

The higher stiffness in the LS-DYNA model was attributed to the inclusion of the out-of-plane resistance of the cross walls rotationally restrained by the floor slabs.

4.1.3.3 Distribution of lateral resistances

Comparing the peak pier forces of the three models (from Table 3.1.9 in Appendix A, Appendix B, and Appendix C) for X-direction pushover in Figure 39, relatively high axial forces were observed for the slender piers (G1 to G4 in Table 3.1.9 of Appendix B) in the TREMURI model, due to flange effects in the equivalent frame model.

In the LS-DYNA output, the transverse walls carry most of the gravity load in axial compression (due to the one-way spanning support condition of the floors), also resulting in them carrying a large proportion of the X-direction pushover shear load out-of-plane; in the TREMURI model, walls are assumed to carry zero lateral force if loaded out-of-plane.

Comparison of the pier forces of the three models (from Table 3.1.10 in Appendix A, Appendix B, and Appendix C) for Y-direction pushover is shown in Figure 40.

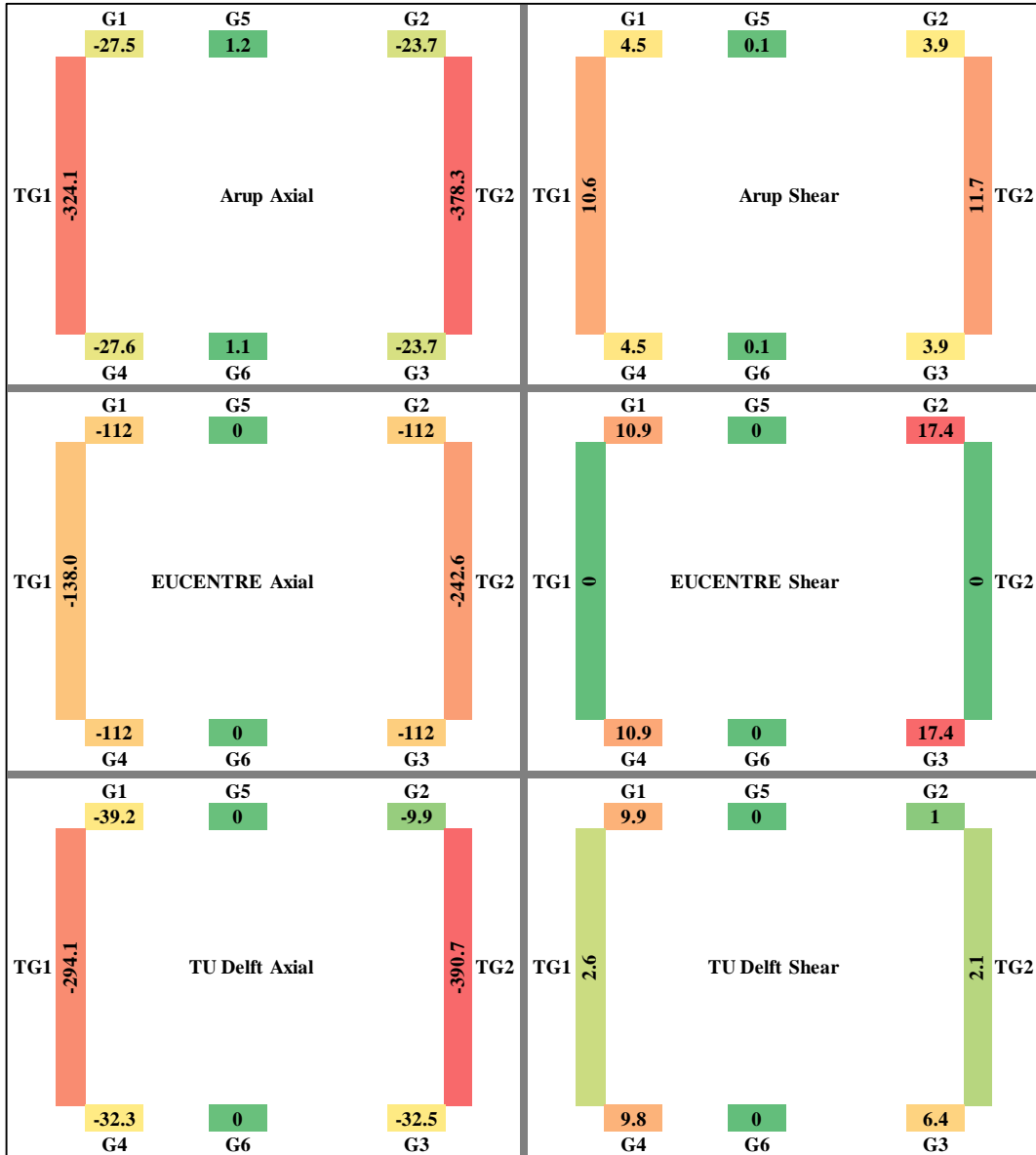


Figure 39 Plan view of the cut-section axial and X shear force distributions at peak/plateau base shear during X-direction pushover for each of the three models. The colour gradient indicates the magnitude of the force distribution – red being the highest magnitude, and green being the lowest.

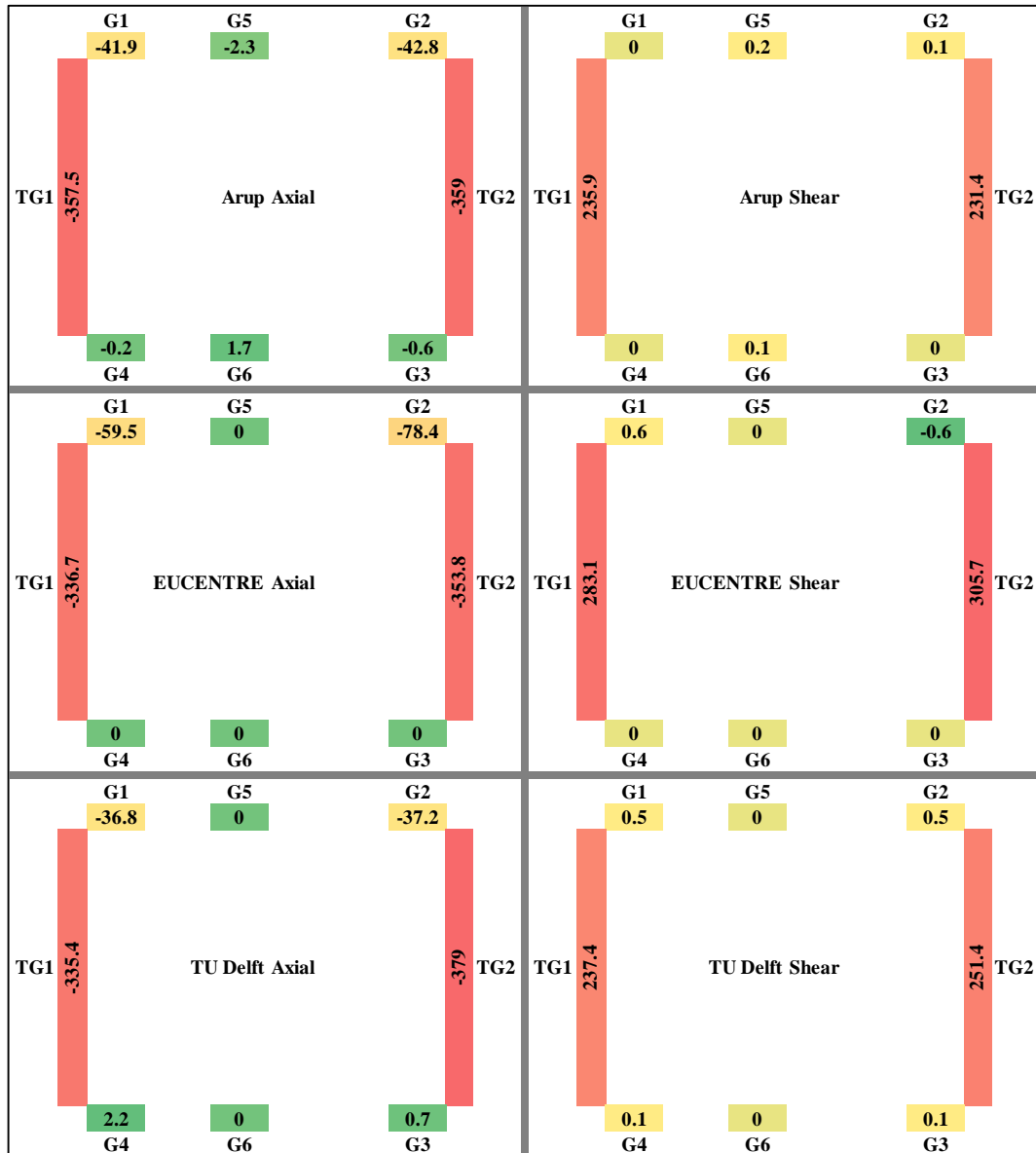


Figure 40 Plan view of the cut-section axial and Y shear force distributions at peak/plateau base shear during Y-direction pushover for each of the three models. The colour gradient indicates the magnitude of the force distribution – red being the highest magnitude, and green being the lowest.

4.1.4 Non-linear response history analysis comparison

Table 7 below compares the peak lateral displacement predicted at the reference roof node by NLRHA analyses using the three software packages for suites of ground motions scaled to three levels of PGA. Rayleigh damping of 1% of critical was implemented in all models (note: The original TREMURI analyses assumed a value of 2%; this was changed to allow direct comparison with the other models).

Table 7 Peak reference node displacement (mm) comparison (three records scaled to three PGA levels each)

PGA	Analysis package	Record 3		Record 6		Record 7	
		X dir.	Y dir.	X dir.	Y dir.	X dir.	Y dir.
0.1g	DIANA	60	0.5	27	1.0	27	0.8
	TREMURI	21	0.8	20	0.5	22	1.0
	LS-DYNA	19	0.9	19	0.9	19	0.9
0.25g	DIANA	>249	2.9	74	2.5	61	1.9
	TREMURI	40	1.0	52	1.3	56	1.8
	LS-DYNA	77	2.7	60	3.1	90	2.5
0.50g	DIANA	>282	7.5	129	5.2	122	6.4
	TREMURI	47	7.8	113	2.6	122	5.3
	LS-DYNA	Collapse	Collapse	Collapse	Collapse	Collapse	Collapse

Figure 37 to 39 below compare the base shear vs roof displacement hysteresis predicted in the Y direction for 0.25g PGA input motions by the three models for the three ground motion sets in turn. The following can be seen:

- The response in TREMUTI is considerably ‘stiffer’ than that predicted by LS-DYNA and DIANA
- Hysteresis loops are of a reasonably conventional form for a structure responding in its stable range
- There is some record to record variation

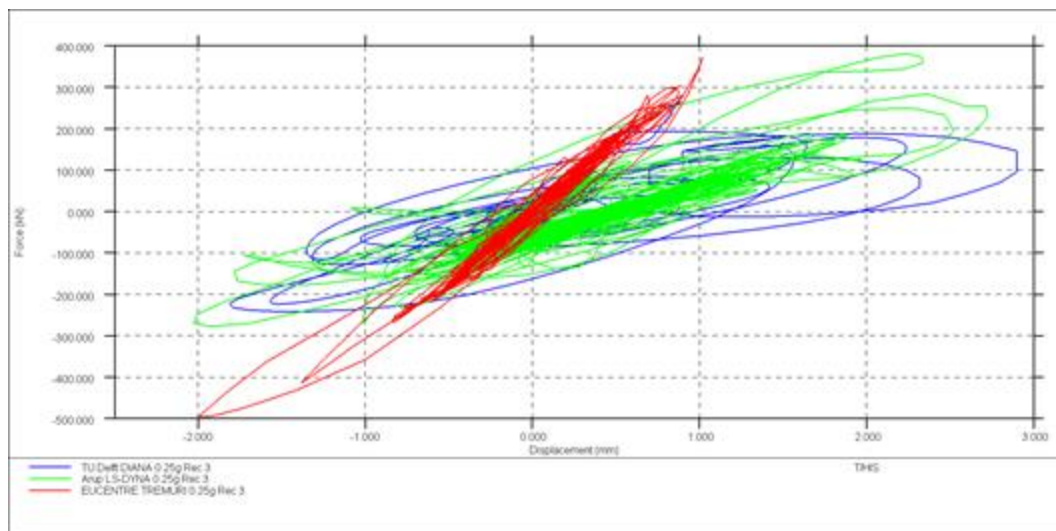


Figure 37 Base shear versus reference node displacement – 0.25g scaled PGA, record 3, Y direction

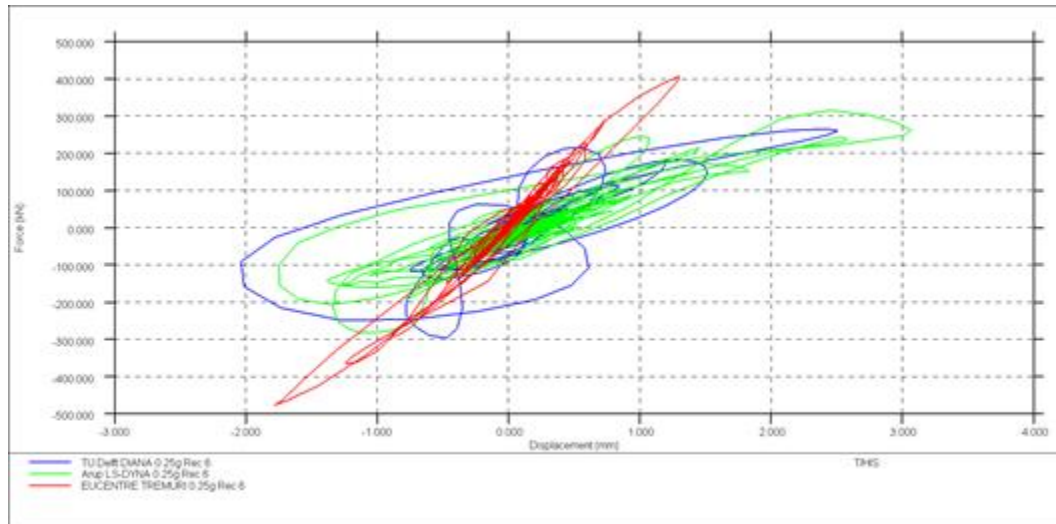


Figure 38 Base shear versus reference node displacement – 0.25g scaled PGA, record 6, Y direction

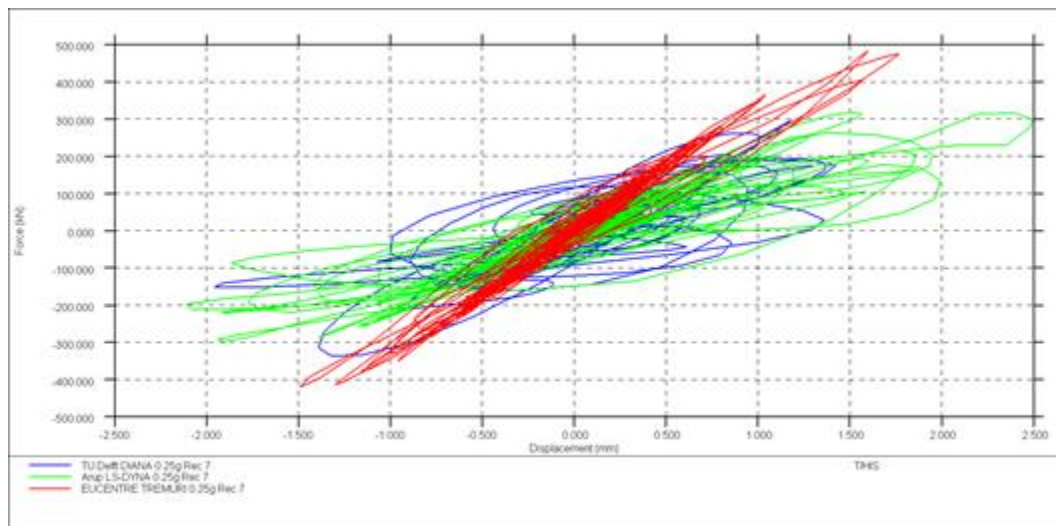


Figure 39 Base shear versus reference node displacement – 0.25g scaled PGA, record 7, Y direction

Figure 40 to 42 below compare the base shear vs roof displacement hysteresis predicted in the X direction for 0.25g PGA input motions by the three models for the three ground motion sets in turn. The following can be seen:

- While the peak forces developed in the three models are comparable, the peak displacement and hysteresis behaviour are completely different
- There is large record to record variation
- The overall hysteresis behaviour in LS-DYNA and DIANA suggests the structure is close to instability, with periods of ‘negative stiffness’ apparent.

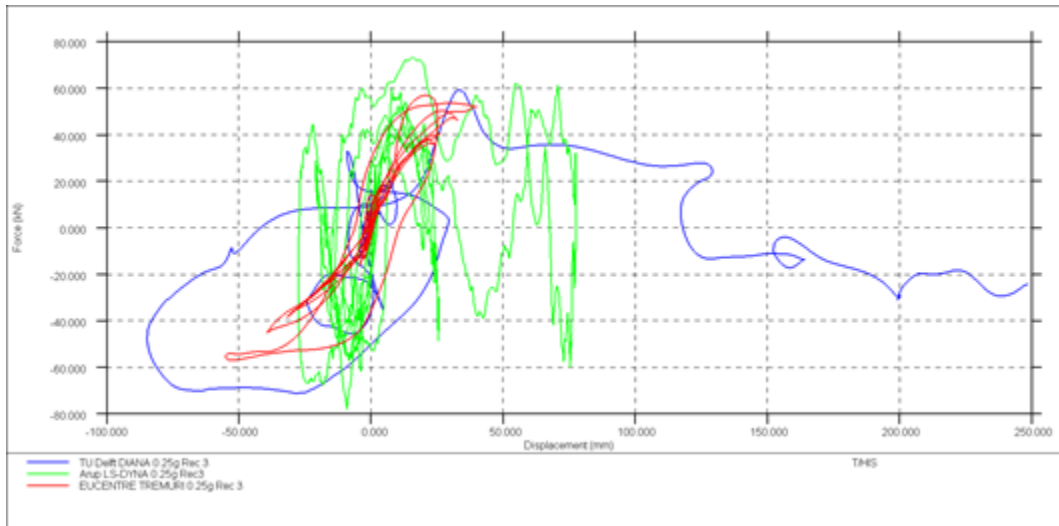


Figure 40 Base shear versus reference node displacement – 0.25g scaled PGA, record 3, X direction

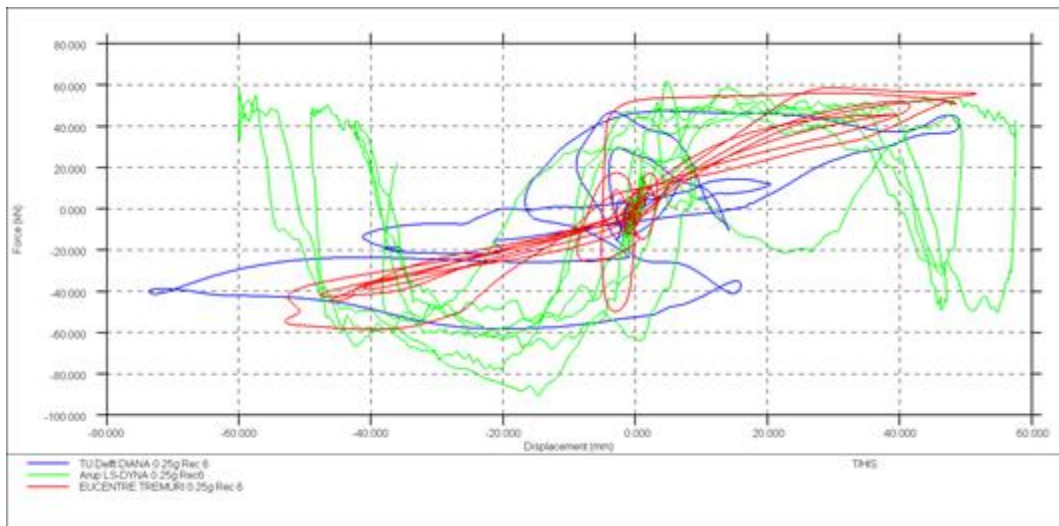


Figure 41 Base shear versus reference node displacement – 0.25g scaled PGA, record 6, X direction

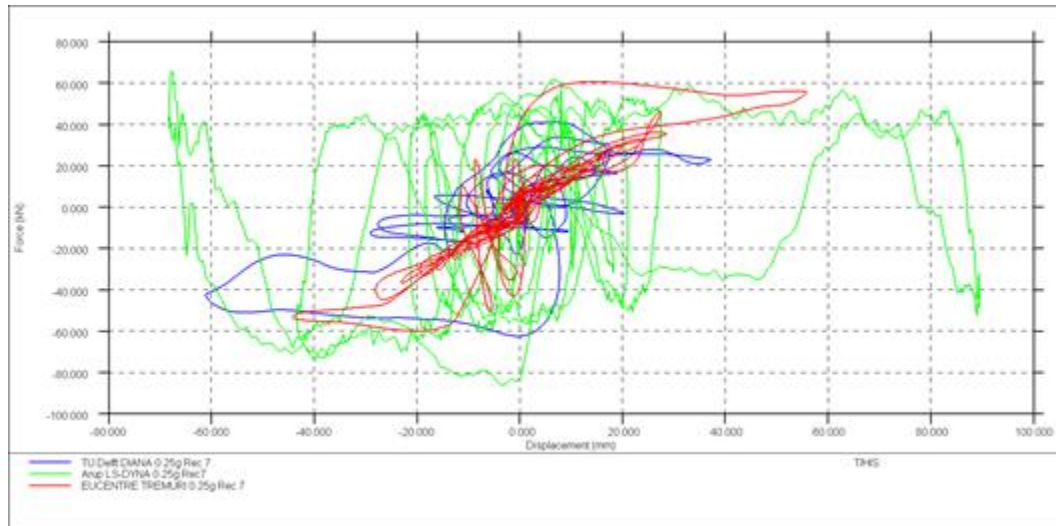


Figure 42 Base shear versus reference node displacement – 0.25g scaled PGA, record 7, X direction

4.1.5 Basis of differences

One reason for the unconventional apparent hysteresis behaviour in the LS-DYNA model is due to very different behaviours in the two storeys – while the upper storey displaces well beyond its ‘yield’ point, the lower storey does not, and the storeys do not move in phase at all times. This means that the response is not well characterised by simple ‘single degree of freedom’ hysteresis between roof displacement and base shear. This behaviour is covered in more detail in [3] Volume 4.

4.1.6 Notes and Discussion

There are several significant differences between the models from the three modelling teams. These include:

- The application of gravity loads and the assumed gravity spanning behaviour of the floor systems
- Different assumptions for dead load, superimposed dead load and live load.
- In the LS-DYNA model the veneer walls were modelled explicitly, unlike the TREMURI and DIANA models where the veneer walls were only included as equivalent added mass on the walls of the weak direction (X).
- The LS-DYNA model includes the out-of-plane resistance of the cross walls – which is significant for X-direction response
- Failure modelling (or lack thereof) in the vertical line joint between the transverse shear wall and the slender pier, affecting the presence of flange effects.
- Whether or not the masonry spandrels act as coupled to the floor structures.

- Modelling and behaviour of the unfilled gaps that are present at the top of the slender piers.

All these contribute to the differences seen in the analytical predictions from the three modelling teams. In the TREMURI model, some of these aspects have been analysed by means of sensitivity studies, as detailed in Appendix B.

4.2 Detached Villa, Timber Floors (T3a)

4.2.1 Modal analysis comparison

The T3a building has timber plank floors and hence flexible diaphragms. This results in a large number of low frequency modes, and dominant lateral modes are not always clear. The lowest modes having significant lateral mass participation modal analysis results are compared in Table 8. In Y direction, the mode shapes of DIANA and LS-DYNA models are slightly different (Figure 43), though the modal frequencies are close. In TREMURI, no dominant mode in the Y direction was observed.

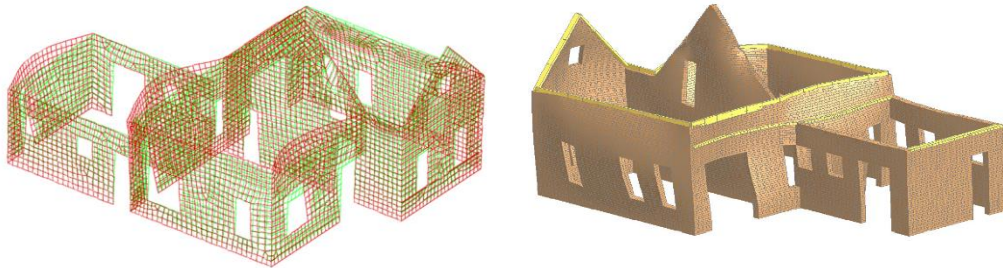


Figure 43 First lateral mode shape (Y direction) – left = DIANA; right = LS-DYNA

Table 8 Modal analysis results comparison of T3a

Modes	Analysis package	Period (s)	Frequency (HZ)	Mode Number	Mass participation %	
					X dir.	Y dir.
1 st fundamental mode in X direction	DIANA	0.094	10.6	16	43	0.39
	TREMURI	0.093	10.7	1	39	0
	LS-DYNA cracked (50% E_{masonry})	0.093	10.8	8	50	0.4
	LS-DYNA uncracked	0.078	12.9	14	23	
1 st fundamental mode in Y direction	DIANA	0.073	13.7	29	0.17	16
	TREMURI	0.069	14.5	2	0.01	12
	LS-DYNA cracked (50% E_{masonry})	0.067	14.8	22	0.37	22
	LS-DYNA uncracked	0.054	18.4	36		31

4.2.2 Gravity comparison

The pier axial forces at ground level under gravity loading are compared in figure 49 between the LS-DYNA and TREMURI models. Values for TU Delft's DIANA model have not been provided. Although the total masses of the building were similar, it is apparent that there was a relatively large difference in the distribution of the loading assumed.

Analysis package	Total Mass (DL+SDL+0.24LL) (t)
DIANA	85.77
TREMURI	90.37
LS-DYNA	89.74

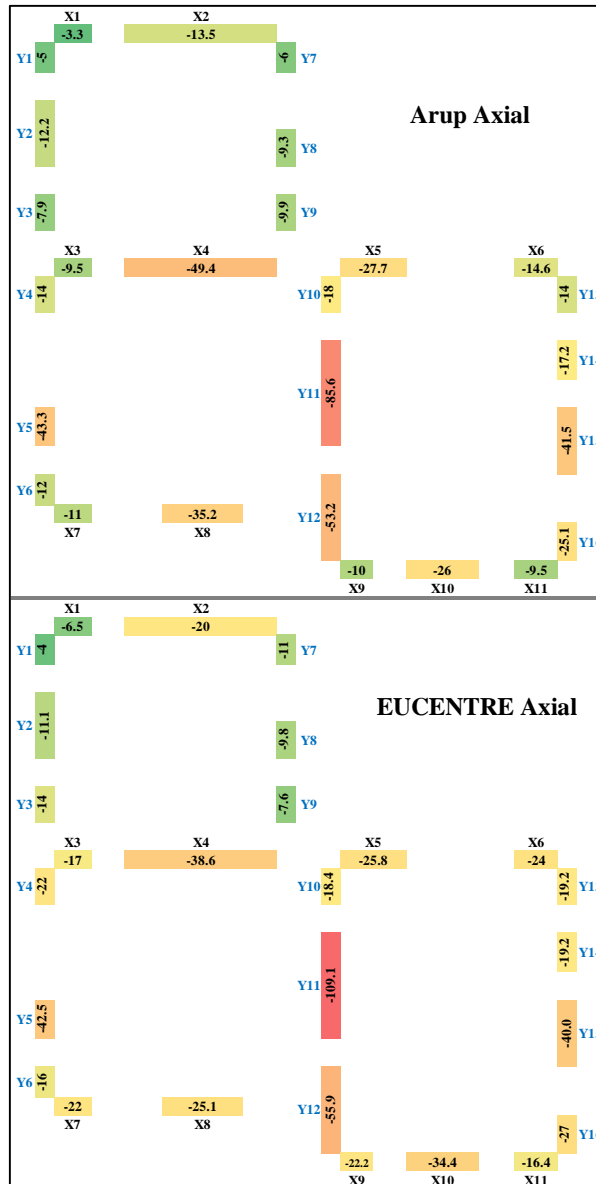


Figure 44 Plan view of the cut-section axial force distributions after initialisation of gravity loading for Arup and EUCENTRE models (TU Delft values n/a). The colour gradient indicates the magnitude of the force distribution – red being the highest magnitude, and green being the lowest.

4.2.3 Pushover comparison

Monotonic and cyclic pushover curves are compared in Figure 45 for the X direction and Figure 46 for the Y direction.

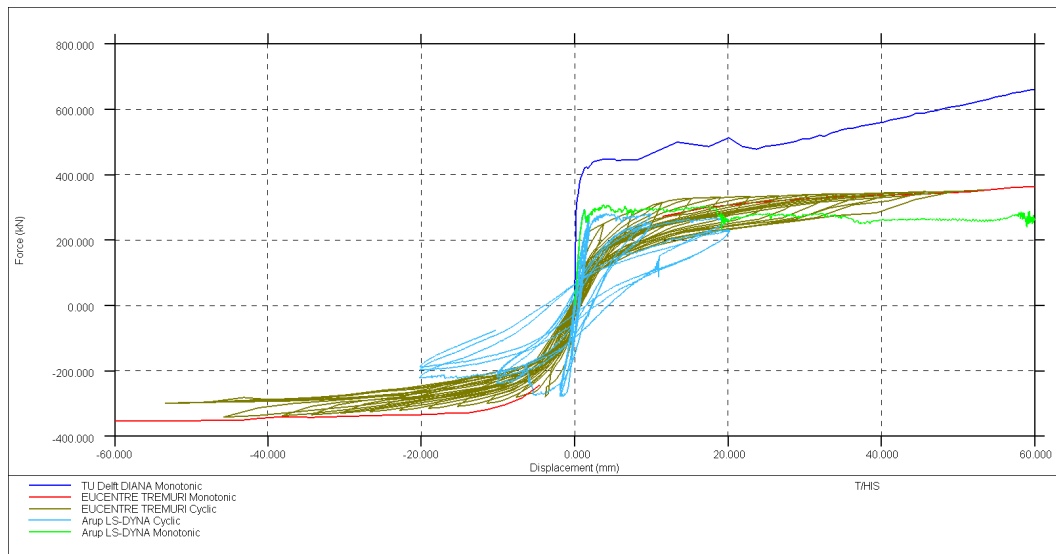


Figure 45 T3a X direction base shear versus average reference height displacement

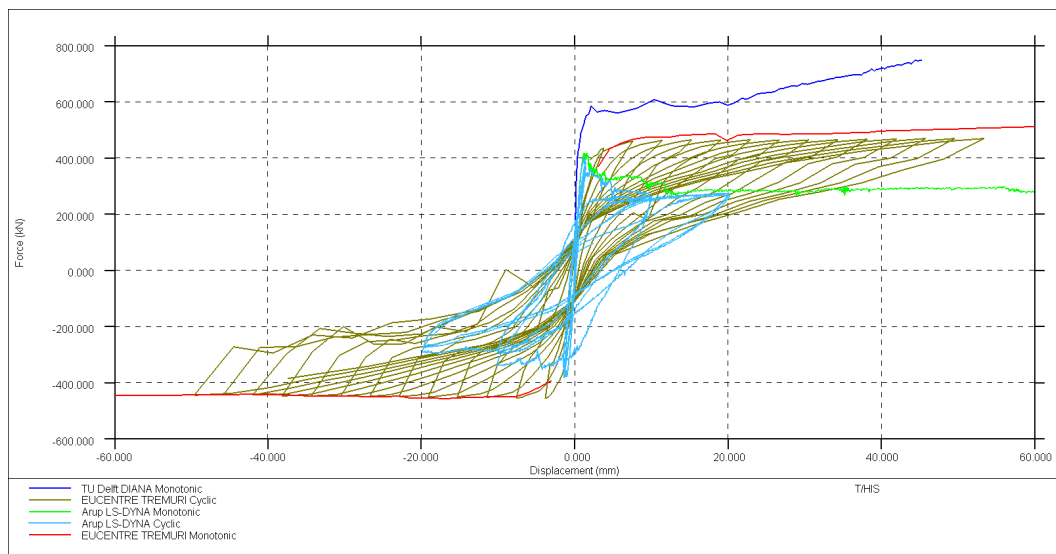


Figure 46 T3a Y direction base shear versus average reference height displacement

In the X direction, the monotonic shear capacities obtained from LS-DYNA, TREMURI and DIANA are 300kN, 370kN and 500kN respectively. Similar trends and differences are apparent in the Y direction. DIANA predicts a higher initial stiffness compared with the other two models and substantially higher ultimate strength, including continuing hardening at large displacement. Under cyclic pushover only the LS-DYNA model predicts significant cyclic degradation. It is observed that TREMURI predicts higher stiffness under cyclic loading than monotonic in small displacement range.

Comparison of the pier forces of the three models (from Table 3.2.9 in Appendix A, Appendix B, and Appendix C) for X-direction pushover is shown in Figure 47. Pier X4 in the LS-DYNA model carries a much lower shear load than the other two models, while pier X10 in the TREMURI model carries much higher shear

load than the other two models. These differences were likely caused by the different diaphragm modelling assumptions in the three models.

Comparison of the pier forces of the three models (from Table 3.2.10 in Appendix A, Appendix B, and Appendix C) for Y-direction pushover is shown in Figure 48. Pier Y9 in the TREMURI model carries much higher shear load than the other two models.

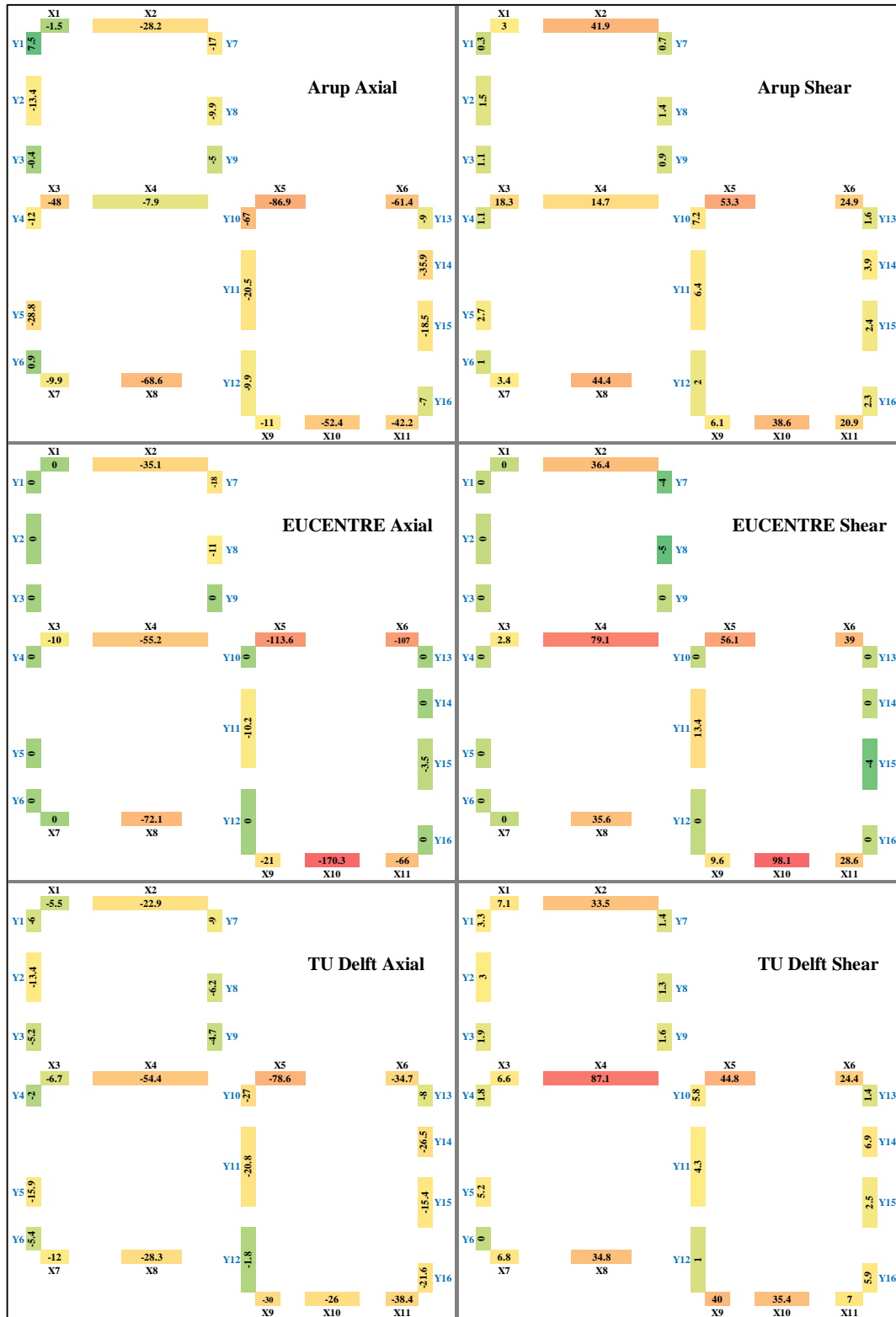


Figure 47 Plan view of the cut-section axial and X shear force distributions at peak/plateau base shear during X-direction pushover for each of the three models. The colour gradient indicates the magnitude of the force distribution – red being the highest magnitude, and green being the lowest.

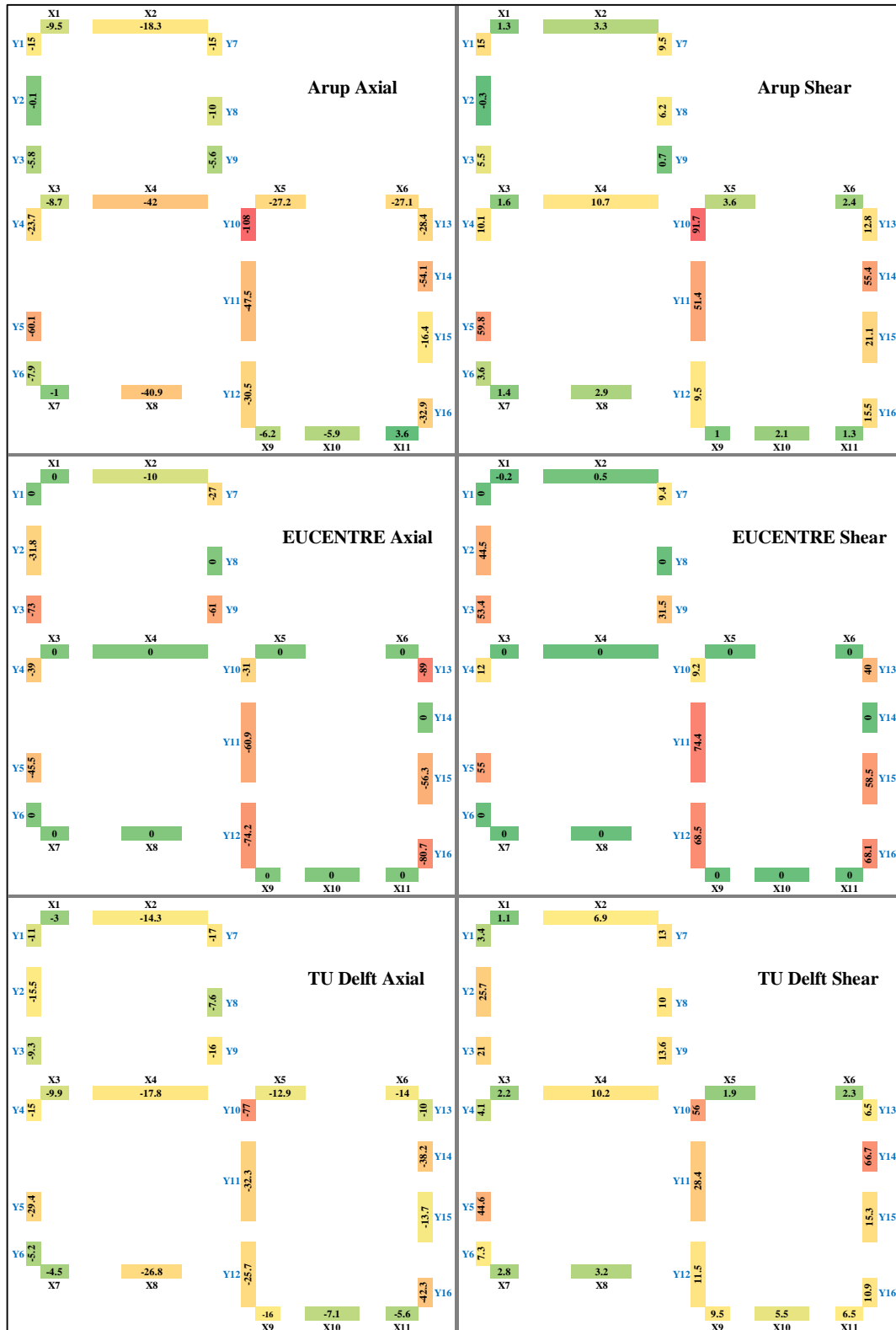


Figure 48 Plan view of the cut-section axial and Y shear force distributions at peak/plateau base shear during Y-direction pushover for each of the three models. The colour gradient indicates the magnitude of the force distribution – red being the highest magnitude, and green being the lowest.

4.2.4 Response history analysis comparison

Table 9 below compares the peak average lateral displacement predicted at roof level by NLRHA analyses using the three software packages for suites of ground motions scaled to three levels of PGA. Rayleigh damping of 1% of critical was implemented in all models.

Table 9 Peak average reference height displacement comparison (three records scaled to three PGA levels each)

PGA	Analysis package	Record 3 (mm)		Record 6 (mm)		Record 7 (mm)	
		X dir.	Y dir.	X dir.	Y dir.	X dir.	Y dir.
0.1g	DIANA	0.15	0.14	0.17	0.14	0.14	0.18
	TREMURI	0.54	0.17	0.47	0.19	0.55	0.16
	LS-DYNA	0.7	0.4	0.6	0.3	0.6	0.3
0.25g	DIANA	0.78	0.7	0.6	0.51	0.92	0.5
	TREMURI	2.13	0.5	1.4	0.51	1.6	0.56
	LS-DYNA	1.9	0.7	2.2	0.8	1.7	0.8
0.50g	DIANA	6.9	4.1	4.2	3.6	6.1	5.8
	TREMURI	4.4	2.5	6.5	1.4	7.2	2.4
	LS-DYNA	21	8.1	9.3	5.0	12	5.6

Figure 49 to 51 below compare the base shear vs roof displacement hysteresis predicted in the X direction for 0.25g PGA input motions by the three models for the three ground motion sets in turn. The following can be seen:

- The difference in stiffness of response is consistent with the pushover curve; DIANA is by far the ‘stiffest’, and LS-DYNA is stiffer than TREMURI
- Hysteresis loops are of a reasonably conventional form for a structure responding in its stable range
- There is some record to record variation

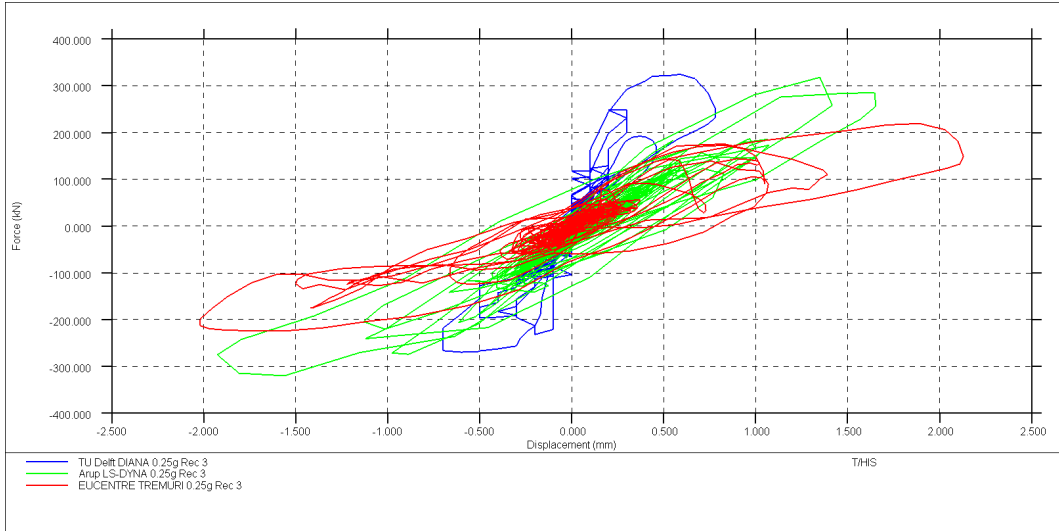


Figure 49 Base shear versus average reference height displacement – 0.25g scaled PGA, record 3, X direction

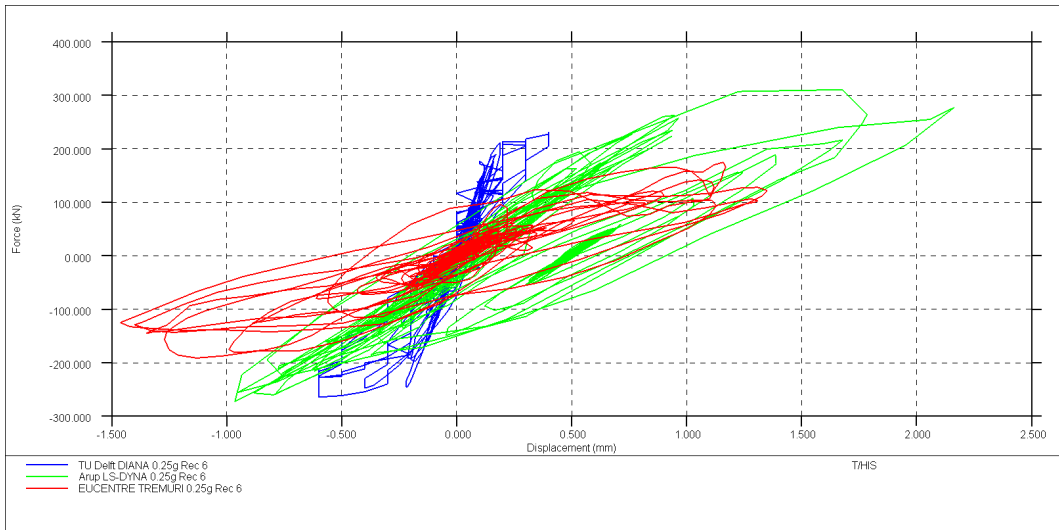


Figure 50 Base shear versus average reference height displacement – 0.25g scaled PGA, record 6, X direction

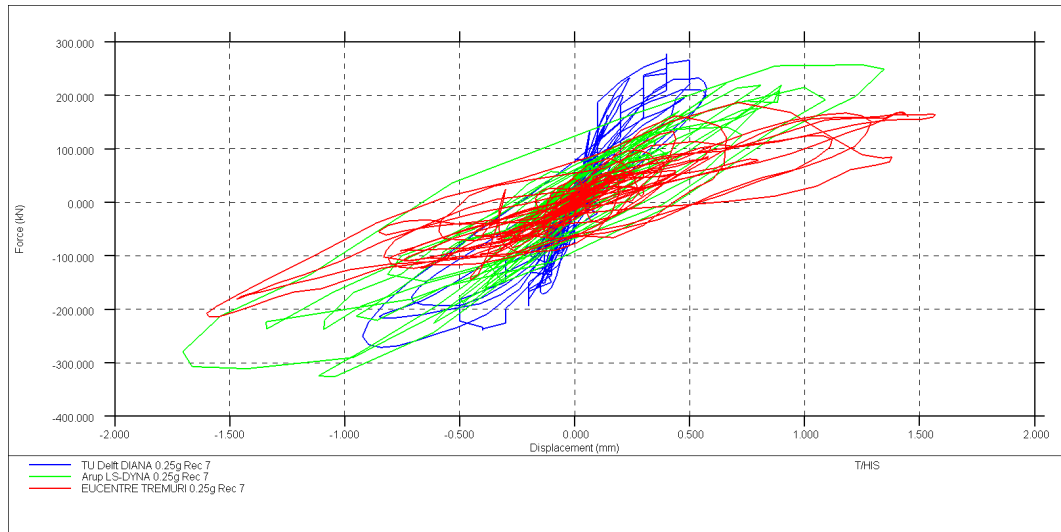


Figure 51 Base shear versus average reference height displacement – 0.25g scaled PGA, record 7, X direction

Figure 52 to 54 below compare the base shear vs roof displacement hysteresis predicted in the Y direction for 0.25g PGA input motions by the three models for the three ground motion sets in turn. The peak displacements are small and the peak forces are lower than the ‘yield’ values in the pushover analysis. The following can be seen:

- The differences in overall response are modest.
- DIANA appears to have ‘fatter’ hysteresis loops and therefore greater energy dissipation. This may account in part for the slightly lower peak responses predicted by DIANA.
- There is some record to record variation

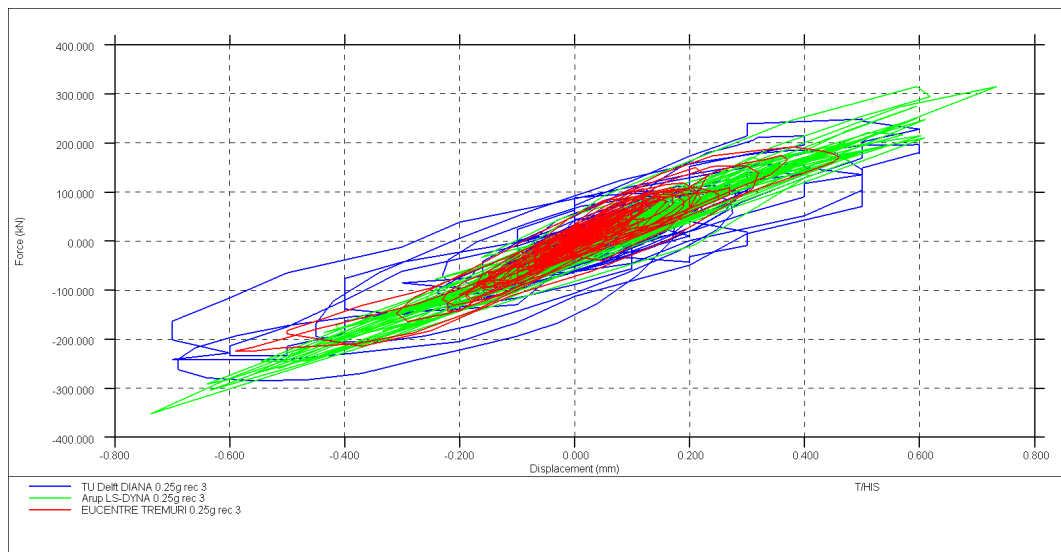


Figure 52 Base shear versus average reference height displacement – 0.25g scaled PGA, record 3, Y direction

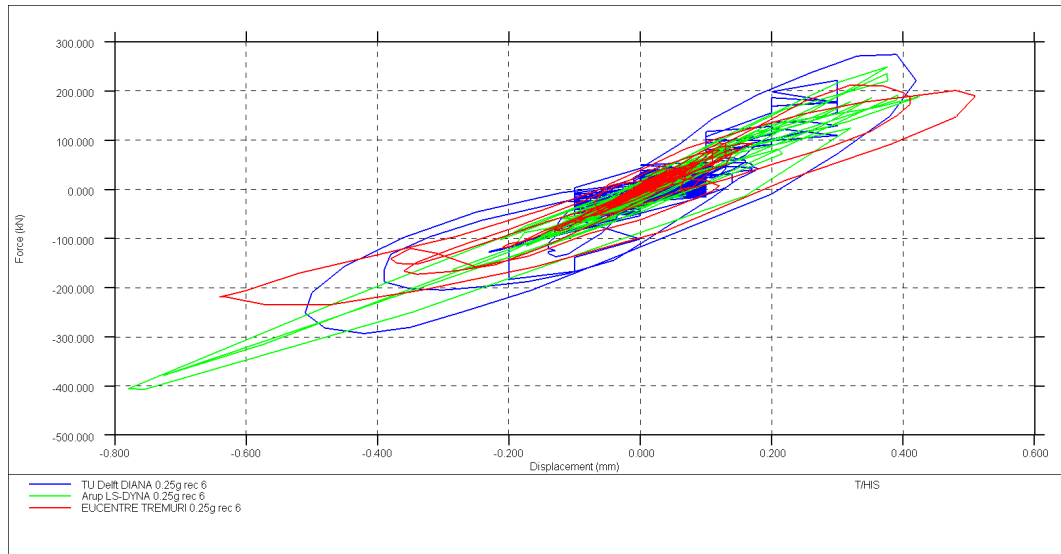


Figure 53 Base shear versus average reference height displacement – 0.25g scaled PGA, record 6, Y direction

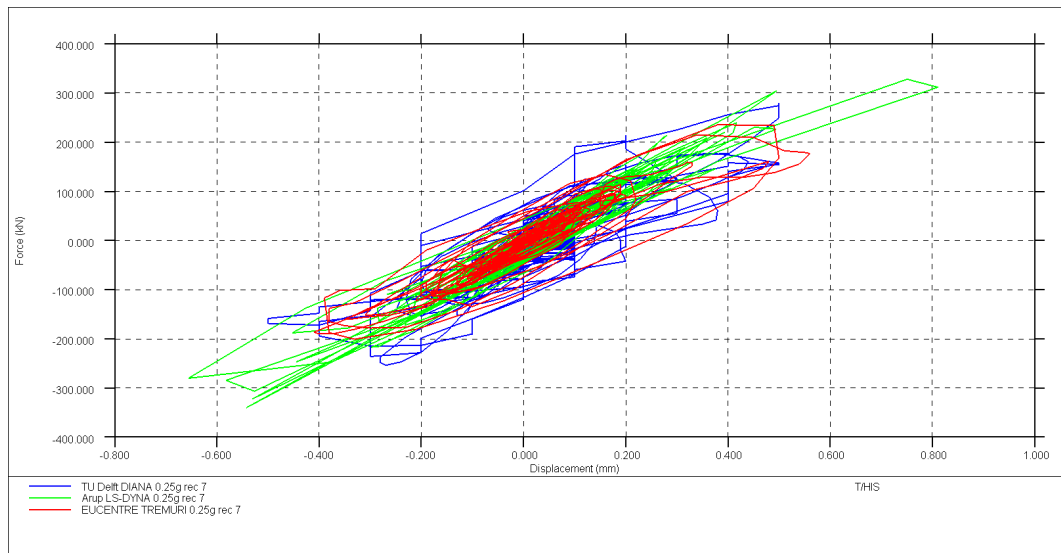


Figure 54 Base shear versus average reference height displacement – 0.25g scaled PGA, record 7, Y direction

4.2.5 Notes and Discussion

The DIANA pushover analysis output showed a hardening phase that requires more investigation and clarification from the TU Delft modelling team.

Compared to the other two models, the LS-DYNA model showed lower peak base shear in the pushover analysis output and greater cyclic degradation (including strength degradation).

5 Conclusions and Recommendations

5.1 Experimental benchmark tests

Where existing results and data were available, the three modelling teams were able to replicate the benchmark tests in analytical models fairly well, albeit with different degrees of “curve-fitting” (e.g. tuning of stiffness in TREMURI as described in Section 3.5.4, and increase of tensile fracture energy in DIANA as described in Sections 3.2.3 and 3.4.3, etc.) in order to match the experimental results realistically.

Differences between predictions and experimental observations are being used to improve the capability of the software analysis programmes.

5.2 Predictions for index buildings

In “blind modelling and prediction” of two index buildings, the three modelling teams predicted performances that were significantly different. In the absence of physical test data it is not possible to make definitive judgements on the relative accuracy or reliability of each prediction. However, some clear differences in modelling assumptions and analysis capabilities have been identified. Reconciliation of these can assist in improving consistency going forward.

5.3 Comparison of modelling approaches

A summary of the comparison between the different modelling approaches is given in Table 10.

Table 10 Comparison summary between different modelling approaches

Modelling Approach	Advantages	Disadvantages	Relative Computational Effort
LS-DYNA brick-by-brick	<p>Near-exact geometry can be modelled, including the effect of brick lay-up patterns and local failure modes.</p> <p>Crack locations and sizes can be tracked explicitly.</p> <p>No need to pre-define the potential failure locations or to pre-calculate the strengths and backbone curves. The masonry material is represented by fundamental properties.</p> <p>Potentially has a low need for curve fitting of experimental results.</p> <p>Distributed or discrete connections to diaphragms are possible.</p> <p>Full 3D simulation including in-plane and out of plane interactions</p> <p>Foundation elements and soil can be modelled using a variety of techniques.</p>	<p>High model complexity, requiring experienced analyst/engineer to build the models and run the analyses.</p> <p>High computational requirement with long run time.</p> <p>Difficulty in replicating dynamic out-of-plane tests on one-way spanning walls without curve fitting of parameters. This is partly due to the limited number of integration points (and their weighting) through the thickness of a wall</p>	High

LS-DYNA 2D shells	<p>Relatively simple model generation – no need to replicate exact brick arrangements.</p> <p>No need to pre-define the potential failure locations or to pre-calculate the strengths and backbone curves. The masonry material is represented by fundamental properties.</p> <p>Potentially has a low need for curve fitting of experimental results.</p> <p>Distributed or discrete connections to diaphragms are possible.</p> <p>Out of plane static and dynamic response is predicted very well</p> <p>Full 3D simulation including in-plane and out of plane interactions\</p> <p>Foundation elements and soil can be modelled using a variety of techniques.</p> <p>Offers a reasonable balance between computational effort and modelling accuracy.</p>	<p>Cannot identify problems associated with individual bricks ‘falling out’.</p> <p>Behaviours controlled by the finite size and shape of the individual bricks cannot be captured easily, which may lead to incorrect prediction of resistance in certain deformation modes, especially modes involving the rotation of individual bricks relative to their neighbours.</p> <p>Overestimated the energy dissipation in some of the benchmark tests.</p>	Medium
TREMURI	<p>Equivalent frame model with low computational requirement.</p> <p>Less complex model where pre- and post-processing are more straightforward.</p> <p>Gives good results for benchmark tests related to in-plane and 2D response of test specimens</p> <p>Not clear how foundation flexibility and SSI can be incorporated</p>	<p>Cannot model out-of-plane dynamic response of walls.</p> <p>Cannot model in-plane and out-of-plane responses simultaneously, as discussed in Section 3.6.3.</p> <p>Requires some ‘case by case calibration’ of the macro-element model parameters governing nonlinear deformability and softening branch (shear behaviour). This requires considerable expertise and judgement unless a specific test result is available.</p>	Low
DIANA	<p>Relatively simple model generation – no need to replicate exact brick arrangements.</p> <p>No need to pre-define the potential failure locations or to pre-calculate the strengths and backbone curves.</p> <p>Distributed or discrete connections to diaphragms are possible.</p> <p>Possible to model foundation elements and soil-structure interactions.</p>	<p>Difficulties in obtaining numerical convergence in implicit time integration scheme may mean solution cannot be obtained.</p> <p>Analysis output shows hardening phase that is unrealistic and not well understood currently.</p> <p>Required different degrees of artificial increases in tensile fracture energy to account for energy dissipations that were not captured in the models.</p>	High

In the context of the Groningen Earthquakes – Structural Upgrading project, it is worth reiterating the following conclusions from [3] Volume 3:

The Groningen Earthquakes – Structural Upgrading project needs to evaluate a very large number of existing unreinforced masonry buildings as accurately as is reasonably possible in order to make sound decisions on the need for and

extent of physical upgrading measures. Confidence in the methods used to assess the seismic performance of these buildings is of paramount importance, and the only means by which methods can be evaluated is by calibration against high quality experimental data.

The quality and completeness of the test data are fundamental to the success of any calibration of computational models. The behaviour of unreinforced masonry in certain modes can be very sensitive to the detail of the experimental setup, the boundary conditions and the mechanical properties of the materials used in the construction of the specimen. Masonry material properties (particularly mortar) have intrinsically high variability, and as was shown in several of the numerical studies, small changes in assumed properties can substantially change the predicted deformation modes and structural characteristics of a component.

Given the intrinsic variability of masonry properties it is not realistic to expect that any calculation method, however sophisticated, will be able to predict the outcome of individual physical tests with very high fidelity. Indeed, if the same experiment were performed several times on notionally identical specimens, the test results themselves would not be exactly the same, particularly in cyclic or dynamic tests where different types of damage accumulate. Therefore, a realistic objective is to show that a computational model is capable of representing all the important failure modes at load or deformation conditions **consistent** with the best estimate material properties and their possible ranges, over a wide variety of tests.

References

- [1] Anthoine A., Magonette G., Magenes G., (1995) “Shear compression testing and analysis of brick masonry walls”, Proc. 10th European conference on earthquake engineering, Vienna.
- [2] Anthoine A. and Capéran, P., (2008) “Enhanced Safety Efficient Construction of Masonry Structures in Europe” – ESECMaSE work package 8, deliverable D 8.3 Earthquake tests and analysis of the experimental results (incl Annex A), ESECMaSE.
- [3] Arup, (2014) 229746_32.0_REP109, "Modelling and Analysis Methods for Unreinforced Masonry Buildings in Groningen Area", 20 December 2014, Draft Rev.0.03.
- [4] Feenstra PH, Rots JG, Arnesen A., Teigen JG, Hoiseth KV, (1998) “A 3D constitutive model for concrete based on co-rotational concept”, Computational modelling of concrete structures. Proc. EURO-C 1998, Eds. R. de Borst et al., pp. 13-22, Bakelma, Rotterdam.
- [5] Griffith MC, Vaculik J., Lam NTK, Wilson J., Lumantarna E., (2007) “Cyclic testing of unreinforced masonry walls in two-way bending”, Earthquake Engineering & Structural Dynamics, 36(6), 801-821.
- [6] Lagomarsino S., Penna A., Galasco A., Cattari S., (2013) “TREMURI Program: an equivalent frame model for the nonlinear seismic analysis of masonry buildings”, ENGINEERING STRUCTURES, 56(11): 1787-1799.
- [7] Lam NTK, Griffith M., Wilson J., Doherty K., (2003) “Time-history analysis of URM walls in out-of-plane flexure”, Engineering Structures 25, 743–754.
- [8] Magenes G., Calvi GM, Kingsley G., (1995) “Seismic Testing of a Full-Scale, Two-Story Masonry Building: Test Procedure and Measured Experimental Response”, University of Pavia, Italy.
- [9] Magenes G., Morandi P., Penna A., (2008) “In-plane cyclic tests of calcium silicate masonry walls”, Proc. 14th IB2MAC, Sydney, CD-ROM paper n. 193.
- [10] Magenes, G., Morandi, P., Penna, A., (2008) “Enhanced Safety Efficient Construction of Masonry Structures in Europe” – ESECMaSE work package 7, deliverable D7.1 c, Test results on the behaviour of masonry under static cyclic in plane lateral loads.
- [11] Mendes N., Lourenco PB, (2010) “Seismic assessment of masonry "Gaioleiro" buildings in Lisbon, Portugal”, Journal of Earthquake Engineering 14:80-101.

- [12] Mendes N., Lourenco PB, (2013) “Seismic performance of ancient masonry buildings”, Proceedings of COMPDYN 2013, eds. Papadrakakis M. et al, Kos Island, Greece.
- [13] Penna A., Lagomarsino S., Galasco A., (2014) “A nonlinear macro-element model for the seismic analysis of masonry buildings”, EARTHQUAKE ENGINEERING & STRUCTURAL DYNAMICS, 43(2): 159-179.
- [14] Rots JG, (2002) “Comparative study of crack models”, Finite Elements in Civil Engineering. Proc. Third DIANA World Conference 2002, Eds. Hendriks MAN & Rots JG, Balkema, Lisse, pp. 17-28.

Appendix A

Modelling Comparison – Arup

1. Solid Modelling – Summary of modelling approach

Table 1.1: General modelling notes

Component	Description
Analysis team	Arup
Analysis software and formulation	LS-DYNA – Explicit time integration scheme and eigensolver are used for different analyses.
Overview of modelling approach	<ul style="list-style-type: none"> • For nonlinear pushover and response history analysis, an explicit time integration scheme was used. • For eigenvalue analysis, the Block Shift and Invert Lanczos eigensolver was used. • Masonry modelled with 3D solid elements (brick-by-brick) with tiebreak contact between bricks to model the mortar. • Shell elements, beam elements, and discrete (spring) elements used to model other components of the benchmark and cross-validation tests. • Material properties and tiebreak contact parameters were defined based on the available test data for masonry – both brick and mortar – characterisation tests, using a consistent methodology across all benchmarks and index buildings models.
Model units	SI units (kg, m, sec)

Table 1.2: Model properties applicable for all benchmark tests and index buildings

Input	Description
Element formulation	Constant stress solid element with single integration point.
Hourglass type	Belytschko-Bindeman assumed strain co-rotational stiffness form for 2D and 3D solid elements only.
Hourglass coefficient	1.0
Brick material type	MAT_WINFRITH [1][2] (MAT_084), with yielding/strain hardening properties.
Contact	AUTOMATIC_SURFACE_TO_SURFACE_TIEBREAK with Dycoss discrete crack model failure surface.
Contact stiffness factor	6
Damping	DAMPING_PART_STIFFNESS, with damping coefficient 0.05. DAMPING_FREQUENCY_RANGE_DEFORM, with damping coefficient 0.01 for frequency range 1–30 Hz.
Brick to brick friction factor	Mean experimental data value when available; 0.75 if no experimental value available.
Tiebreak contact energy release rate – Normal [N/m]	10
Tiebreak contact energy release rate – Shear [N/m]	Mortar shear strength [Pa] / 10000

2. Experimental benchmarks

2.1. Ispra in-plane panel tests

Table 2.1.1: Modelling notes

Component	Description
Analysis software and formulation	LS-DYNA – explicit analysis solver
Walls (in-plane)	Individual bricks modelled with solid elements using nonlinear Winfrith material model. Mortar modelled with tiebreak contact surface (penalty stiffness formulation) with a Mohr-Coulomb failure surface. The stiffness of the bricks was adjusted so that the total masonry stiffness (brick Young's modulus and contact penalty stiffness) matches masonry material test data from laboratory tests.

Table 2.1.2: Nonlinear time history analysis notes

Nonlinear time history analysis notes
<ul style="list-style-type: none">• 1% damping applied using proprietary LS-DYNA constant damping model over 1-30 Hz frequency range.• Additional damping applied at very high frequencies for numerical stability.

Table 2.1.3: Model loading, materials and general comments

Loading	
Dead load	Self-weight of clay brick walls
Overburden	Constant 150 kN applied load (including self-weight of steel beam in test setup)
Materials	
	Material properties including values and stress strain behaviour
Clay bricks	Nonlinear concrete (Winfrith) material model $\rho = 1652 \text{ kg/m}^3$ $E = 2306 \text{ MPa}$ (to match masonry E of 1491 MPa) $\nu = 0.15$ $f_c = 6.2 \text{ MPa}$ $F_t = 1.24 \text{ MPa}$ (lower bound tensile strength)
Mortar	Tensile stress limit = 0.04 MPa Shear stress limit = 0.23 MPa Friction coefficient = 0.58 Modelled using tiebreak contact with Dycoss discrete crack model failure surface. Contact penalty stiffness factor = 6 Tensile energy rate = 10 N/m Shear energy rate = 23 N/m
Steel	Elastic material model $\rho = 7850 \text{ kg/m}^3$ $E = 210 \text{ GPa}$ $\nu = 0.3$
Other key notes	
1) Test data displacement history applied as a velocity sinusoidal input prescribed motion. 2) Rigid shell patches – defined at either end of the steel beam bottom flange – are restrained from rotating but free to translate in-plane and vertically. This maintains a constant overburden throughout the test. 3) Tiebreak contact defined between steel beam and top layer of bricks.	

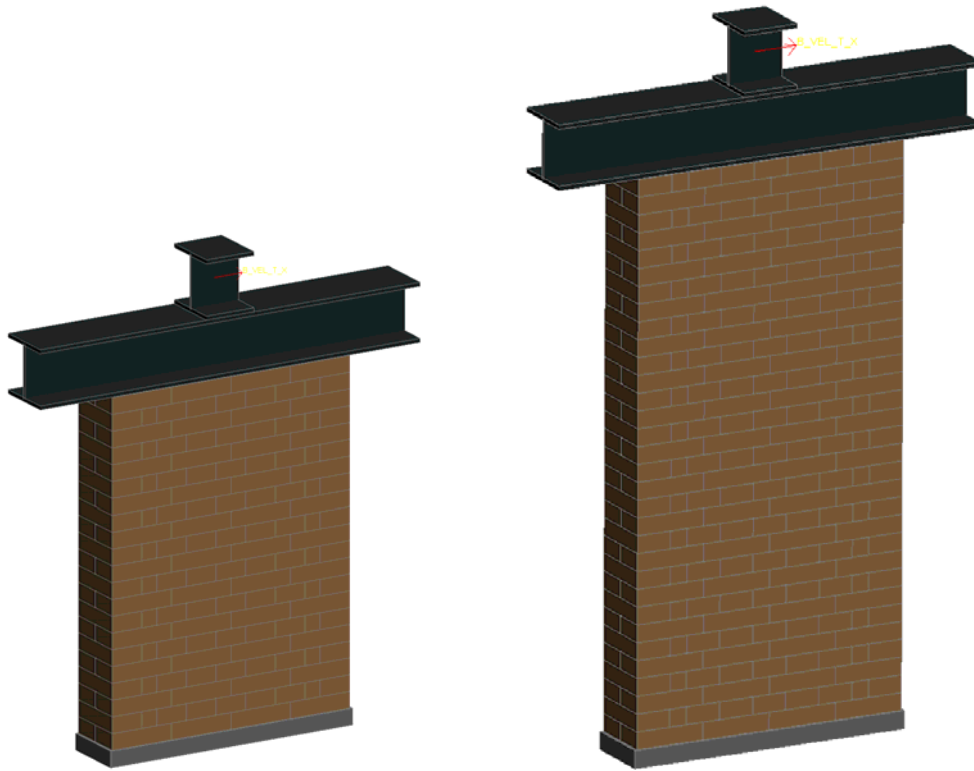


Figure 2.1.1: LS-DYNA models for LOWSTA (left) and HIGSTA1 (right)

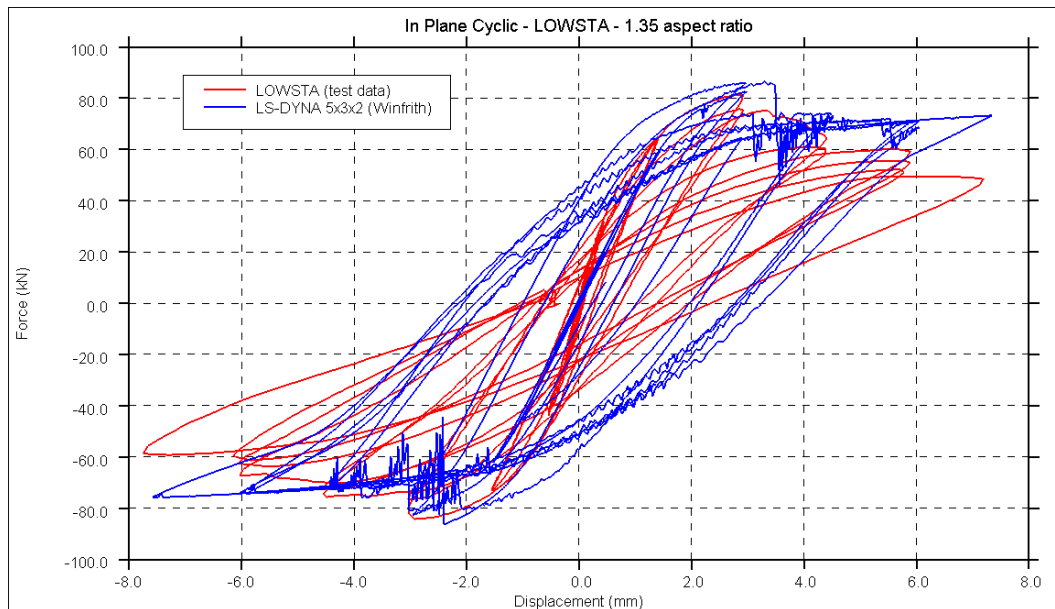


Figure 2.1.2: Shear force-displacement comparison plot for LOWSTA

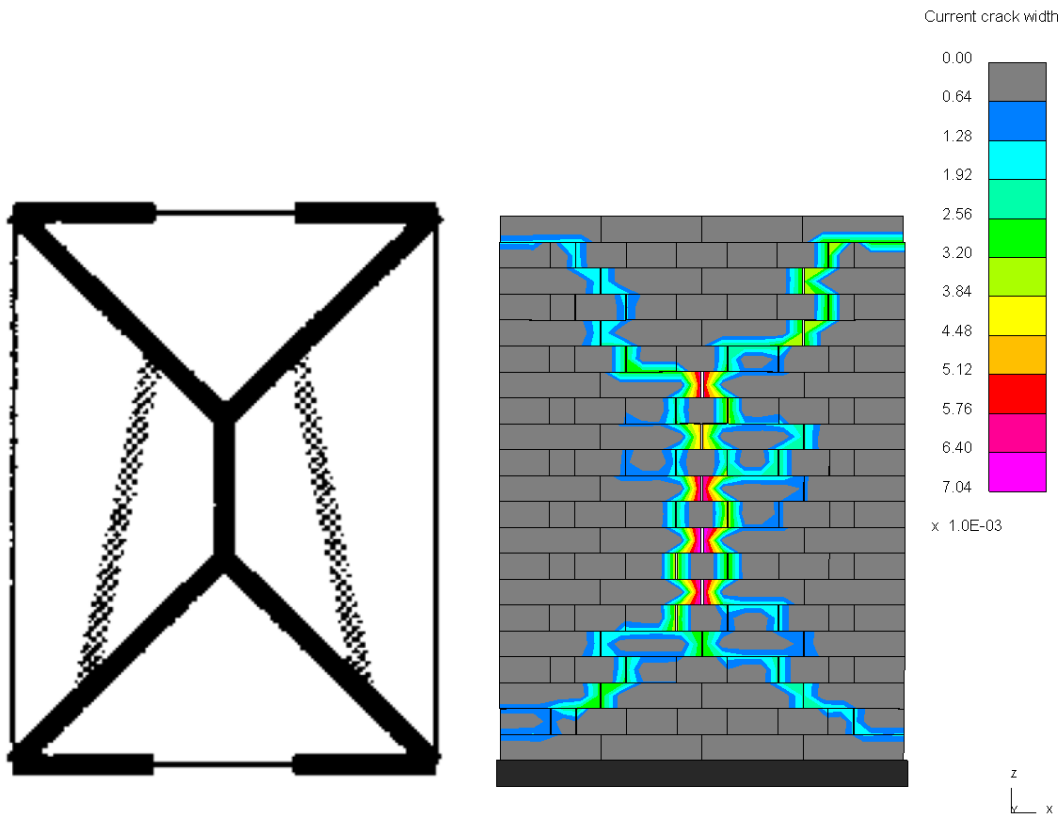


Figure 2.1.3: Final crack pattern for LOWSTA – comparison between test and LS-DYNA

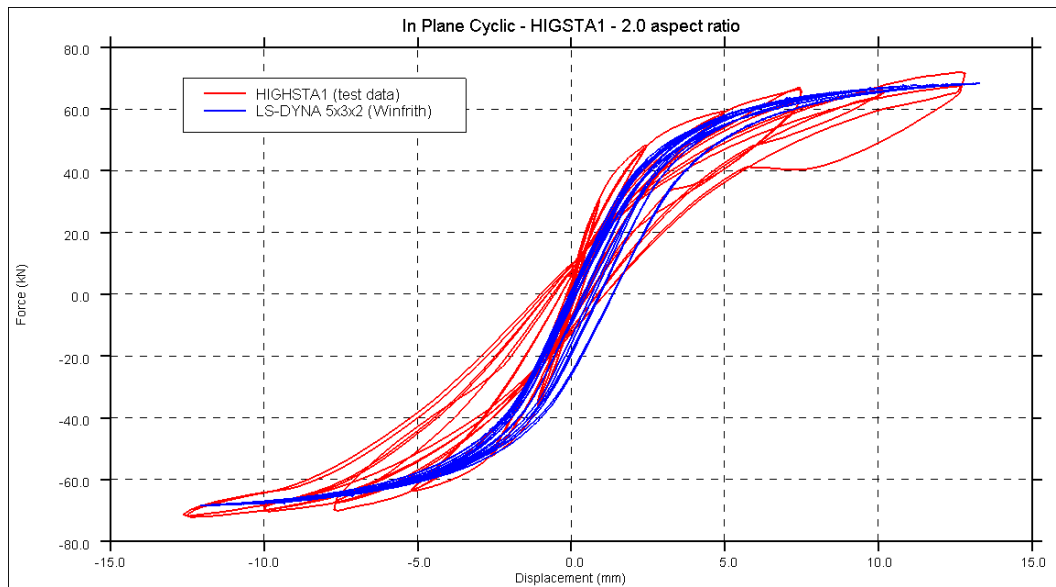


Figure 2.1.4: Shear force-displacement comparison plot for HIGSTA1

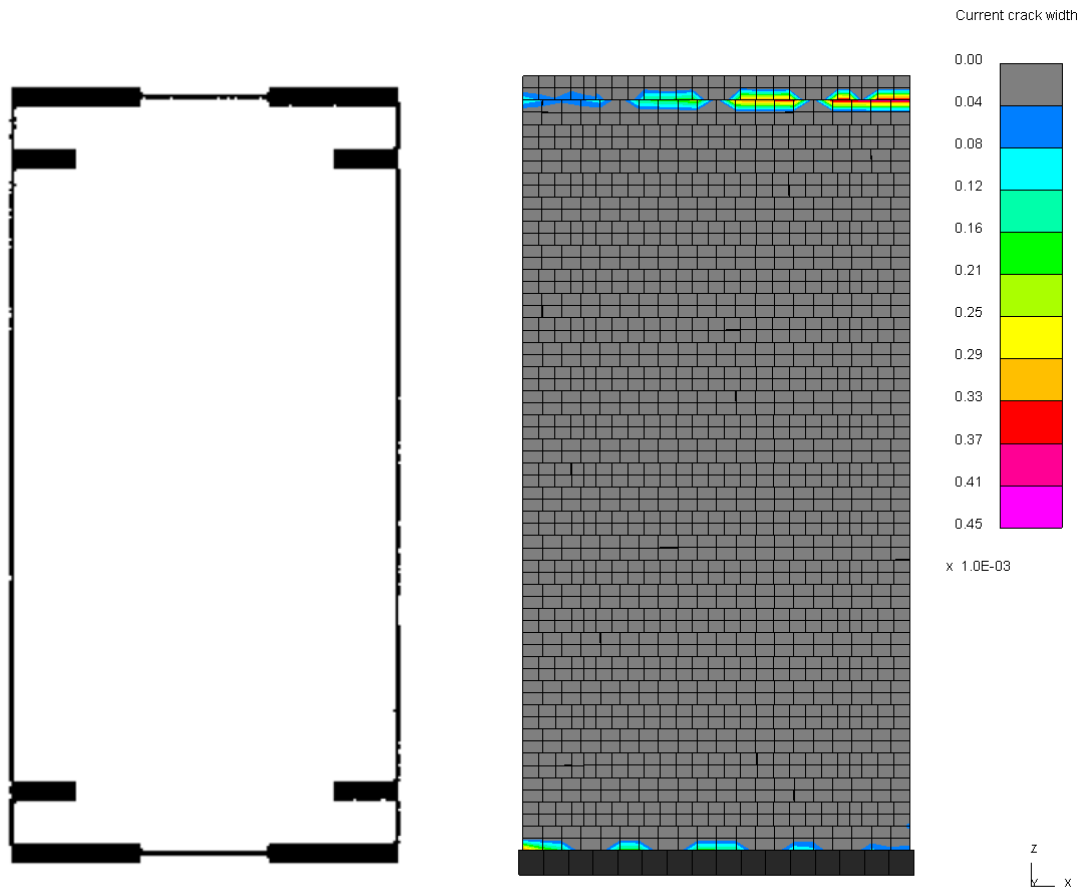


Figure 2.1.5: Final crack pattern for HIGSTA1 – comparison between test and LS-DYNA

2.1.1. Discussion and sensitivity analyses

For the LOWSTA panel, the results of the analysis show good correlation to the test in terms of both crack patterns and force-displacement response. The crack pattern shows a diagonal tension sliding brittle failure mode, similar to the laboratory observations. The analysis force-displacement output shows an ultimate load of 86 kN, which is very close to the laboratory value of 84 kN, at a drift of 2%. The test shows both modest strength degradation and reduction of stiffness during the larger cycles, i.e. above 2.5 mm amplitude. The analysis predicts some strength degradation as the amplitude exceeds 3 mm, but no further degradation for higher amplitudes up to 7 mm.

For the HIGSTA1 panel, the results of the analysis also show good correlation to the test in terms of both crack patterns and force-displacement response. The crack pattern shows a rocking failure mode with cracks forming along the top and bottom of the panel at each corner. The analysis force-displacement output shows an ultimate load of 68 kN, which is very close to the laboratory value of 72 kN, at a drift of 6%. The hysteresis of the test specimen shows some reduction in stiffness and energy dissipation as the amplitude increases. The analysis displays hysteresis with less energy dissipation and less reduction in stiffness at larger amplitudes, consistent with almost pure ‘rigid body’ rocking.

Based on suggestions by EUCENTRE, sensitivity analyses were carried out with 50% reduced tensile strength for mortar head joints (bed joints remained unchanged), i.e. with NFLS value of 0.02 MPa instead of the original 0.04 MPa.

Results are shown in the following figures. The reduced head joint mortar tensile strength did not have a significant effect on the analysis results, as shown in the figures.

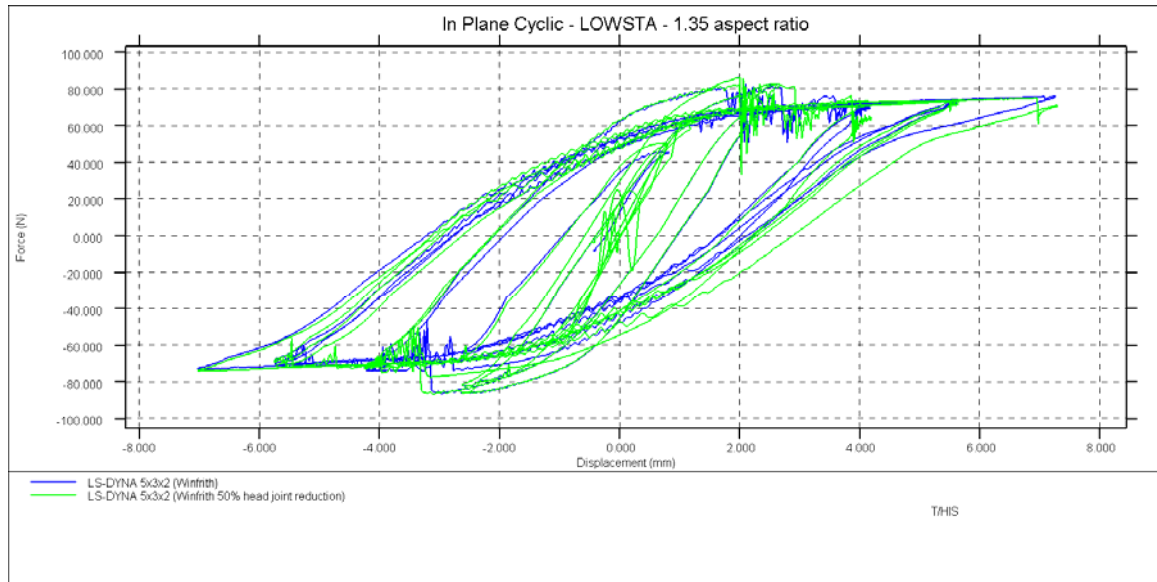


Figure 2.1.1.1: Shear force-displacement sensitivity analysis – LOWSTA

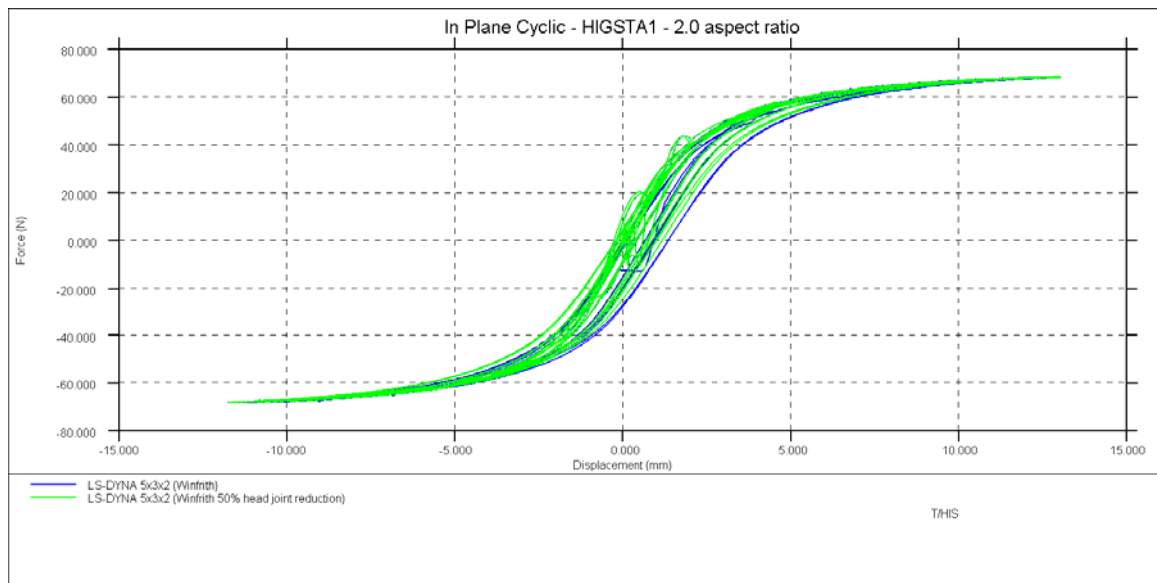


Figure 2.1.1.2: Shear force-displacement sensitivity analysis – HIGSTA1

2.2.Pavia full building tests

Table 2.2.1: Modelling notes

Component	Description
Analysis software and formulation	LS-DYNA – explicit analysis solver
Walls (in-plane)	Individual bricks modelled with solid elements using nonlinear Winfrith material model. Mortar modelled with tiebreak contact surface (penalty stiffness formulation) with a Mohr-Coulomb failure surface. The stiffness of the bricks was adjusted so that the total masonry stiffness (brick Young's modulus and contact penalty stiffness) matches masonry material test data from laboratory tests.
Walls (out-of-plane)	As above.
Spandrels/lintels and wall coupling	Spandrels modelled using the same approach as the walls, with tiebreak contact surface modelling coupling effects. The adjustment of spandrel stiffness (Young's modulus) was treated differently than that for the walls, as the dominant loading on spandrel is along the horizontal direction. Lintels modelled with elastic materials.
Wall to wall connection (incl. flange effects)	Contact surface used for the mortar connection. Refer to the mortar material information for further details. Flange effects are included explicitly.
Wall to diaphragm connection	Contact surface used for the mortar connection between the bricks and the diaphragm.

Table 2.2.2: Nonlinear time history analysis notes

Nonlinear time history analysis notes
<ul style="list-style-type: none"> • 1% damping applied using proprietary LS-DYNA constant damping model over 1–30 Hz frequency range. • Additional damping applied at very high frequencies for numerical stability. • To minimise dynamic effects, the loading was applied on each floor as a prescribed velocity. A maximum velocity magnitude of 15 mm/s was used for the LS-DYNA analysis. The velocities were applied to the constraints at the locations of the flexible diaphragms on each wall.

Table 2.2.3: Model loading, materials and general comments

Loading	
Dead load	Self-weight of clay brick walls
Applied load	248.4 kN on the first floor 236.8 kN on the second floor (This is equivalent to approximately 10 kN/m ² on each floor)
Materials	Material properties including values and stress strain behaviour
Clay bricks	Nonlinear concrete (Winfrith) material model $\rho = 1652 \text{ kg/m}^3$ $E = 2306 \text{ MPa}$ for non-spandrel bricks (to match masonry E of 1491 MPa) $E = 1752 \text{ MPa}$ for spandrel bricks (to match masonry E of 1491MPa; see key note 6 below) $\nu = 0.15$ $f_y = 6.2 \text{ MPa}$ $F_t = 1.24 \text{ MPa}$ (lower bound tensile strength)
Mortar	Tensile stress limit = 0.04 MPa Shear stress limit = 0.23 MPa Friction coefficient = 0.58 Modelled using tiebreak contact with Dycoss discrete crack model failure surface. Contact penalty stiffness factor = 6 Tensile energy rate = 10 N/m Shear energy rate = 23 N/m
Steel	Elastic material model $\rho = 7850 \text{ kg/m}^3$ $E = 210 \text{ GPa}$ $\nu = 0.3$
Other key notes	
<ol style="list-style-type: none"> 1) Brick unit mesh density – $5 \times 3 \times 2$ elements. 2) Flexible diaphragm (steel beams) not modelled to reduce dynamic effects. 3) Superimposed dead load modelled as mass elements at centreline of walls at each floor. 4) Shear and tensile strength of mortar in lintels increased 10 times versus experimental values to model pre-compression of mortar from construction stage. 5) Geometry of bricks in lintels altered to be skewed to prevent premature drop-out of lintel. 6) Stiffness of bricks in spandrels reduced to match masonry E, since loading on spandrels is primarily in the horizontal direction. 7) Frictional coefficient of 0.2 at the interface between the flange walls and the door wall to prevent flange walls moving out of plane (dynamic effect). 	

DSPLOT: Casetta Pavia

DSPLOT: Casetta Pavia

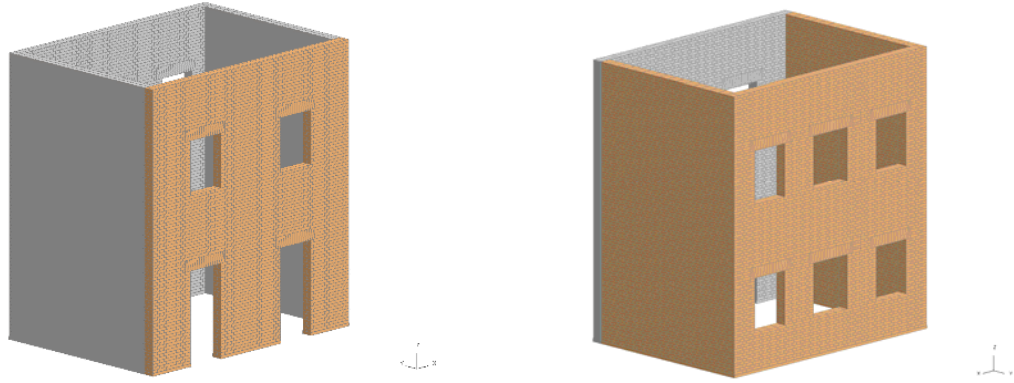


Figure 2.2.1: FE model showing Door Wall (left) and Window Wall (right)

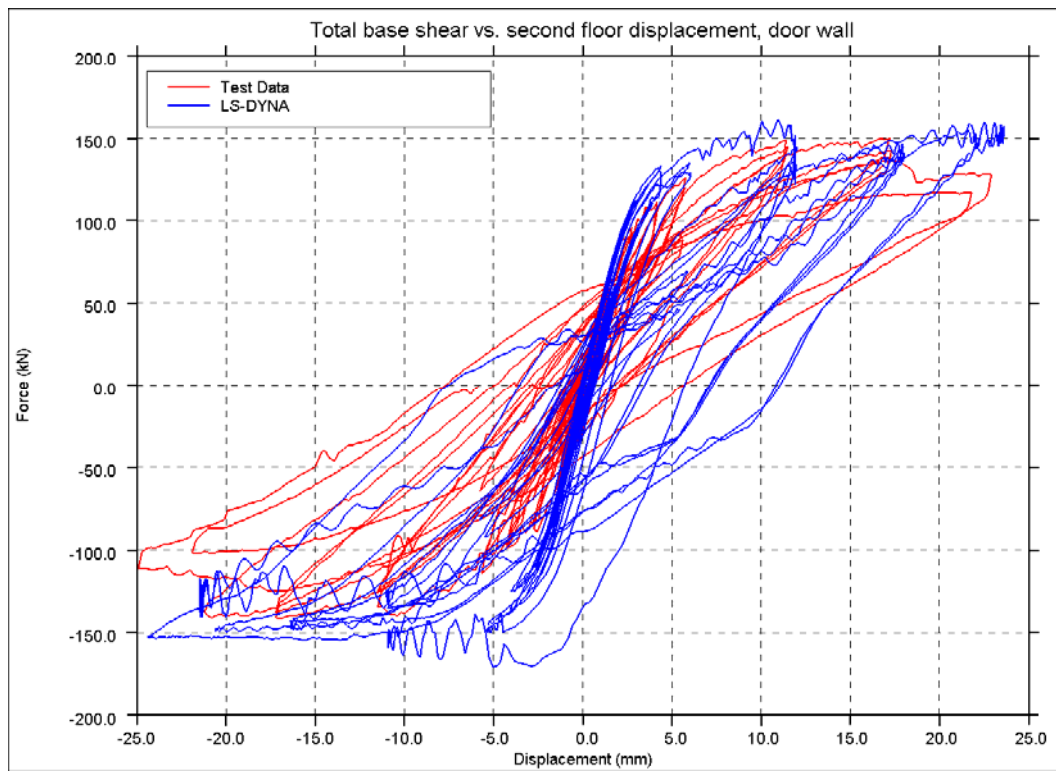


Figure 2.2.2: Total base shear force vs. second floor displacement (Door Wall)

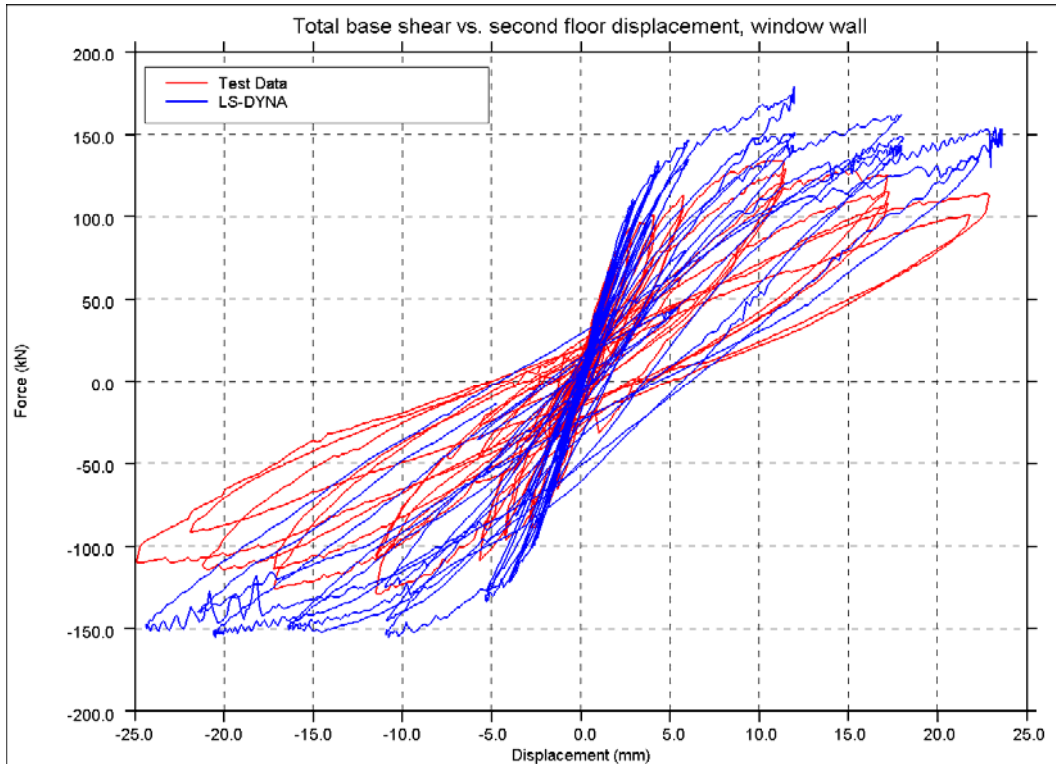


Figure 2.2.3: Total base shear force vs. second floor displacement (Window Wall)

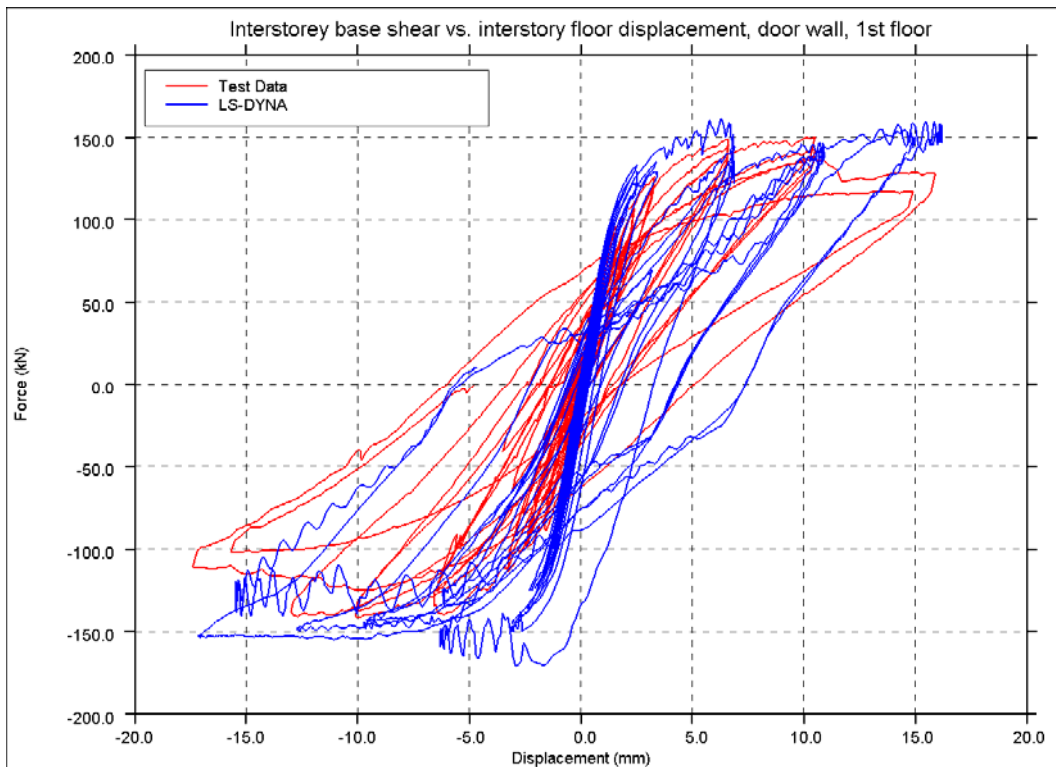


Figure 2.2.4: Interstorey shear force vs. interstorey displacement, 1st floor (Door Wall)

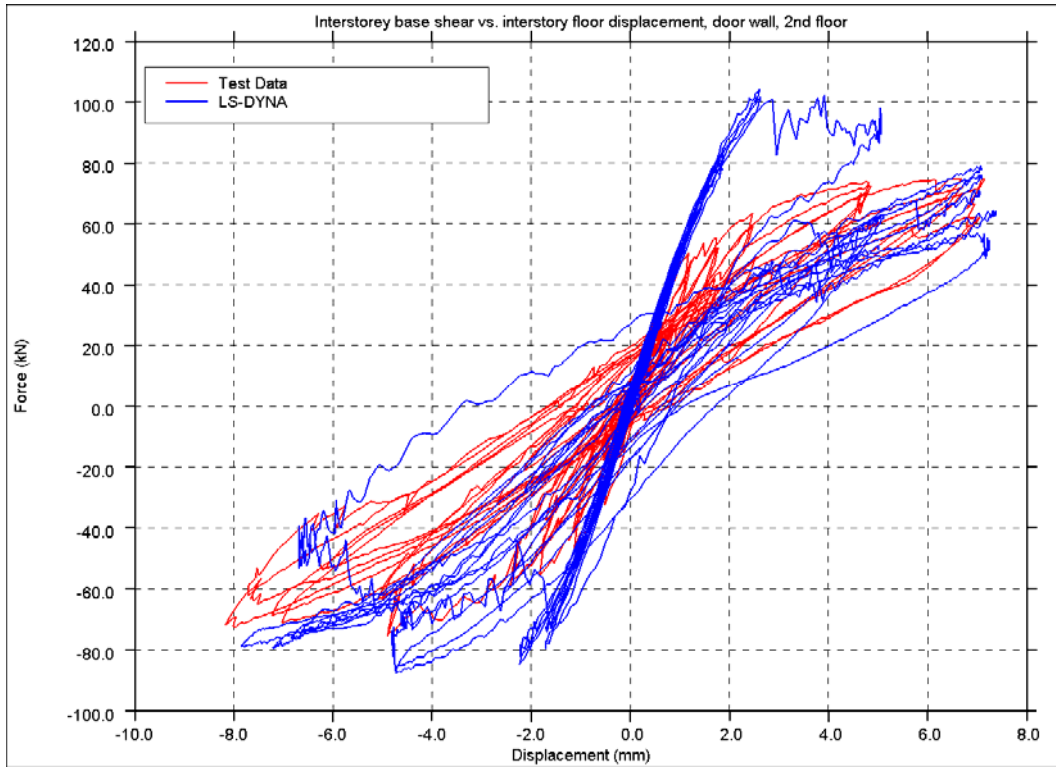


Figure 2.2.5: Interstorey shear force vs. interstorey displacement, 2nd floor (Door Wall)

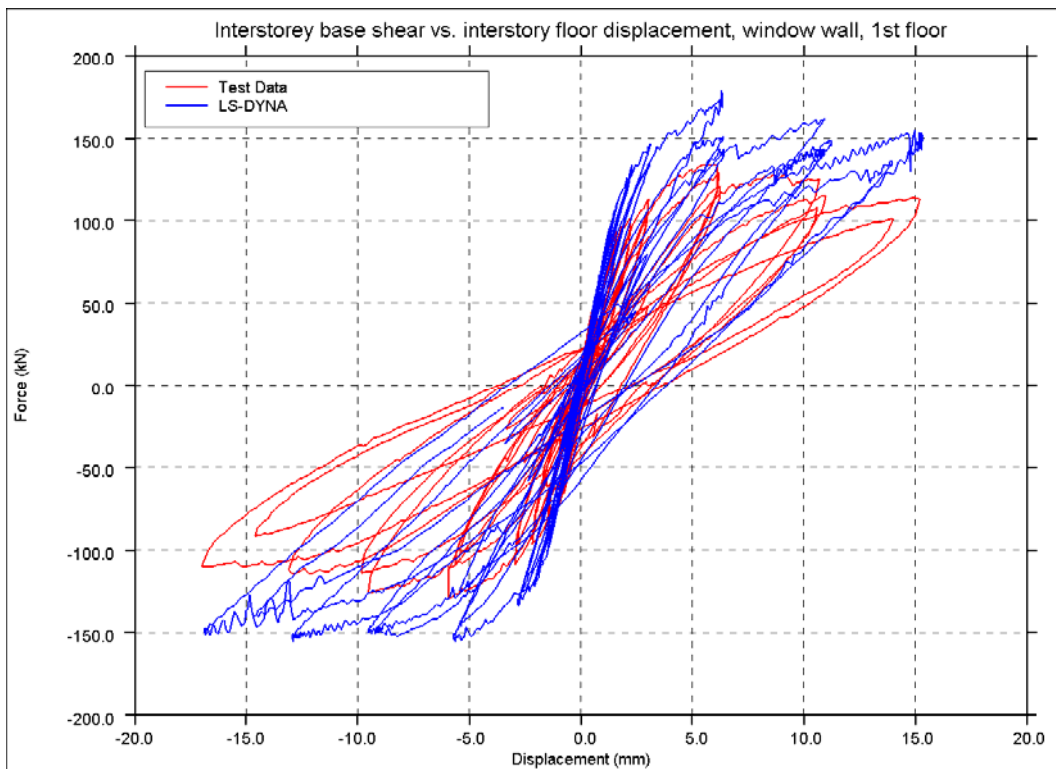


Figure 2.2.6: Interstorey shear force vs. interstorey displacement, 1st floor (Window Wall)

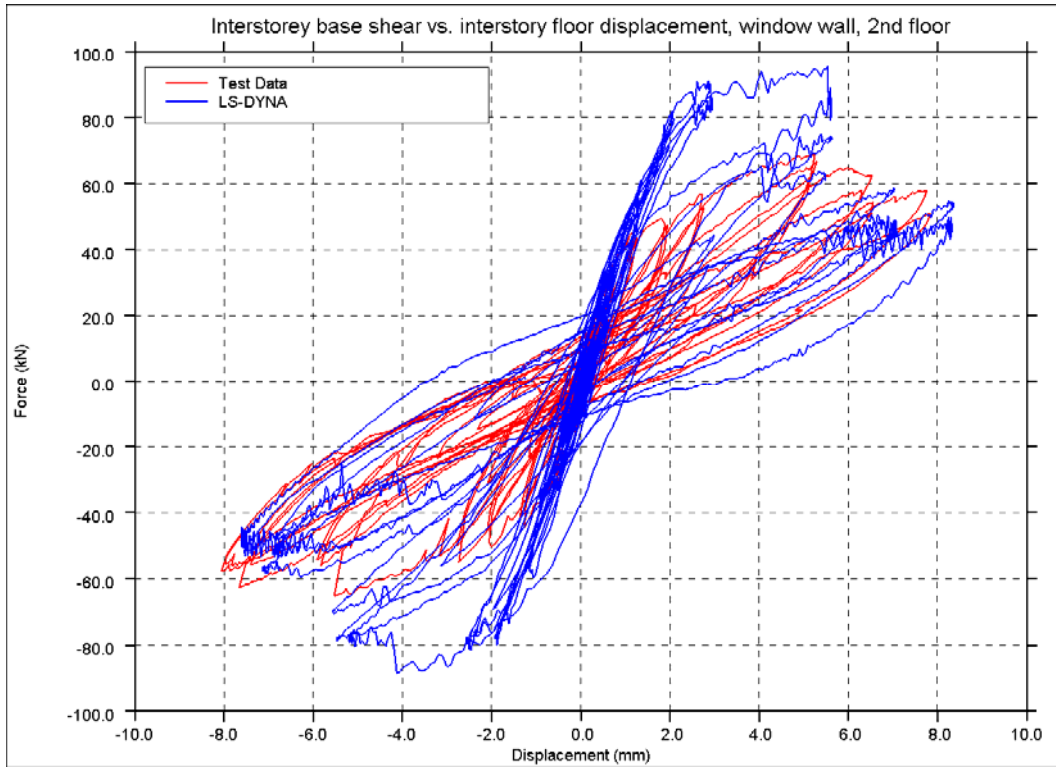


Figure 2.2.7: Interstorey shear force vs. interstorey displacement, 2nd floor (Window Wall)

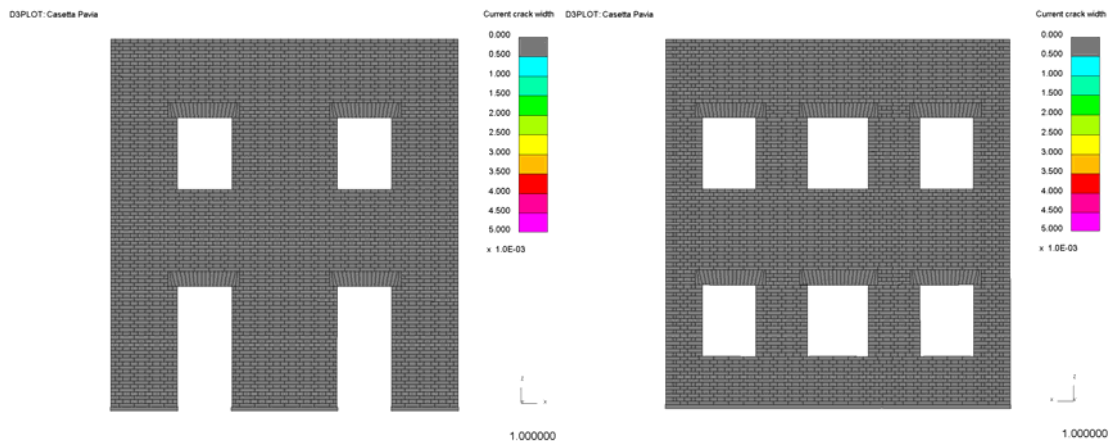


Figure 2.2.8: Crack pattern after Run 1 – Door Wall (left) and Window Wall (right)

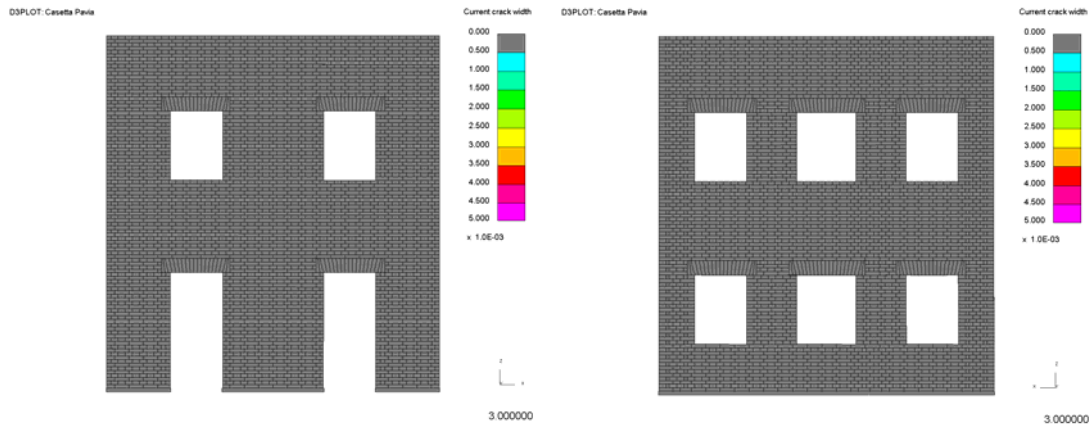


Figure 2.2.9: Crack pattern after Run 2 – Door Wall (left) and Window Wall (right)

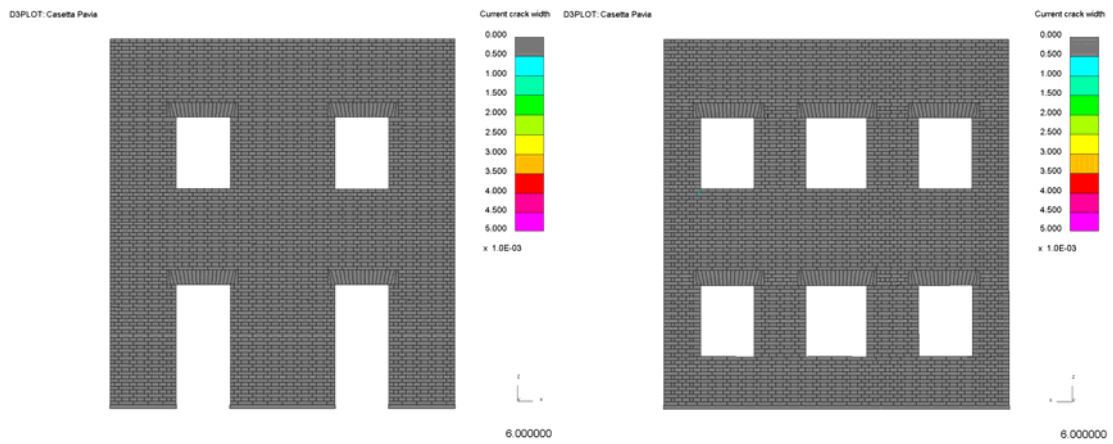


Figure 2.2.10: Crack pattern after Run 3 – Door Wall (left) and Window Wall (right)

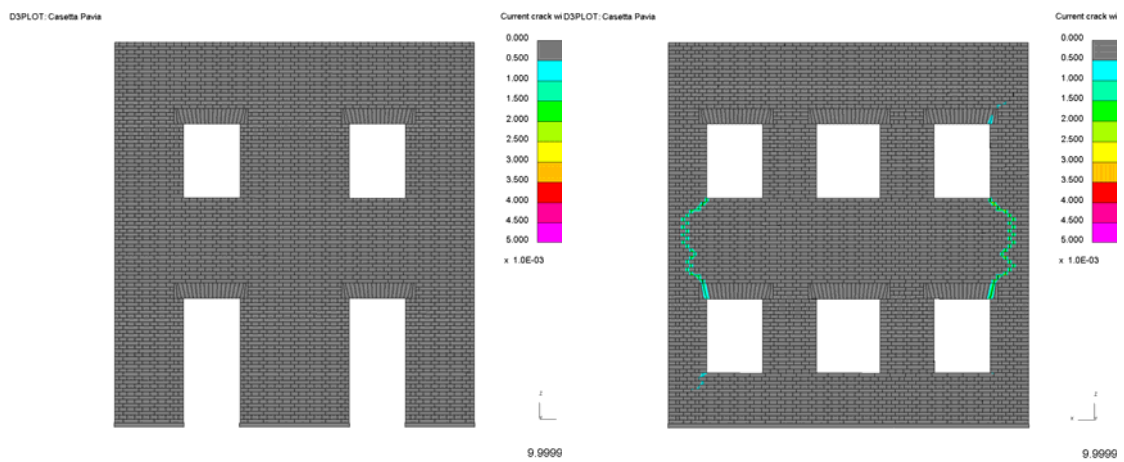


Figure 2.2.11: Crack pattern after Run 4 – Door Wall (left) and Window Wall (right)

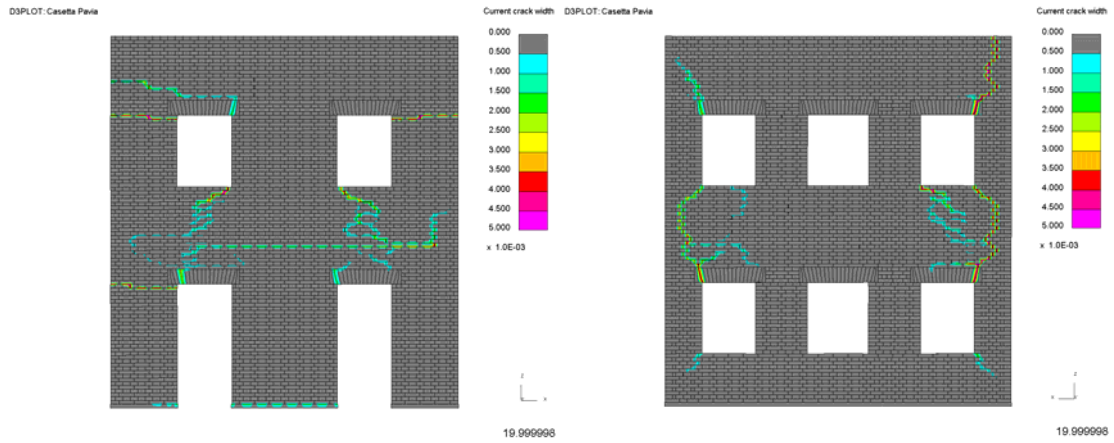


Figure 2.2.12: Crack pattern after Run 5 – Door Wall (left) and Window Wall (right)

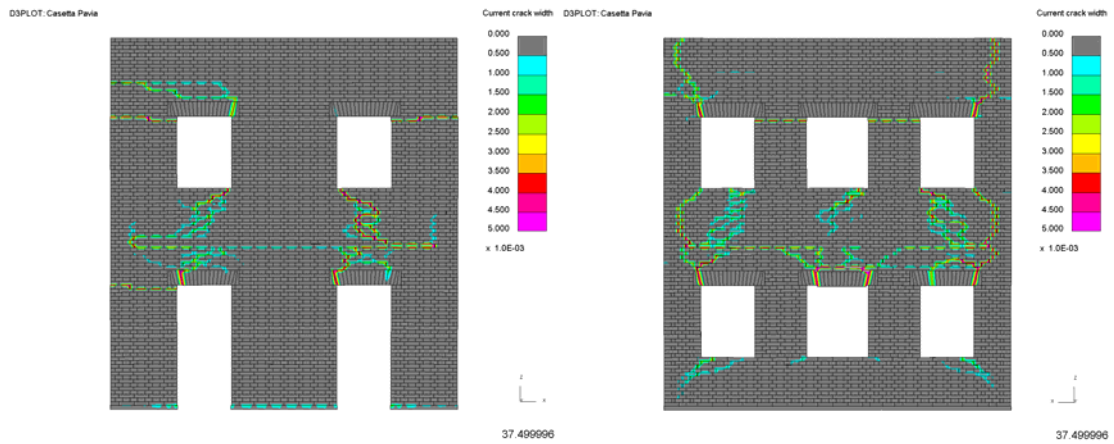


Figure 2.2.13: Crack pattern after Run 6 – Door Wall (left) and Window Wall (right)

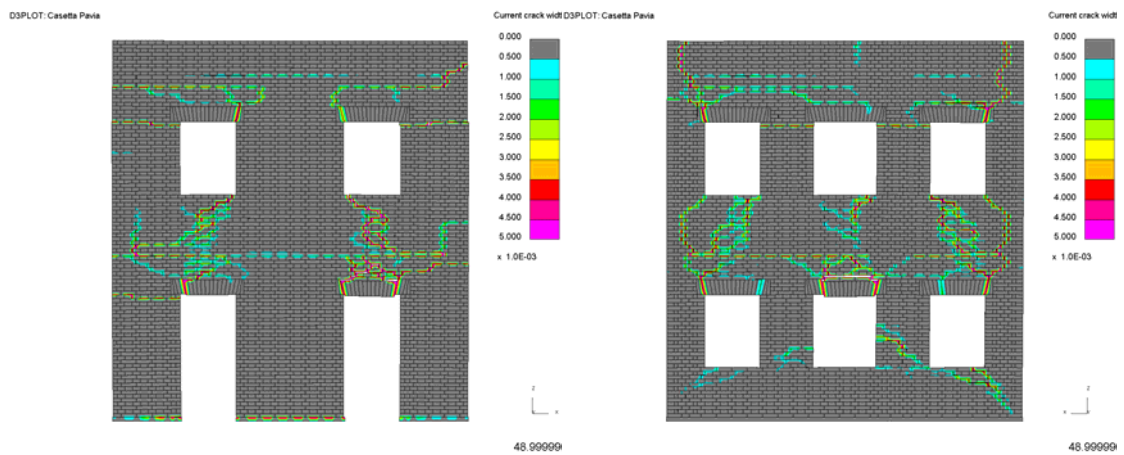


Figure 2.2.14: Crack pattern after Run 7 – Door Wall (left) and Window Wall (right)

2.2.1. Discussion and sensitivity analyses

The main discrepancy came from a lack of stiffness degradation in the LS-DYNA model. The slope of the force-displacement curves from the experiment decreased as the displacement cycles increased, whereas the LS-DYNA slope stayed approximately the same. The lack of degradation was also reflected in the larger peak forces resulting from the LS-DYNA models.

It was clearly observed that the sequence and location of failures was crucial to the final result. In particular, the failure of piers in rocking often caused damage to be concentrated in other parts of the structure, which eventually produced global results with an excess in strength.

Based on suggestions by EUCENTRE, sensitivity analyses were carried out with 50% reduced tensile strength for mortar head joints (bed joints remained unchanged), i.e. with NFLS value of 0.02 MPa instead of the original 0.04 MPa.

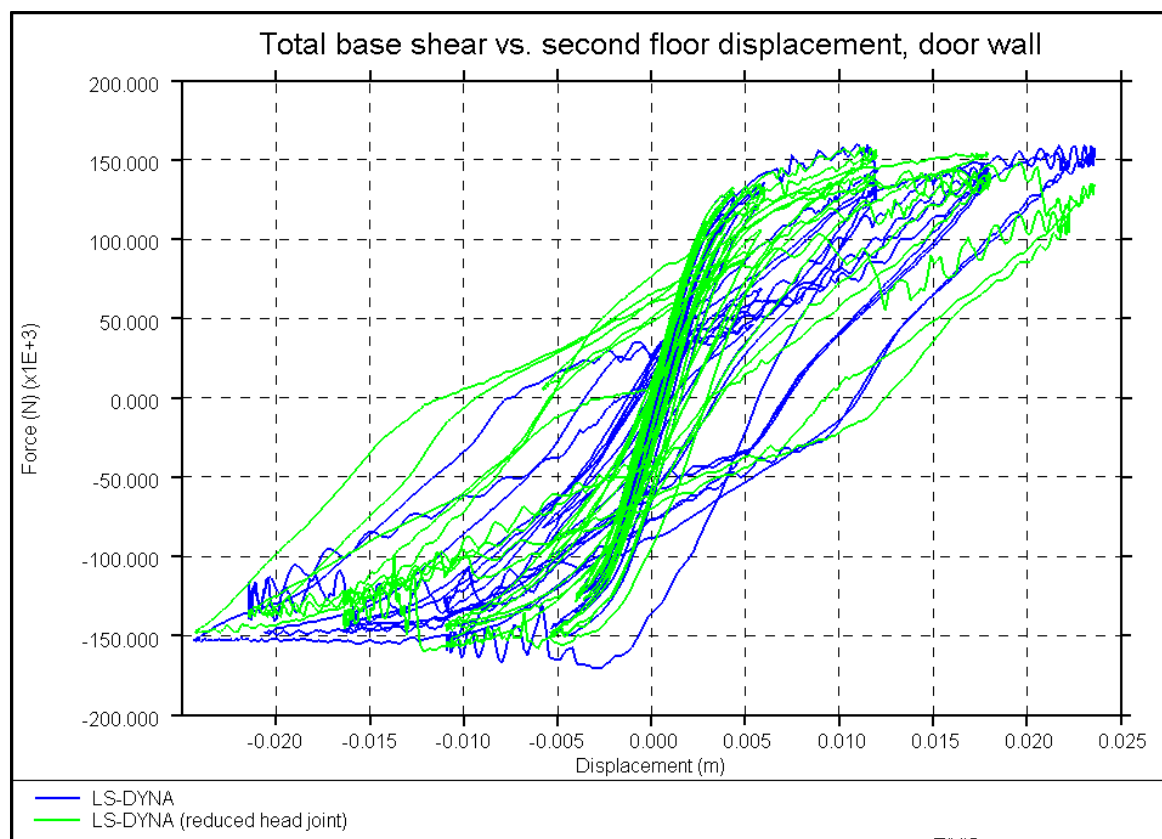


Figure 2.2.1.1: Door Wall LS-DYNA results comparison – original model (blue) vs. 50% reduced headjoint tensile strength (green)

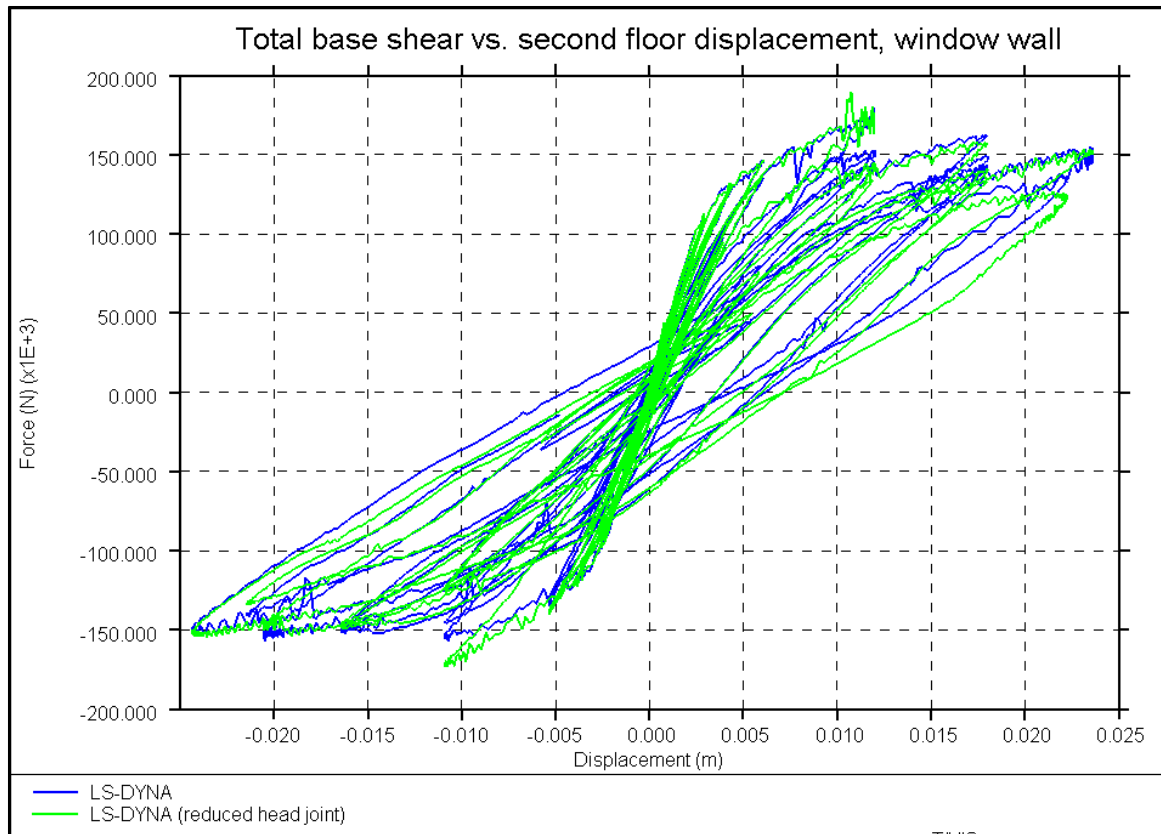


Figure 2.2.1.2: Window Wall LS-DYNA results comparison – original model (blue) vs. 50% reduced headjoint tensile strength (green)

The reduced head joint mortar tensile strength did not have a significant effect on the analysis results, as shown in Figure 2.2.1.1 and Figure 2.2.1.2. The sensitivity analysis did show a final crack pattern on the Door Wall that matches the laboratory test output more closely (Figure 2.2.1.3).

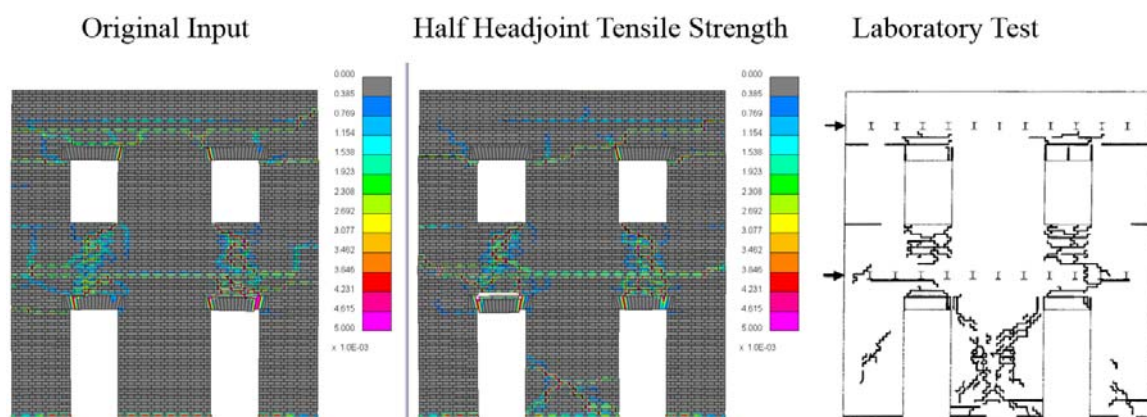


Figure 2.2.1.3: Door Wall final crack pattern comparison

2.3. ESECMaSE calcium silicate in-plane panel tests

Table 2.3.1: Modelling notes

Component	Description
Analysis software and formulation	LS-DYNA – explicit analysis solver
Walls (in-plane)	Individual bricks modelled with solid elements using nonlinear Winfrith material model. Mortar modelled with tiebreak contact surface (penalty stiffness formulation) with a Mohr-Coulomb failure surface. The stiffness of the bricks was adjusted so that the total masonry stiffness (brick Young's modulus and contact penalty stiffness) matches masonry material test data from laboratory tests.

Table 2.3.2: Nonlinear time history analysis notes

Nonlinear time history analysis notes
<ul style="list-style-type: none"> • 1% damping applied using proprietary LS-DYNA constant damping model over 1-30 Hz frequency range. • Additional damping applied at very high frequencies for numerical stability.

Table 2.3.3: Model loading, materials and general comments

Loading	
Dead load	Self-weight of brick wall.
Overburden	<ul style="list-style-type: none"> • 0.5 MPa for CS03 (unfilled headjoint). • 1.0 MPa for CS05 (filled headjoint).
Materials	Material properties including values and stress strain behaviour
Calcium silicate bricks	Winfrith material model (MAT_084) with strain-hardening $\rho = 1800 \text{ kg/m}^3$ $E = 9400 \text{ MPa}$ (to match masonry E of 7562 MPa) $\nu = 0.112$ Compressive strength, UCS = 24 MPa Tensile strength, UTS = 2.24 MPa
Mortar	Tensile stress limit = 0.240 MPa (TNO test data mean) Shear stress limit = 0.245 MPa (TNO test data regression fit) Friction coefficient = 0.677 (TNO test data regression fit) Modelled using tiebreak contact with the Dycoss discrete crack model failure surface. Contact penalty stiffness factor = 6 Tensile energy rate = 10 N/m Shear energy rate = 24.5 N/m
Other key notes	
1) Shear displacement measurements from test data approximated as harmonic input and applied to analysis model as prescribed motion, with peak velocity magnitude capped at 2 mm/s. 2) Separate sensitivity studies were done, where the mortar shear stress limit was better correlated to TNO triplet shear test data, to give a higher value of 0.28 MPa and a correspondingly scaled shear energy rate of 28N/m.	

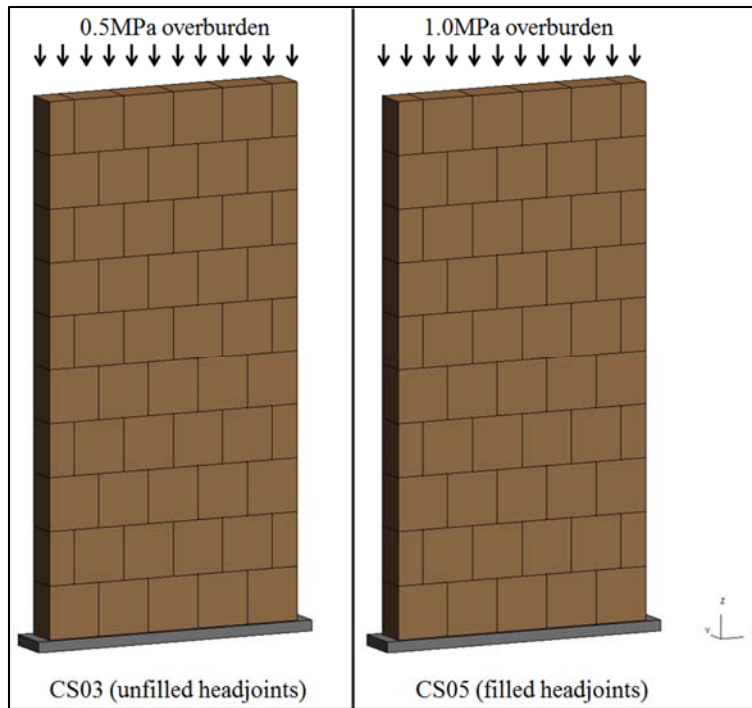


Figure 2.3.1: FE models for CS03 (left) and CS05 (right) panels

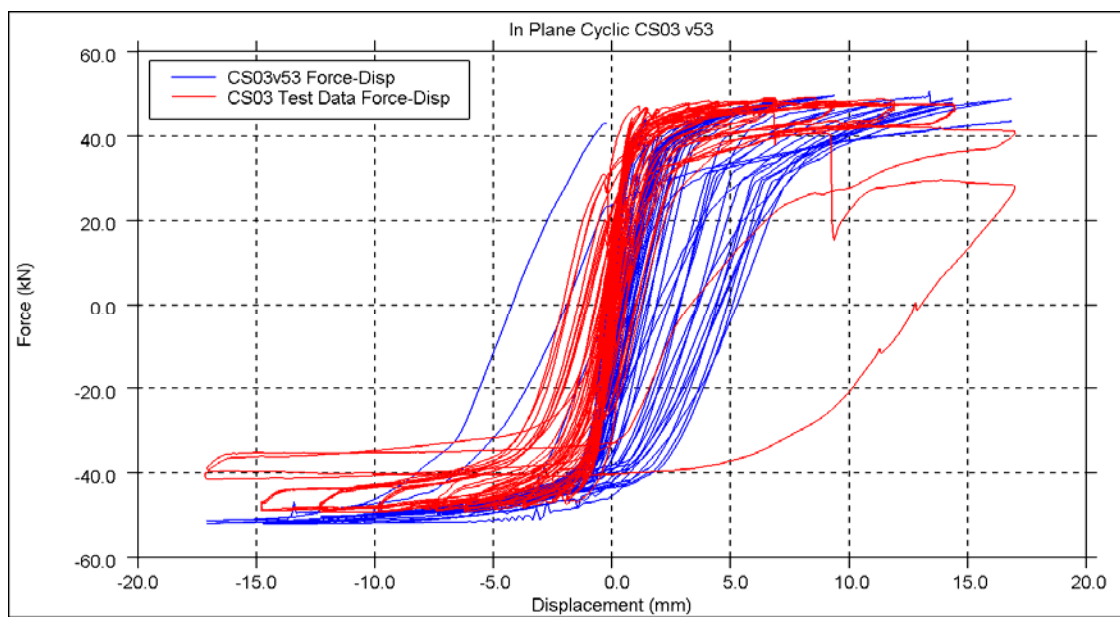


Figure 2.3.2: Shear force-displacement comparison plot for CS03

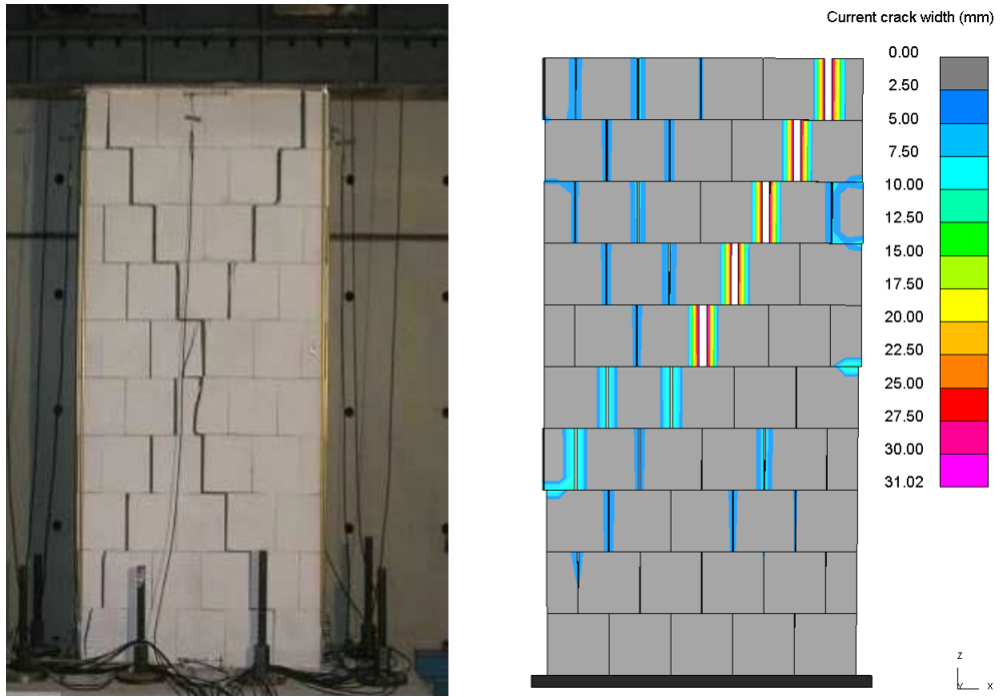


Figure 2.3.3: Final crack pattern for CS03

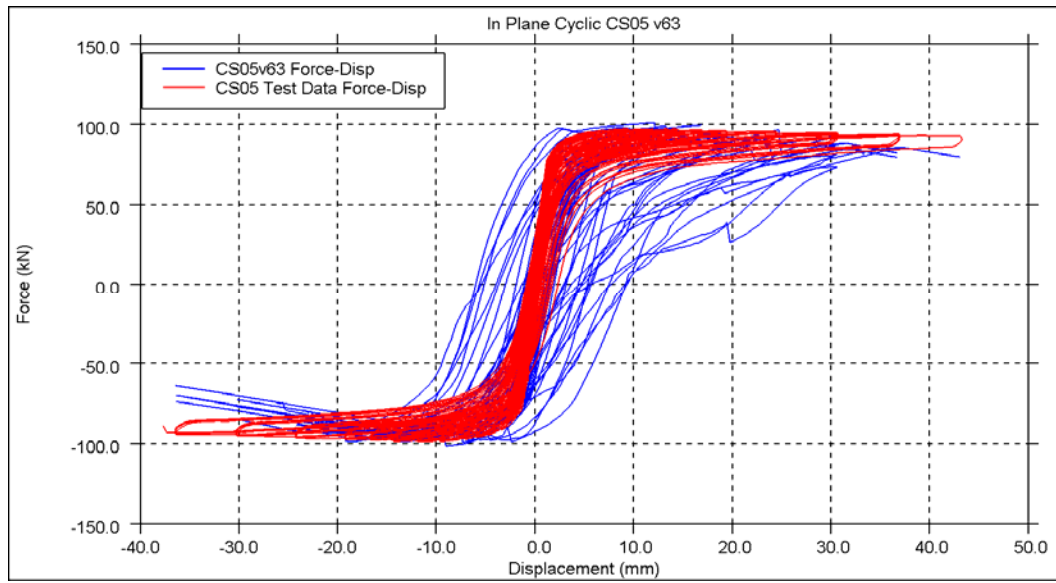


Figure 2.3.4: Shear force-displacement comparison plot for CS05

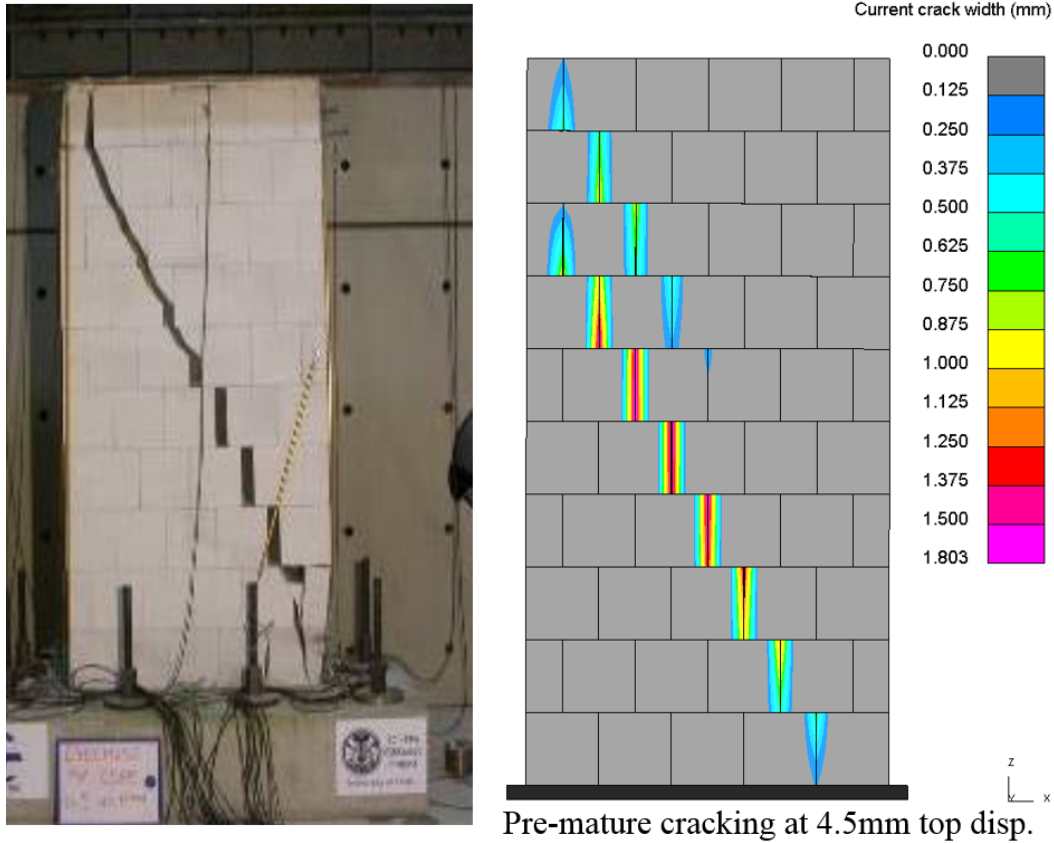


Figure 2.3.5: Final crack pattern for CS05

2.3.1. Discussion and sensitivity analyses

Sensitivity analyses were carried out with a slightly higher shear stress limit for mortar joint (with SFLS value of 0.28 MPa instead of 0.24 MPa) based on correlation of small-scale triplet shear test data conducted at TNO. The results are shown in the following figures.

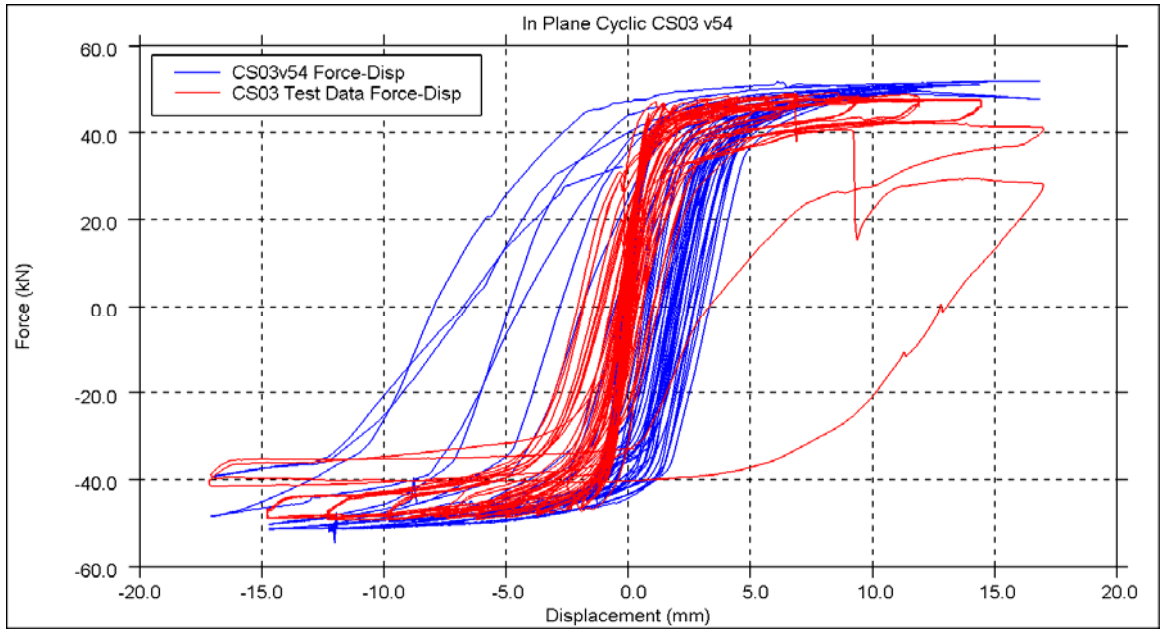


Figure 2.3.1.1: Shear force-displacement comparison graph for CS03 sensitivity run with mortar shear stress limit 0.28 MPa (correlated to TNO triplet shear test)

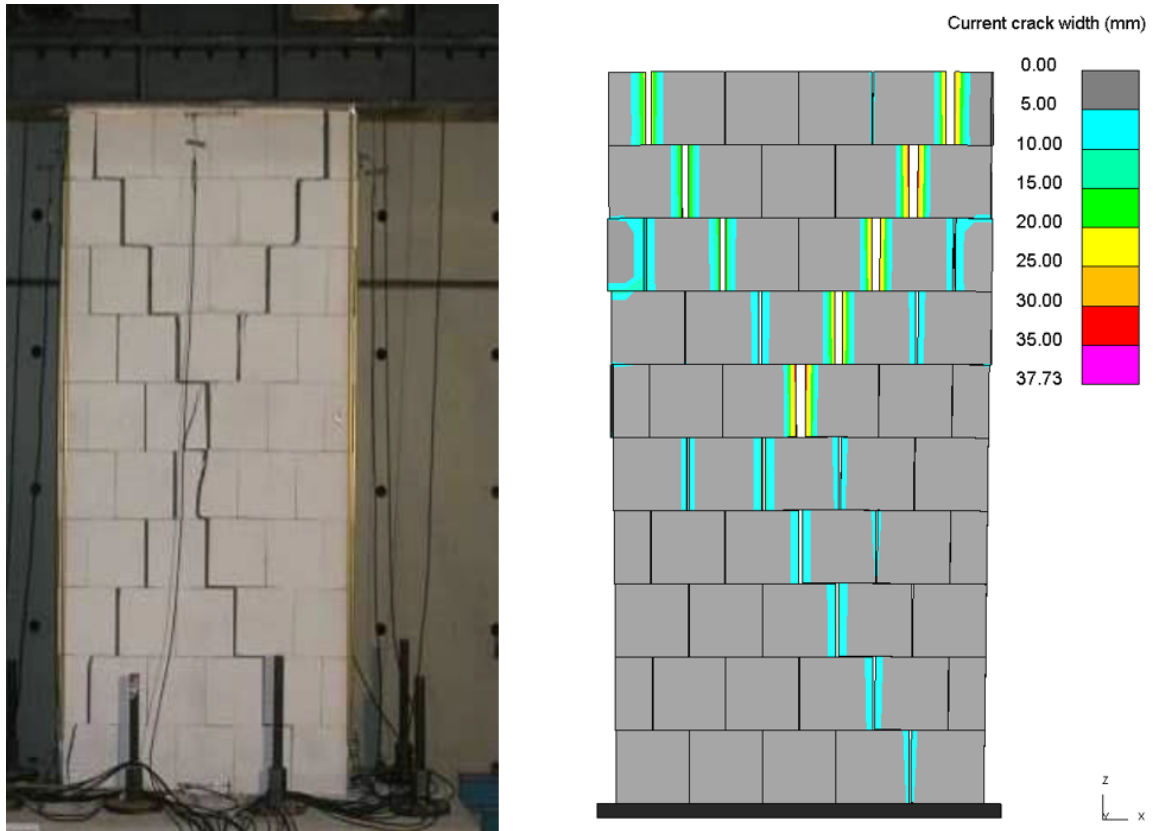


Figure 2.3.1.2: Final crack pattern for CS03 sensitivity run

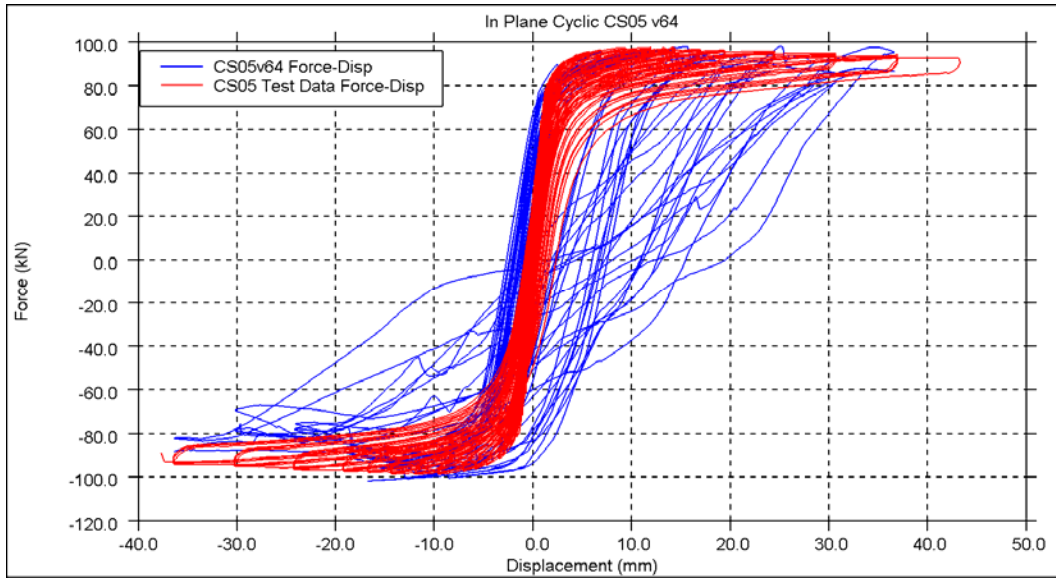
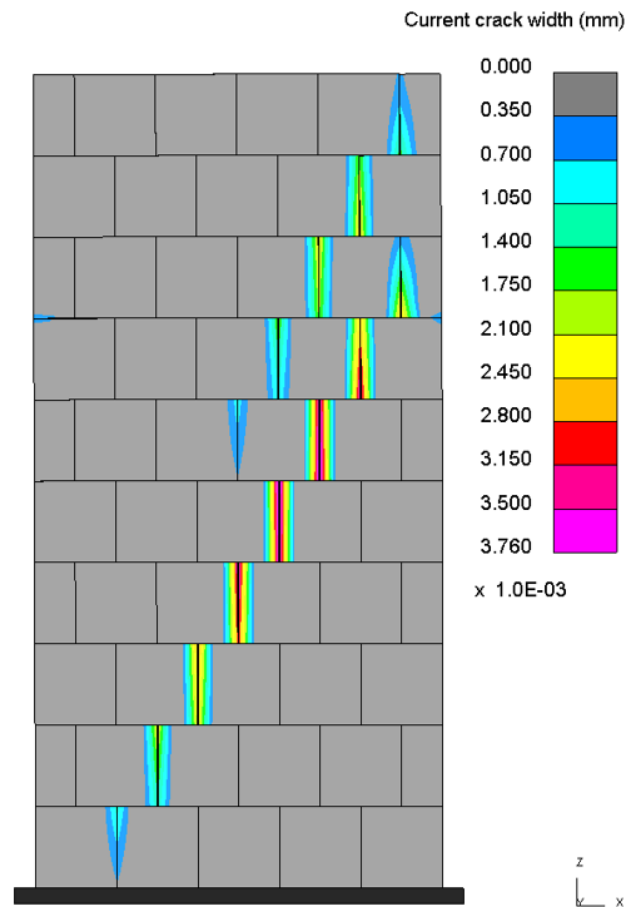
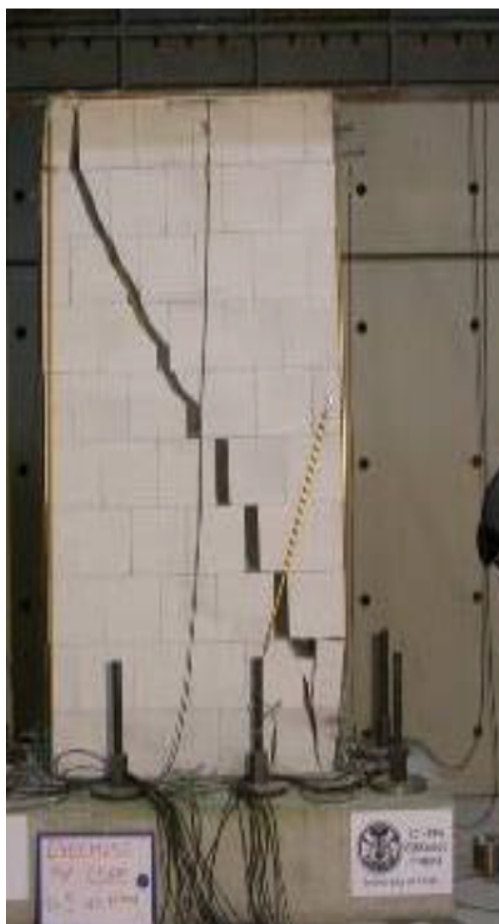


Figure 2.3.1.3: Shear force-displacement comparison graph for CS05 sensitivity run with mortar shear stress limit 0.28 MPa (correlated to TNO triplet shear test)



Pre-mature cracking at 7mm top disp.

Figure 2.3.1.4: Crack pattern for CS05 sensitivity run

2.4. ESECMaSE calcium silicate full-scale half-building test

Table 2.4.1: Modelling notes

Component	Description
Analysis software and formulation	LS-DYNA – explicit analysis solver
Walls (in-plane)	Individual bricks modelled with solid elements using nonlinear Winfrith material model. Mortar modelled with tiebreak contact surface (penalty stiffness formulation) with a Mohr-Coulomb failure surface. The stiffness of the bricks was adjusted so that the total masonry stiffness (brick Young's modulus and contact penalty stiffness) matches masonry material test data from laboratory tests.
Walls (out-of-plane)	As above.
Wall to wall connection (incl. flange effects)	Contact surface used for the mortar connection. Refer to the mortar material information for further details. Flange effects are included explicitly.
Concrete diaphragm	Concrete diaphragm is modelled as 2D shells
Wall to diaphragm connection	Concrete diaphragms are tied to the layers of brick units above and below using CONTACT_TIED_SHELL_EDGE_TO_SURFACE_BEAM_OFFSET in LS-DYNA.

Table 2.4.2: Eigenvalue analysis notes

Eigenvalue analysis notes
<ul style="list-style-type: none"> Masonry Young's modulus of 7562 MPa (from TU Munich test data) was used for the brick material definition in eigenvalue analysis. For LS-DYNA implicit analysis, concrete diaphragms were tied to the layers of brick units above and below using CONTACT_SURFACE_TO_SURFACE_TIED_OFFSET. Masonry wall mass redistribution (described in key note 1 in Table 2.4.5) was not included in the eigenvalue analysis model. The original masonry density of 1800 kg/m³ was used for the brick material definition in eigenvalue analysis.

Table 2.4.3: Nonlinear pushover analysis notes

Nonlinear pushover analysis notes
<ul style="list-style-type: none"> LS-DYNA pushover analysis was not carried out for this benchmark.

Table 2.4.4: Nonlinear time history analysis notes

Nonlinear time history analysis notes
<ul style="list-style-type: none"> 1% damping applied using proprietary LS-DYNA constant damping model over 1–30 Hz frequency range. Additional damping applied at very high frequencies for numerical stability. Measured displacement data were applied in the model as prescribed motions on L1 and L2 floor diaphragms, as per pseudo-dynamic test setup. Prescribed motions applied at half-speed to reduce micro-inertia effects (which will not be present in the pseudo-dynamic laboratory tests), i.e. 12.5-second test data was stretched to 25 seconds.

Table 2.4.5: Model loading, materials and general comments

Loading	
Dead load	Self-weight of brick walls and concrete diaphragms.
Applied load	Mass condition in test (applied using water tanks etc.) modelled with added mass on relevant areas of concrete diaphragms, highlighted in blue in Figure 2.4.1.
Materials	
Calcium silicate bricks	<p>Nonlinear concrete (Winfrith) material model $\rho = 1200 \text{ kg/m}^3$ (see key note 1 below) $E = 9400 \text{ MPa}$ (to match masonry E of 7562 MPa) $\nu = 0.112$ Compressive strength, UCS = 24 MPa Tensile strength, UTS = 2.24 MPa</p>
Mortar	<p>Tensile stress limit = 0.240 MPa (TNO test data mean) Shear stress limit = 0.245 MPa (TNO test data regression fit) Friction coefficient = 0.677 (TNO test data regression fit)</p> <p>Modelled using CONTACT_AUTOMATIC_SURFACE_TO_SURFACE_TIEBREAK with Dycoss discrete crack model failure surface.</p> <p>Contact penalty stiffness factor = 6 Tensile energy rate = 10 N/m Shear energy rate = 24.5 N/m</p>
Concrete	<p>Elastic material model $\rho = 2400 \text{ kg/m}^3$ $E = 38 \text{ GPa}$ $\nu = 0.2$</p>
Other key notes	
<p>1) $\frac{1}{3}$ of calcium silicate wall mass was redistributed as applied mass on the top of the walls, in order to reduce micro-inertia effects of individual brick units without significantly affecting analysis run time. Calcium silicate brick density reduced accordingly from 1800 kg/m^3 to 1200 kg/m^3.</p>	

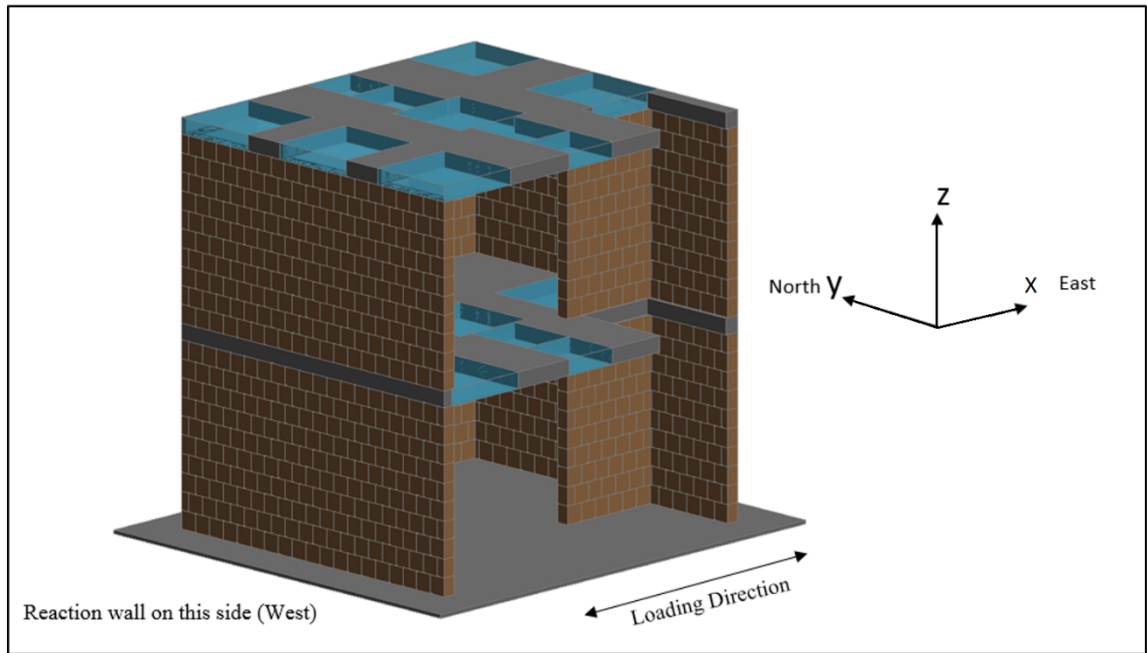


Figure 2.4.1: FE model of ESECMaSE calcium silicate full-scale half-building

Table 2.4.6: Modal period, frequency, description, mass participation

Mode	Period (s)	Frequency (Hz)	Description of mode	Mass participation %	
				X	Y
1	0.14	7.1	1 st flexural mode in x-direction (East-West)	72.9	
2	0.059	16.9	1 st flexural mode in y-direction (North-South)		64.7
3	0.050	20.2	2 nd flexural mode in x-direction	7.7	

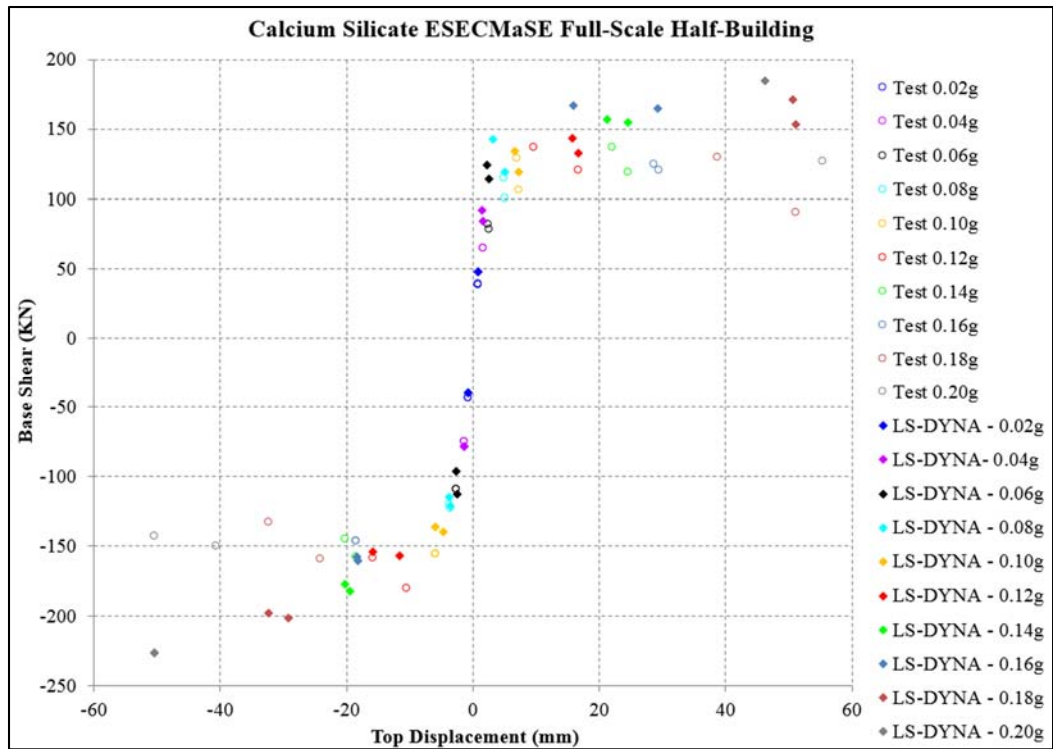


Figure 2.4.2: Envelope of max base shear force vs. max top displacement (0.02g to 0.20g PGA)

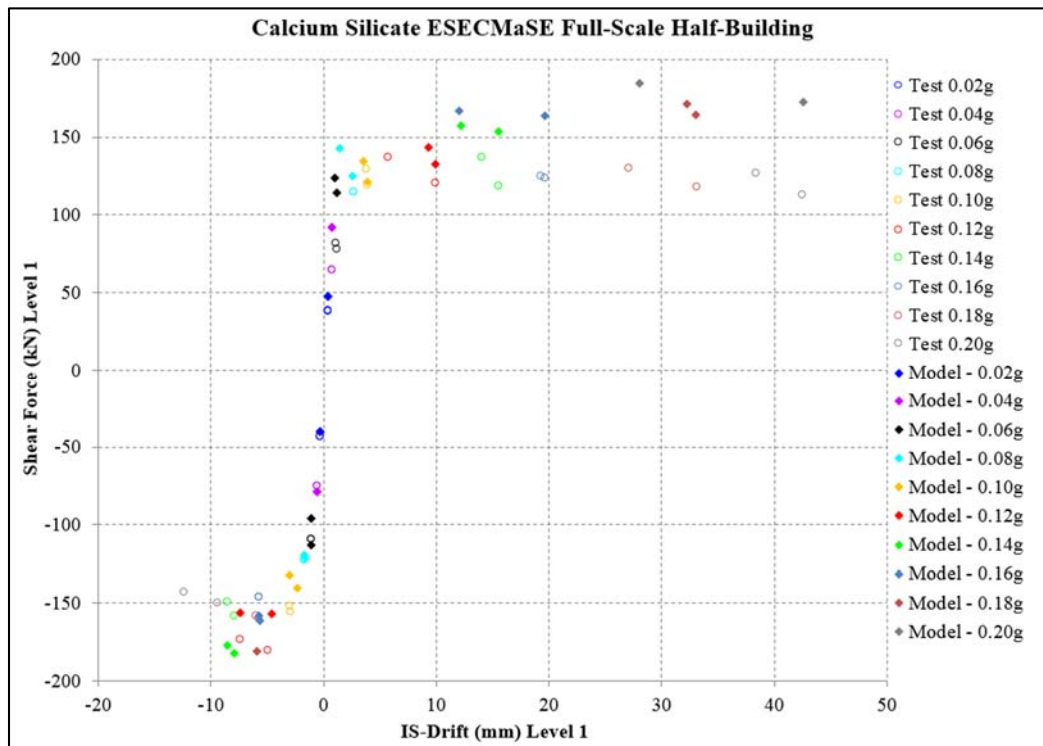


Figure 2.4.3: Envelope of max shear force vs. max inter-storey drift for L1 (0.02g to 0.20g PGA)

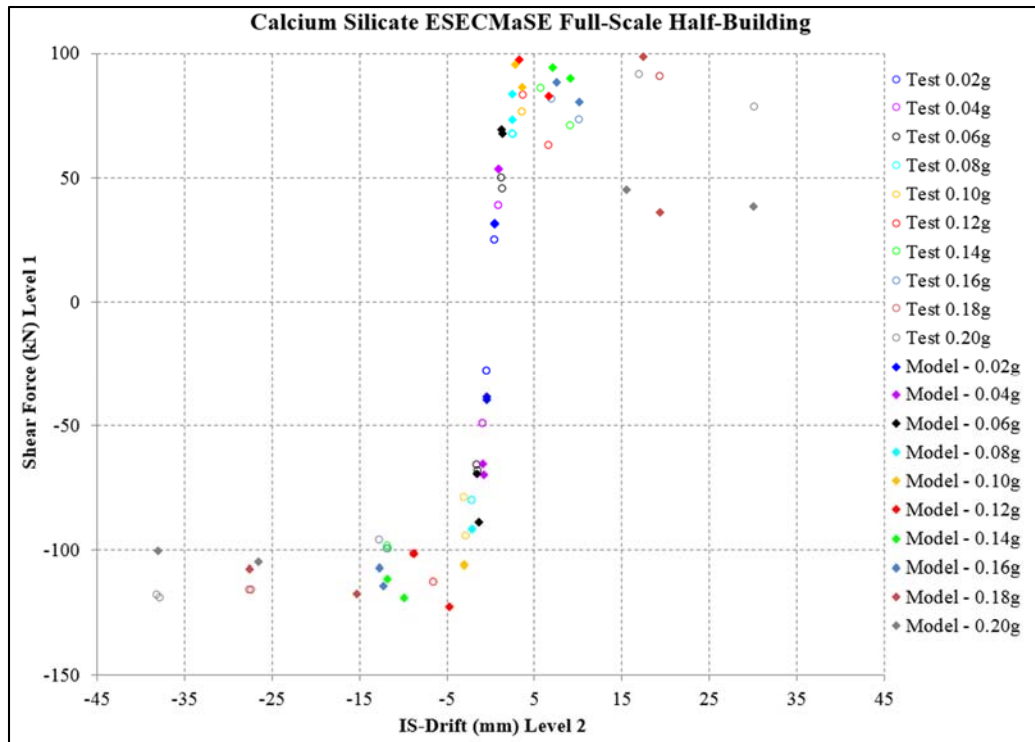
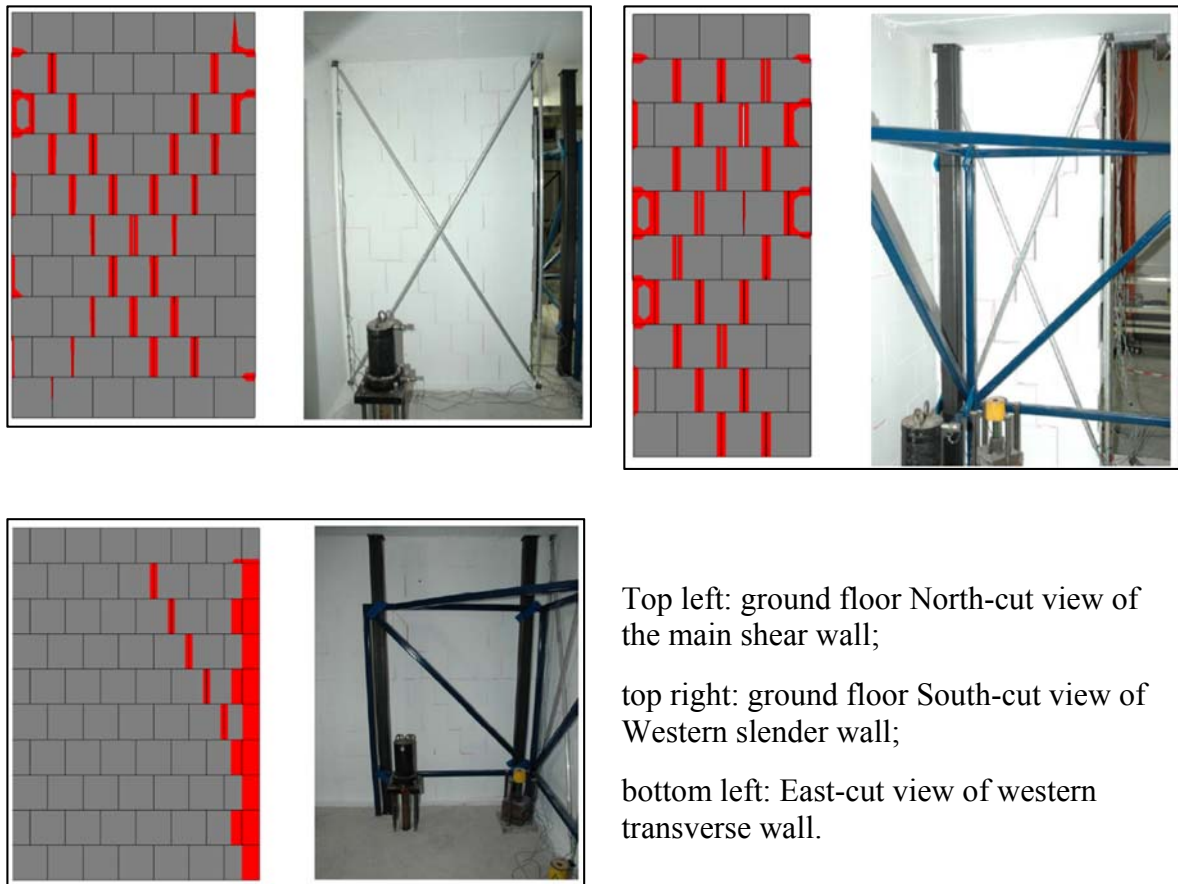


Figure 2.4.4: Envelope of max shear force vs. max inter-storey drift for L2 (0.02g to 0.20g PGA)



Top left: ground floor North-cut view of the main shear wall;
top right: ground floor South-cut view of Western slender wall;
bottom left: East-cut view of western transverse wall.

Figure 2.4.5: Crack pattern after successive loadings of 0.02g–0.12g PGAs, i.e. when damages were first observed in laboratory tests.



Figure 2.4.6: Crack pattern after successive loadings of 0.02g–0.20g PGAs, i.e. after final laboratory test .
(Top left: L1 and L2 view of Eastern slender wall; top right: L1 and L2 view of Western slender wall; bottom left: L1 and L2 view of the main shear wall; bottom right: main shear wall at L1.)

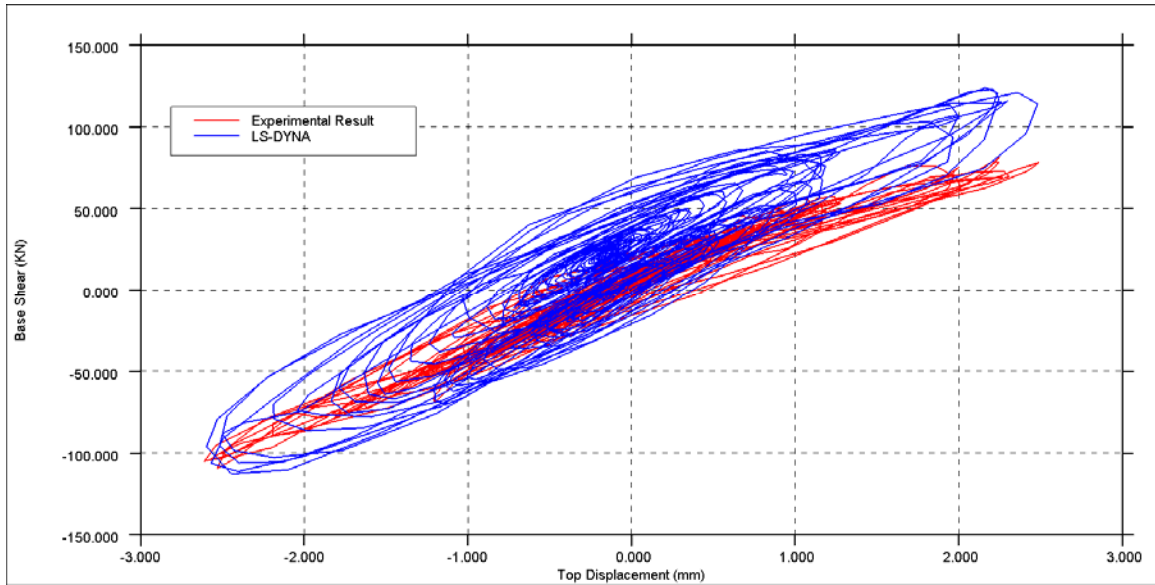


Figure 2.4.7: Base shear force vs. top displacement hysteresis plot during 0.06g PGA

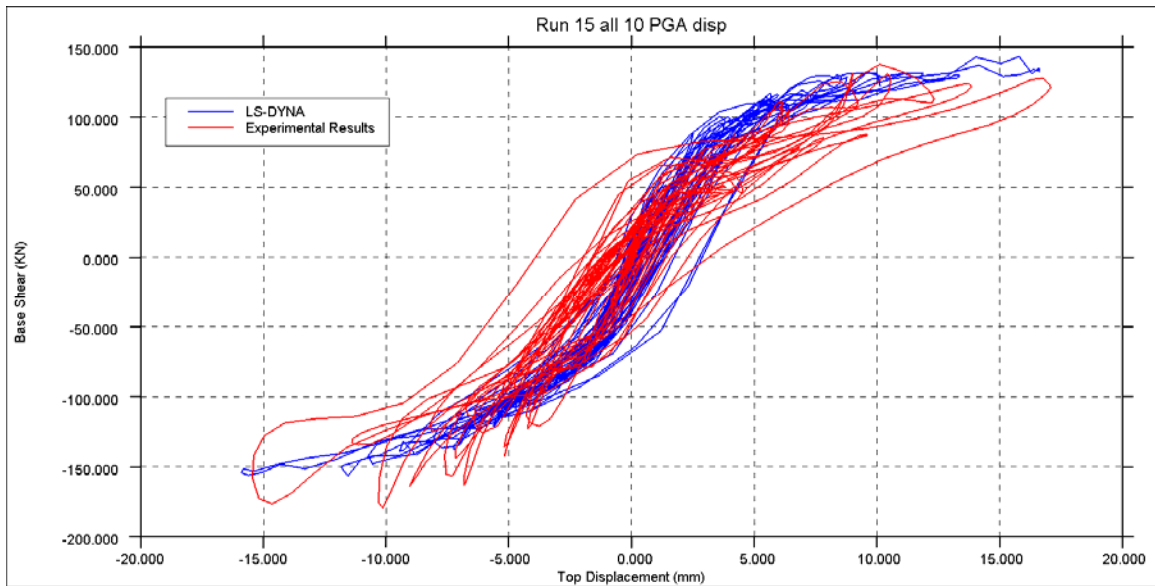


Figure 2.4.8: Base shear force vs. top displacement hysteresis plot during 0.12g PGA

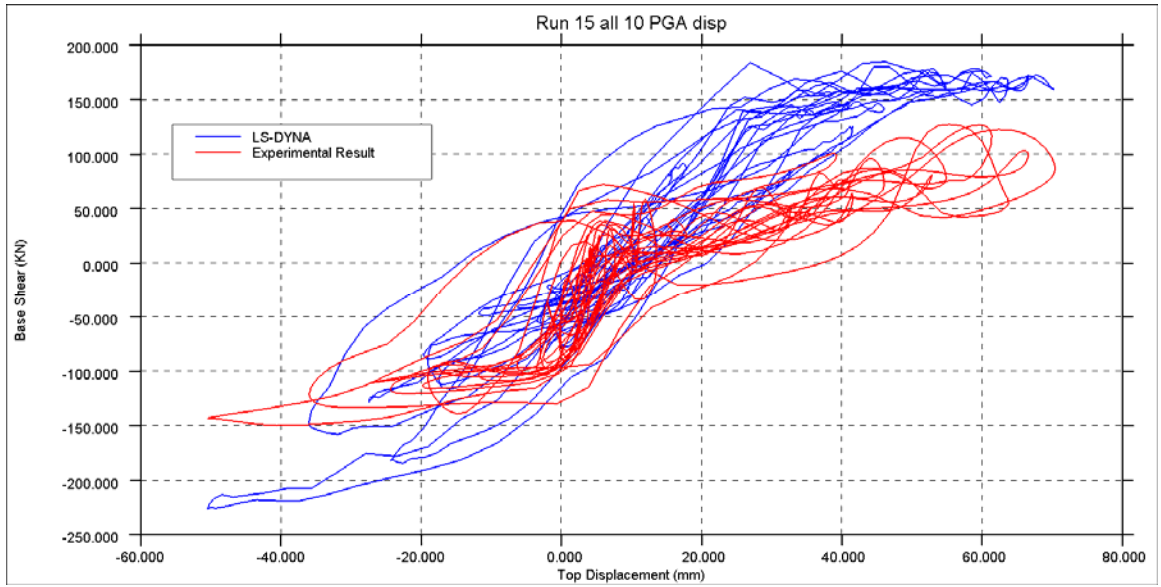


Figure 2.4.9: Base shear force vs. top displacement hysteresis plot during 0.20g PGA

2.4.1. Discussion and sensitivity analyses

A sensitivity analysis was carried out where the reference accelerogram matching the Eurocode 8 design spectrum – used as the basis of the pseudo-dynamic tests – was directly applied as ground motion to the base of the ESECMaSE half-building model.

The results of this sensitivity analysis are presented here.

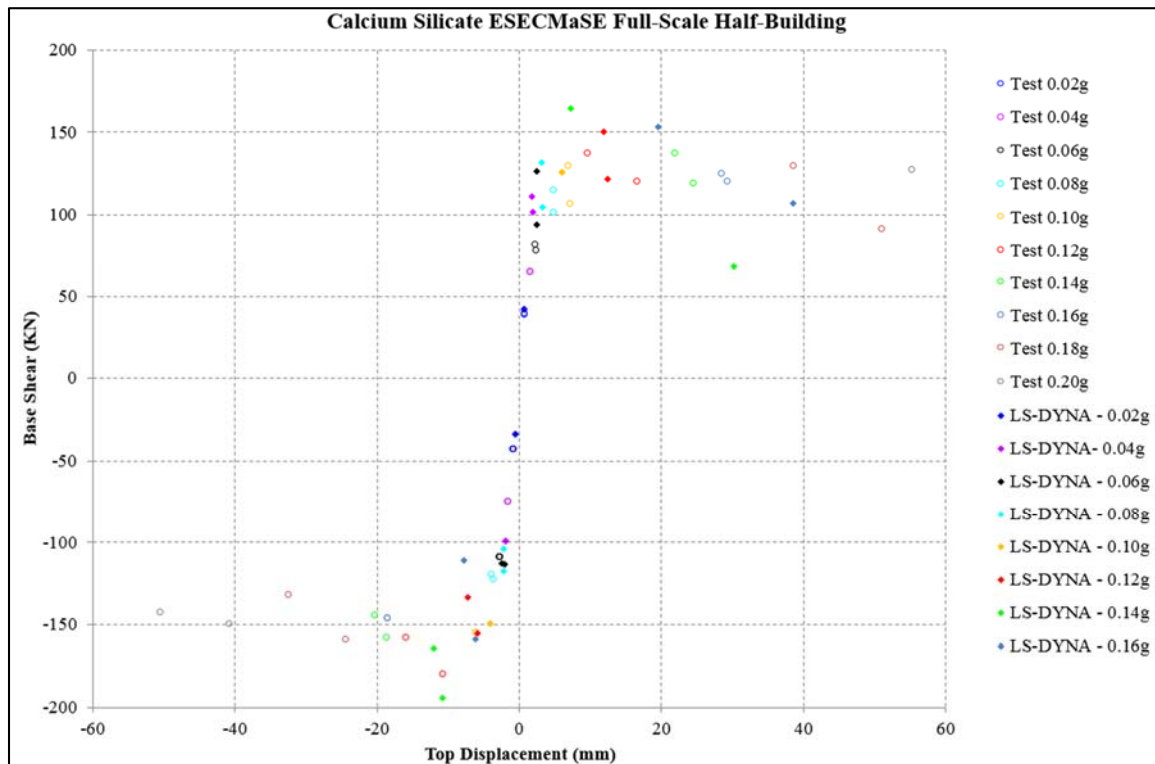


Figure 2.4.1.1: Envelope of max base shear force vs. max top displacement (0.02g to 0.20g PGA). Note: The analysis was stopped after the 0.16g PGA ground motion due to out-of-plane collapse of transverse walls, caused by dynamics and micro-inertia effects of the individual bricks.

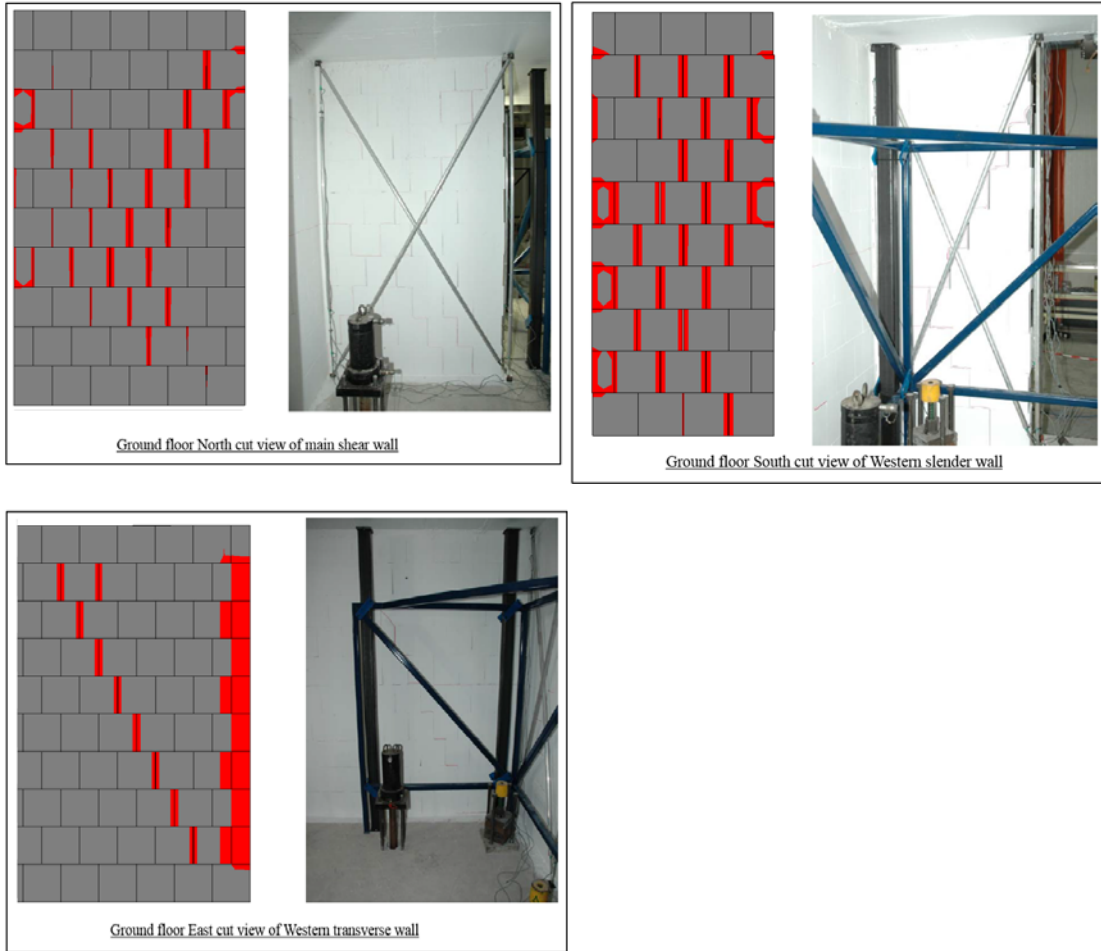


Figure 2.4.1.2: Crack pattern comparison after successive loadings of 0.02g–0.12g PGAs

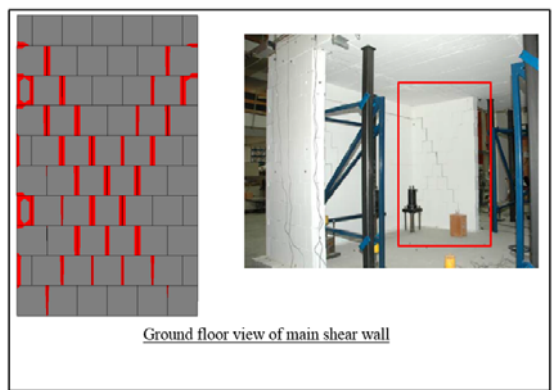
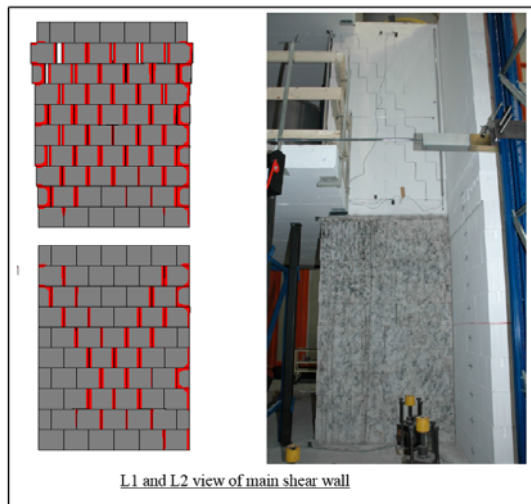
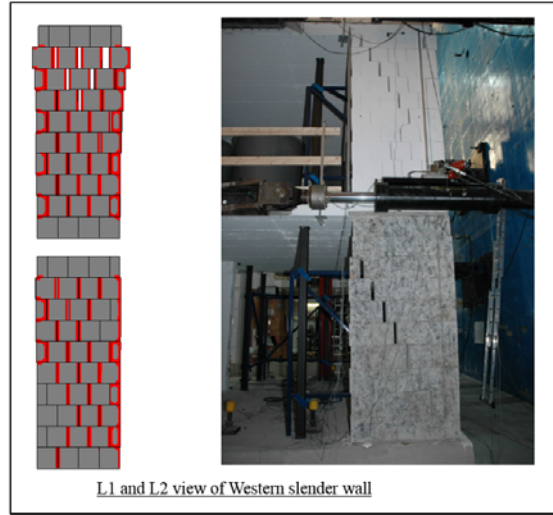
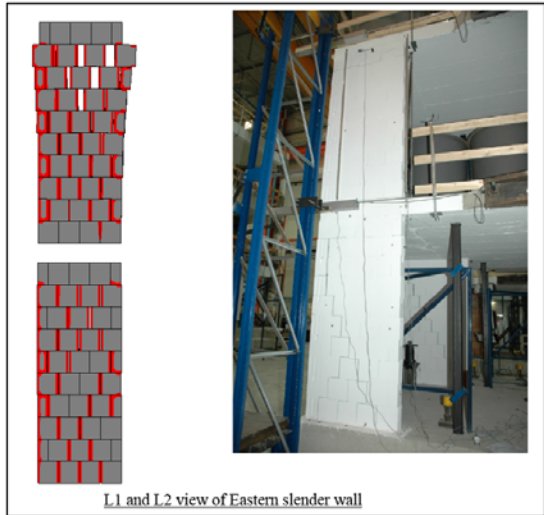


Figure 2.4.1.3: Crack pattern comparison after successive loadings of 0.02g–0.20g PGAs. Note: The analysis was stopped after the 0.16g PGA ground motion due to out-of-plane collapse of transverse walls, caused by dynamics and micro-inertia effects of the individual bricks.

2.5. One-way spanning wall out-of-plane tests (Doherty)

Table 2.5.1: Modelling notes

Component	Description
Analysis software and formulation	LS-DYNA – explicit analysis solver
Walls (in-plane)	Individual bricks modelled with solid elements using nonlinear Winfrith material model. Mortar modelled with tiebreak contact surface (penalty stiffness formulation) with a Mohr-Coulomb failure surface. The stiffness of the bricks was adjusted so that the total masonry stiffness (brick Young's modulus and contact penalty stiffness) matches masonry material test data from laboratory tests.
Walls (out-of-plane)	As above.

Table 2.5.2: Nonlinear time history analysis notes

Nonlinear time history analysis notes
<ul style="list-style-type: none">• 1% damping applied using proprietary LS-DYNA constant damping model over 1-30 Hz frequency range.• Additional damping applied at very high frequencies for numerical stability.

Table 2.5.3: Model loading, materials and general comments

Loading	
Dead load	<i>Specimen 8 and 12:</i> Self-weight of the walls.
Overburden	<i>Specimen 8:</i> 0.15 MPa at top of the wall <i>Specimen 12:</i> No overburden load
Materials	Material properties including values and stress strain behaviour
Clay bricks	<p><i>Specimen 8:</i> Nonlinear concrete (Winfrith) material model $\rho = 1800 \text{ kg/m}^3$ $E = 8635 \text{ MPa}$ (to match masonry E of 5400 MPa) $\nu = 0.15$ $f_c = 9.70 \text{ MPa}$ $f_t = 0.97 \text{ MPa}$ (in the absence of laboratory test results, taken as 10% of compressive strength)</p> <p><i>Specimen 12:</i> Nonlinear concrete (Winfrith) material model $\rho = 1800 \text{ kg/m}^3$ $E = 17944 \text{ MPa}$ (to match masonry E of 11600 MPa) $\nu = 0.15$ $f_c = 15.7 \text{ MPa}$ $f_t = 1.57 \text{ MPa}$ (in the absence of laboratory test results, taken as 10% of compressive strength)</p>
Mortar	<p><i>Specimen 8:</i> Tensile stress limit = 0.45 MPa Shear stress limit = 0.1 MPa Friction coefficient = 0.75</p> <p><i>Specimen 12:</i> Tensile stress limit = 0.30 MPa Shear stress limit = 0.1 MPa Friction coefficient = 0.75</p>
Concrete	<p><i>Specimen 8 and 12:</i> Elastic material model Basic density = 2400 kg/m^3 $E = 11 \text{ GPa}$ $\nu = 0.2$</p>
Steel	<p><i>Specimen 8 and 12:</i> Elastic-plastic material model $\rho = 7850 \text{ kg/m}^3$ $E = 210 \text{ GPa}$ $\nu = 0.3$ $f_y = 300 \text{ MPa}$</p>

Other key notes

- 1) In LS-DYNA overburden load was applied via self-weight of a rigid body, corresponding to an overburden stress of 0.15 MPa. The rigid body was free to move in vertical translation but restrained in rotation, imposing all overburden load on the extreme side of the wall. This modelling approach is not fully accurate as the laboratory pre-compression rig would have some rotational capacity. This is especially important during the elastic response phase of the wall loading.
- 2) In the absence of laboratory spring stiffness and rig rotational capacity, assumptions were made and spring stiffness was calculated by interpolating laboratory test results and rigid body analysis.

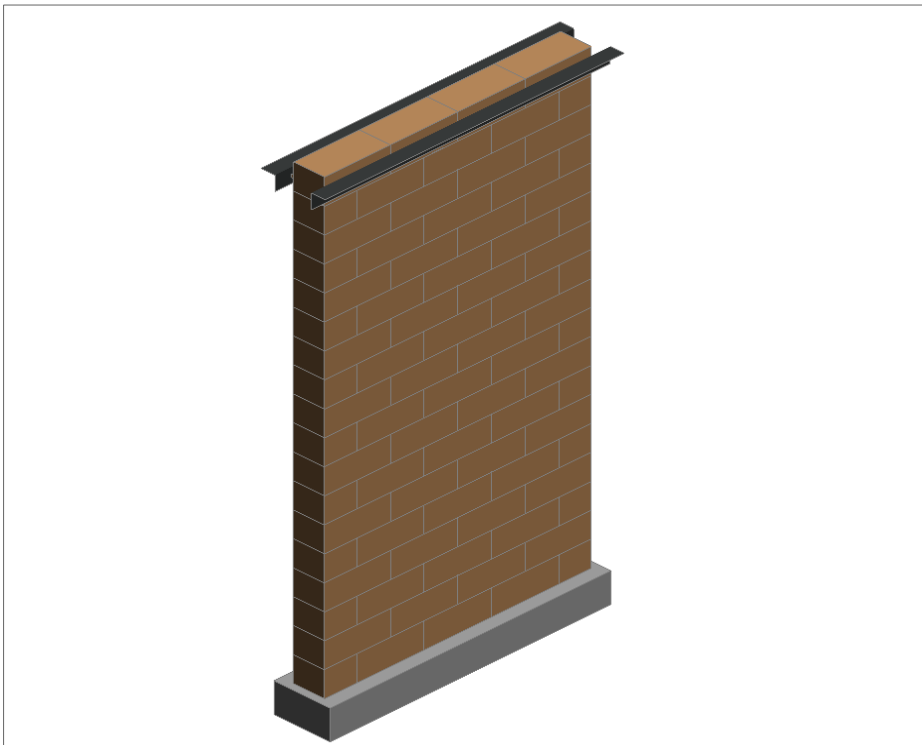


Figure 2.5.1: FE model showing Specimen 8 (isometric view)

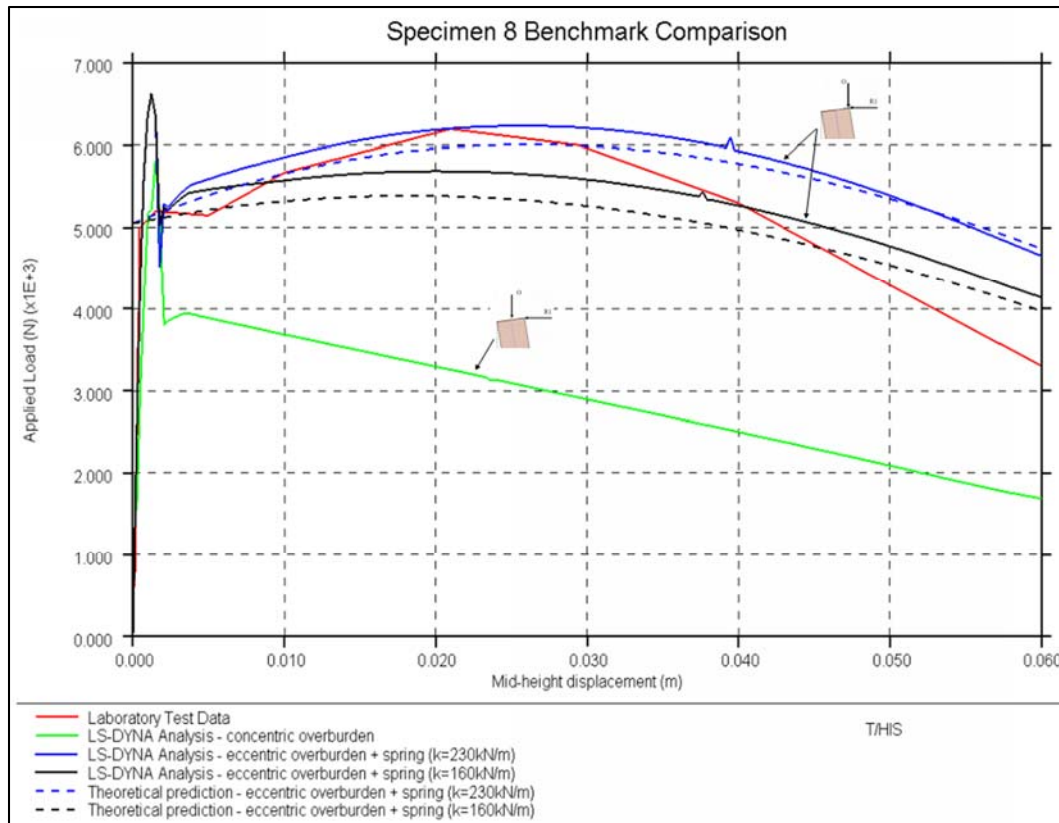


Figure 2.5.2: Total applied force vs. displacement for Specimen 8

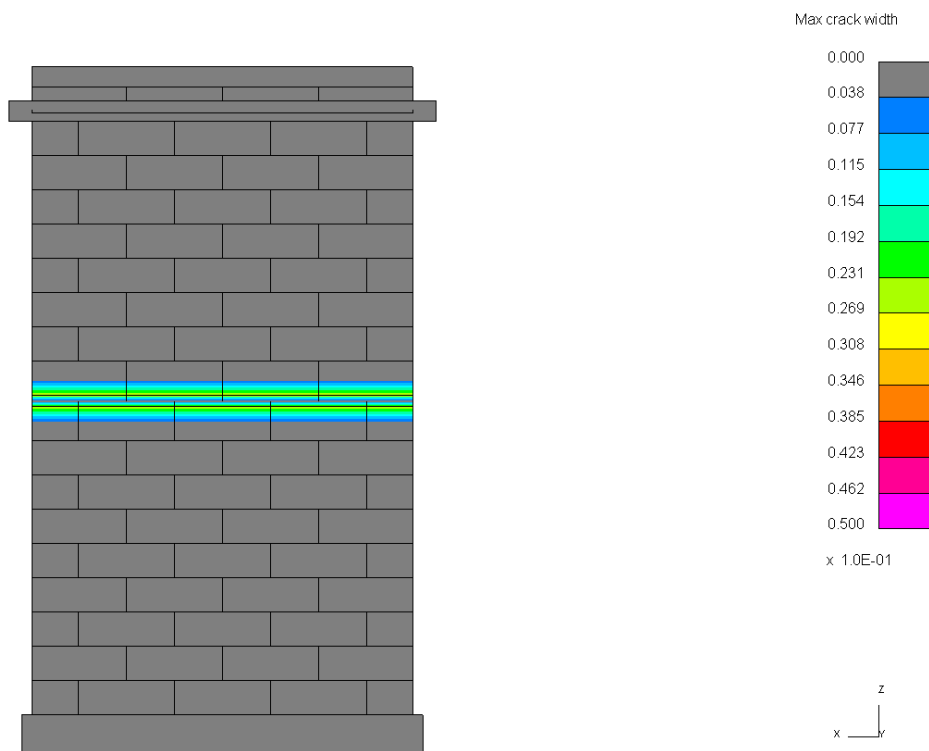


Figure 2.5.3: Final crack pattern – static loading for Specimen 8

Dynamic tests could not be replicated in LS-DYNA. Carrying out the mathematical failure prediction and LS-DYNA analysis, the assumption can be made that the horizontal mortar joint was rounded. LS-DYNA model results showed elastic behaviour throughout the duration of the run and thus the wall did not rock in the analysis.

Figure 2.5.4: Mid-height displacement time history – Specimen 12, 66% EL

Dynamic tests could not be replicated in LS-DYNA. Carrying out the mathematical failure prediction and LS-DYNA analysis, the assumption can be made that the horizontal mortar joint was rounded. LS-DYNA model results showed elastic behaviour throughout the duration of the run and thus the wall did not rock in the analysis.

Figure 2.5.5: Mid-height acceleration time history – Specimen 12, 66% EL

Dynamic tests could not be replicated in LS-DYNA. Carrying out the mathematical failure prediction and LS-DYNA analysis, the assumption can be made that the horizontal mortar joint was rounded. LS-DYNA model results showed elastic behaviour throughout the duration of the run and thus the wall did not rock in the analysis.

Figure 2.5.6: Final crack pattern – Specimen 12, 66% EL

2.5.1. Discussion and sensitivity analyses

Specimen 8 (Static test)

- With the increase of wall rotation (mid-height displacement), the applied pressure on the extreme fibre of the brick increases. This results in mortar damage and rounding at the edges, which decreases the lever arm length and therefore the bending moment carried across the crack.
- The increase in the applied load in laboratory test was caused by the overburden rig used. With increased mid-height displacement, the total wall height also increased slightly, thus increasing the static spring deflection and hence overburden force.
- Degradation of mortar joint, which was observed in the laboratory, cannot be modelled in LS-DYNA. Migration of rotation centre from extreme fibre to the mid-plane would decrease out-of-plane resistance of the specimen.
- In LS-DYNA, overburden load was applied via a self-weight of the rigid body, with the corresponding density of the solid equal to overburden of 0.15 MPa. This element was free to move in a vertical direction but restrained in rotation, imposing all overburden load on the extreme side of the wall. This modelling approach cannot capture the behaviour of the laboratory pre-compression rig having some rotational capacity. This is especially important during the elastic response phase of the wall loading.
- Laboratory test results ‘Specimen 8 pre-cracked’ and ‘post-cracked’ show similar ultimate strength capacity. This indicates that the bond strength of the wall specimen could have been lower than measured in the bond wrench test (0.45 MPa).

Specimen 12 (Nahani)

- Discrepancies in laboratory test results were found and the test could not be replicated. The reported accelerations at the base of the table and the top of the frame do not agree with the reported displacements. There is a large baseline shift when integrating the accelerations. Standard polynomial baseline and piecewise corrections also did not provide satisfactory results.

2.6. Two-way spanning wall out-of-plane tests (Griffith)

Table 2.6.1: Modelling notes

Component	Description
Analysis software and formulation	LS-DYNA – explicit analysis solver
Walls (in-plane)	Individual bricks modelled with solid elements using nonlinear Winfrith material model. Mortar modelled with tiebreak contact surface (penalty stiffness formulation) with a Mohr-Coulomb failure surface. The stiffness of the bricks was adjusted so that the total masonry stiffness (brick Young's modulus and contact penalty stiffness) matches masonry material test data from laboratory tests.
Walls (out-of-plane)	As above.
Wall to wall connection (incl. flange effects)	Contact surface used for the mortar connection. Refer to the mortar material information for further details. Flange effects are included explicitly.

Table 2.6.2: Nonlinear time history analysis notes

Nonlinear time history analysis notes
<ul style="list-style-type: none">• 1% damping applied using proprietary LS-DYNA constant damping model over 1–30 Hz frequency range.• Additional damping applied at very high frequencies for numerical stability.

Table 2.6.3: Model loading, materials and general comments

Loading	
Dead load	<i>Wall 1:</i> Self-weight of the wall and timber spreader beam. <i>Wall 2:</i> Self-weight of the wall.
Overburden	<i>Wall 1:</i> 0.1 MPa applied as point loads at top of the wall. <i>Wall 2:</i> No overburden load.
Materials	Material properties including values and stress strain behaviour
Clay bricks	<p>Wall 1: $\rho = 1500 \text{ kg/m}^3$ (reduced to take into account cored unit) $E = 4931 \text{ MPa}$ (to match masonry E of 3188 MPa) $\nu = 0.15$ $f_c = 17.6 \text{ MPa}$ $f_t = 1.76 \text{ MPa}$ (in the absence of laboratory test results, taken as 10% of compressive strength)</p> <p>Wall 2: $\rho = 1500 \text{ kg/m}^3$ (reduced to take into account cored unit) $E = 3465 \text{ MPa}$ (to match masonry E of 2240 MPa) $\nu = 0.15$ $f_c = 13.6 \text{ MPa}$ $f_t = 1.36 \text{ MPa}$ (in the absence of laboratory test results, taken as 10% of compressive strength)</p>
Mortar	<p>Wall 1: Flexural tensile stress limit = 0.72 MPa Shear stress limit = 0.1 MPa (in the absence of laboratory test results, recommended value used.) Friction coefficient = 0.75</p> <p>Wall 2: Flexural tensile stress limit = 0.52 MPa Shear stress limit = 0.1 MPa (in the absence of laboratory test results, recommended value used.) Friction coefficient = 0.75</p>
Concrete	<p>Wall 1 and 2: Elastic material model Basic density = 2400 kg/m³ $E = 11 \text{ GPa}$ $\nu = 0.2$</p>
Steel	<p>Wall 1 and 2: Elastic-plastic material model $\rho = 7850 \text{ kg/m}^3$ $E = 210 \text{ GPa}$ $\nu = 0.3$ $f_y = 300 \text{ MPa}$</p>

Other key notes

- 1) Pre-compression load in LS-DYNA was applied using rigid bodies (square blocks on top of the wall). The density of each rigid body was estimated to give a total pre-compression stress of 0.1 MPa. This approach provided a better representation of the loads applied in the laboratory in comparison with uniformly distributed pressure load.
- 2) In the absence of the direct tensile strength test results, flexural tensile strength was used in LS-DYNA. Van der Pluijm (1997) suggested a reduction factor of 1.2–1.7 when converting from flexural strength to direct tensile strength.

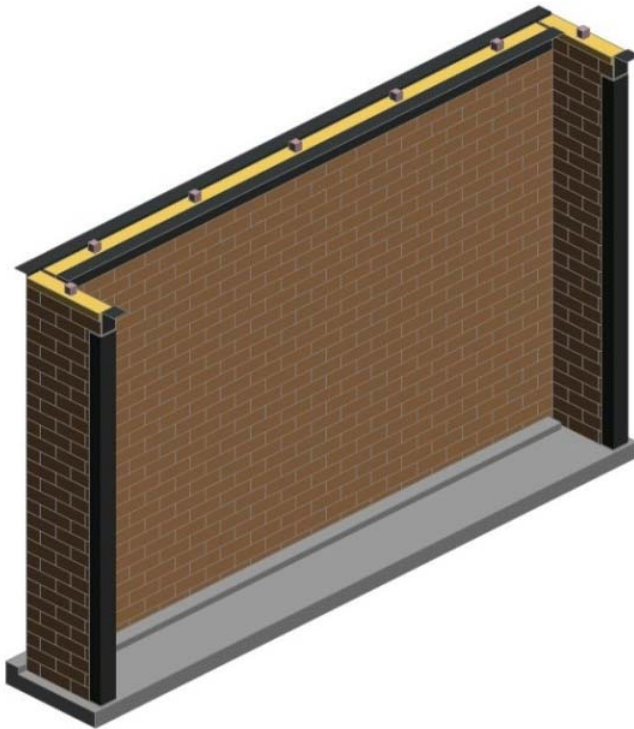


Figure 2.6.1: FE model showing Wall 1 (isometric view)

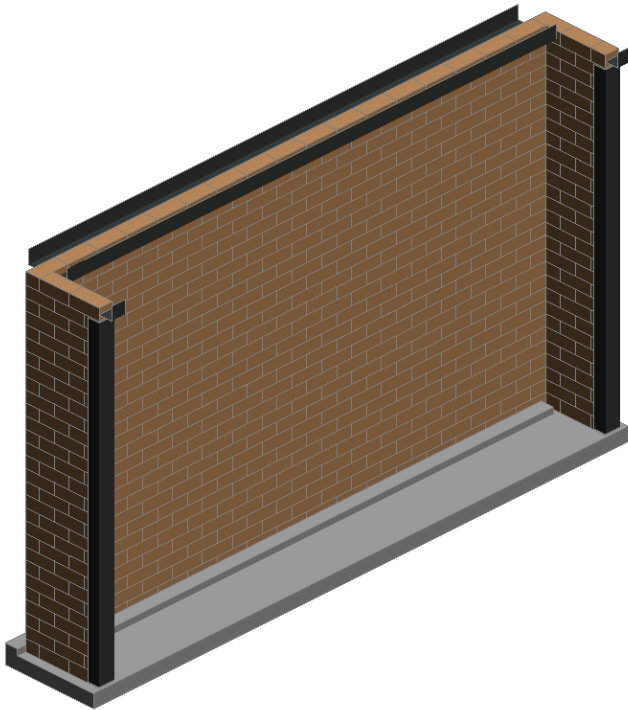


Figure 2.6.2: FE model showing Wall 2 (isometric view)

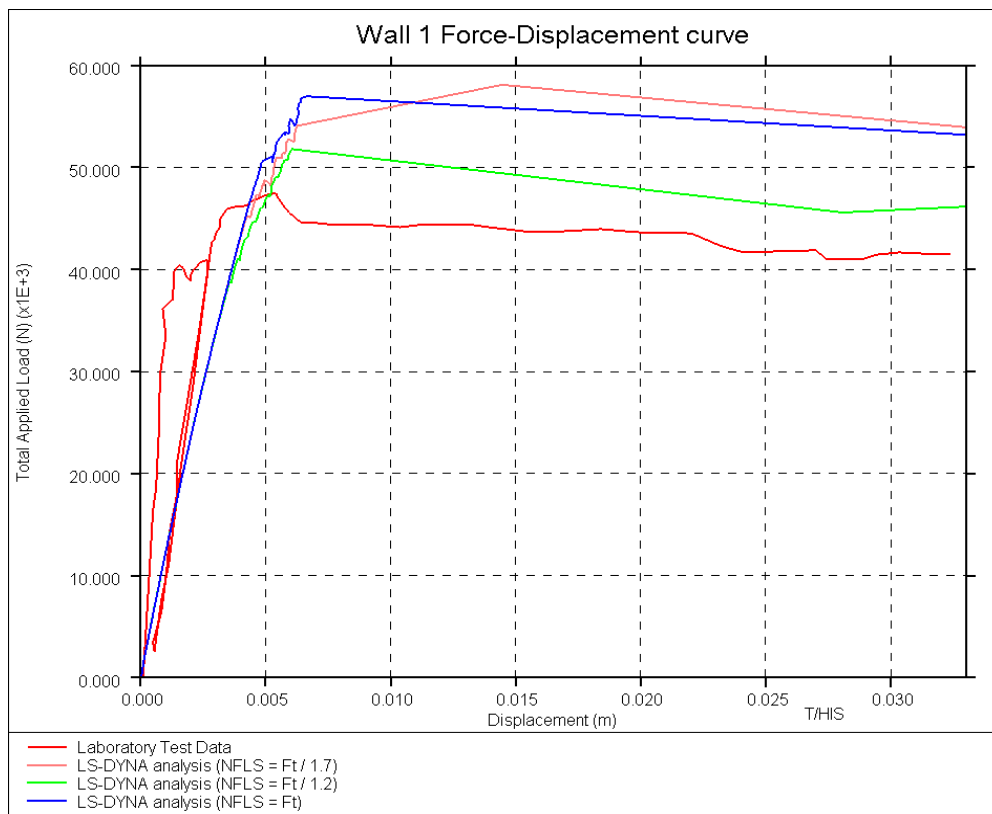


Figure 2.6.3: Load-displacement response plot (Wall 1)

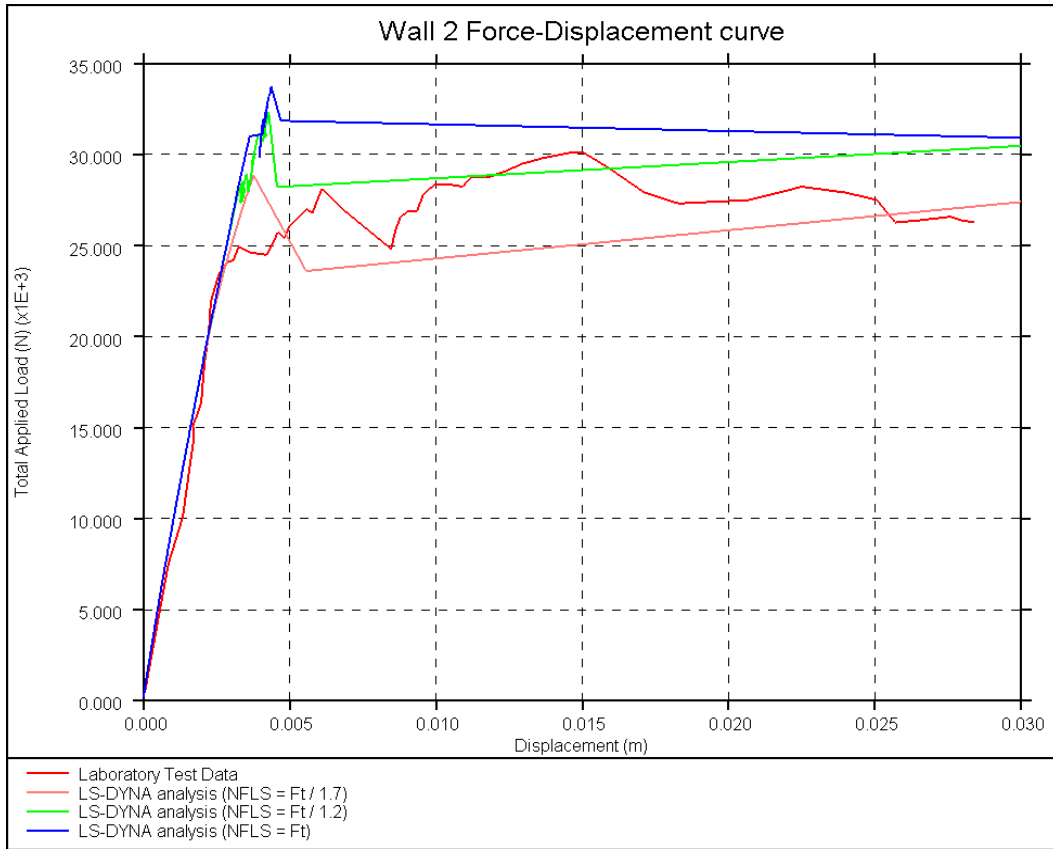


Figure 2.6.4: Load-displacement response plot (Wall 2)

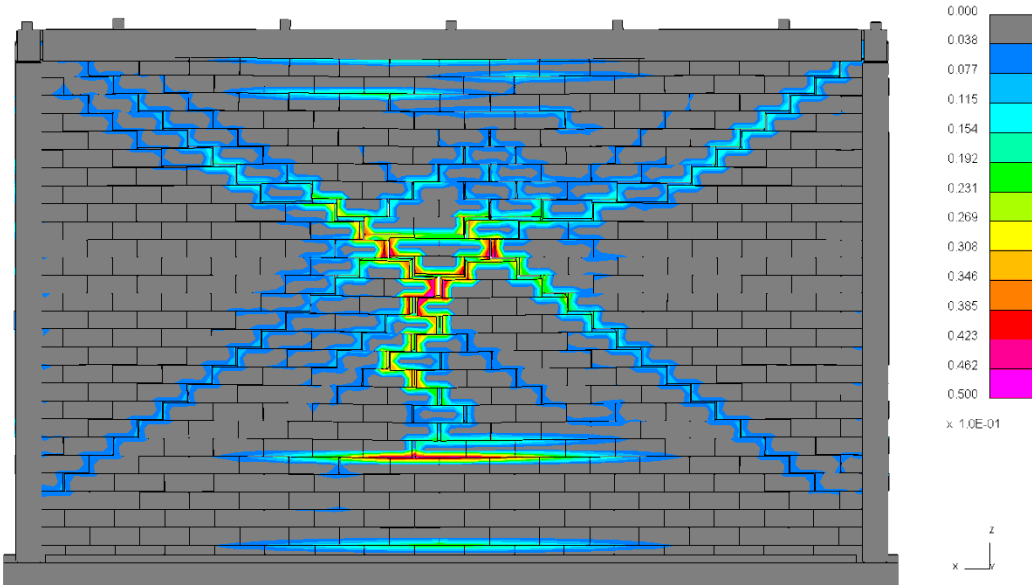


Figure 2.6.5: Final crack pattern for Wall 1

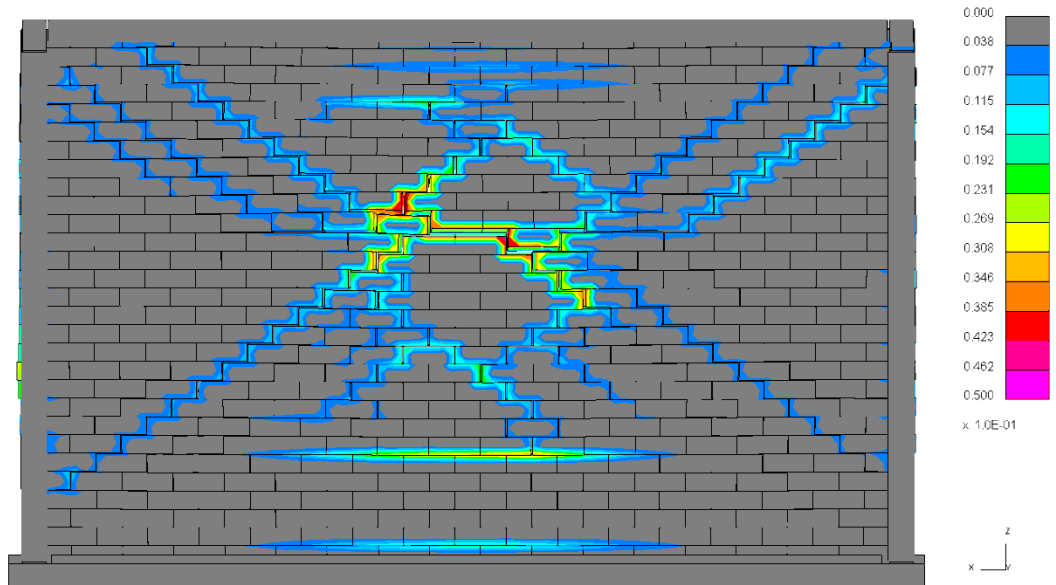


Figure 2.6.6: Final crack pattern for Wall 2

2.6.1. Discussion and sensitivity analyses

Wall 1

- In the absence of the direct tensile strength test results, flexural tensile strength was used in LS-DYNA. Van der Pluijm et al. [3] suggested a reduction factor of 1.2 to 1.7 when converting from flexural strength to direct tensile strength.
- Laboratory records and LS-DYNA load-displacement curves show similar behaviour. However, LS-DYNA elastic response is 'softer'. It was observed that boundary conditions can have a big impact to the analysis results. In the absence of the actual laboratory data, support conditions were assumed in the analysis.
- Load on the wall in LS-DYNA was applied pseudo-statically using force control. This was found to be the most realistic representation of the 'airbag' loading. However, this can result in inertia effects and thus overestimate wall capacity.

Wall 2

- As discussed above, in the absence of the direct tensile strength test results, flexural tensile strength was used in LS-DYNA. Van der Pluijm et al. [3] bounding values are included.
- Similarly, load was applied pseudo-statically using force control, which can cause load overestimation.

Based on suggestions by EUCENTRE, a sensitivity study was carried out with 50% reduced tensile strength of mortar headjoint. The results of this analysis are presented below.

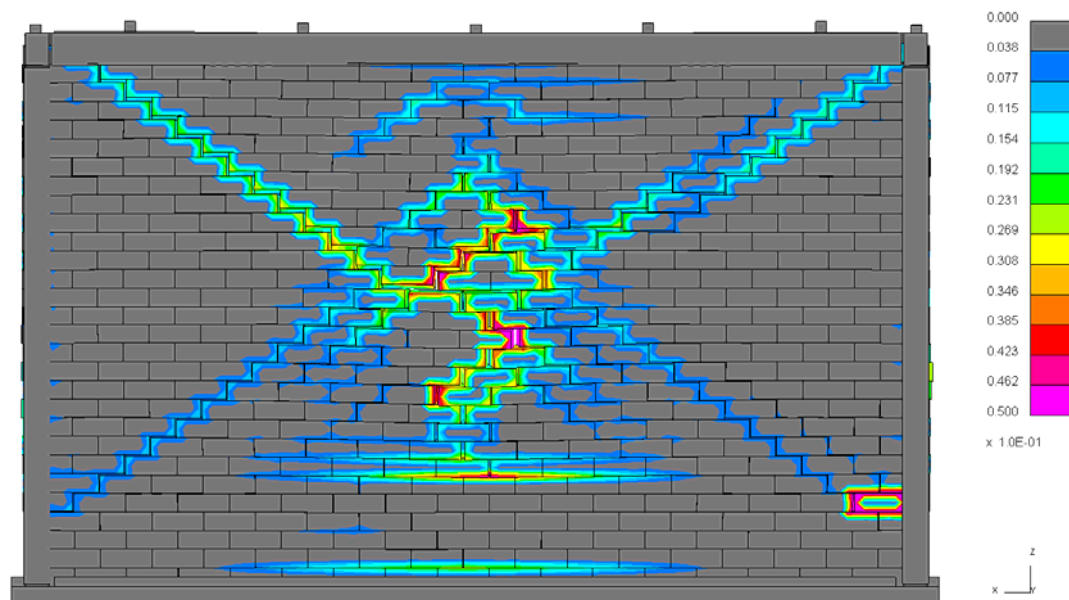


Figure 2.6.1.1: Wall 1, reduced headjoint tensile strength

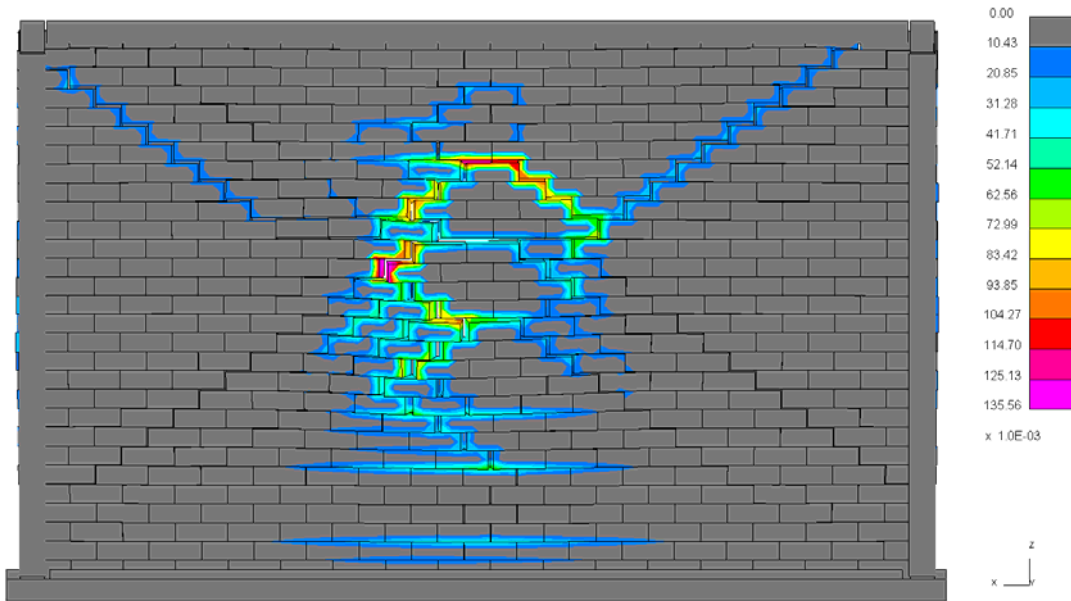


Figure 2.6.1.2: Wall 2, reduced headjoint tensile strength

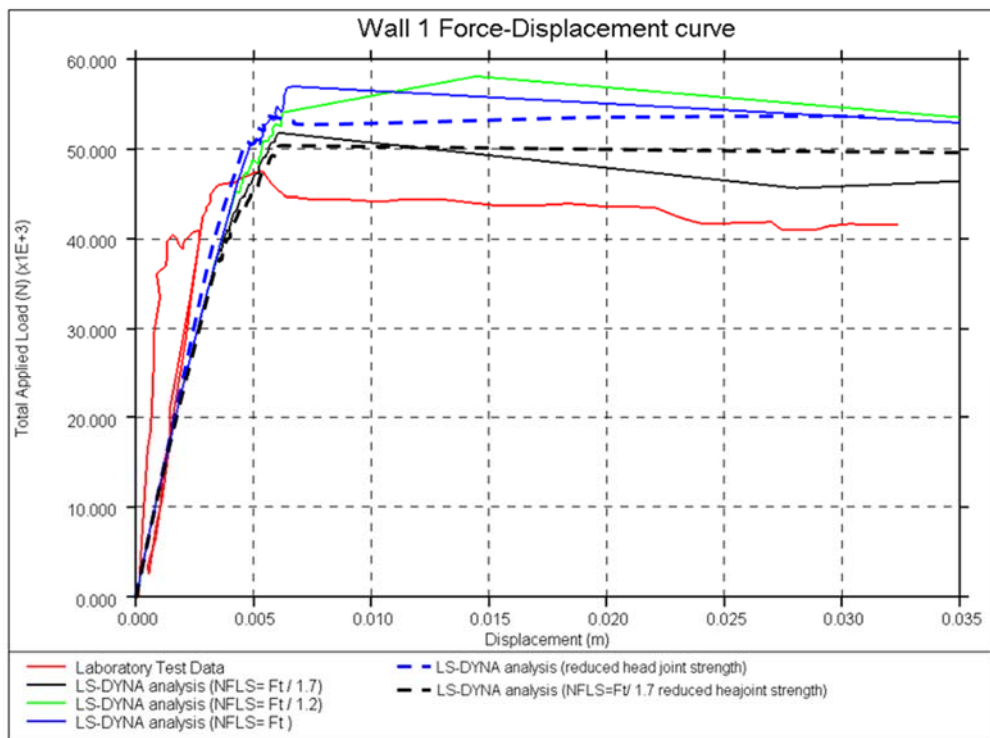


Figure 2.6.1.3: Load-displacement plot Wall 1 (sensitivity analysis)

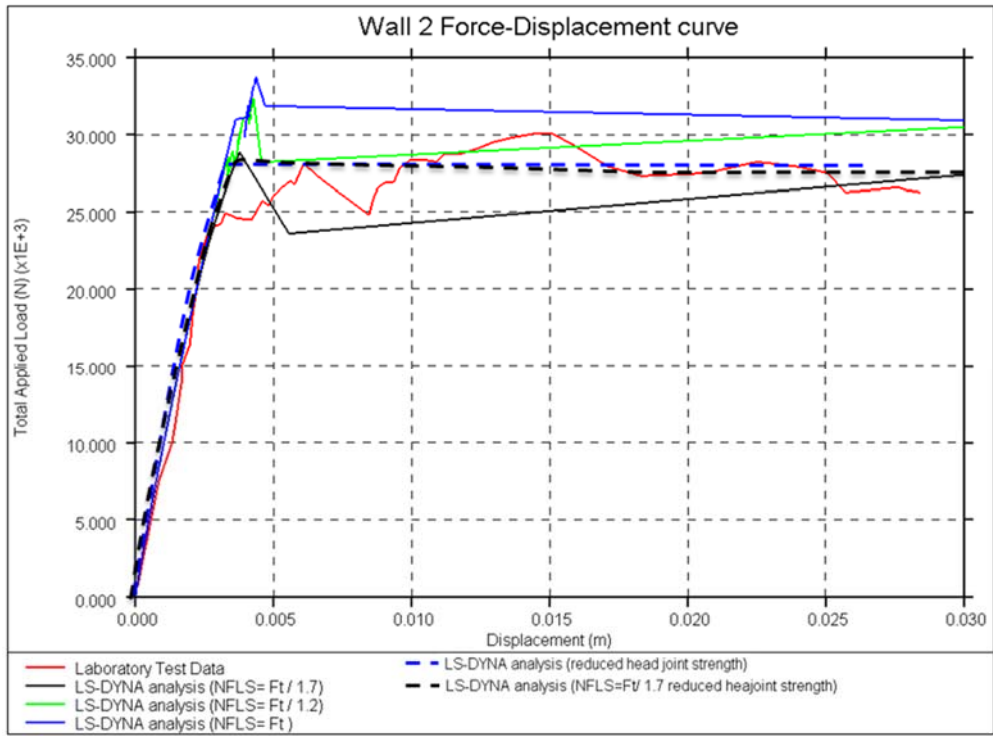


Figure 2.6.1.4: Load-displacement plot Wall 2 (sensitivity analysis)

3. Cross-validation index buildings

3.1. Terraced house (T1*)

Table 3.1.1: Modelling notes

Component	Description
Analysis software and formulation	LS-DYNA – explicit analysis solver
Walls (in-plane)	Individual bricks modelled with solid elements using nonlinear Winfrith material model. Mortar modelled with tiebreak contact surface (penalty stiffness formulation) with a Mohr-Coulomb failure surface. The stiffness of the bricks was adjusted so that the total masonry stiffness (brick Young's modulus and contact penalty stiffness) matches masonry material test data from laboratory tests.
Walls (out-of-plane)	As above.
Spandrels/lintels and wall coupling	Spandrels modelled using the same approach as the walls with the tiebreak contact surface modelling coupling effects. Lintels modelled so that the elements remain elastic.
Wall to wall connection (incl. flange effects)	Contact surface used for the mortar connection. Refer to the mortar material information for further details. Flange effects are included explicitly.
Modelling of veneer walls (outer leaf)	Veneer walls were modelled explicitly using the same technique as the main structure, and was tied to the inner walls with spring (discrete) elements. The tie springs were connected to the masonry at an interior node of the brick mesh. A nonlinear spring has been used with different tensile and compressive limits equal to that of a typical masonry tie.
Wall ties	Spring elements between the inner and outer leaves with different tensile and compressive limits. Tensile limit = 1.4 kN, compressive limit = 0.4 kN, perfectly plastic when the limits are reached.
Concrete diaphragm	The T1* diaphragm is comprised of one-way spanning hollowcore planks. To correctly model the loading and mass distribution, the planks were modelled using shell elements with no gravity loading. The loading from the planks was then applied as a distributed load to the transverse walls supporting the hollowcore planks.
Wall to diaphragm connection	Contact surface used for the mortar connection between the bricks and the diaphragm.
Foundation	Modelled as rigid.

Table 3.1.2: Eigenvalue analysis notes

Eigenvalue analysis notes
<ul style="list-style-type: none"> • Uses the Block Shift and Invert Lanczos eigensolver. • Element formulations modified to be compatible with implicit solver. • Some constraint changes for compatibility with the implicit solver. • Tiebreak contact surfaces removed from the model. • Coincident nodes from adjacent brick parts are merged. • Stiffness of the masonry parts reduced to 50% of E_{masonry} from test data, to account for cracking. A separate sensitivity study was also conducted with the original uncracked 100% E_{masonry}. • All spring (discrete) elements replaced with beam elements.

Table 3.1.3: Nonlinear pushover analysis notes

Nonlinear pushover analysis notes
<ul style="list-style-type: none">• The force profile assumed for the LS-DYNA pushover analysis is a linear distribution. A uniform force distribution was carried out as a sensitivity study.

Table 3.1.4: Nonlinear time history analysis notes

Nonlinear time history analysis notes
<ul style="list-style-type: none">• 1% damping applied using proprietary LS-DYNA constant damping model over 1–30 Hz frequency range.• Additional damping applied at very high frequencies for numerical stability.

Table 3.1.5: Model loading, materials and general comments

Loading	
Dead loads	Self-weight of the walls, hollowcore planks and roof structure.
Superimposed dead loads	Floors = 2.4 kPa (provisions for top layer + interior walls + finishes) Roof = 0.5 kPa
Live loads	Floors = 1.75 kPa Roof = 0 kPa
Load combination	DL + SDL + 0.24LL
Materials	Material properties including values and stress strain behaviour
Clay bricks	Elastic-plastic material model $\rho = 1900 \text{ kg/m}^3$ $E = 6822 \text{ MPa}$ (to match a masonry E of 4410 MPa) $\nu = 0.15$ $f_y = 6.3 \text{ MPa}$ $f_t = 1.26 \text{ MPa}$
Calcium silicate bricks	Elastic-plastic material model $\rho = 1900 \text{ kg/m}^3$ $E = 5452 \text{ MPa}$ (to match a masonry E of 4410 MPa) $\nu = 0.15$ $f_y = 6.3 \text{ MPa}$ $f_t = 1.26 \text{ MPa}$
Mortar	Tensile stress limit = 0.1 MPa Shear stress limit = 0.1 MPa Friction coefficient = 0.75 Modelled using CONTACT_AUTOMATIC_SURFACE_TO_SURFACE with the Dycoss discrete crack model failure surface.
Concrete	Elastic material model Basic density = 2400 kg/m ³ (reduced to 1694 kg/m ³ for effective area) $E = 38 \text{ GPa}$ $\nu = 0.2$
Steel	Elastic-plastic material model $\rho = 7850 \text{ kg/m}^3$ $E = 200 \text{ GPa}$ $\nu = 0.3$ $f_y = 300 \text{ MPa}$
Timber/Plywood	Elastic material model $\rho = 600 \text{ kg/m}^3$ $E = 6000 \text{ MPa}$ $\nu = 0.3$
<u>Other key notes</u>	
1) No additional key notes.	

Table 3.1.6: Breakdown of loading and masses

Loading	DL [kPa]	SDL [kPa]	LL [kPa]	DL+SDL+0.24LL [kPa]	Area [m ²]
1 st Floor	3.25	2.4	1.75	6.07	42.7
2 nd Floor	3.25	2.4	1.75	6.07	42.7
Roof	0.27	0.5	0	0.77	60.0
Total model mass (including DL+SDL+0.24LL) = 96651 kg					
Masonry	Density [kg/m ³]		Thickness [m]		Total masonry mass [kg]
Calcium silicate	1900		0.1 (slender piers) 0.12 (transverse walls)		42342
Clay (vener)	1900		0.1		8185

Table 3.1.7: Cut-section total z-forces (weight from gravity load at t=0) at different cut-plane heights

Cut-plane height (m)	Cut-section z-force (kN)
<Just above ground/base>	937
<Just above L1 diaphragm>	519

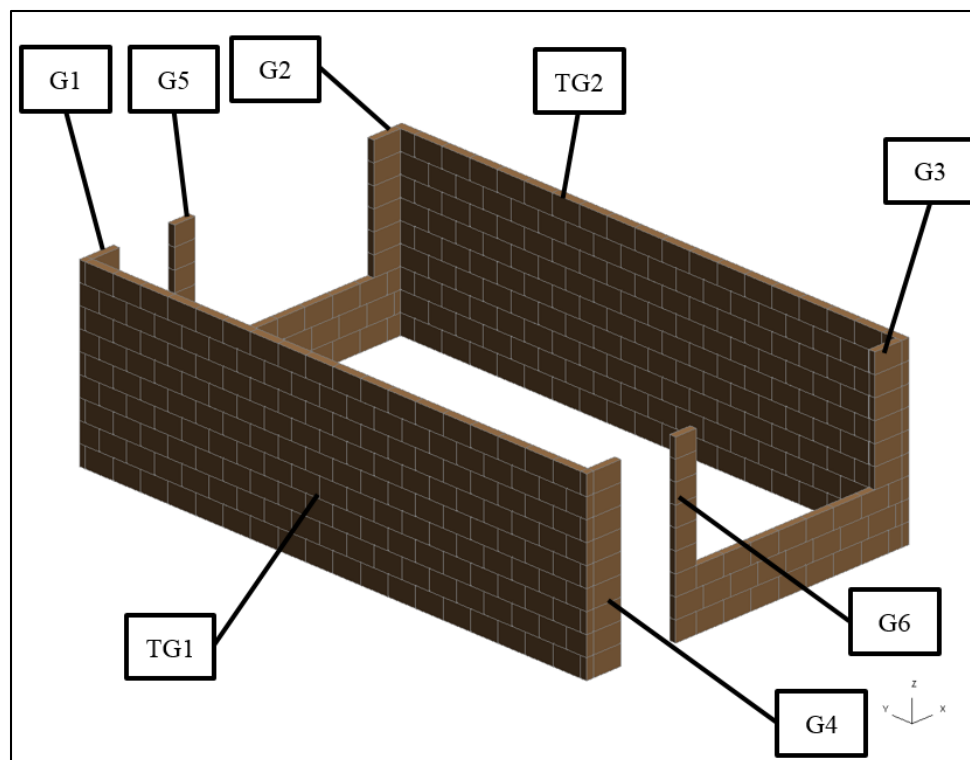


Figure 3.1.1: Pier labelling convention for T1* building (ground floor)

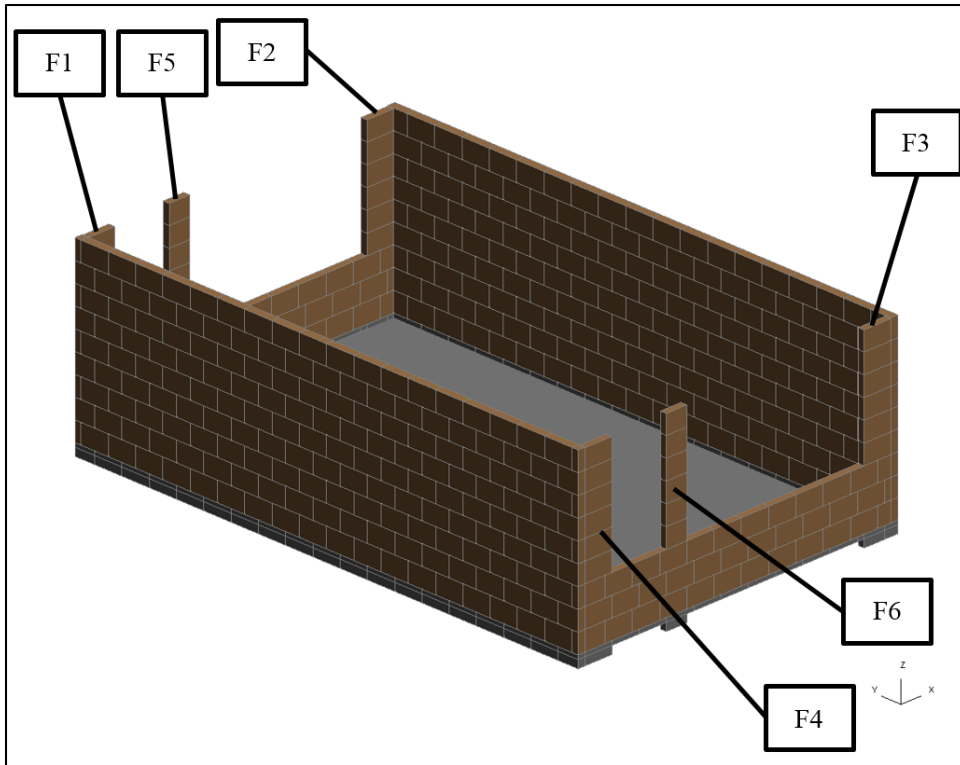


Figure 3.1.2: Pier labelling convention for T1* building (first floor)

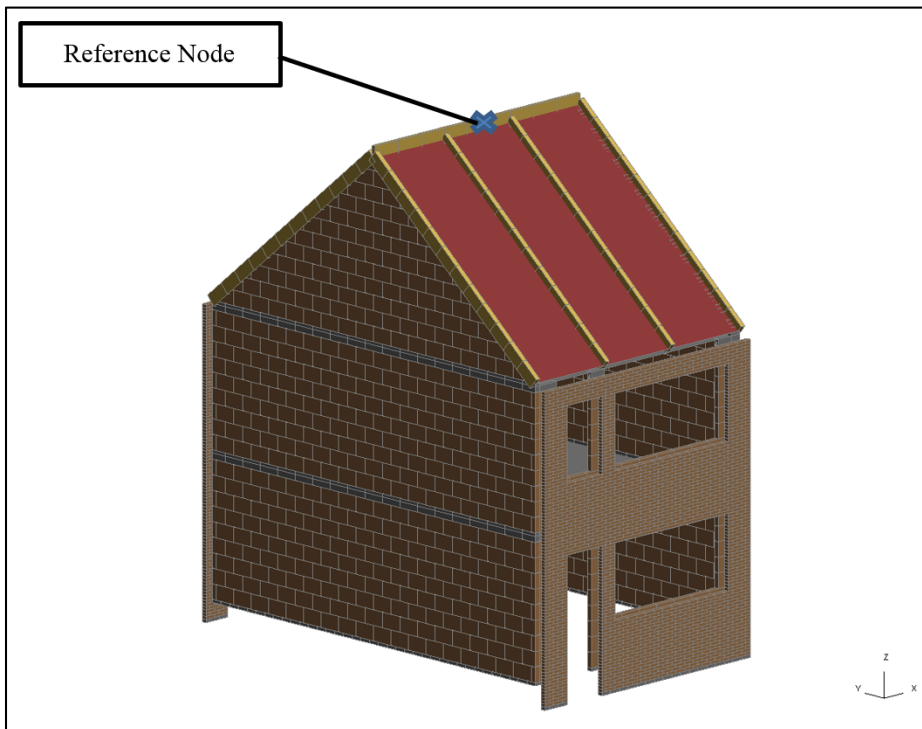


Figure 3.1.3: FE model for T1* model and pushover reference node location

3.1.1. Modal analysis

Table 3.1.8: Modal period, frequency, description, mass participation

Mode	Period (s)	Frequency (Hz)	Description of mode	Mass participation %	
				X	Y
1	0.541	1.85	First lateral X direction sway	76.51%	0.00%
2	0.194	5.15	Second lateral X direction sway	9.73%	0.00%
3	0.160	6.26	Roof out of plane	0.00%	3.13%
4	0.137	7.28	Veneer wall in plane sway (out of phase)	0.00%	0.00%
5	0.137	7.28	Veneer wall in plane sway (in phase)	5.39%	0.00%
6	0.129	7.76	Roof out of plane	0.00%	0.00%
7	0.124	8.07	Roof out of plane	0.00%	0.00%
8	0.111	9.01	First lateral Y direction sway	0.00%	63.67%
9	0.110	9.11	Roof out of plane	0.00%	0.00%
10	0.108	9.27	First torsional	0.00%	0.02%

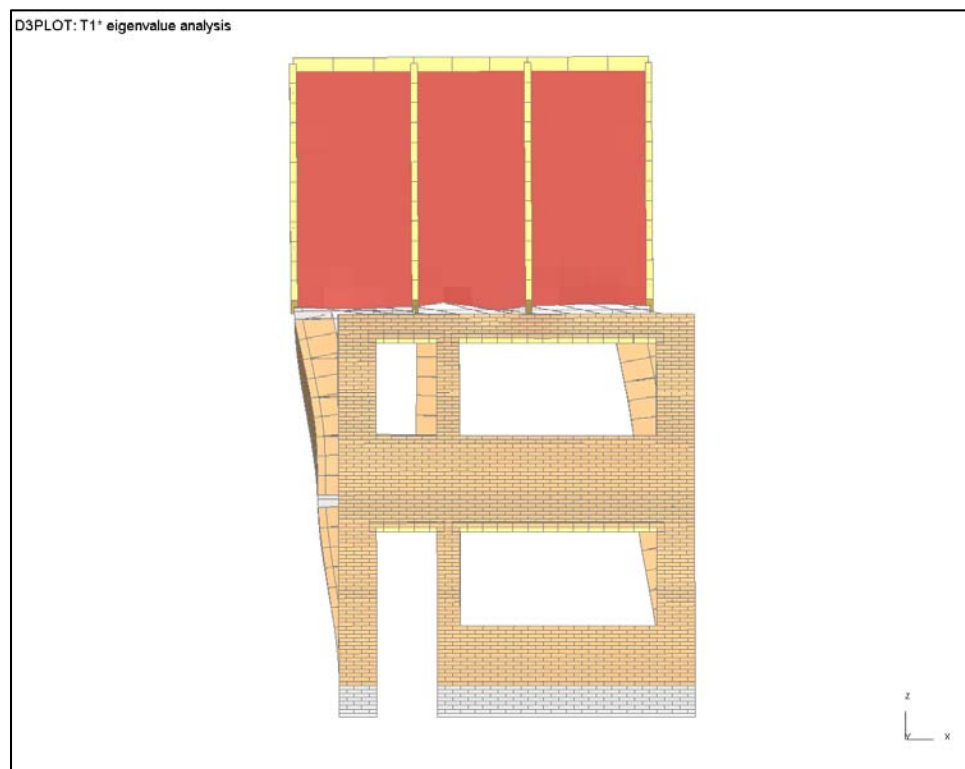


Figure 3.1.4: First lateral mode shape (X-direction)

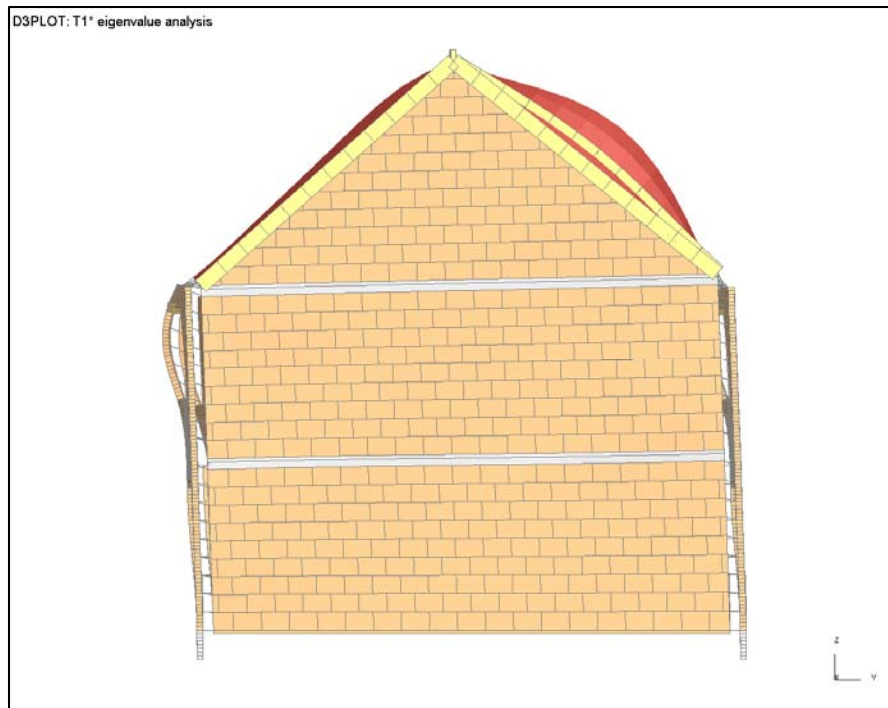


Figure 3.1.5: First lateral mode shape (Y-direction)

3.1.2. Pushover analysis (monotonic and cyclic)

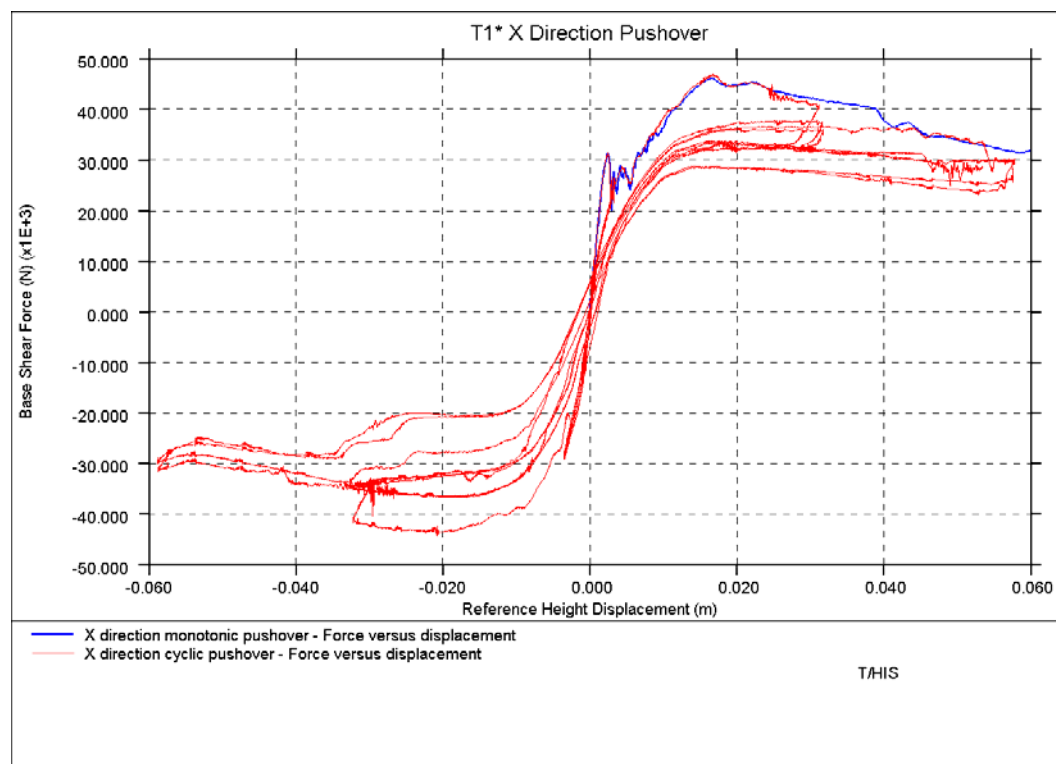


Figure 3.1.6: X-direction base shear versus reference node displacement

Table 3.1.9: Cut-planes pier forces at peak/plateau x-dir pushover base shear

Pier	X-dir pier force (kN) Cut-plane height ~1.65 m		Pier	X-dir pier force (kN) Cut-plane height ~4.65 m	
	Axial	Shear		Axial	Shear
G1	-27.5	4.5	F1	-1.9	1.5
G2	-23.7	3.9	F2	-4.2	1.2
G3	-23.7	3.9	F3	-4.2	1.2
G4	-27.6	4.5	F4	-1.9	1.5
G5	1.2	0.1	F5	0.3	0.08
G6	1.1	0.1	F6	0.2	0.09
TG1	-324.1	10.6	TG1	-196.5	11.3
TG2	-378.3	11.7	TG2	-201.7	8.8
Total	-854.7	46.0	Total	-423.4	29.5

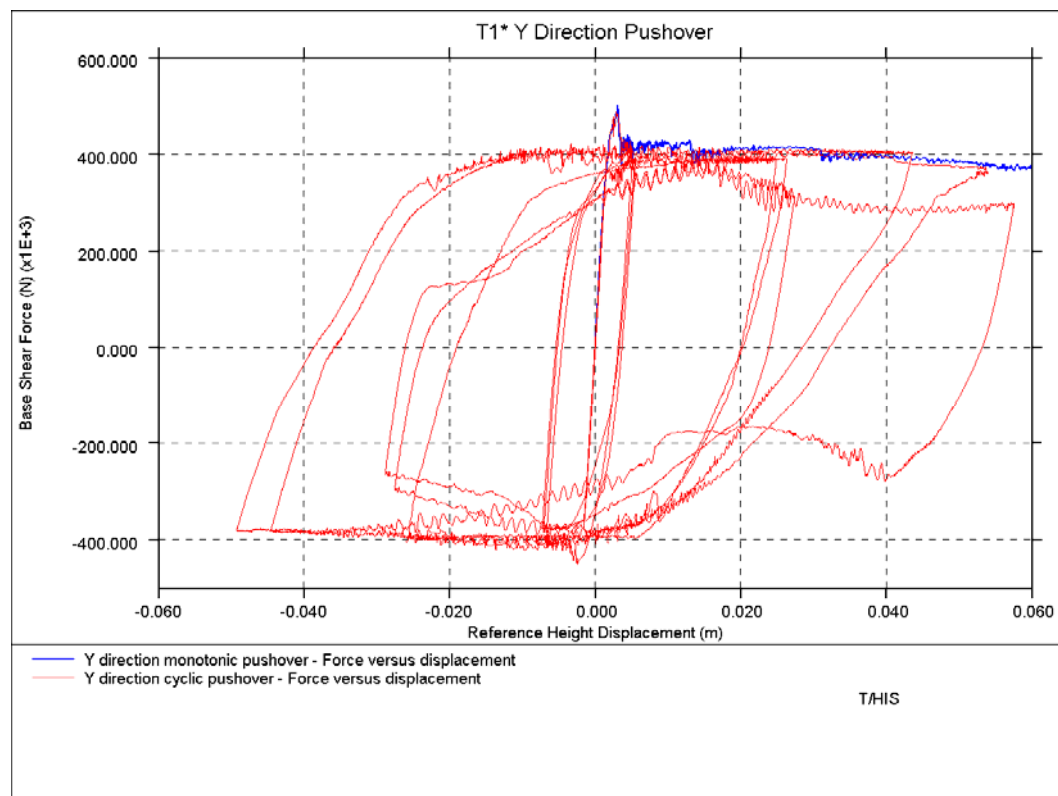


Figure 3.1.7: Y-direction base shear versus reference node displacement

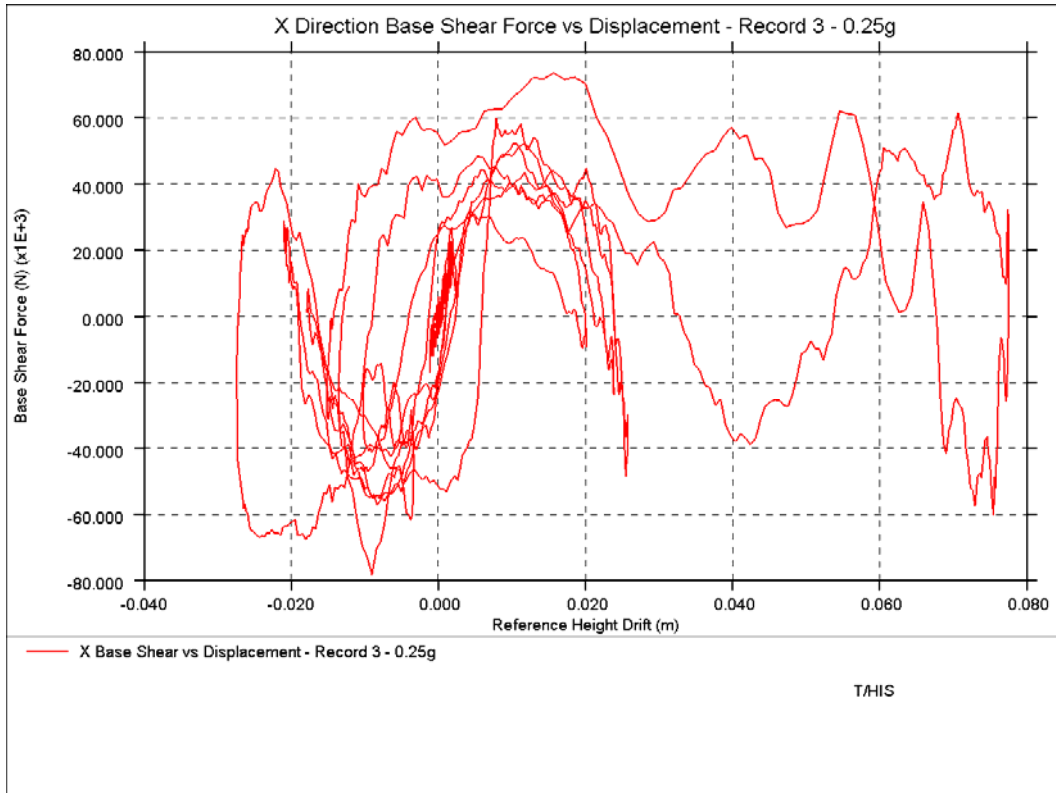


Figure 3.1.8: Base shear versus reference node displacement – 0.25g scaled PGA, record 3, X direction

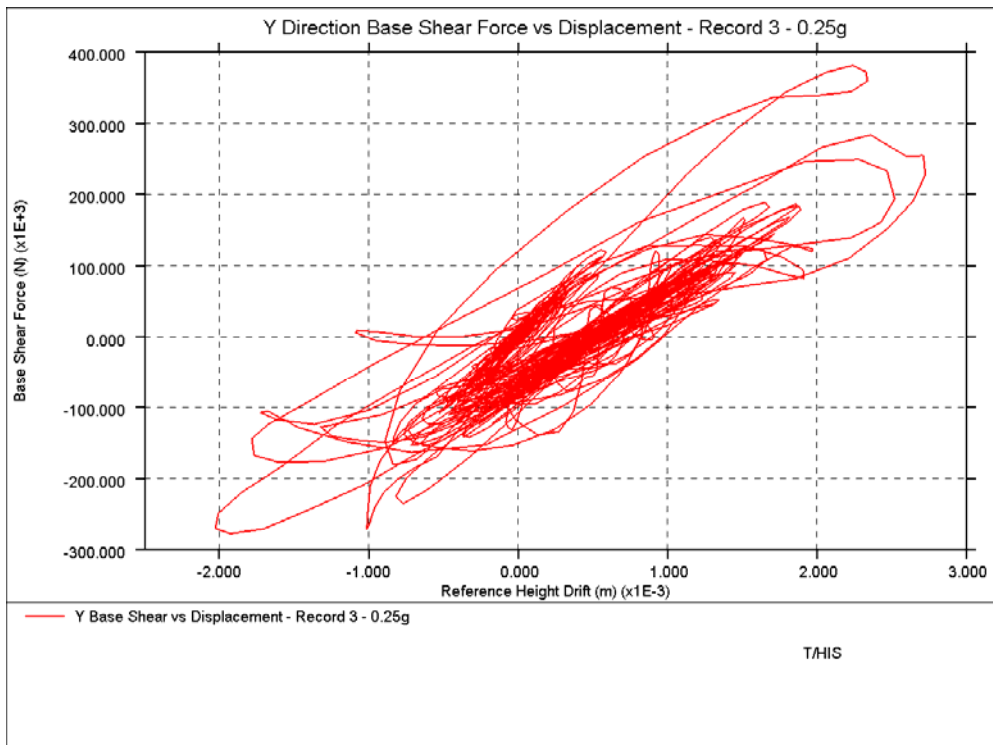


Figure 3.1.9: Base shear versus reference node displacement – 0.25g scaled PGA, record 3, Y direction

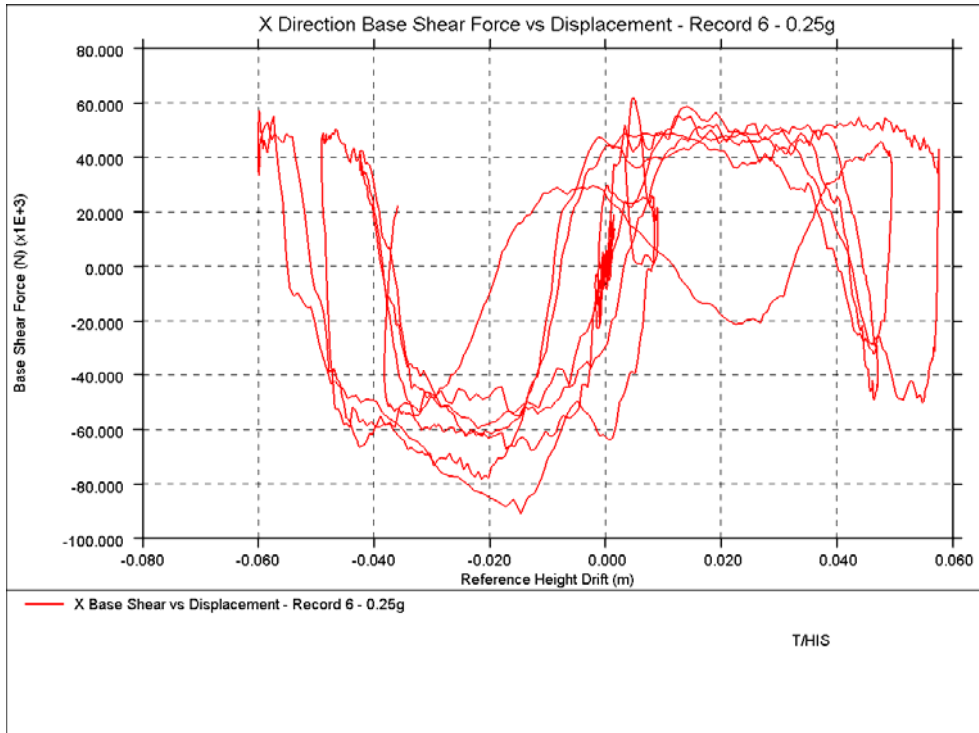


Figure 3.1.10: Base shear versus reference node displacement – 0.25g scaled PGA, record 6, X direction

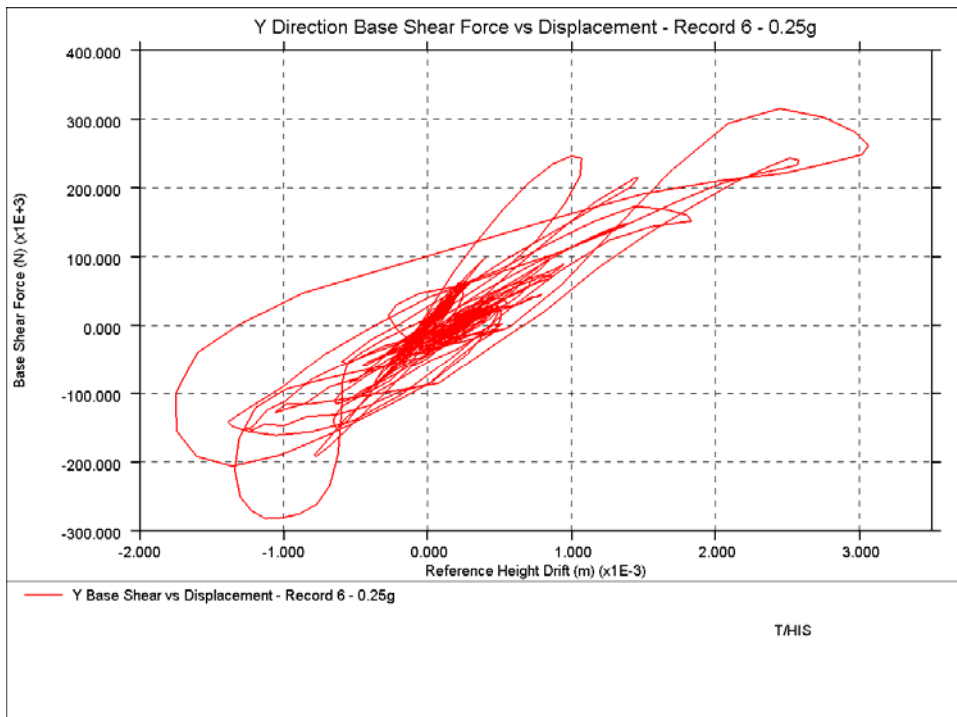


Figure 3.1.11: Base shear versus reference node displacement – 0.25g scaled PGA, record 6, Y direction

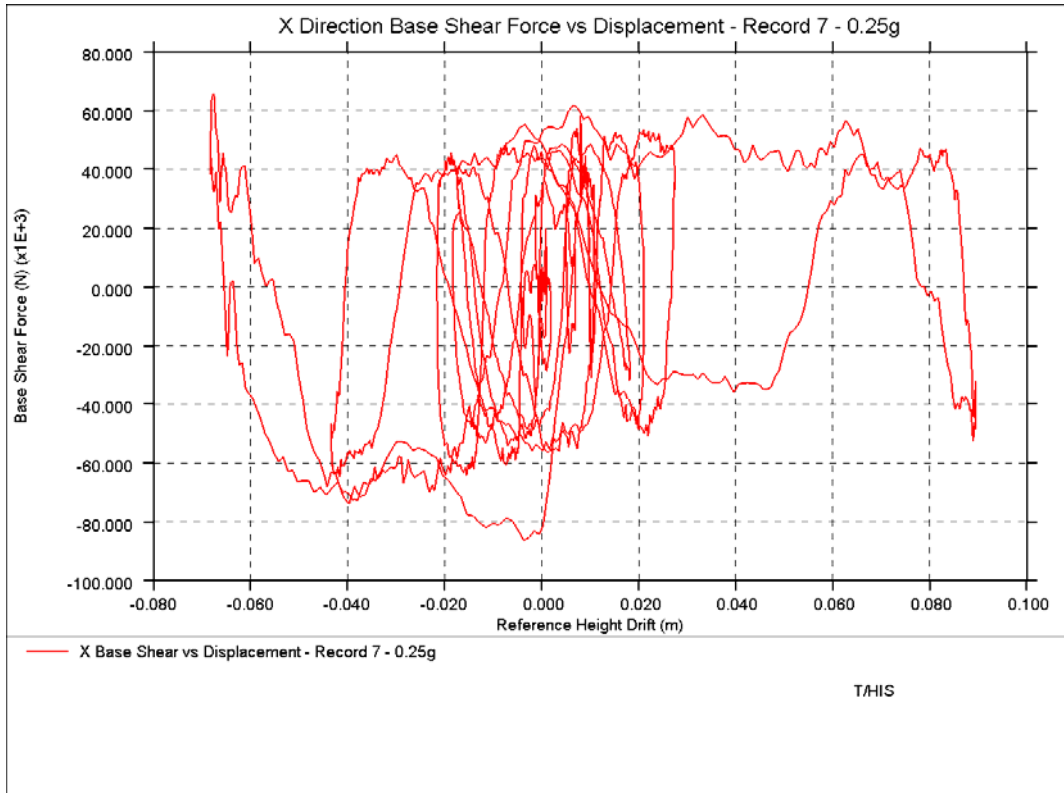


Figure 3.1.12: Base shear versus reference node displacement – 0.25g scaled PGA, record 7, X direction

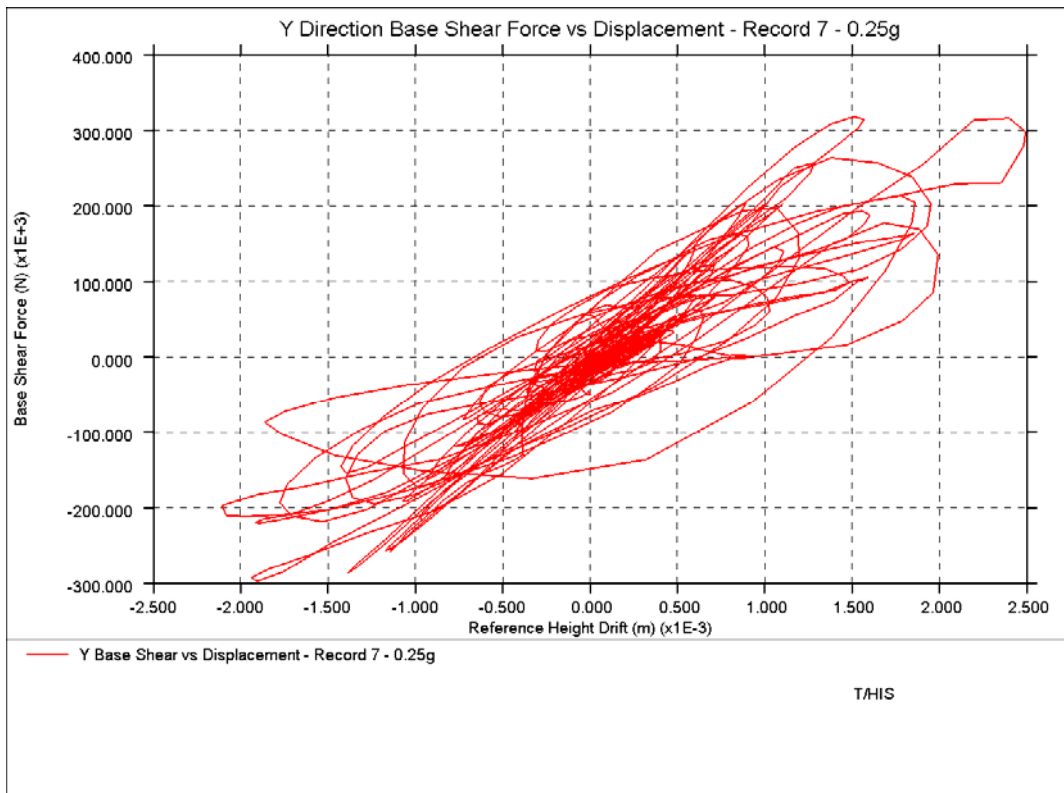


Figure 3.1.13: Base shear versus reference node displacement – 0.25g scaled PGA, record 7, Y direction

3.1.4. Discussion and sensitivity analyses

Several sensitivity analyses were carried out.

In the first study, an eigenvalue analysis was performed where bricks were modelled with the uncracked Young's Modulus (4410 MPa). The results in terms of periods, frequency and participating mass are compared with the original model with the 50% cracked Young's Modulus and are presented below.

Table 3.1.4.1: Modal period, frequency, description, mass participation – x-direction

x-dir	Mode No.	Period (s)	Freq (Hz)	Participating mass %	Participating mass (tonne)
Uncracked	1	0.41	2.5	76.2	73.1
Cracked (50% E)	1	0.54	1.8	76.5	73.4

Table 3.1.4.2: Modal period, frequency, description, mass participation – y-direction

y-dir	Mode No.	Period (s)	Freq (Hz)	Participating mass %	Participating mass (tonne)
Uncracked	15	0.081	12.3	11.3	10.8
Uncracked	16	0.080	12.5	43.9	42.2
Cracked (50% E)	8	0.111	9.0	63.7	61.1

In the second study, carried out on monotonic pushover analyses, the sensitivity of the results to a model with adjusted spandrel stiffness and uniform force distribution was studied. The results are presented and compared with the original analysis results.

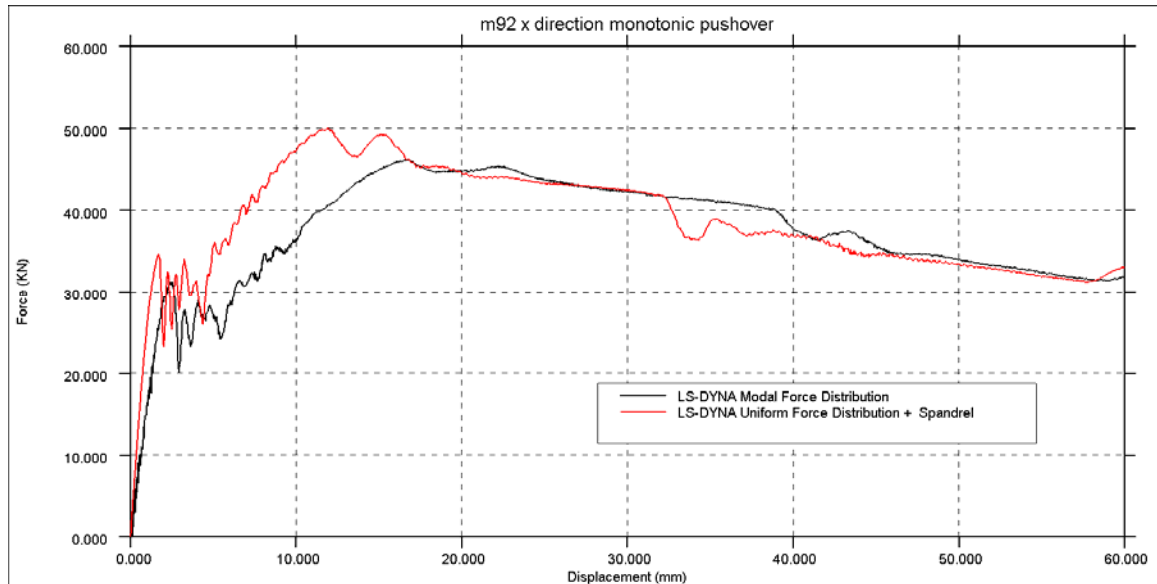


Figure 3.1.4.1: X-direction base shear versus reference node displacement

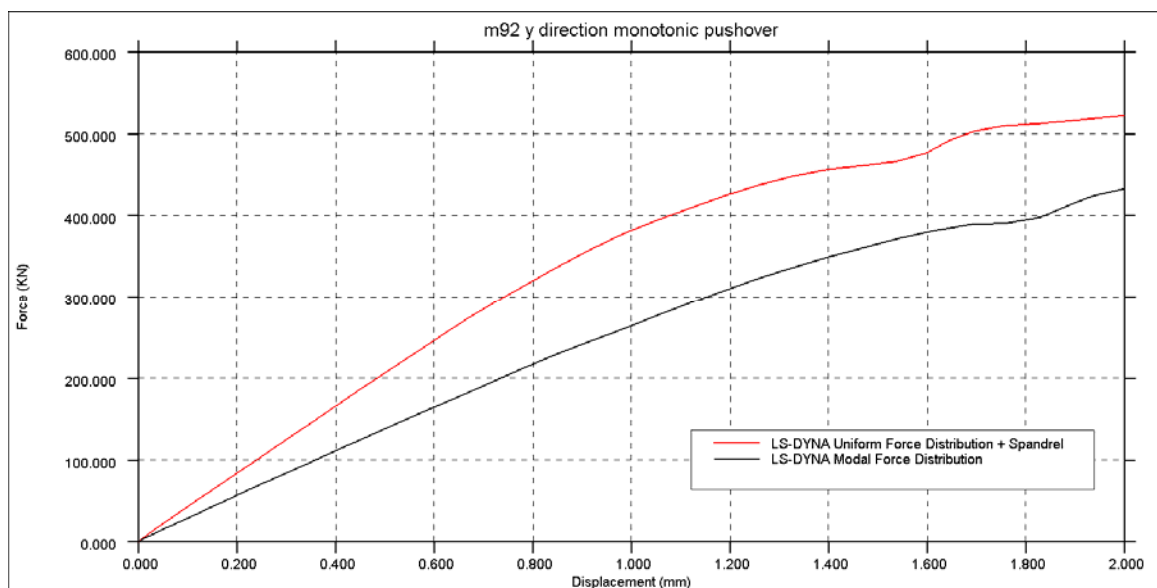


Figure 3.1.4.2: Y-direction base shear versus reference node displacement. Note: Y-direction pushover continue beyond 2 mm displacement, with a base shear force plateau of approximately 400 kN.

In the third sensitivity study, the monotonic pushover analysis was repeated with 50% reduced tensile strength of the headjoints, as per suggestion by EUCENTRE. The output was not sensitive to the reduced headjoint tensile strength.

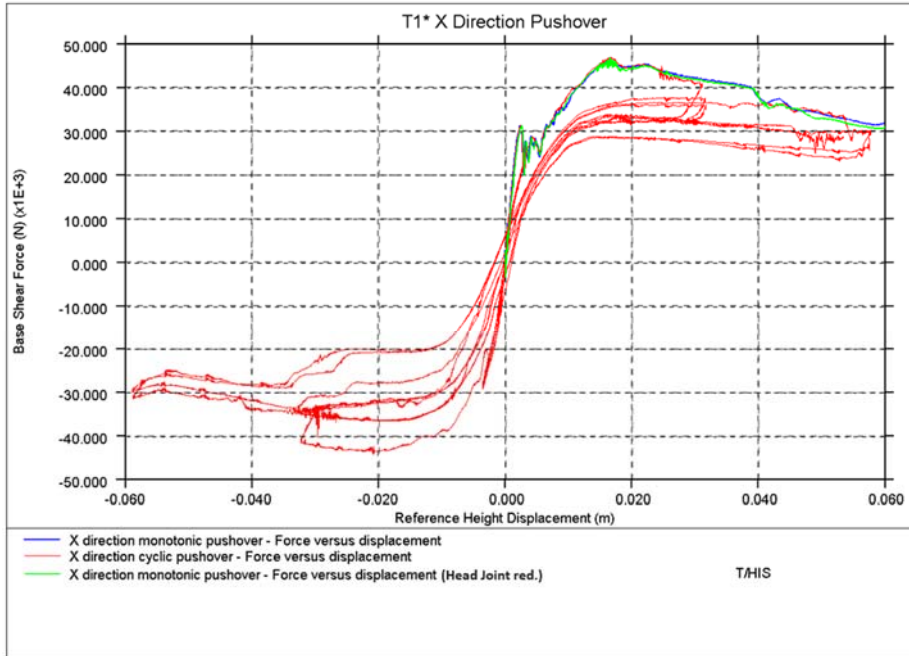


Figure 3.1.4.3: X-direction base shear versus reference node displacement

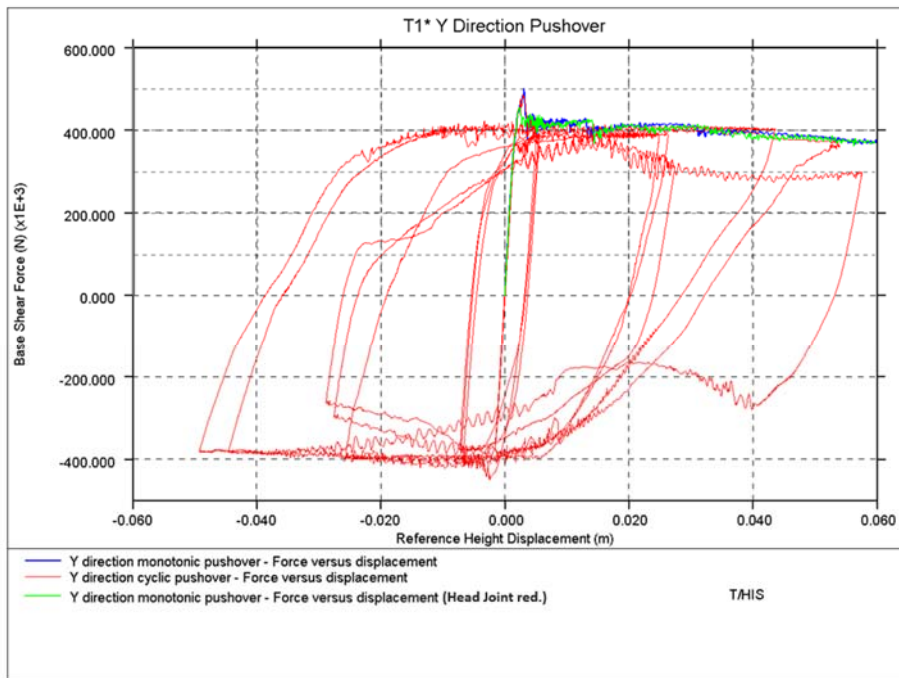


Figure 3.1.4.4: Y-direction base shear versus reference node displacement

In order to estimate the initial elastic stiffness of the models, linear elastic “pushover” analyses (scaled linearly up to 1g acceleration) were conducted in each direction. The linear elastic “pushover” was performed on the original nonlinear model used for the pushover (with modal force distribution), with relevant modifications and elastic material definitions from the eigenvalue analysis.

As shown in the following figures, the linear elastic “pushover” initial stiffness is higher than that for the nonlinear pushover, due to the differences in the modelling of the masonry stiffness – the linear elastic model has the masonry Young’s modulus directly applied to the material model; whereas the nonlinear model contains the combined stiffness of MAT_WINFRITH Young’s modulus and penalty stiffness of the tiebreak contacts for the mortar modelling.

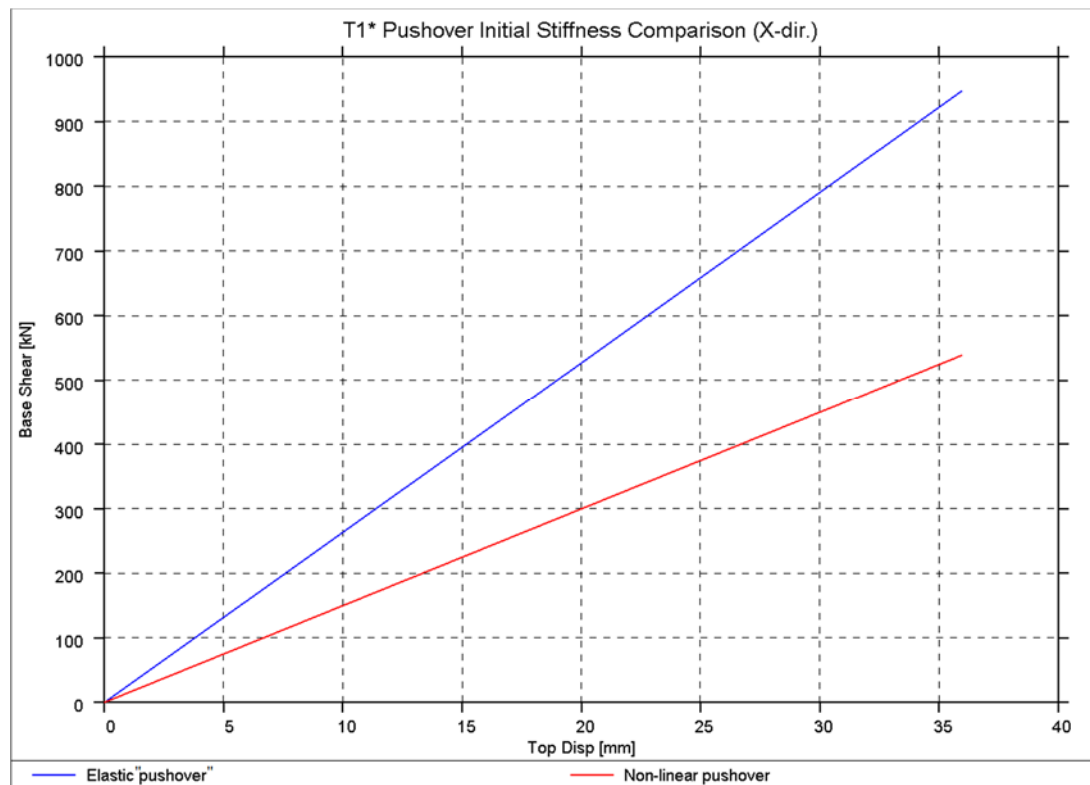


Figure 3.1.4.5: T1* initial stiffness (x-direction)

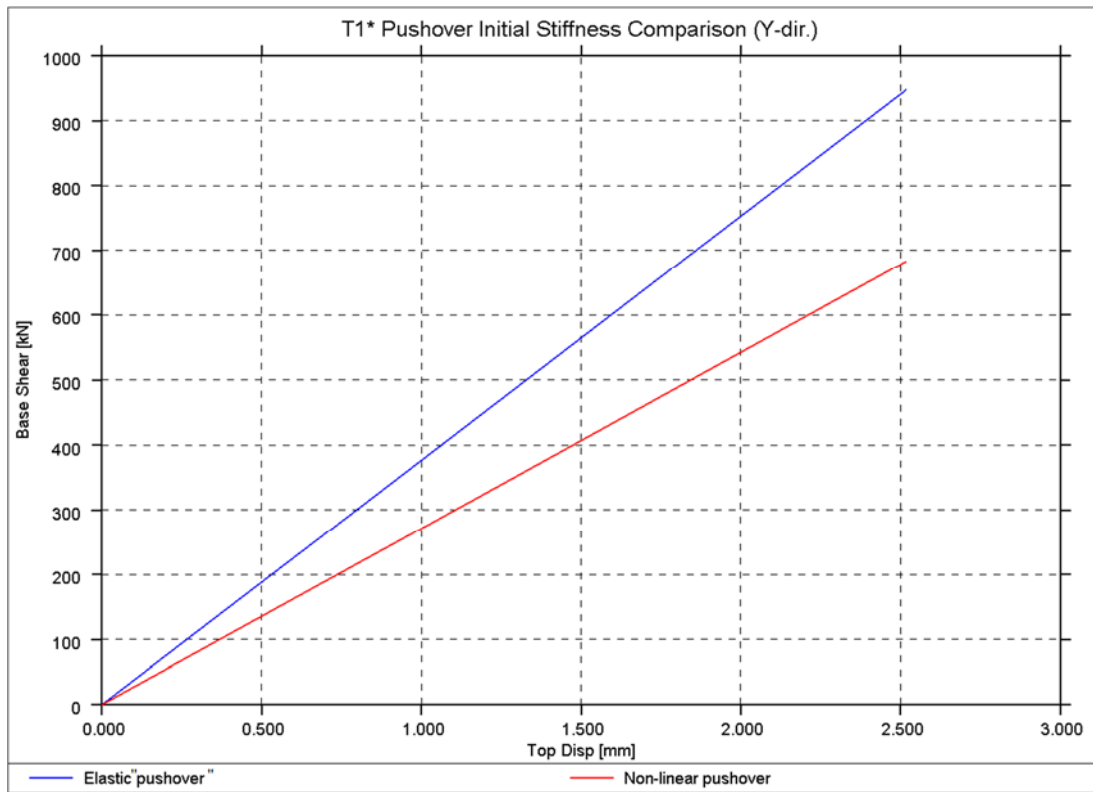


Figure 3.1.4.6: T1* initial direction (y-direction)

3.2. Detached villa, timber floors (T3a)

Table 3.2.1: Modelling notes

Component	Description
Analysis software and formulation	LS-DYNA – explicit analysis solver
Walls (in-plane)	Individual bricks modelled with solid elements using nonlinear Winfrith material model. Mortar modelled with tiebreak contact surface (penalty stiffness formulation) with a Mohr-Coulomb failure surface. The stiffness of the bricks was adjusted so that the total masonry stiffness (brick Young's modulus and contact penalty stiffness) matches masonry material test data from laboratory tests.
Walls (out-of-plane)	As above.
Spandrels/lintels and wall coupling	Spandrels modelled using the same approach as the walls with the tiebreak contact surface modelling coupling effects. Lintels modelled so that the elements remain elastic.
Wall to wall connection (incl. flange effects)	Contact surface used for the mortar connection. Refer to the mortar material information for further details. Flange effects are included explicitly.
Wall ties	Spring elements between the inner and outer leaves with different tensile and compressive limits. Tensile limit = 1.4 kN, compressive limit = 0.4 kN, perfectly plastic when the limits are reached.
Timber diaphragm	Timber diaphragms modelled with beam elements for the joists and the individual floor boards. Null shells used to apply load to the floor.
Wall to diaphragm connection	Contact surface used for the mortar connection between the bricks and the diaphragm. Contact surface is also used for the interface with the rigid foundation.
Foundation	Modelled as rigid.

Table 3.2.2: Eigenvalue analysis notes

Eigenvalue analysis notes
<ul style="list-style-type: none"> Eigenvalue analysis was conducted for the LS-DYNA modal analyses, using the Block Shift and Invert Lanczos eigensolver. Due to the detail of the 3D brick-by-brick model where structural components were modelled explicitly, many local modes were identified during the analysis. They have been summarised in the table of results.

Table 3.2.3: Nonlinear pushover analysis notes

Nonlinear pushover analysis notes
<ul style="list-style-type: none"> The force profile assumed for the LS-DYNA pushover analysis is a linear distribution. A uniform distribution has been carried out as a sensitivity study.

Table 3.2.4: Nonlinear time history analysis notes

Nonlinear time history analysis notes
<ul style="list-style-type: none"> 1% damping applied using proprietary LS-DYNA constant damping model over 1–30 Hz frequency range. Additional damping applied at very high frequencies for numerical stability.

Table 3.2.5: Model loading, materials and general comments

Loading	
Dead loads	Self-weight of the walls and roof structure.
Superimposed dead loads	Floor = 1.0 kPa Barn roof = 0.5 kPa Main roof = 1.0 kPa
Live loads	Floor = 1.75 kPa Barn roof = 0 kPa Main roof = 0 kPa
Load combination	DL + SDL + 0.24LL
Materials	
Clay bricks	Elastic-plastic material model $\rho = 1900 \text{ kg/m}^3$ $E = 6822 \text{ MPa}$ (to match masonry E of 4410 MPa) $\nu = 0.15$ $f_y = 6.3 \text{ MPa}$ $f_t = 1.26 \text{ MPa}$
Mortar	Tensile stress limit = 0.1 MPa Shear stress limit = 0.1 MPa Friction coefficient = 0.75 Modelled using CONTACT_AUTOMATIC_SURFACE_TO_SURFACE with the Dycoss discrete crack model failure surface.
Concrete	Elastic material model Basic density = 2400 kg/m^3 $E = 38 \text{ GPa}$ $\nu = 0.2$
Steel	Elastic-plastic material model $\rho = 7850 \text{ kg/m}^3$ $E = 200 \text{ GPa}$ $\nu = 0.3$ $f_y = 300 \text{ MPa}$
Timber/Plywood	Elastic material model $\rho = 600 \text{ kg/m}^3$ $E = 6000 \text{ MPa}$ $\nu = 0.3$
Other key notes	
1) No additional key notes.	

Table 3.2.6: Breakdown of loading and masses

Loading	DL [kPa]	SDL [kPa]	LL [kPa]	DL+SDL+0.24LL [kPa]	Area [m ²]
Floor	0.5	1.0	1.75	1.92	55.37
Barn roof	0.5	0.5	0.0	1.0	20.58
Main roof	0.72	1.0	0.0	1.72	80.38
Total model mass (including DL+SDL+0.24LL) = 89743 kg					
Masonry	Density [kg/m ³]		Thickness [m]		Total masonry mass [kg]
Clay	1900		0.22		61527

Table 3.2.7: Cut-section z-forces (weight from gravity load at t=0) at different cut-plane heights

Cut-plane height (m)	Cut-section z-force (kN)
At the Base	889
Just above diaphragm	146

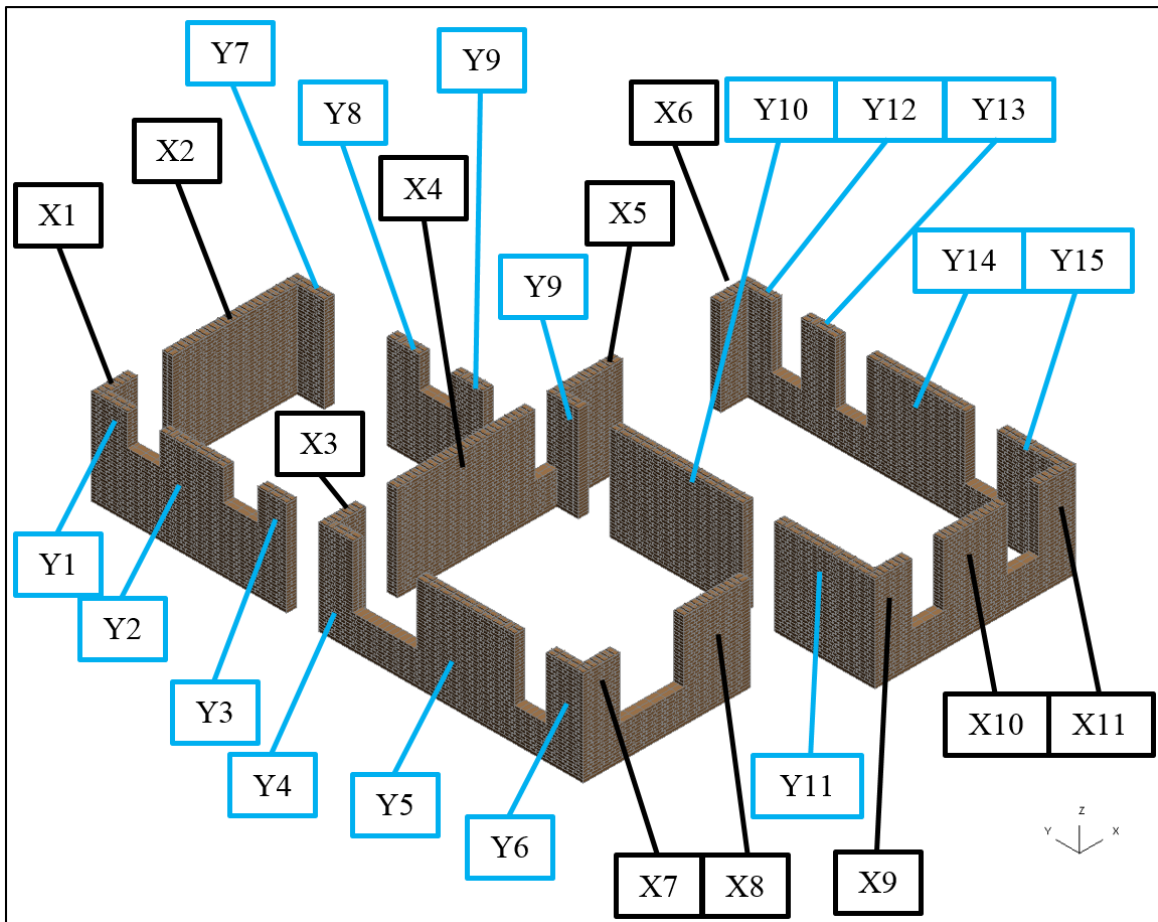


Figure 3.2.1: Pier labelling convention for T3a building

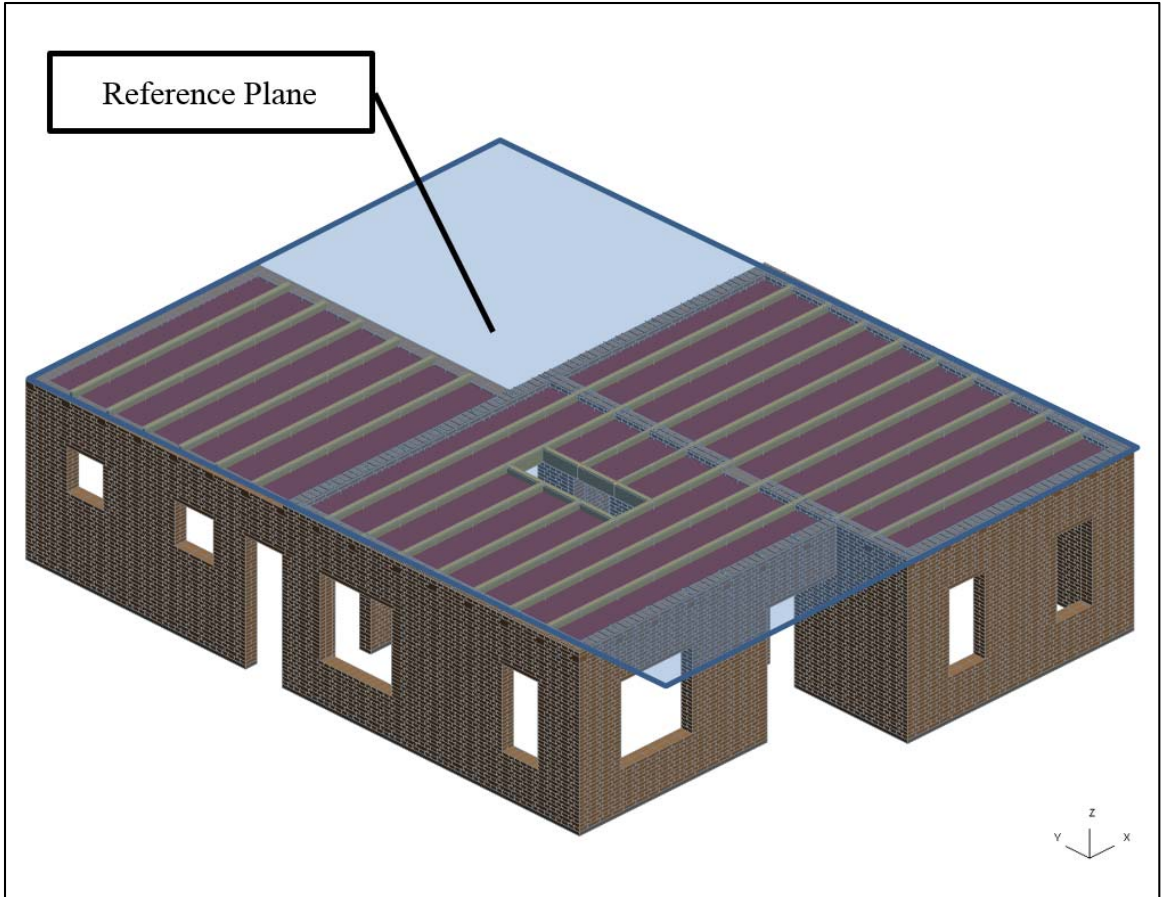


Figure 3.2.2: T3a model pushover reference plane location/height



Figure 3.2.3: FE model for T3a model

3.2.1. Modal analysis

Table 3.2.8: Modal period, frequency, description, mass participation

Mode	Period (s)	Frequency (Hz)	Description of mode	Mass participation %	
				X	Y
1-6	0.1322-0.0962	7.6-10.4	Floor diaphragm/roof out of plane	0.10%	2.49%
7	0.0942	10.6	First lateral X direction sway	7.76%	0.02%
8	0.0927	10.8	Second lateral X direction sway	50.20%	0.40%
9-18	0.0881-0.0753	11.4-13.3	Floor diaphragm/roof out of plane	2.80%	1.76%
19	0.0745	13.4	First lateral Y direction sway	0.43%	4.85%
20	0.0718	13.9	Roof out of plane	0.57%	0.28%
21	0.0709	14.1	Floor diaphragm out of plane	0.00%	0.00%
22	0.0677	14.8	Second lateral Y direction sway	0.37%	22.17%
23	0.0673	14.9	Floor diaphragm and roof out of plane	0.09%	1.80%
24	0.0665	15.0	Third lateral Y direction sway	0.12%	11.16%
25	0.0664	15.1	Fourth lateral Y direction sway	0.22%	18.37%

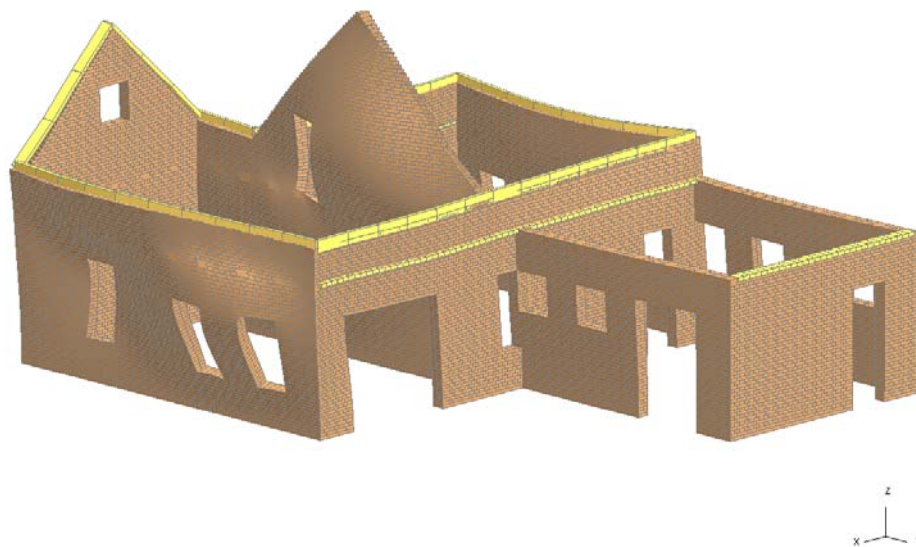


Figure 3.2.4: First lateral mode shape (X direction)

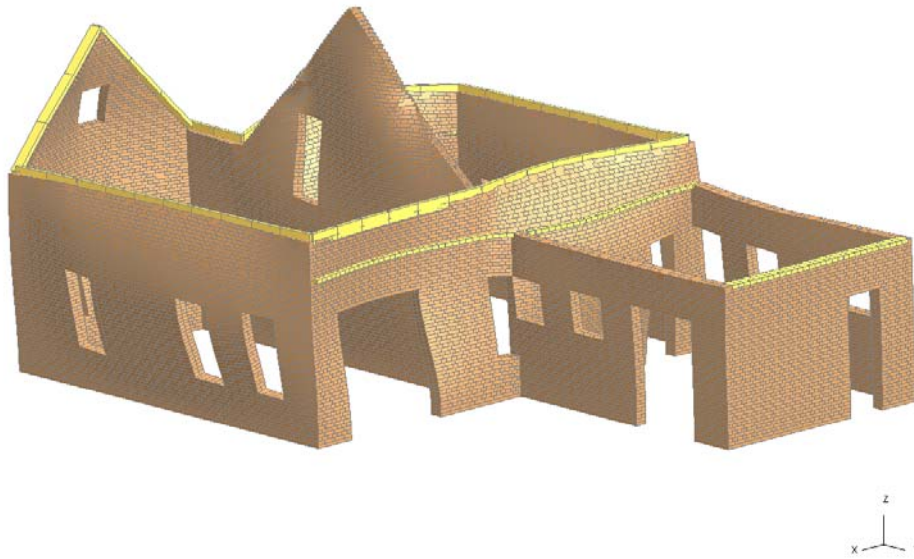


Figure 3.2.5: First lateral mode shape (Y direction)

3.2.2. Pushover analysis (monotonic and cyclic)

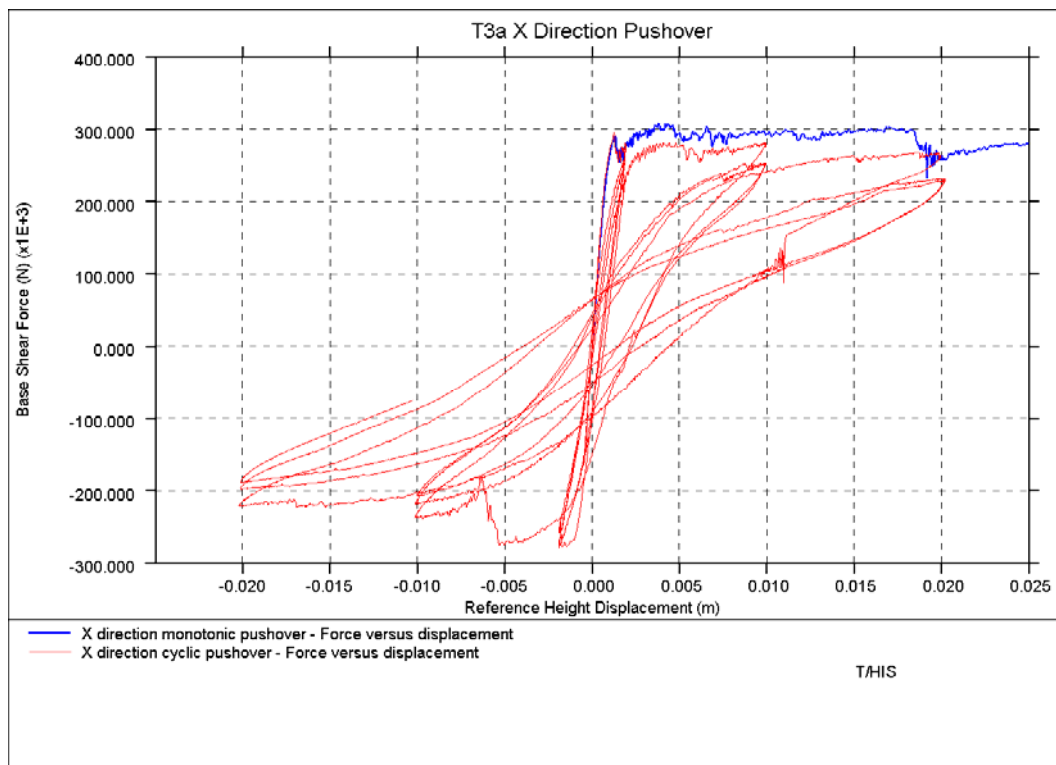


Figure 3.2.6: X direction base shear versus average reference height displacement (monotonic and cyclic)

Table 3.2.9: Cut-plane pier forces at peak/plateau x-dir pushover base shear

Pier	X-dir pier force (kN) Cut-plane height ~1.4 m	
	Axial	Shear
X1	-1.5	3.0
X2	-28.2	41.9
X3	-48.2	18.3
X4	-7.9	14.7
X5	-86.9	53.3
X6	-61.4	24.9
X7	-9.9	3.4
X8	-68.6	44.4
X9	-10.9	6.1
X10	-52.4	38.6
X11	-42.2	20.9
Y1	7.5	0.3
Y2	-13.4	1.5
Y3	-0.4	1.1
Y4	-12.0	1.1
Y5	-28.8	2.7
Y6	0.9	1.0
Y7	-17.2	0.7
Y8	-9.9	1.4
Y9	-5.0	0.9
Y10	-67.2	7.2
Y11	-20.5	6.4
Y12	-9.9	2.0
Y13	-8.7	1.6
Y14	-35.9	3.9
Y15	-18.5	2.4
Y16	-7.0	2.3
Total	-664.2	306.4

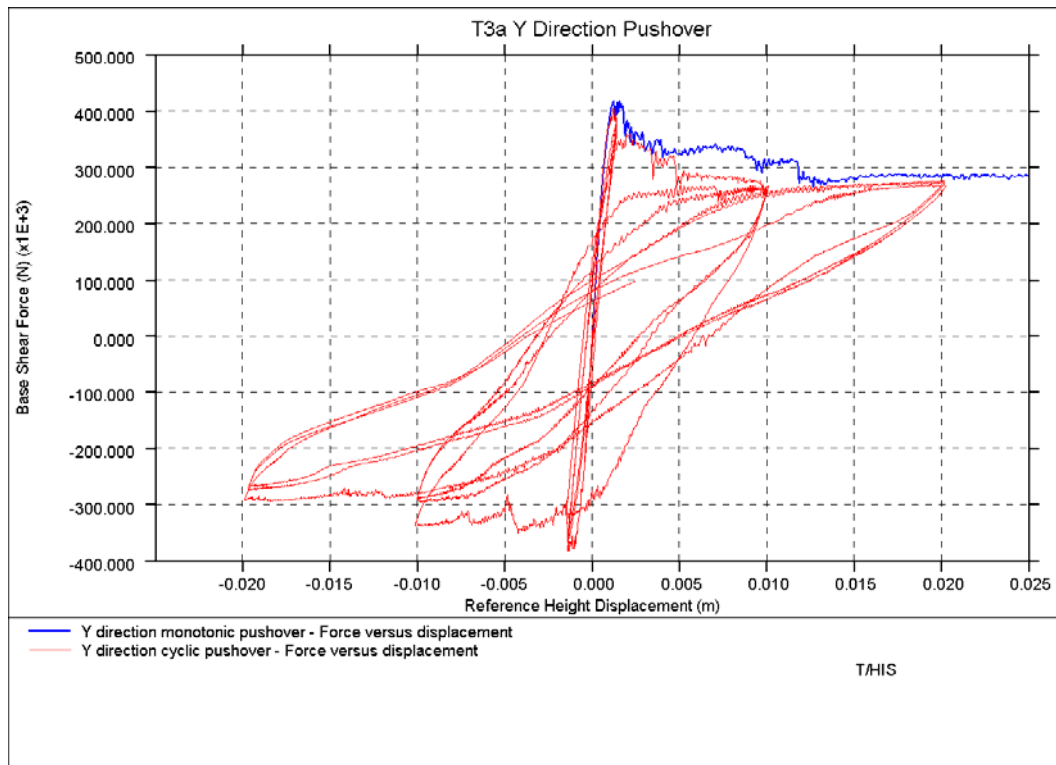


Figure 3.2.7: Y direction base shear versus average reference height displacement (monotonic and cyclic)

Table 3.2.10: Cut-plane pier forces at peak/plateau y-dir pushover base shear

Pier	Y-dir pier force (kN) Cut-plane height ~1.4 m	
	Axial	Shear
X1	-9.5	1.3
X2	-18.3	3.3
X3	-8.7	1.6
X4	-42.0	10.7
X5	-27.2	3.6
X6	-27.1	2.4
X7	-1.0	1.4
X8	-40.9	2.9
X9	-6.2	0.97
X10	-5.9	2.1
X11	3.6	1.3
Y1	-14.97	15.0
Y2	-0.1	-0.3
Y3	-5.8	5.45
Y4	-23.7	10.1
Y5	-60.1	59.8
Y6	-7.9	3.6

Pier	Y-dir pier force (kN) Cut-plane height ~1.4 m	
	Axial	Shear
Y7	-15.2	9.5
Y8	-10.1	6.2
Y9	-5.6	0.7
Y10	-107.6	91.7
Y11	-47.5	51.4
Y12	-30.5	9.5
Y13	-28.4	12.8
Y14	-54.1	55.4
Y15	-16.4	21.1
Y16	-32.9	15.5
Total	-644.0	398.99

3.2.3. Time history analysis

Table 3.2.11: Peak average reference height displacement (3 records at each PGA level)

PGA	RECORD 3		RECORD 6		RECORD 7	
	X direction	Y direction	X direction	Y direction	X direction	Y direction
0.1g	0.7 mm	0.4 mm	0.6 mm	0.3 mm	0.6 mm	0.3 mm
0.25g	1.9 mm	0.7 mm	2.2 mm	0.8 mm	1.7 mm	0.8 mm
0.5g	21.0 mm	8.1 mm	9.3 mm	5.0 mm	12.1 mm	5.6 mm

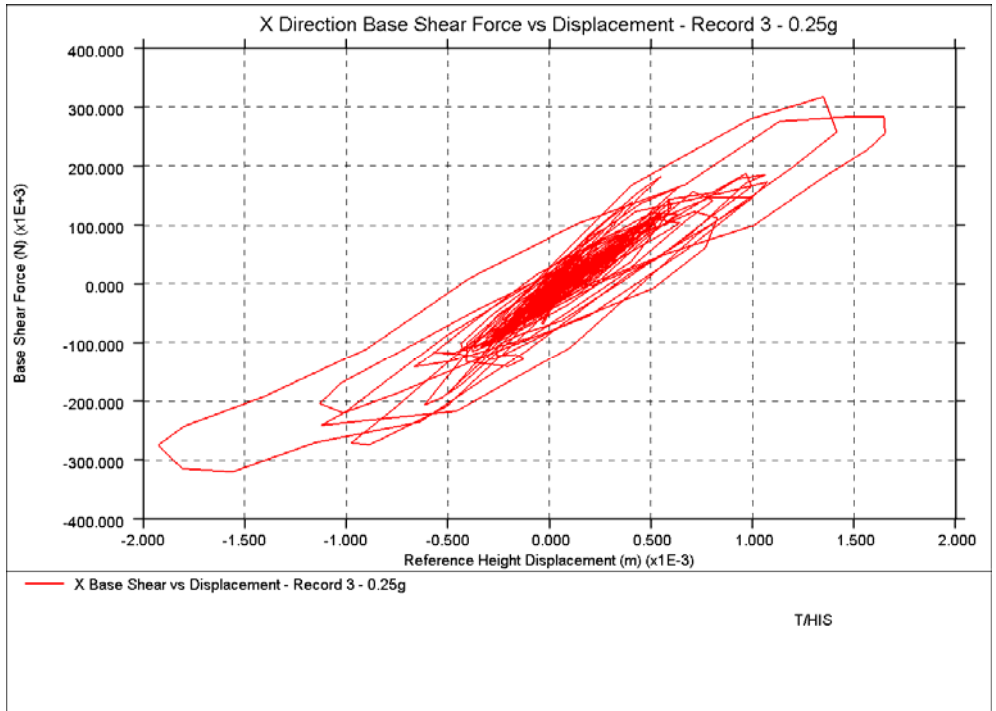


Figure 3.2.8: Base shear versus average reference height displacement – 0.25g scaled PGA, record 3, X direction

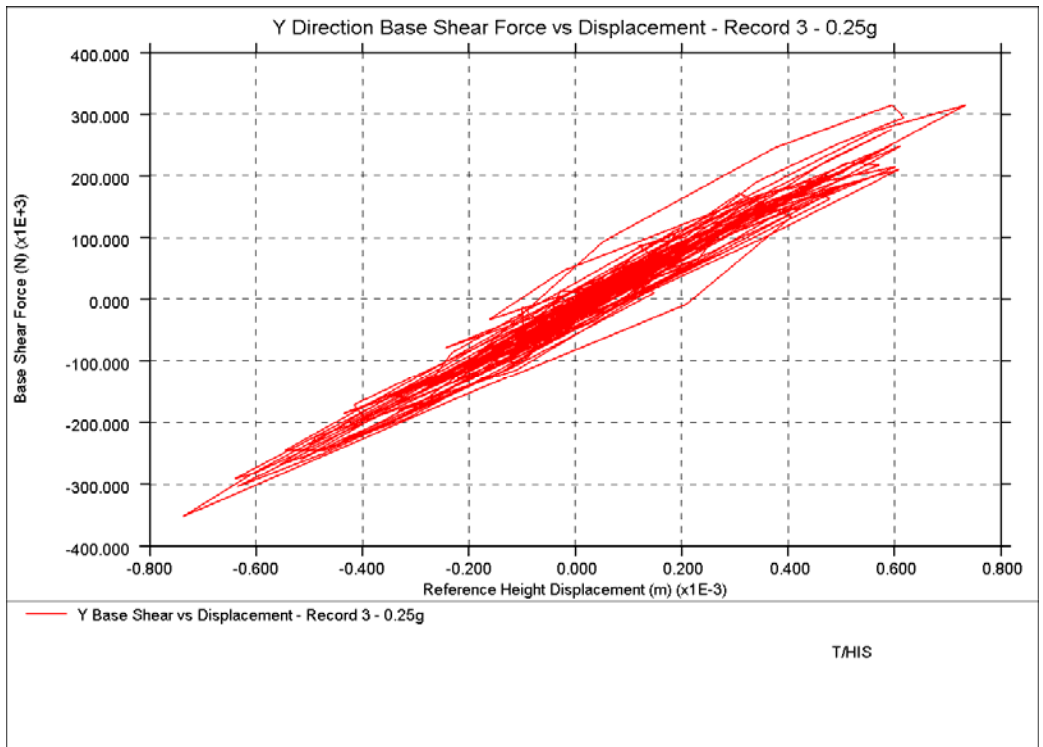


Figure 3.2.9: Base shear versus average reference height displacement – 0.25g scaled PGA, record 3, Y direction

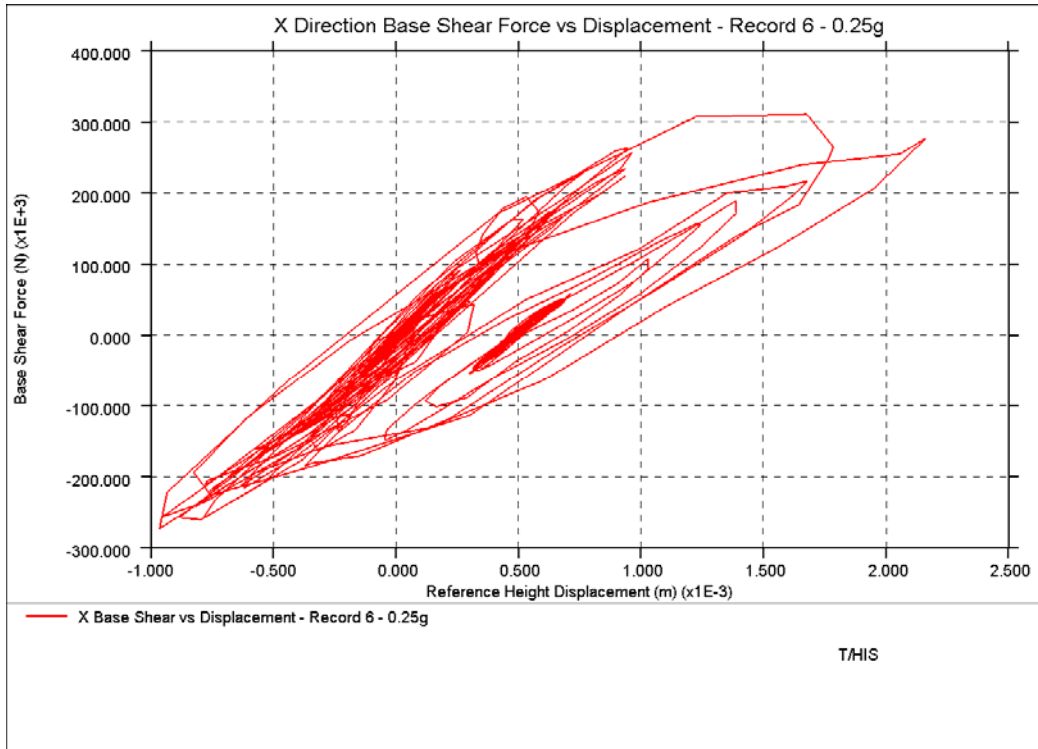


Figure 3.2.10: Base shear versus average reference height displacement – 0.25g scaled PGA, record 6, X direction

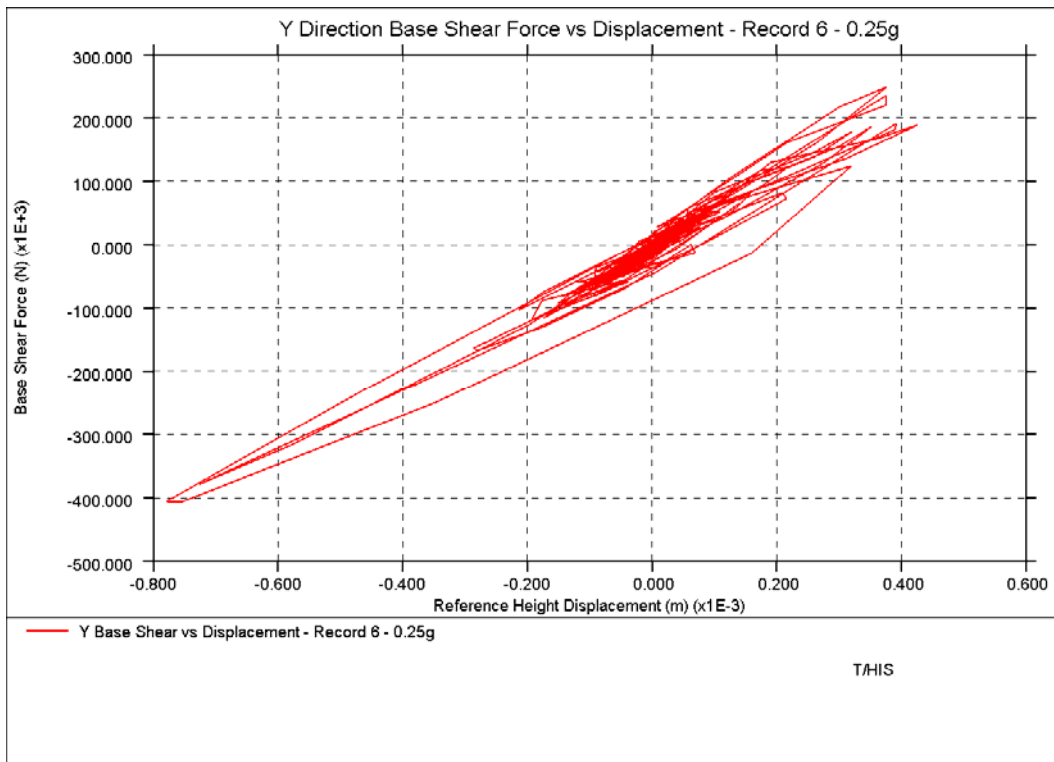


Figure 3.2.11: Base shear versus average reference height displacement – 0.25g scaled PGA, record 6, Y direction

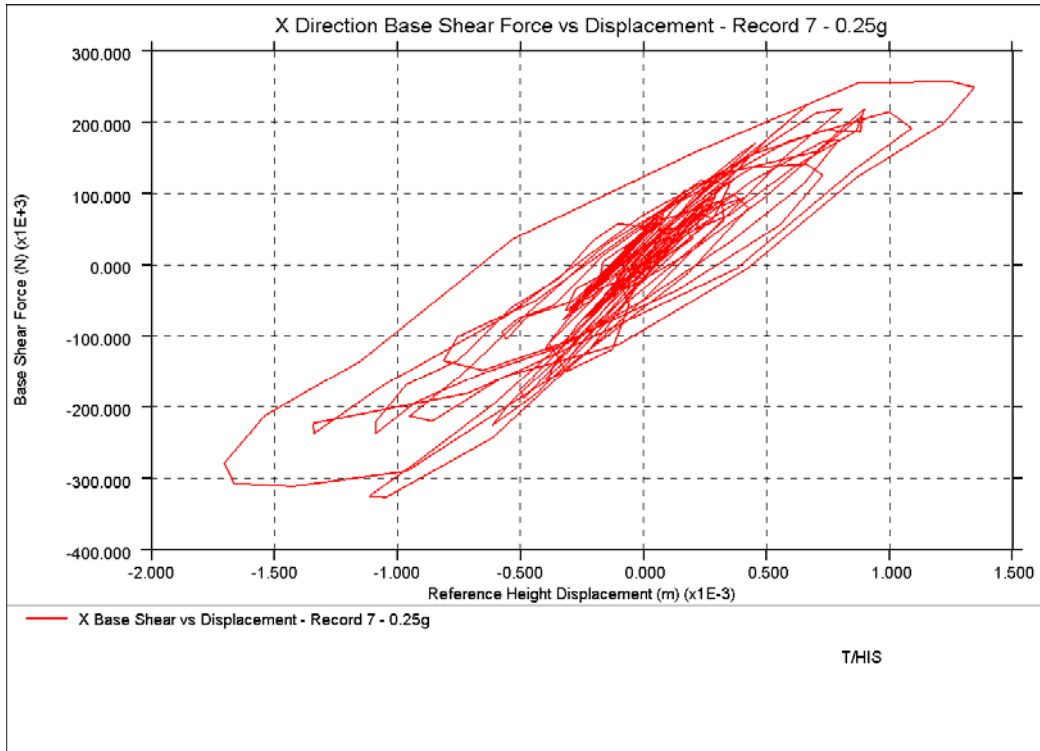


Figure 3.2.12: Base shear versus average reference height displacement – 0.25g scaled PGA, record 7, X direction

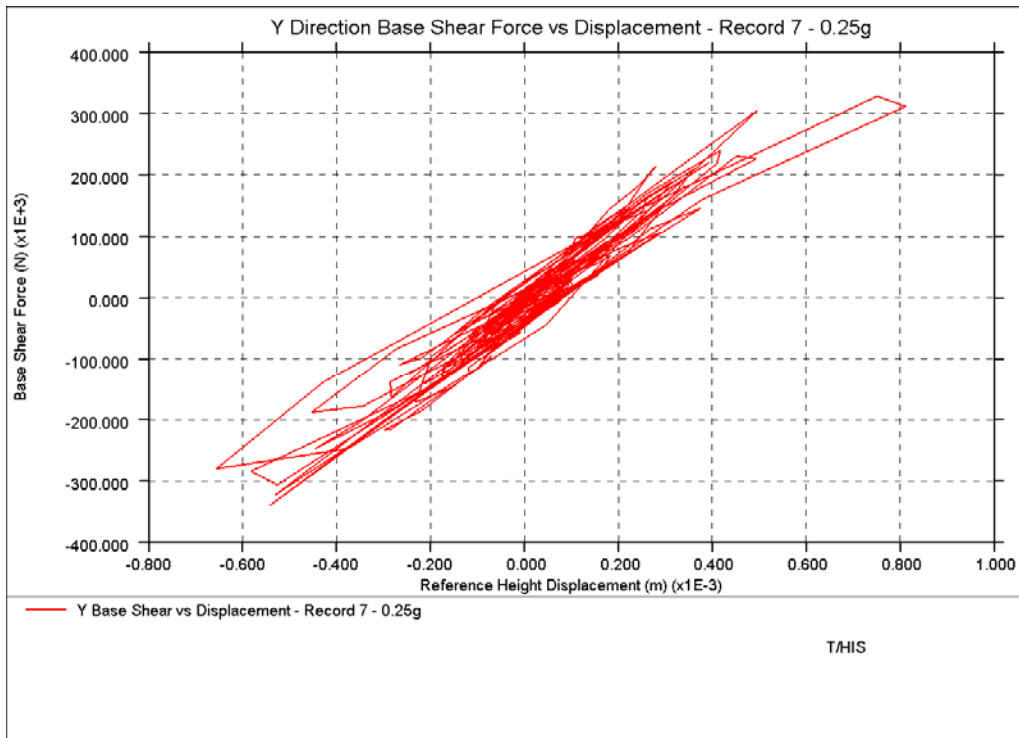


Figure 3.2.13: Base shear versus average reference height displacement – 0.25g scaled PGA, record 7, Y direction

3.2.4. Discussion and sensitivity analyses

A sensitivity study was performed where the eigenvalue analysis was repeated with the uncracked 100% Young's Modulus (4410 MPa).

Table 3.2.4.1: Modal period, frequency, description, mass participation – x-direction

X-dir	Mode No.	Period (s)	Freq (Hz)	Participating mass %	Participating mass (tonne)
Uncracked	14	0.078	12.9	23.3	20.5
Uncracked	21	0.070	14.3	19.6	17.3
Cracked (50% E)	7	0.094	10.6	7.8	6.8
Cracked (50% E)	8	0.093	10.8	50.2	44.2

Table 3.2.4.2: Modal period, frequency, description, mass participation – y-direction

Y-dir	Mode No.	Period (s)	Freq (Hz)	Participating mass %	Participating mass (tonne)
Uncracked	36	0.054	18.4	30.6	27.0
Cracked (50% E)	22	0.068	14.8	22.2	19.5

The sensitivity of the monotonic and cyclic pushover analyses of T3a to adjusted spandrel stiffness was studied. The results are presented here.

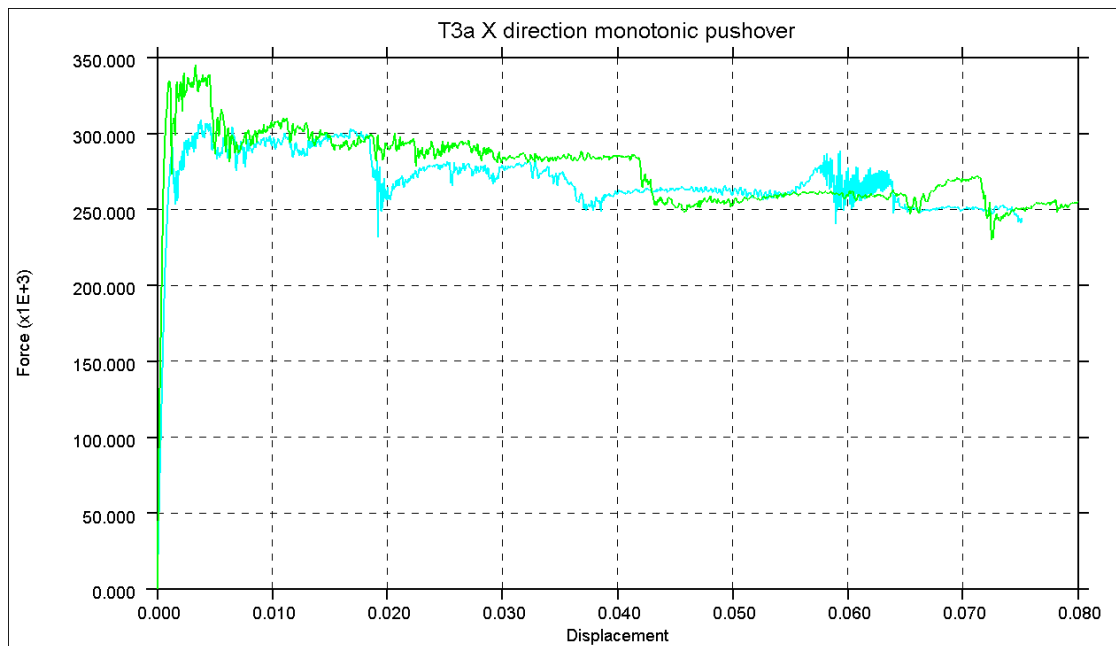


Figure 3.2.4.1: X-direction base shear versus average reference height displacement. The original model in cyan and the adjusted spandrel stiffness model in green.

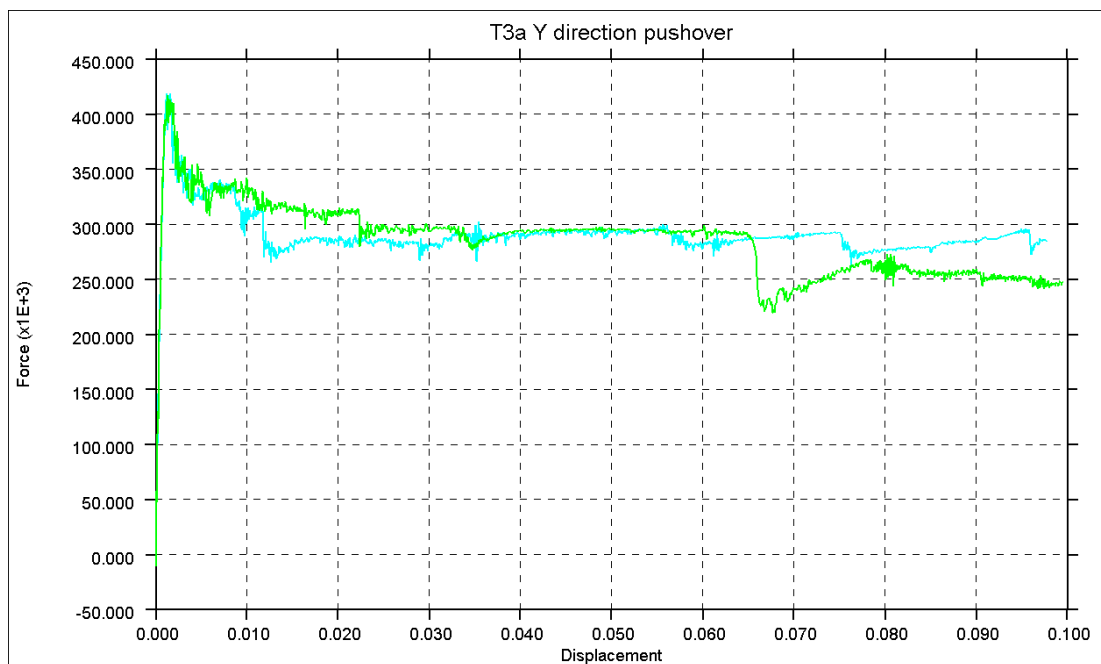


Figure 3.2.4.2: Y-direction base shear versus average reference height displacement. The original model in cyan and the adjusted spandrel stiffness model in green.

In another sensitivity study, the monotonic pushover analysis was repeated with 50% reduced headjoint tensile strength, as per suggestion by EUCENTRE.

The reduced headjoint tensile strength did not have a significant effect on the analysis output, as shown in the following figures.

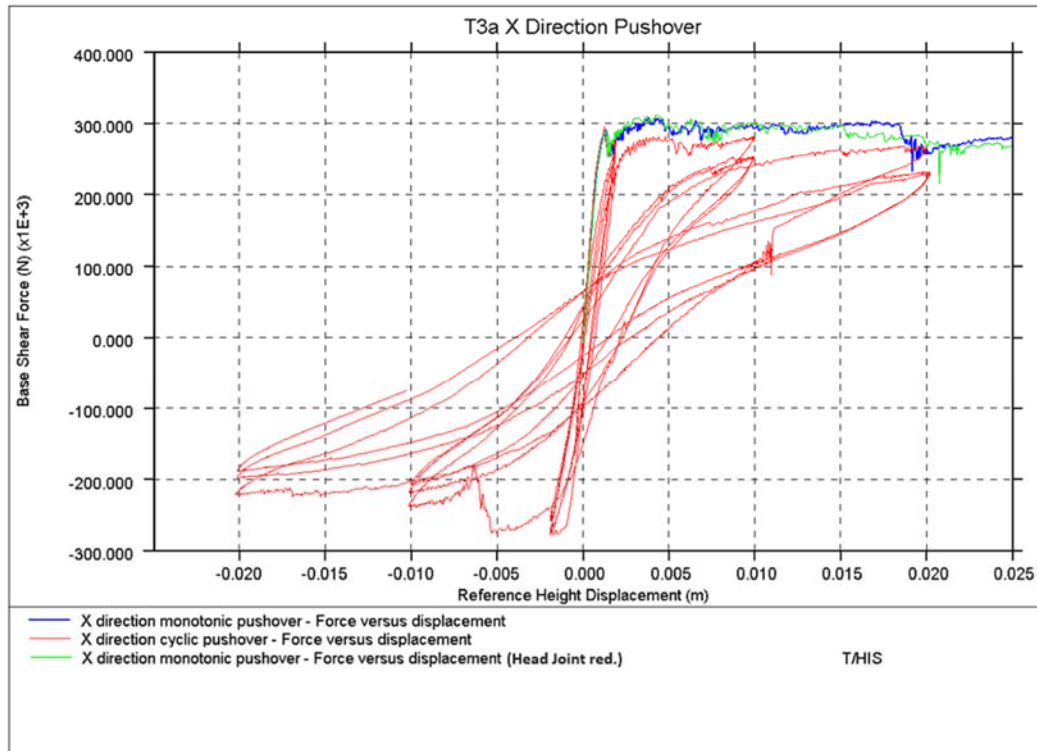


Figure 3.2.4.3: X-direction base shear versus average reference height displacement

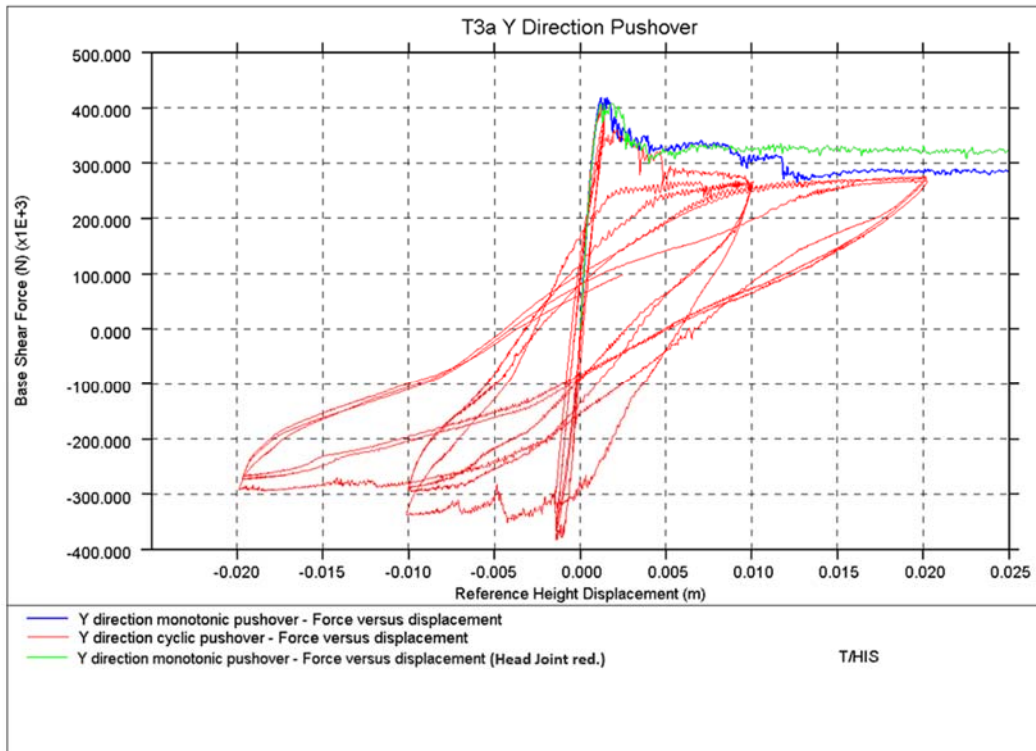


Figure 3.2.4.4: Y-direction base shear versus average reference height displacement

In order to estimate the initial elastic stiffness of the models, linear elastic “pushover” analyses (scaled linearly up to 1g acceleration) were conducted for each index building in each direction. The linear elastic “pushover” was performed on the original nonlinear model used for the pushover (with modal force distribution), with relevant modifications and elastic material definitions from the eigenvalue analysis.

As shown in the following figures, the linear elastic “pushover” initial stiffness is higher than that for the nonlinear pushover, due to the differences in the modelling of the masonry stiffness – the linear elastic model has the masonry Young’s modulus directly applied to the material model; whereas the nonlinear model contains the combined stiffness of MAT_WINFRITH Young’s modulus and penalty stiffness of the tiebreak contacts for the mortar modelling.

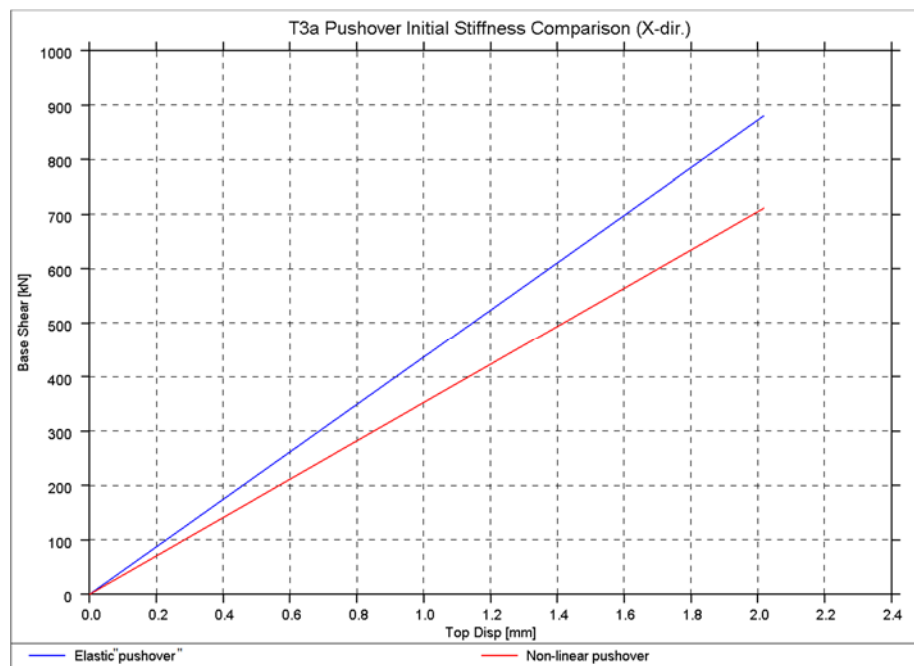


Figure 3.2.4.5: T3a initial stiffness (x-direction)

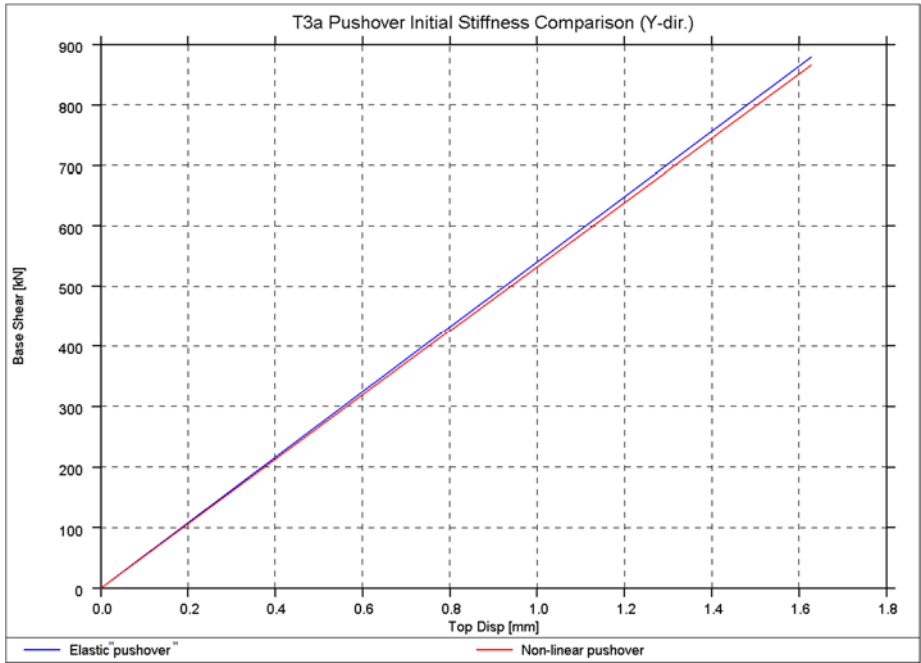


Figure 3.2.4.6: T3a initial stiffness (y-direction)

4. Shell Modelling – Summary of modelling approach

A development material model, suitable for modelling masonry using shell element was developed part way through the initial scope of this report. The results from this model are reproduced in the following sections.

Table 4.1: General modelling notes

Component	Description
Analysis team	Arup
Analysis software and formulation	LS-DYNA – Explicit time integration scheme and eigensolver are used for different analyses.
Overview of modelling approach	<ul style="list-style-type: none"> • For nonlinear pushover and response history analysis, an explicit time integration scheme was used. • For eigenvalue analysis, the Block Shift and Invert Lanczos eigensolver was used. • Masonry modelled with fully integrated shell elements where damage is smeared across each element and crack plane directions are pre-defined to model mortar bonds • Shell elements, beam elements, and discrete (spring) elements are used to model other components of the benchmark and cross-validation tests. • Material properties and bond parameters are defined based on the available test data for masonry – both brick and mortar – characterisation tests, using a consistent methodology across all benchmarks and index buildings models.
Model units	SI units (kg, m, sec)

Table 4.2: Model properties applicable for all benchmark tests and index buildings

Input	Description
Element formulation	Fully integrated shell elements with nine through-thickness integration points
Shell material type	MAT_SHELL_MASONRY. For more guidance refer to Volume 1 Appendix C
Damping	DAMPING_PART_STIFFNESS, with damping coefficient 0.05, for numerical stability without affecting primary behaviours DAMPING_FREQUENCY_RANGE_DEFORM, with damping coefficient 0.01 for frequency range 1–30 Hz.

5. Experimental benchmarks

5.1. Ispra in-plane panel tests

Table 5.1.1: Modelling notes

Component	Description
Analysis software and formulation	LS-DYNA – explicit analysis solver
Walls (in-plane)	Masonry modelled with shell elements with damage smeared across each element using nonlinear MAT_SHELL_MASONRY material model. Crack plane directions are pre-defined to model mortar bonds.

Table 5.1.2: Nonlinear time history analysis notes

Nonlinear time history analysis notes
<ul style="list-style-type: none"> • 1% damping applied using proprietary LS-DYNA constant damping model over 1-30 Hz frequency range. • Additional damping applied at very high frequencies for numerical stability.

Table 5.1.3: Model loading, materials and general comments

Loading	
Dead load	Self-weight of clay brick walls
Overburden	Constant 150 kN applied load (including self-weight of steel beam in test setup)
Materials	Material properties including values and stress strain behaviour
2D Shell Masonry	Nonlinear masonry material model $\rho = 1652 \text{ kg/m}^3$ $E = 1491 \text{ MPa}$ $\nu = 0.15$ $f_c = 6.2 \text{ MPa}$ $f_t = 0.04 \text{ MPa}$ (tensile stress limit of mortar joints) $f_s = 0.23 \text{ MPa}$ (shear stress limit of mortar joints) $G_t = 10 \text{ N/m}$ (Mortar joint tensile energy rate) $G_s = 23 \text{ N/m}$ (Mortar joint shear energy rate) Friction coefficient = 0.58 $F_{sd} = 0.23 \text{ MPa}$ (diagonal tension strength) $G_{sd} = 2300 \text{ N/m}$ (diagonal tension energy release rate)
Other key notes	
4) Test data displacement history is applied as a velocity sinusoidal input prescribed motion. 5) Top nodes of wall form a rigid body that is free to translate in-plane and vertically. This maintains a constant overburden throughout the test.	

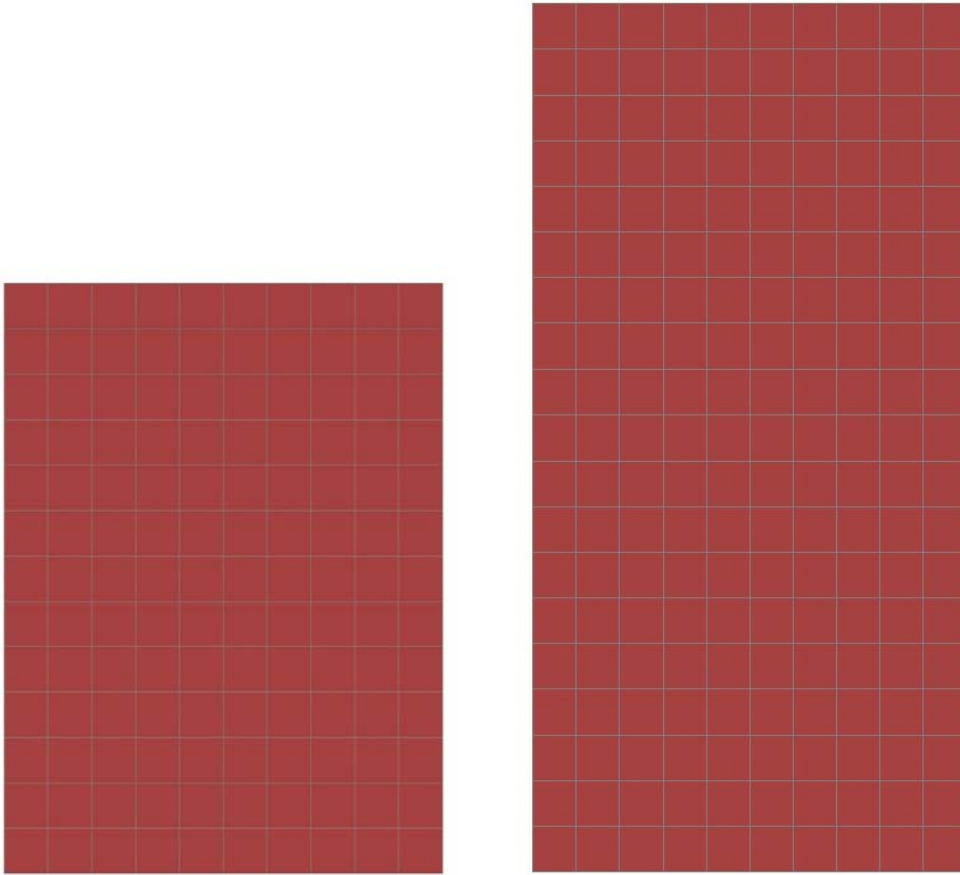


Figure 5.1.1: LS-DYNA shell models for LOWSTA (left) and HIGSTA1 (right)

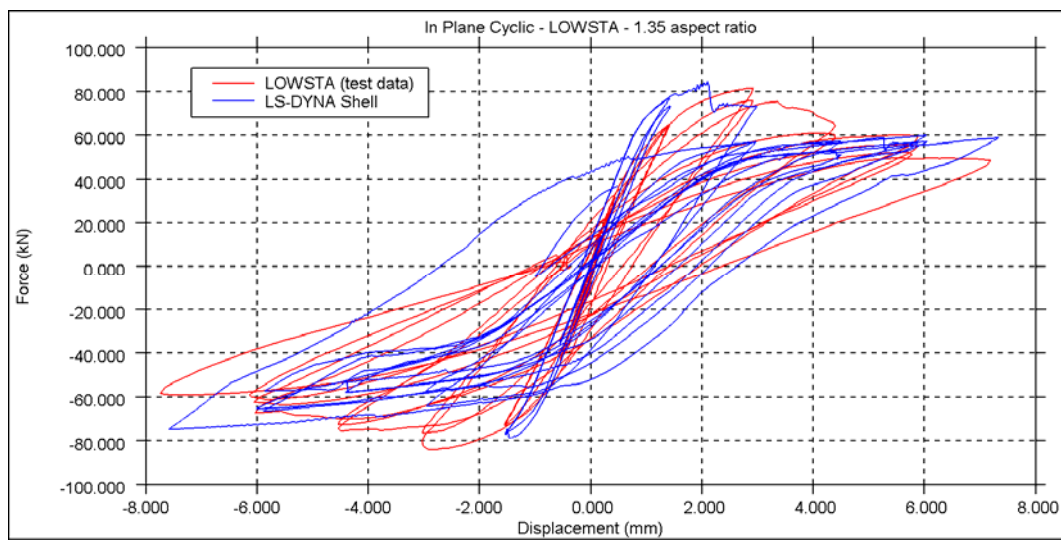


Figure 5.1.2: Shear force-displacement comparison plot for LOWSTA

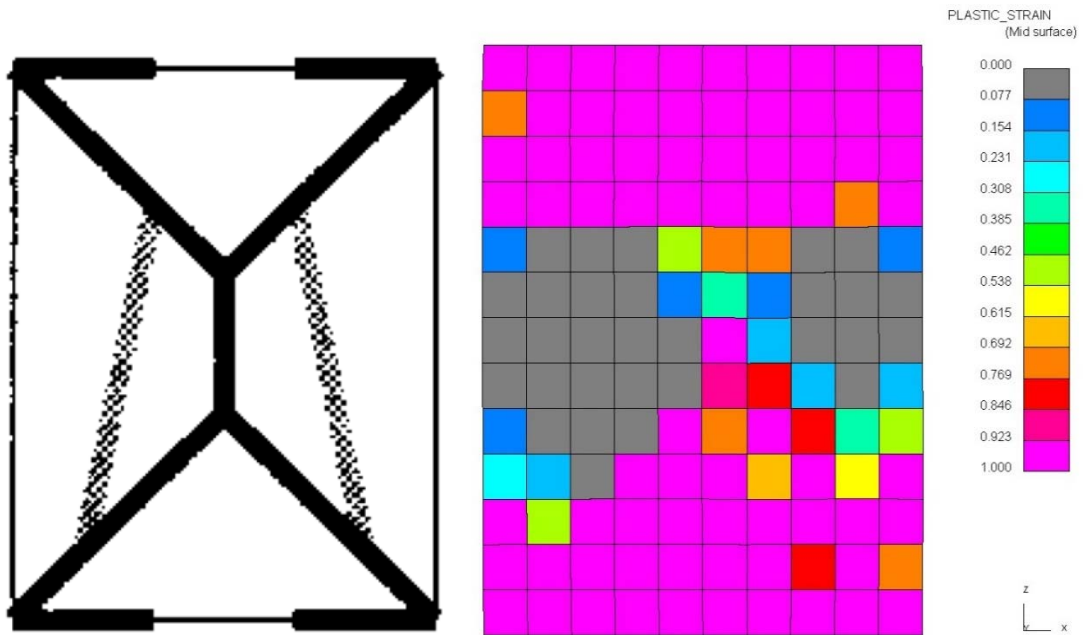


Figure 5.1.3: Final damage plot for LOWSTA – comparison between test and LS-DYNA

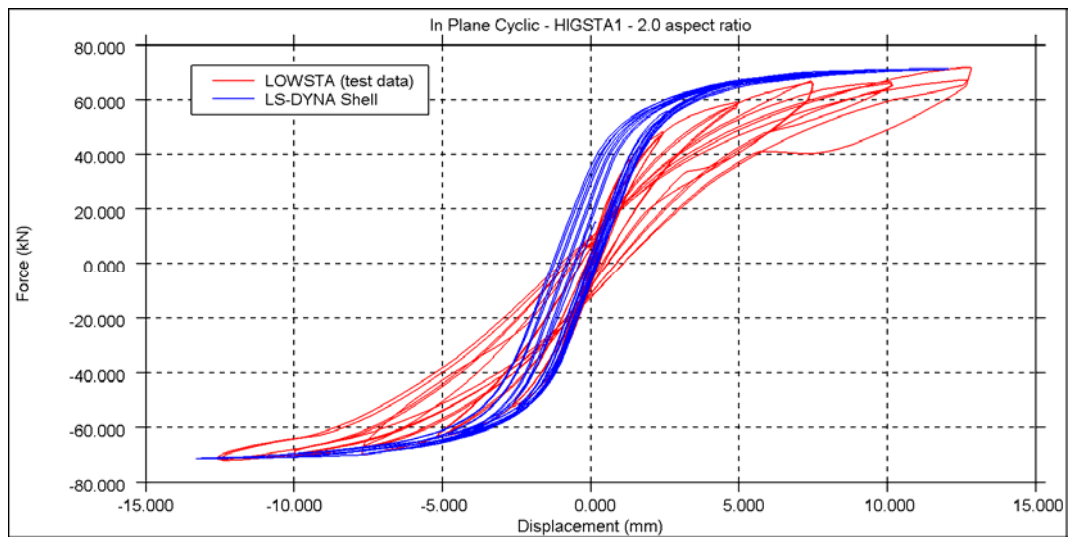


Figure 5.1.4: Shear force-displacement comparison plot for HIGSTA1

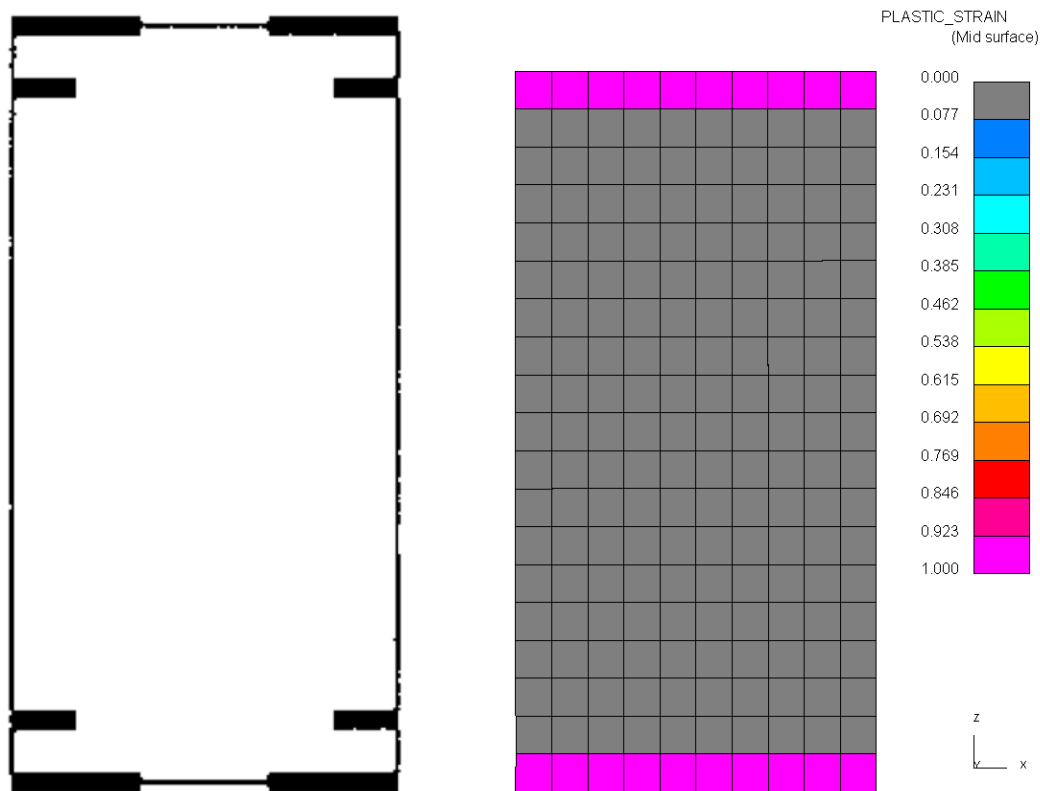


Figure 5.1.5: Final damage plot for HIGSTA1 – comparison between test and LS-DYNA

5.1.1. Discussion

For the LOWSTA panel, the results of the analysis show fairly good correlation to the test in terms of both damage plot and force-displacement response. The damage plot shows a diagonal tension sliding brittle failure mode, similar to the laboratory observations, although the damage plot appears to be slightly less symmetrical than the experimental results. The analysis force-displacement output shows an ultimate load of 86 kN, which is very close to the laboratory value of 84 kN, at a drift of 2%. The test shows both modest strength degradation and reduction of stiffness during the larger cycles, i.e. above 2.5 mm amplitude. The analysis predicts similar strength degradation as well as some reduction in stiffness.

For the HIGSTA1 panel, the results of the analysis also show good correlation to the test in terms of both damage plot and force-displacement response. The damage plot shows a rocking failure mode with cracks forming along the top and bottom of the panel. The analysis force-displacement output shows an ultimate load of 71 kN, which is very close to the laboratory value of 72 kN, at a drift of 0.6%. The hysteresis of the test specimen shows some reduction in stiffness and energy dissipation as the amplitude increases. The analysis displays hysteresis with less energy dissipation and less reduction in stiffness at larger amplitudes, consistent with almost pure ‘rigid body’ rocking.

5.2.Pavia full building tests

Table 5.2.1: Modelling notes

Component	Description
Analysis software and formulation	LS-DYNA – explicit analysis solver
Walls (in-plane)	Masonry modelled with shell elements with damage smeared across each element using nonlinear MAT_SHELL_MASONRY material model. Crack plane directions are pre-defined to model mortar bonds.
Walls (out-of-plane)	As above.
Spandrels/lintels and wall coupling	Spandrels are modelled using the same approach as the walls. Lintels modelled with MAT_SHELL_MASONRY with increased joint strength in the vertical direction to account for pre-compression and highly increased joint strength in the horizontal direction since the bricks in the lintel were constructed without horizontal joints.
Wall to wall connection (incl. flange effects)	Merged nodes
Wall to diaphragm connection	Nodes of steel beam elements representing the diaphragm merged with encountering wall nodes.

Table 5.2.2: Nonlinear time history analysis notes

Nonlinear time history analysis notes
<ul style="list-style-type: none"> • 1% damping applied using proprietary LS-DYNA constant damping model over 1–30 Hz frequency range. • Additional damping applied at very high frequencies for numerical stability. • To minimise dynamic effects, the loading is applied on each floor as a prescribed velocity. A maximum velocity magnitude of 15 mm/s is used for the LS-DYNA analysis. The velocities are applied to the constraints at the locations of the flexible diaphragms on each wall.

Table 5.2.3: Model loading, materials and general comments

Loading	
Dead load	Self-weight of clay brick walls
Applied load	265 kN on the first floor 265 kN on the second floor (This is equivalent to approximately 10 kN/m ² on each floor)
Materials	
2D Shell Masonry	Nonlinear masonry material model $\rho = 1652 \text{ kg/m}^3$ $E = 1494 \text{ MPa}$ $G = 224 \text{ MPa}$ $\nu = 0.15$ $f_y = 6.2 \text{ MPa}$ $f_t = 0.04 \text{ MPa}$ (tensile stress limit of mortar joints) $f_s = 0.23 \text{ MPa}$ (shear stress limit of mortar joints) $G_t = 10 \text{ N/m}$ (Mortar joint tensile energy rate) $G_s = 23 \text{ N/m}$ (Mortar joint shear energy rate) Friction coefficient = 0.58 $F_{sd} = 0.23 \text{ MPa}$ (diagonal tension strength) $G_{sd} = 2300 \text{ N/m}$ (diagonal tension energy release rate)
Steel	Elastic material model $\rho = 370,200 \text{ kg/m}^3$ $E = 200 \text{ GPa}$ $\nu = 0.3$
Other key notes	
8) Flexible diaphragm (steel beams) modelled. Density adjusted in order to represent overburden. 9) Shear and tensile strength of mortar in lintels is increased 10 times in vertical direction and 100 times in horizontal direction versus experimental values to model pre-compression of mortar from construction stage and lack of horizontal joints, respectively. 10) Stiffness of bricks in spandrels is reduced to match masonry E, since loading on spandrels is primarily in the horizontal direction.	

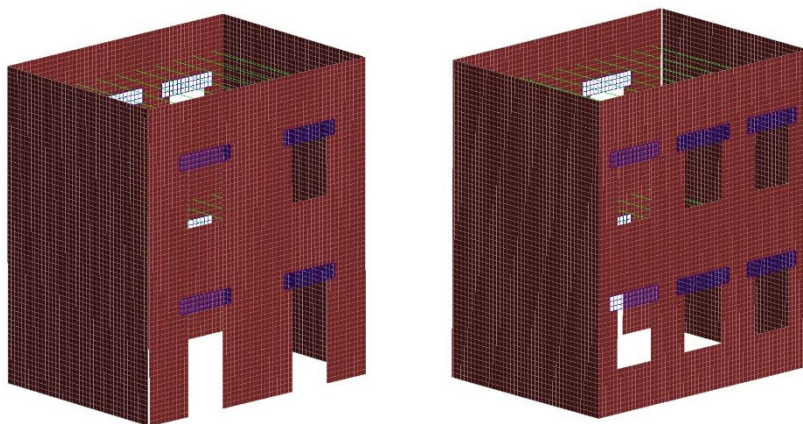


Figure 5.2.1: FE model showing Door Wall (left) and Window Wall (right)

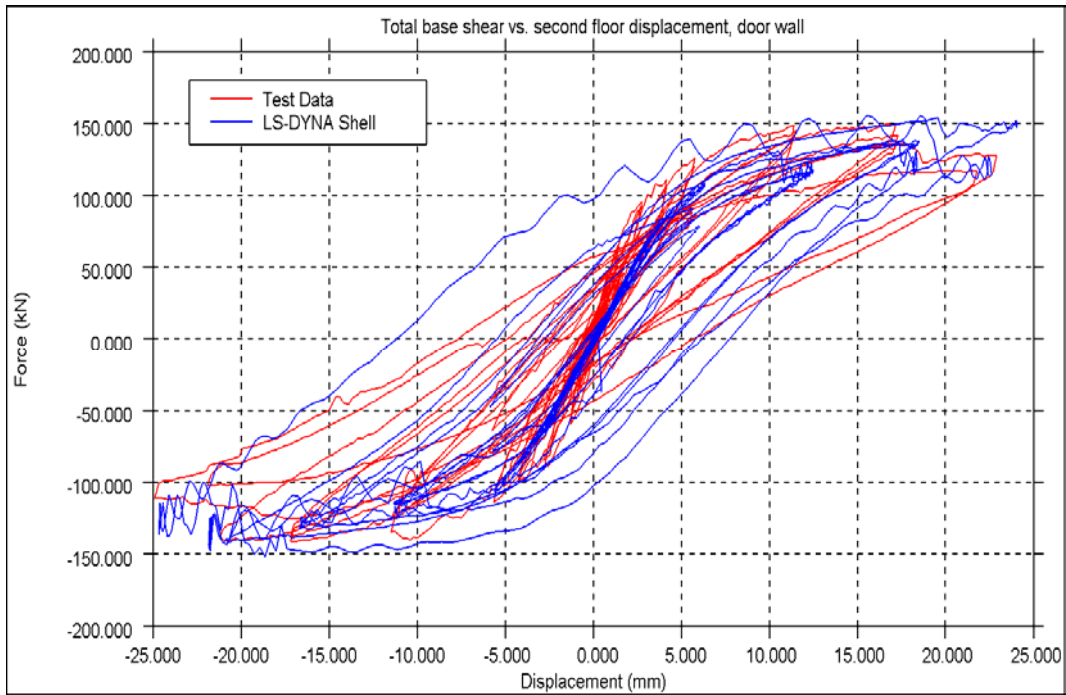


Figure 5.2.2: Total base shear force vs. second floor displacement (Door Wall)

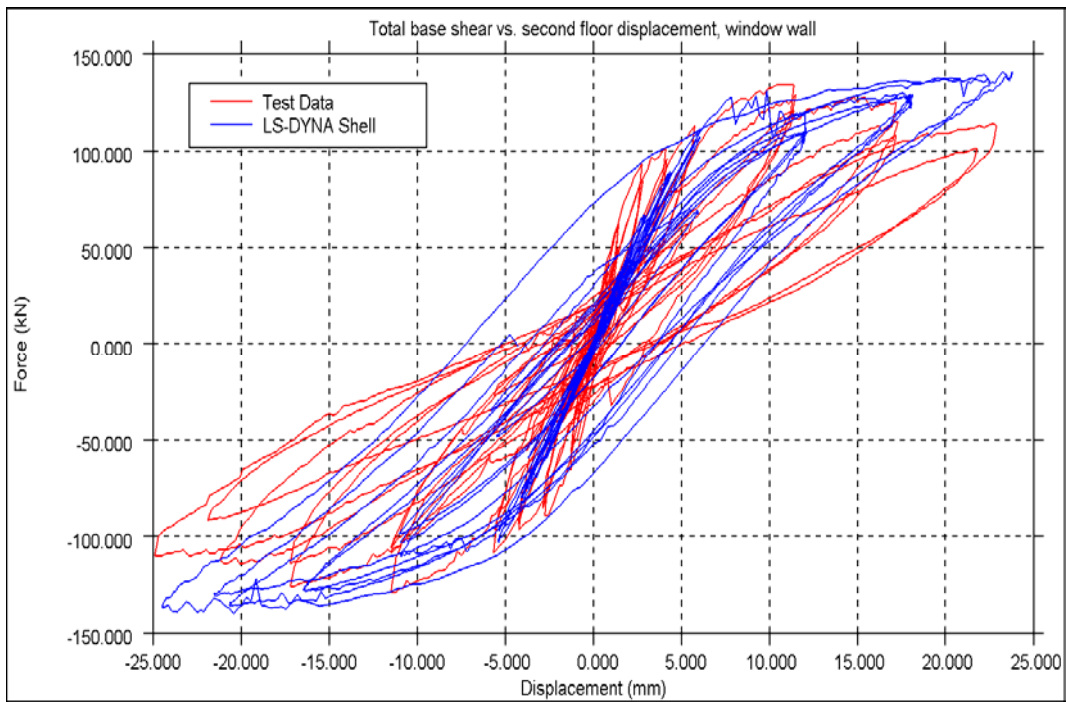


Figure 5.2.3: Total base shear force vs. second floor displacement (Window Wall)

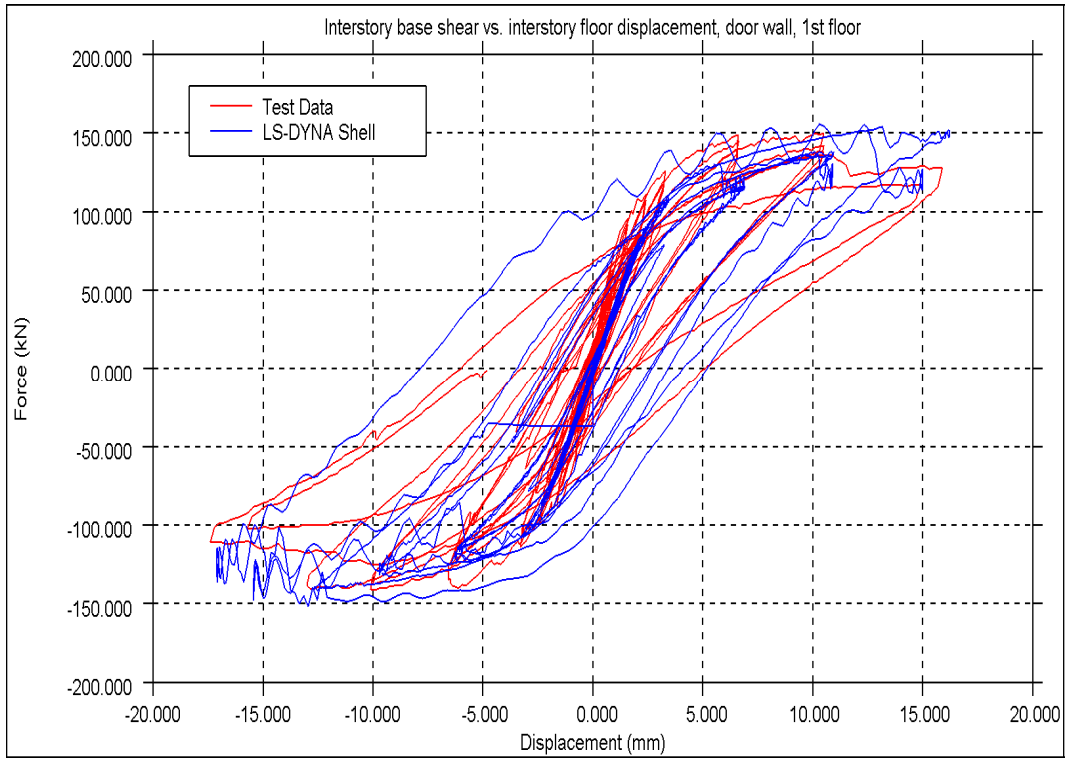


Figure 5.2.4: Interstorey shear force vs. interstorey displacement, 1st floor (Door Wall)

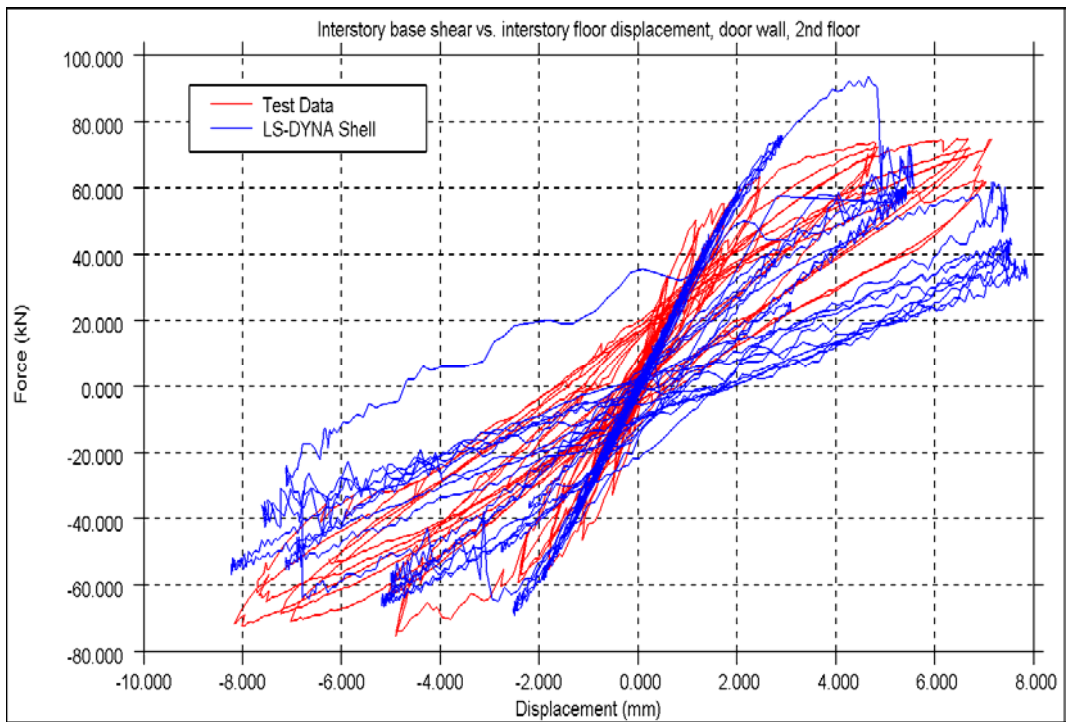


Figure 5.2.5: Interstorey shear force vs. interstorey displacement, 2nd floor (Door Wall)

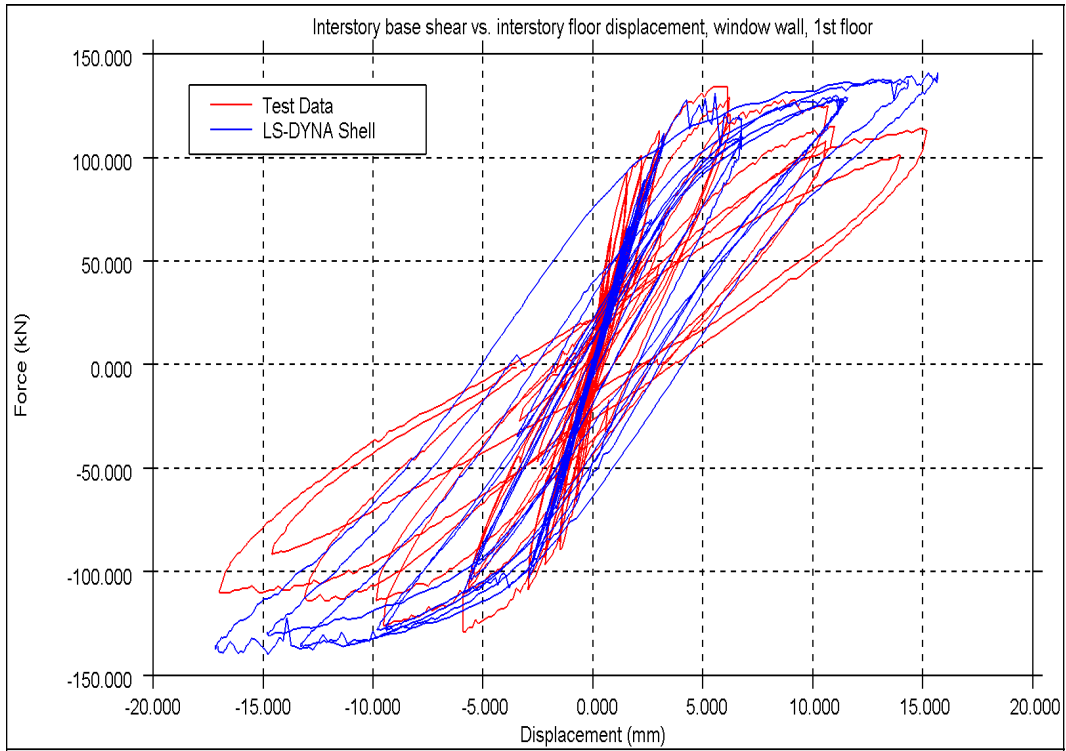


Figure 5.2.6: Interstorey shear force vs. interstorey displacement, 1st floor (Window Wall)

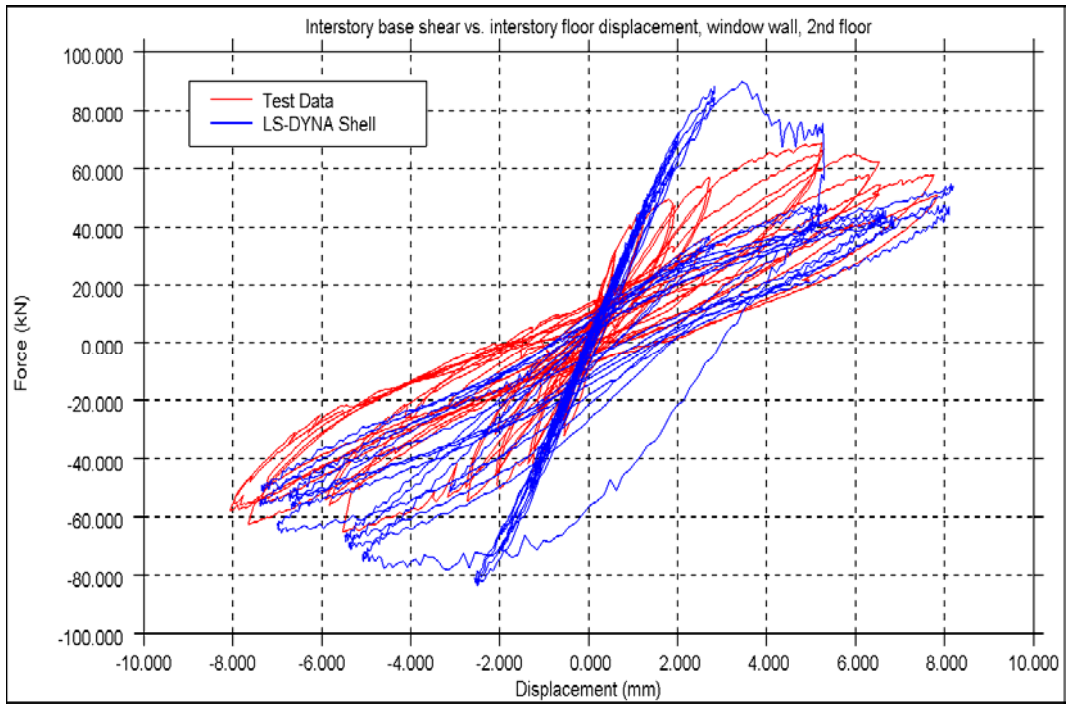


Figure 5.2.7: Interstorey shear force vs. interstorey displacement, 2nd floor (Window Wall)

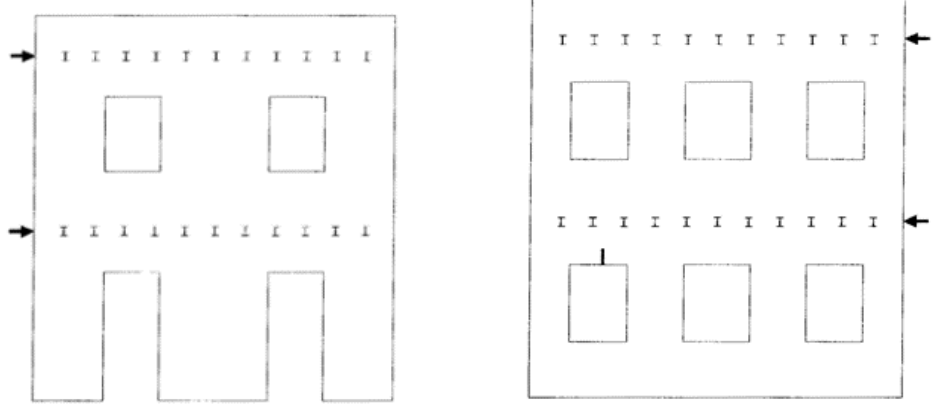
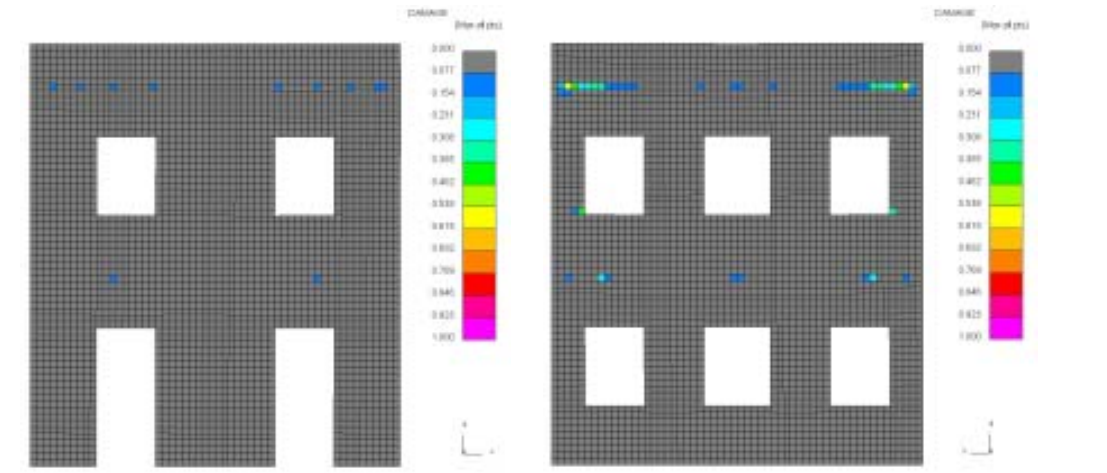


Figure 5.2.8: Damage plot after Run 1 – Door Wall (left) and Window Wall (right). Respective laboratory test results below.

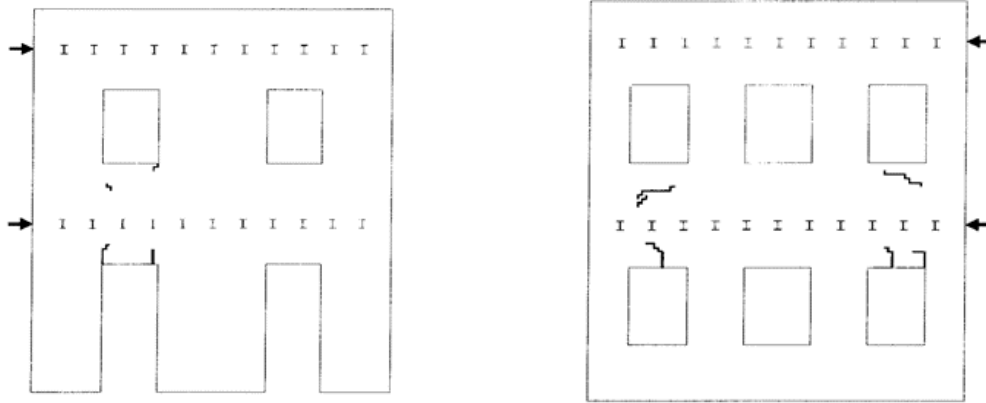
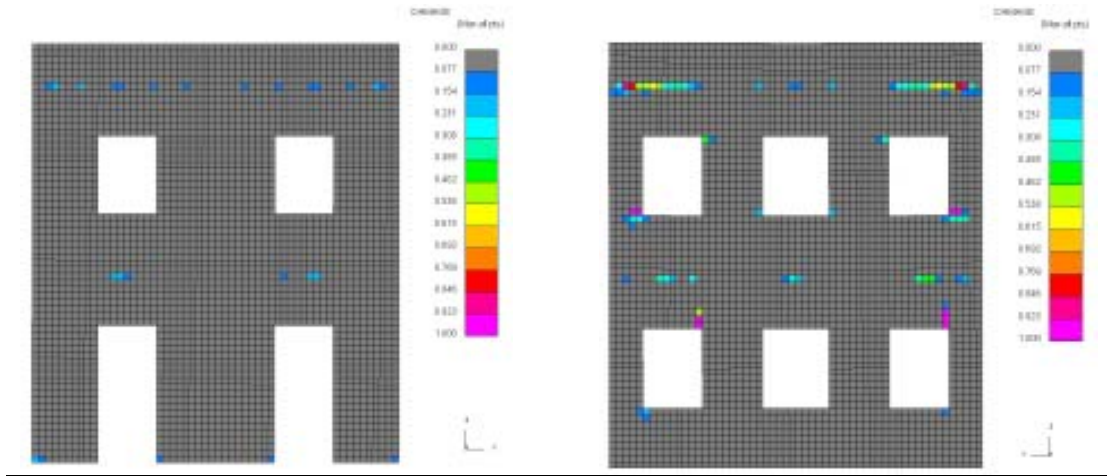


Figure 5.2.9: Damage plot after Run 2 – Door Wall (left) and Window Wall (right). Respective laboratory test results below.

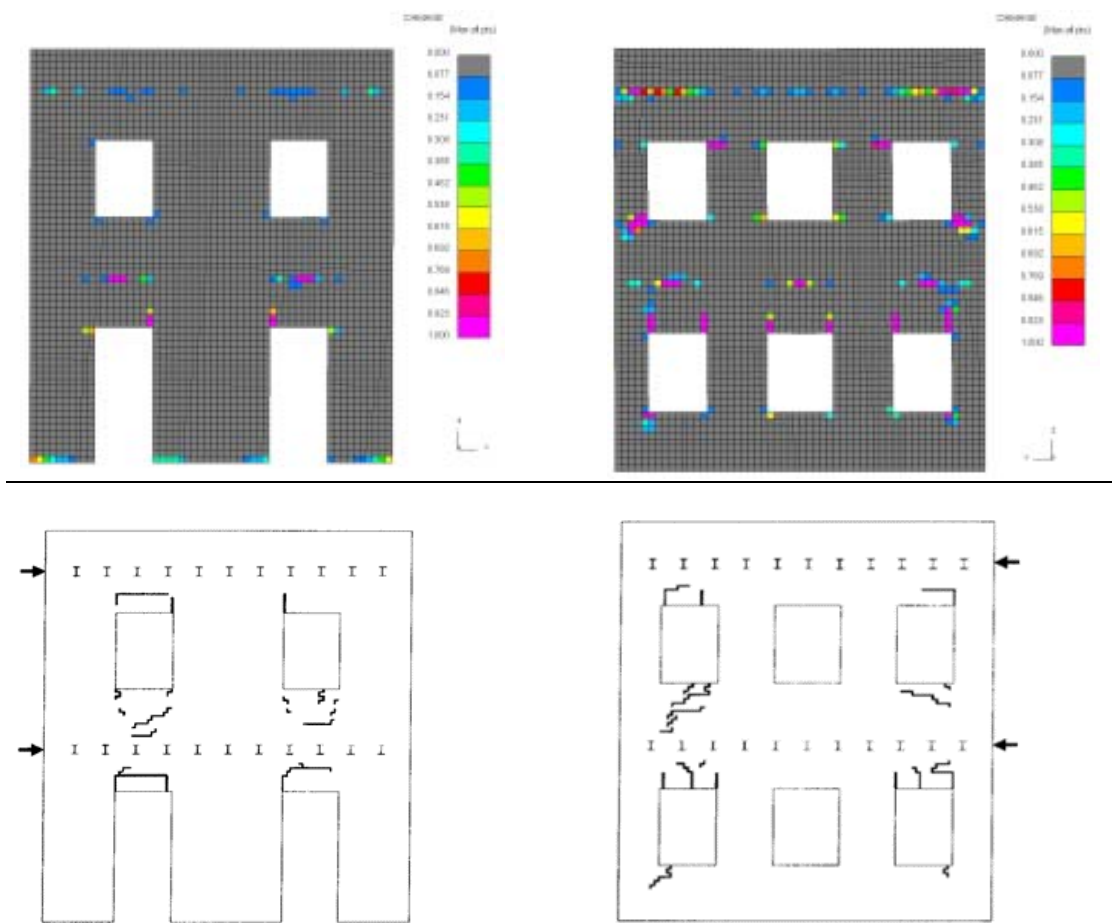


Figure 5.2.10: Damage plot after Run 3 – Door Wall (left) and Window Wall (right). Respective laboratory test results below.

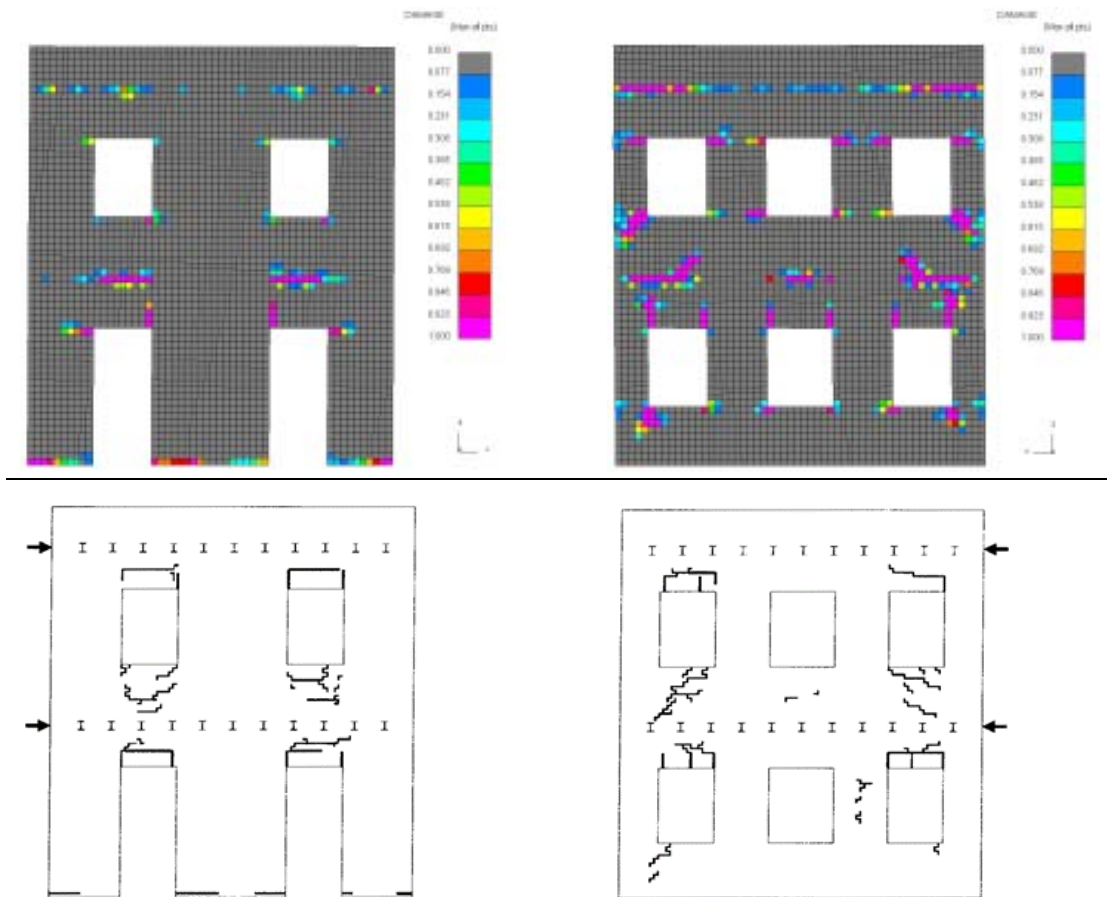


Figure 5.2.11: Damage plot after Run 4 – Door Wall (left) and Window Wall (right). Respective laboratory test results below.

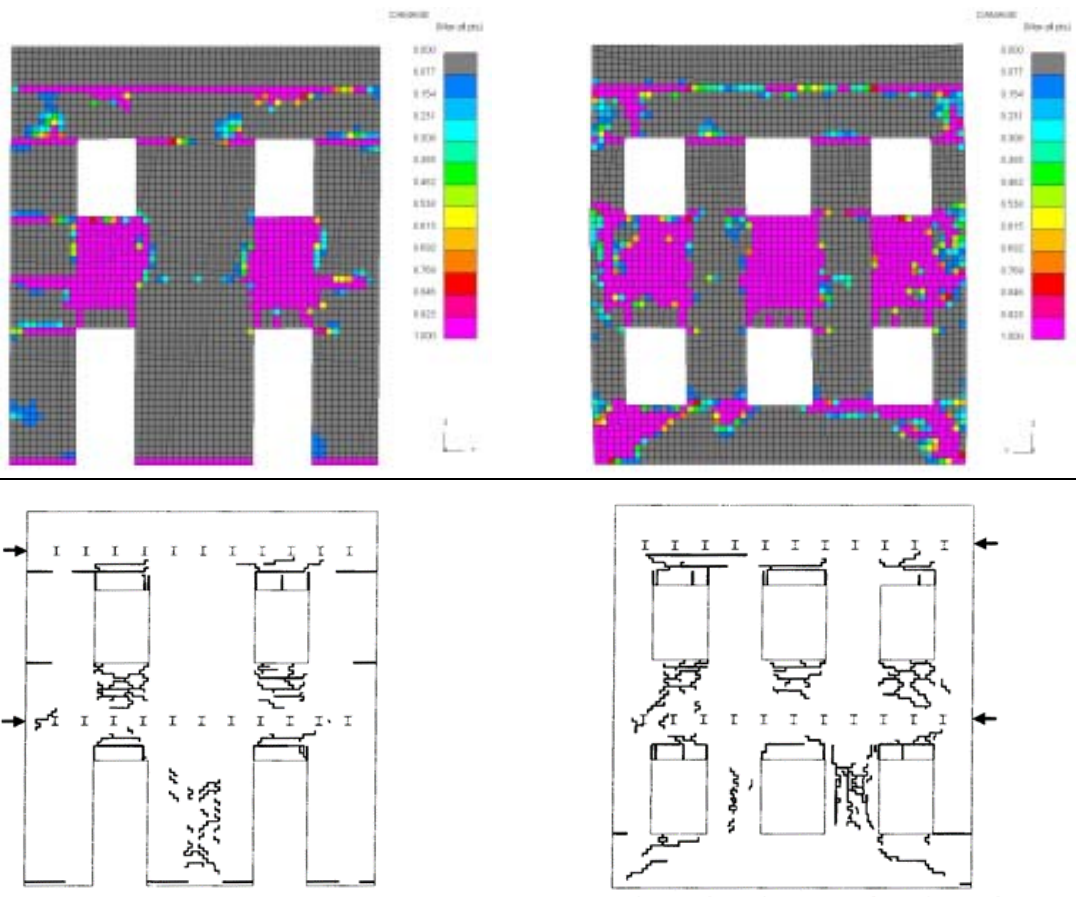


Figure 5.2.12: Damage plot after Run 5 – Door Wall (left) and Window Wall (right). Respective laboratory test results below.

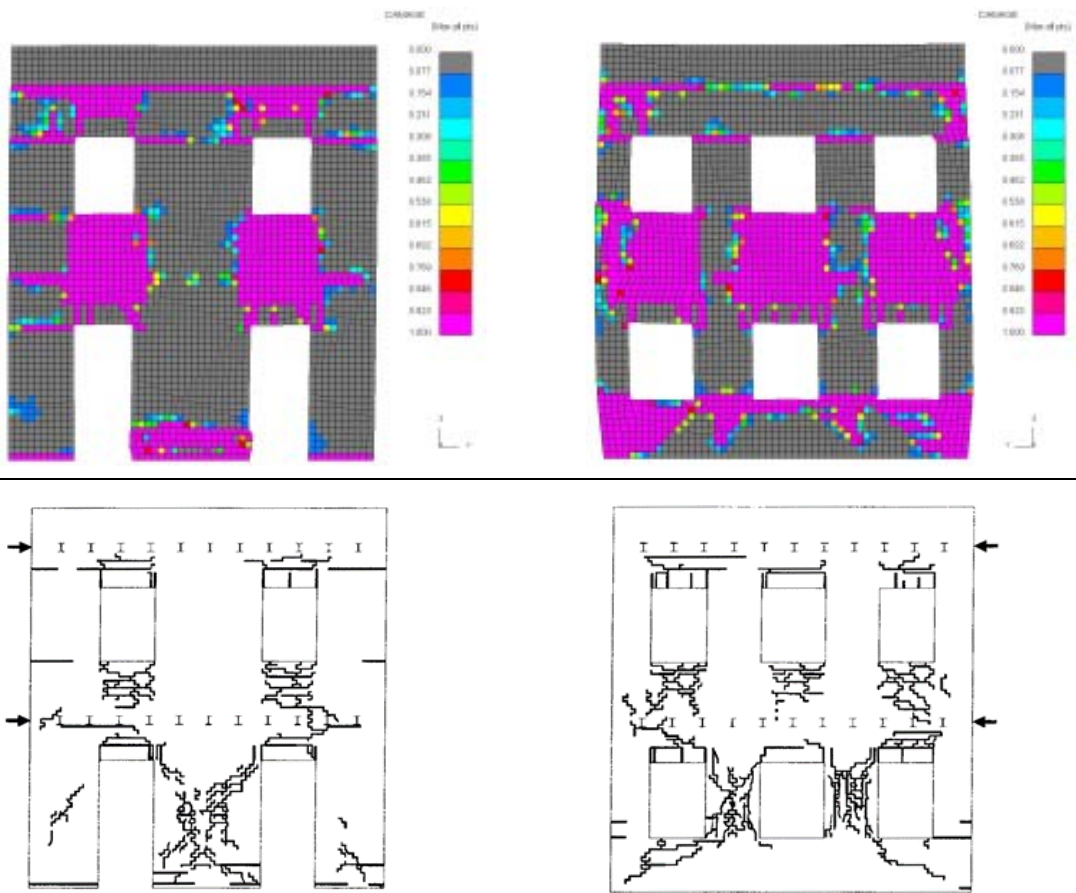


Figure 5.2.13: Damage plot after Run 6 – Door Wall (left) and Window Wall (right). Respective laboratory test results below.

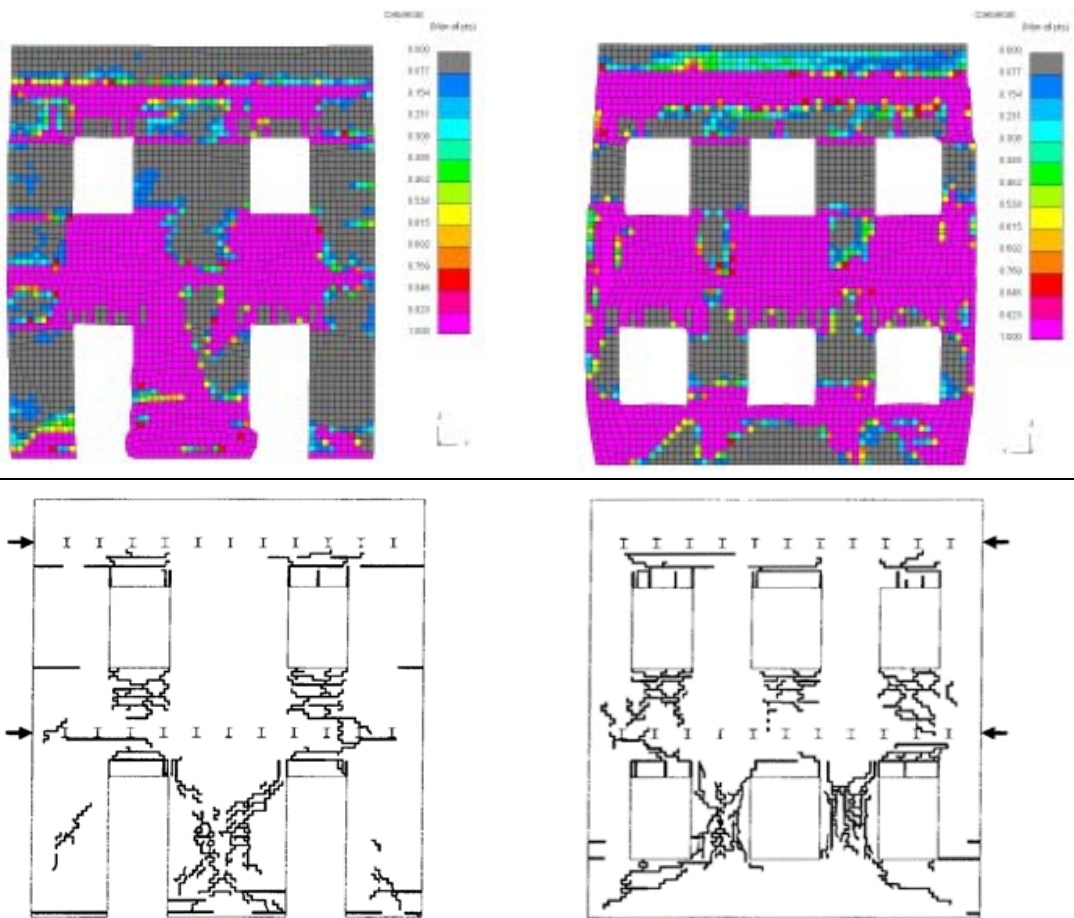


Figure 5.2.14: Damage plot after Run 7 – Door Wall (left) and Window Wall (right). Respective laboratory test results below.

5.2.1. Discussion

The curve comparisons show that the initial stiffness is fairly well captured, although the LS-DYNA shell model is slightly on the stiffer side.

The main discrepancy in the curve comparisons comes generally from a lack of stiffness degradation in the shell model. The slope of the force-displacement curves from the experiment decreases as the displacement cycles increased, whereas the shell model slope stays approximately the same over the last number of cycles. The lack of degradation is also reflected in the larger peak forces resulting from the shell model.

It is clearly observed that the sequence and location of failures is crucial to the final result. In particular, the failure of piers in rocking often causes damage to be concentrated in other parts of the structure, such as the spandrels, which experience heavy damage over the progression of the ground motions. This occurrence eventually produces global results with an excess in strength.

5.3. ESECMaSE calcium silicate in-plane panel tests

Table 5.3.1: Modelling notes

Component	Description
Analysis software and formulation	LS-DYNA – explicit analysis solver
Walls (in-plane)	Masonry modelled with shell elements with damage smeared across each element using nonlinear MAT_SHELL_MASONRY material model. Crack plane directions are pre-defined to model mortar bonds.

Table 5.3.2: Nonlinear time history analysis notes

Nonlinear time history analysis notes
<ul style="list-style-type: none"> 1% damping applied using proprietary LS-DYNA constant damping model over 1-30 Hz frequency range. Additional damping applied at very high frequencies for numerical stability.

Table 5.3.3: Model loading, materials and general comments

Loading	
Dead load	Self-weight of brick wall.
Overburden	<ul style="list-style-type: none"> 0.5 MPa for CS03 (unfilled headjoint). 1.0 MPa for CS05 (filled headjoint).
Materials	Material properties including values and stress strain behaviour
2D Shell Masonry	Nonlinear masonry material model $\rho = 1800 \text{ kg/m}^3$ $E = 7560 \text{ MPa}$ $\nu = 0.112$ $f_c = 24 \text{ MPa}$ $f_t = 0.24 \text{ MPa}$ (tensile stress limit of mortar joints) $f_s = 0.245 \text{ MPa}$ (shear stress limit of mortar joints) $G_t = 10 \text{ N/m}$ (Mortar joint tensile energy rate) $G_s = 24.5 \text{ N/m}$ (Mortar joint shear energy rate) Friction coefficient = 0.677
Other key notes	
3) Shear displacement measurements from test data is approximated as harmonic input and applied to analysis model as prescribed motion, with peak velocity magnitude capped at 2 mm/s. 4) Top nodes of wall form a rigid body that is free to translate in-plane and vertically. This maintains a constant overburden throughout the test.	

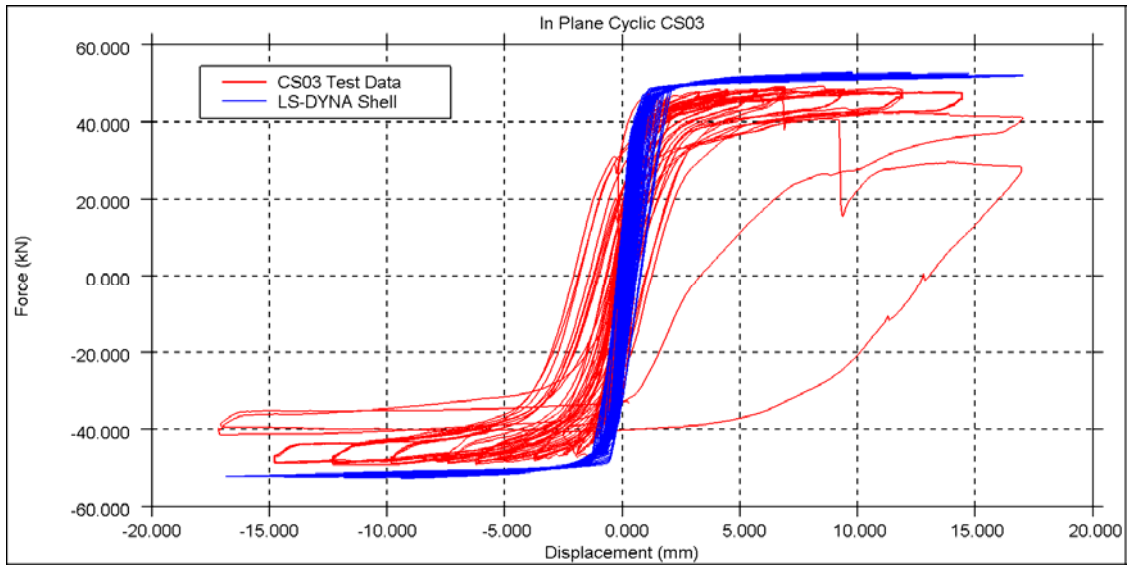


Figure 5.3.1: Shear force-displacement comparison plot for CS03

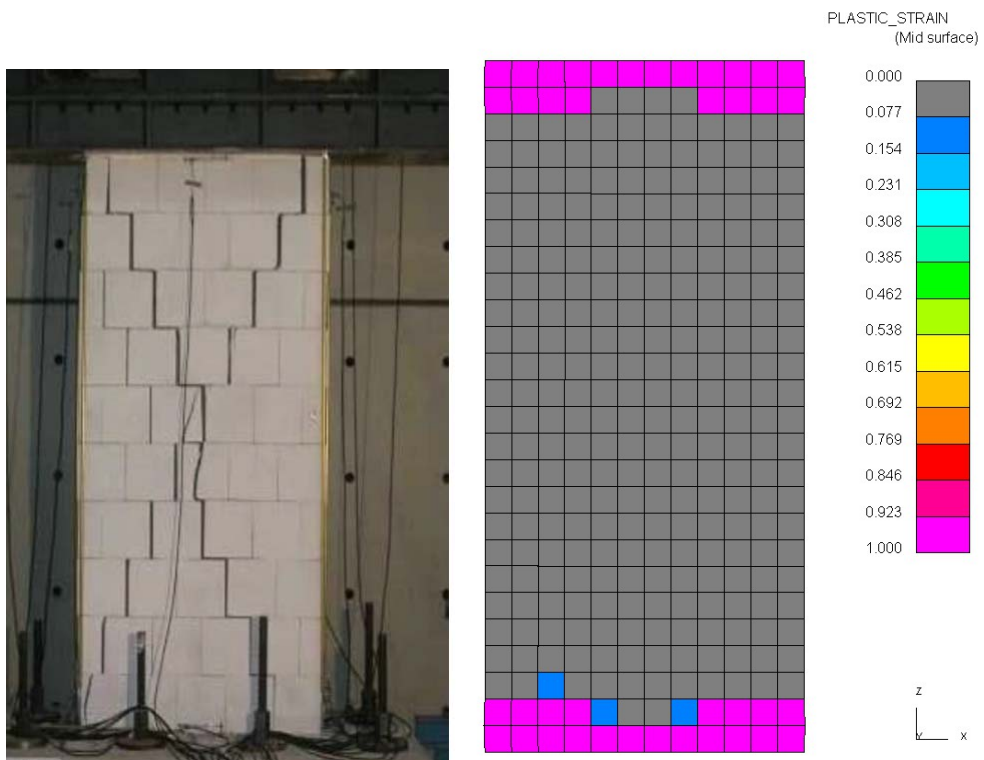


Figure 5.3.2: Final damage plot for CS03

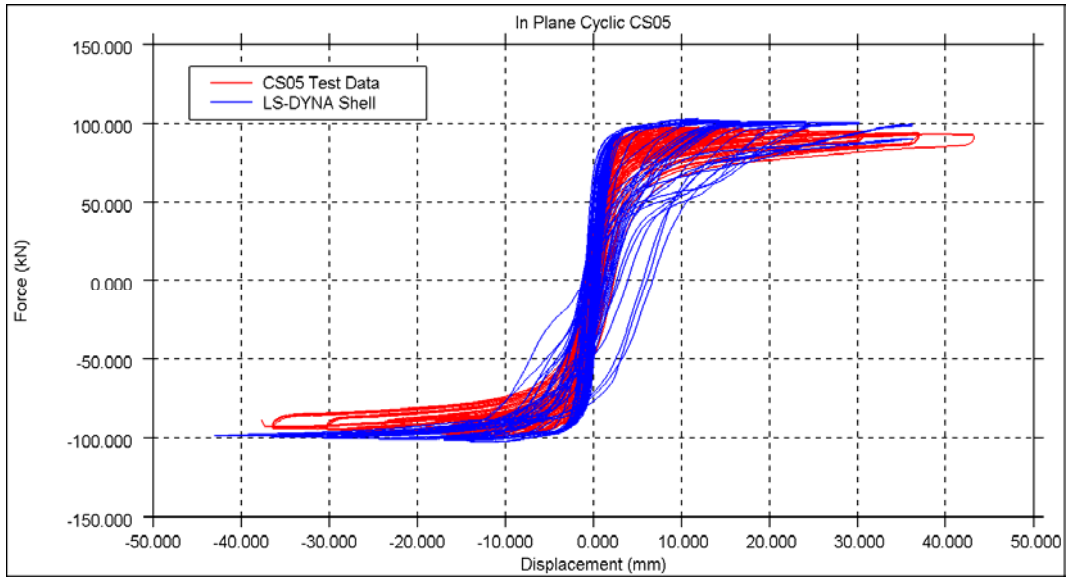


Figure 5.3.3: Shear force-displacement comparison plot for CS05



Figure 5.3.4: Final damage plot for CS05

5.3.1. Discussion

For both CS03 and CS05, the LS-DYNA shell models predict similar peak shear forces compared to the experiments.

For CS03, the specimen in the laboratory test experiences a stepwise diagonal crack. The LS-DYNA shell model does not predict such failure mode. In fact, the shell model does not exhibit failure of the wall panel at the end of the loading. In addition, the shell model predicts a slightly higher initial stiffness in comparison to the experimental results.

For CS05, comparing the shear force-displacement curves, it is observed that the LS-DYNA shell model predicts slightly more energy dissipation than the experimental data during the last few cycles. This occurs as the wall no longer experiences pure rocking and damage spreads further into the wall, releasing more energy than would a wall undergoing rocking behaviour. The initial stiffness is captured fairly well with the shell model.

5.4. ESECMaSE calcium silicate full-scale half-building test

Table 5.4.1: Modelling notes

Component	Description
Analysis software and formulation	LS-DYNA – explicit analysis solver
Walls (in-plane)	Masonry modelled with shell elements with damage smeared across each element using nonlinear MAT_SHELL_MASONRY material model. Crack plane directions are pre-defined to model mortar bonds.
Walls (out-of-plane)	As above.
Wall to wall connection (incl. flange effects)	Merged nodes
Concrete diaphragm	Concrete diaphragm is modelled as 2D shells
Wall to diaphragm connection	Merged nodes

Table 5.4.2: Eigenvalue analysis notes

Eigenvalue analysis notes
<ul style="list-style-type: none"> Masonry Young's modulus of 7560 MPa (from TU Munich test data) is used for the elastic masonry material definition in eigenvalue analysis. The original masonry density of 1800 kg/m³ is used for the masonry material definition in eigenvalue analysis.

Table 5.4.3: Nonlinear pushover analysis notes

Nonlinear pushover analysis notes
<ul style="list-style-type: none"> LS-DYNA pushover analysis was not carried out for this benchmark.

Table 5.4.4: Nonlinear time history analysis notes

Nonlinear time history analysis notes
<ul style="list-style-type: none"> 1% damping applied using proprietary LS-DYNA constant damping model over 1–30 Hz frequency range. Additional damping applied at very high frequencies for numerical stability. Measured displacement data are applied in the model as prescribed motions on L1 and L2 floor diaphragms, as per pseudo-dynamic test setup. Prescribed motions are applied at half-speed to reduce micro-inertia effects (which will not be present in the pseudo-dynamic laboratory tests), i.e. 12.5-second test data is stretched to 25 seconds.

Table 5.4.5: Model loading, materials and general comments

Loading	
Dead load	Self-weight of brick walls and concrete diaphragms.
Applied load	Mass condition in test (applied using water tanks etc.) modelled with added mass on relevant areas of concrete diaphragms, highlighted in various colours in Figure 2.4.1.
Materials	Material properties including values and stress strain behaviour
Calcium silicate bricks	Nonlinear masonry material model $\rho = 1800 \text{ kg/m}^3$ $E = 7560 \text{ MPa}$ $\nu = 0.112$ $f_c = 24 \text{ MPa}$ $f_t = 0.24 \text{ MPa}$ (tensile stress limit of mortar joints) $f_s = 0.245 \text{ MPa}$ (shear stress limit of mortar joints) $G_t = 10 \text{ N/m}$ (Mortar joint tensile energy rate) $G_s = 24.5 \text{ N/m}$ (Mortar joint shear energy rate) Friction coefficient = 0.677
Concrete	Elastic material model $\rho = 2400 \text{ kg/m}^3$ $E = 38 \text{ GPa}$ $\nu = 0.2$

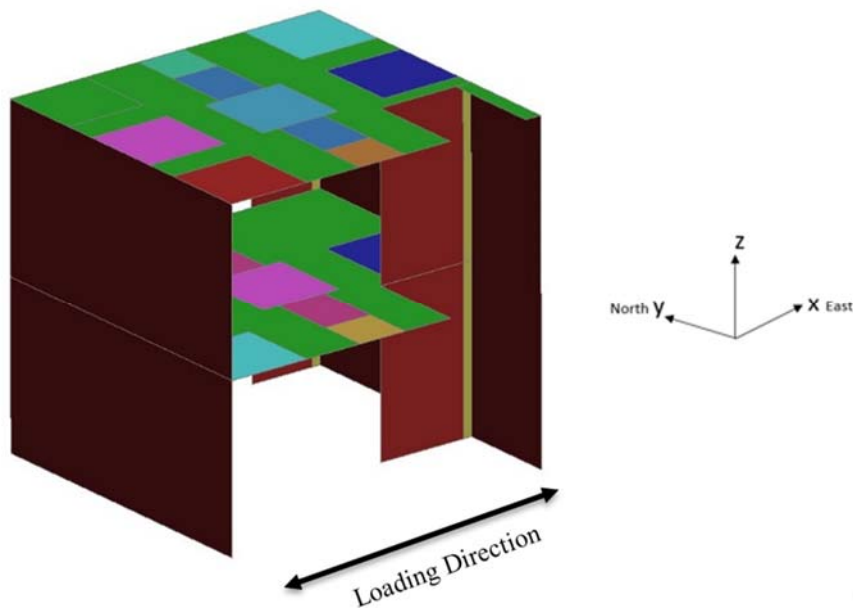


Figure 5.4.1: FE model of ESECMaSE calcium silicate full-scale half-building

Table 5.4.6: Modal period, frequency, description, mass participation

Mode	Period (s)	Frequency (Hz)	Description of mode	Mass participation %	
				X	Y
1	0.128	7.79	1 st flexural mode in x-direction (East-West)	77.0	0.04
2	0.052	19.31	1 st flexural mode in y-direction (North-South)	0.02	65.5
3	0.039	25.36	1 st torsional mode	0.18	0.26

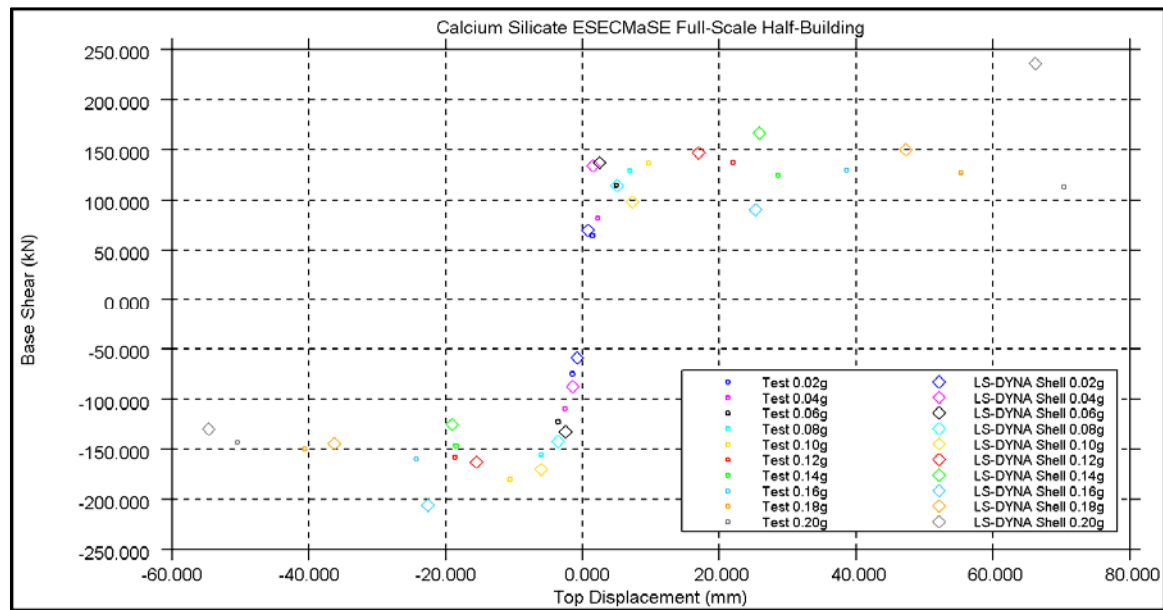


Figure 5.4.2: Envelope of max base shear force vs. max top displacement (0.02g to 0.20g PGA)

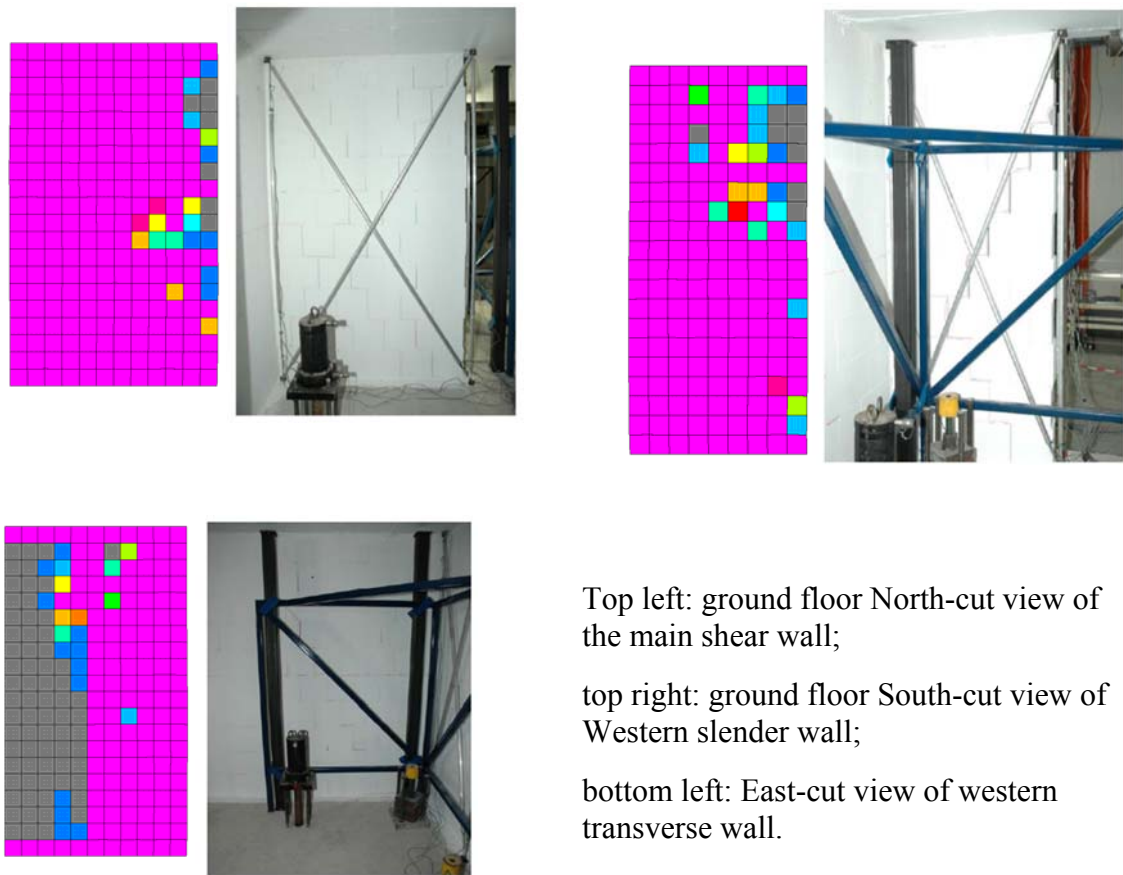


Figure 5.4.5: Damage plot after successive loadings of 0.02g–0.12g PGAs, i.e. when damages were first observed in laboratory tests.

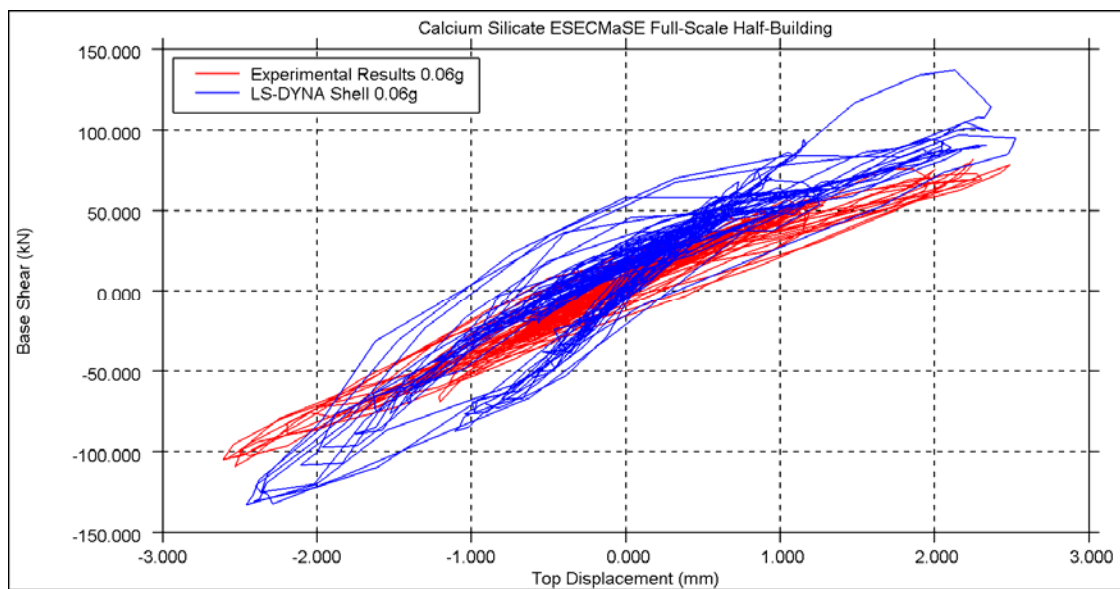


Figure 5.4.7: Base shear force vs. top displacement hysteresis plot during 0.06g PGA

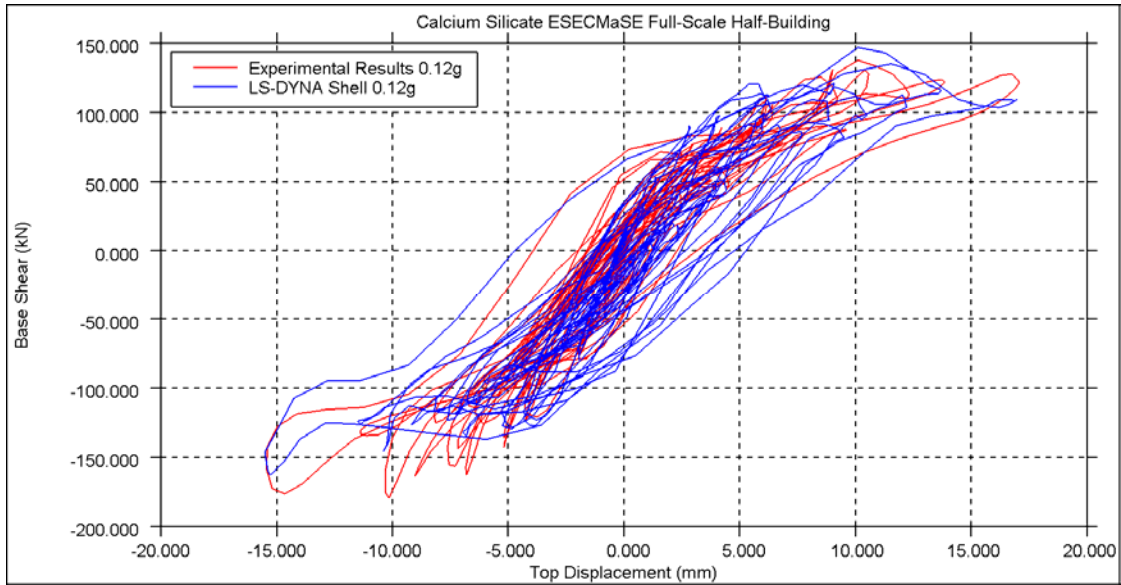


Figure 5.4.8: Base shear force vs. top displacement hysteresis plot during 0.12g PGA

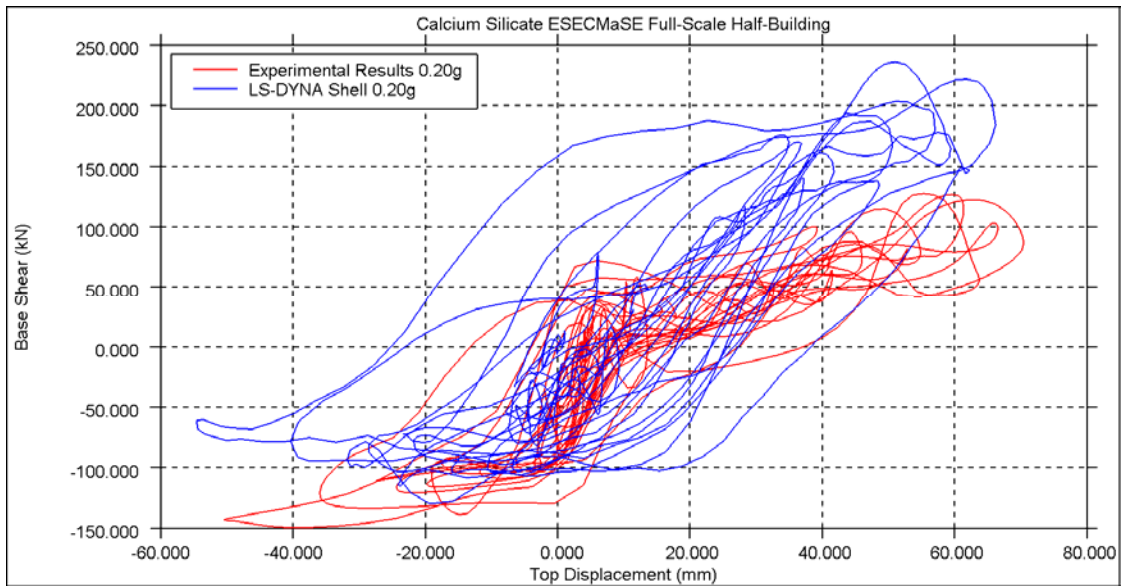


Figure 5.4.9: Base shear force vs. top displacement hysteresis plot during 0.20g PGA

5.4.1. Discussion

The LS-DYNA shell model exhibits a comparatively higher initial stiffness than the experimental results, but the strength and stiffness degradation at subsequently higher PGAs lead to a good match to the experimental values up through 0.14g PGA. The shell model shows much higher energy dissipation than the experimental results, particularly from 0.16g PGA upwards. This is due to the higher levels of damage to the in-plane wall panels than those observed in the experiment (Figure)

The crack patterns from the LS-DYNA shell analysis at the end of the 0.12g PGA bears some resemblance to the experimental output, however the degree of damage is much higher in the analysis model. At the final PGA, the shell model displays significant cracking in almost every in-plane and out-of-plane wall.

5.5. One-way spanning wall out-of-plane tests (Doherty)

Specimen 8 only

Table 5.5.1: Modelling notes

Component	Description
Analysis software and formulation	LS-DYNA – explicit analysis solver
Walls (in-plane)	Masonry modelled with shell elements with damage smeared across each element using nonlinear MAT_SHELL_MASONRY material model. Crack plane directions are pre-defined to model mortar bonds.
Walls (out-of-plane)	As above.

Table 5.5.2: Nonlinear time history analysis notes

Nonlinear time history analysis notes
<ul style="list-style-type: none"> • 1% damping applied using proprietary LS-DYNA constant damping model over 1-30 Hz frequency range. • Additional damping applied at very high frequencies for numerical stability.

Table 5.5.3: Model loading, materials and general comments

Loading	
Dead load	Self-weight of the walls.
Overburden	0.15 MPa at top of the wall
Materials	Material properties including values and stress strain behaviour
2D Shell Masonry	Nonlinear masonry material model $\rho = 1800 \text{ kg/m}^3$ $E = 5400 \text{ MPa}$ $\nu = 0.15$ $f_c = 9.70 \text{ MPa}$ $f_t = 0.45 \text{ MPa}$ (tensile stress limit of mortar joints) $f_s = 0.34 \text{ MPa}$ (shear stress limit of mortar joints. In absence of laboratory test results, min value used.) $G_t = 10 \text{ N/m}$ (Mortar joint tensile energy rate) $G_s = 34 \text{ N/m}$ (Mortar joint shear energy rate) Friction coefficient = 0.75
Other key notes	
3) In LS-DYNA overburden load is applied via self-weight of a rigid body, corresponding to an overburden stress of 0.15 MPa. The rigid body was free to move in vertical translation but restrained in rotation, imposing all overburden load on the extreme side of the wall. This modelling approach is not fully accurate as the laboratory pre-compression rig would have some rotational capacity. This is especially important during the elastic response phase of the wall loading.	
4) In the absence of laboratory spring stiffness and rig rotational capacity, assumptions were made and spring stiffness was calculated by interpolating laboratory test results and rigid body analysis.	

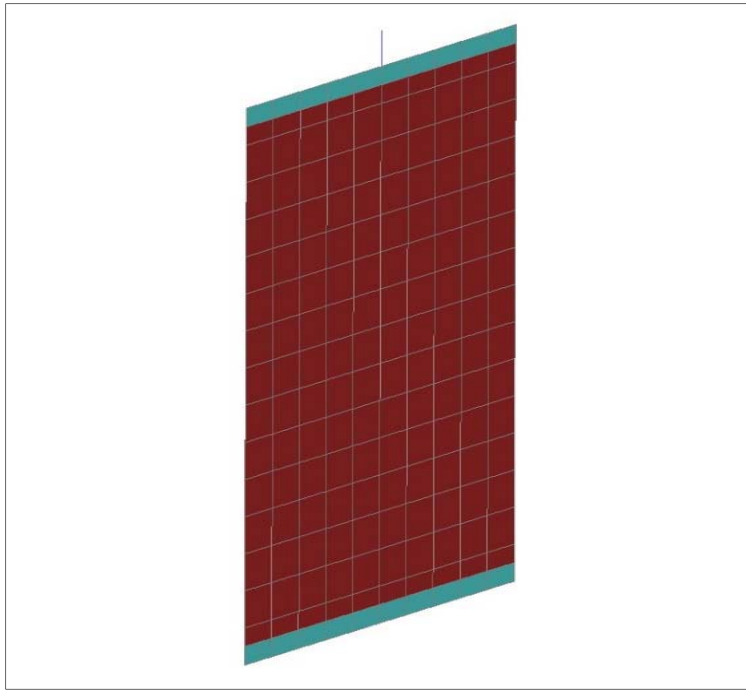


Figure 5.5.1: FE model showing Specimen 8 (isometric view)

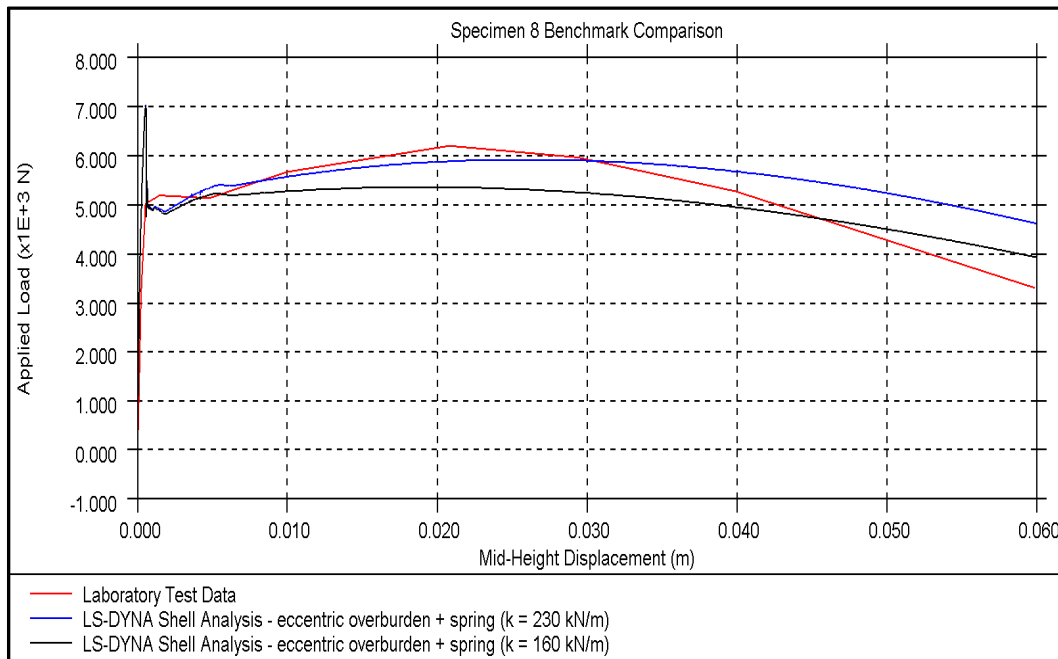
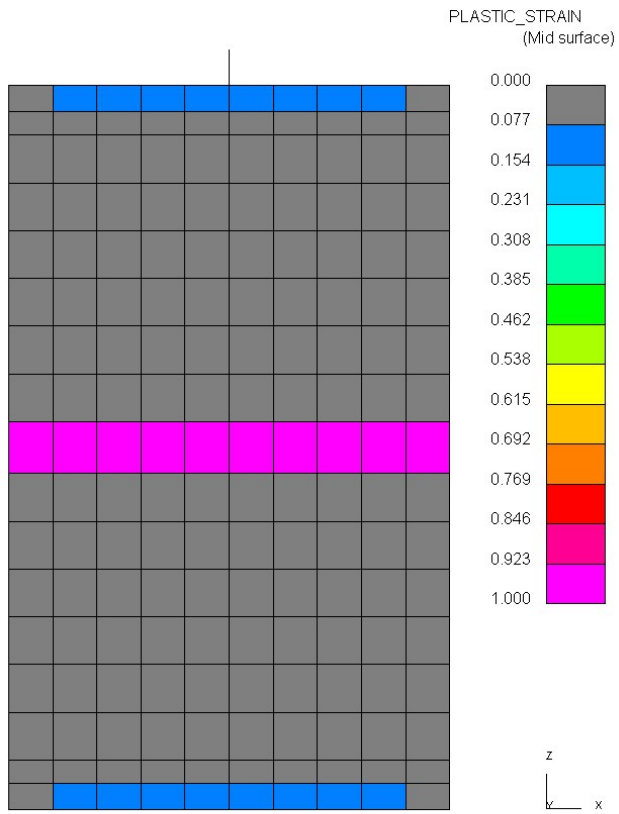


Figure 5.5.2: Total applied force vs. displacement for Specimen 8



62.000015

Figure 5.5.3: Final damage plot – static loading for Specimen 8

5.5.1. Discussion

As shown in Figure 5.5.2, the overall response of the specimen was predicted well by the LS-DYNA shell model. The pre-crack load resistance obtained in the shell model analysis, however, is higher than the test value. This resistance is governed by the mortar tensile strength. It is possible that the bond strength of the wall specimen could have been lower than measured in the bond wrench test (0.45 MPa).

Other notes to consider:

- With the increase of wall rotation (mid-height displacement), the applied pressure on the extreme fibre of the brick increases. This results in mortar damage and rounding at the edges, which decreases the lever arm length and therefore the bending moment carried across the crack.
- The increase in the applied load in laboratory test was caused by the overburden rig used. With increased mid-height displacement, the total wall height also increased slightly, thus increasing the static spring deflection and hence overburden force.
- In LS-DYNA, overburden load was applied via a self-weight of the rigid body, with the corresponding density of the solid equal to overburden of 0.15 MPa. This element was free to move in a vertical direction but restrained in rotation, imposing all overburden load on the extreme side of the wall. This modelling approach cannot capture the behaviour of the laboratory pre-compression rig having some rotational capacity. This is especially important during the elastic response phase of the wall loading.

5.6. Two-way spanning wall out-of-plane tests (Griffith)

Table 5.6.1: Modelling notes

Component	Description
Analysis software and formulation	LS-DYNA – explicit analysis solver
Walls (in-plane)	Masonry modelled with shell elements with damage smeared across each element using nonlinear MAT_SHELL_MASONRY material model. Crack plane directions are pre-defined to model mortar bonds.
Walls (out-of-plane)	As above.
Wall to wall connection (incl. flange effects)	Merged nodes.

Table 5.6.2: Nonlinear time history analysis notes

Nonlinear time history analysis notes
<ul style="list-style-type: none">• 1% damping applied using proprietary LS-DYNA constant damping model over 1–30 Hz frequency range.• Additional damping applied at very high frequencies for numerical stability.

Table 5.6.3: Model loading, materials and general comments

Loading	
Dead load	<i>Wall 1 & 2: Self-weight of the wall</i>
Overburden	<i>Wall 1: 0.1 MPa applied as point loads at top of the wall. Wall 2: No overburden load.</i>
Materials	Material properties including values and stress strain behaviour
2D Shell Masonry	<p>Wall 1: $\rho = 1500 \text{ kg/m}^3$ (reduced to take into account cored unit) $E = 3190 \text{ MPa}$ $\nu = 0.15$ $f_c = 17.6 \text{ MPa}$ $f_t = 0.614 \text{ MPa}$ (tensile stress limit of mortar joints) $f_s = 0.461 \text{ MPa}$ (shear stress limit of mortar joints. In absence of laboratory test results, min value used.) $G_t = 10 \text{ N/m}$ (Mortar joint tensile energy rate) $G_s = 46 \text{ N/m}$ (Mortar joint shear energy rate) Friction coefficient = 0.75</p> <p>Wall 2: $\rho = 1500 \text{ kg/m}^3$ (reduced to take into account cored unit) $E = 2240 \text{ MPa}$ $\nu = 0.15$ $f_c = 13.6 \text{ MPa}$ $f_t = 0.52 \text{ MPa}$ (tensile stress limit of mortar joints) $f_s = 0.391 \text{ MPa}$ (shear stress limit of mortar joints. In absence of laboratory test results, min value used.) $G_t = 10 \text{ N/m}$ (Mortar joint tensile energy rate) $G_s = 39 \text{ N/m}$ (Mortar joint shear energy rate) Friction coefficient = 0.75</p>
Other key notes	
<p>3) Pre-compression load in LS-DYNA is applied as uniformly distributed pressure load.</p> <p>4) In the absence of the direct tensile strength test results, flexural tensile strength is used in LS-DYNA. Van der Pluijm (1997) suggests a reduction factor of 1.2–1.7 when converting from flexural strength to direct tensile strength.</p>	

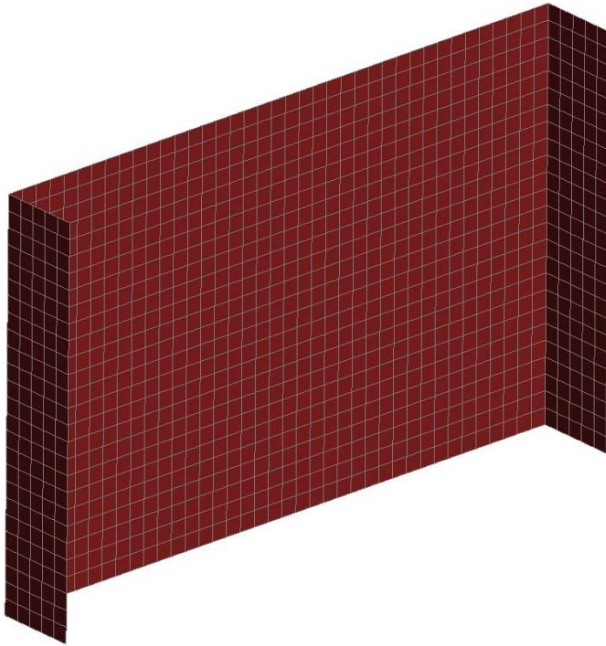


Figure 5.6.1: FE model showing Wall 1 / Wall 2 (isometric view)

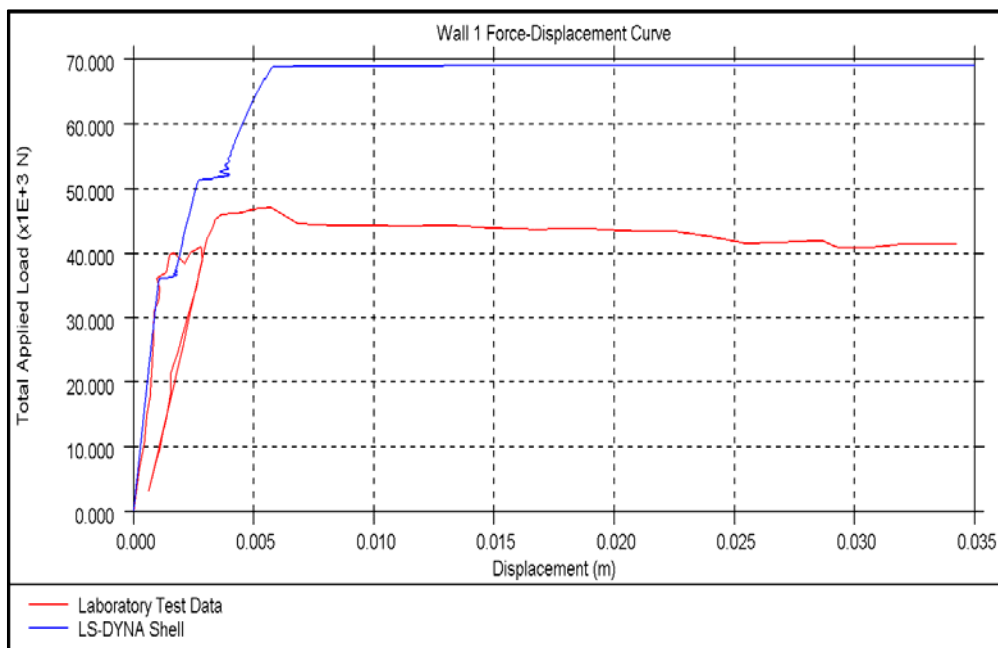


Figure 5.6.2: Load-displacement response plot (Wall 1)

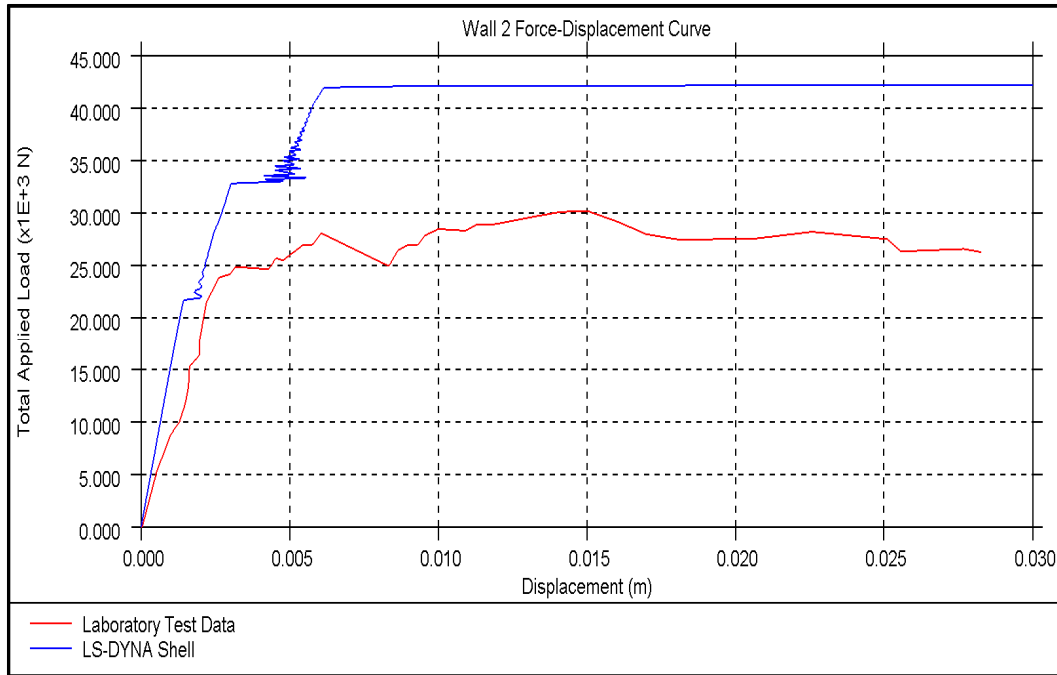


Figure 5.6.3: Load-displacement response plot (Wall 2)

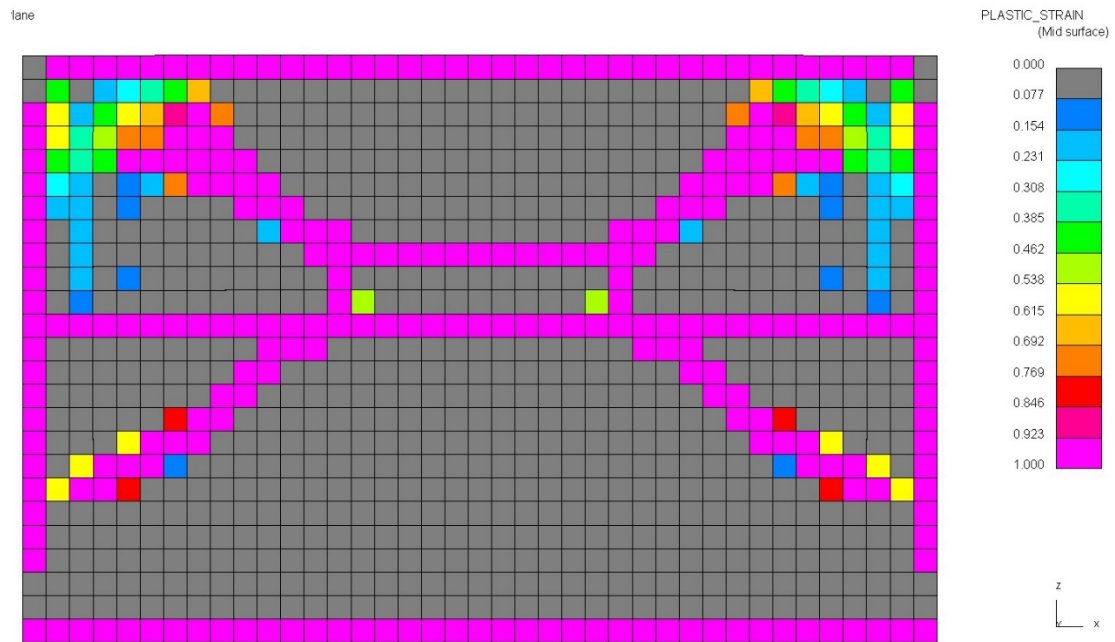


Figure 5.6.4: Final crack pattern for Wall 1

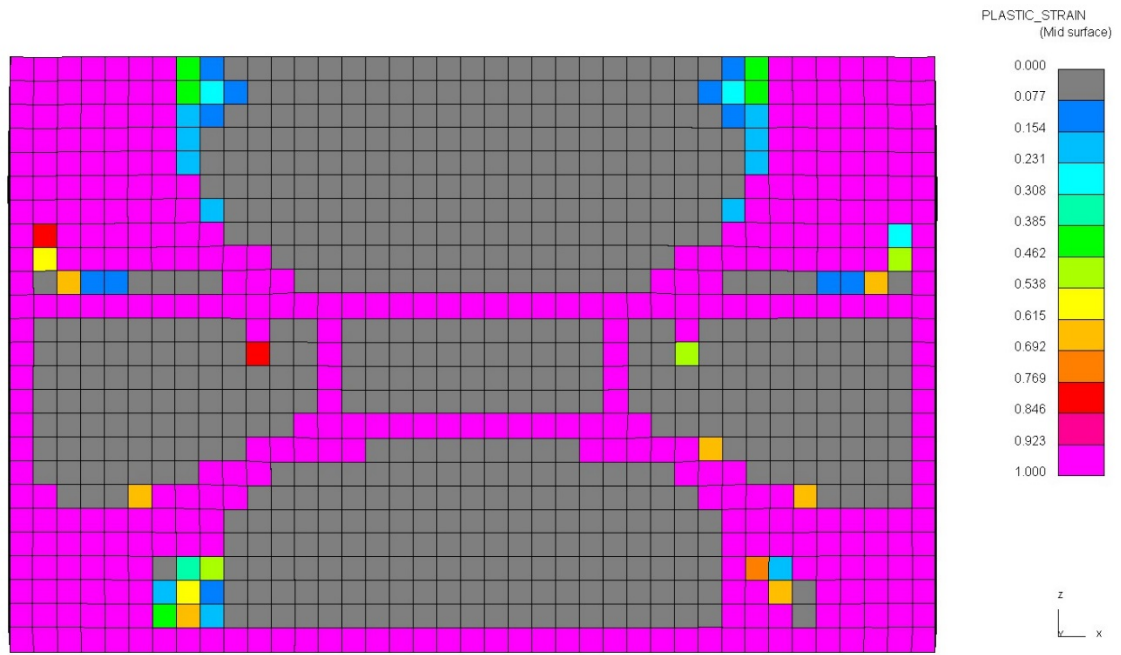


Figure 5.6.5: Final crack pattern for Wall 2

5.6.1. Discussion

- In the absence of the direct tensile strength test results, flexural tensile strength was used in LS-DYNA. Van der Pluijm et al. [3] suggested a reduction factor of 1.2 to 1.7 when converting from flexural strength to direct tensile strength.
- Laboratory records and LS-DYNA load-displacement curves for both Wall 1 and Wall 2 show similar behaviour. However, shell model results reach a much larger peak strength.
- Load on the wall in LS-DYNA was applied pseudo-statically using force control. This was found to be the most realistic representation of the 'airbag' loading. However, this can result in inertia effects and thus overestimate wall capacity.

6. References

- [1] Broadhouse, B. J. (1995). *The Winfrith concrete model in LS-DYNA3D*. Structural Performance Department, AEA Technology, Winfrith Technology Centre.
- [2] Broadhouse, B. J., and Neilson, A. J. (1987). "Modelling reinforced concrete structures in DYNA3D." *DYNA3D User Group Conference*, Safety and Engineering Science Division, AEE Winfrith, London, UK.
- [3] Van der Pluijm, R. (1997). *Non-linear behaviour of masonry under tension*. Eindhoven University of Technology, Faculty of Architecture, Building and Planning. Building and Construction Research.

Appendix B

Modelling Comparison – EUCENTRE



Numerical modelling report

June 2015



1. Summary of modelling approach

Table 1.1: General modelling notes

Component	Description
Analysis team	EU CENTRE-Pavia
Analysis software and formulation	TREMURI – Equivalent-frame formulation based on a macro-element model
Overview of modelling approach	<p>The adopted equivalent-frame modelling strategy implemented in the Tremuri program [Lagomarsino et al., 2013] is based on the effective non-linear macro-element modelling approach.</p> <p>The macro-element model represents the cyclic non-linear behaviour associated with the two main in-plane masonry failure modes, bending-rocking and shear mechanisms, with a limited number of degrees of freedom (8 d.o.f) and internal variables which describe the damage evolution [Penna et al., 2014]. The two-node macro-element, suitable for modelling piers and spandrel beams, can be ideally subdivided into three parts: a central body where only shear deformation can occur and two interfaces, where the external degrees of freedom are placed, which can have relative axial displacements and rotations with respect to those of the extremities of the central body. In the two interfaces, infinitely rigid in shear, the axial deformations are due to distributed system of zero-length springs with no-tension and limited compression behaviour.</p> <p>Due to the concentration of the axial and flexural deformations in the interfaces, the spring stiffness equal to $k = 2E'/h$, where E' is an effective elastic modulus and h is the element length (height in case of pier elements), is set differently as far as axial or lateral stiffness need to be more accurately reproduced. The following settings apply for E':</p> <ul style="list-style-type: none">• $E' = E$ (masonry Young's modulus in compression) when axial stiffness is concerned;• $E' = 1.5E$ when lateral stiffness is concerned in a cantilever wall;• $E' = 3E$ when lateral stiffness is concerned in a double-fixed wall;• E' is usually set to $2E$ when lateral stiffness is concerned in a building model with intermediate boundary conditions for the different structural elements.



<p>Overview of modelling approach</p>	<p>The macroscopic shear model is based on a combination of equivalent cohesion, \bar{c}, and friction, $\bar{\mu}$, parameters. The determination of the model parameters from the “local” mechanical parameters derived from characterisation tests depends on the governing shear failure mode:</p> <ul style="list-style-type: none"> For diagonal shear cracking (with cracks passing through bricks), the following relations apply, $\begin{cases} \bar{\mu} = \frac{1}{4.6(1+\alpha_v)\sqrt{1+N_o/f_{bt}lt}} \\ \bar{c} = \frac{f_{bt}}{2.3(1+\alpha_v)}\sqrt{1+N_o/f_{bt}lt} - \bar{\mu}\frac{N_o}{lt} \end{cases}$ <p>where f_{bt} is the longitudinal unit tensile strength, N_o is the axial force and $\alpha_v=h_o/l$ is the shear span ratio (ratio between the zero moment height and the wall length);</p> <ul style="list-style-type: none"> For shear failure with sliding along bed-joints the following relations apply, $\begin{cases} \bar{\mu} = \frac{\mu}{(1+\alpha_v)\left(1+\frac{2\mu\Delta_y}{\Delta_x}\right)} \\ \bar{c} = \frac{c}{(1+\alpha_v)\left(1+\frac{2\mu\Delta_y}{\Delta_x}\right)} \end{cases}$ <p>where c and μ are the joint cohesion and friction coefficient, and Δ_y and Δ_x are the unit height and length, respectively. Reduced values of μ (50%) can be used to account for loading reversal effects.</p> <p>The Tremuri computer program performs several types of linear and nonlinear analyses: modal analysis, incremental static analyses (Newton-Raphson) with force or displacement control, 3D pushover analyses with fixed and adaptive load pattern and 3D time-history dynamic analysis (Newmark integration method; Rayleigh viscous damping).</p> <p>Floor and roof diaphragms are modelled by means of linear 3-node and 4-node orthotropic membrane elements.</p>
<p>Model units</p>	<p>SI units (kg, m, sec)</p>



2. Experimental benchmarks

2.1. Ispra in-plane panel tests

Table 2.1.1: Modelling notes

Component	Description
Analysis software and formulation	TREMURI – Equivalent-frame formulation based on a macro-element model
Walls (in-plane)	See Table 1.1 and Penna et al. [2014]

Table 2.1.2: Nonlinear pushover analysis notes

Nonlinear pushover analysis notes
<ul style="list-style-type: none">• Seismic load applied as equivalent horizontal load pattern (imposed displacement of a control node and relative force ratios kept constant)• +/- load directions considered• Cyclic load cases considered• The solution of the static equilibrium equations is obtained by iteration (Newton-Raphson)

Table 2.1.3: Model loading, materials and general comments

Loading	
Dead load	Self-weight of the walls
Overburden	0.6 MPa
Materials	Material properties including values and stress strain behaviour
Masonry (Clay bricks)	Model Parameters (as described in Penna et al. [2014]) $\rho = 1650 \text{ kg/m}^3$ $E' = 4473 \text{ MPa} (= 3E = 3 \cdot 1491 \text{ MPa})$ $G = 445 \text{ MPa}$ $f_m = 6.2 \text{ MPa}$ $\bar{c} = 0.29 \text{ MPa}$ (cohesion also referred as f_{vmo} in Penna et al. [2014]) Equivalent Friction coefficient = 0.09
Other key notes	
1) Double-bending test configuration	

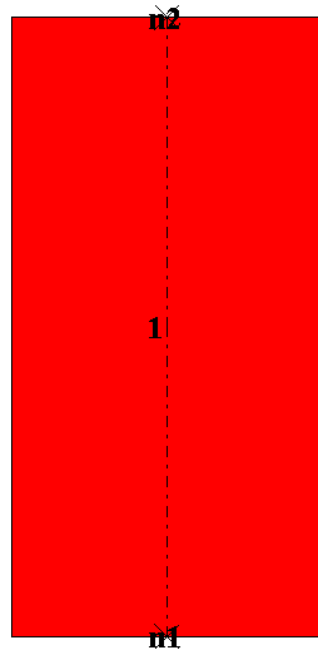


Figure 2.1.1: Tremuri model

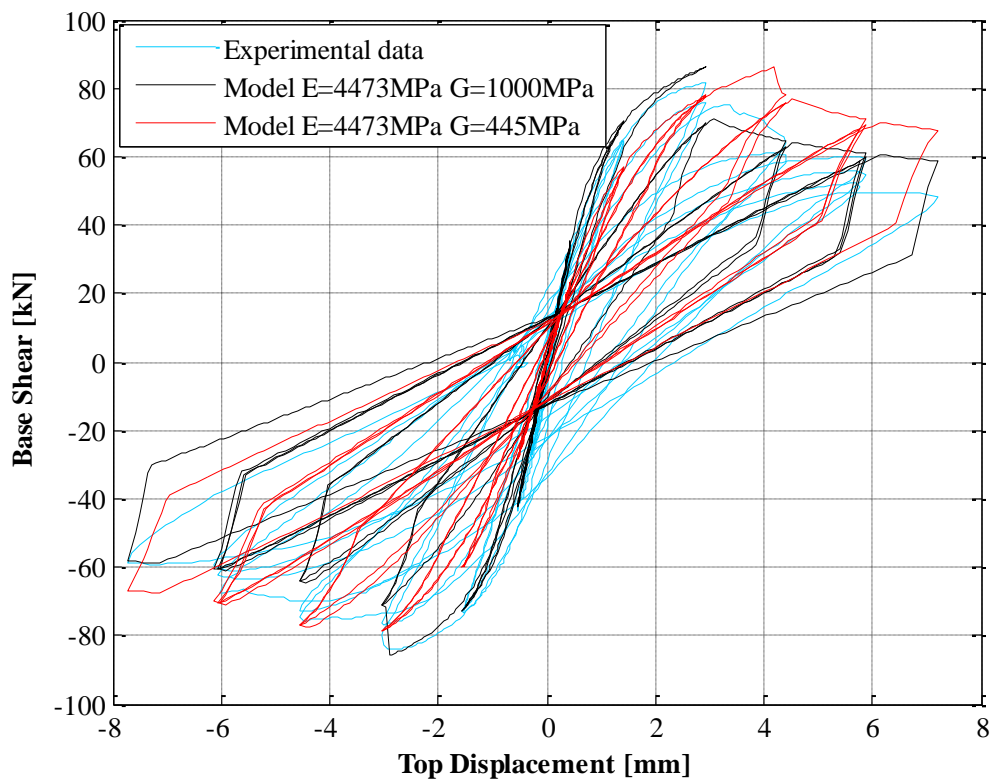
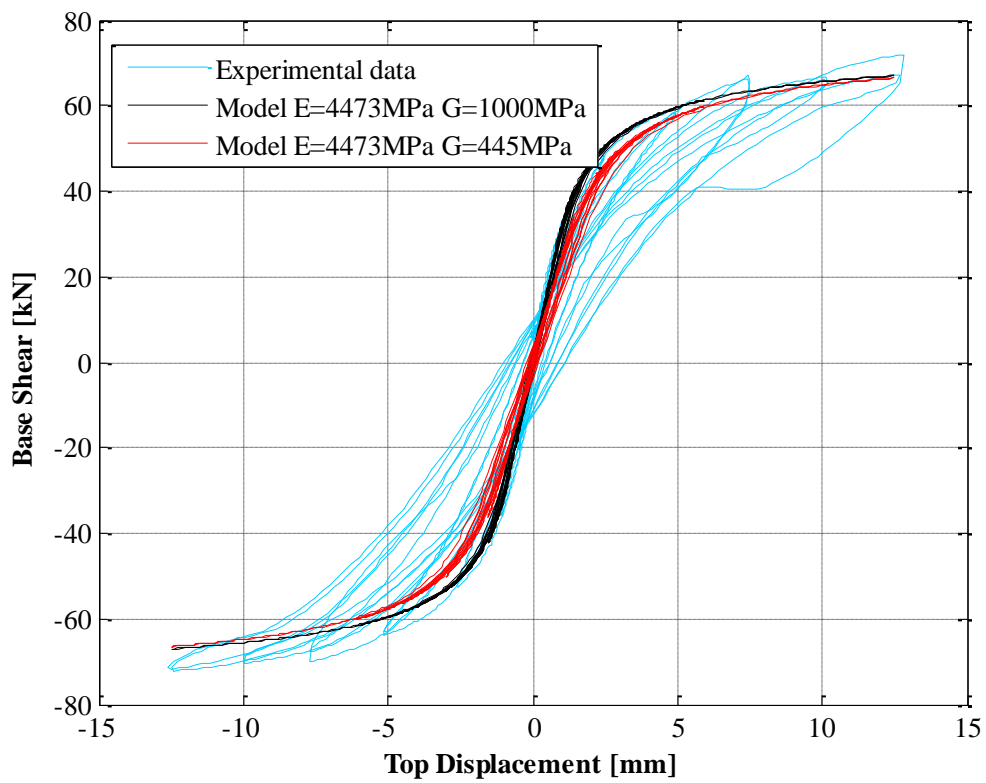


Figure 2.1.2: Shear force-displacement comparison plot for LOWSTA





2.2. Pavia full building tests

Table 2.2.1: Modelling notes

Component	Description
Analysis software and formulation	TREMURI – Equivalent-frame formulation based on a macro-element model
Walls (in-plane)	See Table 1.1, Lagomarsino et al. [2013] and Penna et al. [2014]
Walls (out-of-plane)	The walls out-of-plane response is not computed because it is considered generally negligible with respect to the global building response if suitable wall-to-floor connections are present. The 3D models are created assembling equivalent frames representing the wall in-plane response and membrane elements representative of diaphragms. Only the wall and diaphragm in-plane behaviour is modelled [Lagomarsino et al., 2013]. 2D macro-element models accounting for 2 nd order effects can be suitably applied for the analysis of local out-of-plane wall response [Penna & Galasco, 2013].
Spandrels/lintels and wall coupling	Spandrels modelled using the same approach as piers (rotated macro-elements).
Wall to wall connection (incl. flange effects)	The kinematics of 3D nodes connecting walls at intersections is defined by 5 d.o.f. in the global coordinate system ($u_x, u_y, u_z, rot_x, rot_y$). Ideal connections are usually assumed (full transmission of nodal forces and moments in the vertical planes, no transmission of moments around the vertical axis) Flange effects considered in the default options can be reduced or neglected by introducing (linear/nonlinear) deformable elements, if required.
Wall to diaphragm connection	Ideal connection, with perfect displacement coupling, no (out-of-plane) moment transfer

Table 2.2.2: Nonlinear pushover analysis notes

Nonlinear Pushover analysis notes
<ul style="list-style-type: none">• Seismic load applied as equivalent horizontal load pattern (imposed displacement of a control node and relative force ratios kept constant)• Pushover analysis constant load pattern consisting of 4 equal forces applied to “window” and “door” walls at the floor levels• +/- load directions considered• Cyclic load cases considered• The solution of the static equilibrium equations is obtained by iteration (Newton-Raphson)

Table 2.2.3: Model loading, materials and general comments

Loading	
Dead load	Masonry self-weight and weight of floor joists and testing (steel) beams
Applied load	Total added vertical load of 248.4 kN at the first floor and 236.8 kN at the second floor (approximately 10 kN/m ² per floor)
Materials	
Masonry (Clay bricks)	Model Parameters (as described in Penna et al. [2014]) $\rho = 1650 \text{ kg/m}^3$ $E' = 2982 \text{ MPa}$ ($= 2E = 2 \cdot 1491 \text{ MPa}$) $G = 445 \text{ MPa}$ $f_m = 6.2 \text{ MPa}$ $\bar{c} = 0.13 \text{ MPa}$ (cohesion also referred as f_{vmo} in Penna et al. [2014]) Equivalent Friction coefficient = 0.16 (obtained considering 50% of the friction coefficient from characterisation tests)
Other key notes	
	1) “Door” wall loaded by the floors but structurally disconnected from the rest of the specimen (“Window” wall). See figures below.

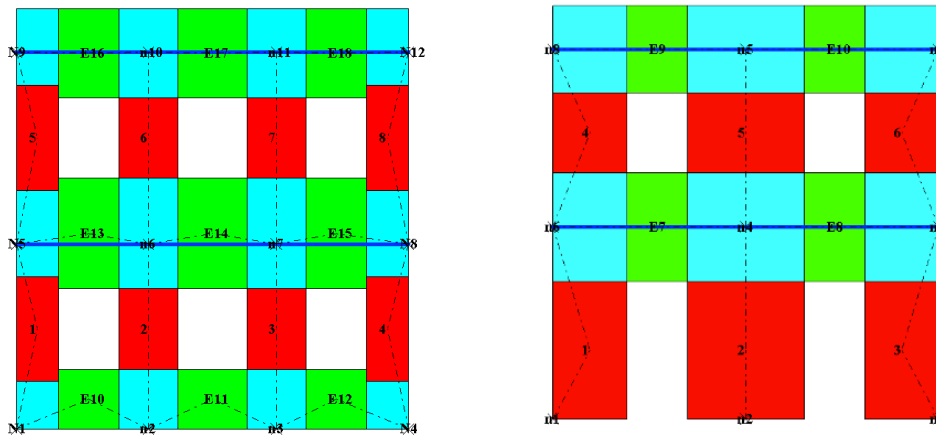


Figure 2.2.1: Tremuri model showing Window Wall and Door Wall (front view)

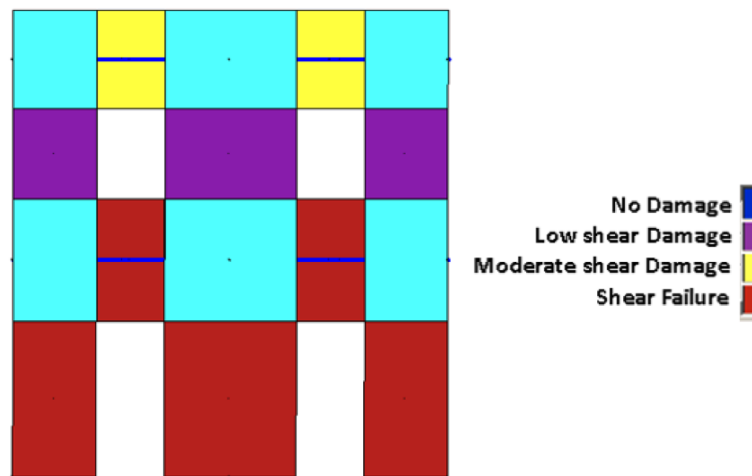
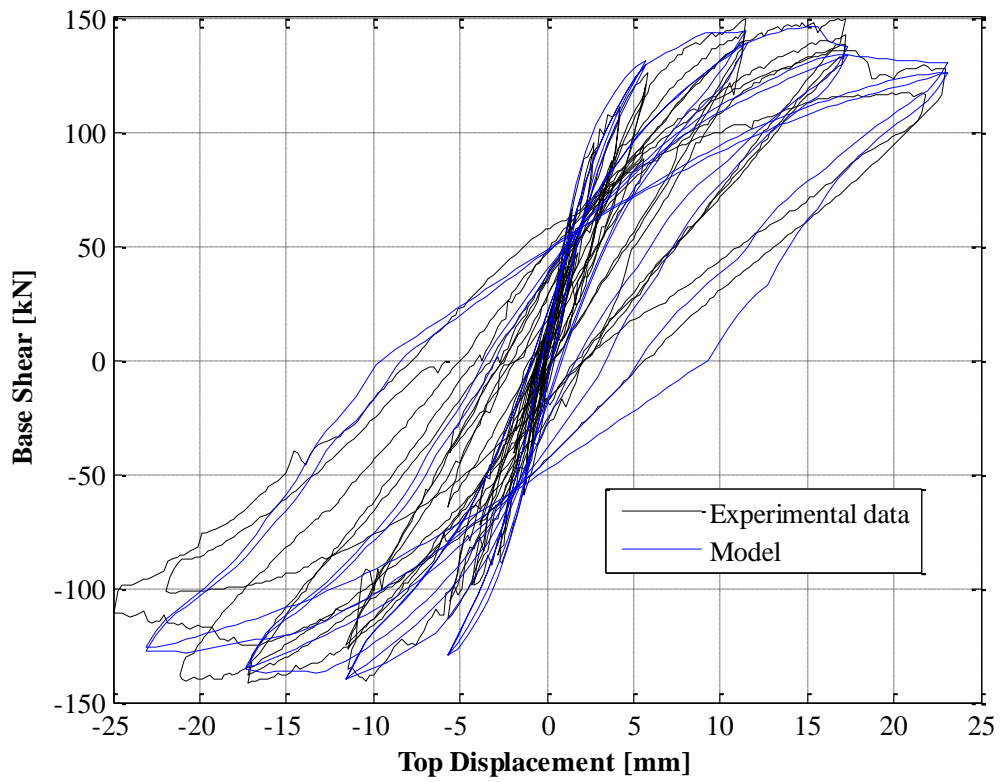


Figure 2.2.2: Top: Total base shear force vs. 2nd floor displacement (Door Wall); Bottom: Final Damage Pattern.

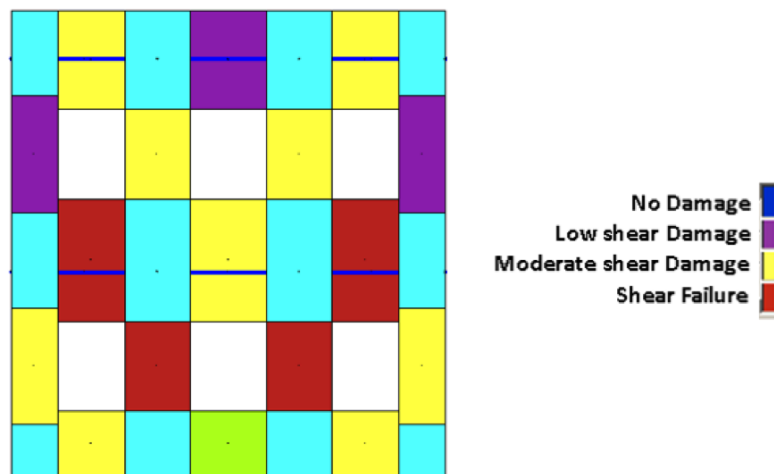
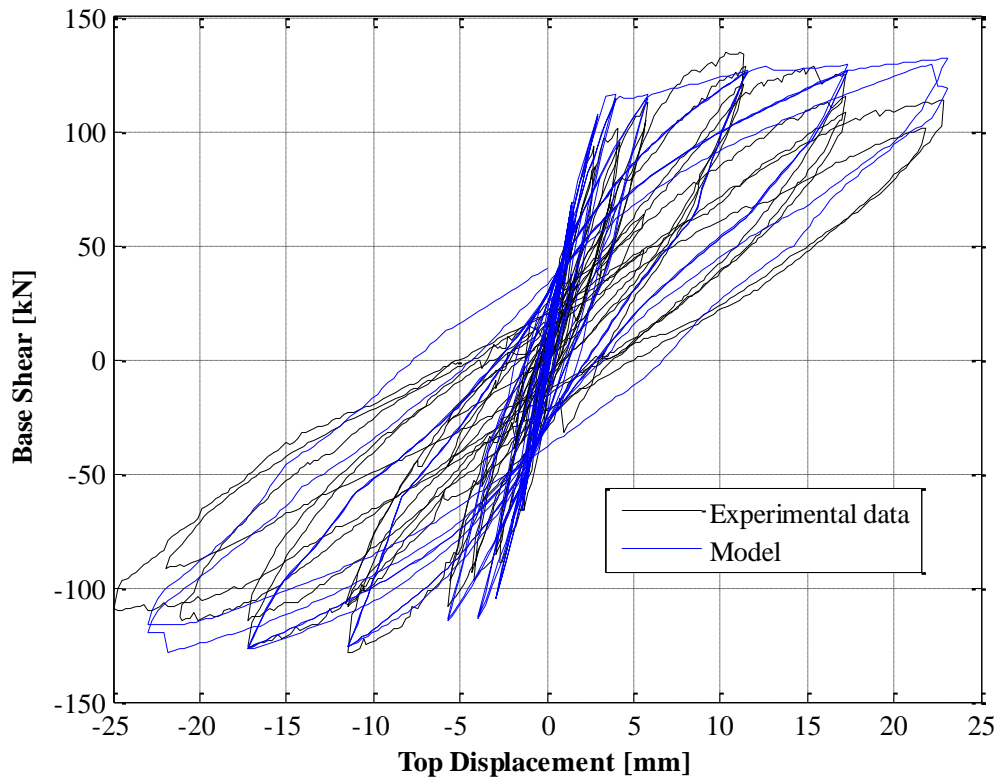


Figure 2.2.3: Top: Total base shear force vs. 2nd floor displacement (Window Wall); Bottom: Final Damage Pattern.

2.2.1. Discussion and sensitivity analyses

Sensitivity analyses have been carried out with different combinations of material properties (according to the results obtained from characterisation tests), summarised in the table below. An additional investigation has been carried out to evaluate the effect of the effective height of the masonry piers.

Table 2.2.4: Summary of the material properties

E [MPa]	G [MPa]	ρ [kg/m ³]	f_m [MPa]	f_{vm0} [MPa]	Equivalent friction coefficient
2982	445	1650	6.2	0.13	0.16
1491	400	1650	6.2	0.29	0.09
4250	1000	1650	6.2	0.29	0.09

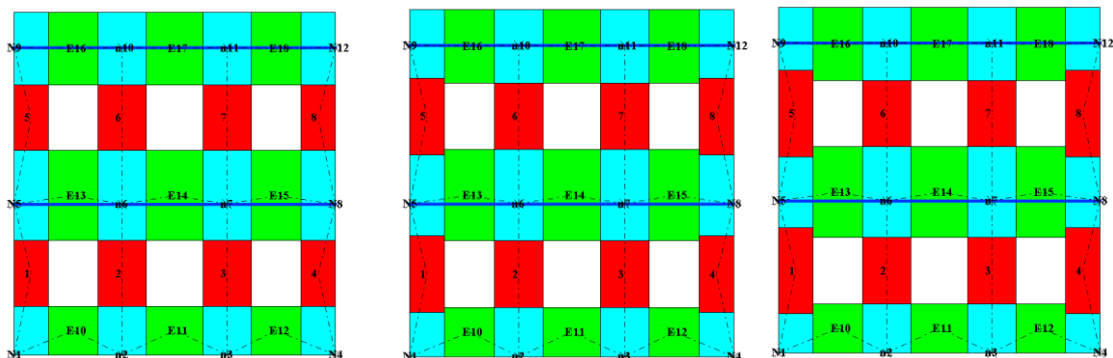


Figure 2.2.4: Window Wall: Tremuri model showing the different effective height assumed (from left to right: min, interm and max)

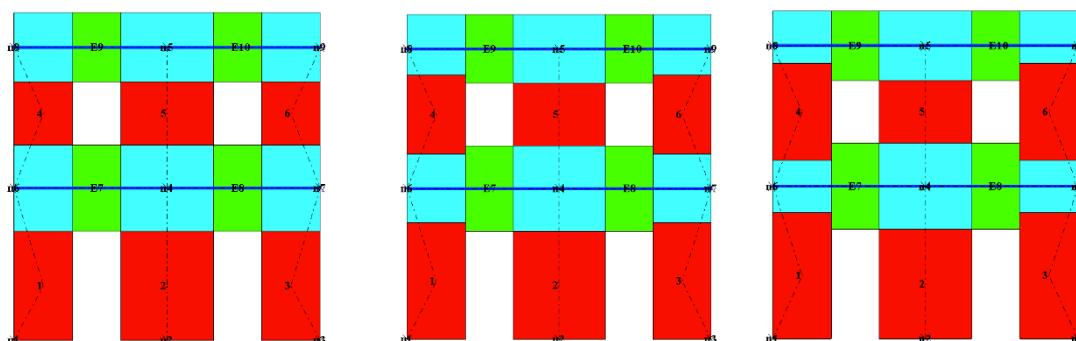


Figure 2.2.5: Door Wall: Tremuri model showing the different effective height assumed (from left to right: min, interm and max)

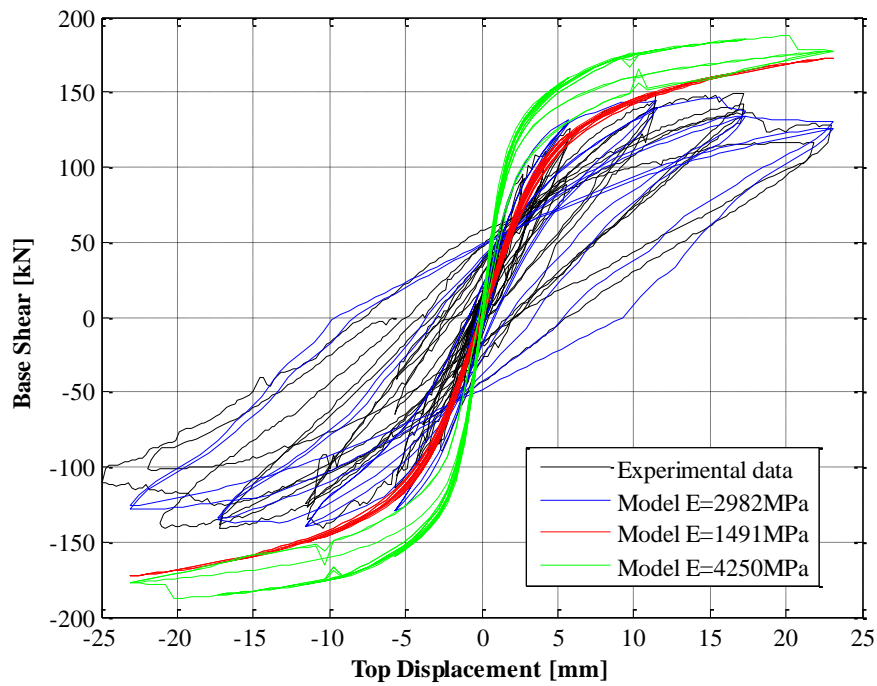


Figure 2.2.6: Total base shear force vs. 2nd floor displacement (Door Wall, $H_{eff} = H_{min}$).

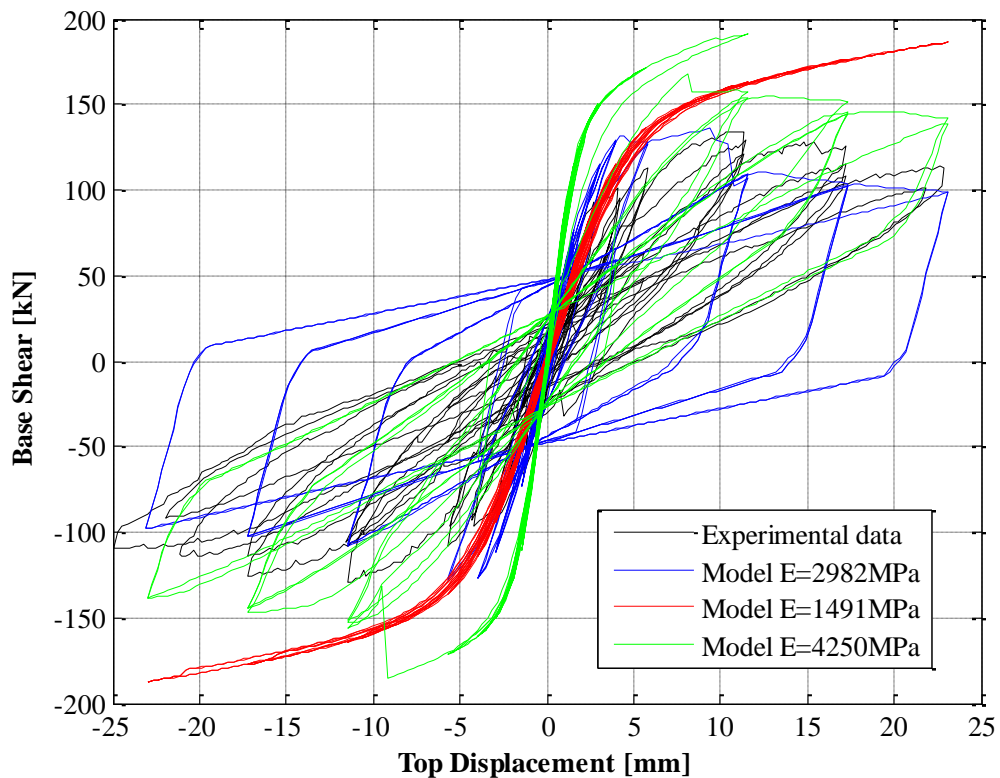


Figure 2.2.7: Total base shear force vs. 2nd floor displacement (Window Wall, $H_{eff} = H_{min}$)

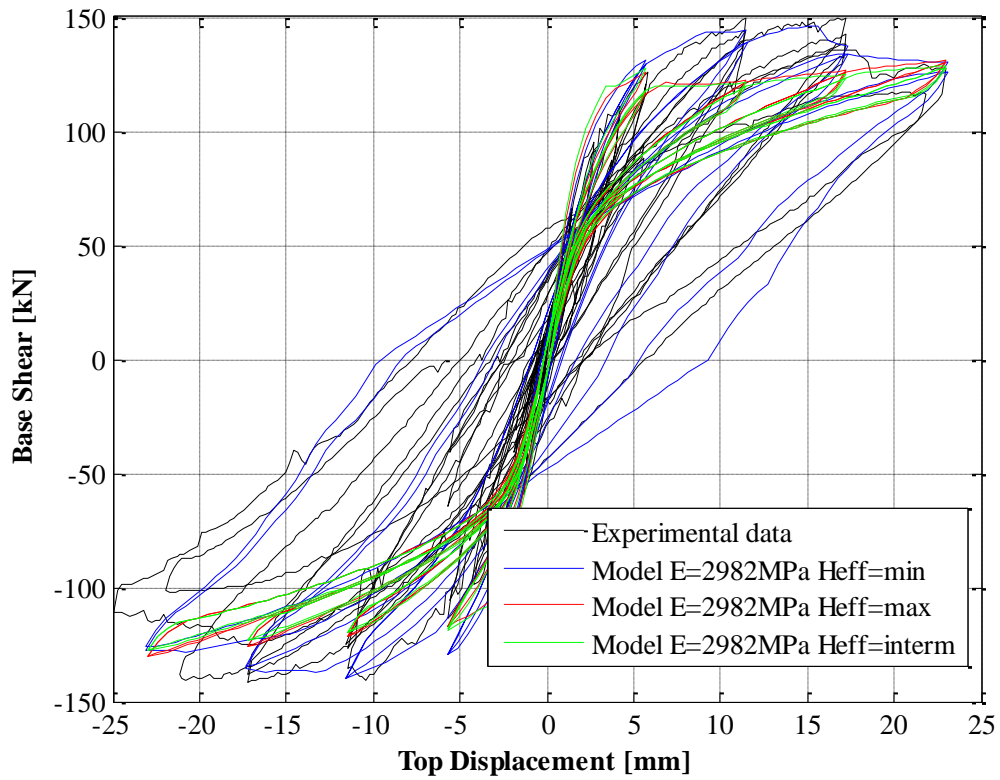


Figure 2.2.8: Door Wall: Total base shear force vs. 2nd floor displacement (Effects of H_{eff})

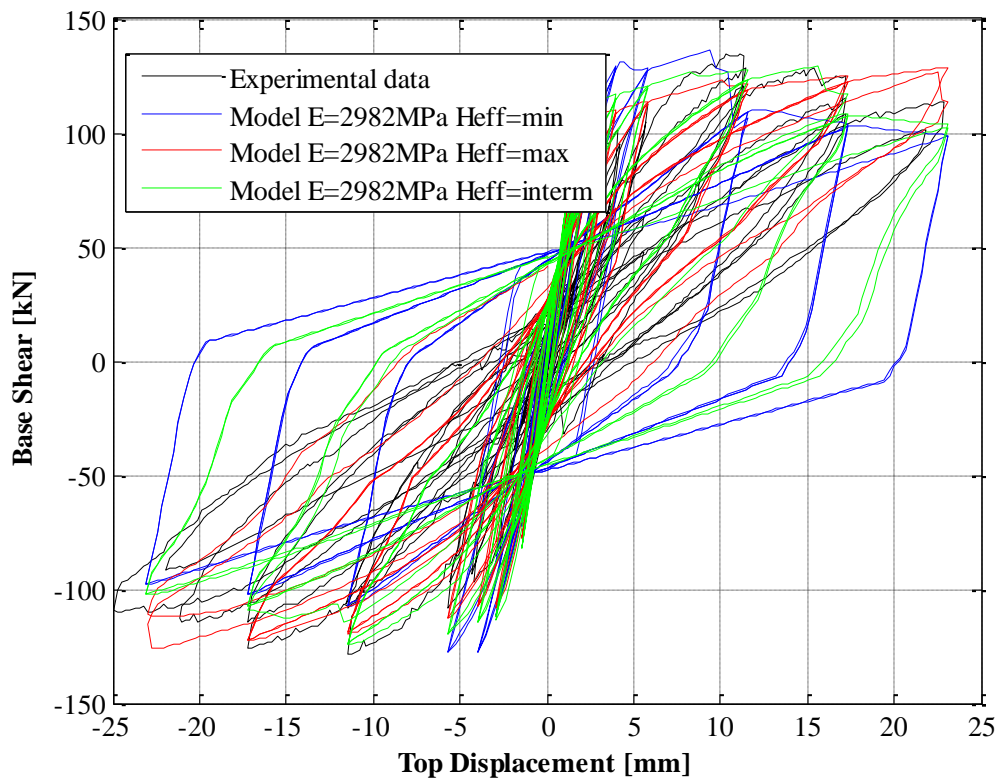


Figure 2.2.9: Window Wall: Total base shear force vs. 2nd floor displacement (Effects of H_{eff})

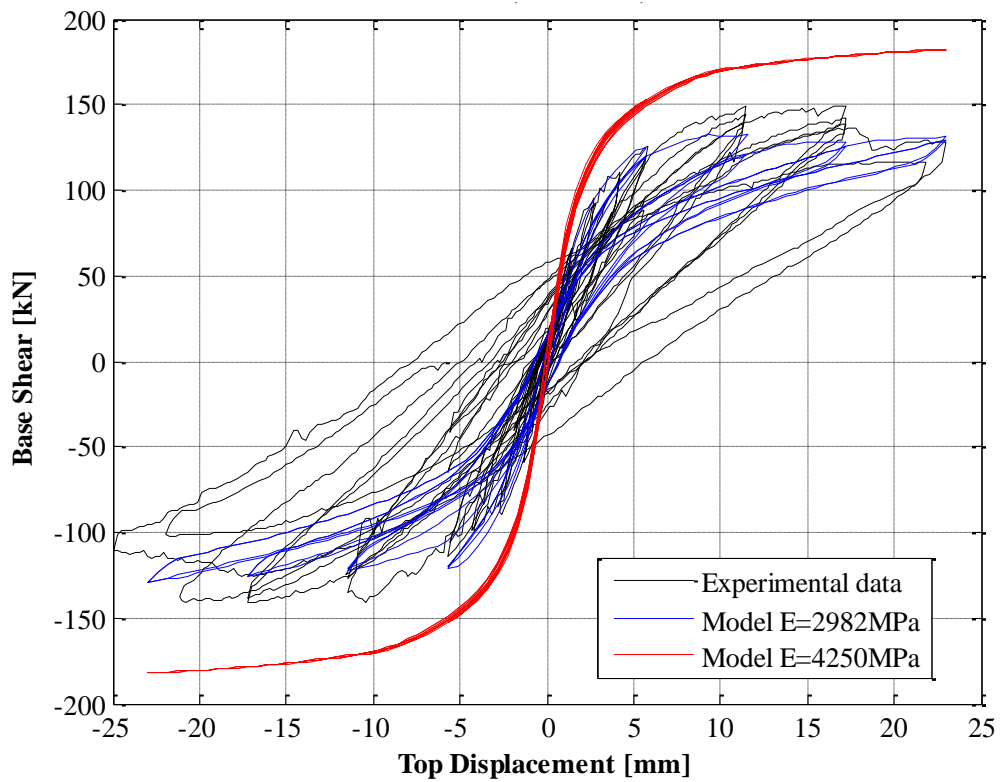


Figure 2.2.10: Total base shear force vs. 2nd floor displacement (Door Wall, $H_{eff} = H_{max}$)

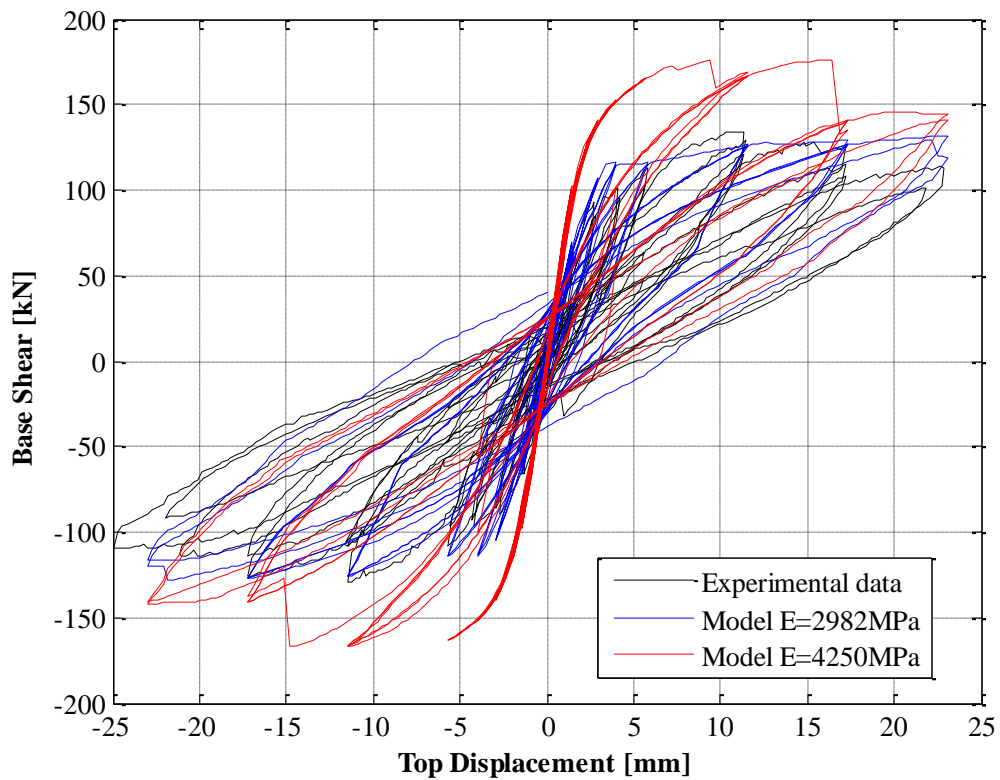


Figure 2.2.11: Total base shear force vs. 2nd floor displacement (Window Wall, $H_{eff} = H_{max}$).



2.3. ESECMaSE calcium silicate in-plane panel tests

Table 2.3.1: Modelling notes

Component	Description
Analysis software and formulation	TREMURI – Equivalent-frame formulation based on a macro-element model
Walls (in-plane)	See Table 1.1 and Penna et al. [2014]

Table 2.3.2: Nonlinear Pushover analysis notes

Nonlinear Pushover analysis notes
<ul style="list-style-type: none"> • Seismic load applied as equivalent horizontal load pattern (imposed displacement of a control node and relative force ratios kept constant) • +/- load directions considered • Cyclic load cases considered • The solution of the static equilibrium equations is obtained by iteration (Newton-Raphson)

Table 2.3.3: Model loading, materials and general comments

Loading	
Dead load	Self-weight of the walls
Overburden	CS03= 0.5 MPa CS05= 1 MPa
Materials	Material properties including values and stress strain behaviour
Masonry (CS bricks)	Model Parameters (as described in Penna et al. [2014]) $\rho = 1800 \text{ kg/m}^3$ $E' = 11343 \text{ MPa}$ (CS03), 18000 MPa (CS05) $G = 1134 \text{ MPa}$ (CS03), 6000 MPa (CS05) $f_m = 7.5 \text{ MPa}$ $\bar{c} = 0.25 \text{ MPa}$ (for CS03; cohesion also referred as f_{vmo} in Penna et al. [2014]) Equivalent Friction coefficient = 0.1 (CS03)
Other key notes	
1) Cyclic incremental static analyses (in displacement control) performed. 2) Second order effects (p-delta) included in the analyses [Penna & Galasco, 2013].	

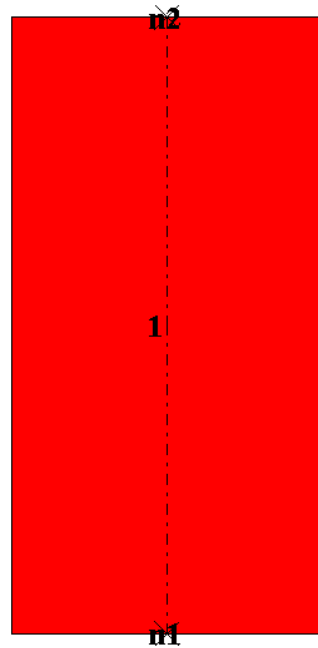


Figure 2.3.1: Tremuri model for CS03 and CS05 panels

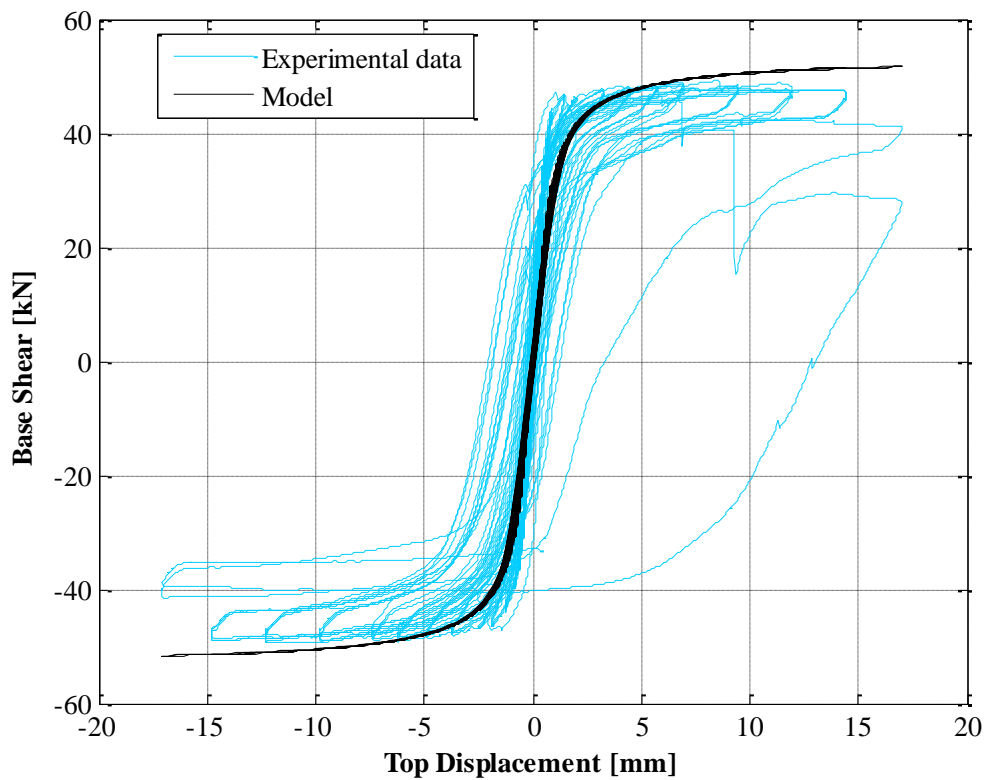


Figure 2.3.2: Shear force-displacement comparison plot for CS03

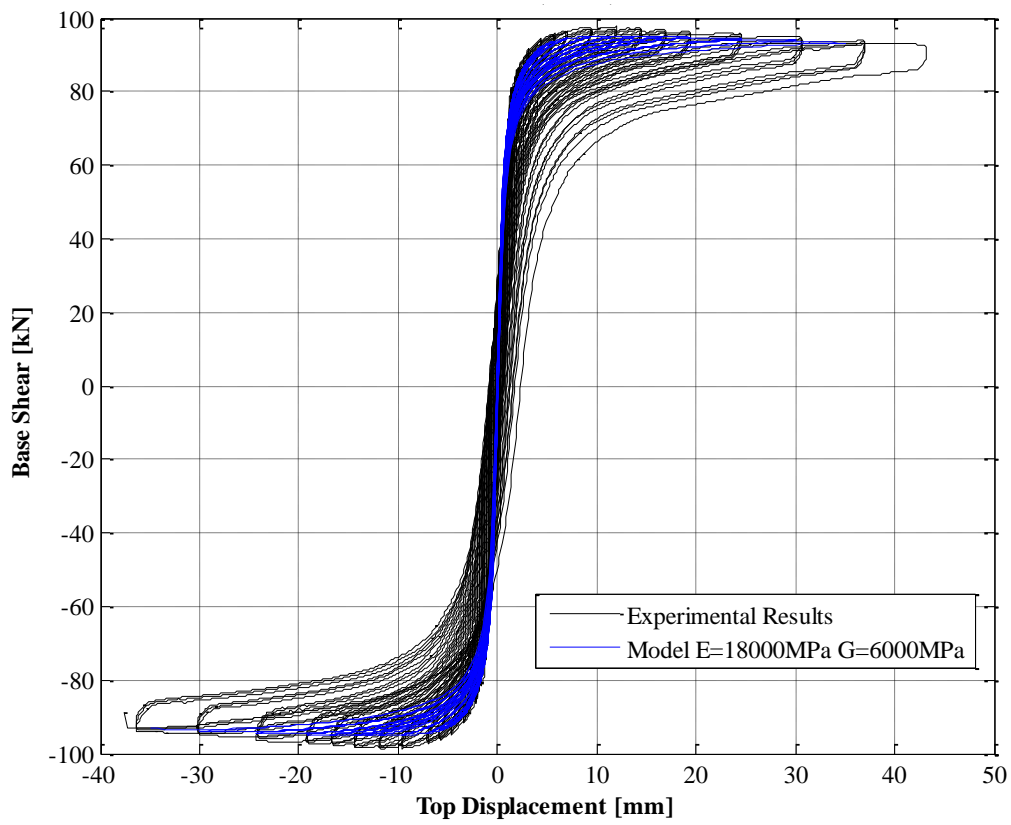


Figure 2.3.3: Shear force-displacement comparison plot for CS05



2.4. ESECMaSE calcium silicate full-scale half-building test

Table 2.4.1: Modelling notes

Component	Description
Analysis software and formulation	TREMURI – Equivalent-frame formulation based on a macro-element model
Walls (in-plane)	See Table 1.1, Lagomarsino et al. [2013] and Penna et al. [2014]
Walls (out-of-plane)	See Table 2.2.1
Wall to wall connection (incl. flange effects)	See Table 2.2.1
Concrete diaphragm	The floor elements are modelled as orthotropic membrane finite elements, identified by a main (spanning) direction, with Young’s moduli in the two perpendicular directions, shear modulus and Poisson ratio [Lagomarsino et al., 2013]
Wall to diaphragm connection	See Table 2.2.1

Table 2.4.2: Eigenvalue analysis notes

Eigenvalue analysis notes
<ul style="list-style-type: none">• Modal analysis is currently performed by means of the Jacobi algorithm on a reduced model with condensed rotational degrees of freedom.

Table 2.4.3: Nonlinear pushover analysis notes

Nonlinear pushover analysis notes
<ul style="list-style-type: none">• Seismic load applied as equivalent horizontal load pattern (imposed displacement of a control node and relative force ratios kept constant)• Pushover analysis with (uniform) mass proportional load pattern assumed• +/- load directions considered• Monotonic and cyclic load cases considered• The solution of the static equilibrium equations is obtained by iteration (Newton-Raphson)



Table 2.4.4: Nonlinear time history analysis notes

Nonlinear time history analysis notes	
	<ul style="list-style-type: none"> • Single-component ground motions applied (x and y separately) • Newmark integration method (constant mean acceleration formulation) implemented • Classical Rayleigh damping model implemented (damping matrix obtained as a linear combination of mass and initial stiffness matrices)

Table 2.4.5: Model loading, materials and general comments

Loading	
Dead load	Self-weight of the walls
Applied load	Additional masses (testing set-up, self-weight of the slab, safety frames...): Floor = 7.3 kN/m ² Roof = 8.9 kN/m ²
Materials	
	Material properties including values and stress strain behaviour
Masonry (CS bricks)	Model Parameters (as described in Penna et al. [2014]) $\rho = 1800 \text{ kg/m}^3$ $E' = 7562 \text{ MPa}$ $G = 2000 \text{ MPa}$ $f_m = 10 \text{ MPa}$ $\bar{c} = 0.25 \text{ MPa}$ (cohesion also referred as f_{vmo} in Penna et al. [2014]) Equivalent Friction coefficient = 0.1
Concrete	Elastic-perfectly plastic formulation (equivalent beams) $\rho = 2500 \text{ kg/m}^3$ $E = 30000 \text{ MPa}$ $G = 12500 \text{ MPa}$ $f_m = 28 \text{ MPa}$
Other key notes	
	<ol style="list-style-type: none"> 1) The out of plane stiffness of the slab has been modelled using fictitious r.c. ring beams, at the top of all the walls, with an equivalent width. The self-weight of the r.c. ring beams have been fixed to 0, in order to avoid any alterations in the total model mass. 2) The presence of the hole in the slab has been taken into account by modelling the self weight of the adjacent portion of slab (and all the additional masses on it) as a linear distributed load acting on the main shear wall. In particular: Floor = 8.8 kN/m Roof = 8.9 kN/m 3) Cyclic incremental static analyses (in displacement control) performed, in addition to pushover (monotonic and cyclic) and incremental static (displacement control) analyses. 4) Second order effects (p-delta) included in the analyses. 5) Time-history analyses performed with reduced stiffness (calibrated, see the Discussion section for details). 6) Need for some additional viscous damping (2%) to simulate the first stages of the pseudodynamic tests (in which no viscous damping was considered). Values of viscous damping close to 0 (1.5% → 0.1%) used in the following stages, in which nonlinearities are activated in the model. 7) Good agreement of simulations accounting for cumulated damage with calibrated viscous damping (Rayleigh) up to test at 0.16g.

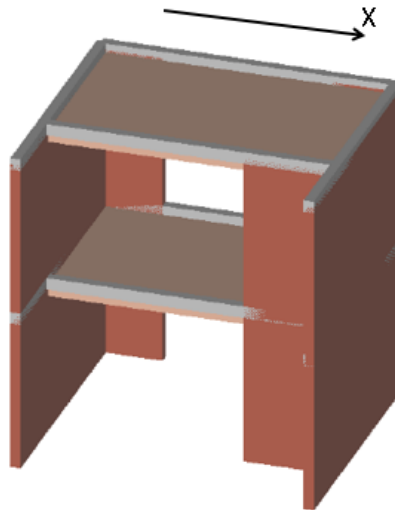


Figure 2.4.1: Tremuri model of the tested half-building specimen

Table 2.4.6: Modal period, frequency, description, mass participation

Mode	Period (s)	Frequency (Hz)	Description of mode	Mass participation %	
				X	Y
1	0.166	6.017	1 st Flexural mode in X direction	80.202	0
2	0.057	17.645	2 nd Flexural mode in X direction	10.509	0
3	0.025	40.794	3 rd Flexural mode in X direction	0.0258	0

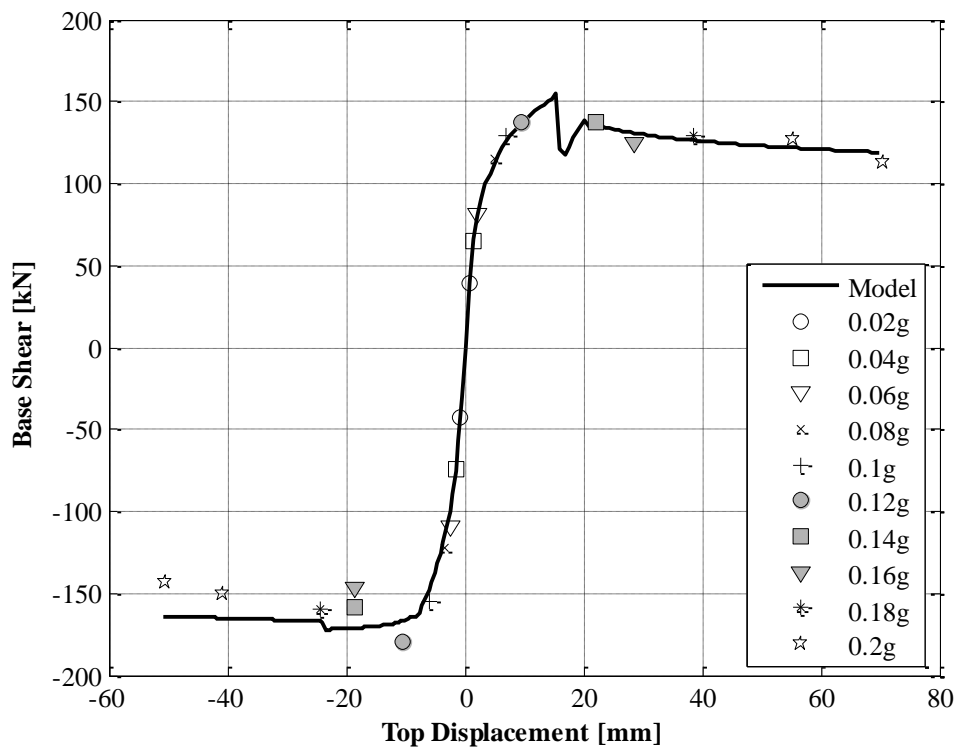


Figure 2.4.2: Monotonic push-over analysis: shear force vs. top displacement (0.02g to 0.20g PGA)

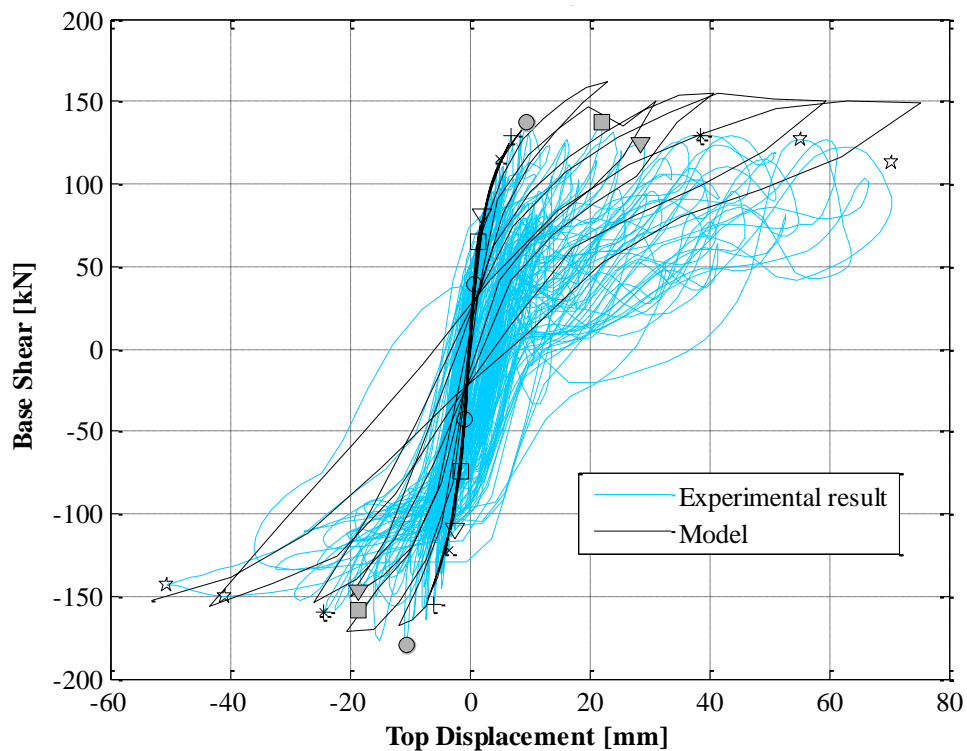


Figure 2.4.3: Cyclic push-over analysis: shear force vs. top displacement (0.02g to 0.20g PGA)

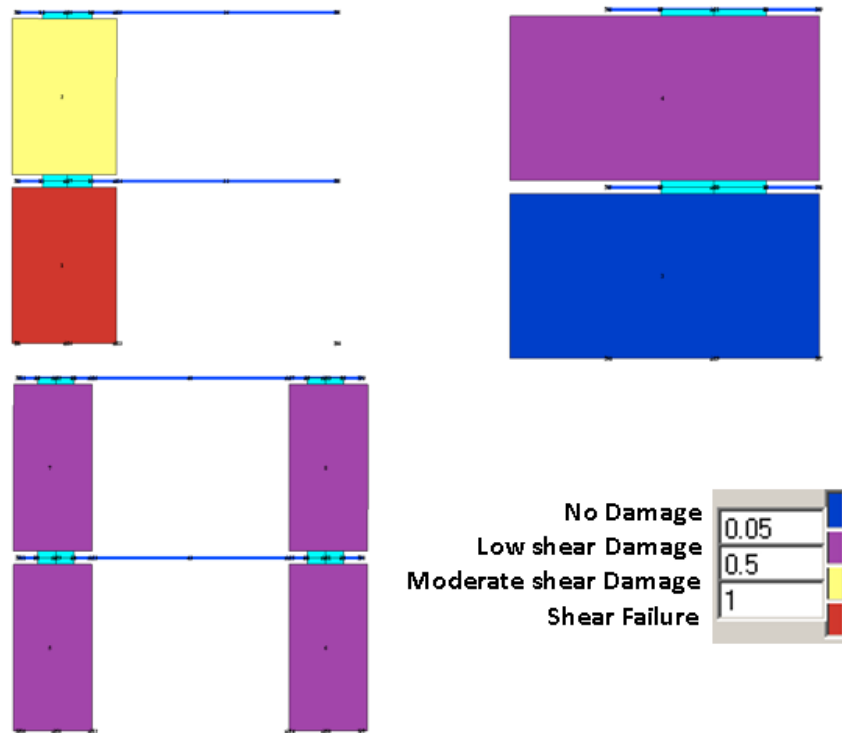


Figure 2.4.4: Crack pattern after successive loadings of 0.02g–0.12g PGAs, i.e. when damages were first observed in laboratory tests

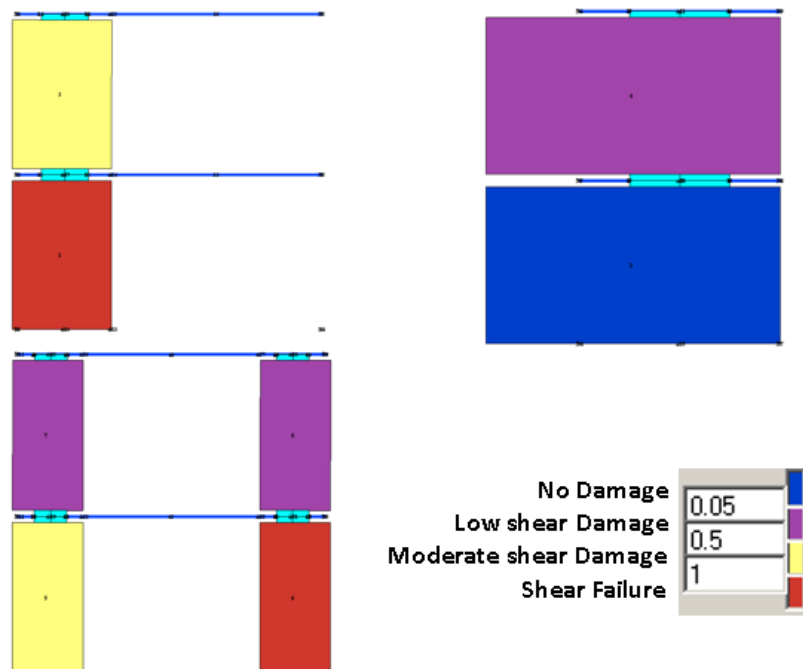


Figure 2.4.5: Crack pattern after successive loadings of 0.02g–0.20g PGAs, i.e. after final laboratory test

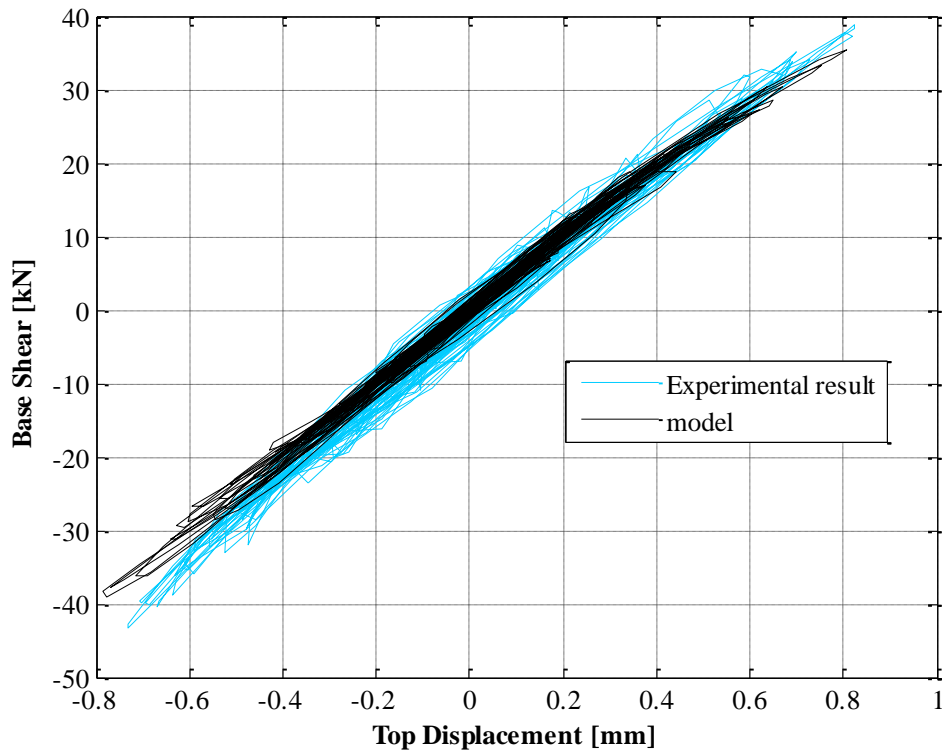


Figure 2.4.6: Base shear force vs. top displacement hysteresis plot during 0.02g PGA

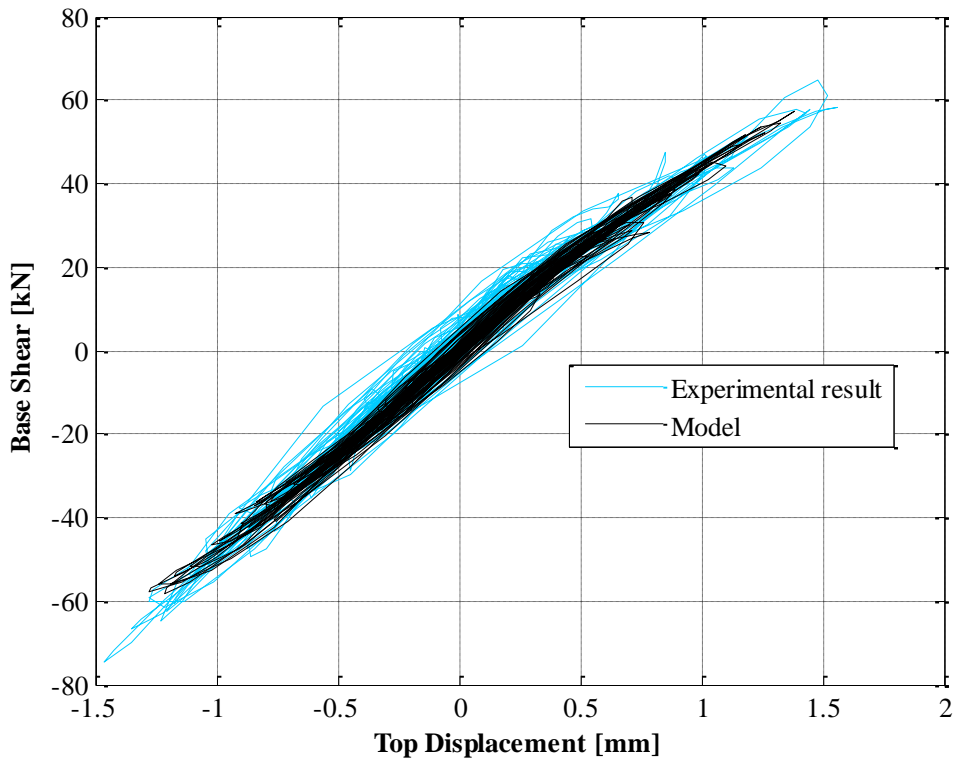


Figure 2.4.7: Base shear force vs. top displacement hysteresis plot during 0.04g PGA

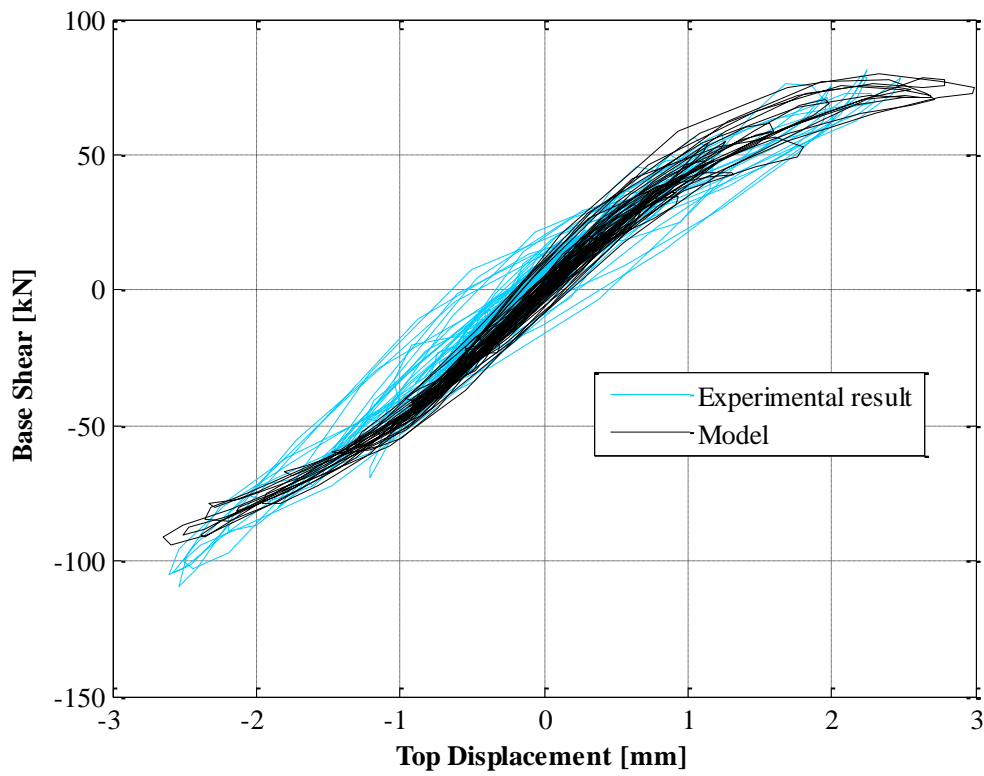


Figure 2.4.8: Base shear force vs. top displacement hysteresis plot during 0.06g PGA

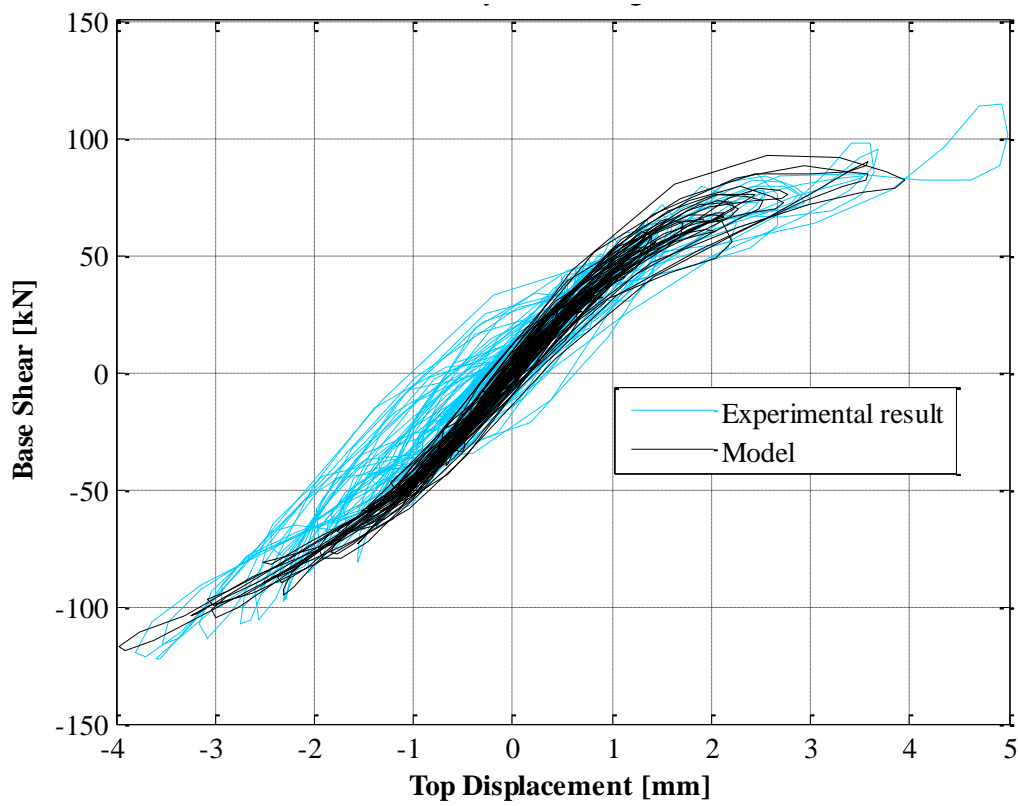


Figure 2.4.9: Base shear force vs. top displacement hysteresis plot during 0.08g PGA

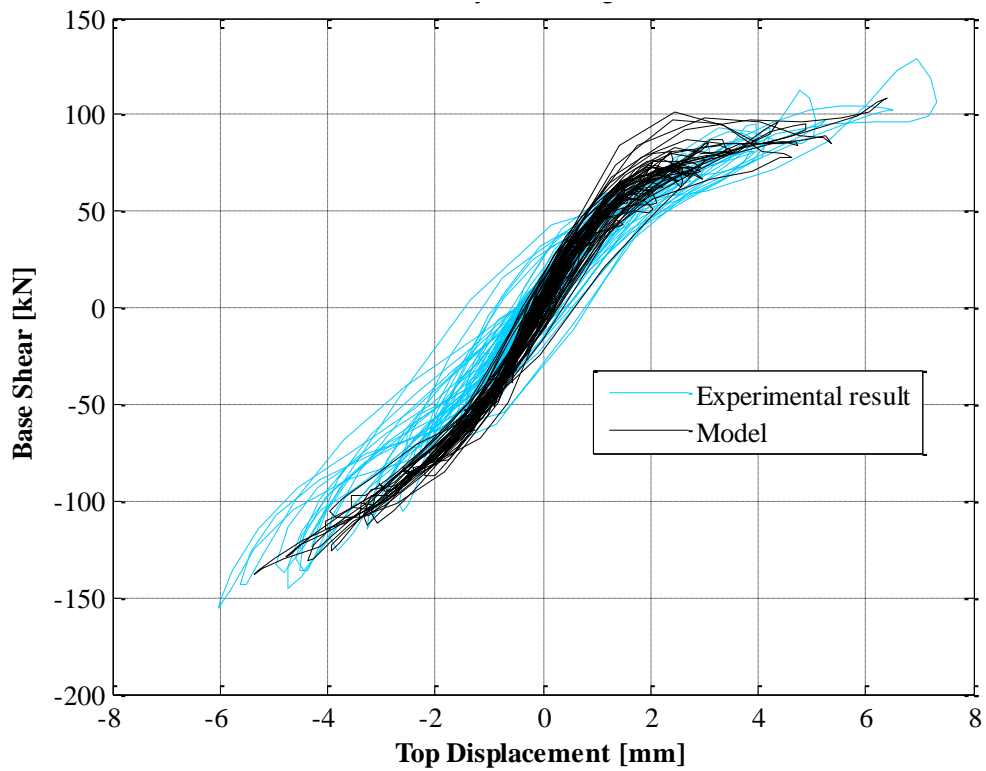


Figure 2.4.10: Base shear force vs. top displacement hysteresis plot during 0.1g PGA

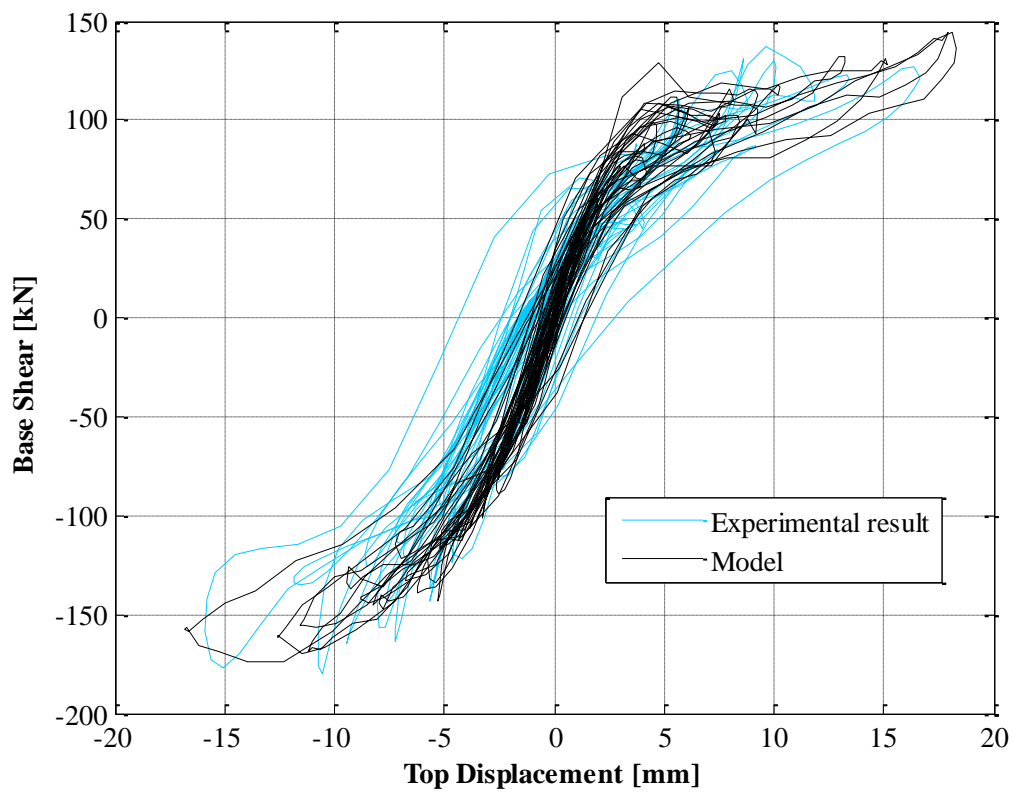


Figure 2.4.11: Base shear force vs. top displacement hysteresis plot during 0.12g PGA

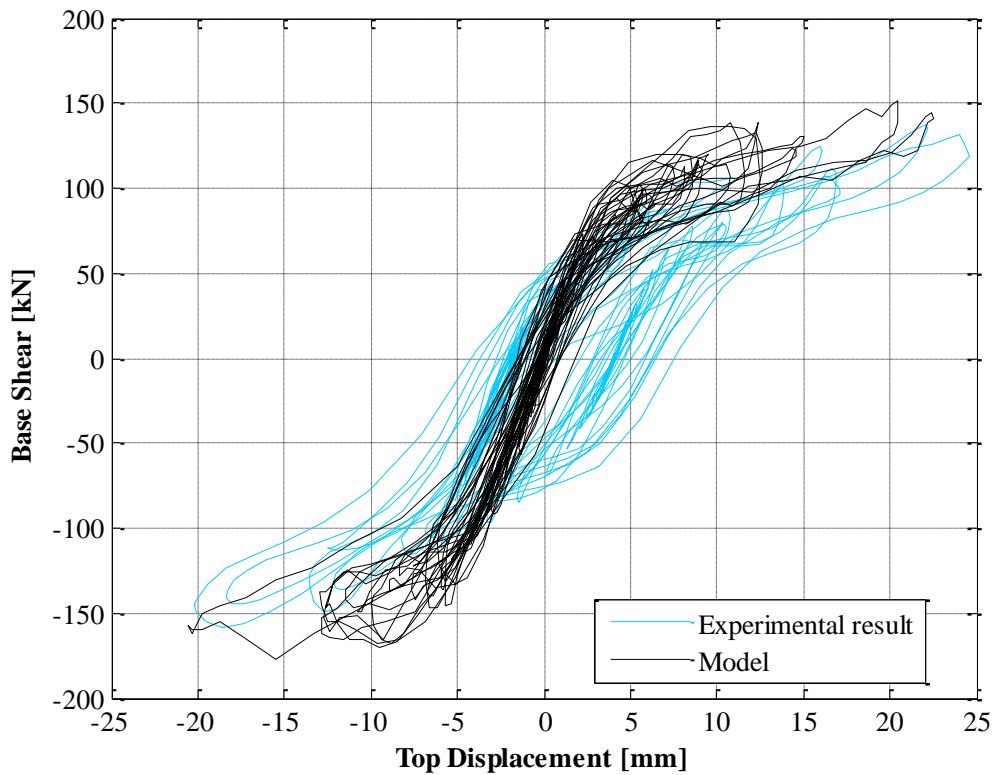


Figure 2.4.12: Base shear force vs. top displacement hysteresis plot during 0.14g PGA

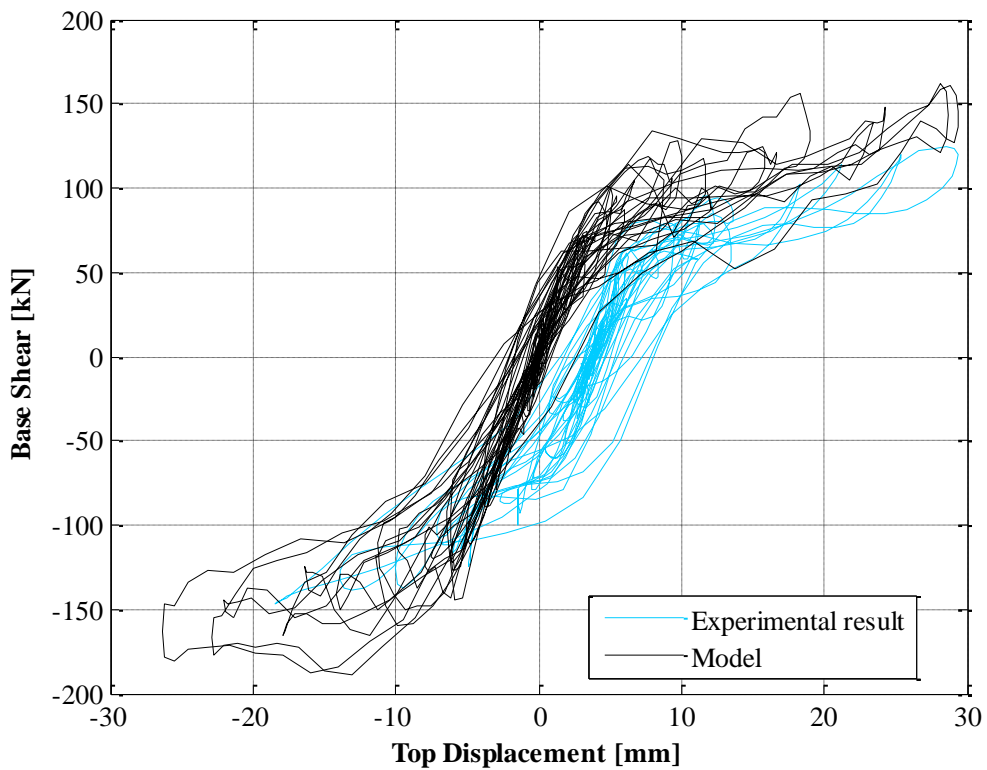


Figure 2.4.13: Base shear force vs. top displacement hysteresis plot during 0.16g PGA

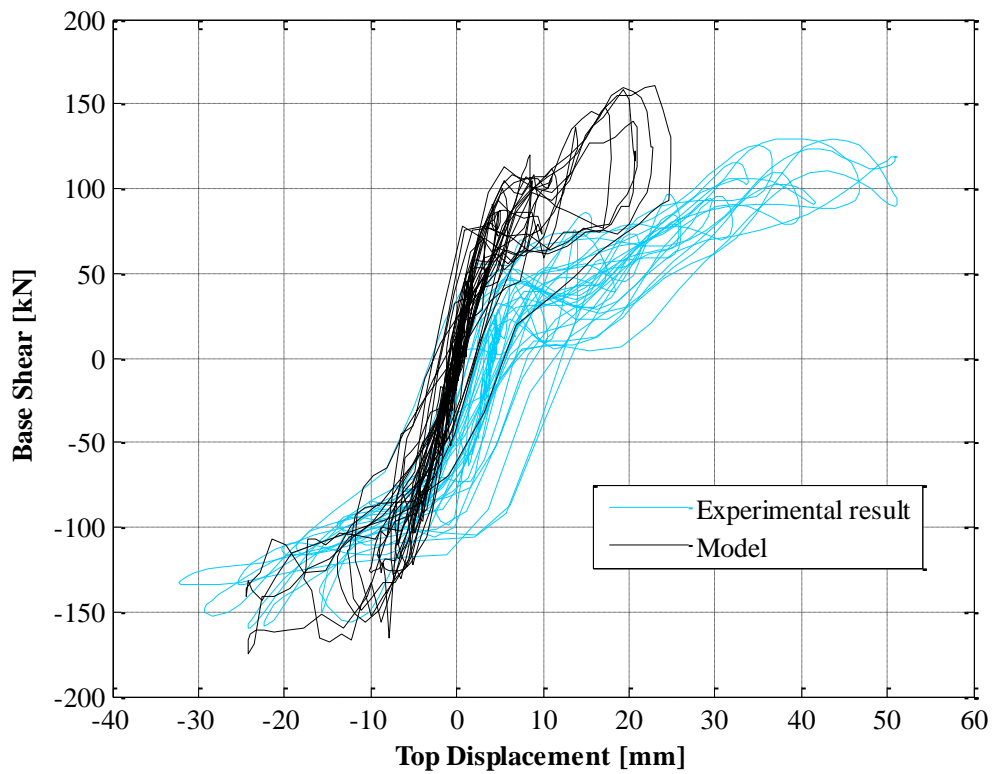


Figure 2.4.14: Base shear force vs. top displacement hysteresis plot during 0.18g PGA

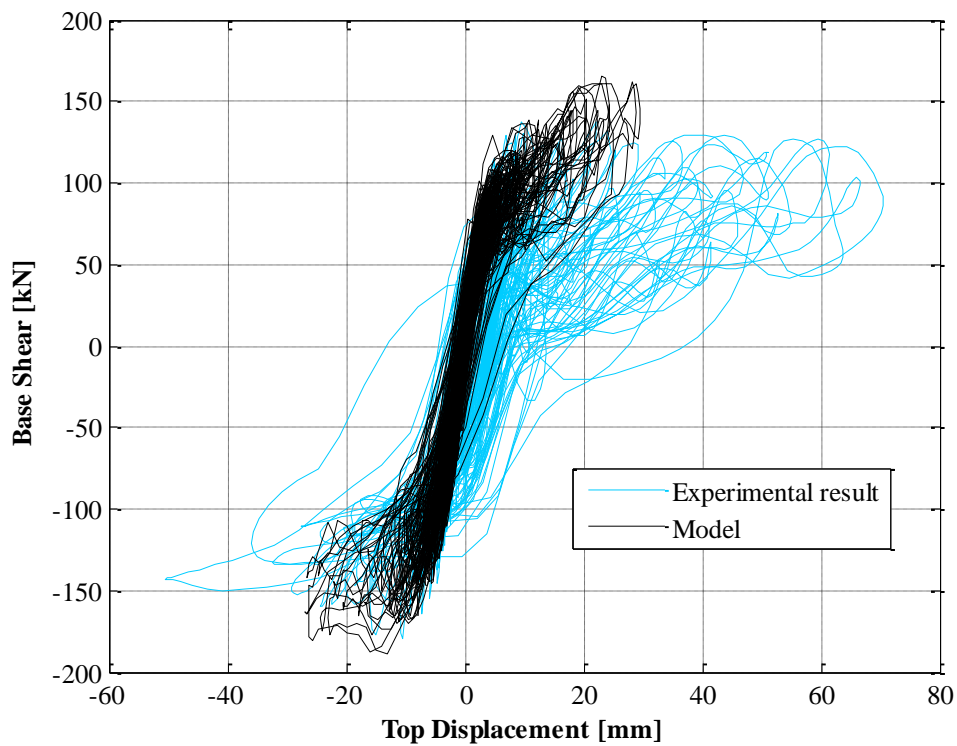


Figure 2.4.15: Base shear force vs. top displacement hysteresis plot during 0.2g PGA



2.4.1. Discussion

The table below summarises the values of stiffness and equivalent viscous damping implemented in the Tremuri model during the dynamic analyses.

A change in the model properties in the degraded model is expected as damage evolution affects the boundary conditions of the structural members during the analysis.

A higher damping ratio at the early stages of the simulated excitation was necessary to match the experimental response in the nonlinear time-history analyses.

Table 2.4.7: Stiffness and Damping implemented in the model during the dynamic tests

PGA [g]	0.02	0.04	0.06	0.08	0.1	0.12	0.14	0.16	0.18	0.2
E' [MPa]	7562	7562	7562	7562	7562	6000	6000	5000	5000	5000
G [MPa]	2000	2000	2000	2000	2000	1800	1800	1500	1500	1500
ξ_v [%]	2	2	1.5	1.5	0.5	0.3	0.2	0.15	0.1	0.1



2.5. One-way spanning wall out-of-plane tests (Doherty)

Table 2.5.1: Modelling notes

Component	Description
Analysis software and formulation	a) TREMURI – Equivalent-frame formulation based on a macro-element model b) Trilinear model for dynamic analysis with secant-stiffness proportional damping, calibrated on TREMURI pushover curves
Walls (out-of-plane)	See Penna & Galasco [2013]

Table 2.5.2: Nonlinear time history analysis notes

Nonlinear time history analysis notes
<ul style="list-style-type: none">• Single-component ground motions applied• Newmark integration method (constant mean acceleration formulation) implemented• A) Classical Rayleigh damping model implemented (damping matrix obtained as a linear combination of mass and initial stiffness matrices)• B) Secant-stiffness proportional viscous damping

Table 2.5.3: Model loading, materials and general comments

Loading	
Dead load	Self-weight of the masonry wall
Overburden	Specimen 8: 0.15 MPa Specimen 12: no overburden
Materials	Material properties including values and stress strain behaviour
Masonry (Clay bricks)	Model parameters: $\rho = 1800 \text{ kg/m}^3$ $E = 5400 \text{ MPa}$ $f_m = 9.7 \text{ MPa}$ (the shear model parameters are not relevant in this case)
Other key notes	
<ol style="list-style-type: none">1) The stiffness of the top spring used in the experimental setup has been explicitly modelled by means of an equivalent beam model2) A limitation to the bending moment transmitted by the spring to the top of the wall has been also considered3) A fair agreement has been achieved for the “cracked” tests on specimen 8	

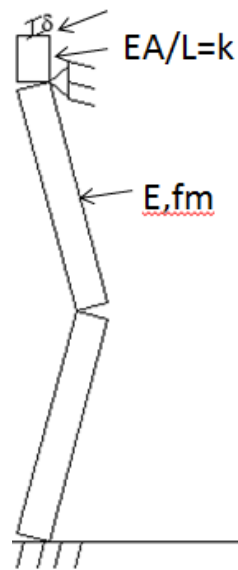


Figure 2.5.1: Scheme of the 2D macroelement model

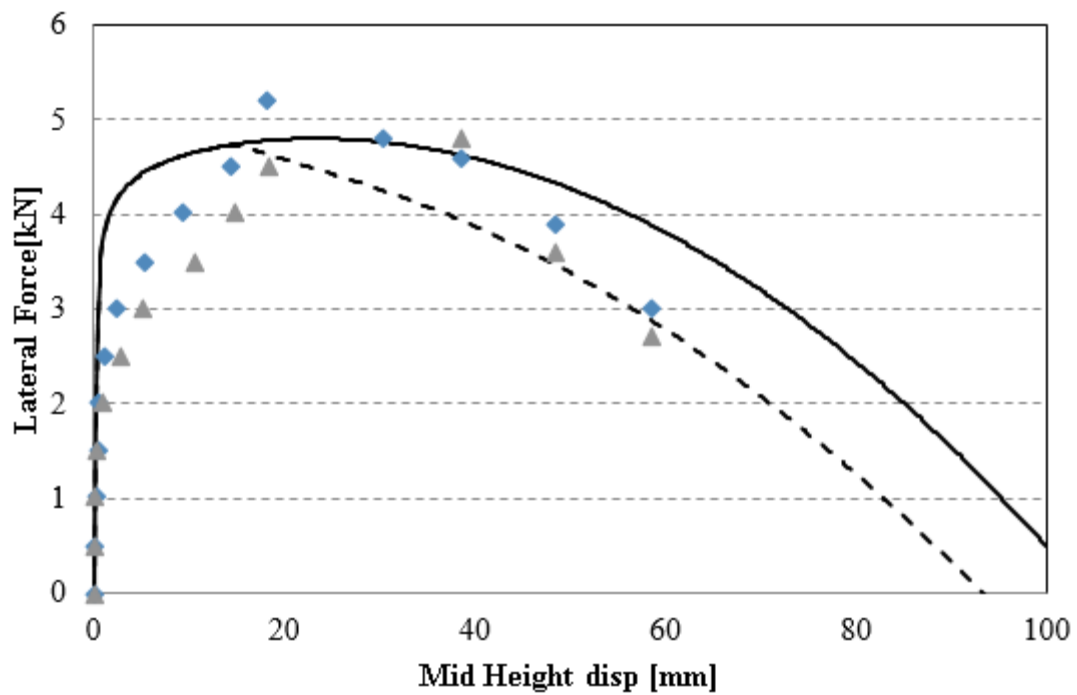


Figure 2.5.2: Comparison of experimental (“cracked” tests) and numerical force-displacement curves for Specimen 8 (dashed line with limited bending moment on top of the wall)

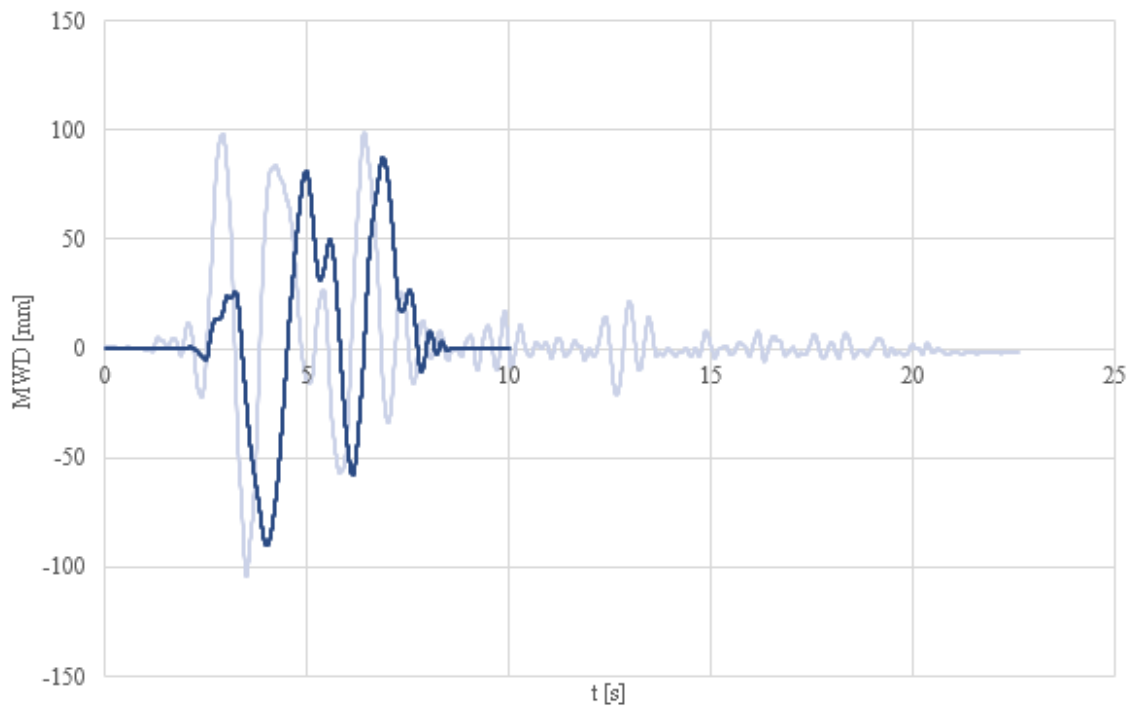


Figure 2.5.3: Example of mid-height displacement time-history (numerical results in blue) – Specimen 12, 66% EL

2.5.1. Discussion and sensitivity analyses (if relevant)

As the dynamic model implemented in TREMURI is still under development, an alternative trilinear model was developed for the dynamic simulation. The trilinear envelope is calibrated against the Tremuri pushover analysis curves.



Force-Disp Curve Comparison

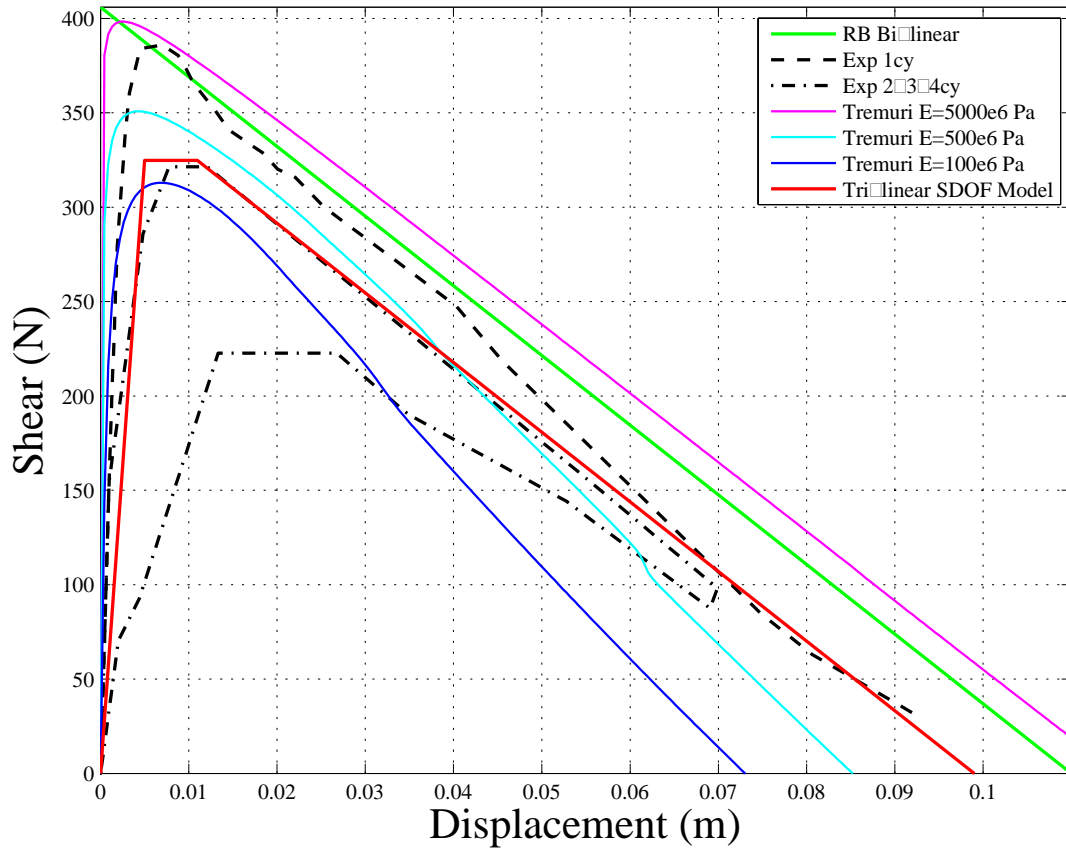


Figure 2.5.4: Comparison of experimental envelope force-displacement curves, Tremuri pushover curves and simplified trilinear model curves.

The results of the trilinear model are in fair agreement with the experimental results (see following figures).

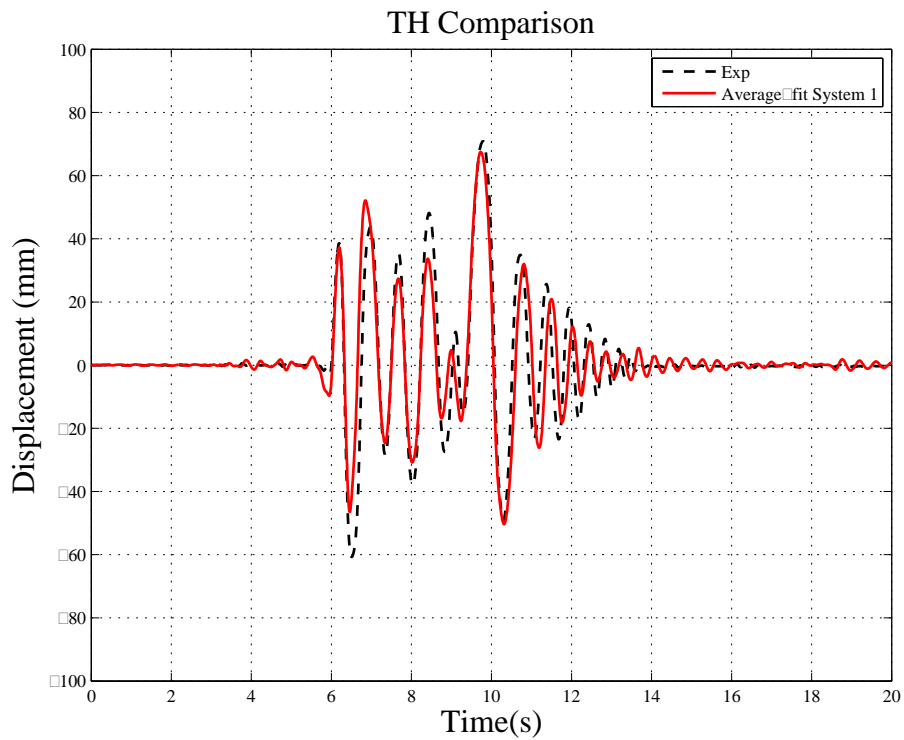


Figure 2.5.5: Comparison of experimental and numerical displacement time-history for Specimen 13 –September- Paicoma Dam 80%.

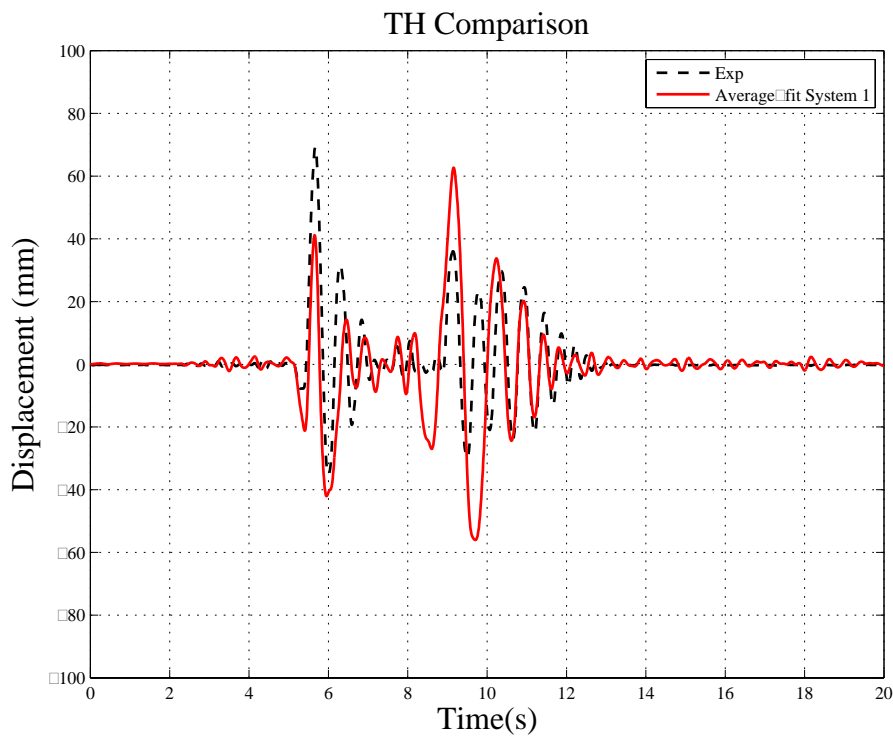


Figure 2.5.6: Comparison of experimental and numerical displacement time-history for Specimen 13 –September- Paicoma Dam 100%.

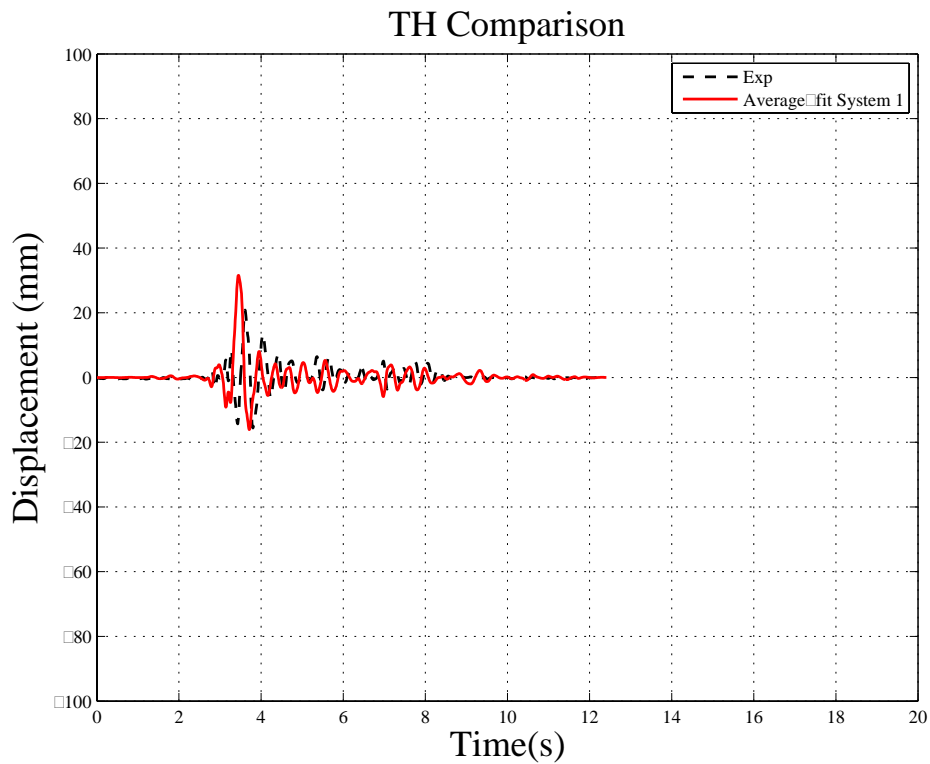


Figure 2.5.7: Comparison of experimental and numerical displacement time-history for Specimen 12 –September- Nahanni 200%.

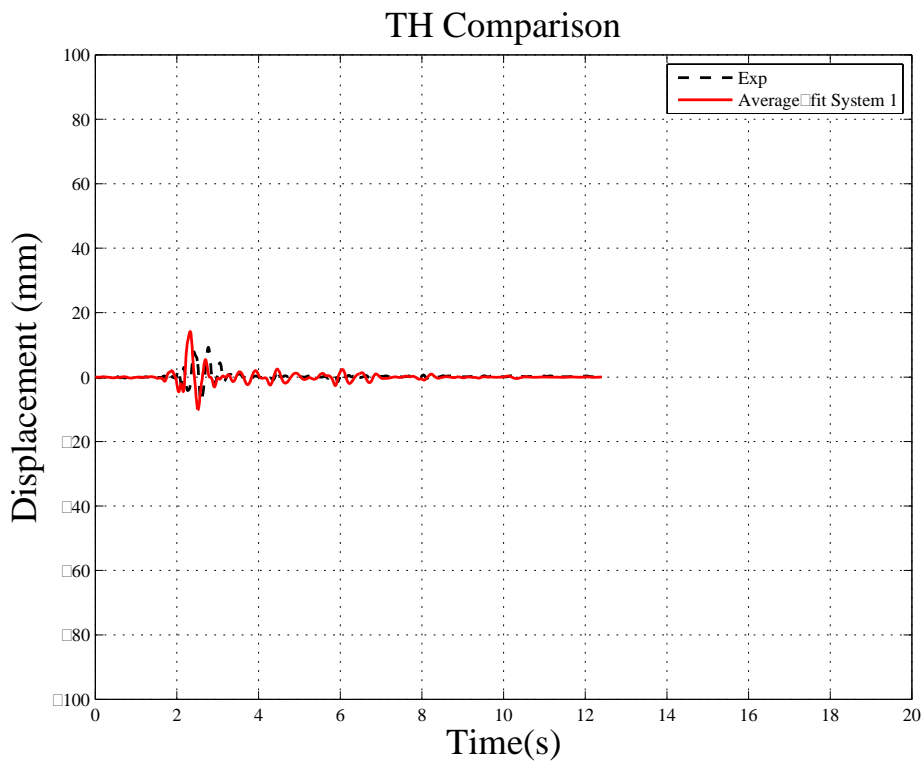


Figure 2.5.8: Comparison of experimental and numerical displacement time-history for Specimen 12 –September- Nahanni 100%.

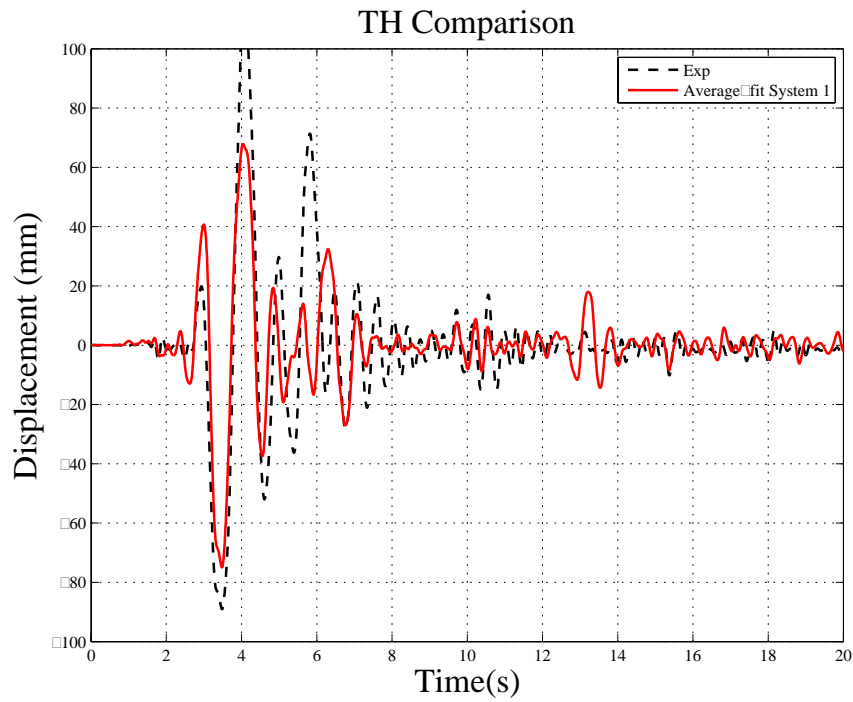


Figure 2.5.9: Comparison of experimental and numerical displacement time-history for Specimen 13 –September- El Centro 66%.

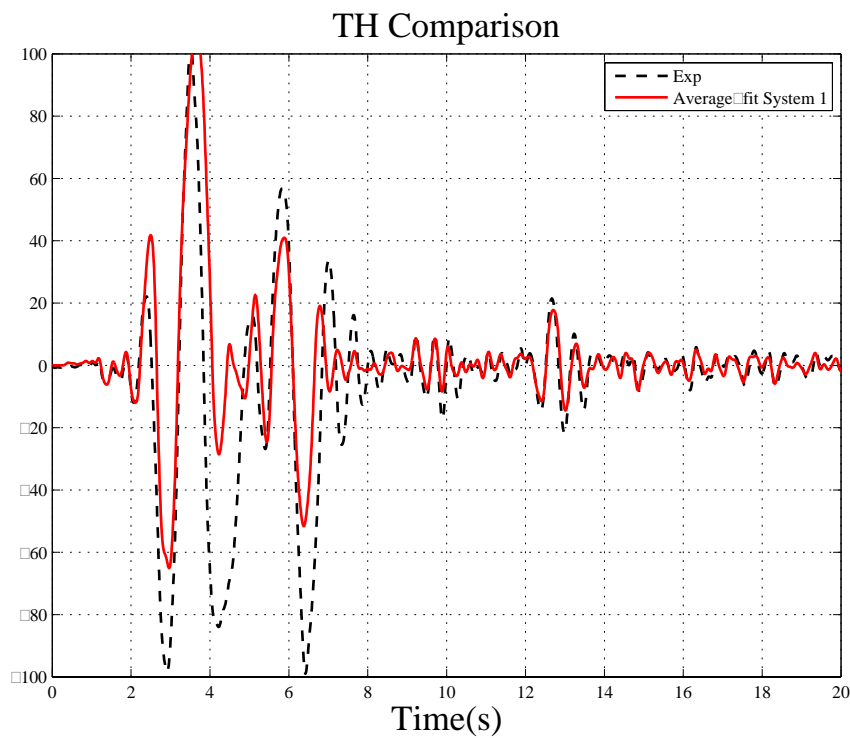


Figure 2.5.10: Comparison of experimental and numerical displacement time-history for Specimen 12 –September- El Centro 66%.



3. Cross-validation index buildings

3.1. Terraced house (T1*)

Table 3.1.1: Modelling notes

Component	Description
Analysis software and formulation	TREMURI – Equivalent-frame formulation based on a macro-element model
Walls (in-plane)	See Table 1.1, Lagomarsino et al. [2013] and Penna et al. [2014]
Walls (out-of-plane)	See Table 2.2.1
Spandrels/lintels and wall coupling	See Table 2.2.1
Wall to wall connection (incl. flange effects)	See Table 2.2.1
Modelling of veneer walls (outer leaf)	The external clay veneer of the gable walls has been modelled as an equivalent additional inertial mass applied to the wall (only for horizontal components).
Wall ties	See above.
Concrete/Timber diaphragm	The floor elements are modelled as orthotropic membrane finite elements, identified by a main (spanning) direction, with Young’s moduli in the two perpendicular directions, shear modulus and Poisson ratio (see Lagomarsino et al., 2013). In particular the numerical values implemented are: E1 = 210000 MPa (concrete*); 5000MPa (Timber Roof*) E2 = 30000 MPa (concrete); 50MPa (Timber Roof) G = 12500 MPa (concrete); 35MPa (Timber Roof) $\nu = 0.2$ (concrete); *in both cases a thickness of 20 mm was adopted for the equivalent membrane elements
Wall to diaphragm connection	See Table 2.2.1
Foundation	Modelled as rigid (fixed restrain).

Table 3.1.2: Eigenvalue analysis notes

Eigenvalue analysis notes
<ul style="list-style-type: none"> Modal analysis is currently performed by means of the Jacobi algorithm on a reduced model with condensed rotational degrees of freedom.



Table 3.1.3: Nonlinear pushover analysis notes

Nonlinear pushover analysis notes
<ul style="list-style-type: none">• Seismic load applied as equivalent horizontal load pattern (imposed displacement of a control node and relative force ratios kept constant)• Pushover analysis with (uniform) mass proportional and inverse triangular load pattern assumed• +/- load directions considered• Monotonic and cyclic load cases considered• The solution of the static equilibrium equations is obtained by iteration (Newton-Raphson)

Table 3.1.4: Nonlinear time history analysis notes

Nonlinear time history analysis notes
<ul style="list-style-type: none">• Single-component ground motions applied to the foundation(x and y separately)• Newmark integration method (constant mean acceleration formulation) implemented• Classical Rayleigh damping model implemented (damping matrix obtained as a linear combination of mass and initial stiffness matrices)



Table 3.1.5: Model loading, materials and general comments

Loading	
Dead loads	Self-weight of the walls, hollowcore planks and roof/floor structure.
Superimposed dead loads	Floors = 2.4kPa Roof = 0.5kPa
Live loads	Floors = 1.75kPa Roof = 0kPa
Load combination	DL + SDL + 0.24LL
Materials	
Masonry (CS bricks)	Model Parameters (as described in Penna et al. [2014]) $\rho = 1900 \text{ kg/m}^3$ $E' = 8820 \text{ MPa} (= 2E = 2*4410 \text{ MPa})$ $G = 1300 \text{ MPa}$ $f_m = 6.3 \text{ MPa}$ $\bar{c} = 0.22 \text{ MPa}$ (cohesion also referred as f_{vmo} in Penna et al. [2014]) Equivalent Friction coefficient = 0.27
Timber/Plywood	Elastic-plastic material model (beams) $\rho = 600 \text{ kg/m}^3$ $E = 6000 \text{ MPa}$ $G = 370 \text{ MPa}$
Other key notes	
1) The external clay ($\rho = 1900 \text{ kg/m}^3$, $s = 0.1 \text{ m}$) veneer of the gable walls has been modelled as an equivalent additional mass applied to the wall. 2) Analyses have been performed also on an equivalent 2D model (accounting for out-of-plane response) 3) Second order effects (p-delta) included in the analyses. 4) Rayleigh damping implemented with $\xi_v = 2\%$ set for the following range of frequency: X direction: $f_1=1.51 \text{ Hz}$ and $f_2=0.49 \text{ Hz}$ Y direction: $f_1=12.20 \text{ Hz}$ and $f_2=1.44 \text{ Hz}$	

Table 3.1.6: Breakdown of loading and masses

Loading	DL [kPa]	SDL [kPa]	LL [kPa]	DL+SDL+0.24LL [kPa]	Area [m ²]
1 st Floor	3.25	2.4	1.75	6.07	42.7
2 nd Floor	3.25	2.4	1.75	6.07	42.7
Roof	0.27	0.5	0	0.77	60.5
Total model mass (including DL+SDL+0.24LL) = 99062 kg					
Masonry	Density [kg/m ³]		Thickness [m]	Total masonry mass [kg]	
Calcium silicate	1900		0.1 / 0.12	34100	
Clay (veneer)	1900		0.1	7372	

Table 3.1.7: Cut-section total z-forces (weight from gravity load at $t=0$) at different cut-plane heights

Cut-plane height (m)	Cut-section z-force (kN)
<Just above ground/base>	971.8
<Just above L1 diaphragm>	457.84

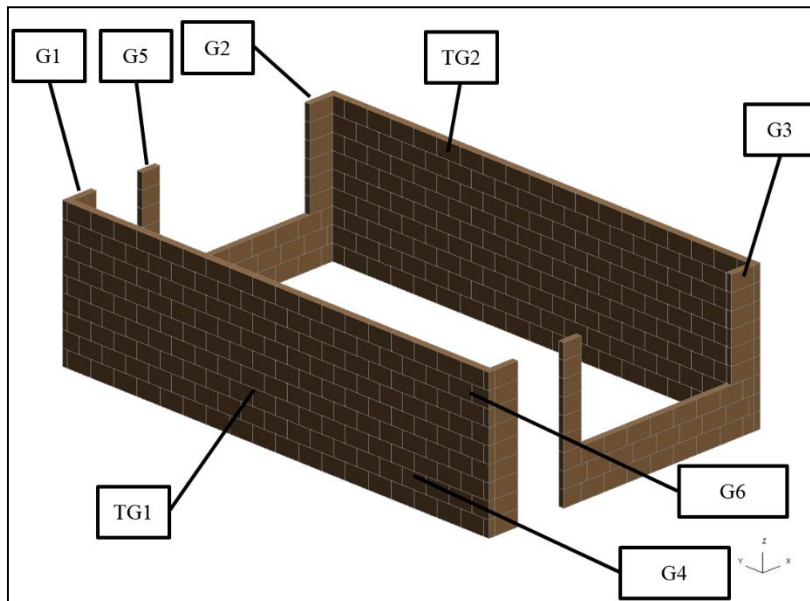


Figure 3.1.1: Pier labelling convention for T1* building (ground floor)

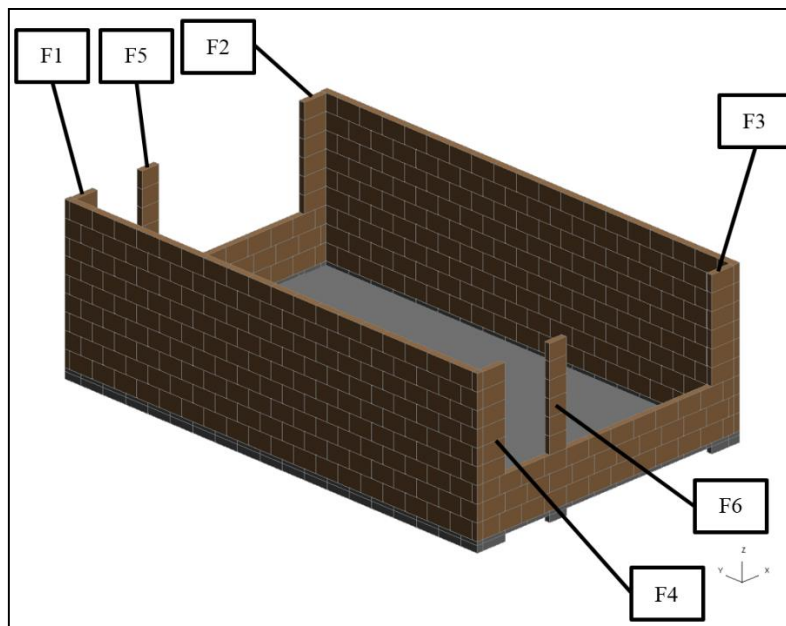


Figure 3.1.2: Pier labelling convention for T1* building (first floor)

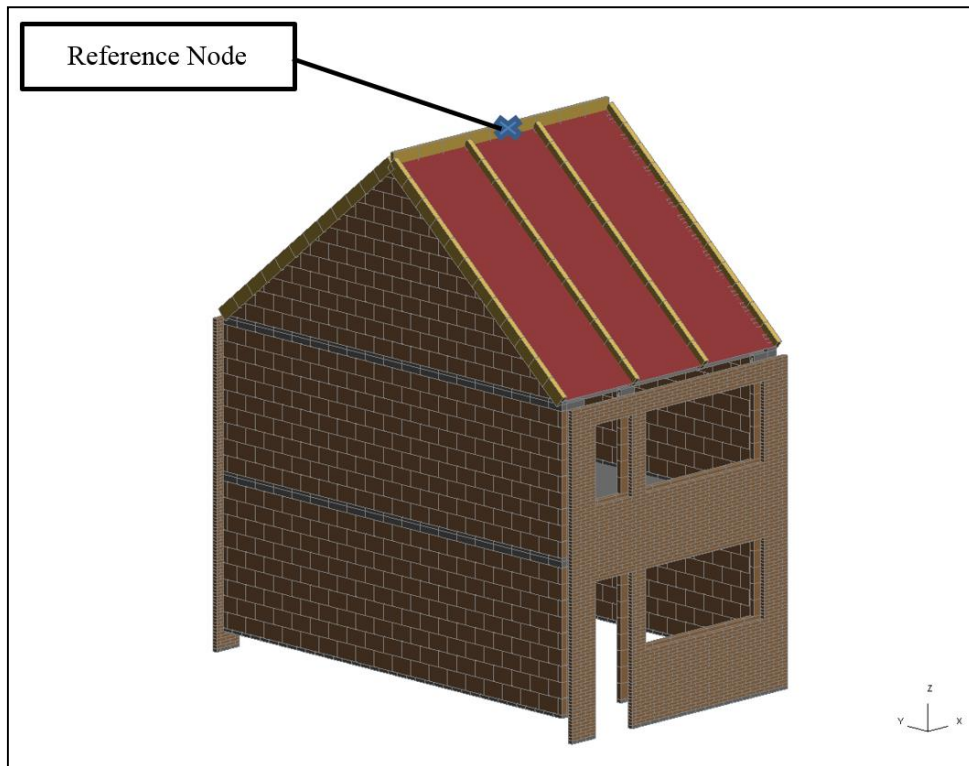


Figure 3.1.3: T1* model pushover reference node location

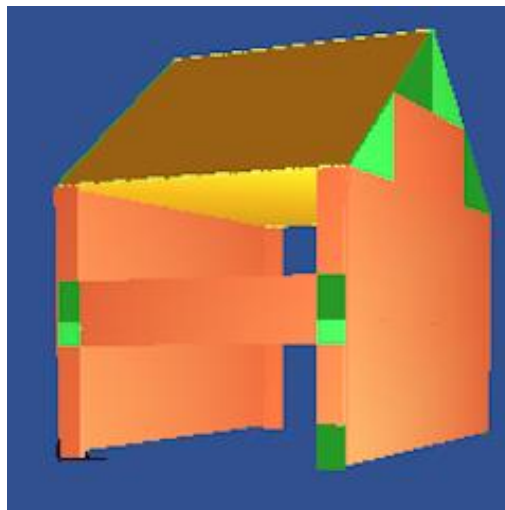
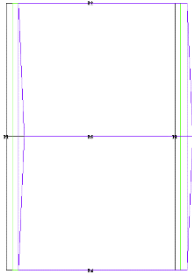
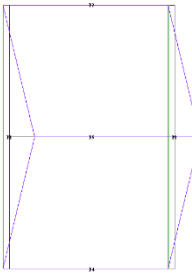
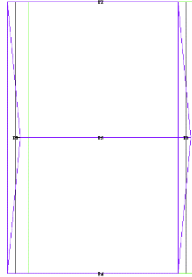
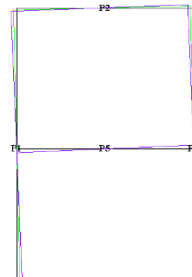
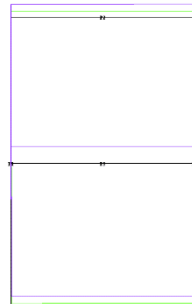


Figure 3.1.4: Tremuri model for T1*

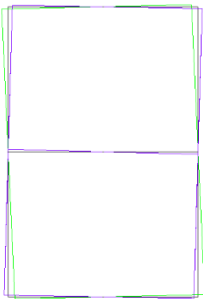
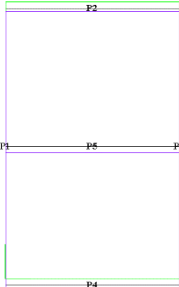
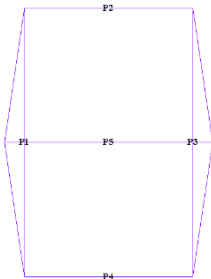
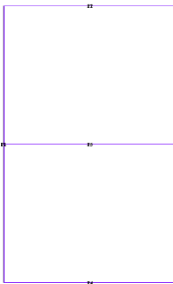
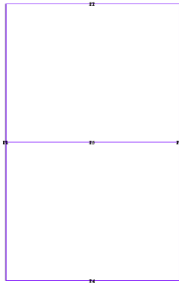


3.1.1. Modal analysis

Table 3.1.8: Modal period, frequency, description, mass participation

Mode	Period (s)	Frequency (Hz)	Description of mode	Mass participation %	
				X	Y
1	0.661	1.512		81.955	0
2	0.287	3.488		6.086	0
3	0.236	4.235		4.669	0
4	0.144	6.945		0	0.050
5	0.082	12.141		0	83.861



Mode	Period (s)	Frequency (Hz)	Description of mode	Mass participation %	
				X	Y
6	0.067	14.976		0	0.000
7	0.032	31.699		0	8.756
8	0.029	34.407		0	0
9	0.027	37.169		0	0
10	0.026	38.033		0	0

3.1.2. Pushover analysis (monotonic and cyclic)

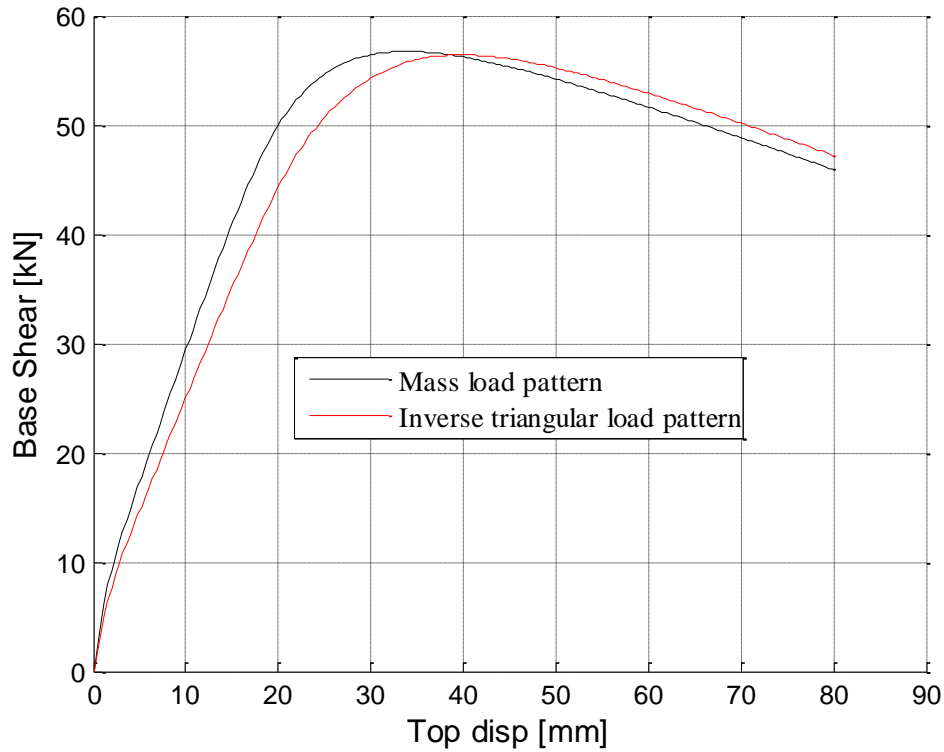


Figure 3.1.5: X direction base shear versus reference node displacement (monotonic)

Table 3.1.9: Cut-planes pier forces at peak/plateau x-dir pushover (mass load pattern) base shear

Pier	X- dir pier force (kN) Cut-plane height ~1.65m		Pier	X-dir pier force (kN) Cut-plane height ~4.65m	
	Axial	Shear		Axial	Shear
G1	-112.124	10.948	F1	-79.144	11.160
G2	-111.878	17.411	F2	-78.993	2.794
G3	-111.868	17.411	F3	-78.896	2.784
G4	-112.128	10.949	F4	-79.129	11.159
TG1	-138.003	0.000	TG1	-36.974	-0.008
TG2	-242.597	0.000	TG2	-75.508	0.008
Total	-828.598	56.720	Total	-428.645	27.897

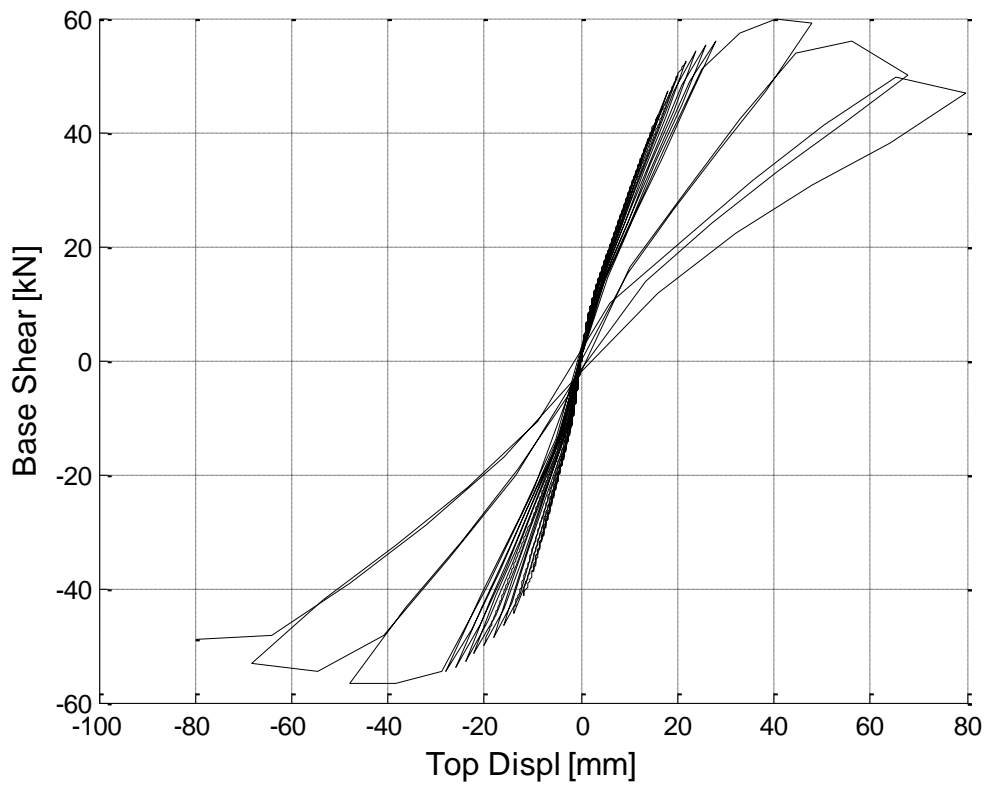


Figure 3.1.6: X direction base shear versus reference node displacement (cyclic)

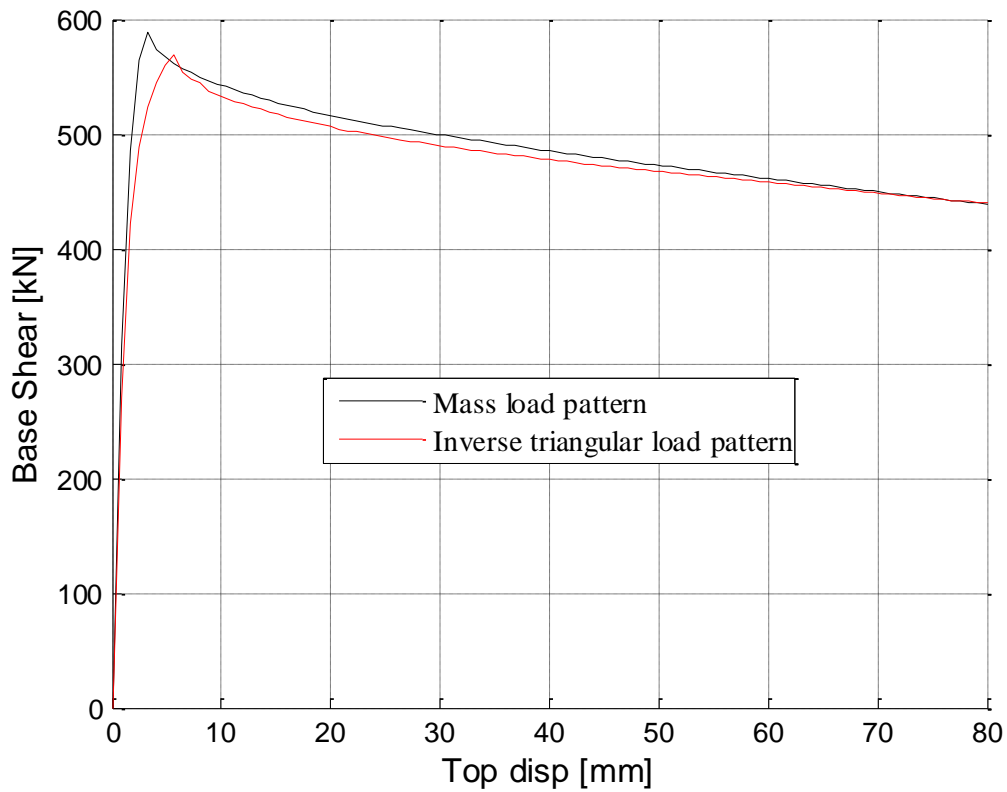


Figure 3.1.7: Y direction base shear versus reference node displacement (monotonic)



Table 3.1.10: Cut-planes pier forces at peak/plateau y-dir pushover (mass load pattern) base shear

Pier	Y- dir pier force (kN) Cut-plane height ~1.65m		Pier	Y-dir pier force (kN) Cut-plane height ~4.65m	
	Axial	Shear		Axial	Shear
G1	-59.547	0.633	F1	-22.465	1.290
G2	-78.412	-0.635	F2	-29.609	-1.608
G3	0	0	F3	-3.989	0.466
G4	0	0	F4	-2.308	-0.149
TG1	-336.707	283.143	TG1	-180.007	139.347
TG2	-353.821	305.685	TG2	-190.276	150.278
Total	-828.487	588.827	Total	-428.654	289.625

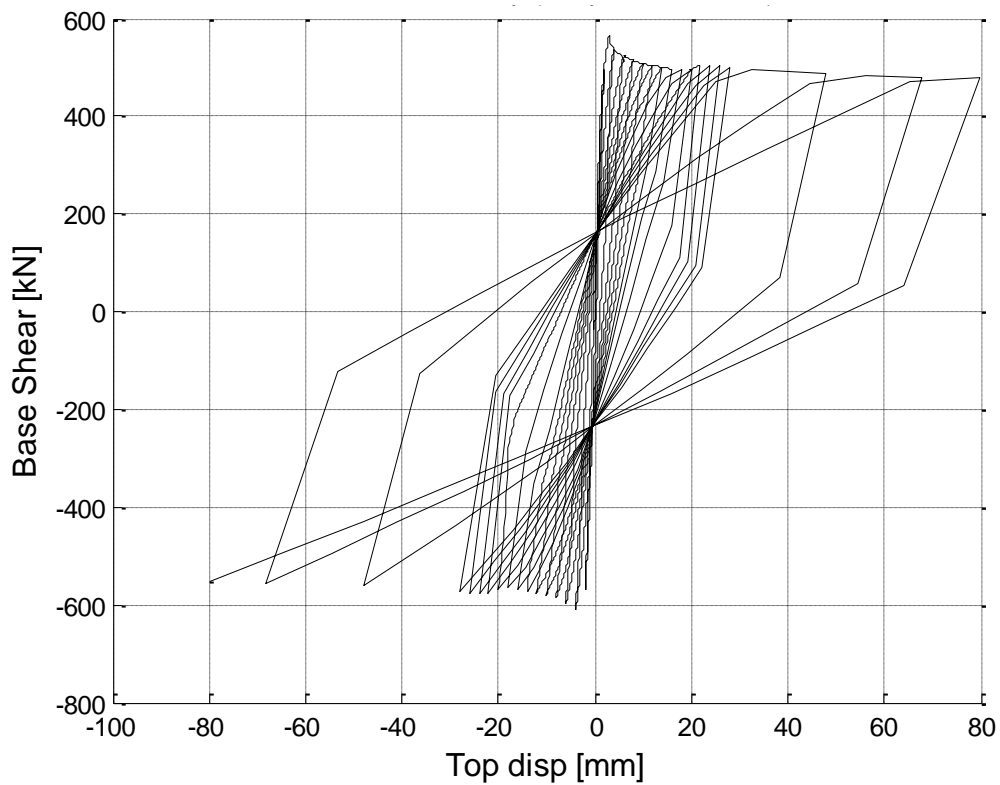


Figure 3.1.8: Y direction base shear versus reference node displacement (cyclic)



3.1.3. Time history analysis

Table 3.1.11: Peak reference node displacement (3 records at each PGA level)

PGA	RECORD 3 (mm)		RECORD 6 (mm)		RECORD 7 (mm)	
	X direction	Y direction	X direction	Y direction	X direction	Y direction
0.1g	18.89	0.71	17.49	0.5	18.05	0.84
0.25g	35.95	1.12	45.24	1.26	50.26	1.61
0.5g	47.99	6.28	98.98	2.52	113.67	4.17

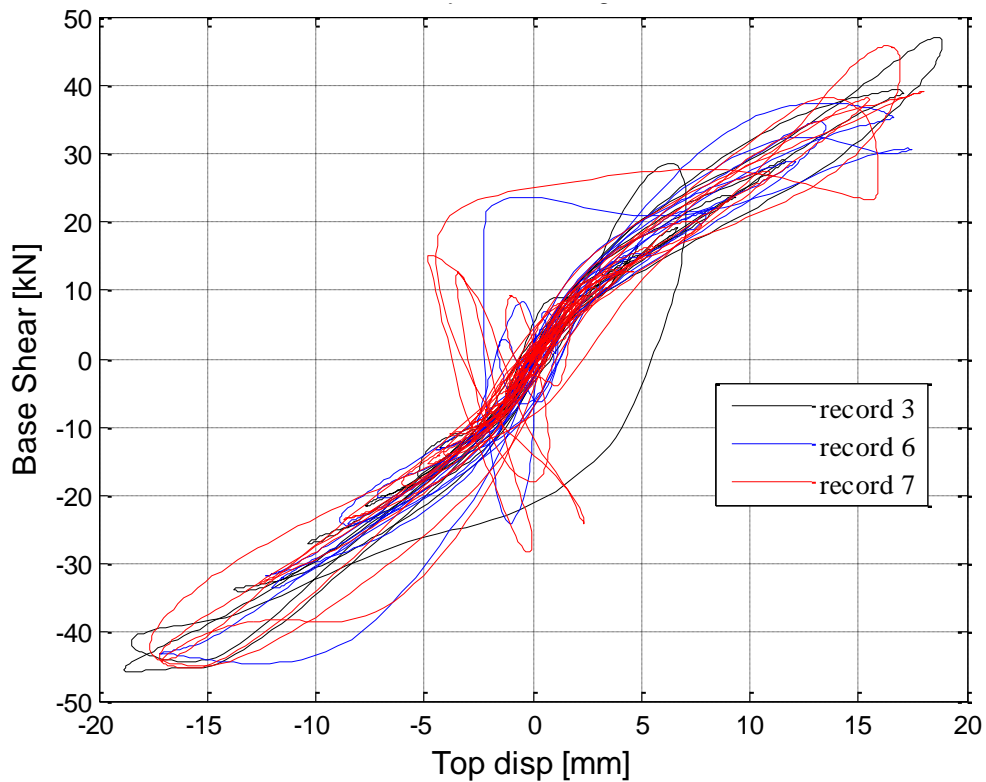


Figure 3.1.9: Base shear versus reference node displacement – 0.1g scaled PGA, record 3, 6 and 7 (X direction).

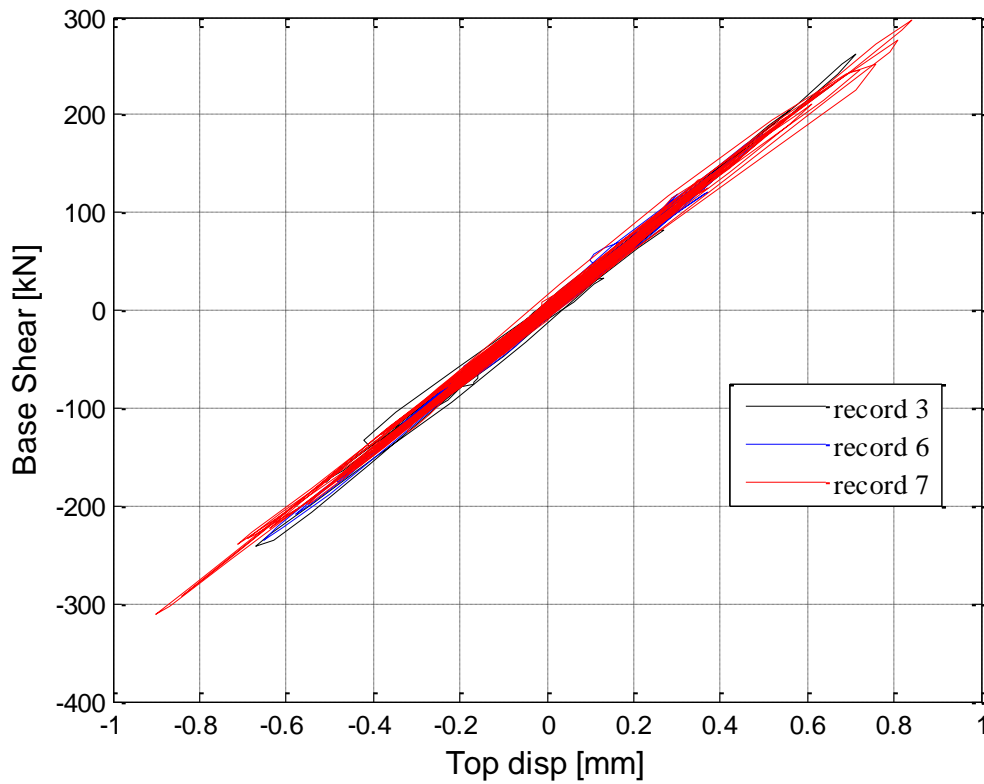


Figure 3.1.10: Base shear versus reference node displacement – 0.1g scaled PGA, record 3, 6 and 7 (Y direction).

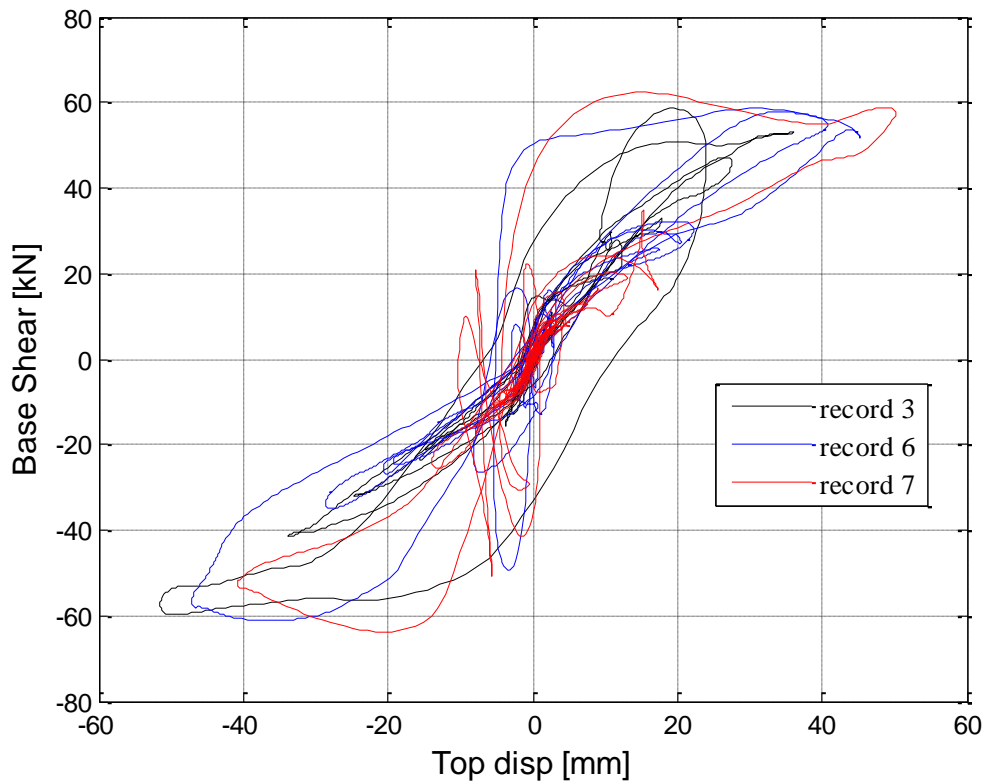


Figure 3.1.11: Base shear versus reference node displacement – 0.25g scaled PGA, record 3, 6 and 7 (X direction).

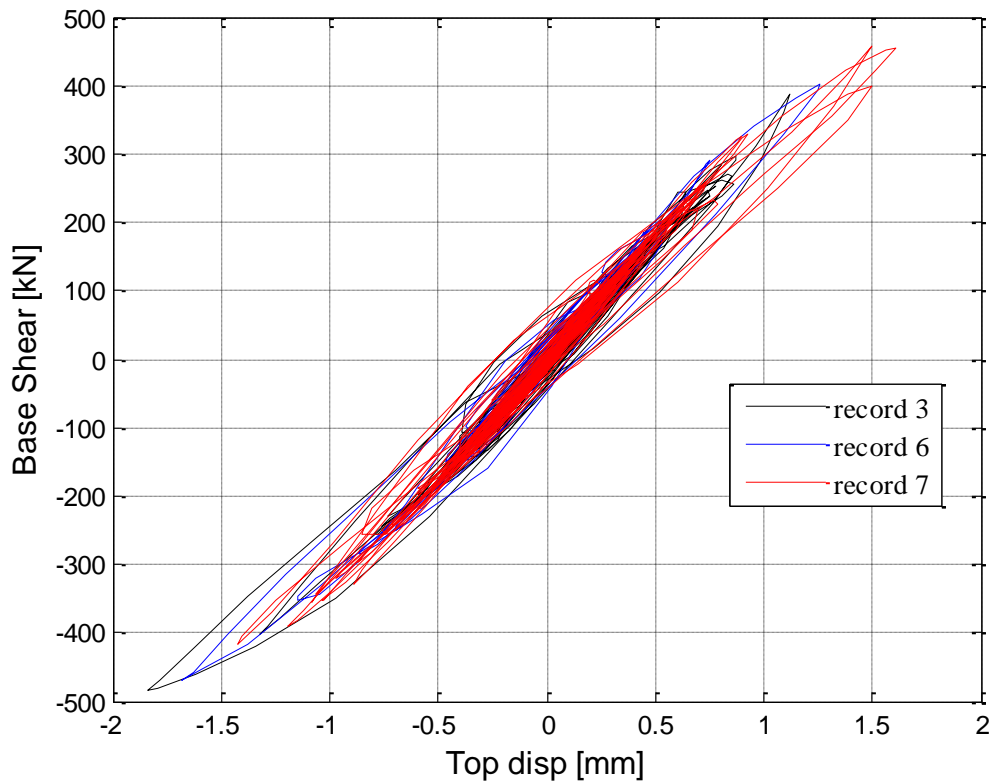


Figure 3.1.12: Base shear versus reference node displacement – 0.25g scaled PGA, record 3, 6 and 7 (Y direction).

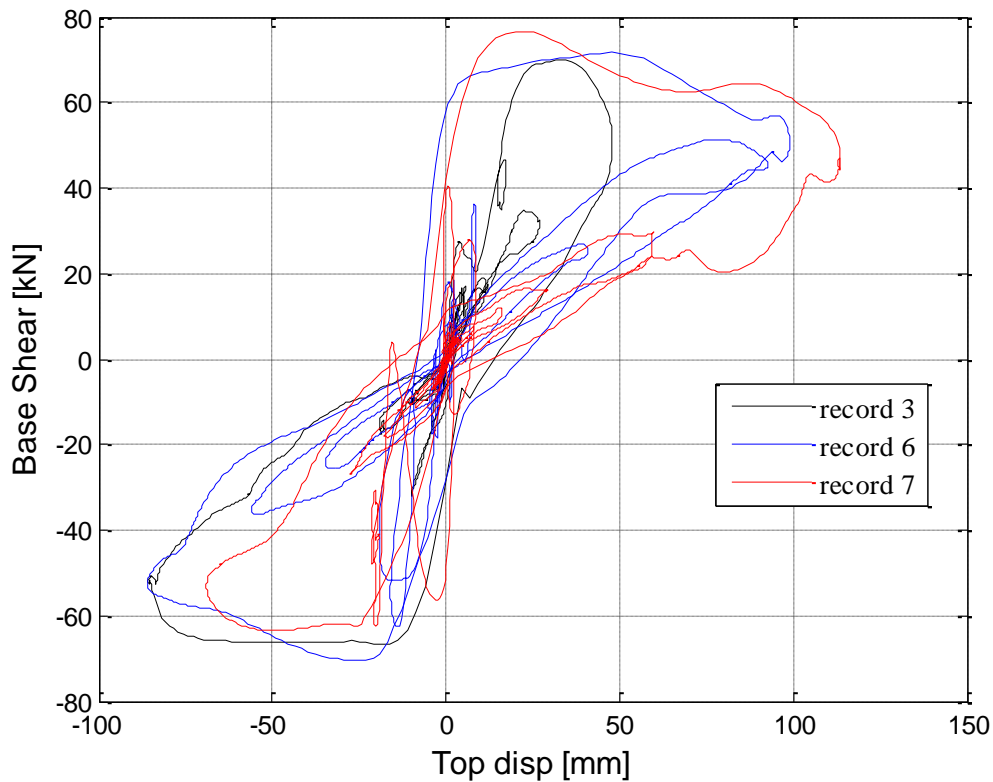


Figure 3.1.13: Base shear versus reference node displacement – 0.5g scaled PGA, record 3, 6 and 7 (X direction).

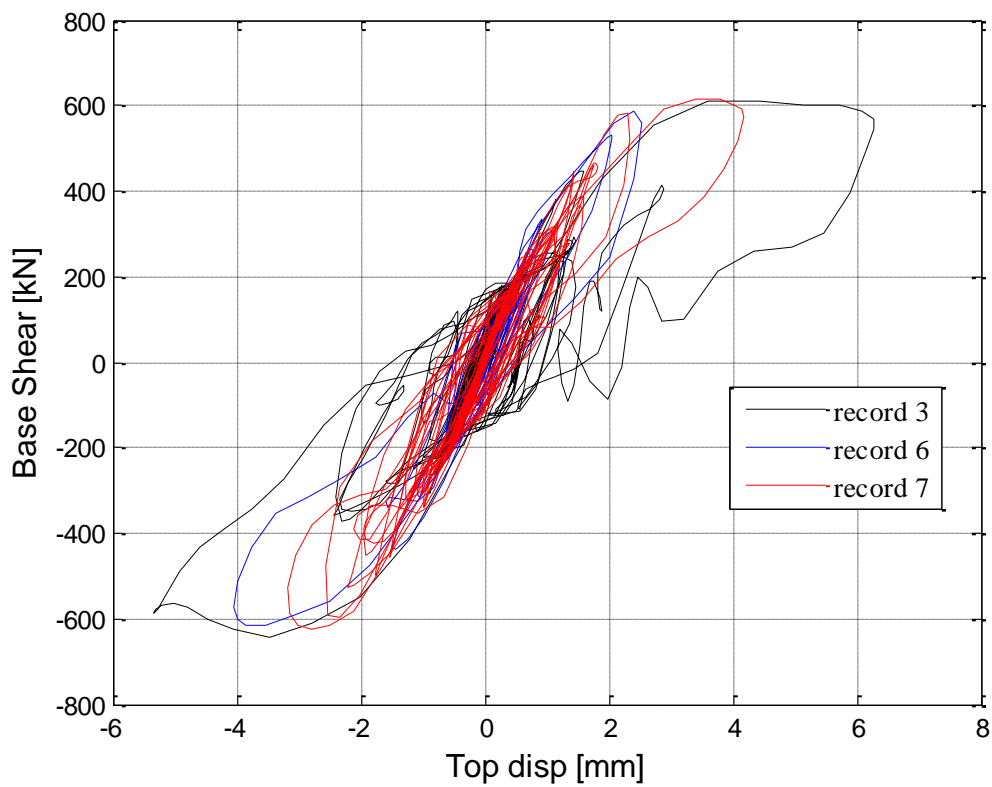


Figure 3.1.14: Base shear versus reference node displacement – 0.5g scaled PGA, record 3, 6 and 7 (Y direction).

3.1.4. Discussion and sensitivity analyses

Analyses have been performed also on an equivalent 2D model (accounting for out-of-plane response of TG walls) and on an additional model in which the modelling of the wall-to-wall interaction has been modified introducing an element to limit flange effects. Both the models have been also analysed with a fictitious ring beam (with zero mass and equivalent inertia) at the top of each piers in order to provide the horizontal diaphragms with a more realistic flexural stiffness (frame action).

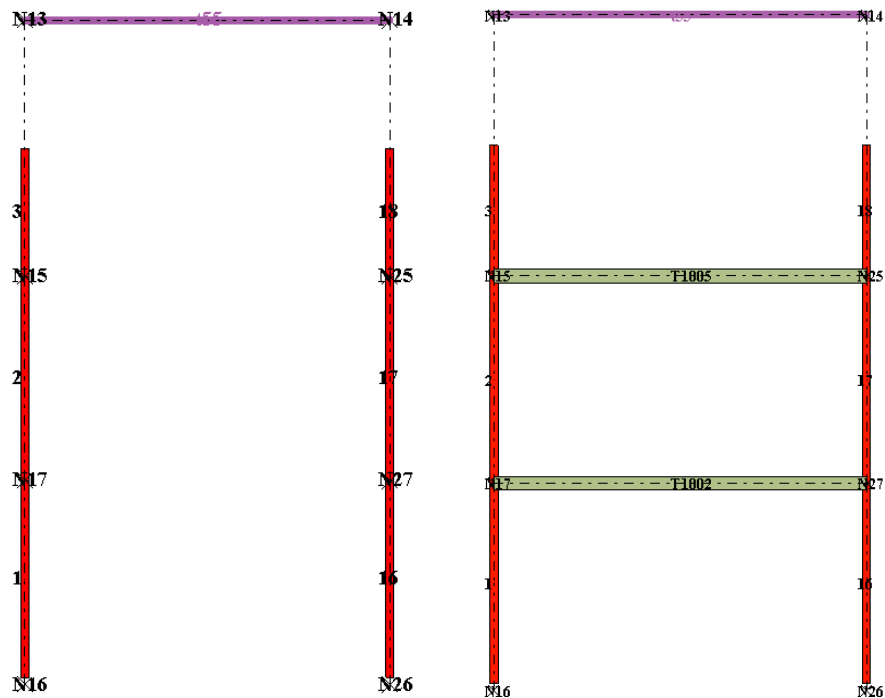


Figure 3.1.15: Out-of-plane walls in X direction: 2D model with (right) and without (left) ring beam.

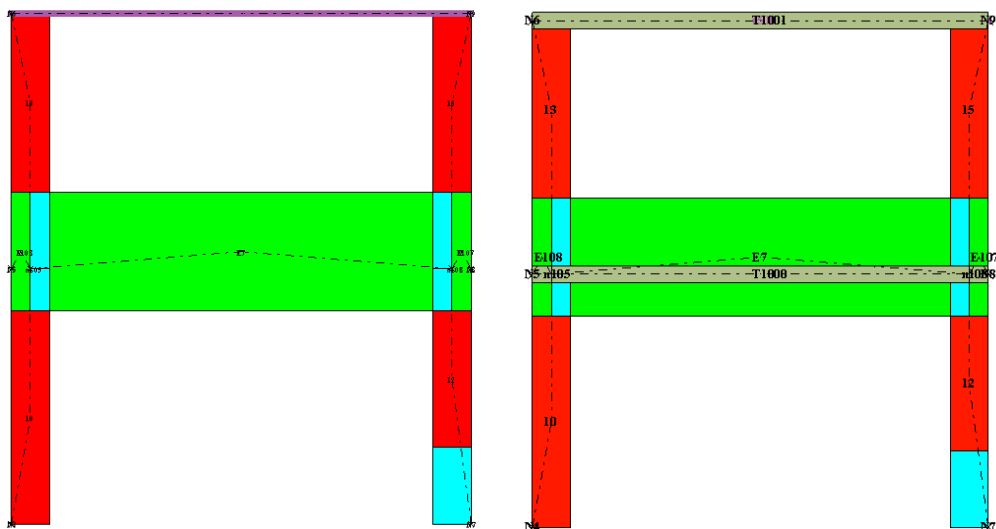


Figure 3.1.16: Wall in X direction with the connection to the orthogonal walls modelled by means of double corner nodes (to control flange effects).

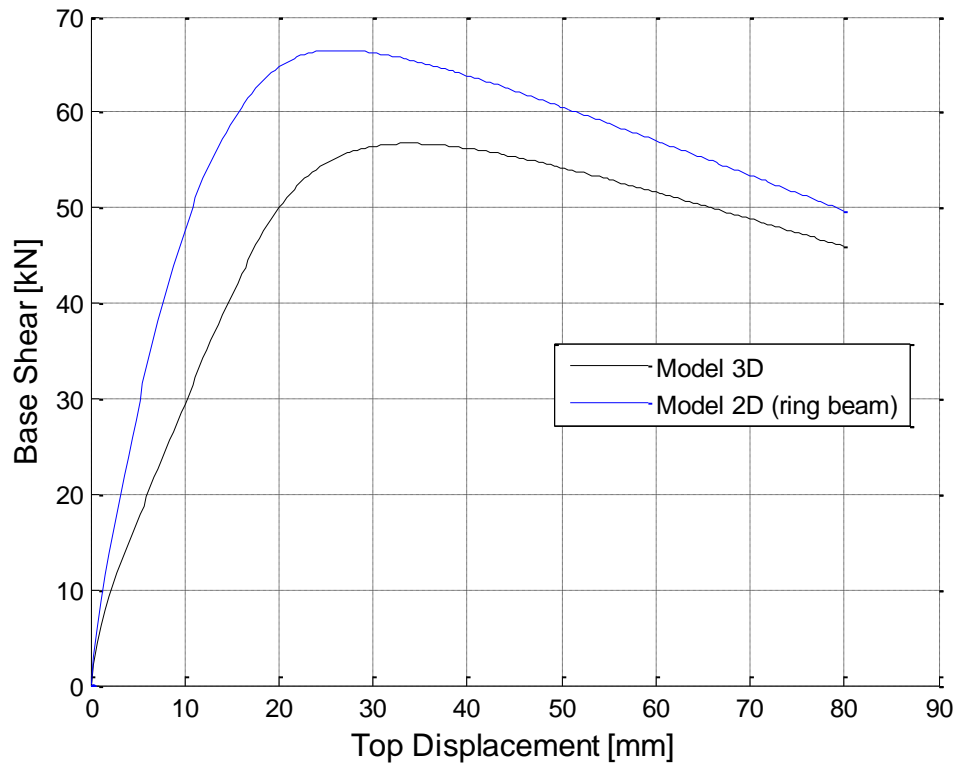


Figure 3.1.17: Monotonic Pushover Analysis in X direction: Out-of-plane investigation

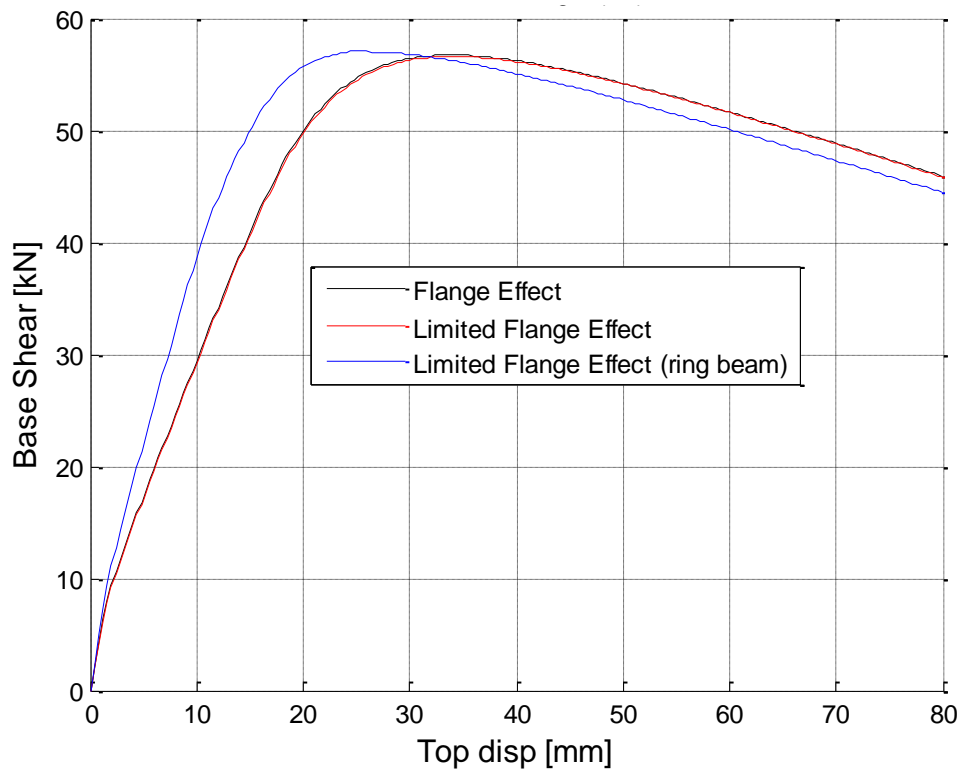


Figure 3.1.18: Monotonic Pushover Analysis in X direction: effect of limited flange effects (red line)

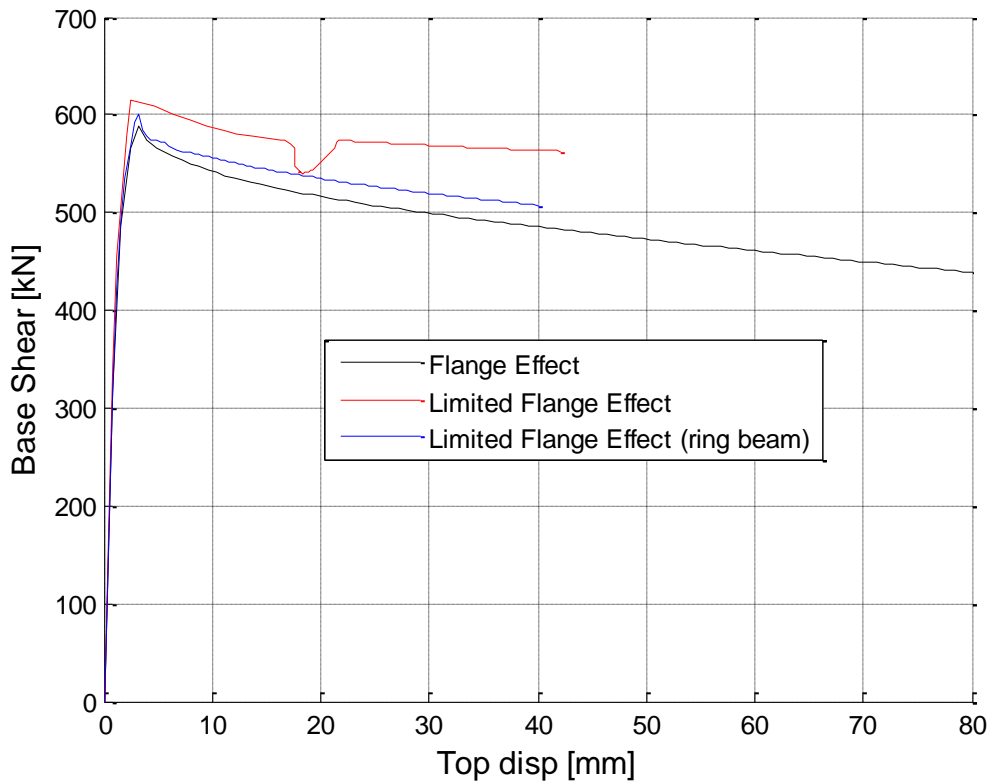


Figure 3.1.19: Monotonic Pushover Analysis in Y direction: effect of limited flange effects (red line)

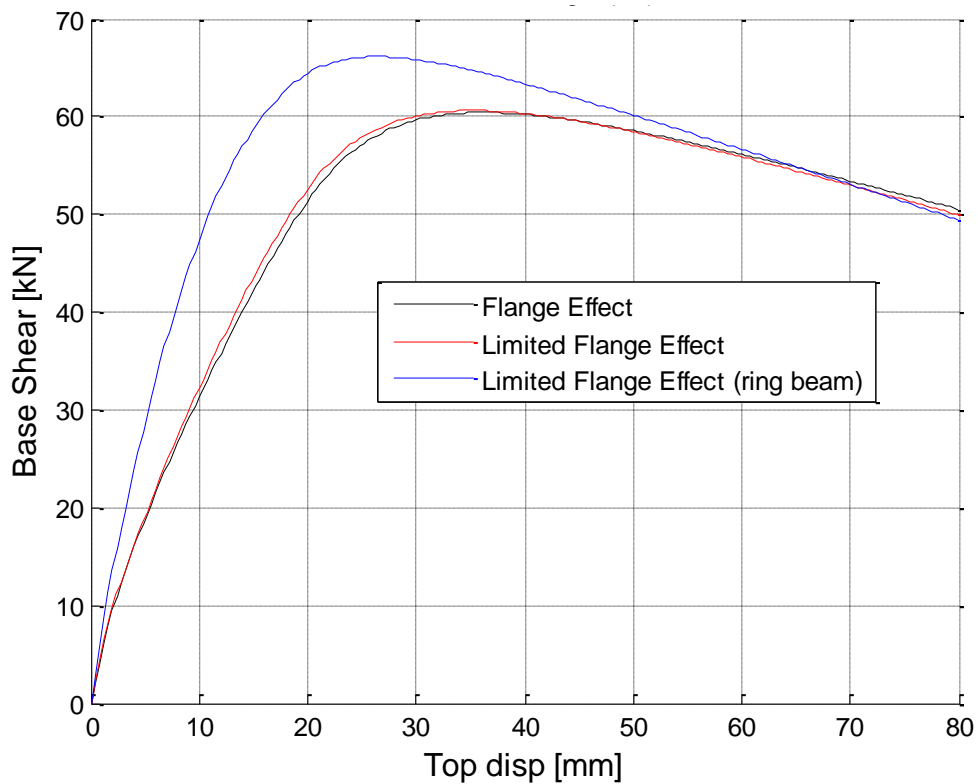


Figure 3.1.20: Monotonic Pushover Analysis in X direction: effect of limited flange effects on the 2D model



In order to estimate initial elastic stiffness of the model, elastic pushover analyses (until 1g) in both the directions have been performed.

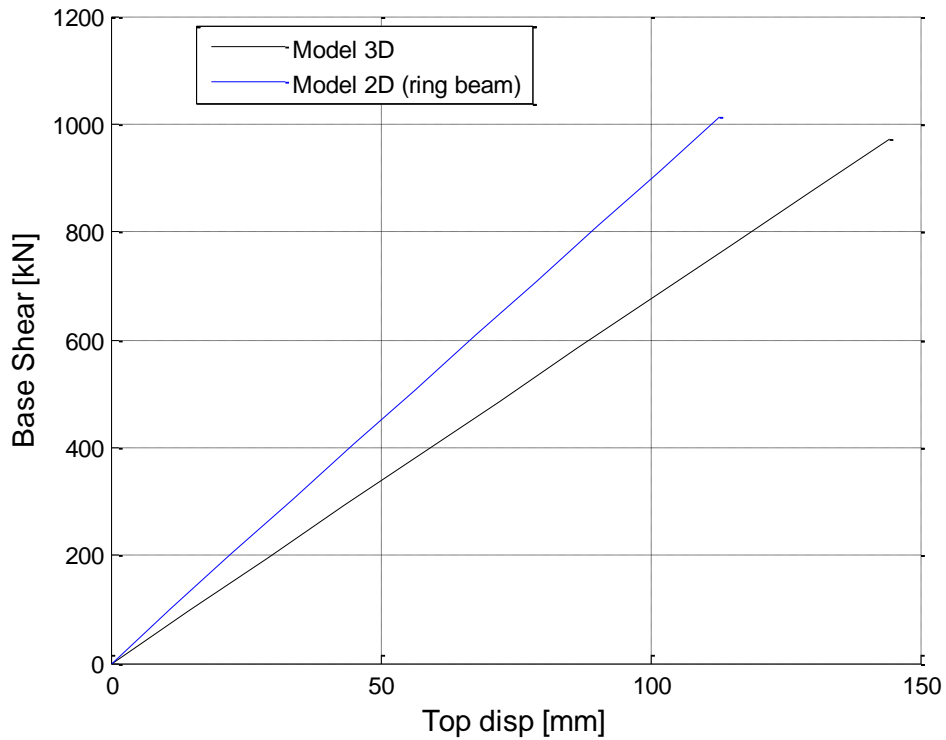


Figure 3.1.21: Elastic Pushover Analysis for model T1* (in X direction)

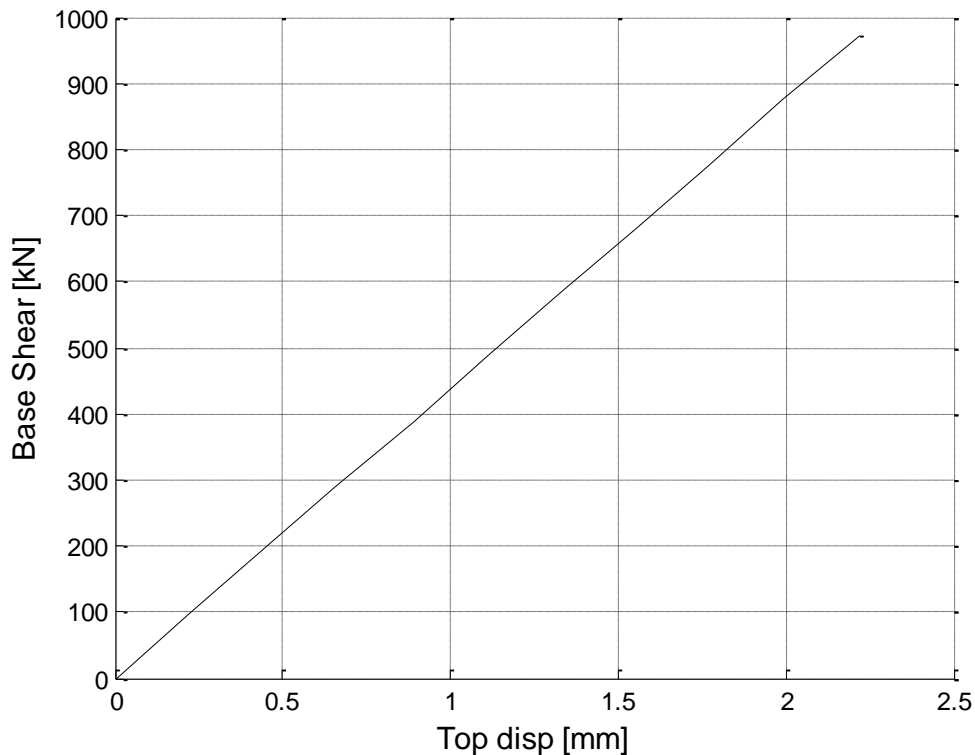


Figure 3.1.22: Elastic Pushover Analysis for model T1* (in Y direction)



In order to guarantee a more meaningful comparison of the results, the Rayleigh damping implemented in the Tremuri models (2%) have been realigned to the one adopted by the other teams (1%). The results are reported in the following.

Table 3.1.12: Peak reference node displacement (3 records at each PGA level)-Damping 1%

PGA	RECORD 3 (mm)		RECORD 6 (mm)		RECORD 7 (mm)	
	X direction	Y direction	X direction	Y direction	X direction	Y direction
0.1g	21.3	0.79	20.34	0.55	21.52	1.01
0.25g	40.2	1.02	51.62	1.3	55.8	1.77
0.5g	47.4	7.84	113.07	2.63	121.96	5.34

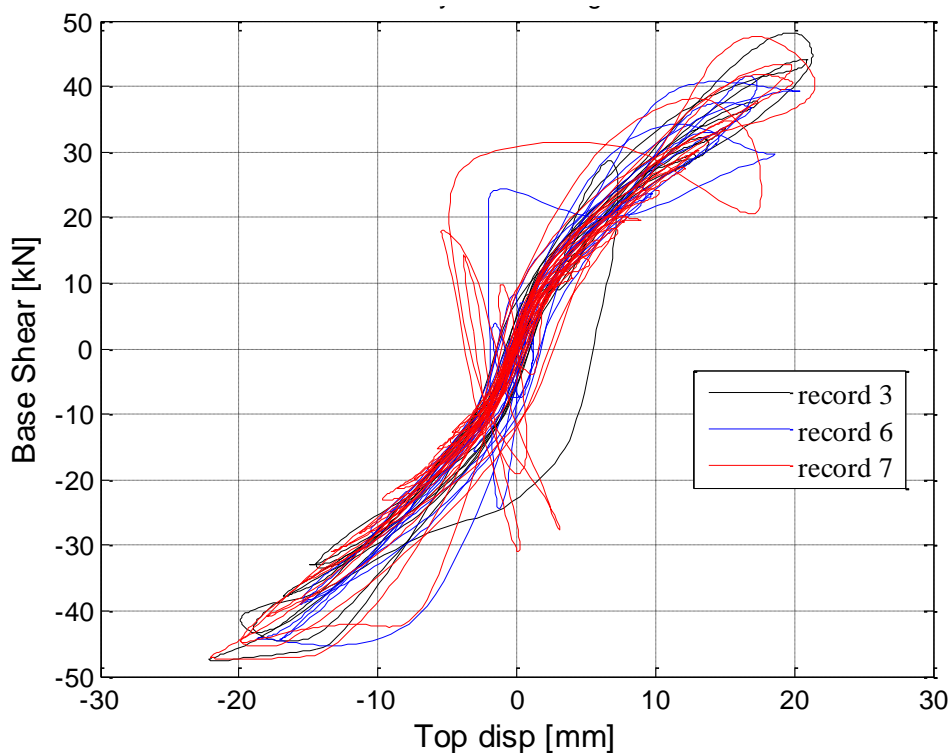


Figure 3.1.23: Base shear versus reference node displacement – 0.1g scaled PGA, record 3, 6 and 7 (X direction, Damping 1%).

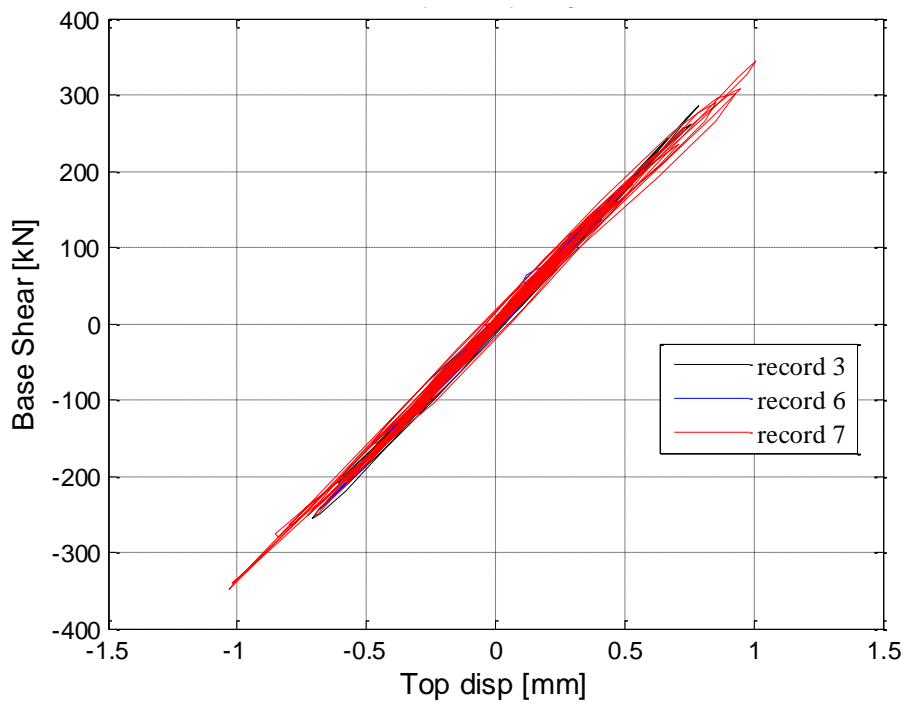


Figure 3.1.24: Base shear versus reference node displacement – 0.1g scaled PGA, record 3, 6 and 7 (Y direction, Damping 1%).

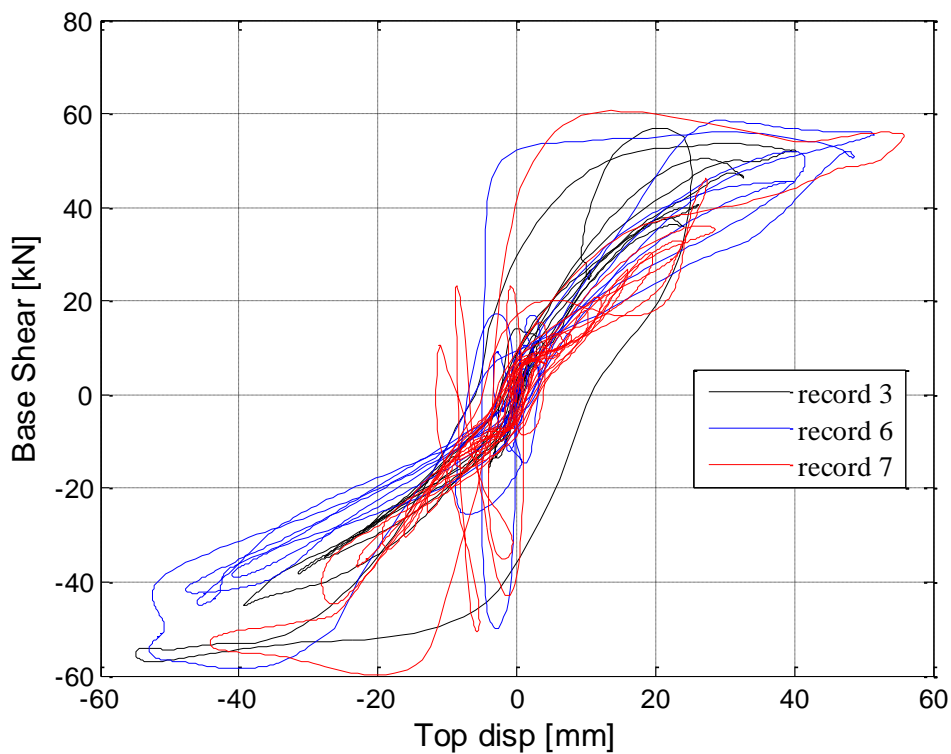


Figure 3.1.25: Base shear versus reference node displacement – 0.25g scaled PGA, record 3, 6 and 7 (X direction, Damping 1%).

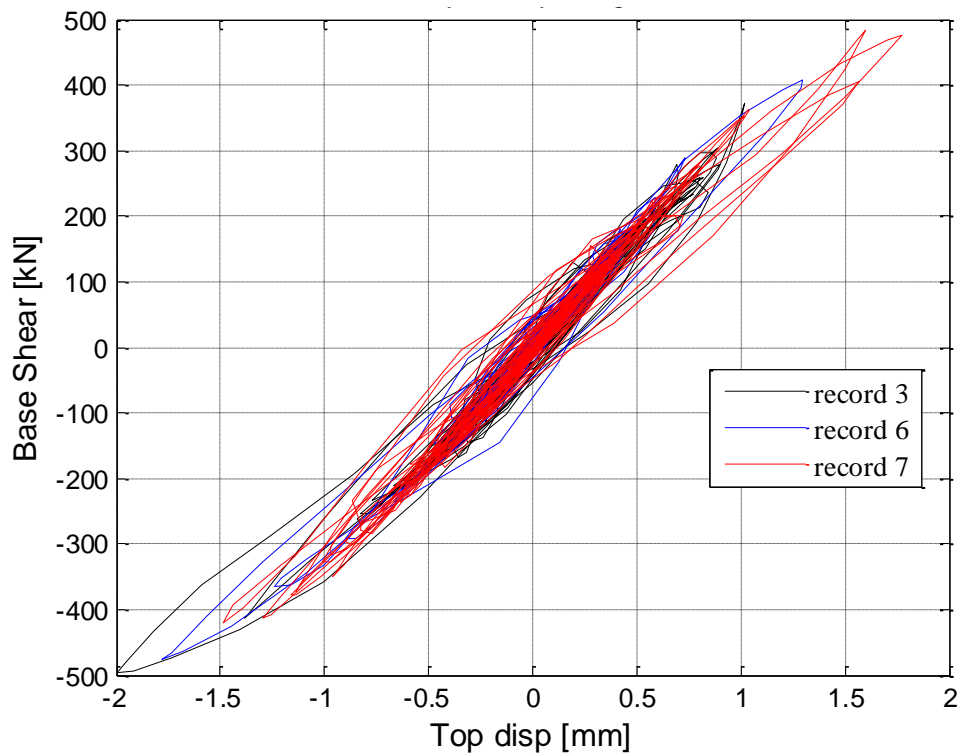


Figure 3.1.26: Base shear versus reference node displacement – 0.25g scaled PGA, record 3, 6 and 7 (Y direction, Damping 1%).

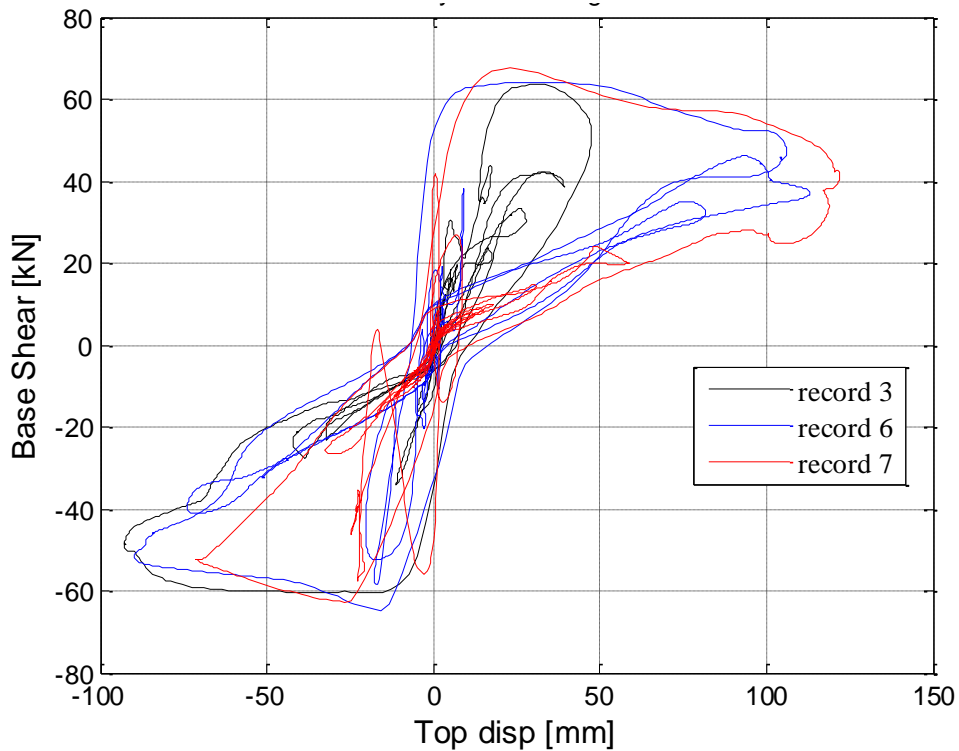


Figure 3.1.27: Base shear versus reference node displacement – 0.5g scaled PGA, record 3, 6 and 7 (X direction, Damping 1%).

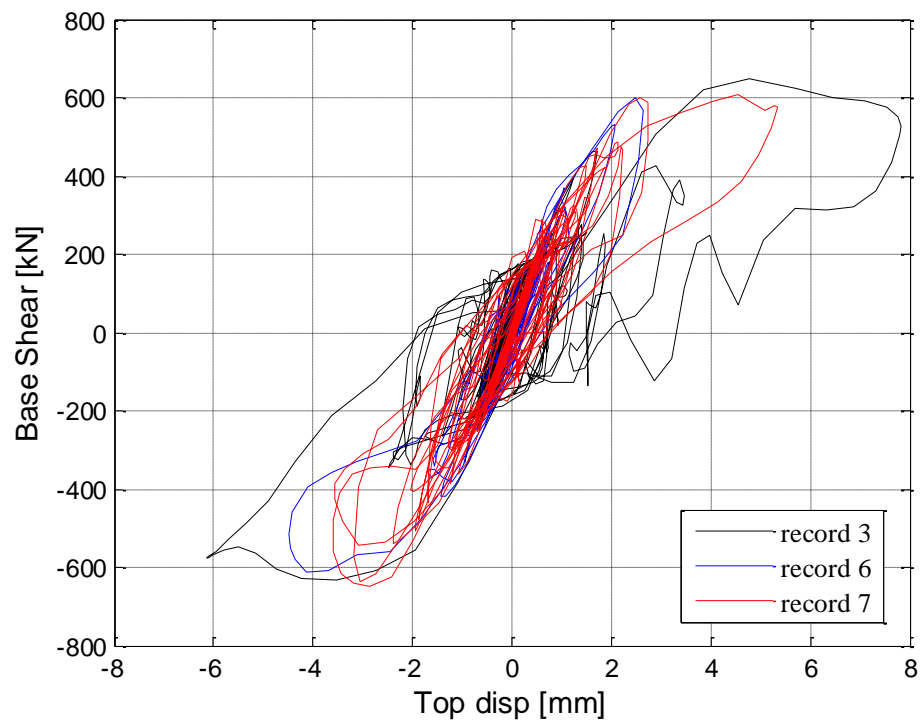


Figure 3.1.28: Base shear versus reference node displacement – 0.5g scaled PGA, record 3, 6 and 7 (Y direction, Damping 1%).



3.2. Detached villa, timber floors (T3a)

Table 3.2.1: Modelling notes

Component	Description
Analysis software and formulation	TREMURI – Equivalent-frame formulation based on a macro-element model
Walls (in-plane)	See Table 1.1, Lagomarsino et al. [2013] and Penna et al. [2014]
Walls (out-of-plane)	See Table 2.2.1
Spandrels/lintels and wall coupling	See Table 2.2.1
Wall to wall connection (incl. flange effects)	See Table 2.2.1
Timber diaphragm	The floor elements are modelled as orthotropic membrane finite elements, identified by a main (spanning) direction, with Young’s moduli in the two perpendicular directions, shear modulus and Poisson ratio [Lagomarsino et al., 2013]. In particular the numerical values implemented are: E1 = 3536 MPa E2 = 0 MPa G = 10 MPa
Wall to diaphragm connection	See Table 2.2.1
Foundation	Modelled as rigid (fixed restrain).

Table 3.2.2: Eigenvalue analysis notes

Eigenvalue analysis notes
<ul style="list-style-type: none"> Modal analysis is currently performed by means of the Jacobi algorithm on a reduced model with condensed rotational degrees of freedom.

Table 3.2.3: Nonlinear pushover analysis notes

Nonlinear pushover analysis notes
<ul style="list-style-type: none"> Seismic load applied as equivalent horizontal load pattern (imposed displacement of a control node and relative force ratios kept constant) Pushover analysis with (uniform) mass proportional and inverse triangular load pattern assumed +/- load directions considered Monotonic and cyclic load cases considered The solution of the static equilibrium equations is obtained by iteration (Newton-Raphson)



Table 3.2.4: Nonlinear time history analysis notes

Nonlinear time history analysis notes	
•	Single-component ground motions applied to the foundation (x and y separately)
•	Newmark integration method (constant mean acceleration formulation) implemented
•	Classical Rayleigh damping model implemented (damping matrix obtained as a linear combination of mass and initial stiffness matrices)

Table 3.2.5: Model loading, materials and general comments

Loading	
Dead loads	Self-weight of the walls and roof/floor structure.
Superimposed dead loads	Floor = 1kPa Barn roof = 0.5 kPa Main roof = 1 kPa
Live loads	Floor = 1.75 kPa Barn roof = 0 kPa Main roof = 0 kPa
Load combination	DL + SDL + 0.24LL
Materials	
Masonry (Clay bricks)	Model Parameters (as described in Penna et al. [2014]) $\rho = 1900 \text{ kg/m}^3$ $E' = 8820 \text{ MPa} (= 2E = 2*4410 \text{ MPa})$ $G = 1300 \text{ MPa}$ $f_m = 6.3 \text{ MPa}$ $\bar{c} = 0.12 \text{ MPa}$ (cohesion also referred as f_{vmo} in Penna et al. [2014]) Equivalent Friction coefficient = 0.3
Timber/Plywood	Elastic-plastic material model (beams) $\rho = 600 \text{ kg/m}^3$ $E = 6000 \text{ MPa}$ $G = 370 \text{ MPa}$
Other key notes	
1) Rayleigh damping implemented with $\xi_v = 2\%$ set for the following range of frequency: X direction: $f_1=10.75 \text{ Hz}$ and $f_2=3.14 \text{ Hz}$ Y direction: $f_1=19.23 \text{ Hz}$ and $f_2=3.80 \text{ Hz}$	

Table 3.2.6: Breakdown of loading and masses

Loading	DL [kPa]	SDL [kPa]	LL [kPa]	DL+SDL+0.24LL [kPa]	Area [m ²]
Floor	0.5	1	1.75	1.92	55.72
Barn roof	0.5	0.5	0	1	20.58
Main roof	0.72	1	0	1.72	80.2
Total model mass (including DL+SDL+0.24LL) = 90370 kg					
Masonry	Density [kg/m ³]		Thickness [m]	Total masonry mass [kg]	
Clay	1900		0.22	63305	

Table 3.2.7: Cut-section z-forces (weight from gravity load at t=0) at different cut-plane heights

Cut-plane height (m)	Cut-section z-force (kN)
<Just above ground/base>	886.52
<Just above diaphragm>	159

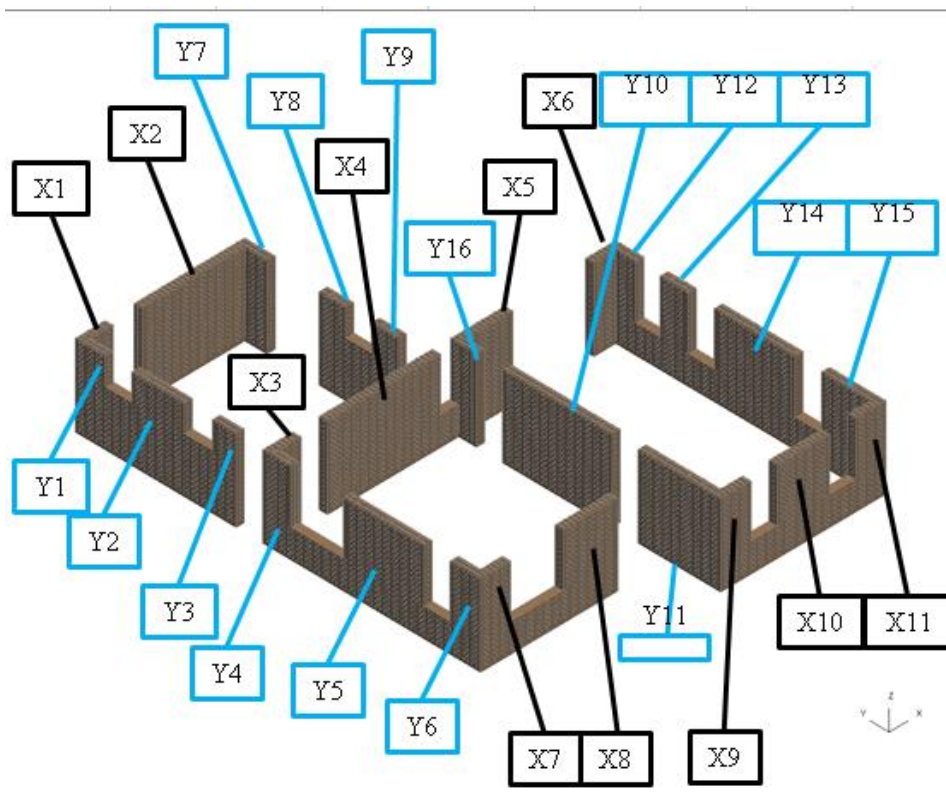


Figure 3.2.1: Pier labelling convention for T3a building

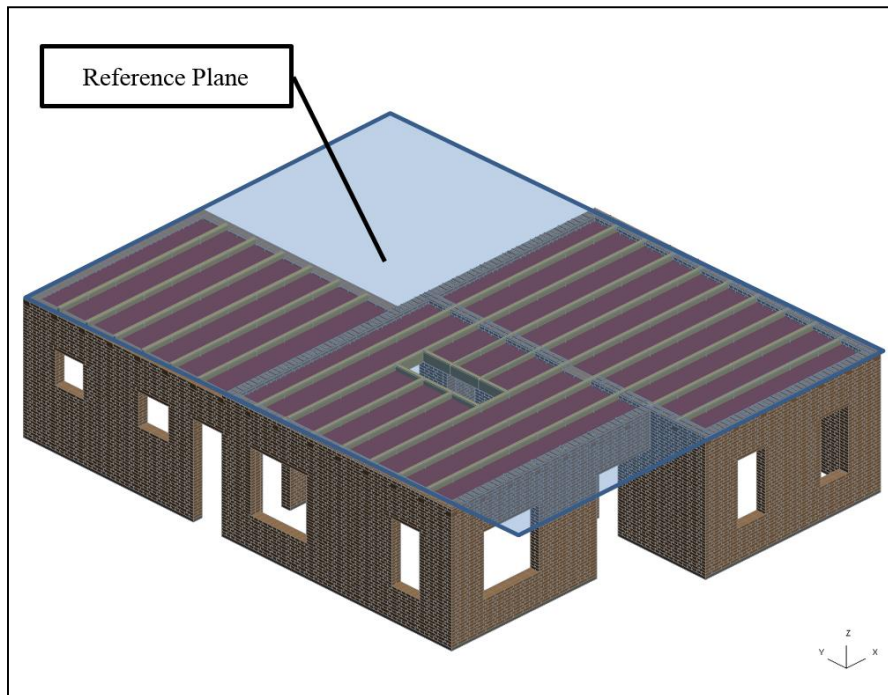


Figure 3.2.2: T3a model pushover reference plane location/height

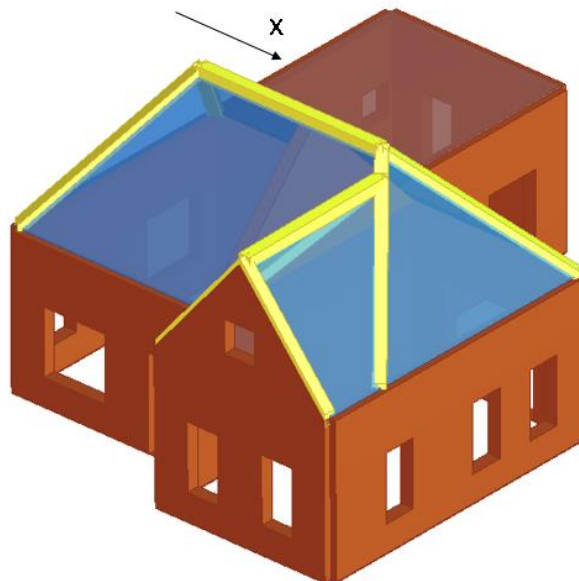
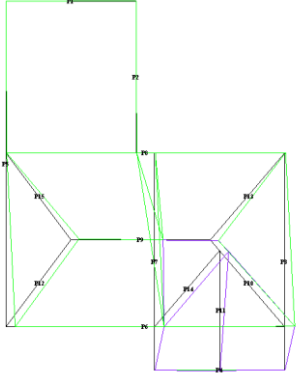
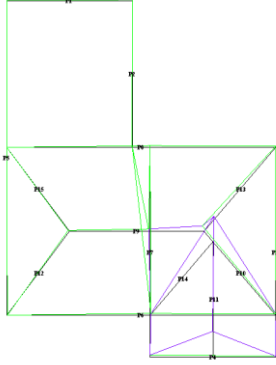
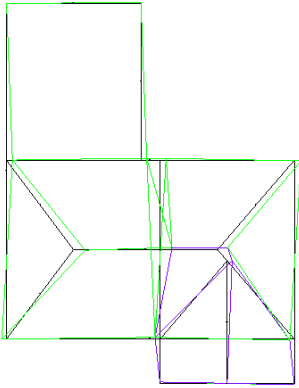


Figure 3.2.3: Tremuri model for T3a



3.2.1. Modal analysis

Table 3.2.8: Modal period, frequency, description, mass participation

Mode	Period (s)	Frequency (Hz)	Description of mode	Mass participation %	
				X	Y
1	0.093	10.713		39.213	0.002
2	0.069	14.502		0.006	12.247
3	0.055	18.17		8.809	1.108



4	0.052	19.241		1.541	33.303
5	0.046	21.698		3.721	1.200
6	0.045	21.996		14.854	2.399
7	0.042	23.753		0.822	3.354



8	0.04	25.292		0.578	5.895
9	0.035	28.399		0.053	12.683
10	0.033	30.317		5.964	0.134

3.2.2. Pushover analysis (monotonic and cyclic)

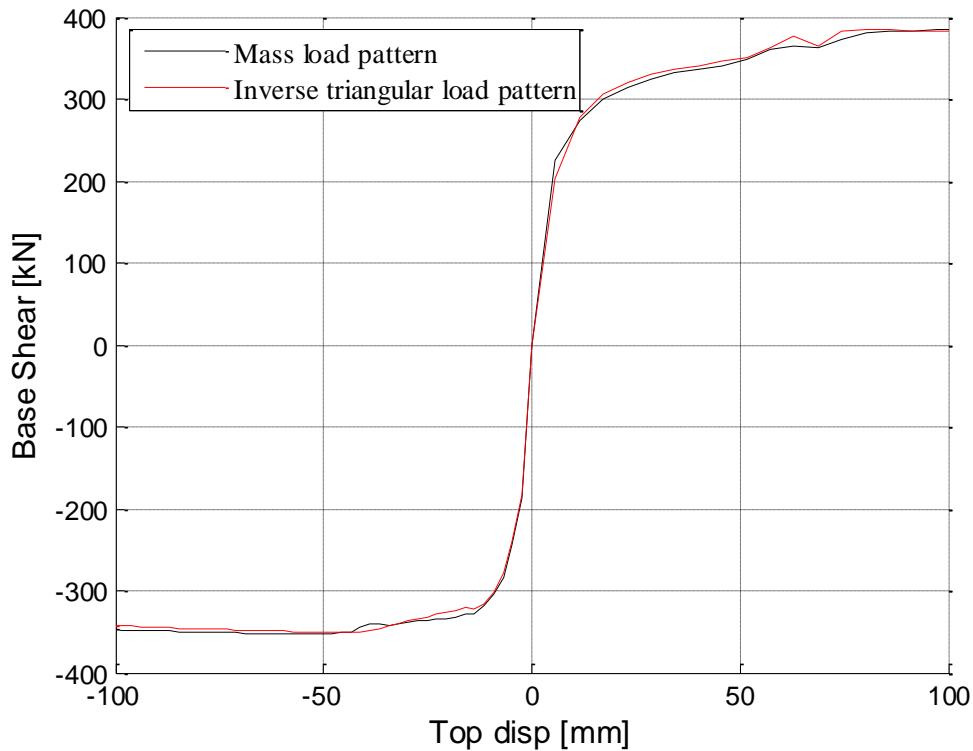


Figure 3.2.4: Monotonic Pushover: X direction base shear versus average reference height displacement

Table 3.2.9: Cut-plane pier forces at peak/plateau x-dir (positive, mass proportional load pattern) pushover base shear

Pier	X-dir pier force (kN) Cut-plane height ~1.4m	
	Axial	Shear
X1	0	0
X2	-35.095	36.426
X3	-9.995	2.845
X4	-55.225	79.084
X5	-113.594	56.066
X6	-106.933	39.043
X7	0	0
X8	-72.079	35.616
X9	-20.784	9.639
X10	-170.328	98.134
X11	-65.890	28.645



Pier	X-dir pier force (kN) Cut-plane height ~1.4m	
	Axial	Shear
Y1	0	0
Y2	0	0
Y3	0	0
Y4	0	0
Y5	0	0
Y6	0	0
Y7	-18.162	-4.133
Y8	-11.160	-4.887
Y9	0	0
Y10	0	0
Y11	-10.156	13.353
Y12	0	0
Y13	0	0
Y14	0	0
Y15	-3.461	-3.995
Y16	0	0
Total	-692.862	385.836

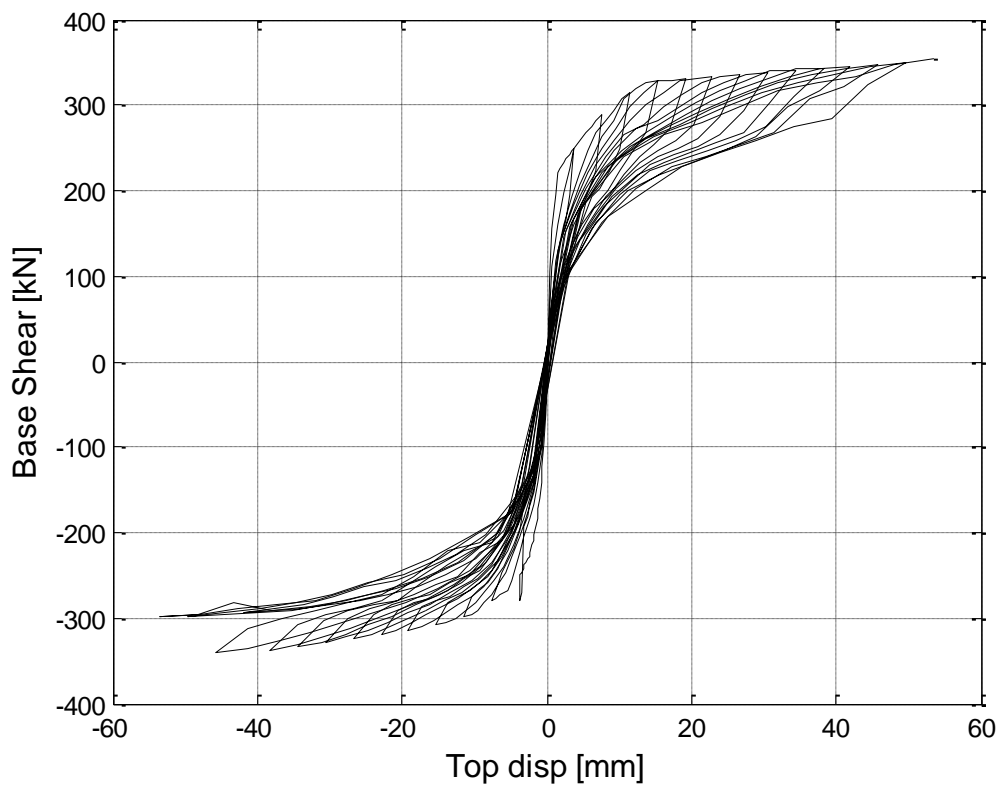


Figure 3.2.5: Cyclic Pushover: X direction base shear versus average reference height displacement

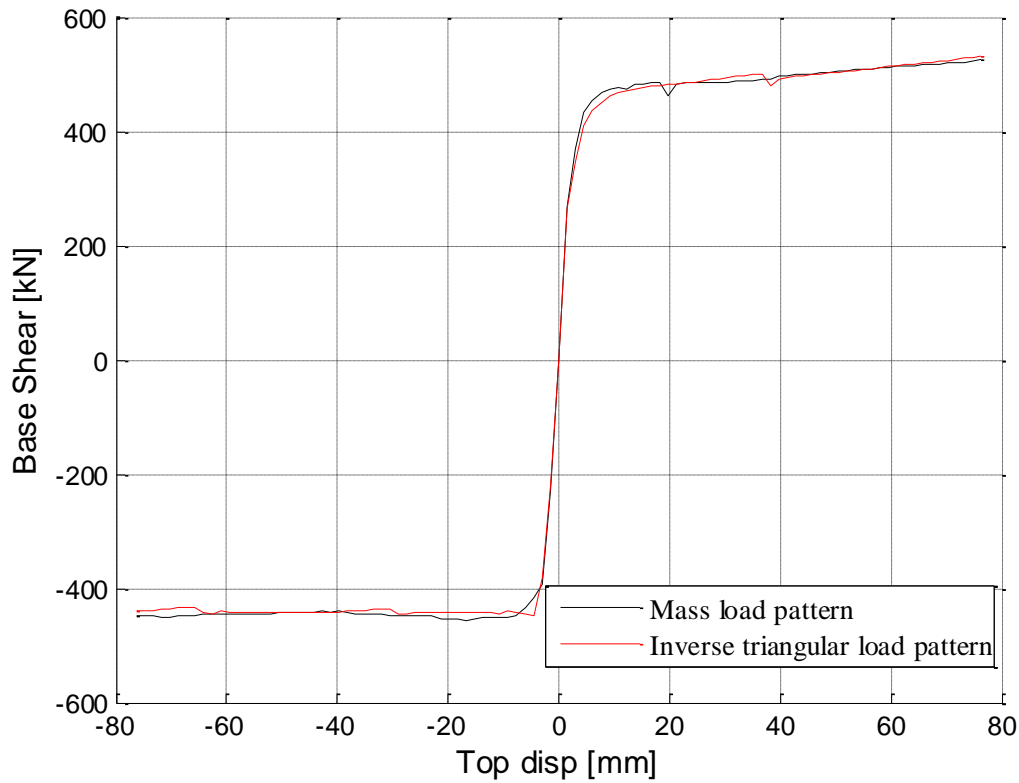


Figure 3.2.6: Y direction base shear versus average reference height displacement

Table 3.2.10: Cut-plane pier forces at peak/plateau y-dir (positive, mass proportional load pattern) pushover base shear

Pier	Y-dir pier force (kN) Cut-plane height ~1.4m	
	Axial	Shear
X1	-0.001	-0.182
X2	-9.958	0.489
X3	0	0
X4	0	0
X5	0	0
X6	0	0
X7	0	0
X8	0	0
X9	0	0
X10	0	0
X11	0	0
Y1	0	0
Y2	-31.765	44.467
Y3	-73.400	53.365



Pier	Y-dir pier force (kN) Cut-plane height ~1.4m	
	Axial	Shear
Y4	-39.424	12.460
Y5	-45.538	55.045
Y6	0	0
Y7	-26.482	9.373
Y8	0	0
Y9	-60.917	31.497
Y10	-31.294	9.197
Y11	-60.935	74.448
Y12	-74.192	68.545
Y13	-89.058	39.889
Y14	0	0
Y15	-56.345	58.493
Y16	-80.722	68.134
Total	-680.031	525.221

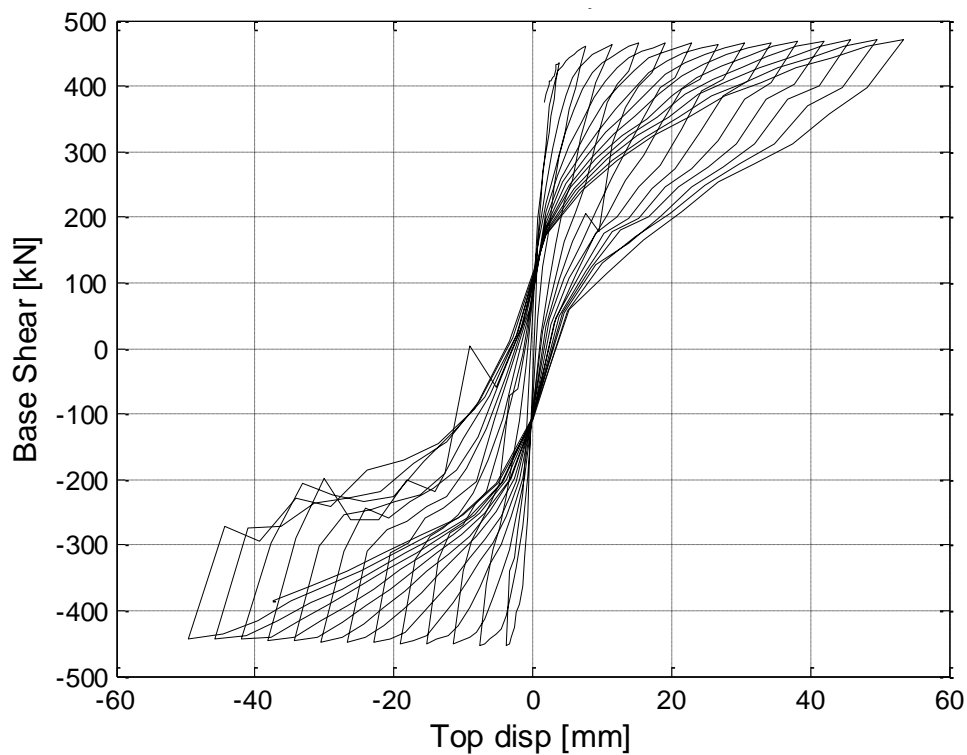


Figure 3.2.7: Cyclic Pushover: Y direction base shear versus average reference height displacement



3.2.3. Time history analysis

Table 3.2.11: Peak average reference height displacement (3 records at each PGA level)

PGA	RECORD 3		RECORD 6		RECORD 7	
	X direction	Y direction	X direction	Y direction	X direction	Y direction
0.1g	0.480	0.158	0.380	0.157	0.430	0.136
0.25g	1.430	0.410	1.140	0.460	1.340	0.480
0.5g	3.870	1.850	4.230	1.250	5.020	1.850

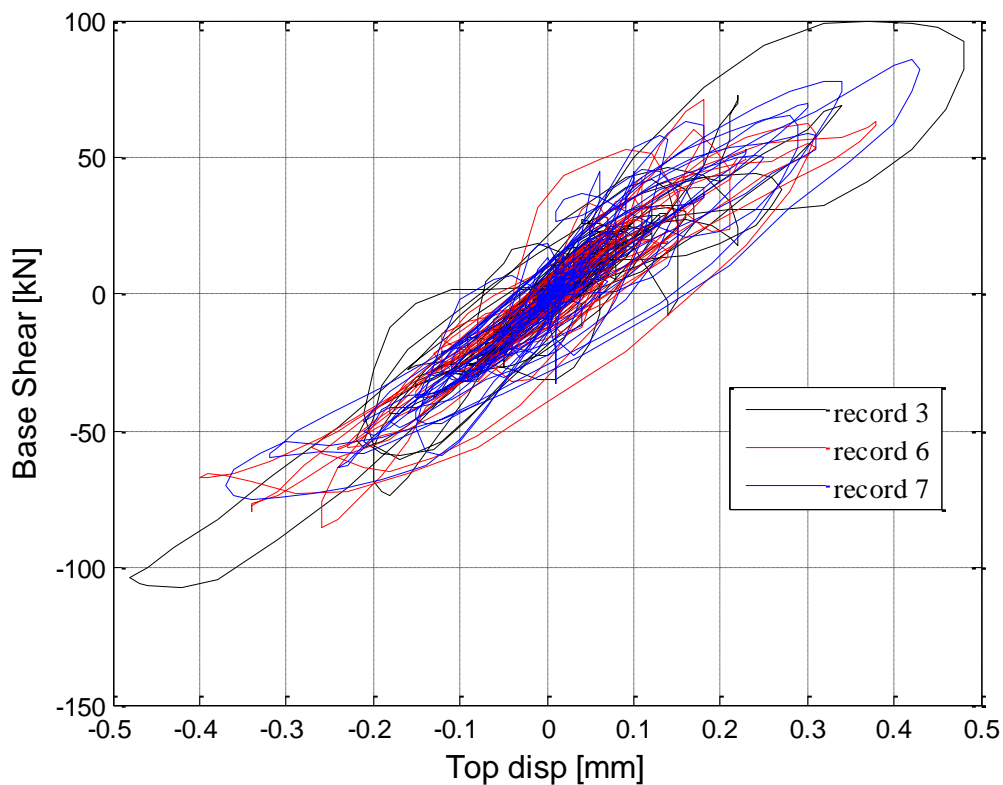


Figure 3.2.8: Base shear versus average reference floor displacement – 0.1g scaled PGA, record 3, 6 and 7 (X direction).

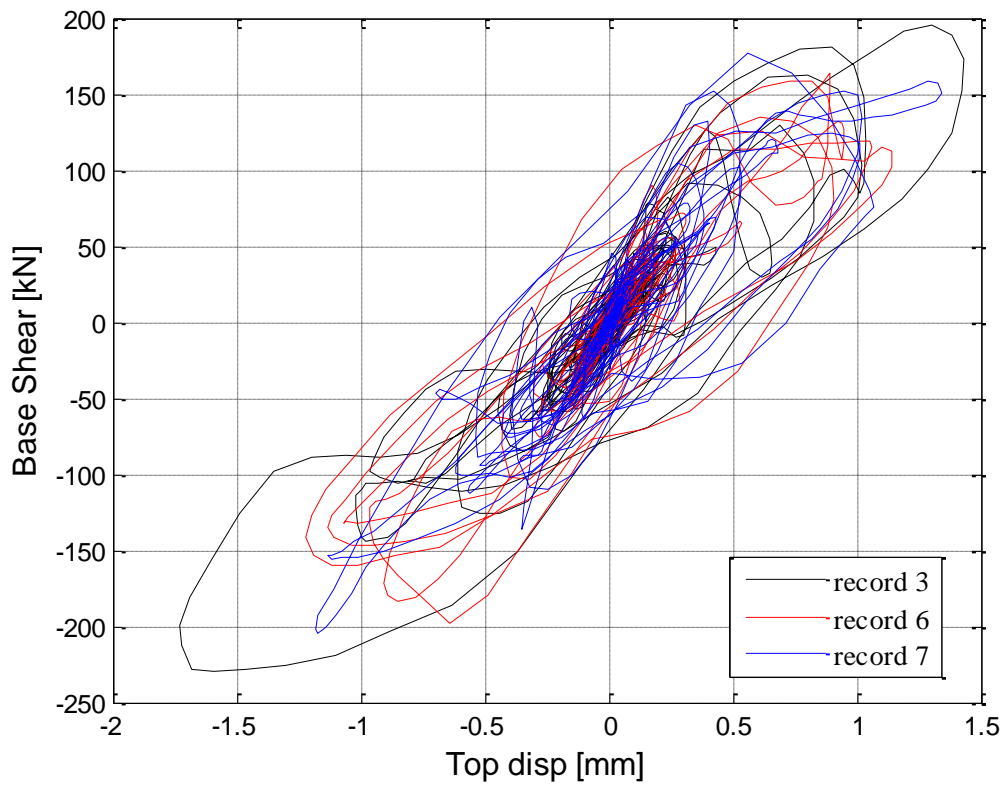


Figure 3.2.9: Base shear versus average reference floor displacement – 0.25g scaled PGA, record 3, 6 and 7 (X direction).

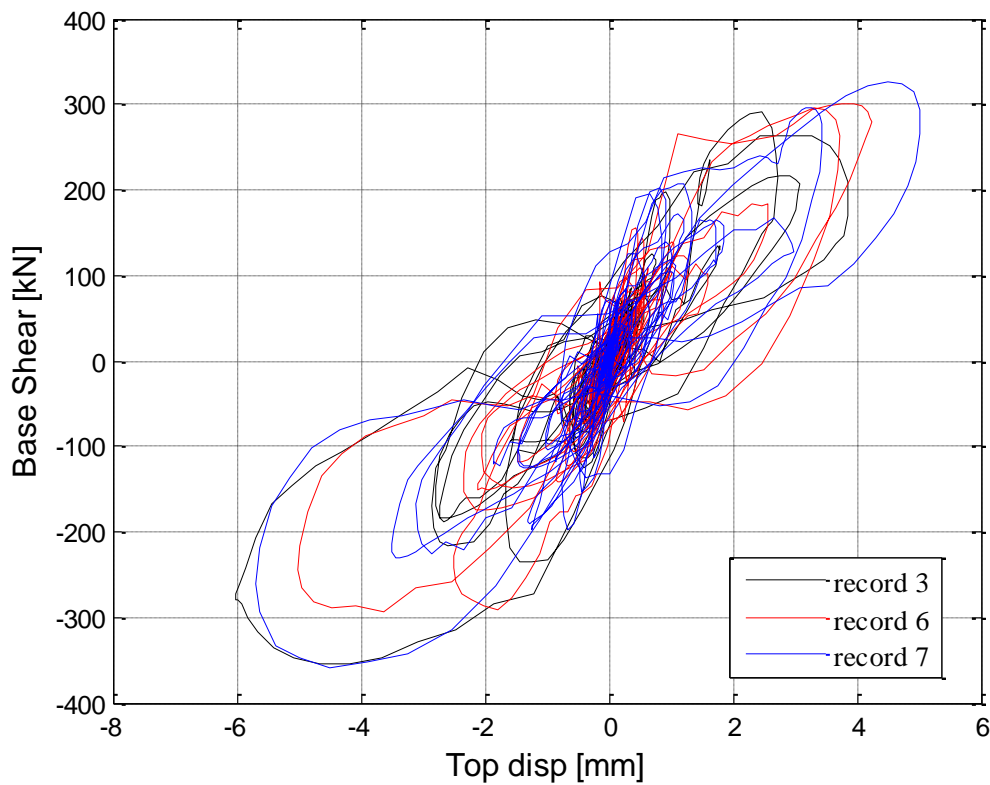


Figure 3.2.10: Base shear versus average reference floor displacement – 0.5g scaled PGA, record 3, 6 and 7 (X direction).

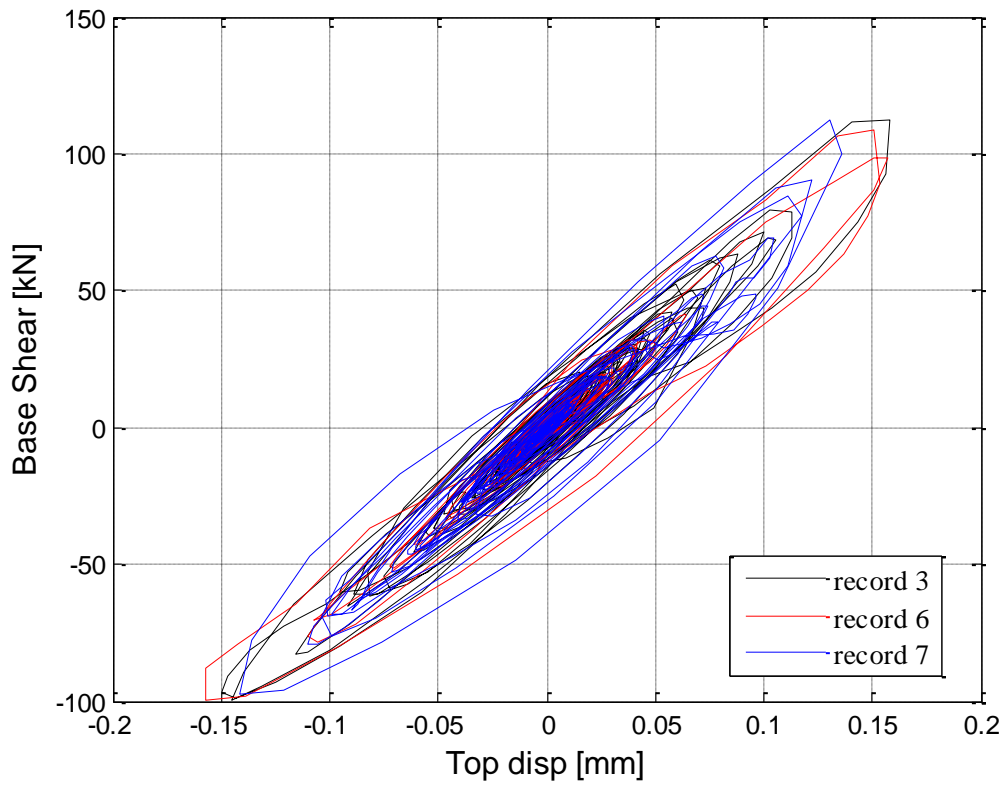


Figure 3.2.11: Base shear versus average reference floor displacement – 0.1g scaled PGA, record 3, 6 and 7 (Y direction).

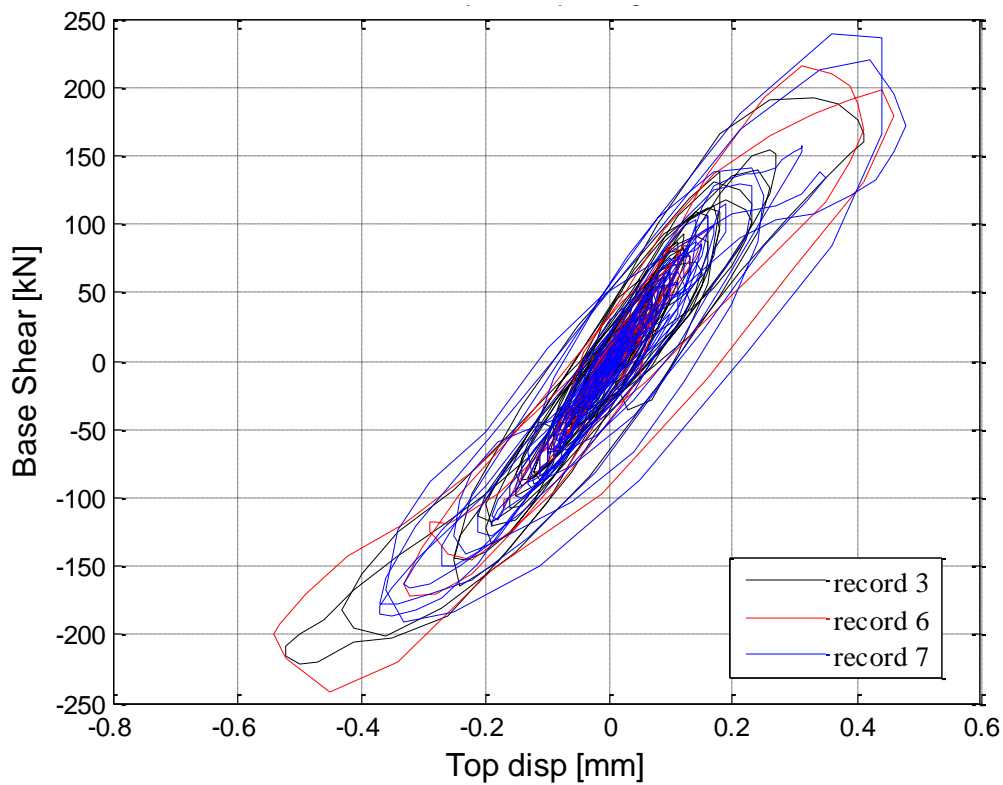


Figure 3.2.12: Base shear versus average reference floor displacement – 0.25g scaled PGA, record 3, 6 and 7 (Y direction).

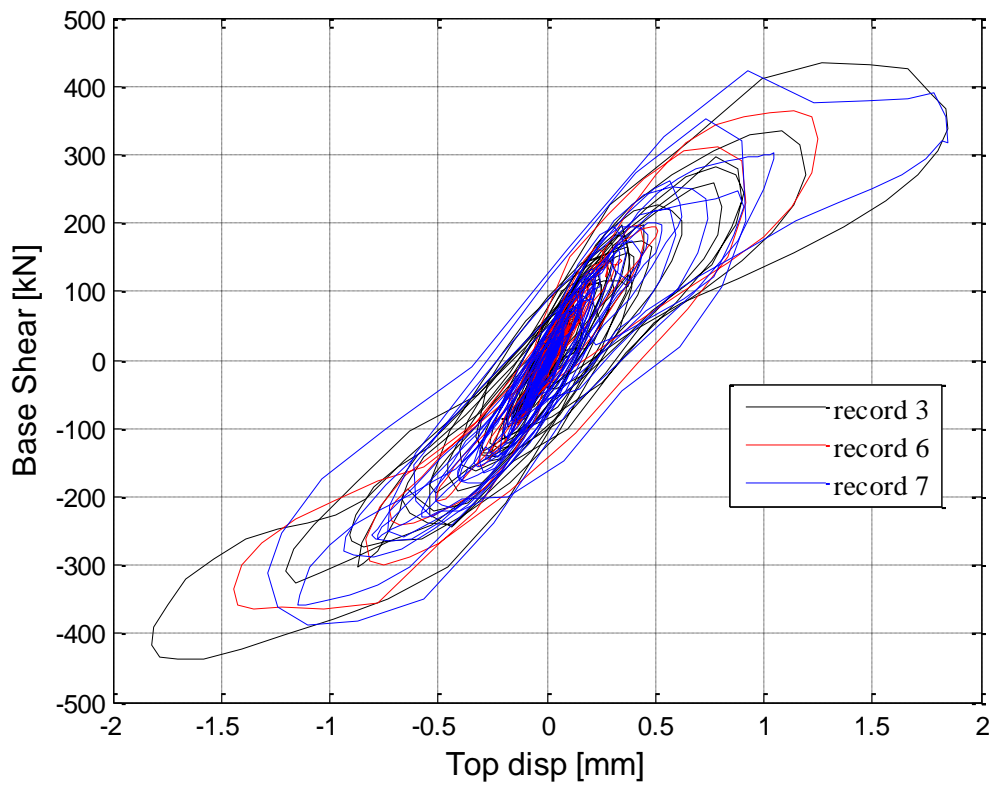


Figure 3.2.13: Base shear versus average reference floor displacement – 0.5g scaled PGA, record 3, 6 and 7 (Y direction).

3.2.4. Discussion

In order to have a more complete idea on the dynamic behavior of the building, the damage patterns at the end of a selected time-history analysis (0.1g PGA - record 7), have been analysed and reported in the following. As expected, the most vulnerable elements are often spandrel beams followed by short and squat piers.

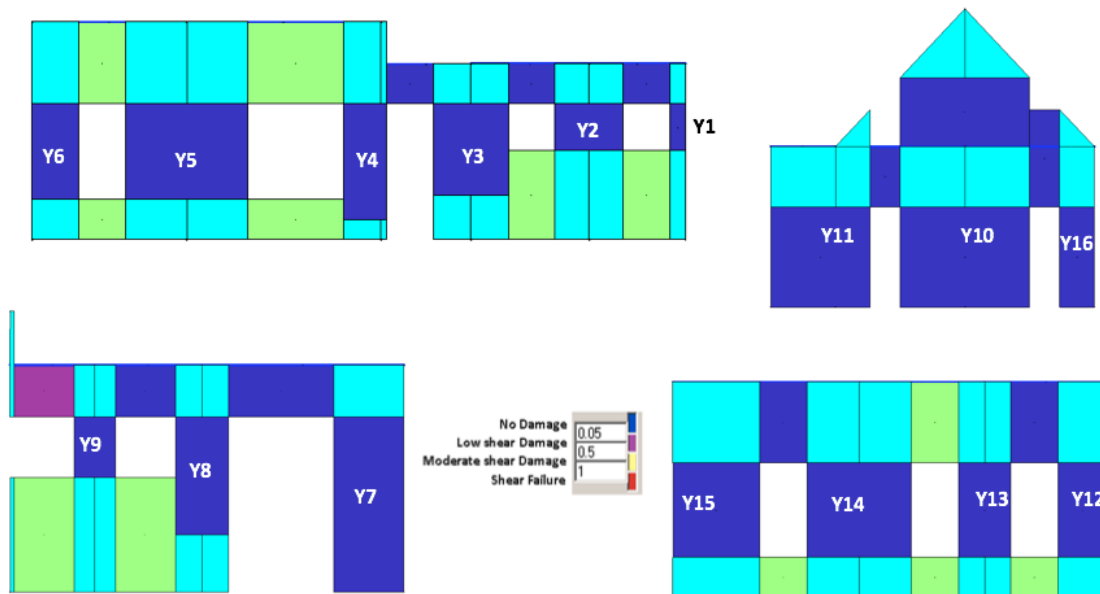


Figure 3.2.14: Damage pattern of the Y-walls at the end of the dynamic analysis (PGA 0.1g – Record 7- X direction)

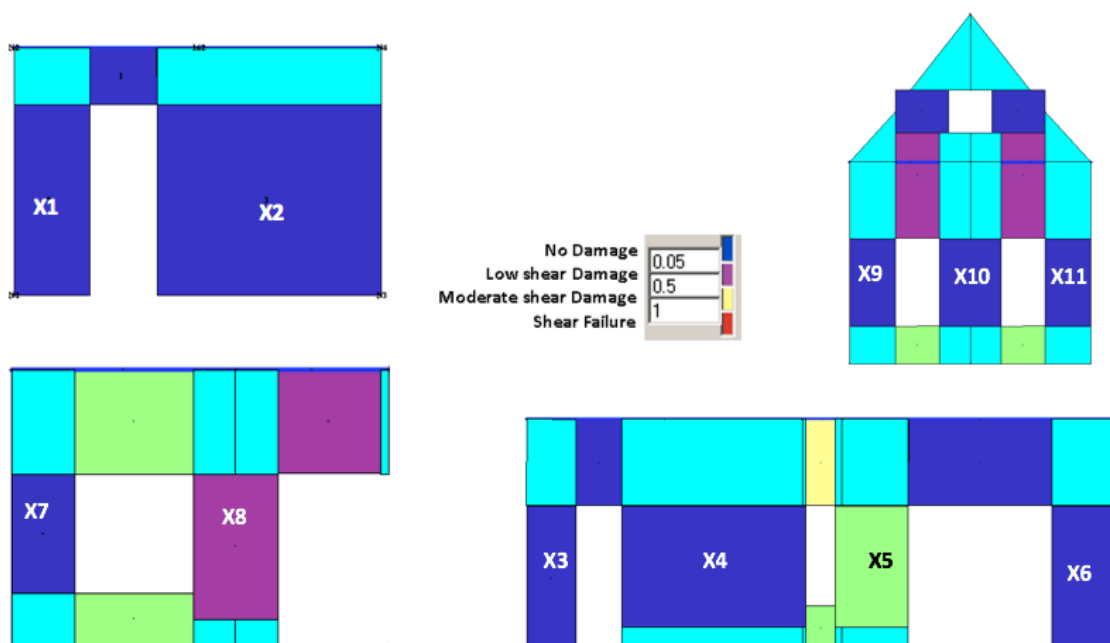


Figure 3.2.15: Damage pattern of the X-walls at the end of the dynamic analysis (PGA 0.1g – Record 7- X direction)

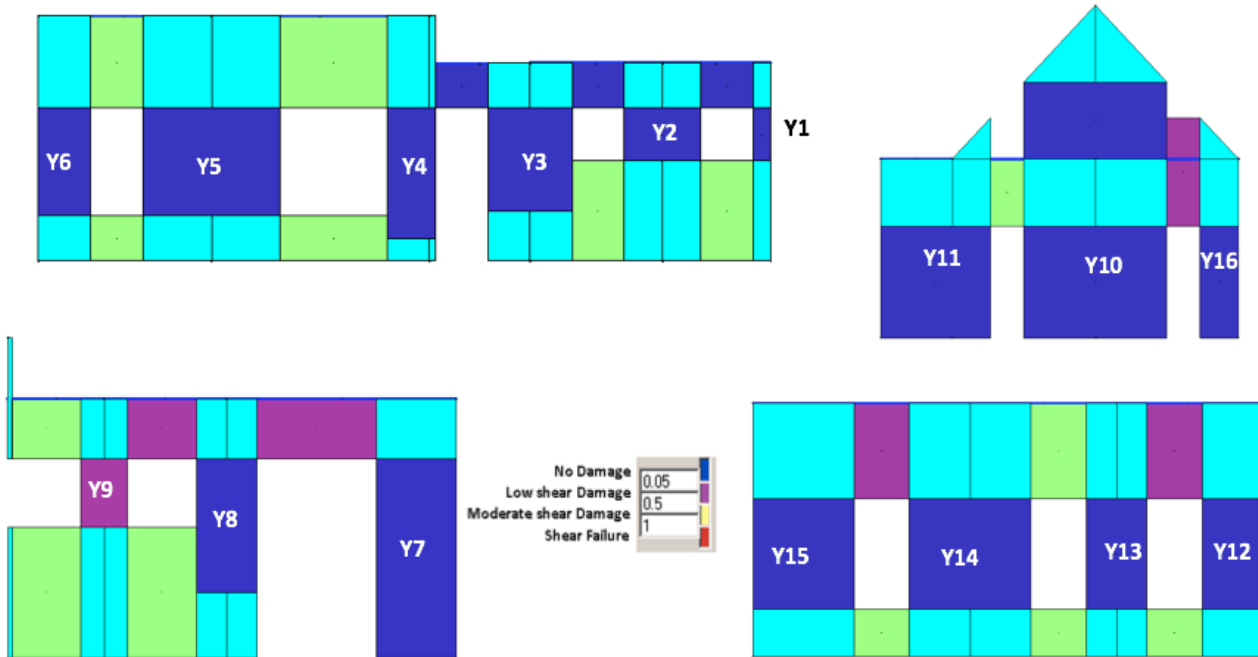


Figure 3.2.16: Damage pattern of the Y-walls at the end of the dynamic analysis (PGA 0.1g – Record 7- Y direction)

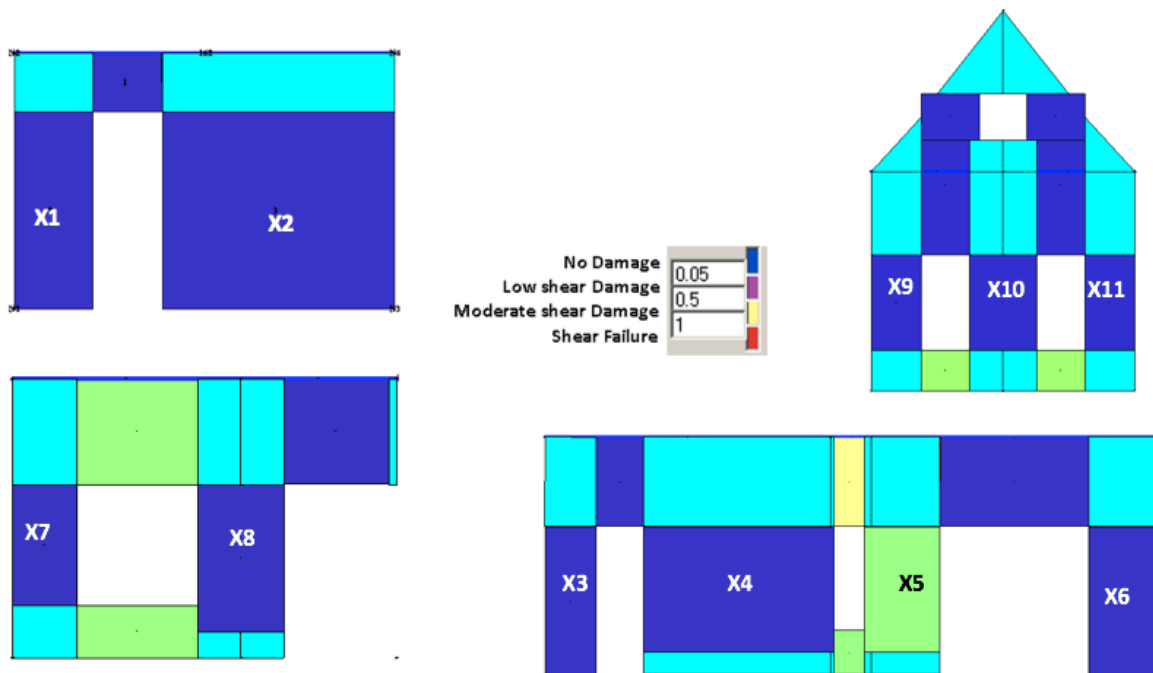


Figure 3.2.17: Damage pattern of the X-walls at the end of the dynamic analysis (PGA 0.1g – Record 7- Y direction)



In order to estimate the initial elastic stiffness of the model, elastic pushover analyses (by imposing a horizontal acceleration of 1g) in both the directions have been performed.

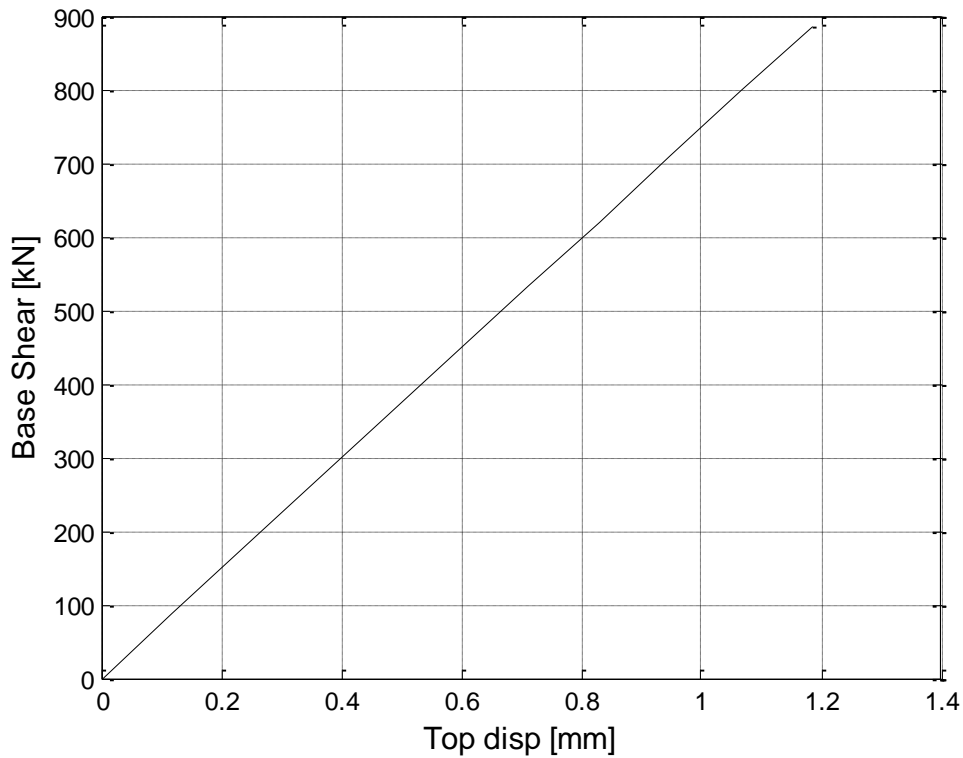


Figure 3.2.18: Elastic Pushover Analysis for model T3A (in X direction)

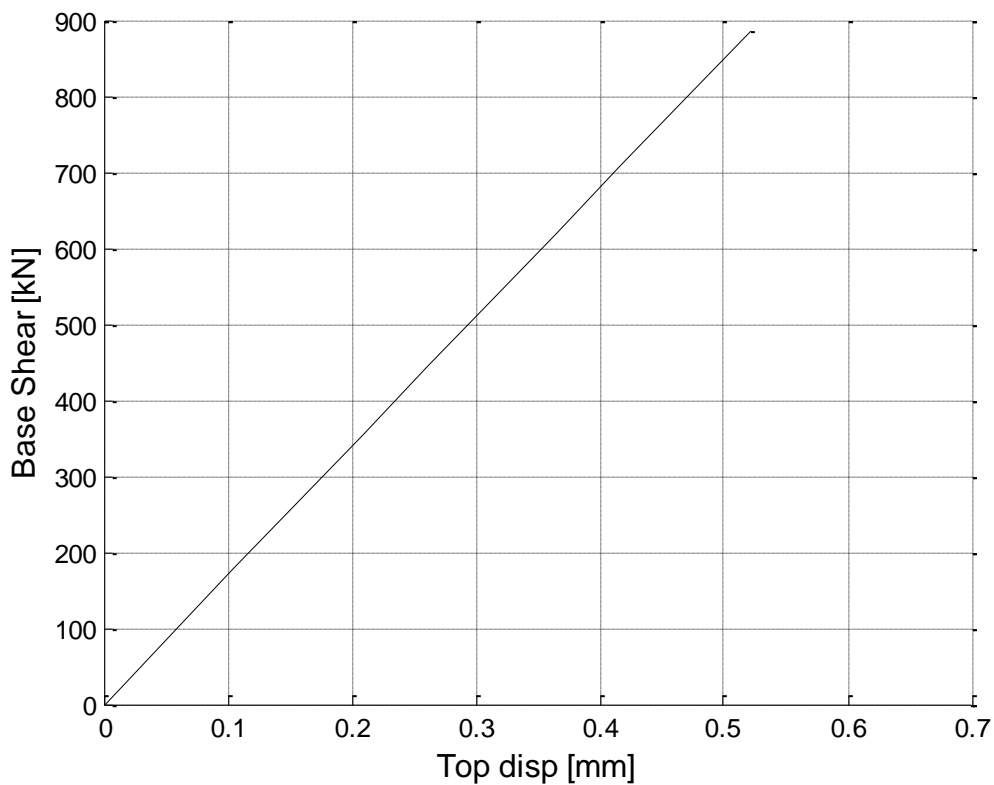


Figure 3.2.19: Elastic Pushover Analysis for model T3A (in Y direction)



In order to obtain a meaningful comparison of the results, the Rayleigh damping implemented in the Tremuri models (2%) have been set to the same level adopted by the other teams (1%). The results are reported in the following. As expected maximum displacement slightly increase.

Table 3.2.12: Peak reference node displacement (3 records at each PGA level)-Damping 1%

PGA	RECORD 3 (mm)		RECORD 6 (mm)		RECORD 7 (mm)	
	X direction	Y direction	X direction	Y direction	X direction	Y direction
0.1g	0.54	0.175	0.47	0.19	0.55	0.156
0.25g	2.13	0.46	1.35	0.51	1.57	0.56
0.5g	4.41	2.48	6.47	1.42	7.17	2.44

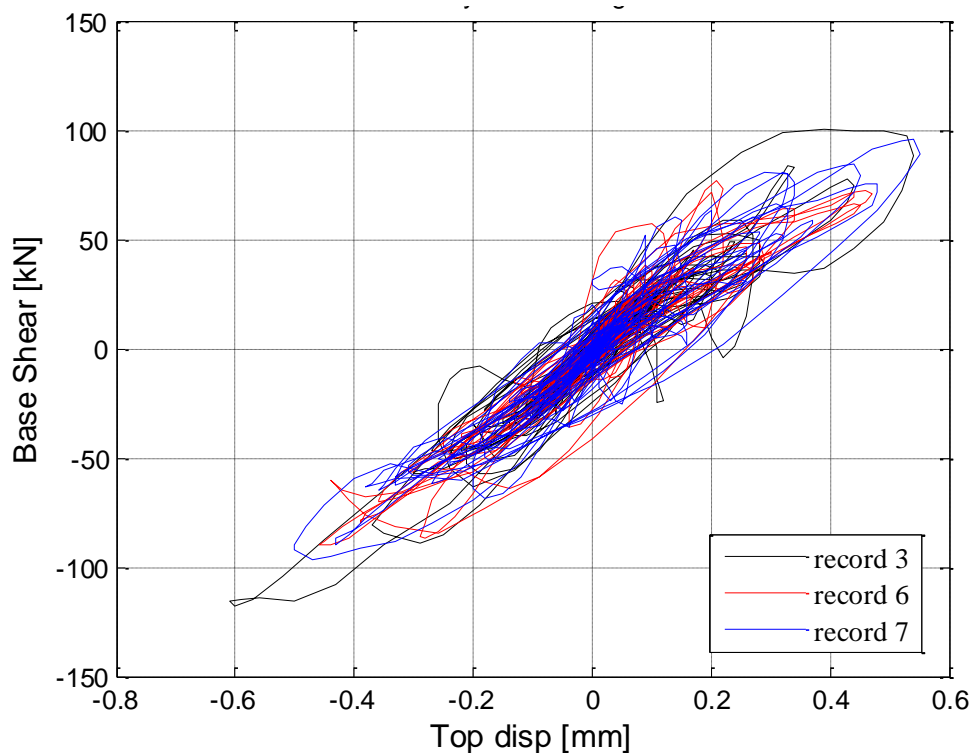


Figure 3.2.20: Base shear versus reference node displacement – 0.1g scaled PGA, record 3, 6 and 7 (X direction, Damping 1%).

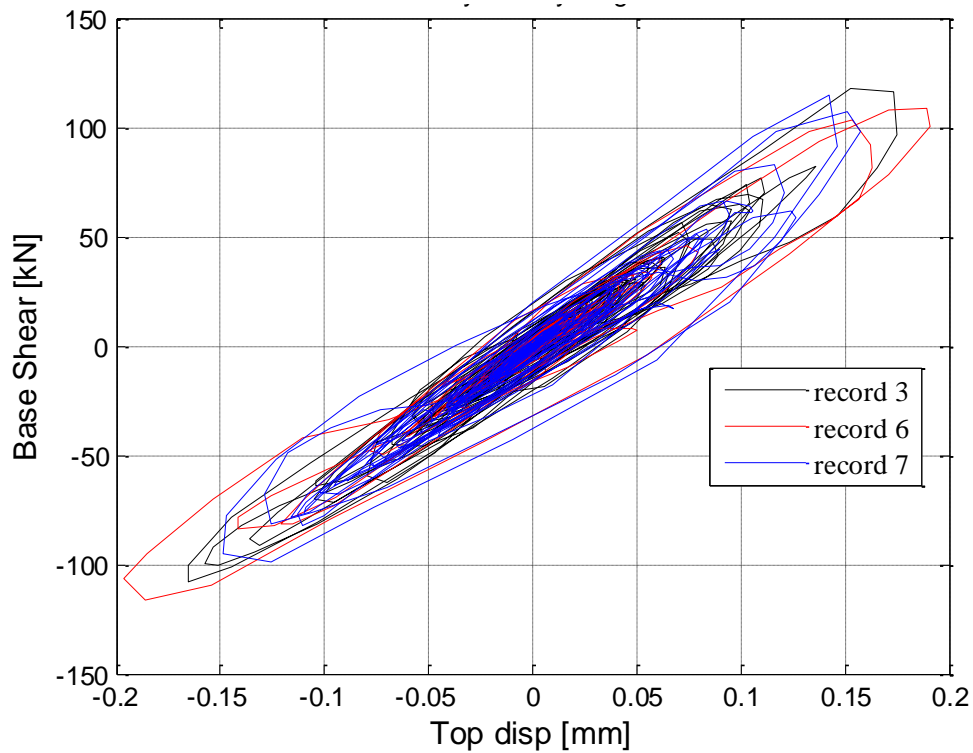


Figure 3.2.21: Base shear versus reference node displacement – 0.1g scaled PGA, record 3, 6 and 7 (Y direction, Damping 1%).

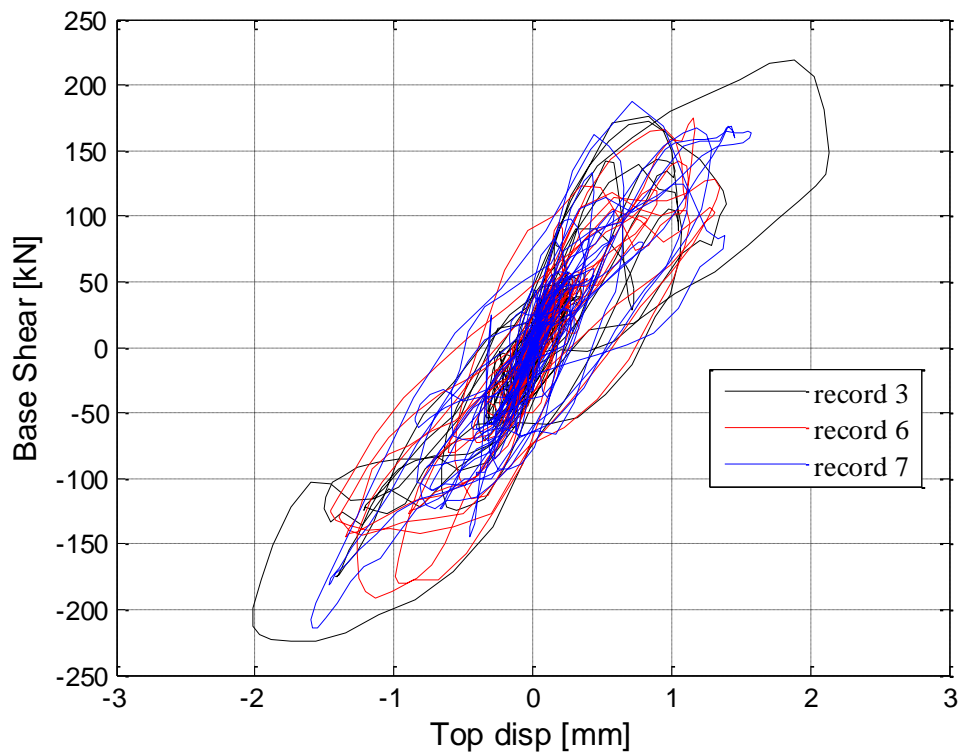


Figure 3.2.22: Base shear versus reference node displacement – 0.25g scaled PGA, record 3, 6 and 7 (X direction, Damping 1%).

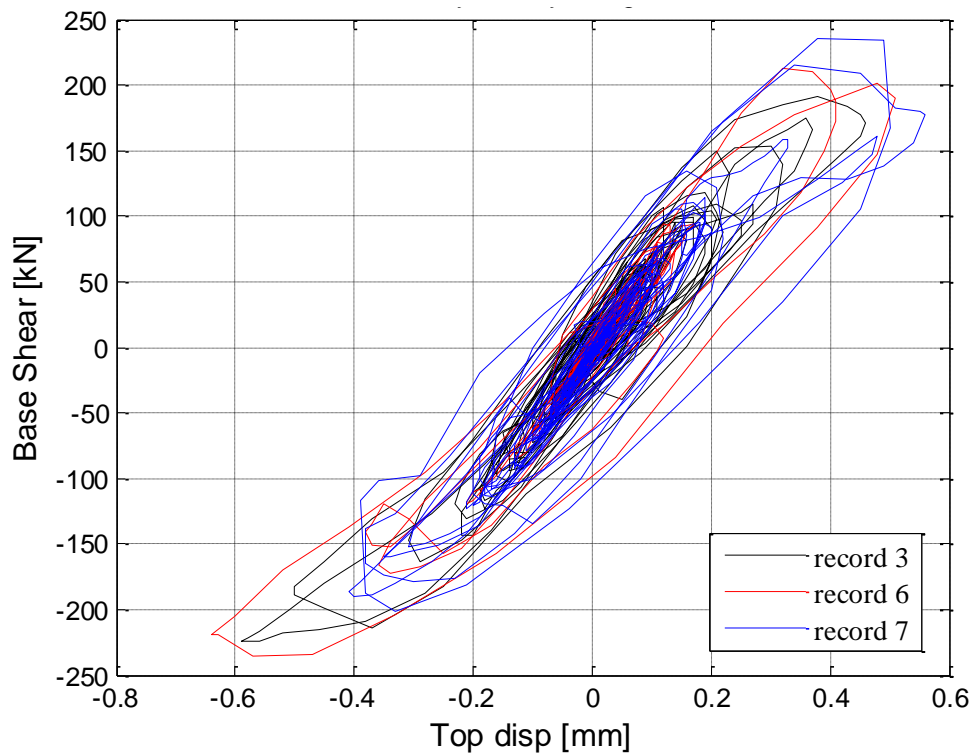


Figure 3.2.23: Base shear versus reference node displacement – 0.25g scaled PGA, record 3, 6 and 7 (Y direction, Damping 1%).

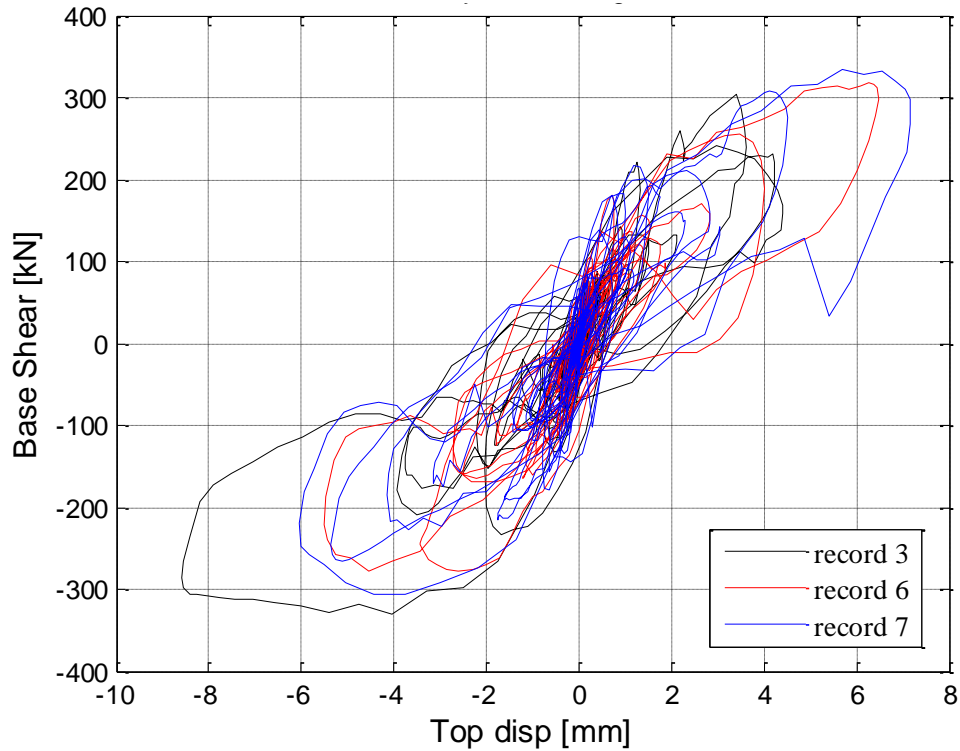


Figure 3.2.24: Base shear versus reference node displacement – 0.5g scaled PGA, record 3, 6 and 7 (X direction, Damping 1%).

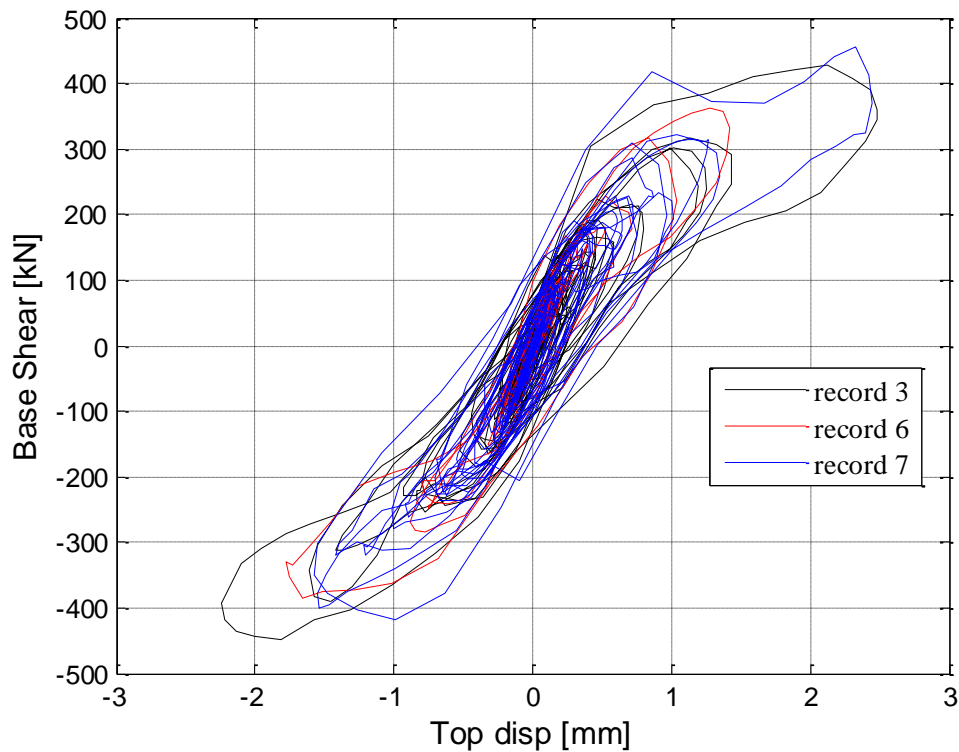


Figure 3.2.25: Base shear versus reference node displacement – 0.5g scaled PGA, record 3, 6 and 7 (Y direction, Damping 1%).

4. References

- Lagomarsino S., Penna A., Galasco A., Cattari S. [2013] “TREMURI Program: an equivalent frame model for the nonlinear seismic analysis of masonry buildings”, *ENGINEERING STRUCTURES*, 56(11): 1787-1799.
- Penna A., Lagomarsino S., Galasco A. [2014] “A nonlinear macro-element model for the seismic analysis of masonry buildings”, *EARTHQUAKE ENGINEERING & STRUCTURAL DYNAMICS*, 43(2): 159-179.
- Penna A., Galasco A. (2013). A macro-element model for the nonlinear analysis of masonry members including second order effects. In: Papadrakakis M., Papadopoulos V., Plevris V. Proceedings 4th ECCOMAS Thematic Conference on Computational Methods in Structural Dynamics and Earthquake Engineering (COMPdyn 2013). Kos Island, Grecia, 12-14 June 2013.

Appendix C

Modelling Comparison – TU
Delft

1. Summary of modelling approach

Table 1.1: General modelling notes

Component	Description
Analysis team	TU DELFT
Analysis software and formulation	DIANA implicit solver
Overview of modelling approach	Total strain based smeared crack model optionally with non-linearity in compression [1-4].
Model units	SI units (kg, m, sec)

Table 1.2: Model properties applicable for all benchmark tests and index buildings

Input	Description
Element formulation	Quadratic plane stress elements for in-plane cases and 2D configurations. Quadratic shell elements for combined in-plane and out-of-plane cases and 3D configurations.
Solution procedure	Incremental iterative Newton Raphson technique. If possible displacement control otherwise load control optionally with arc-length techniques.
Masonry constitutive model	Total strain based smeared crack model optionally with non-linearity in compression. The specific material properties will be included in the tables for the specific benchmarks

2. Experimental benchmarks

2.1. Ispra in-plane panel tests

Table 2.1.1: Modelling notes

Component	Description
Analysis software and formulation	DIANA
Walls (in-plane)	Masonry modelled with quadratic plane stress elements using Total Strain Fixed Smeared Crack Model with Exponential Tensile Softening, Elastic Compression and Variable Shear Reduction factor. Secant unloading.

Table 2.1.2: Nonlinear time history analysis notes

Nonlinear pushover analysis notes
<ul style="list-style-type: none"> Displacement control

Table 2.1.2: Model loading, materials and general comments

Loading	
Dead load	1800kg/m ³
Overburden	140kN/m uniformly distributed on top layer
Materials	Material properties including values and stress strain behaviour
Masonry	Total Strain Fixed Smeared Crack Model with Exponential Tensile Softening, Elastic Compression and Variable Shear Reduction factor. Secant unloading $\rho = 1800 \text{ kg/m}^3$ $E = 1410 \text{ MPa}$ $\nu = 0.15$ with reduction $f_t = 0.1 \text{ MPa}$ (Tensile strength) $G_f = 50 \text{ N/m}$ (Tensile fracture energy) β Variable
Steel	Linear Elastic model $\rho = 7860 \text{ kg/m}^3$ $E = 200 \text{ GPa}$ $\nu = 0.3$
<u>Other key notes</u>	
1) Tyings for equal vertical displacement were placed at the top nodes	

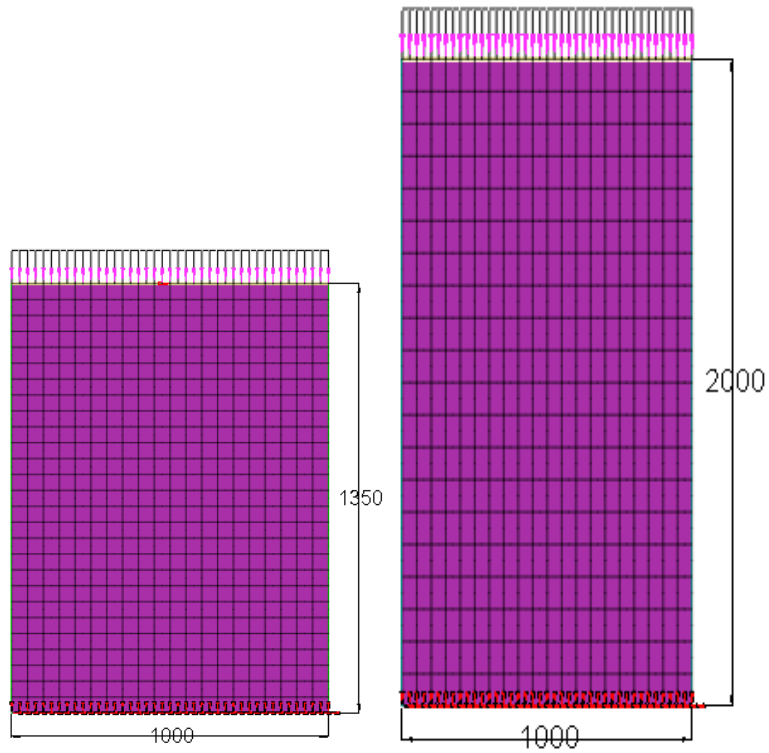


Figure 2.1.1: FE models for (a) LOWSTA and (b) HIGSTA1, measures in mm

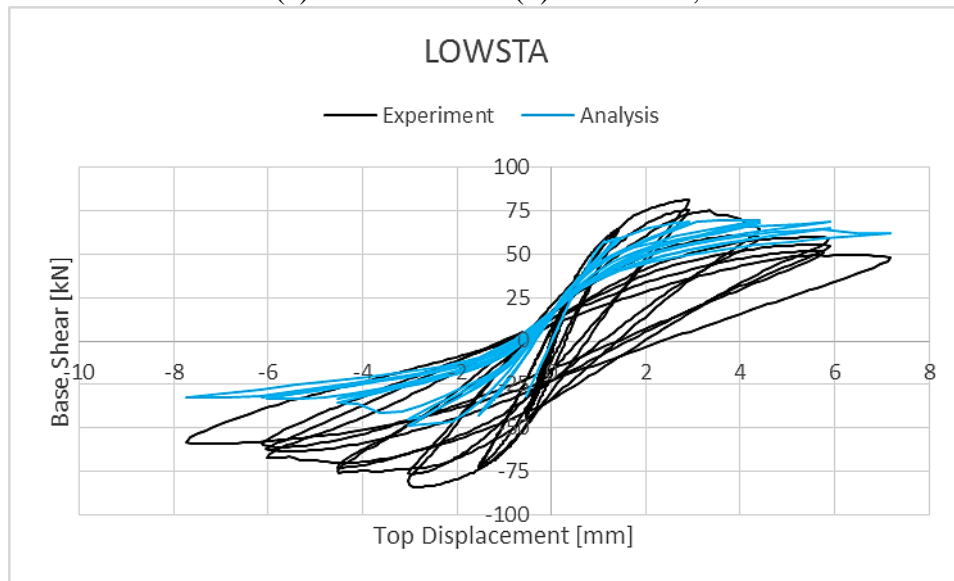


Figure 2.1.2: Shear force-displacement comparison plot for LOWSTA

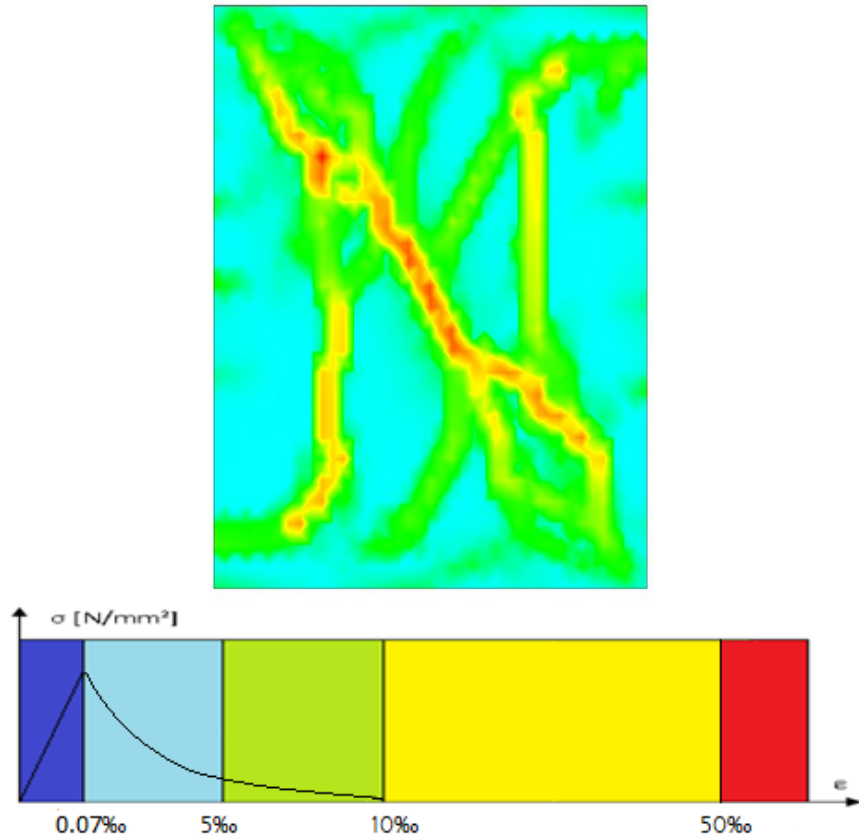


Figure 2.1.3: Final crack pattern for LOWSTA (if relevant)

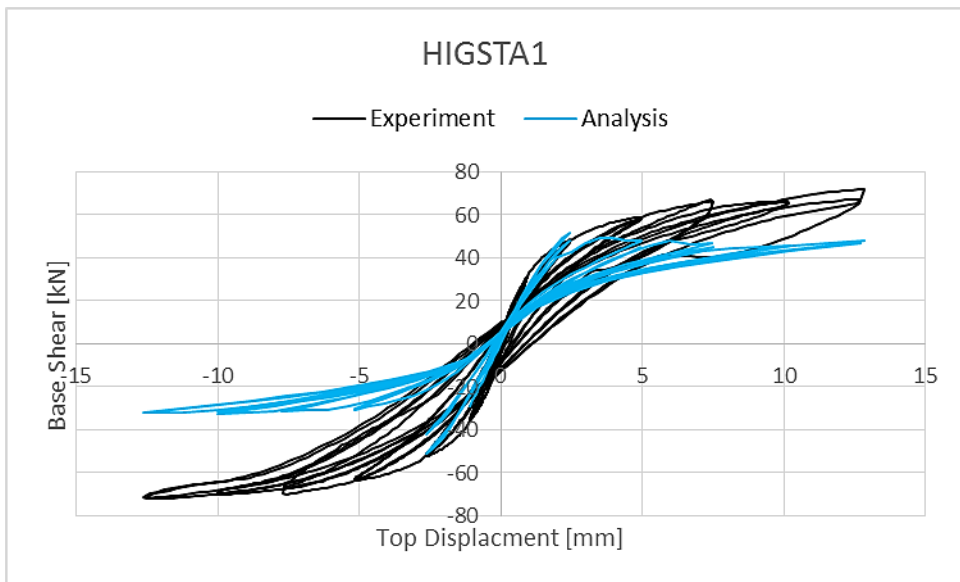


Figure 2.1.4: Shear force-displacement comparison plot for HIGSTA1

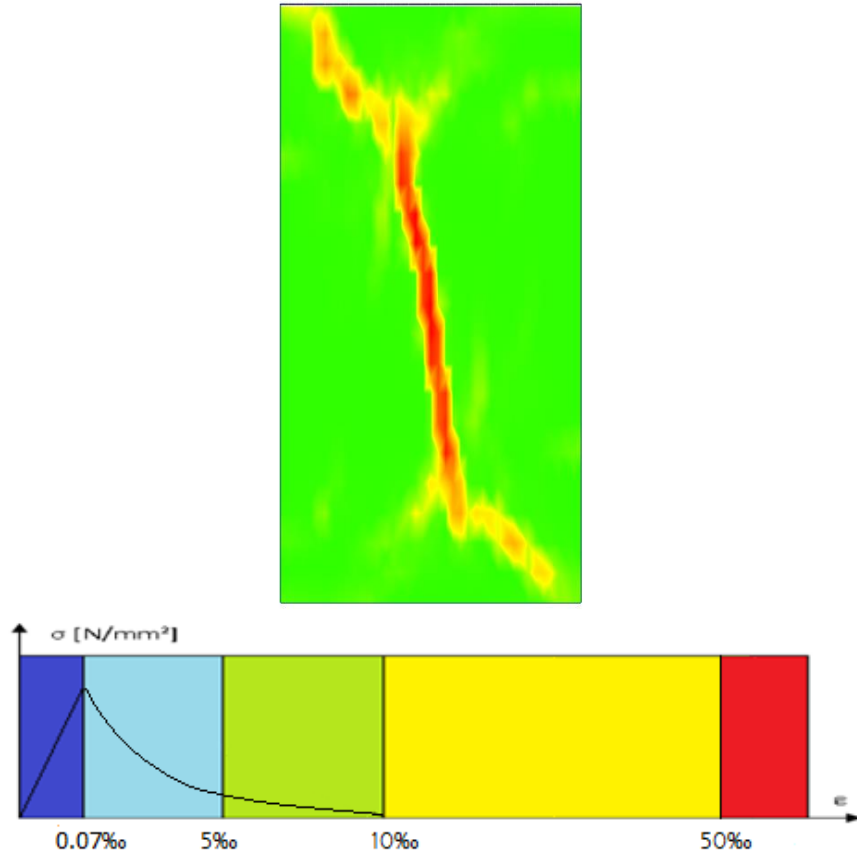


Figure 2.1.5: Final crack pattern for HIGSTA1 (if relevant)

2.1.1. Discussion and sensitivity analyses (if relevant)

Sensitivity Analyses

Materials	Material properties including values and stress strain behaviour
Masonry	Total Strain Fixed Smeared Crack Model with Linear Tensile Softening, Elastic Compression and Variable Shear Reduction factor. Secant unloading $\rho = 1800 \text{ kg/m}^3$ $E = 1410 \text{ MPa}$ $\nu = 0.15$ with reduction $f_t = 0.2 \text{ MPa}$ (Tensile strength) $G_f = 100 \text{ N/m}$ (Tensile fracture energy) β Variable

Sensitivity on mesh size for variable beta with Poisson's ratio reduction

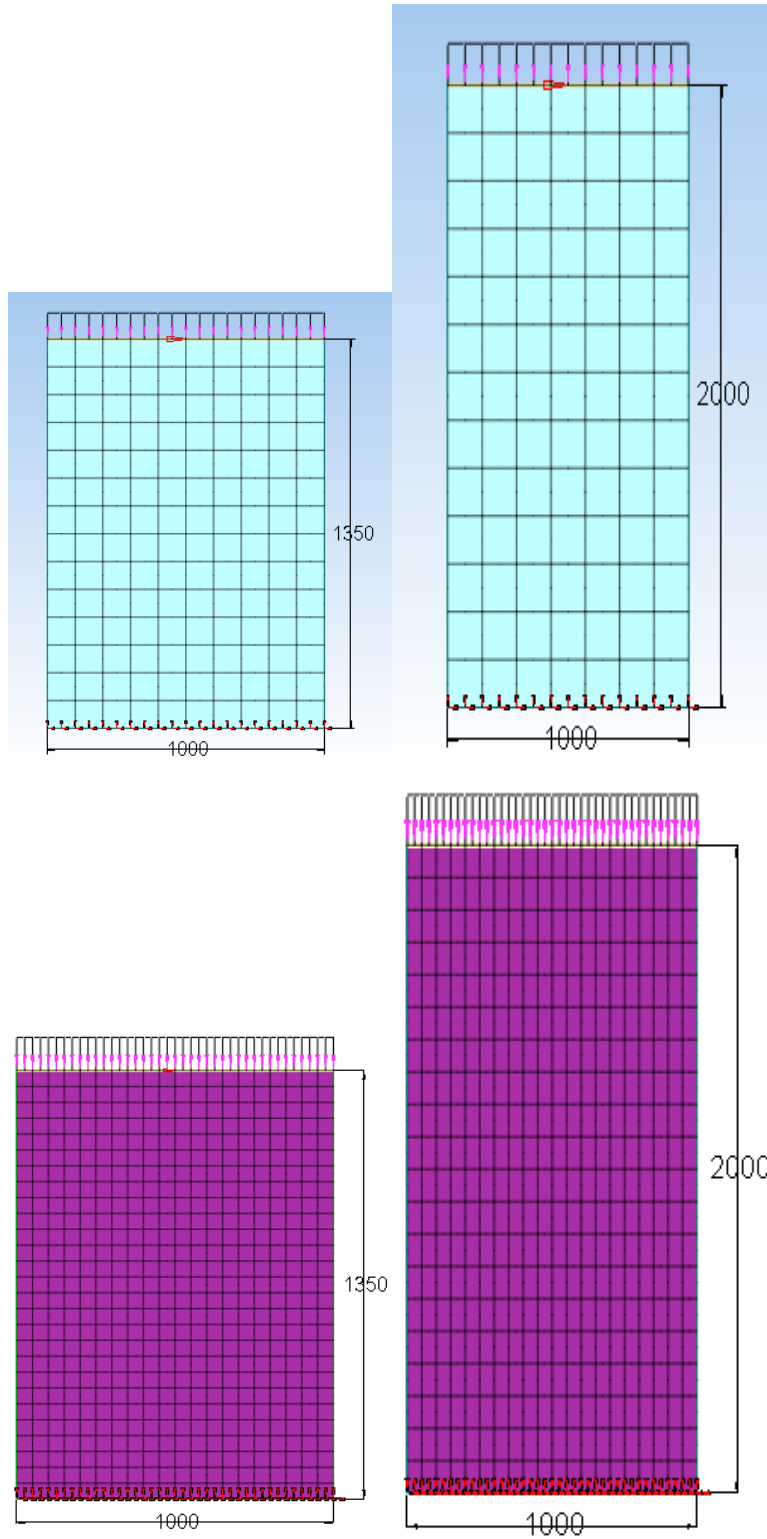


Figure 2.1.6 Coarse and fine mesh for LOWSTA and HIGHSTA1

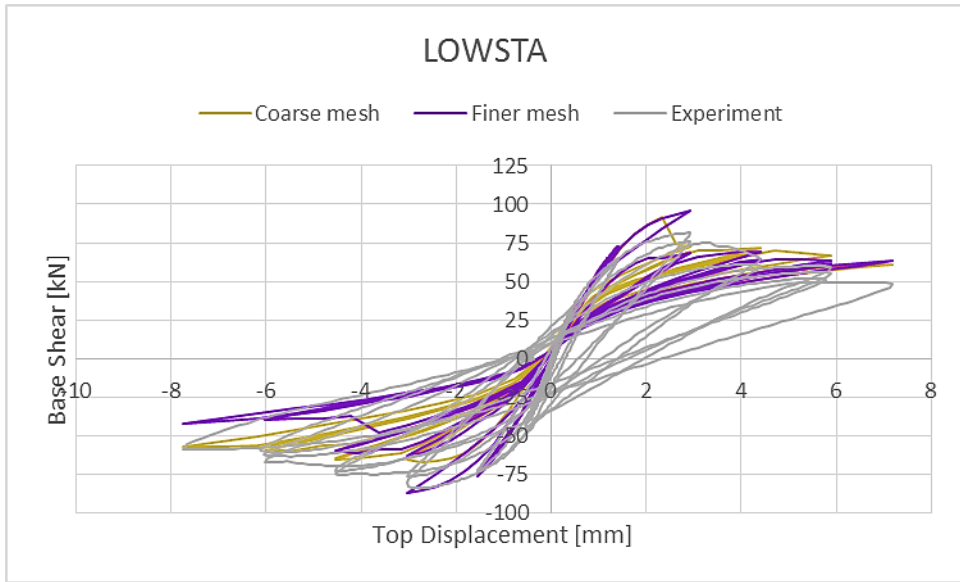


Figure 2.1.7 Comparison between coarse and finer mesh for TSCF model with variable beta and Poisson's ratio reduction, LOWSTA

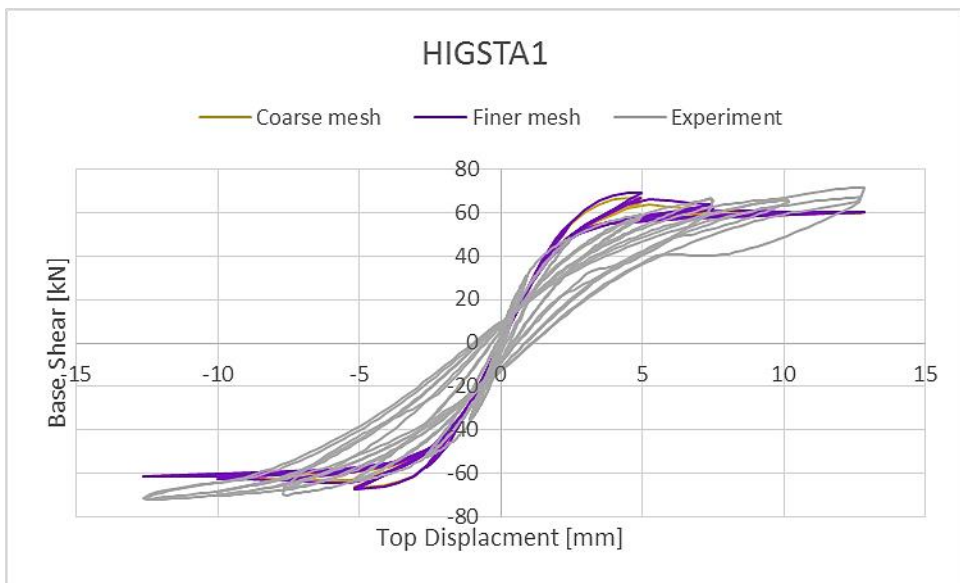


Figure 2.1.8 Comparison between coarse and finer mesh for TSCF model with variable beta and Poisson's ratio reduction, HIGSTA1

Sensitivity on Variable and Constant shear reduction factor with $\beta=0.01$

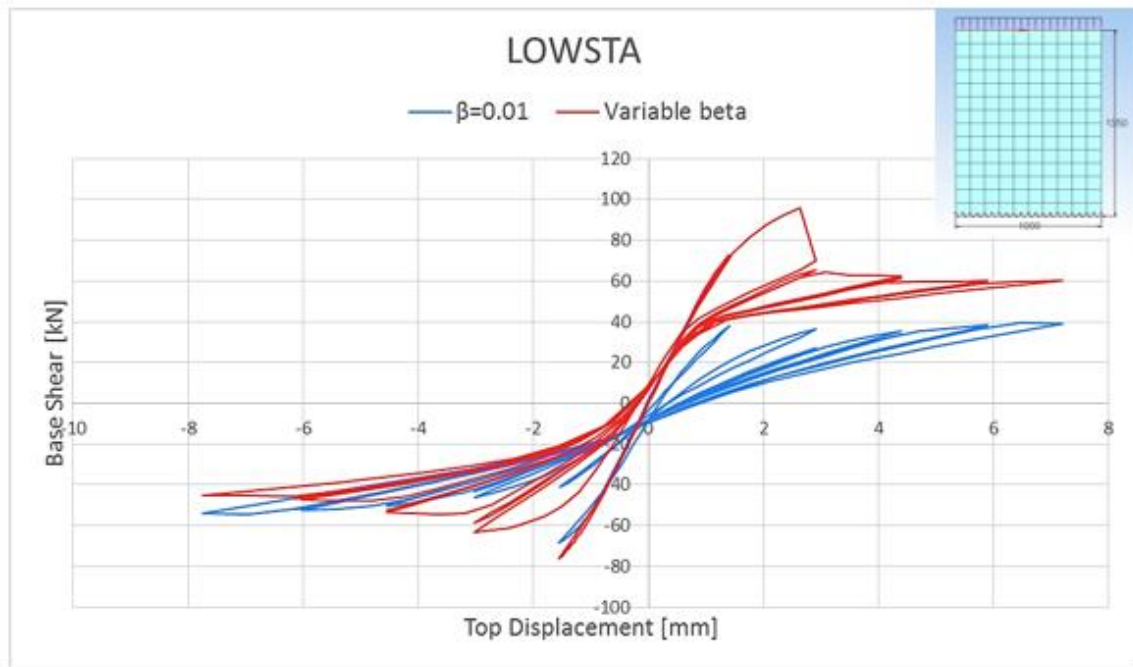


Figure 2.1.9 Comparison between constant shear reduction factor ($\beta=0.01$) and variable beta LOWSTA, coarse mesh LOWSTA

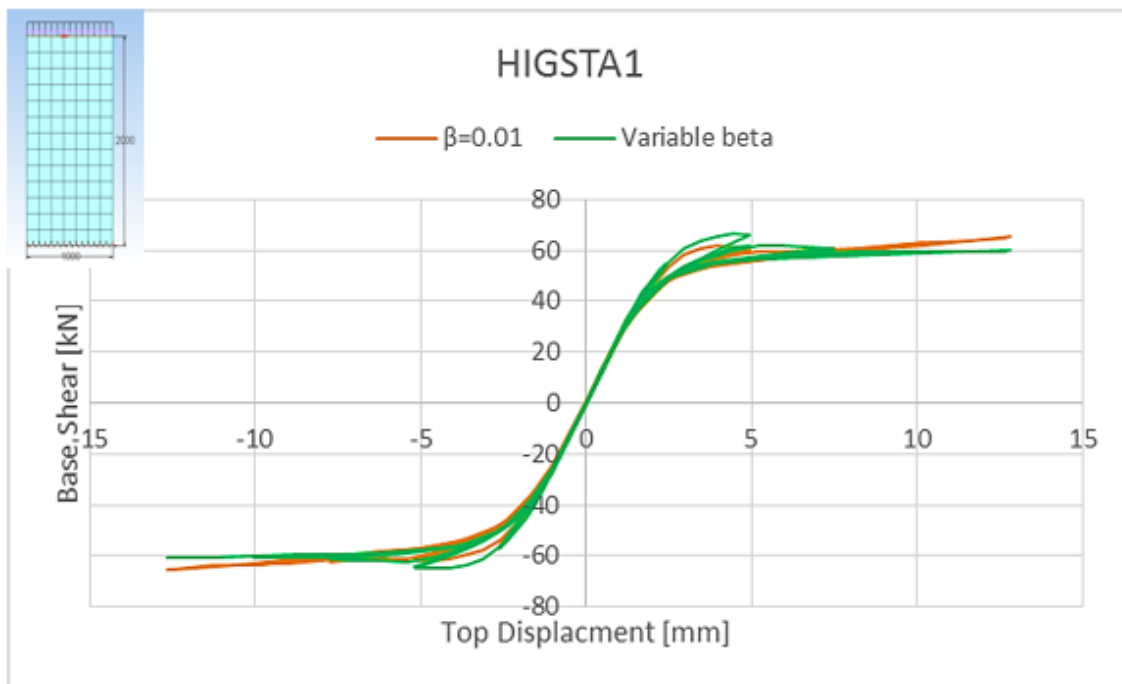


Figure 2.1.10 Comparison between constant shear reduction factor ($\beta=0.01$) and variable beta, coarse mesh HIGSTA1

Sensitivity on Hysteresis Model and Total Strain model with Fixed orthogonal cracks with secant unloading

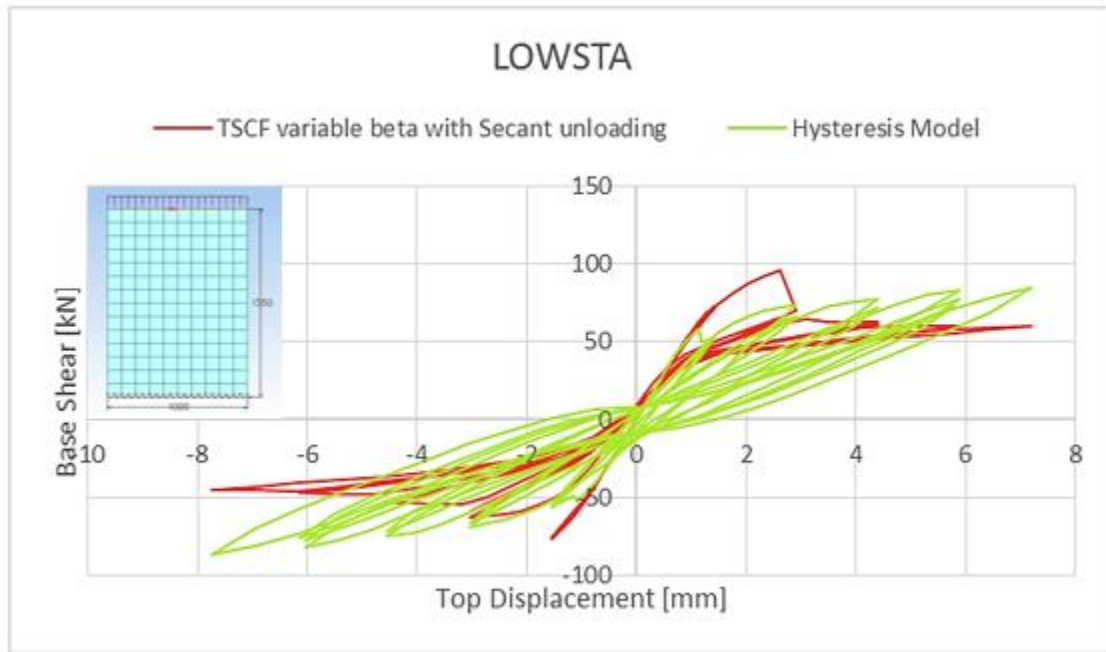


Figure 2.1.11 Comparison between Total Strain Crack model with secant unloading and Hysteresis model, coarse mesh LOWSTA

Sensitivity on Poisson's ratio reduction

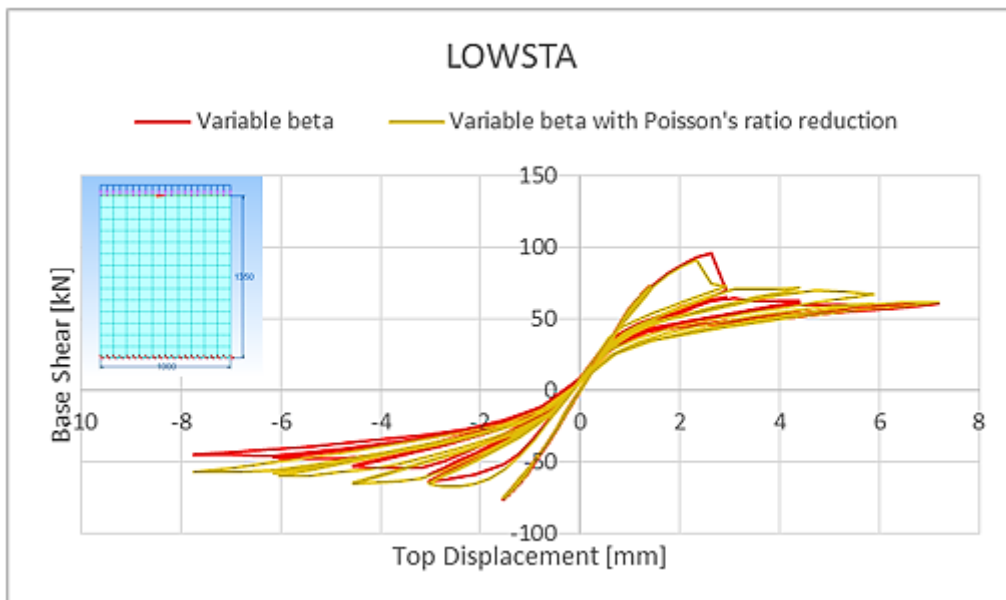


Figure 2.1.12 Comparison between Variable beta and Variable beta with Poisson's ratio reduction, coarse mesh LOWSTA

2.2. Pavia full building tests

Table 2.2.1: Modelling notes

Component	Description
Analysis software and formulation	DIANA
Walls (in-plane)	Masonry modelled with quadratic plane stress elements (Door Wall-2D model) and shell elements (Window Wall-3D model) using Total Strain Fixed smeared Crack Model with Exponential Tensile Softening, Elastic Compression and Variable Shear Reduction factor. Secant unloading.
Walls (out-of-plane)	As above.
Spandrels/lintels and wall coupling	Spandrels modelled using the same approach as the walls. Clamped connection between spandrels and walls. Lintels were not modelled.
Wall to wall connection (incl. flange effects)	Clamped connection. Flange effects are included explicitly.
Wall to diaphragm connection	Diaphragm is not included as the two walls (Door Wall and Window Wall) behaved as independent structures [Seismic Testing of a Full-Scale, Two-Story Masonry Building: Test Procedure and Measured Experimental Response G. Magenes, G.M. Calvi, G.R. Kingsley]

Table 2.2.2: Pushover analysis notes

Nonlinear pushover analysis notes
<ul style="list-style-type: none"> Indirect displacement control with auxiliary beam which loads the structure with equal forces on the two floor levels

Table 2.2.2: Model loading, materials and general comments

Loading	
Dead load	1800kg/m ³
Applied load	First floor: 20.7kN/m Second floor: 19.7kN/m
Materials	
Masonry	Material properties including values and stress strain behaviour Total Strain Fixed Smeared Crack Model with Exponential Tensile Softening, Elastic Compression and Variable Shear Reduction factor. Secant unloading $\rho = 1800 \text{ kg/m}^3$ $E = 1410\text{MPa}$ $\nu = 0.15$ with reduction $f_t = 0.1\text{MPa}$ (Tensile strength) $G_f = 50\text{N/m}$ (Tensile fracture energy) Variable β
Other key notes	
1) Indirect displacement control with auxiliary beam which loads the structure with equal forces on the two floor levels 2) Tyings for equal horizontal displacement were placed at the floor levels	

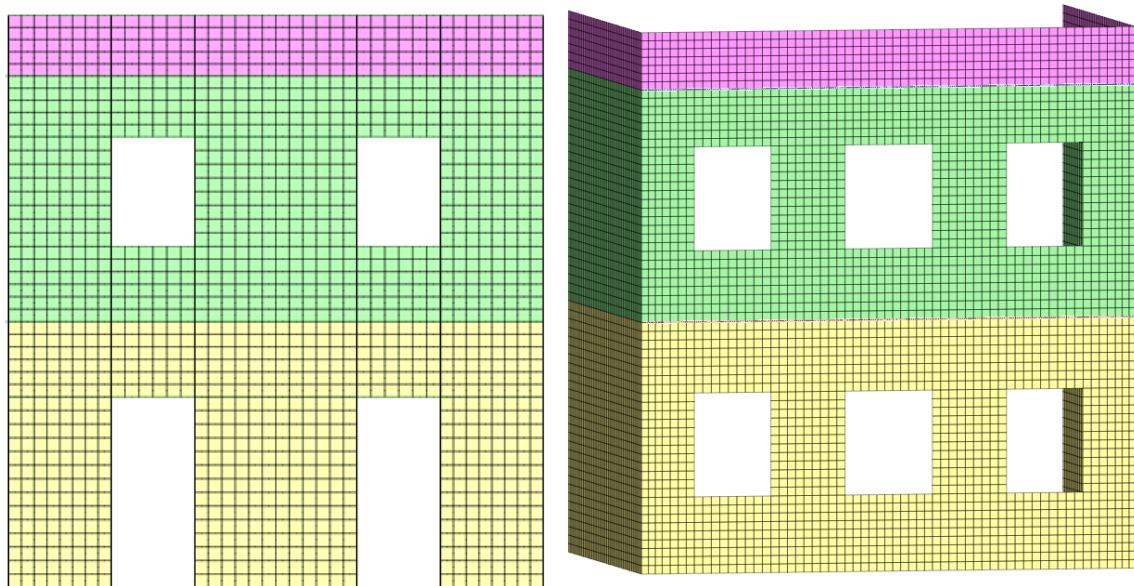


Figure 2.2.1: FE model showing Window Wall and Door Wall (isometric view)

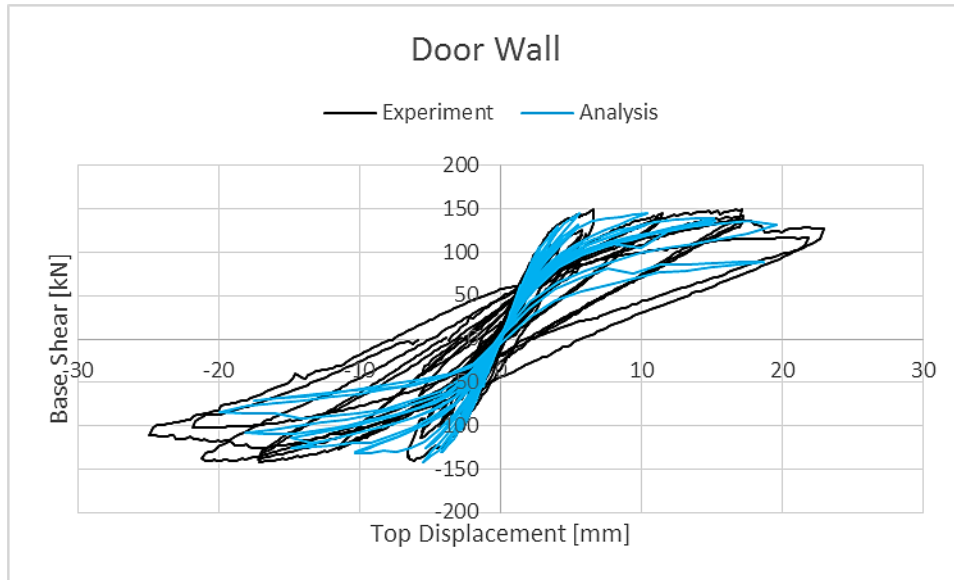


Figure 2.2.2: Total base shear force vs. 2nd floor displacement (Door Wall)

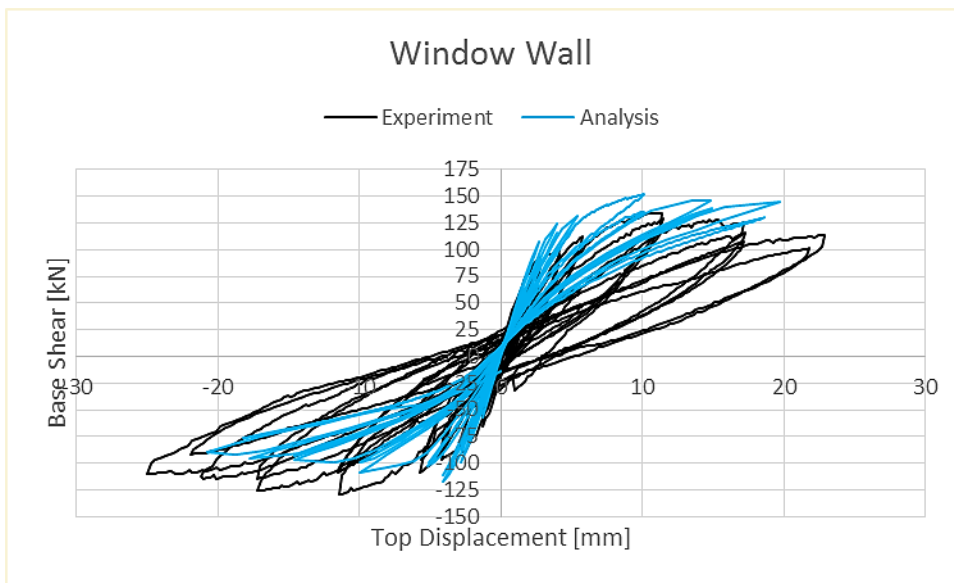


Figure 2.2.3: Total base shear force vs. 2nd floor displacement (Window Wall)

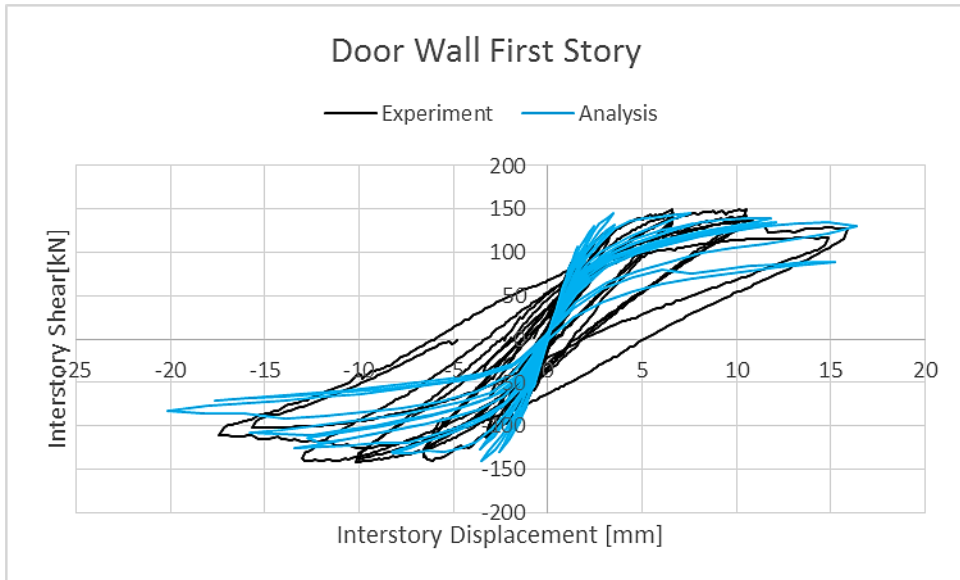


Figure 2.2.4: Interstorey shear force vs. interstorey displacement, 1st floor (Door Wall)

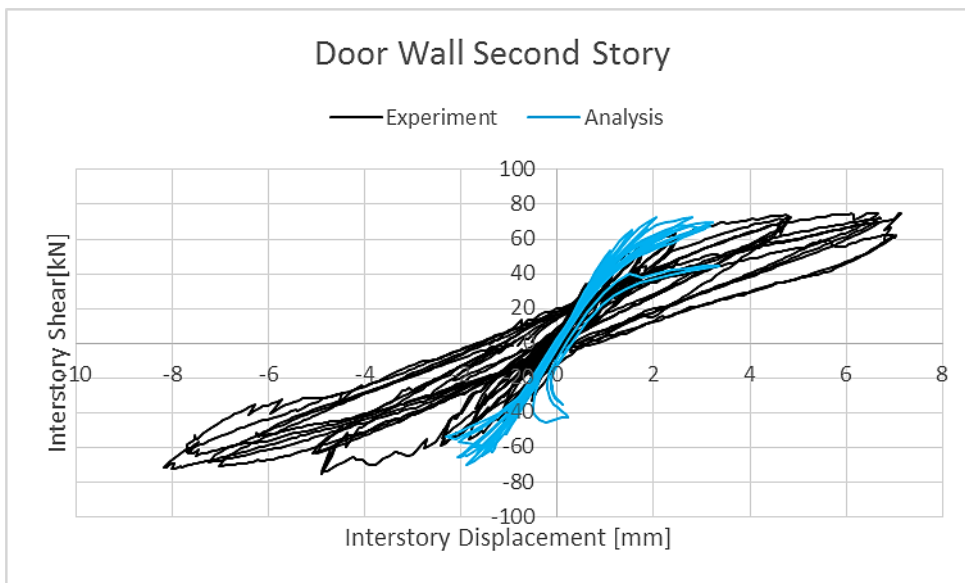


Figure 2.2.5: Interstorey shear force vs. interstorey displacement, 2nd floor (Door Wall)

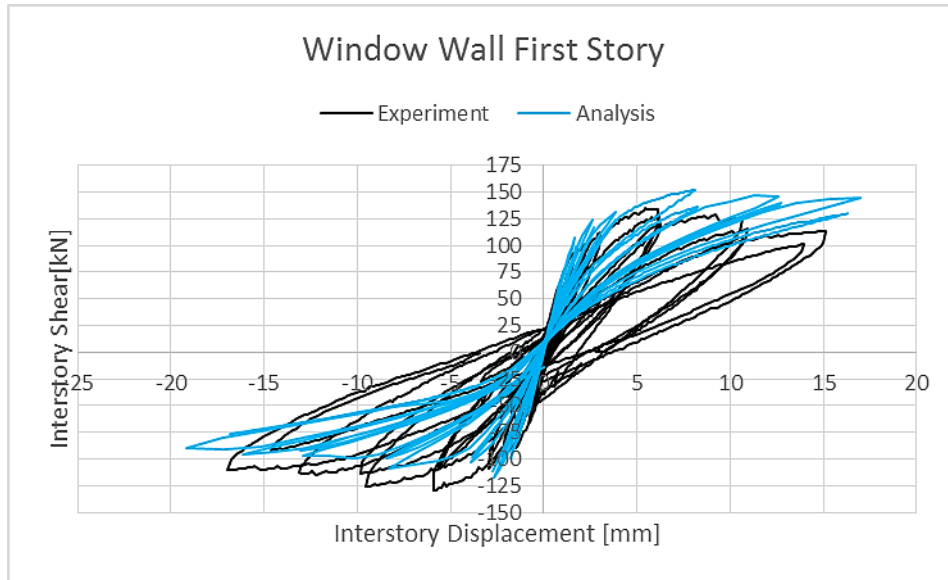


Figure 2.2.6: Interstorey shear force vs. interstorey displacement, 1st floor (Window Wall)

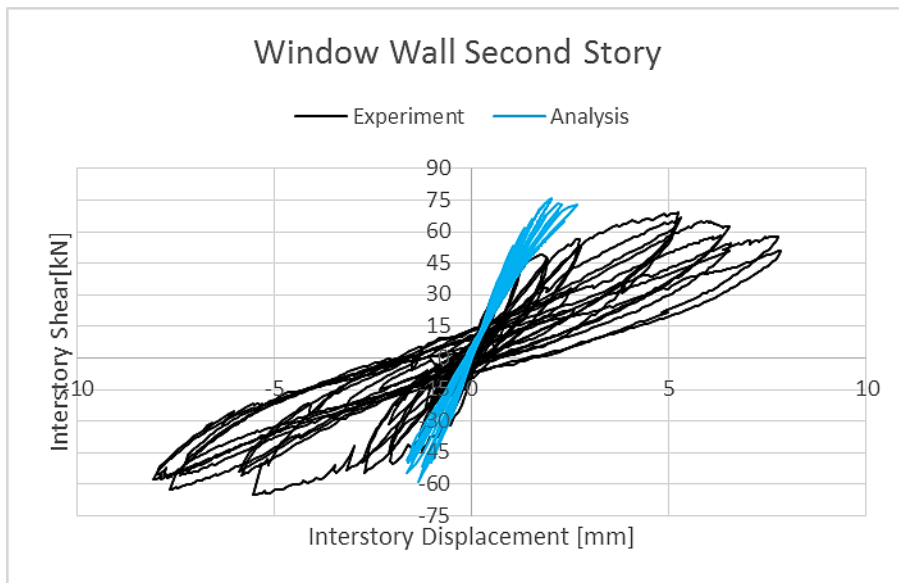


Figure 2.2.7: Interstorey shear force vs. interstorey displacement, 2nd floor (Window Wall)

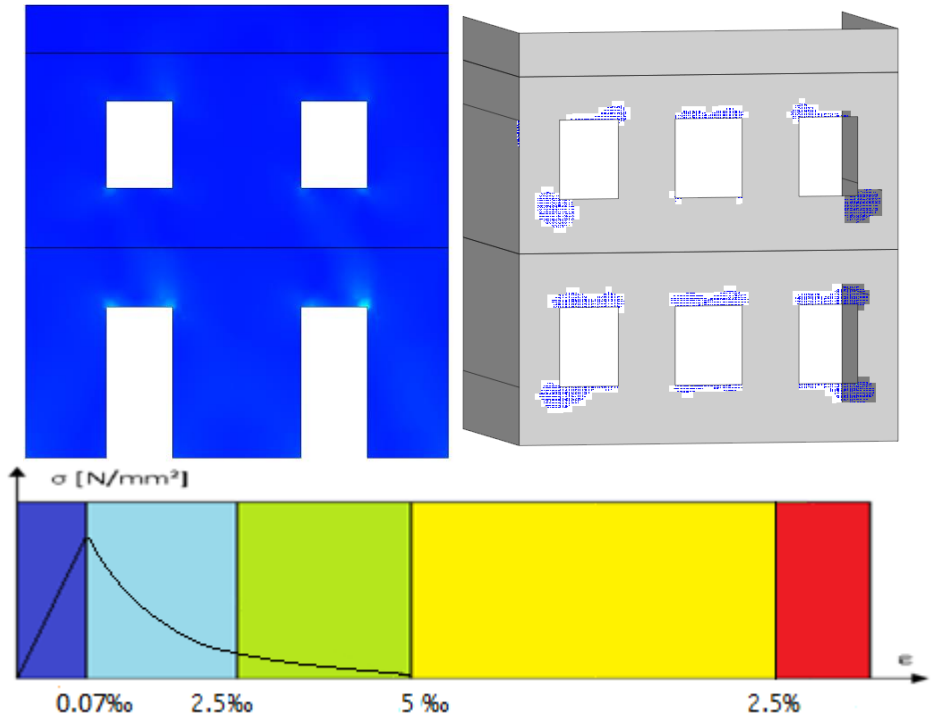


Figure 2.2.8: Crack pattern after Run 1 – Door Wall and Window Wall (if relevant)

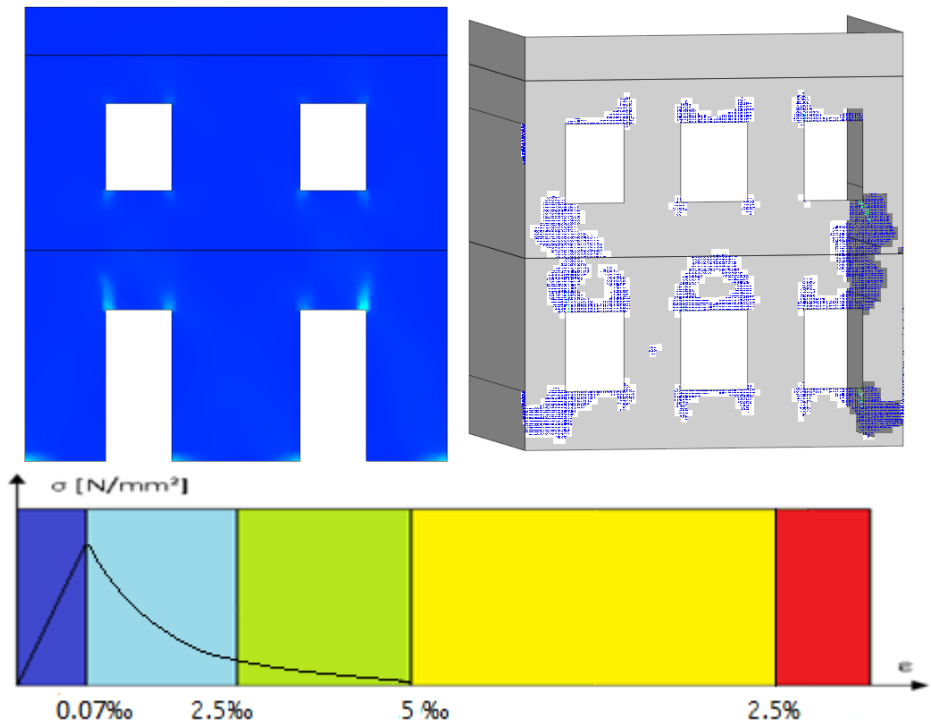


Figure 2.2.9: Crack pattern after Run 2 – Door Wall and Window Wall (if relevant)

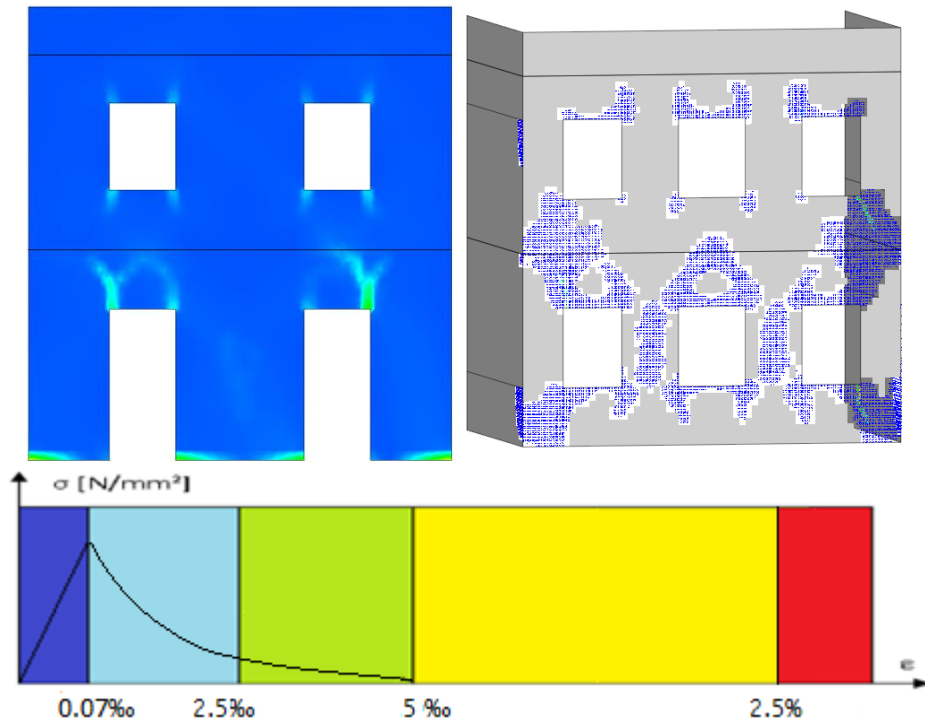


Figure 2.2.10: Crack pattern after Run 3 – Door Wall and Window Wall (if relevant)

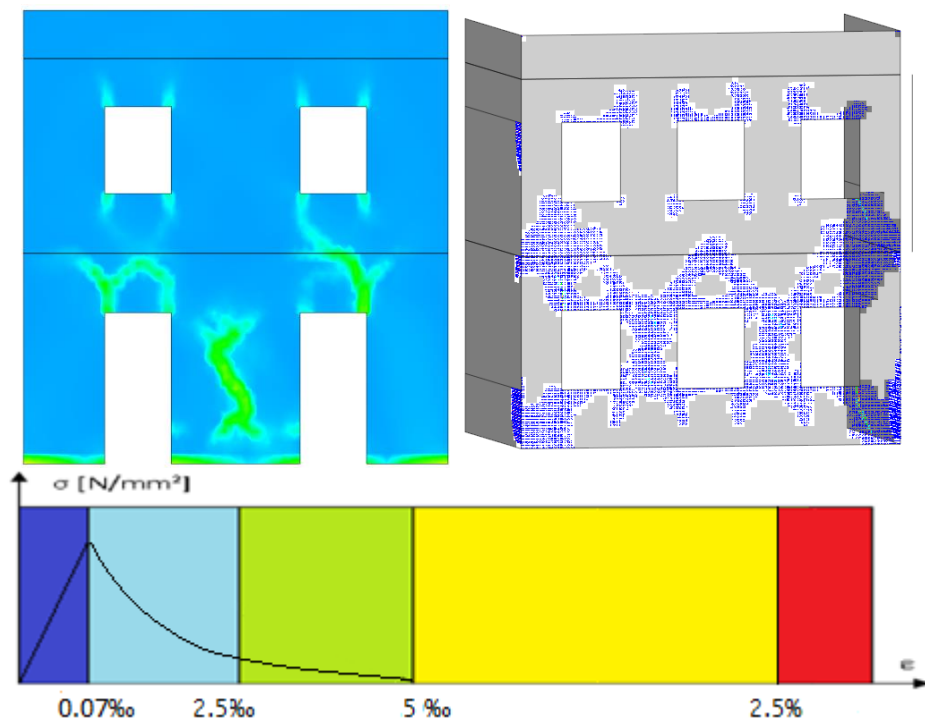


Figure 2.2.11: Crack pattern after Run 4 – Door Wall and Window Wall (if relevant)

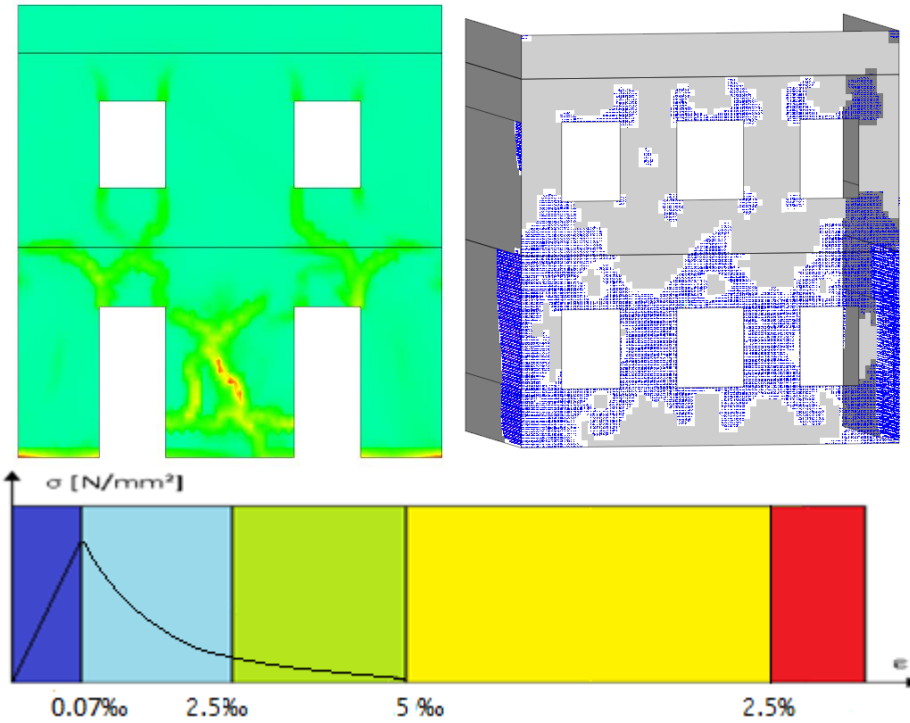


Figure 2.2.12: Crack pattern after Run 5 – Door Wall and Window Wall (if relevant)

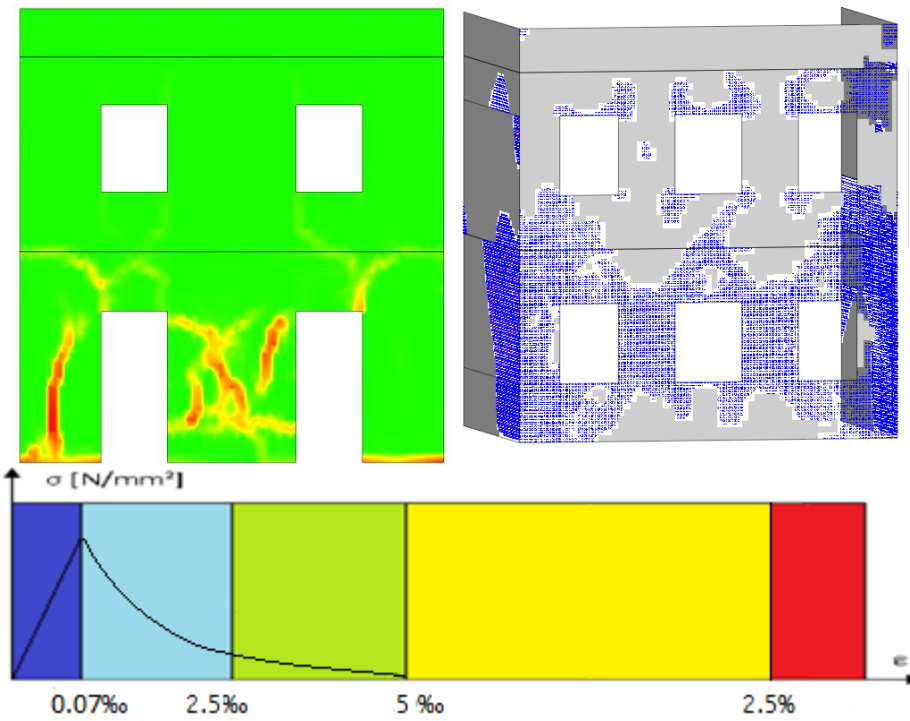


Figure 2.2.13: Crack pattern after Run 6 – Door Wall and Window Wall (if relevant)

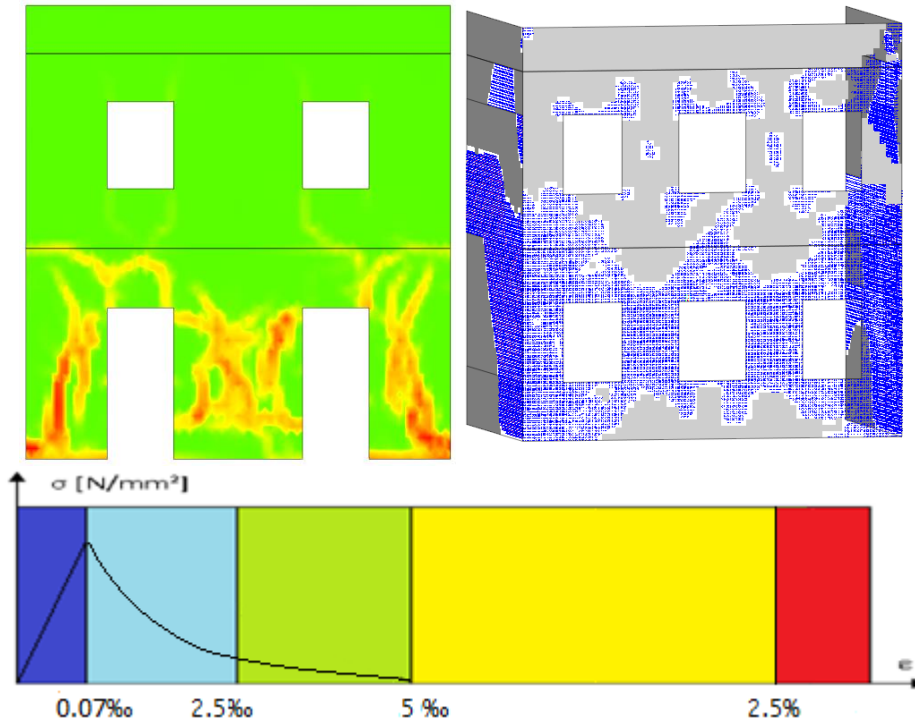


Figure 2.2.14: Crack pattern after Run 7 – Door Wall and Window Wall (if relevant)

2.2.1. Discussion and sensitivity analyses

Materials	Material properties including values and stress strain behaviour
Masonry	Total Strain Fixed Smeared Crack Model with Linear Tensile Softening, Elastic Compression and Constant Shear Reduction factor. Secant unloading $\rho = 1800 \text{ kg/m}^3$ $E = 1410 \text{ MPa}$ $\nu = 0.15$ $f_t = 0.1 \text{ MPa}$ (Tensile strength) $G_f = 50 \text{ N/m}$ (Tensile fracture energy) $\beta = 0.01$ (Constant Shear Reduction)

Variation on the application of the lateral load for monotonic pushover on 2D models:

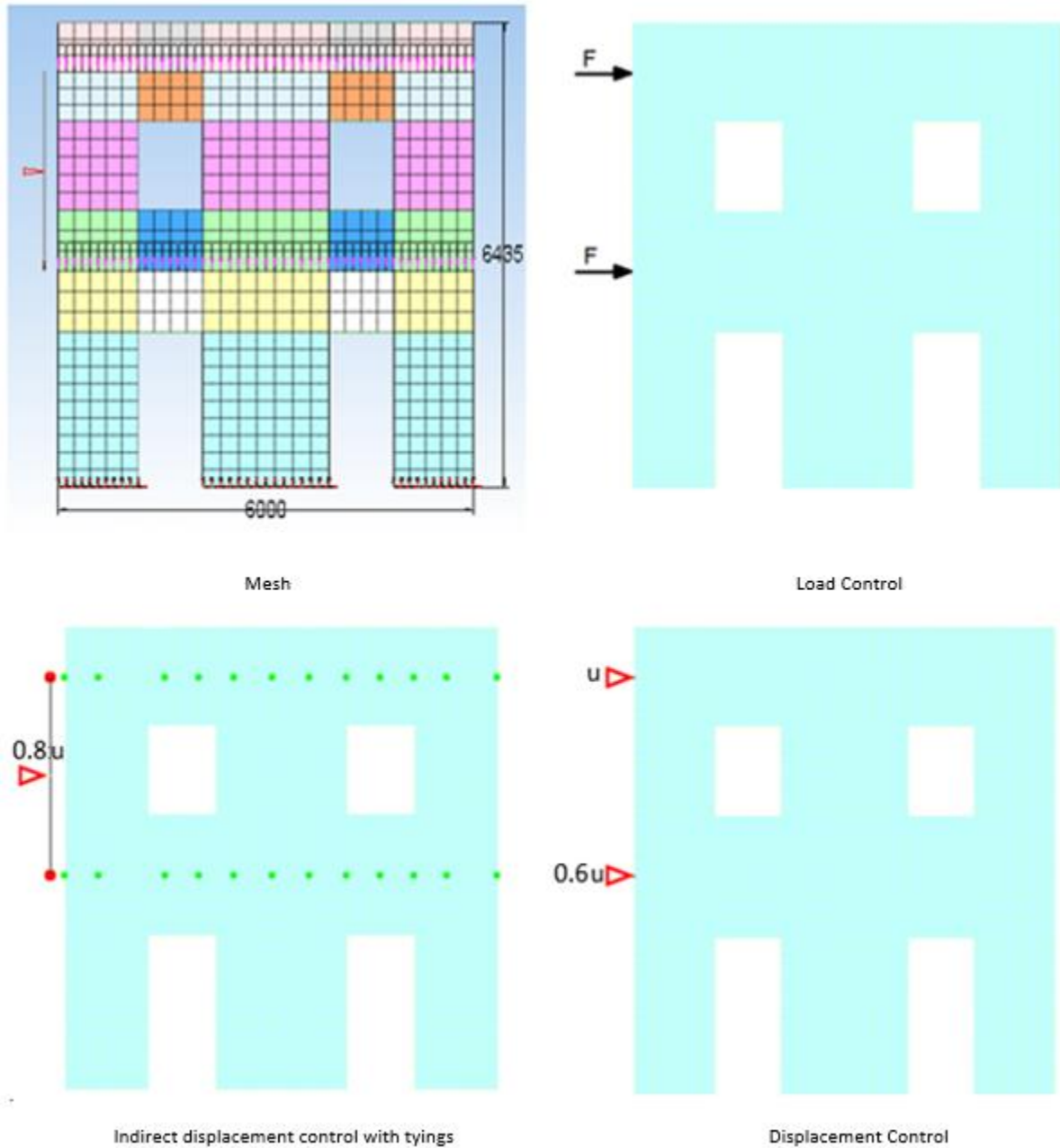


Figure 2.2.15 Mesh size, load and boundary conditions for the Door Wall Load Control Model, Indirect displacement control with tyings Model using an auxiliary beam and Displacement Control Model. The green colored nodes have the same horizontal displacement as the corresponding red ones, measures in mm

i. Load Control

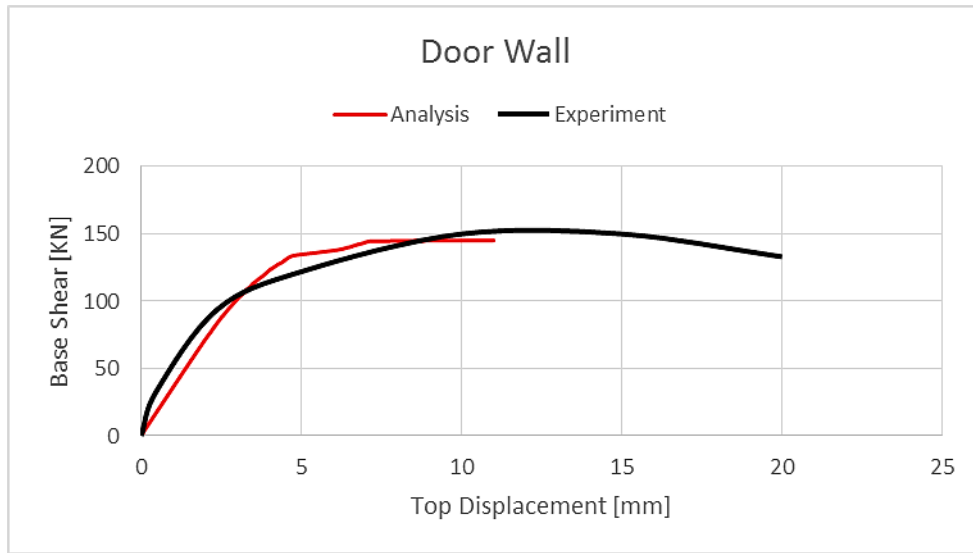


Figure 2.2.16 Comparison between analysis and experiment for the Door Wall (Load Control)

ii. Indirect displacement control without tyings

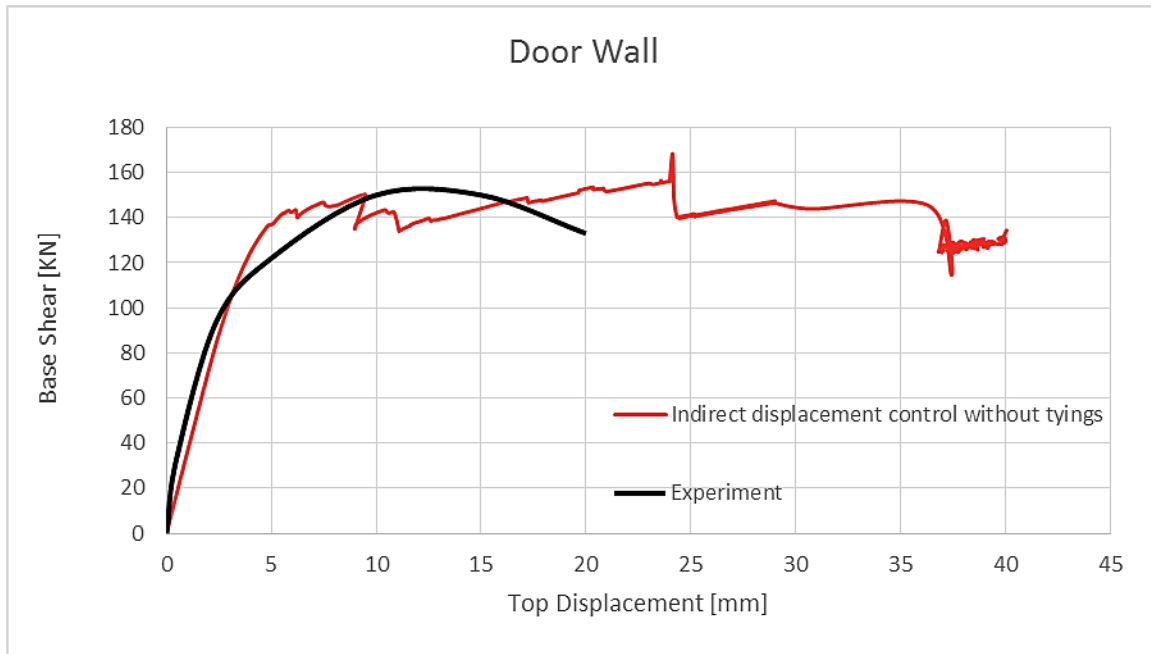


Figure 2.2.17 Comparison between analysis and experiment for the Door Wall Indirect displacement control without tyings

iii. Indirect displacement control with tyings

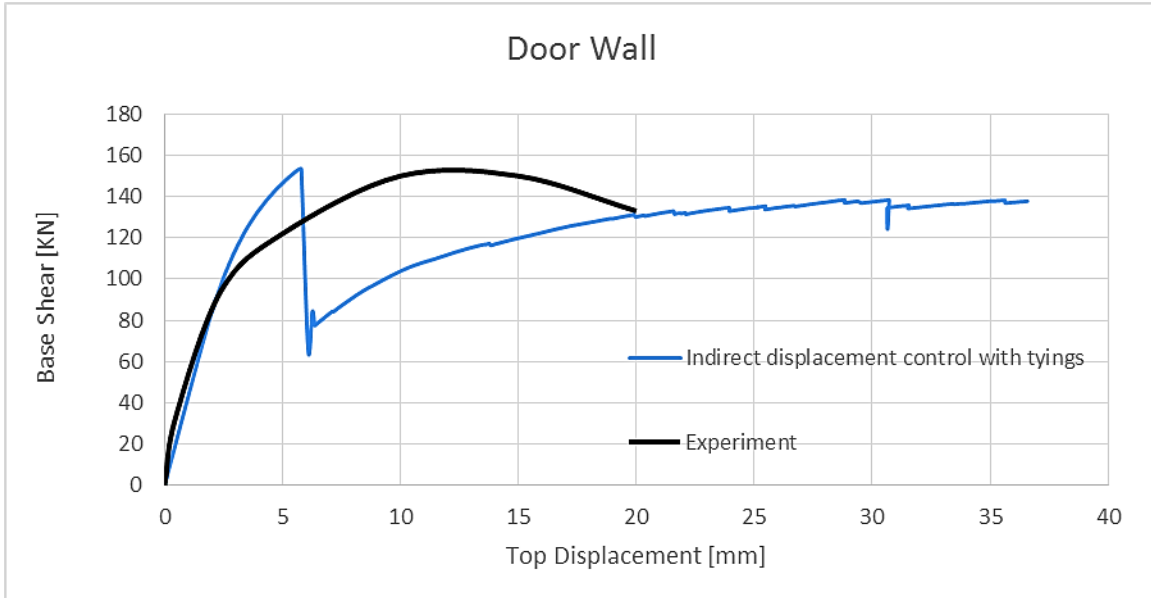


Figure 2.2.18 Comparison between analysis and experiment for the Door Wall (Indirect displacement control with tyings)

iv. Displacement Control

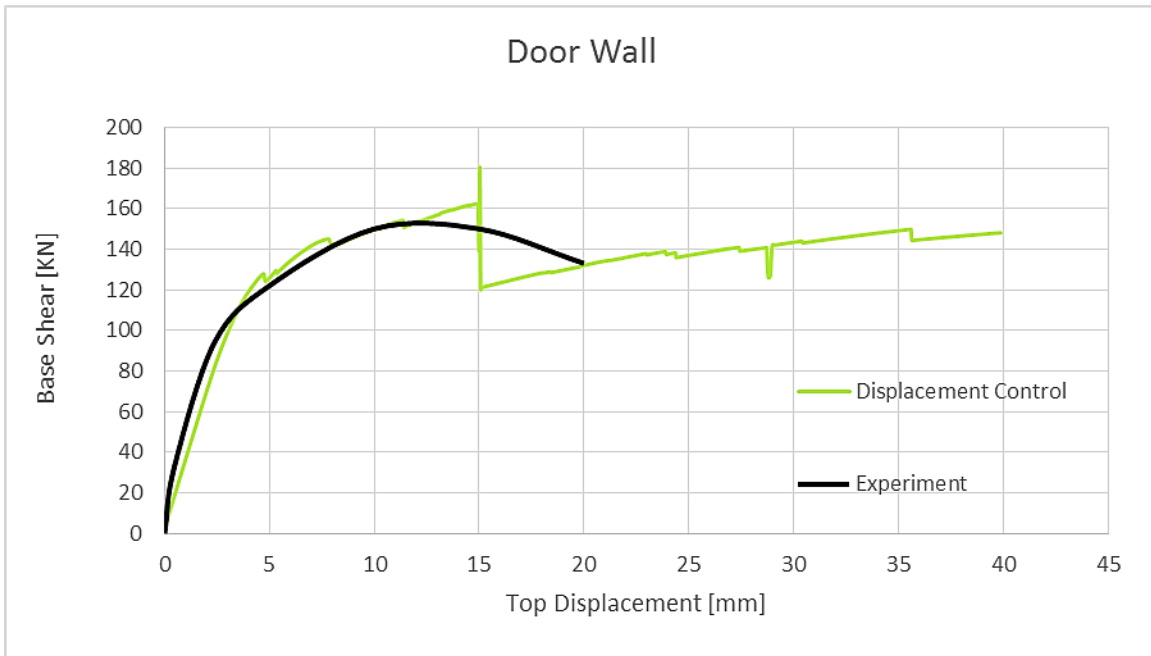


Figure 2.2.19 Comparison between analysis and experiment for the Door Wall (Displacement Control)

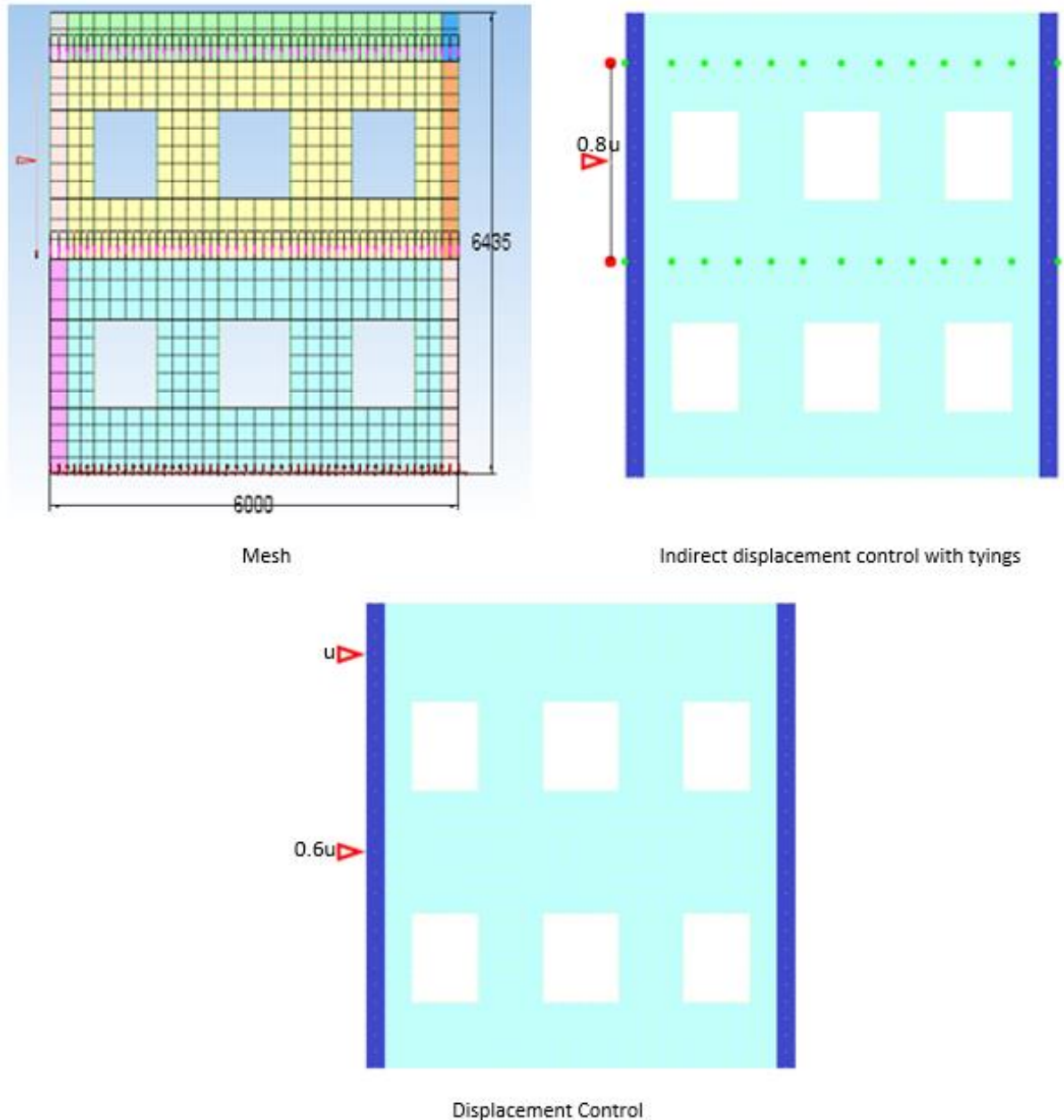


Figure 2.2.20 Mesh size, load and boundary conditions for the Window Wall Indirect displacement control with tyings Model using an auxiliary beam and Displacement Control Model. The leftmost and rightmost elements have 2200mm (half the length of the orthogonal walls) thickness. The green colored nodes have the same horizontal displacement as the corresponding red ones, measures in mm

v. Indirect displacement control without tyings

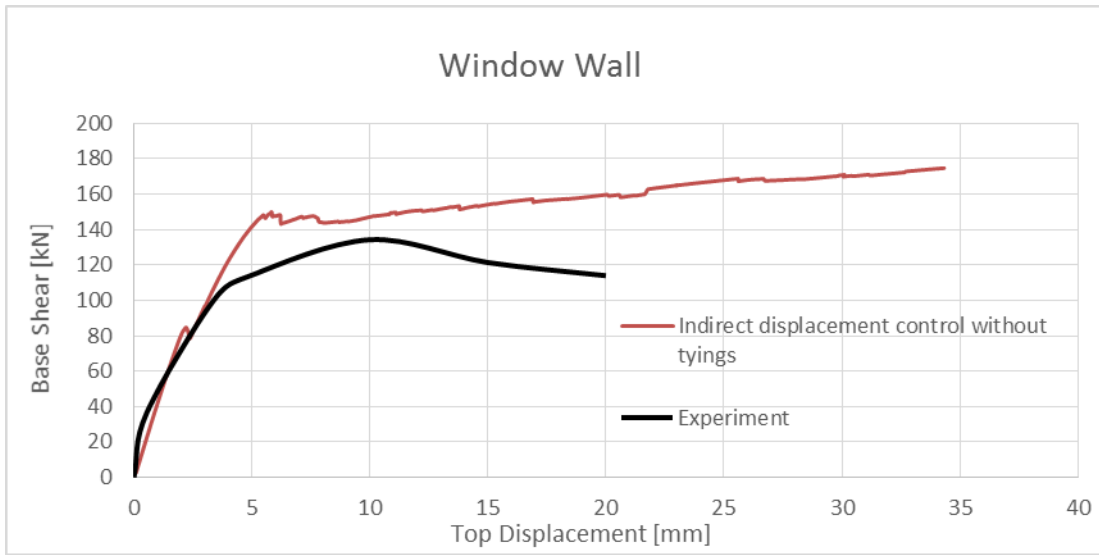


Figure 2.2.21: Comparison between analysis and experiment for the Window Wall Indirect displacement control without tyings

vi. Indirect displacement control with tyings

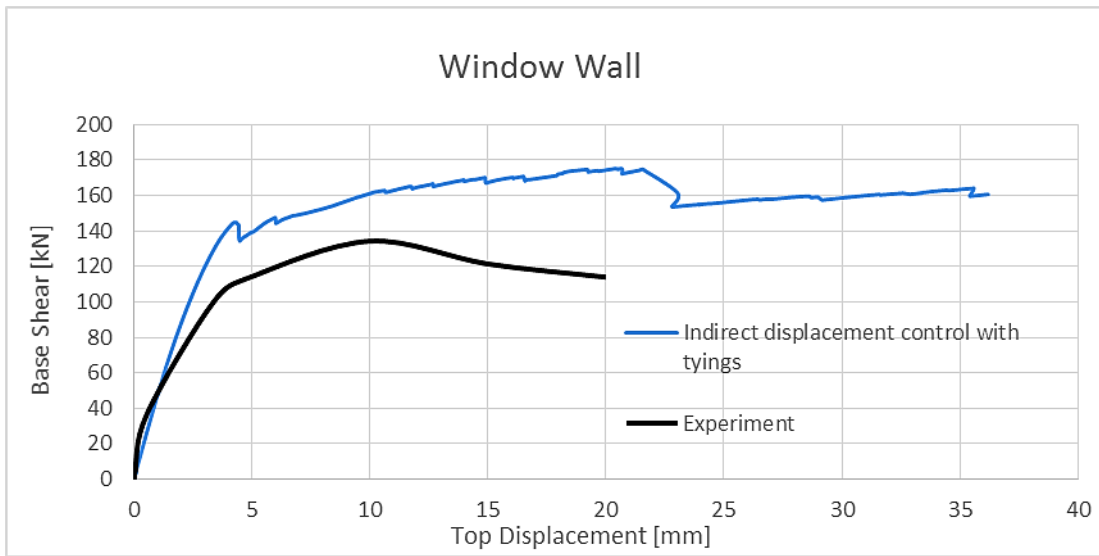


Figure 2.2.22 Comparison between analysis and experiment for the Window Wall Indirect displacement control with tyings

vii. Displacement control

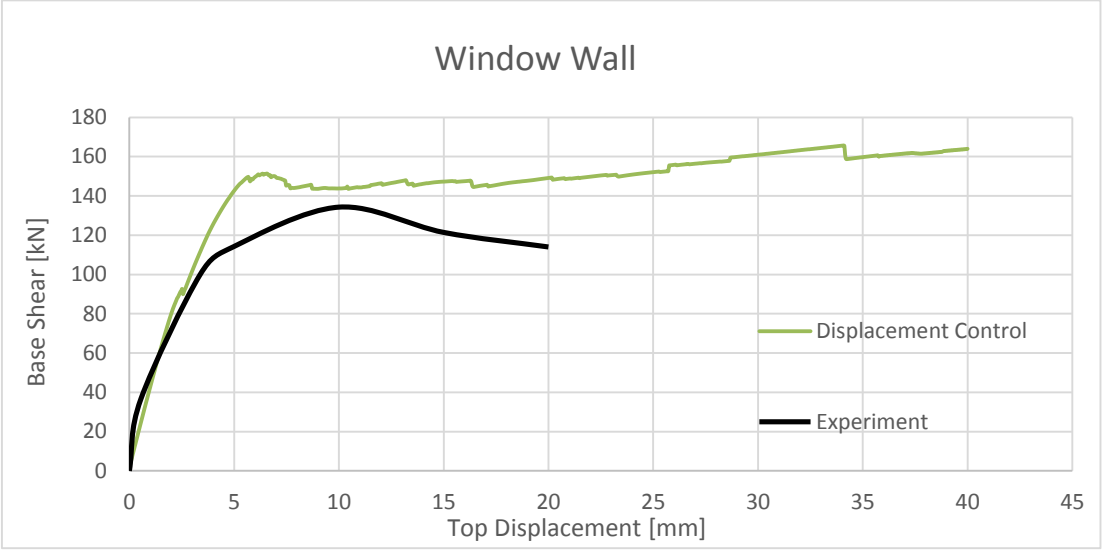


Figure 2.2.23 Comparison between analysis and experiment for the Window Wall Displacement Control

Variation between 2D and 3D model for Window Wall:

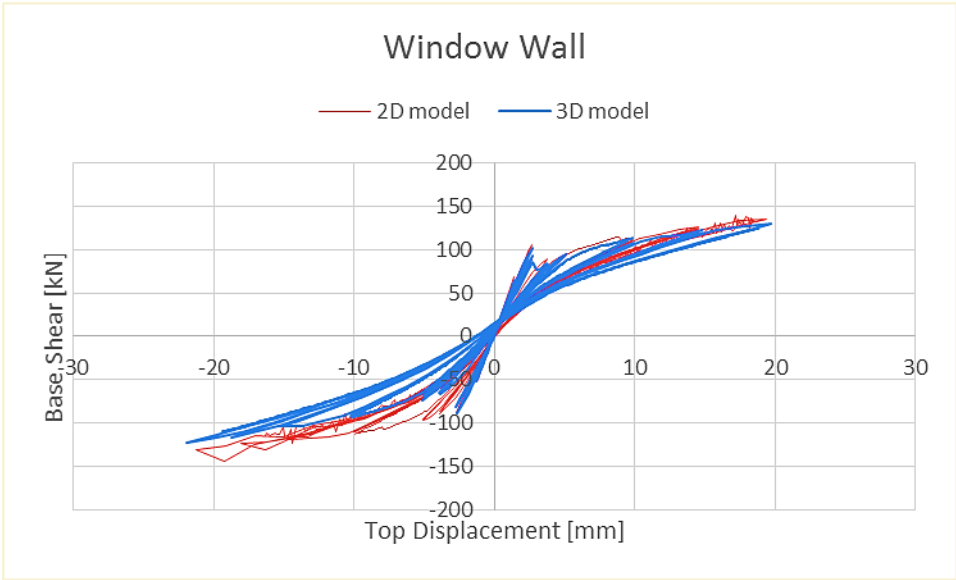


Figure 2.2.24 Comparison between 2D model and 3D model for Window Wall

Variation between Linear and Exponential Softening for Door Wall

Materials	Material properties including values and stress strain behaviour
Masonry	Total Strain Fixed Smeared Crack Model with Linear Tensile Softening, Elastic Compression and Variable Shear Reduction factor. Secant unloading $\rho = 1800 \text{ kg/m}^3$ $E = 1410 \text{ MPa}$ $\nu = 0.15$ with reduction $f_t = 0.1 \text{ MPa}$ (Tensile strength) $G_f = 50 \text{ N/m}$ (Tensile fracture energy) β Variable

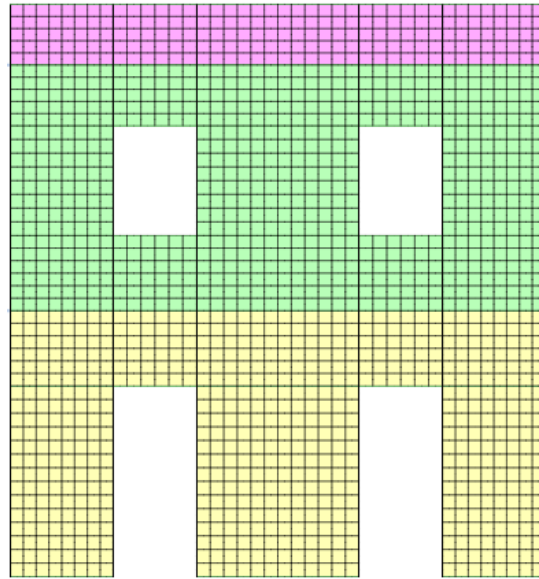


Figure 2.2.25 Door Wall

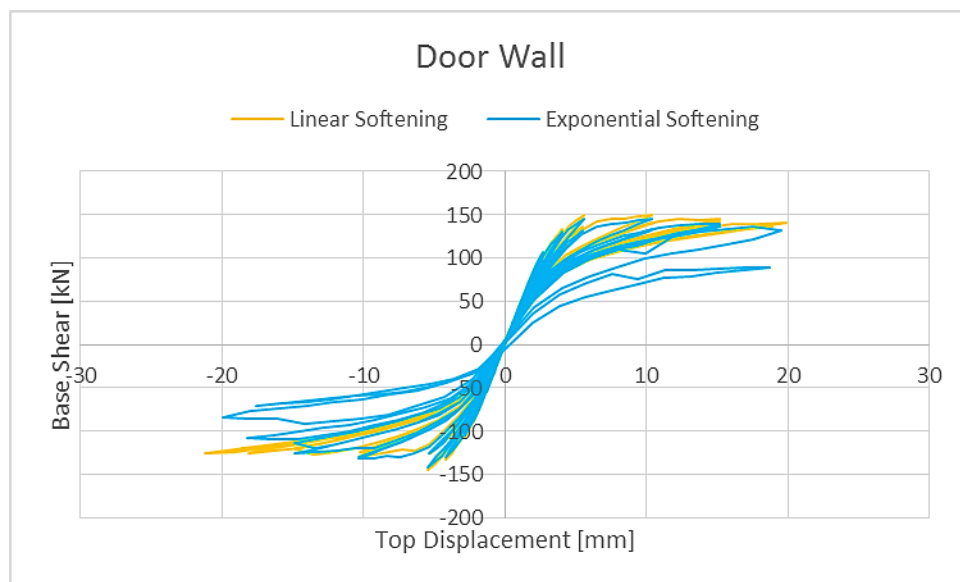


Figure 2.2.26 Comparison between Linear and Exponential Softening, Door Wall

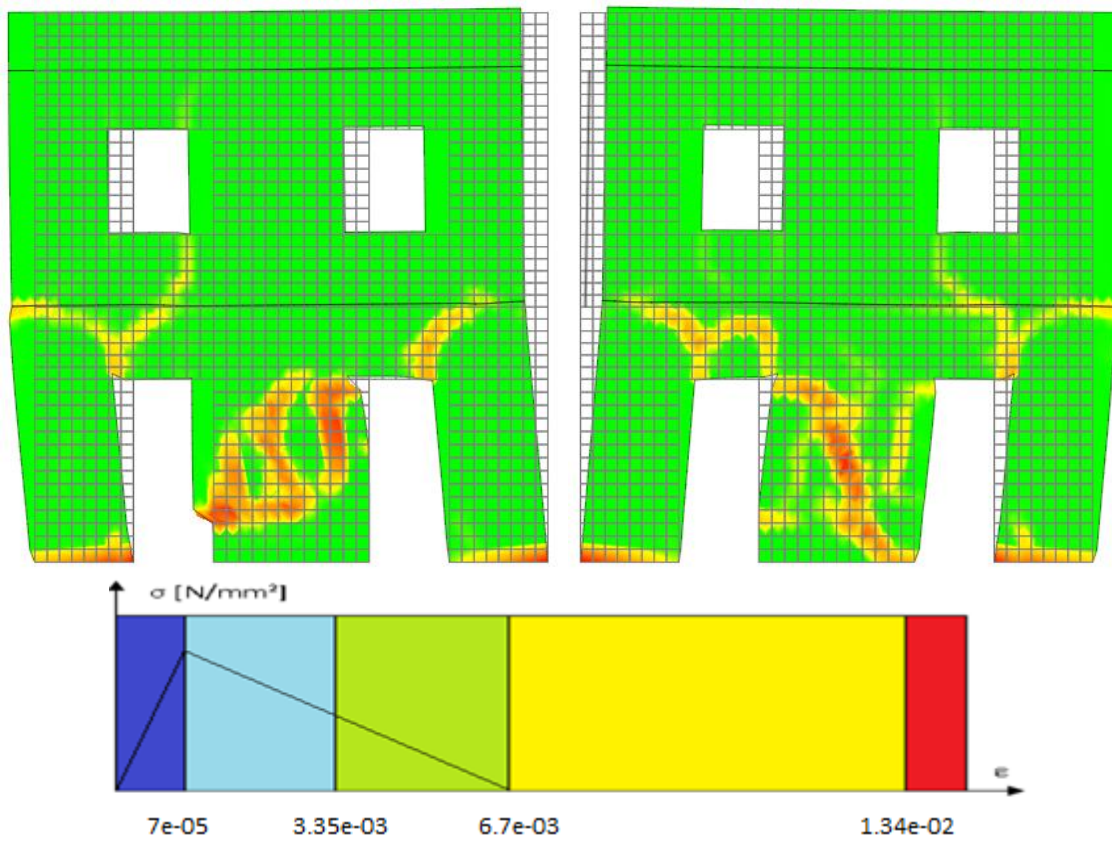


Figure 2.2.27 Crack pattern after Run 7, Door Wall with Linear Softening

2.3. ESECMaSE calcium silicate in-plane panel tests

Table 2.3.1: Modelling notes

Component	Description
Analysis software and formulation	Diana - implicit integration
Walls (in-plane)	The panels have been modelled with a macro-continuum approach, with 2D plane stress finite elements, using the Total Strain Fixed Crack Model, with nonlinear behaviour both in tension and compression.

Table 2.3.2: Pushover analysis notes

Pushover analysis notes
<ul style="list-style-type: none"> Increasing cyclic displacement applied on top of the wall

Table 2.3.3: Model loading, materials and general comments

Loading	
Dead load	Self-weight of masonry wall
Overburden	0.5 MPa for CS03 1.0 MPa for CS05
Materials	Material properties including values and stress strain behaviour
Masonry	<p>According to Total Strain Smeared Crack Model:</p> <p>$E=7562$ MPa Young modulus</p> <p>$\nu_0=0.112$ Poisson coefficient variable (reducing with damage)</p> <p>$\rho=1800$ kg/m³ Unit mass</p> <p>$f_t=0.3$ MPa Tensile strength</p> <p>$G_t=15$ N/m (CS03) Tensile fracture energy</p> <p>$G_t=75$ N/m (CS05)</p> <p>Exponential tension softening</p> <p>β variable Shear retention factor (reducing to zero with damage)</p> <p>$f_c=10$ MPa Compressive strength</p> <p>$G_c=5000$ N/m Compressive fracture energy</p> <p>Parabolic compressive softening</p>
Other key notes	
<ol style="list-style-type: none"> To reproduce the “double fixed” condition a “TYING” has been assigned to the top edge of the panel so as to constraint all nodes belonging to that edge to have the same horizontal and vertical displacement during the analysis. The middle edge node has been assumed as master node. The vertical load (0.5-1.0 MPa) has been assigned as a concentrated force in the master node, resulting equal to 109375 N for CS03 and 218750 N for CS05. Second order effects included. 	

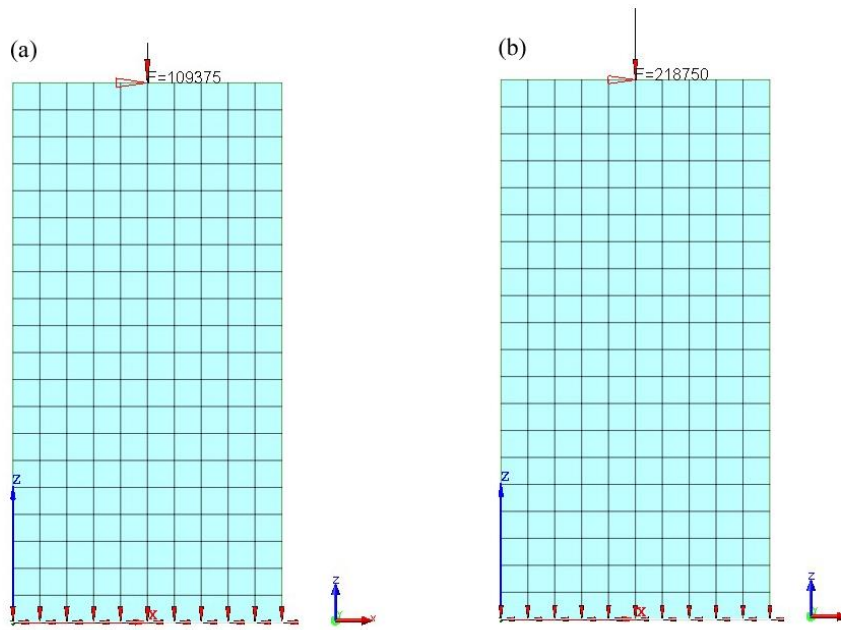


Figure 2.3.1: FE models for (a) CS03 and (b) CS05 panels

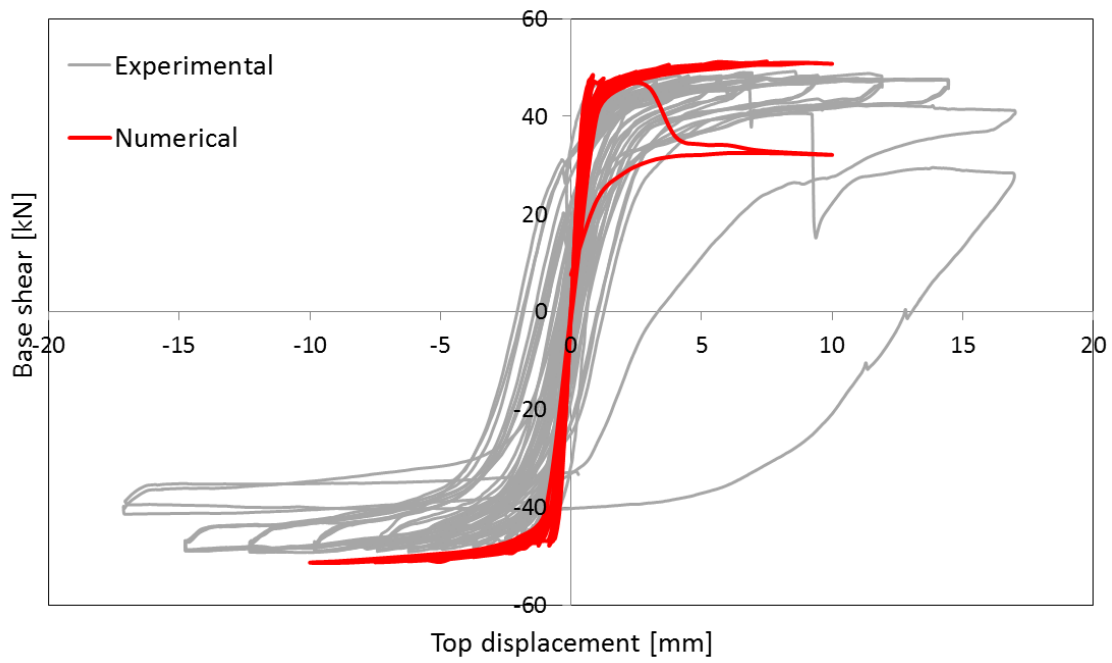


Figure 2.3.2: Shear force-displacement comparison plot for CS03

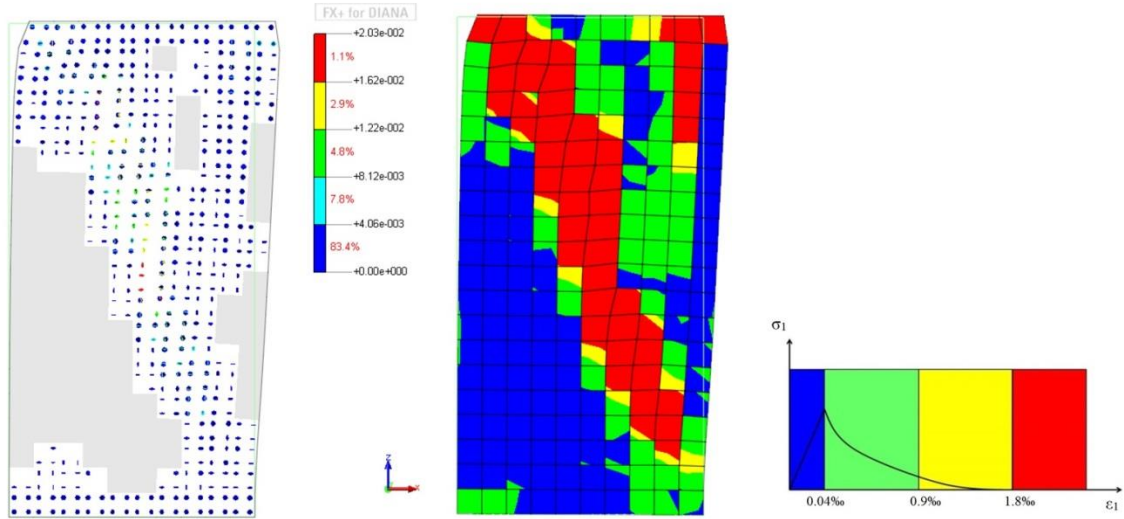


Figure 2.3.3: Final crack pattern for CS03: crack strains (left) and representation of the active cracks by means of the principal strains (right).

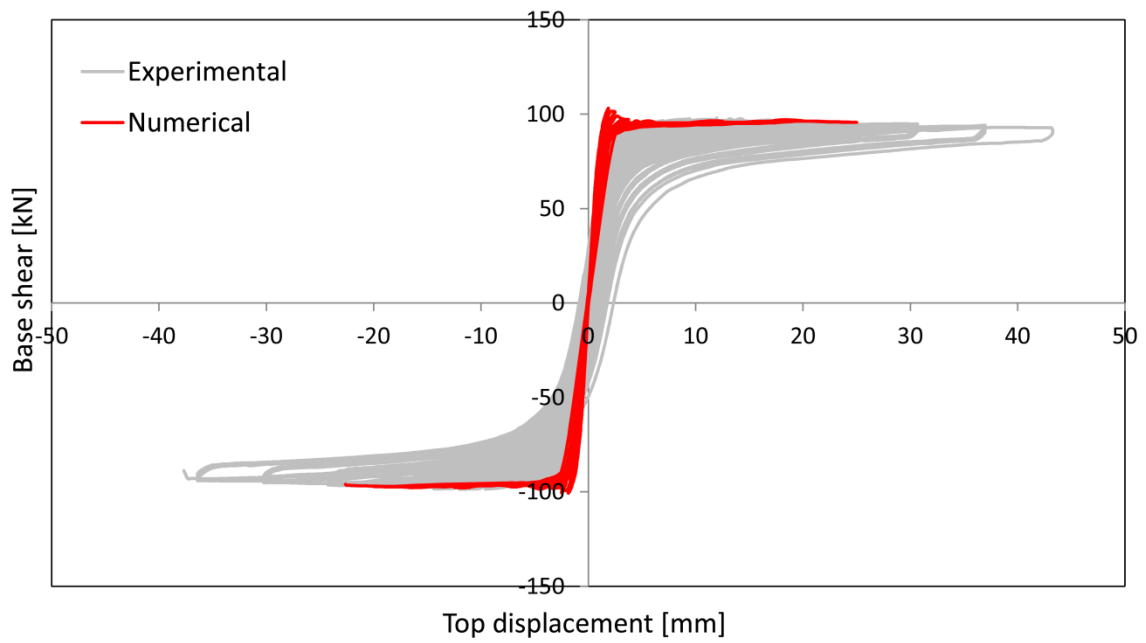


Figure 2.3.4: Shear force-displacement comparison plot for CS05.

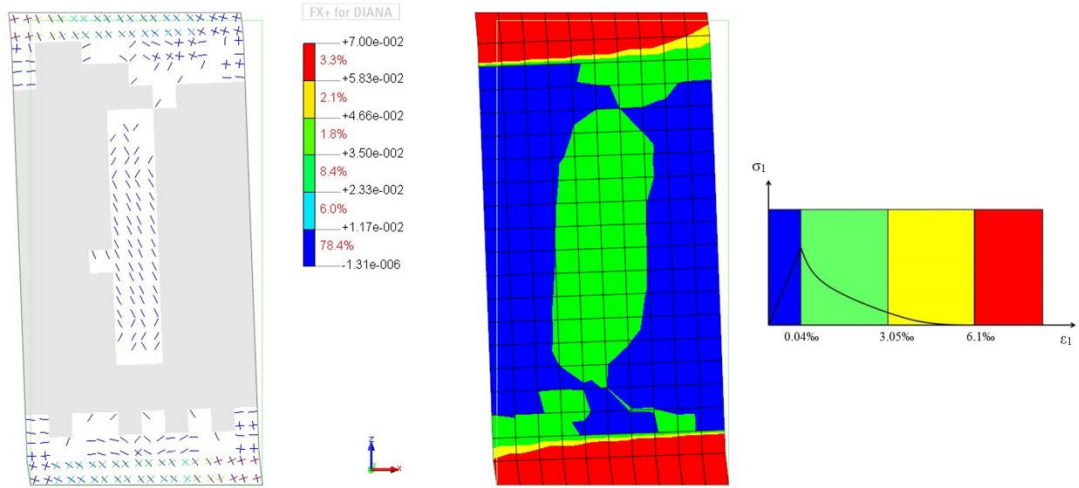


Figure 2.3.5: Final crack pattern for CS05: crack strains (left) and representation of the active cracks by means of the principal strains (right).

2.3.1. Discussion and sensitivity analyses

Comments on obtained results

- good agreement of the analytical results with the experimental ones, both for the envelope of shear-displacement curves and for the damage patterns;
- slight underestimation of the displacement capacity observed for panel CS05;
- the analytical model was not able to reproduce the hysteresis loops of the experiments. Possible causes: high value of compressive strength (no energy consumption in compression), secant unloading;
- need for the increase of tensile fracture energy (especially for higher vertical loads, i.e. for CS05) to account for the energy consumption in the stepwise diagonal crack associated to friction due to horizontal sliding of the blocks (see Fig.2.3.7).

Additional modelling and analyses

A macro-crack model has been also developed: the panel has been modelled with pre-defined potential crack lines, through line interface elements. The rest of the panel has been modelled with plane stress elements. The tensile and shear nonlinear behaviour has been lumped in those crack lines, while the compressive nonlinearity has been included in the plane stress elements.

Table 2.3.4: Material properties to be assigned to the 2D quadratic plane stress elements.

Parameter	Value	units	Description	Notes
YOUNG	7562	MPa	Elastic modulus	
POISON	0.112	/	Poisson ratio	
DENSIT	1800	kg/m ³	Unit mass	
TOTCRK	FIXED	/	Total Strain Fixed Crack Model	
COMCRV	PARABO	/	Parabolic compressive softening	
COMSTR	10	MPa	Compressive strength	
GC	5000	N/m	Compressive fracture energy	

Table 2.3.5: Material properties to be assigned to the interfaces that reproduce the potential diagonal cracks (line quadratic interface elements).

Parameter	Value	units	Description	Notes
DISCRA	1	/	Discrete cracking	
DSTIF	1e ⁵ 1e ⁵	N/mm ³	Normal and shear stiffness values	
DCRVAL	0.6	N/mm ²	Tensile strength	
MODE1	1	/	Tensile linear softening	
UNLO1	1	/	Secant unloading	
MO1VAL	100	N/m	Tensile fracture energy	High value as to simulate a “perfect plastic” behaviour along the diagonal cracks
MODE2	1	/	Constant shear stiffness after cracking	
MO2VAL	1e ⁵	N/mm ³	Shear stiffness after cracking	no reduction

Table 2.3.6: Material properties to be assigned to the interfaces that reproduce the potential cracks at the boundary edges of the panel (line quadratic interface elements).

Parameter	Value	Units	Description	Notes
DISCRA	1	/	Discrete cracking	
DSTIF	$1e^5$ $1e^5$	N/mm ³	Normal and shear stiffness values	
DCRVAL	0.6	N/mm ²	Tensile strength	
MODE1	1	/	Tensile linear softening	
UNLO1	1	/	Secant unloading	
MO1VAL	15	N/m	Tensile fracture energy	
MODE2	1	/	Constant shear stiffness after cracking	
MO2VAL	$1e^3$	N/mm ³	Shear stiffness after cracking	As if BETA=0.01

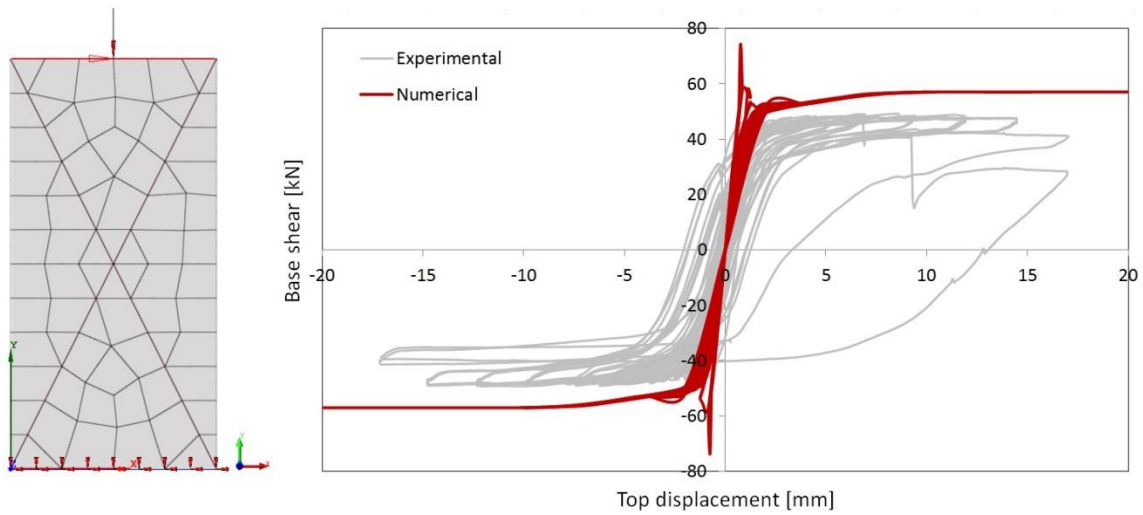


Figure 2.3.6: CS03: Macro-crack model and results of cyclic pushover analysis.

Sensitivity studies

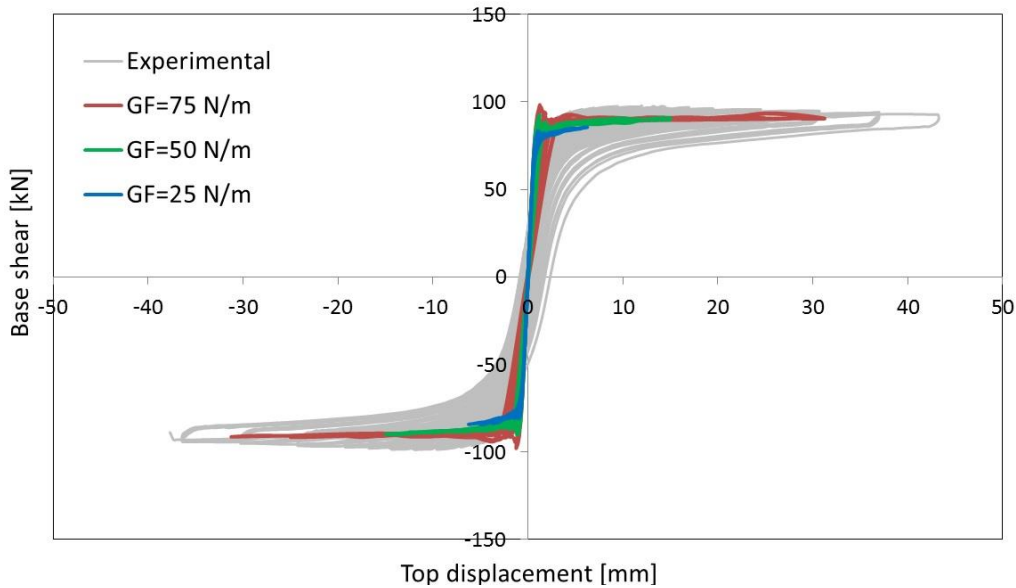


Figure 2.3.7: CS05: Sensitivity analysis to tensile fracture energy G_f .

2.4. ESECMaSE calcium silicate full-scale half-building test

Table 2.4.1: Modelling notes

Component	Description
Analysis software and formulation	Diana - implicit integration
Walls (in-plane)	The building has been modelled with a macro-continuum approach, with 2D plane stress finite elements, using the Total Strain Fixed Crack Model, with nonlinear behaviour both in tension and compression.
Walls (out-of-plane)	As above.
Wall to wall connection (incl. flange effects)	Fully connected
Concrete diaphragm	Modelled with 2D plane stress finite elements with linear elastic behaviour: $E=30000$ MPa Young modulus $\nu=0.15$ Poisson coefficient $\rho=0$ kg/m ³ Unit mass (assigned directly on top of the walls)
Wall to diaphragm connection	Fully connected

Table 2.4.2: Eigenvalue analysis notes

Eigenvalue analysis notes
<ul style="list-style-type: none"> Performed with elastic Young Modulus $E=7562$ MPa coming from experimental tests

Table 2.4.3: Nonlinear pushover analysis notes

Nonlinear pushover analysis notes
<ul style="list-style-type: none"> Mass proportional loading profile Forces applied in the centres of masses of the two floors

Table 2.4.4: Nonlinear time history and pseudo-dynamic analysis notes

Nonlinear time history analysis notes
<ul style="list-style-type: none"> The pseudo-dynamic (PSD) analysis has been performed applying displacement time-histories at centres of masses of the two floors. The analysis has been performed with “accumulated damages”, i.e. by applying subsequent increasing levels of PGA, as in the real experimental test.

Table 2.4.5: Model loading, materials and general comments

Loading	
Dead load	Self-weight of the masonry walls
Applied load	1 st floor: 7.65 kN/m ² – 2 nd floor 8.85 kN/m ² Including concrete slabs, additional permanent loads and 30% of the live loads.
Materials	
	Material properties including values and stress strain behaviour
Masonry	<p>According to Total Strain Smeared Crack Model:</p> <p>E=7562 MPa Young modulus</p> <p>$\nu=0.112$ Poisson coefficient</p> <p>$\rho=1800 \text{ kg/m}^3$ Unit mass</p> <p>$f_t=0.3 \text{ MPa}$ Tensile strength</p> <p>$G_t=50 \text{ N/m}$ Tensile fracture energy</p> <p>Exponential tension softening</p> <p>β variable Shear retention factor (reducing to zero with damage)</p> <p>$f_c=10 \text{ MPa}$ Compressive strength</p> <p>$G_c=5000 \text{ N/m}$ Compressive fracture energy</p> <p>Parabolic compressive softening</p>
Concrete	<p>Linear elastic behaviour:</p> <p>E=30000 MPa Young modulus</p> <p>$\nu=0.15$ Poisson coefficient</p> <p>$\rho=0 \text{ kg/m}^3$ Unit mass (assigned directly on top of the walls)</p>
Other key notes	
<ol style="list-style-type: none"> 1) To perform the pushover and PSD analysis, the vertical loads (including self-weight of the slabs) have been assigned directly on the top of the walls, to avoid cracking at the wall-slab connections during the preliminary application of dead and live loads; 2) To perform eigenvalue analysis an equivalent self-weight has been assigned to the two floors, so as to include also the mass contribution of additional dead and live loads. The resulting equivalent self-weights of the floors are respectively equal to $W^*1 = 38.25 \text{ kN/m}^3$ $W^*2 = 41.25 \text{ kN/m}^3$; 3) The numerical PSD analysis has been carried out up to a PGA equal to 0.12 g, at which a divergence of the numerical procedure has been observed; 4) Geometrical nonlinearities included. 	

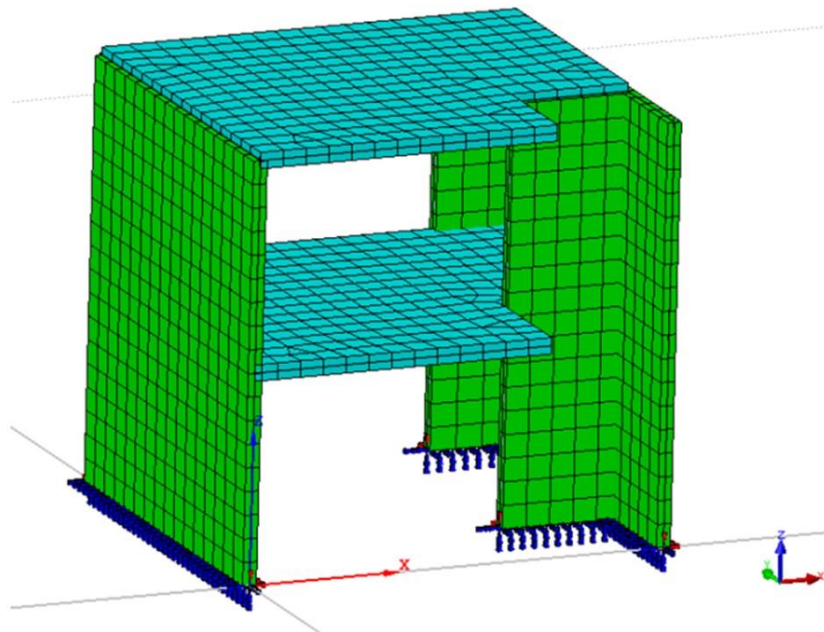


Figure 2.4.1: FE model of ESECMaSE calcium silicate full-scale half-building

Table 2.4.6: Modal period, frequency, description, mass participation

Mode	Period (s)	Frequency (Hz)	Description of mode	Mass participation %	
				X	Y
1	0.148	6.75	1 st fundamental bending mode in x-dir.	75.3	0.053
2	0.058	17.34	Bending of the 2 nd floor	1.38	5.56
3	0.054	18.67	1 st fundamental bending mode in y-dir.	0.30	55.16
4	0.049	20.26	Bending of the 1 st floor	0.53	4.38
5	0.044	22.50	Bending of the 2 nd floor	0.20	8.10
6	0.041	24.22	Bending of the 1 st floor	1.50	1.14
7	0.039	25.60	Out of plane bending of free portion of the longitudinal wall	0.044	2.79
8	0.037	27.26	2 nd bending mode in x-dir.	12.44	1.06

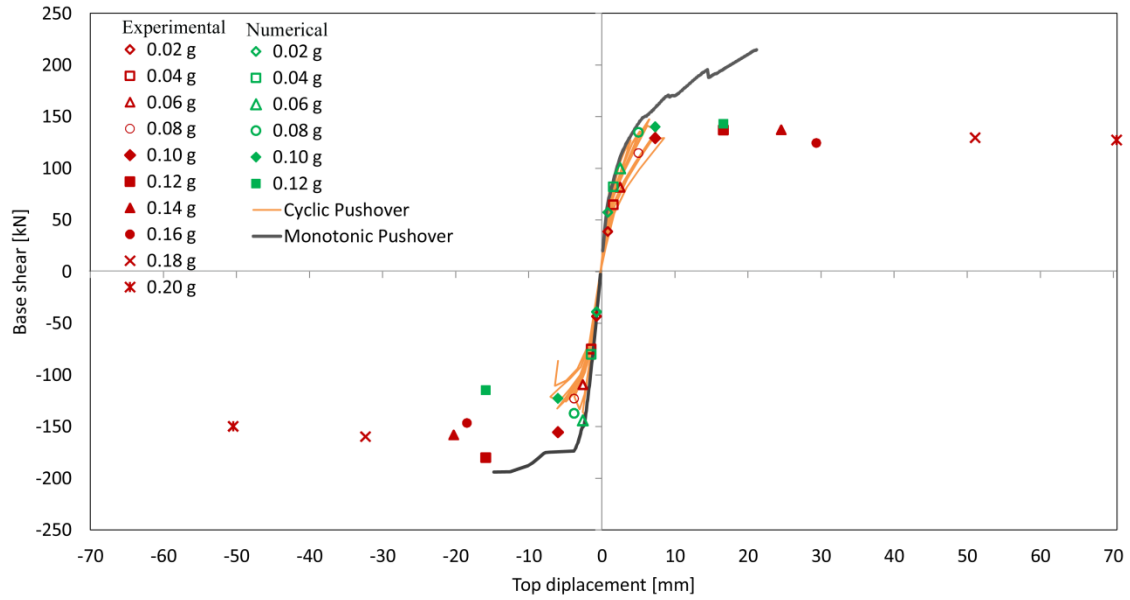


Figure 2.4.2: Envelope of max base shear force vs. max top displacement (0.02g to 0.20g PGA)

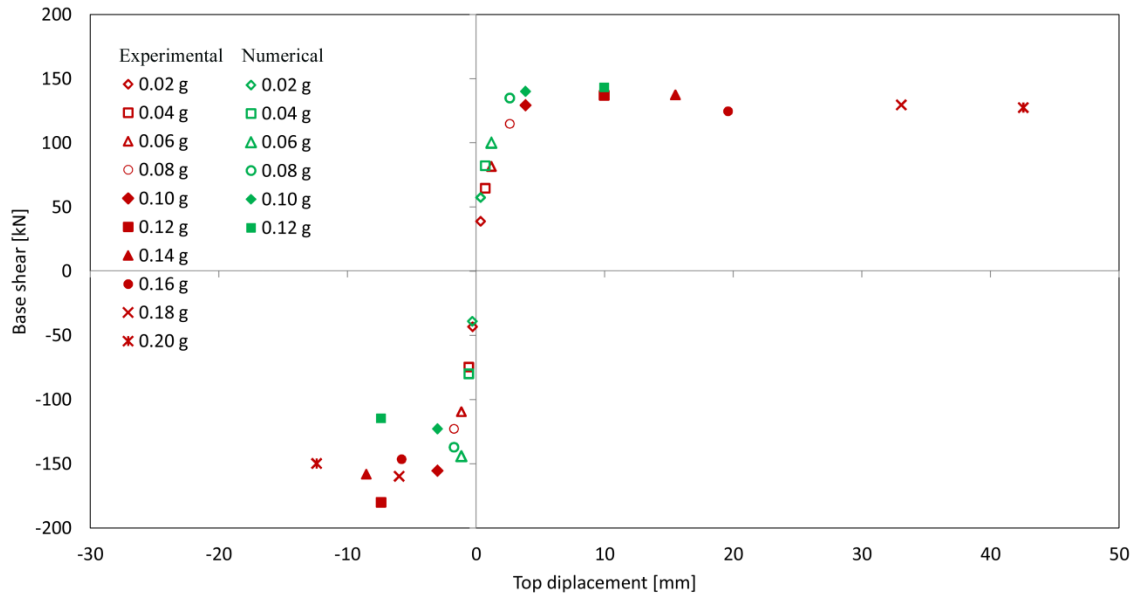


Figure 2.4.3: Envelope of max shear force vs. max inter-storey drift for L1 (0.02g to 0.20g PGA)

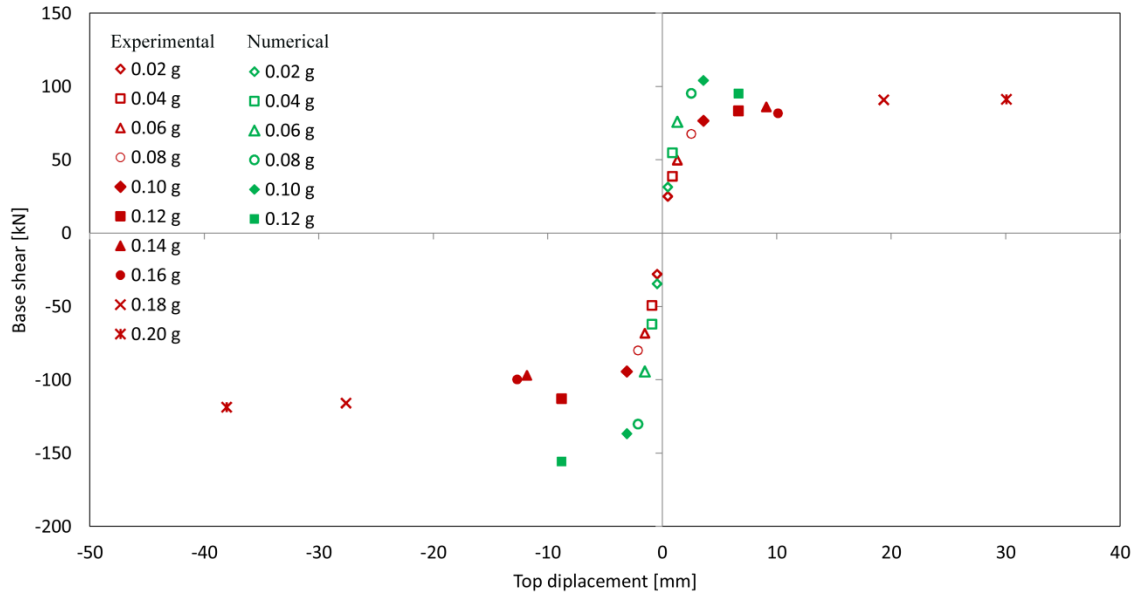


Figure 2.4.4: Envelope of max shear force vs. max inter-storey drift for L2 (0.02g to 0.20g PGA)

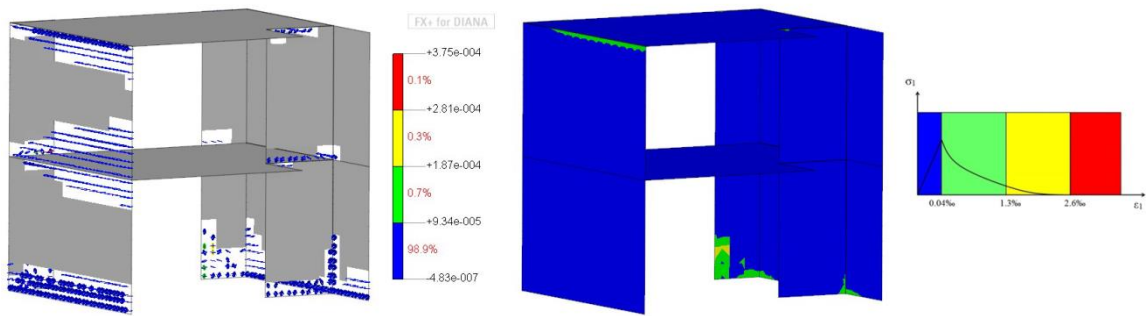


Figure 2.4.5: Crack pattern after successive loadings of 0.02g–0.06g PGAs.

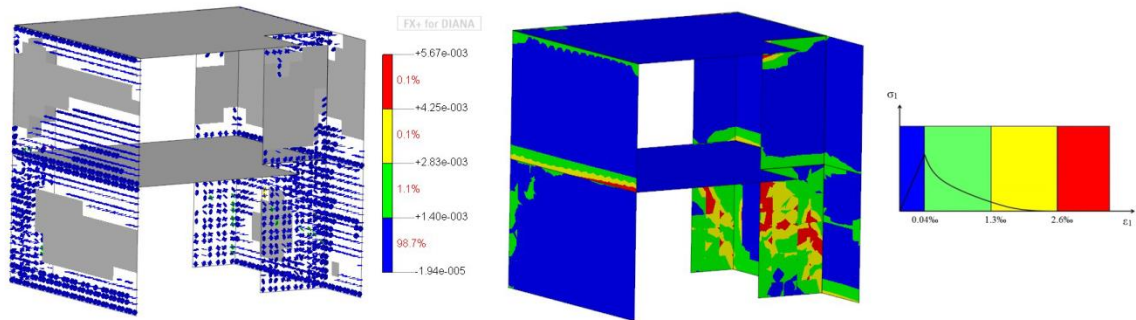


Figure 2.4.6: Crack pattern after successive loadings of 0.02g–0.12g PGAs.

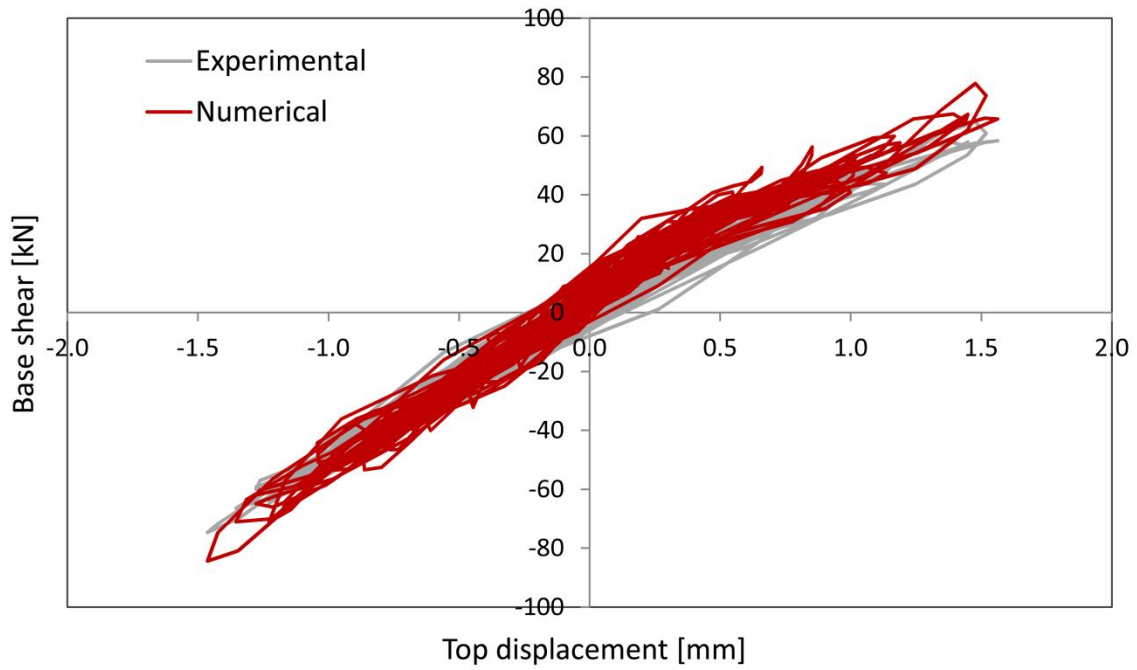


Figure 2.4.7: Base shear force vs. top displacement hysteresis plot during 0.04g PGA.

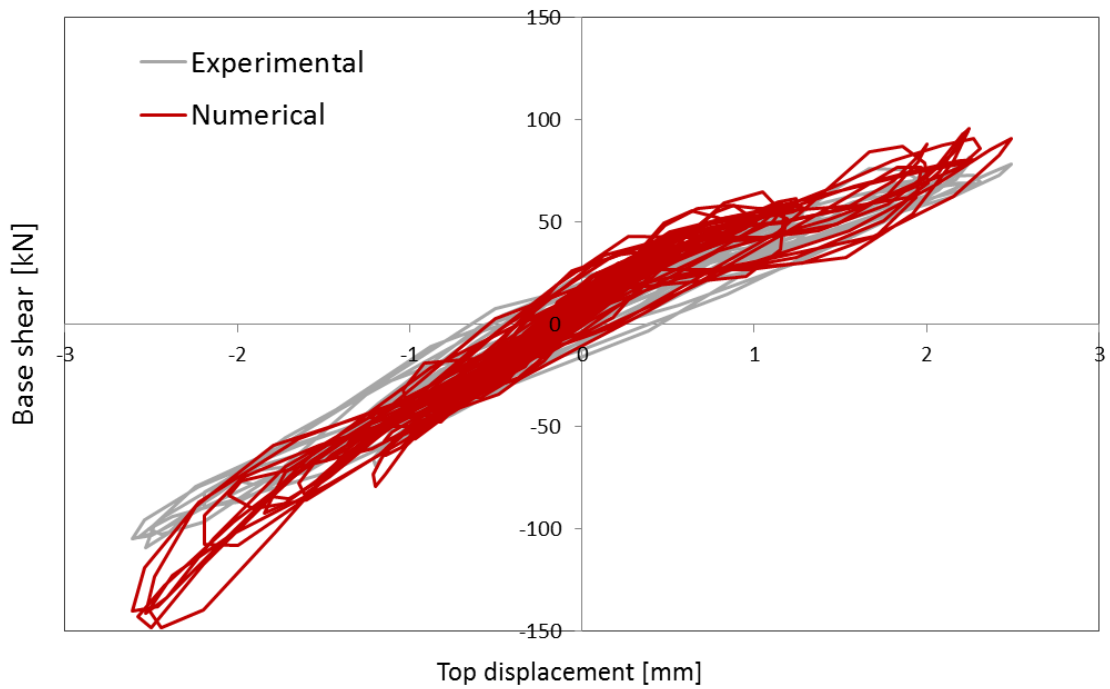


Figure 2.4.8: Base shear force vs. top displacement hysteresis plot during 0.06g PGA.

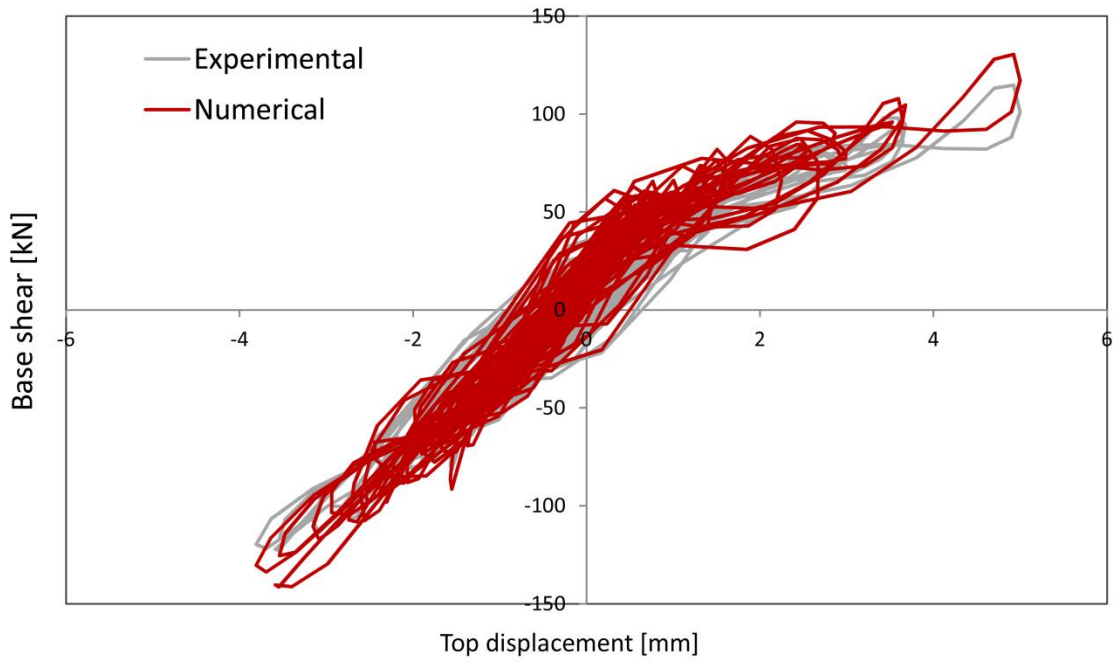


Figure 2.4.9: Base shear force vs. top displacement hysteresis plot during 0.08g PGA.

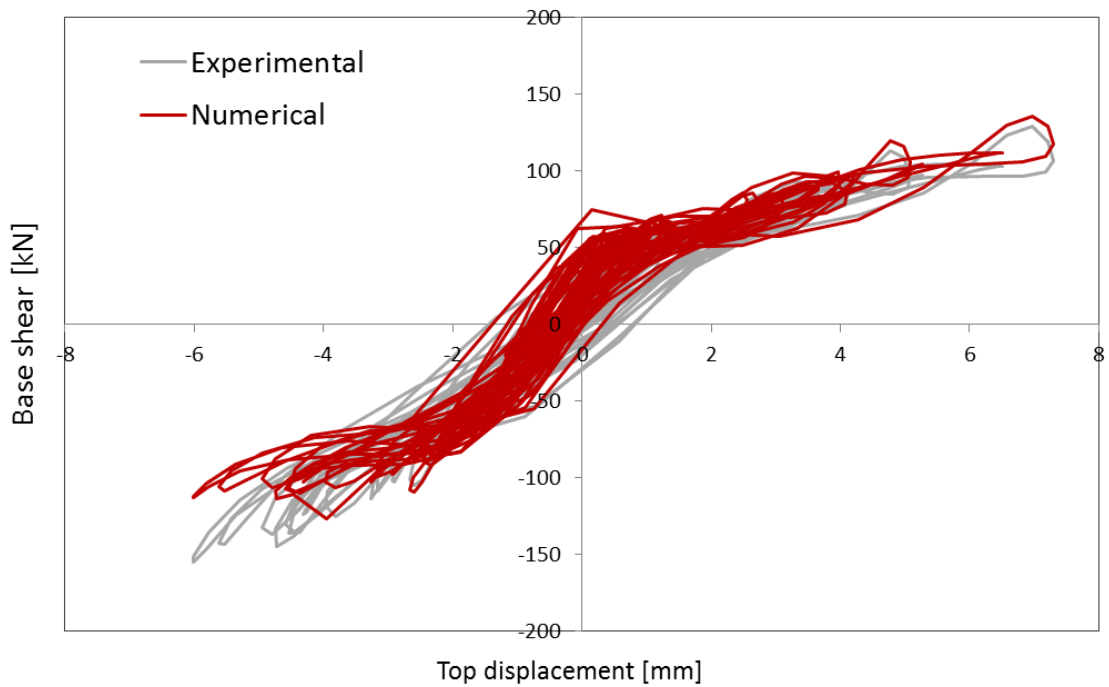


Figure 2.4.10: Base shear force vs. top displacement hysteresis plot during 0.10g PGA.

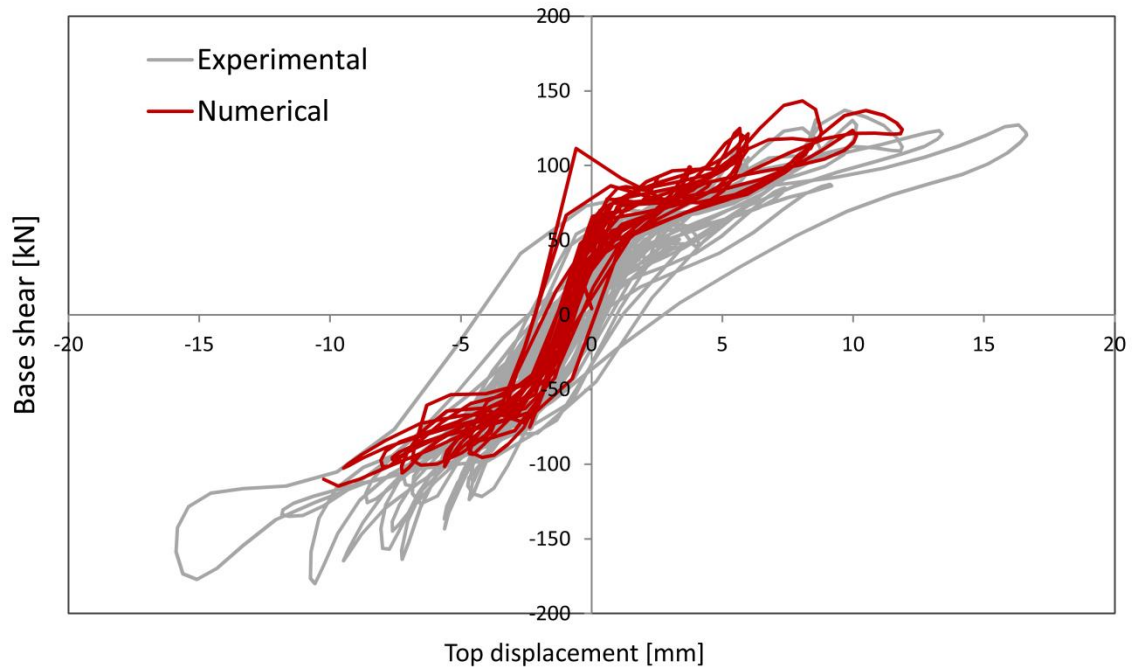


Figure 2.4.11: Base shear force vs. top displacement hysteresis plot during 0.12g PGA.

2.4.1. Discussion and sensitivity analyses (if relevant)

Comments on obtained results

- Good agreement is found between experimental and numerical PSD results in terms of base shear-top displacement trends up to 0.12 g.
- Further calibration of the parameters could be desirable to investigate the behaviour for PGA values higher than 0.12 g at which the divergence of the numerical procedure has been detected;
- Consistent reproduction of the damage pattern in terms of out-of-plane and in-plane flexural failures. Also vertical cracks developing at the connection between orthogonal walls correctly reproduced.
- Detection of severe diagonal cracks in the shear walls, confirming the ultimate shear failure observed in the experimental test.
- Concerning the pushover analysis, the numerical procedure was not able to follow the almost horizontal softening branch. A sensitivity analysis to the main parameters has been carried out to investigate this issue (see Fig. 2.4.12). A hardening effect has been detected with increasing load. This can be due to the fully clumped connection through the orthogonal walls. Further studies can be developed on that.

Sensitivity studies

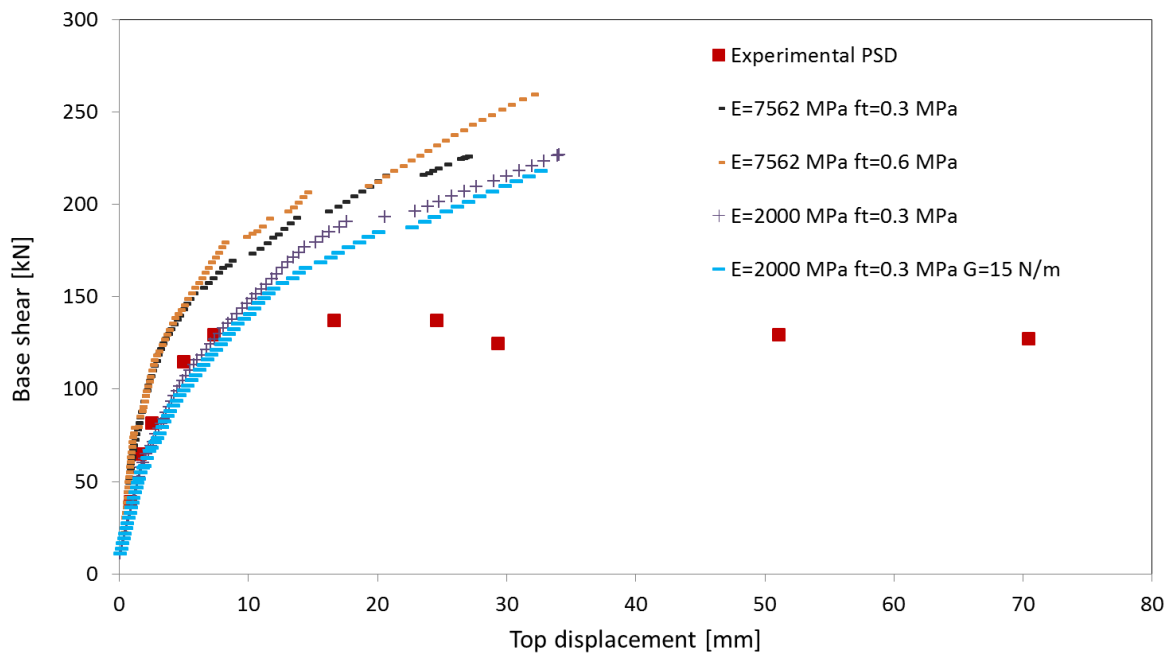


Figure 2.4.12: Sensitivity analysis to E , f_t and G_f to investigate the hardening effect observed in the monotonic pushover analysis.

2.5. One-way spanning wall out-of-plane tests (Doherty)

Table 2.5.1: Modelling notes

Component	Description
Analysis software and formulation	LS-DYNA – explicit analysis solver
Walls (in-plane)	The wall is modelled as a continuous plate with curved shell elements. The Total Strain Rotating Crack material model is applied.
Walls (out-of-plane)	As above.

Table 2.5.2: Nonlinear time history analysis notes

Nonlinear time history analysis notes
<ul style="list-style-type: none">• 1% Rayleigh damping applied. Rayleigh damping coefficients are determined from modal analysis.• Spurious modes are constraint by applying ‘symmetry’ boundary conditions on the sides of the shell elements.• An extra interface at mid-height is used during time history analysis to predefine the crack, which is also present at the start of the experiment.

Table 2.5.3: Model loading, materials and general comments

Loading	
Dead load	Self-weight of masonry wall
Overburden	Specimen 8: Overburden 0.15 MPa Specimen 12: No overburden
Materials	Material properties including values and stress strain behaviour
Masonry	<p><u>Specimen 8:</u> $E=5400$ MPa Young modulus $f_t=0.45$ MPa Tensile strength</p> <p><u>Specimen 12:</u> $E=11600$ MPa Young modulus $f_t=0.3$ MPa Tensile strength</p> <p><u>Both Specimen</u> Total Strain Rotating Crack: $\nu=0.0$ - Poisson coefficient (to prevent splitting of the wall due to overburden.) $\rho=1800$ kg/m³ Unit mass $G_f=35$ N/m Tensile fracture energy Exponential tension softening $\beta = 0.01$ - Shear retention factor (reducing to zero with damage) $f_c=4.41$ MPa Compressive strength $G_c=5000$ N/m Compressive fracture energy Parabolic compressive softening</p>
Interface elements	<p><u>Specimen 8 Curved Shell Model:</u> Non-linear elasticity, zero normal and shear stiffness for positive deformation in normal direction. $k_n = 1.6E+13$ N/m³ $k_t = 1.0E+13$ N/m³</p> <p><u>Specimen 12 Curved Shell Model:</u> Non-linear elasticity, zero normal and shear stiffness for positive deformation in normal direction. $k_n = 1.0E+6$ N/m³ $k_t = 1.0E+11$ N/m³</p> <p><u>Specimen 8/12 Plane Strain Model:</u> Non-linear elasticity, zero normal and shear stiffness for positive deformation in normal direction. $k_n = 1.0E+13$ N/m³ $k_t = 1.0E+13$ N/m³</p>
Overburden spring	<p><u>Specimen 8 Curved Shell Model:</u> $K = 1.01E+5$ N/m (Modelled 100 mm of wall)</p> <p><u>Specimen 8 Plane Strain Model</u> $K = 9.6E+5$ N/m</p> <p><u>Specimen 12:</u> No overburden</p>

Other key notes

- 1) For the transient analysis an extra interface element was added at mid-height to model the crack at mid-height that was already present at the start of the shake table test.
- 2) The top constraint is assumed to be rotational free and the overburden rig to remain horizontal. This causes the point of rotation to shift over the thickness from the inner to the outer fibre during rocking. Similar behaviour is found at the mid-height and bottom interface element.
- 3) For the Plane Strain Model a sensitivity analysis for the thickness at the mid-height and bottom interface element was performed. This was done to study the influence of damage due to rounding of the edges and crushing of the mortar. The elements above and below the interface are narrowed at the bottom to achieve the thickness reduction.

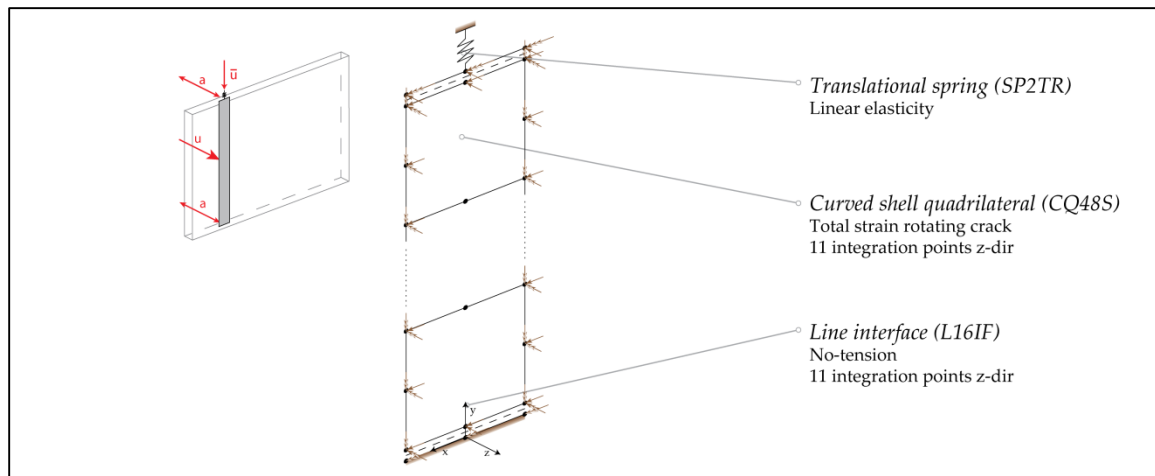


Figure 2.5.1: FE Curved Shell Model showing Specimen 8 (isometric view)

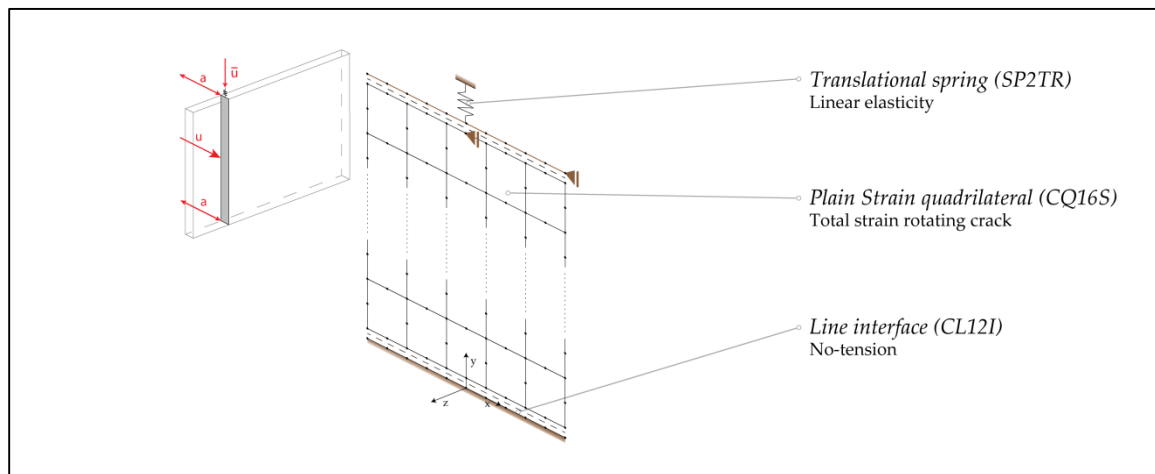


Figure 2.5.2: FE Plane Strain Model showing Specimen 8 (isometric view)

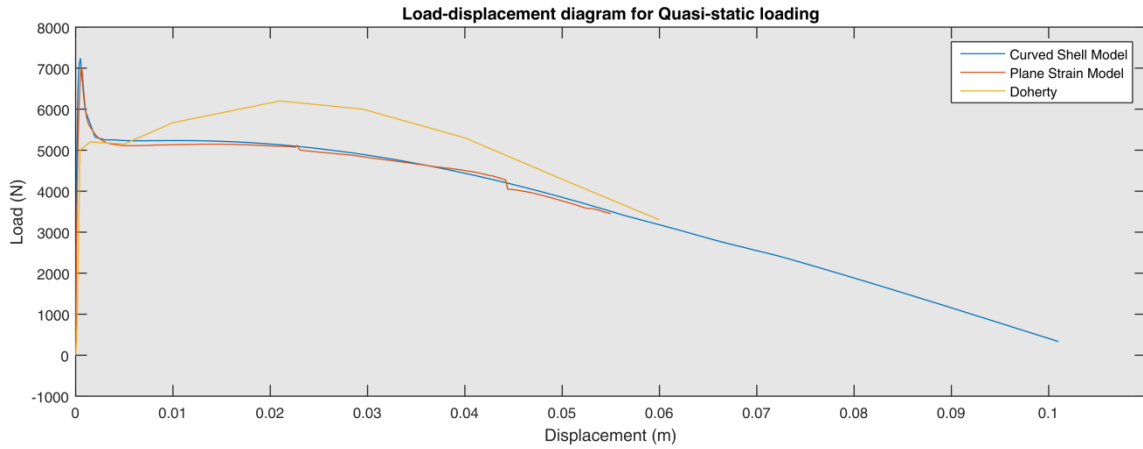


Figure 2.5.3: Total applied force vs. displacement for Specimen 8

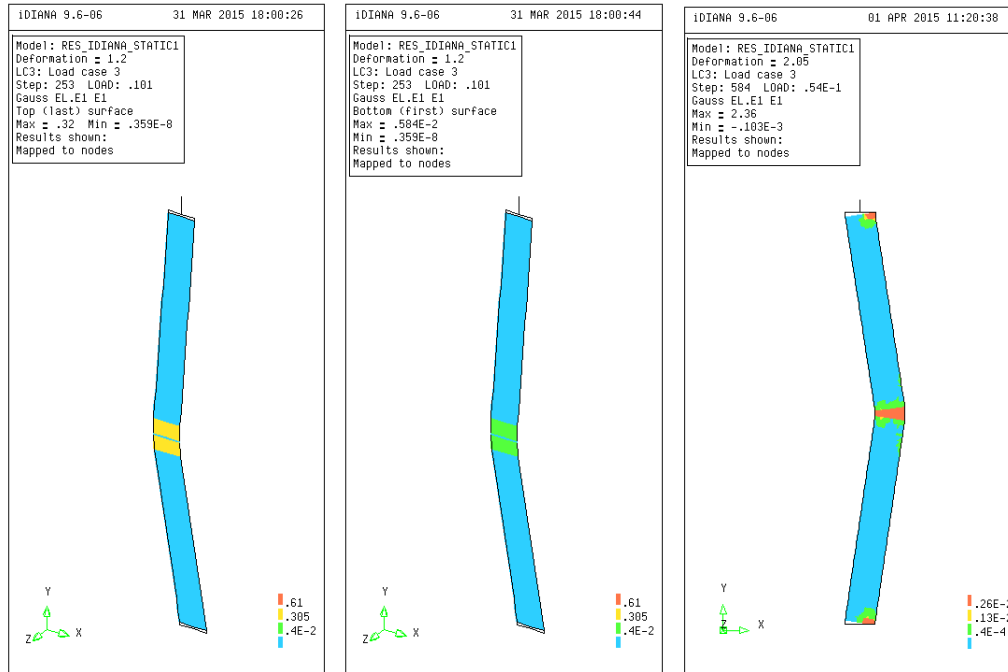


Figure 2.5.4: Final crack pattern – static loading for Specimen 8, (a) & (b) for Curved Shell Model and (c) for Plane Strain Model

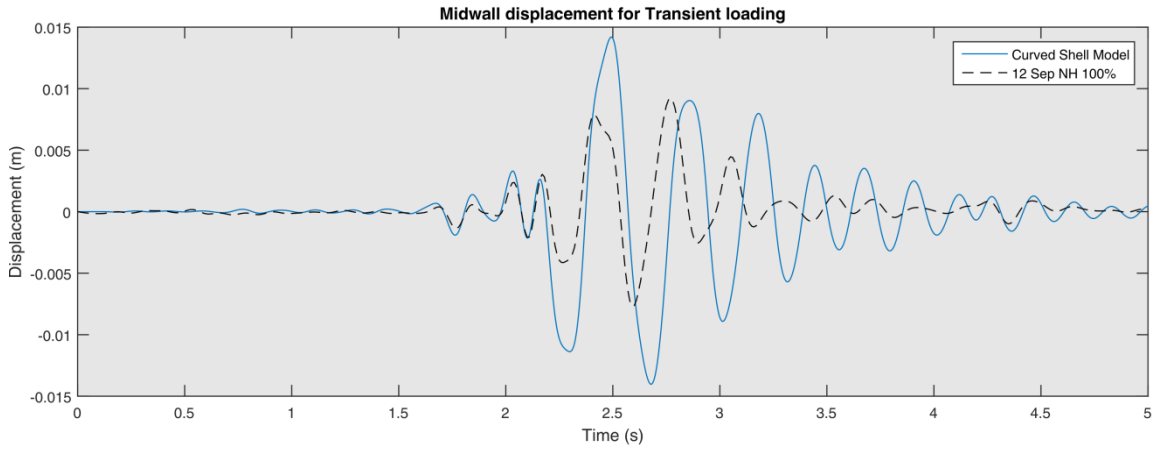


Figure 2.5.5: Mid-height displacement time history – Specimen 12, NH 100% for Curved Shell Model

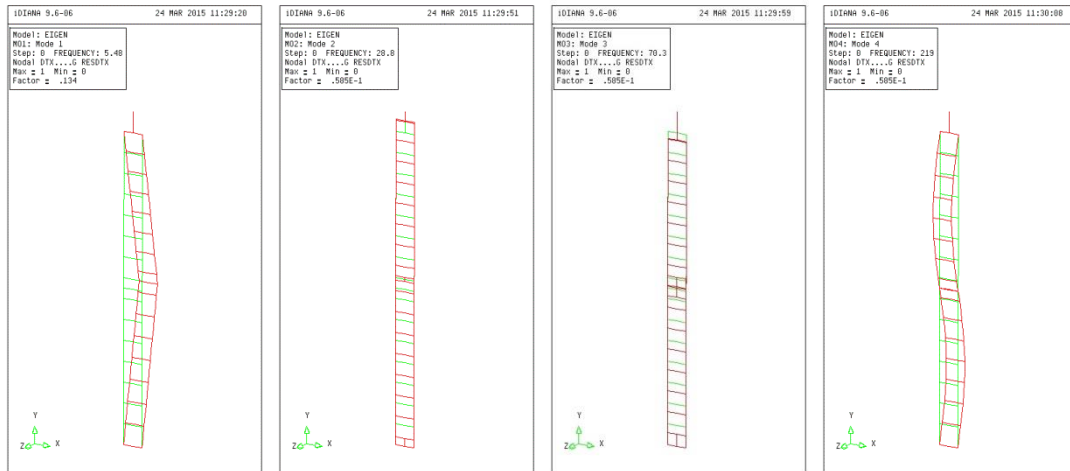
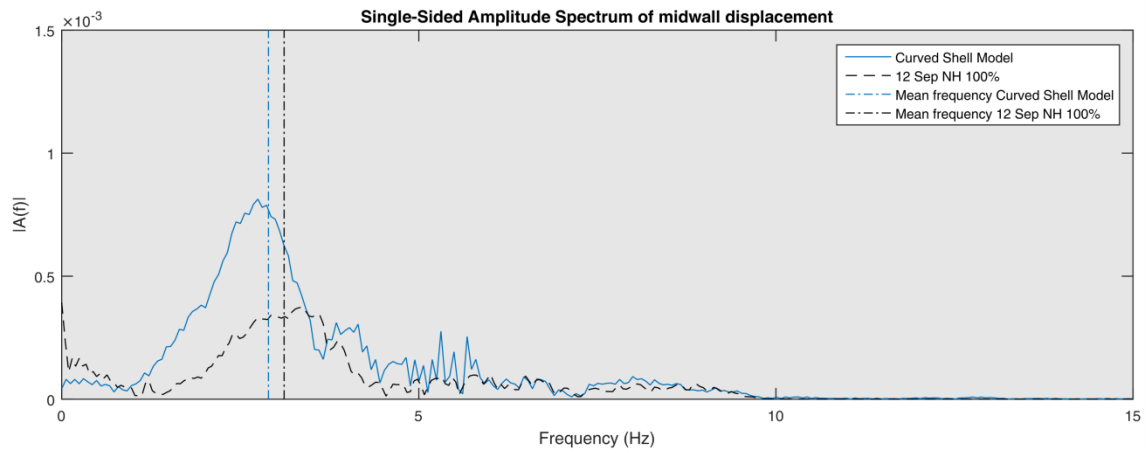


Figure 2.5.6: Eigenmodes of Curved Shell Model

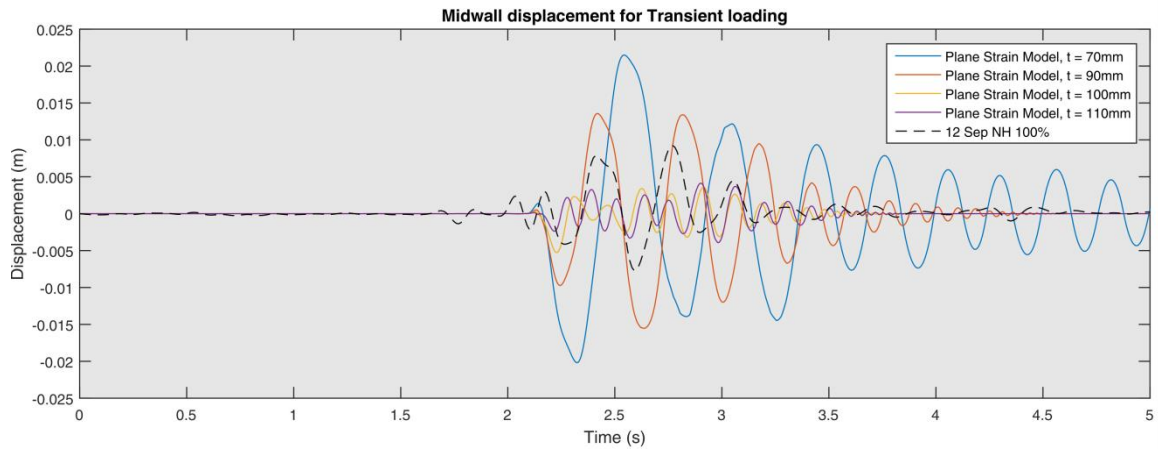


Figure 2.5.7: Mid-height displacement time history – Specimen 12, NH 100% for Plane Strain Model for different midwall and bottom thicknesses to account for damage.

2.5.1. Discussion and sensitivity analyses (if relevant)

For the transient analysis the influence of the normal stiffness of the line interface elements is considerable. This is caused by the way the deformations of the wall over the thickness are modelled. The shell elements are not able to follow this deformation pattern due to the Euler-Bernoulli's hypothesis: plane sections remain plane. To compensate for this stiff behavior of the shell elements a reduced interface stiffness is used and accurate results can be found. To verify and calibrate the stiffness properties of the interface elements the wall is also modelled with plane strain elements in the thickness direction (see Fig. 2.5.2).

For the plane strain model a sensitivity analysis was performed for the thickness of the wall at mid-height and at the bottom support. The idea is that a smaller thicknesses at mid-height and bottom support represents effects like: rounding of the edges of the mortar layer and initial crushing damage in the mortar layer at the start of the experiment.

At this moment the slip of the bottom support is neglected. During dynamic analysis the wall did show some slip, see Fig. 2.5.8d.

Acceleration signals

On the next pages a compatibility check is performed on the acceleration signals as reported by Doherty. The table and frame accelerations are compared with their displacements by differentiating the displacements twice. As Fig. 2.5.8 and 2.5.9 there is a small difference for the table accelerations of the 12 Sep NH100% signal. However the results from analysis show that experimental values for the midwall displacements in a transient analysis can be found. Thus the signal is not incorrect.

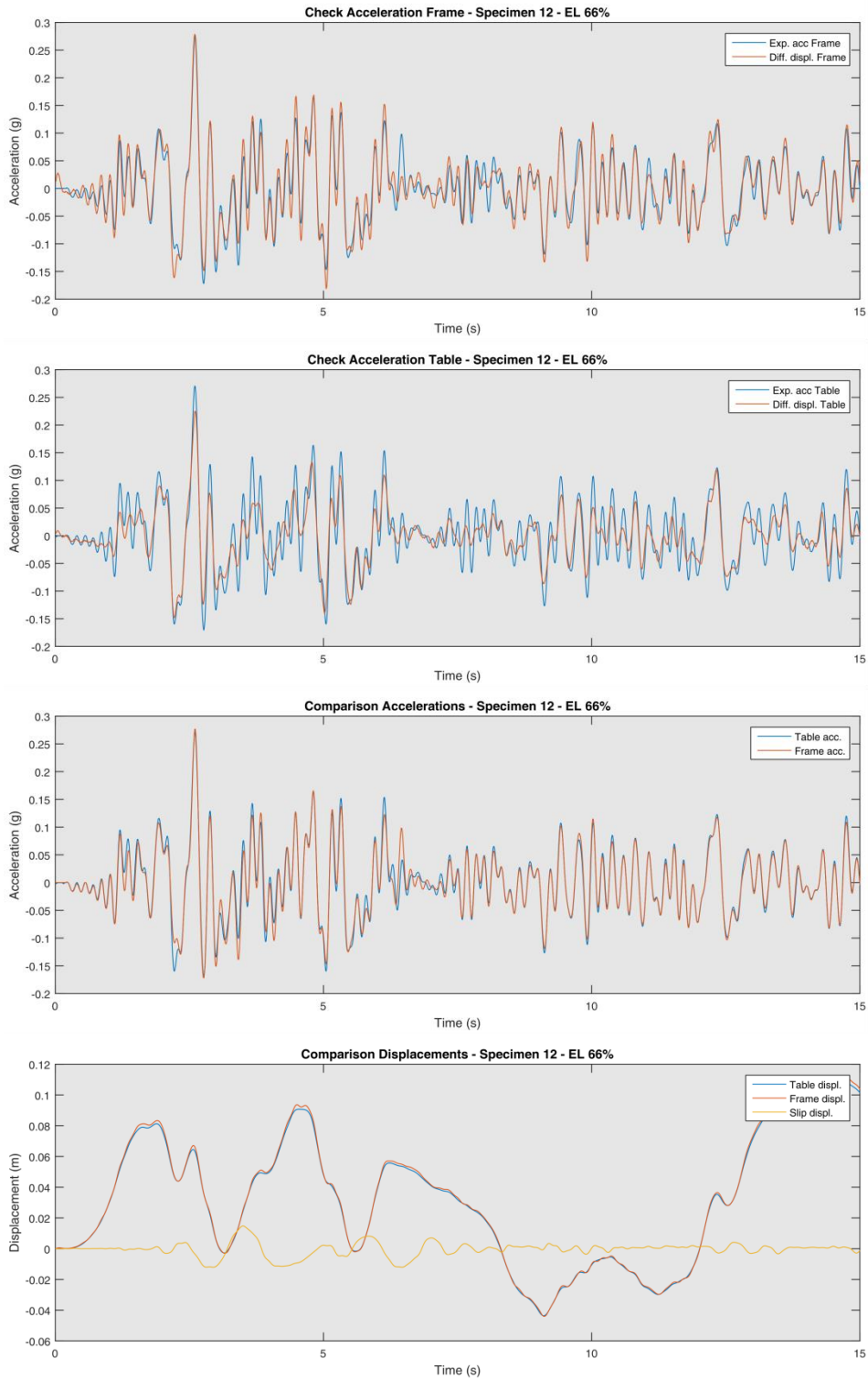


Figure 2.5.8: Mid-height acceleration time history with differentiated midwall displacement – Specimen 12, EL 66%

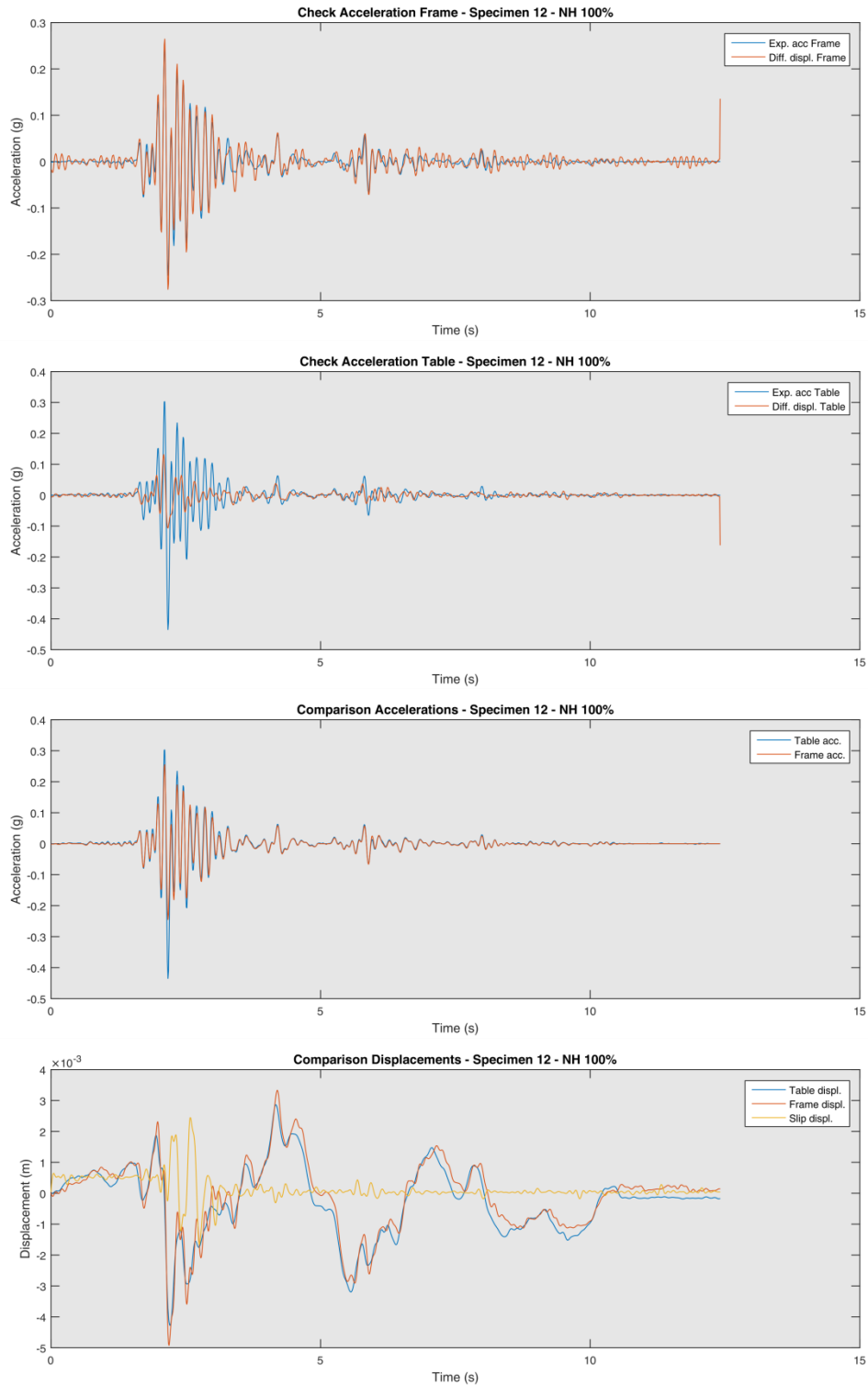


Figure 2.5.9: Mid-height acceleration time history with differentiated midwall displacement – Specimen 12, NH 100%

2.6. Two-way spanning wall out-of-plane tests (Griffith)

Table 2.6.1: Modelling notes

Component	Description
Analysis software and formulation	DIANA
Walls (in-plane)	Masonry modelled with shell elements using Total Strain Fixed Smearred Crack Model with Linear Tensile Softening, Elastic Compression and Constant Shear Reduction factor. Secant unloading
Walls (out-of-plane)	As above.
Wall to wall connection (incl. flange effects)	Clamped connection. Flange effects are included explicitly.

Table 2.6.2: Nonlinear time history analysis notes

Nonlinear time history analysis notes
-

Table 2.6.3: Model loading, materials and general comments

Loading	
Dead load	1900kg/m ³
Overburden	11kN/m for Wall 1
Materials	Material properties including values and stress strain behaviour
Masonry Wall 1	Total Strain Fixed Smeared Crack Model with Linear Tensile Softening, Elastic Compression and Constant Shear Reduction factor. Secant unloading $\rho = 1900 \text{ kg/m}^3$ $E = 3188\text{MPa}$ $\nu = 0.15$ $f_t = 0.721\text{MPa}$ (Tensile strength) $G_f=20\text{N/m}$ (Tensile fracture energy) $\beta=0.01$
Masonry Wall 2	Total Strain Crack Fixed Model with Linear Tensile Softening, Elastic Compression and Constant Shear Reduction factor. Secant unloading $\rho = 1900 \text{ kg/m}^3$ $E = 2240\text{MPa}$ $\nu = 0.15$ $f_t = 0.52\text{MPa}$ (Tensile strength) $G_f=20\text{N/m}$ (Tensile fracture energy) $\beta=0.01$
Timber beam for Wall 1	Linear Elastic model $\rho = 600 \text{ kg/m}^3$ $E = 6000\text{MPa}$ $\nu = 0.3$
<u>Other key notes</u>	
1) Tyings for equal vertical displacement where placed at the top nodes	

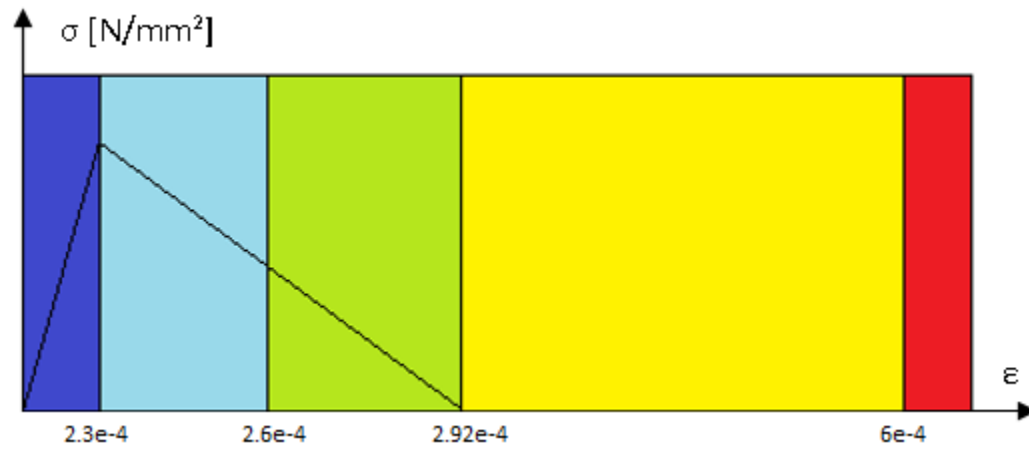
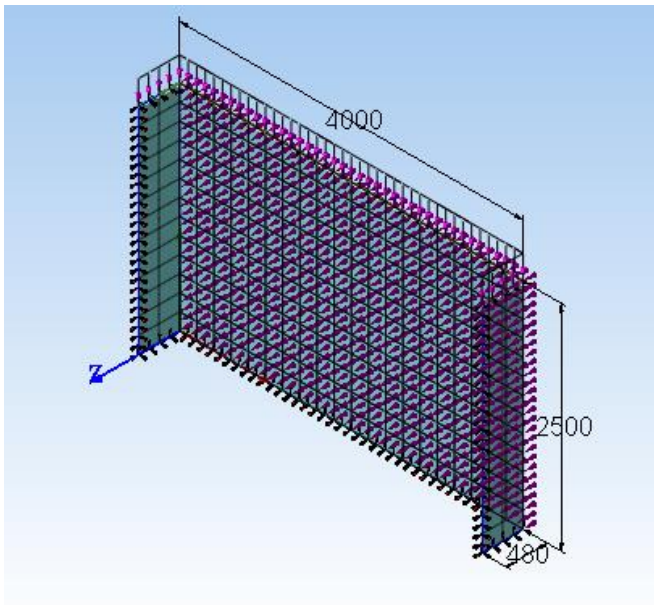


Figure 2.6.1: FE model showing Wall 1 and color ranks used for maximum principal strains (ϵ_1) plots

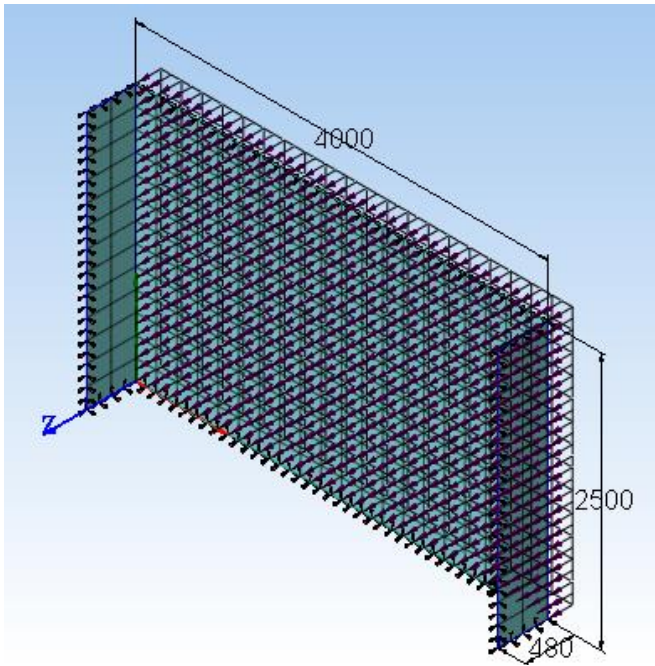


Figure 2.6.2: FE model showing Wall 2 and color ranks used for maximum principal strains (ϵ_1) plots

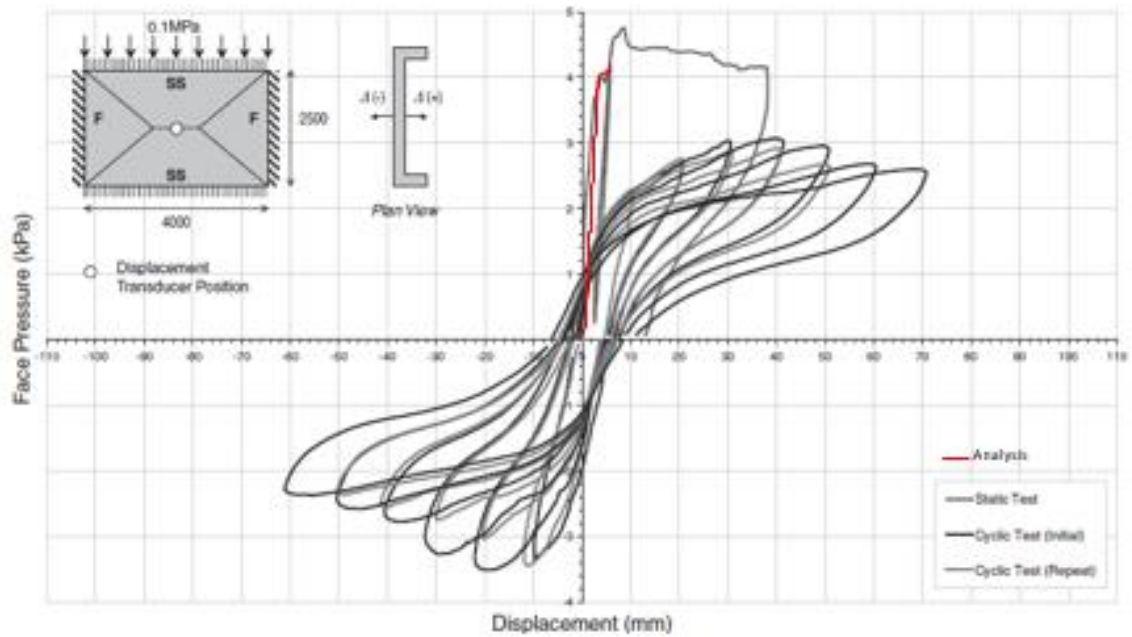


Figure 2.6.3: Load-displacement response plot (Wall 1)

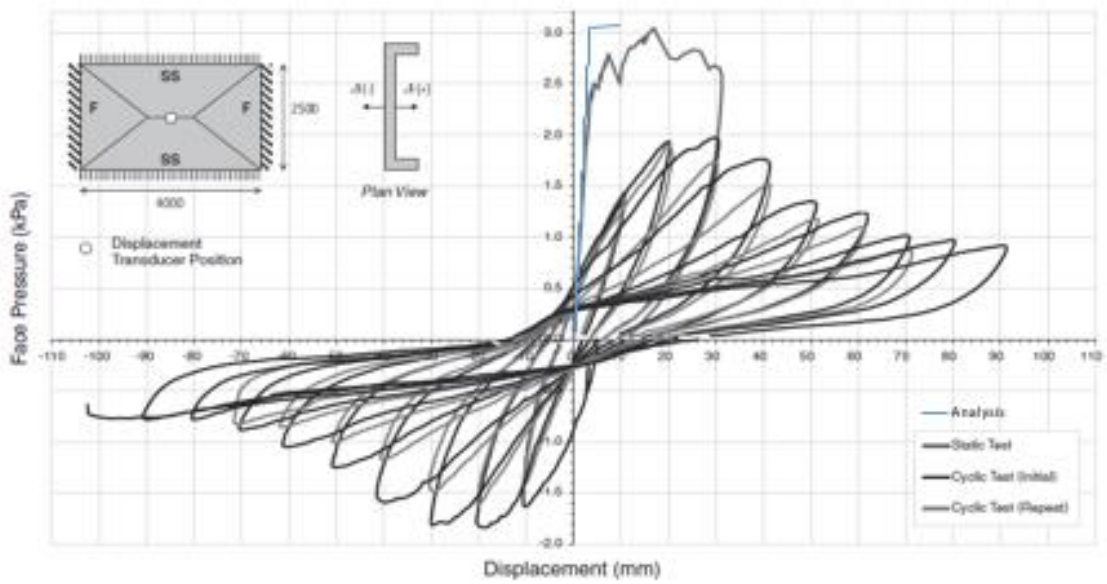


Figure 2.6.4: Load-displacement response plot (Wall 2)

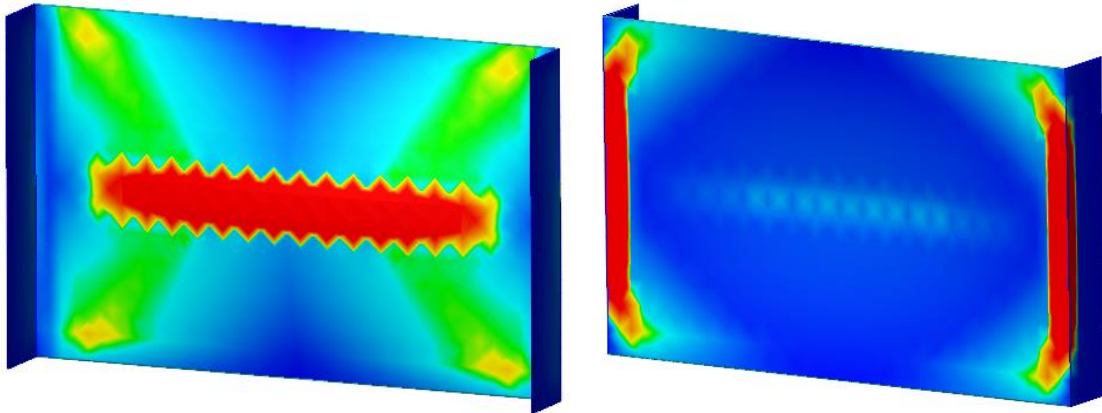


Figure 2.6.5: Corresponding representation of the active cracks, by means of the principal strain ϵ_1 of the outmost part of Wall 1 $\Delta(+)$ at displacement 5mm and of the inmost part of Wall 1 $\Delta(-)$ at displacement 5mm

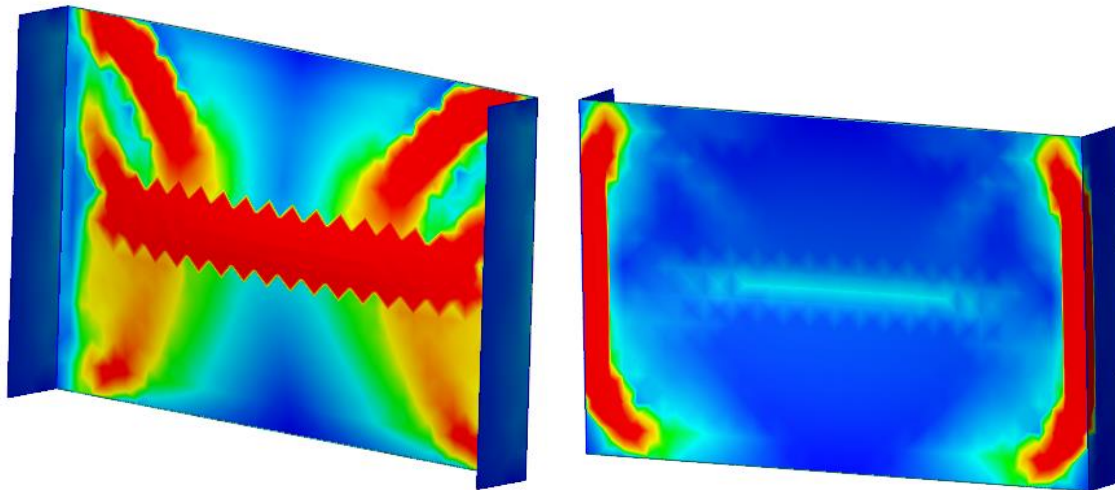


Figure 2.6.6: Corresponding representation of the active cracks, by means of the principal strain ϵ_1 of the outmost part of Wall 2 $\Delta(+)$ at displacement 9mm and of the inmost part of Wall 2 $\Delta(-)$ at displacement 9mm

2.6.1. Discussion and sensitivity analyses (if relevant)

Comments on obtained results

- Good prediction of the crack pattern for both walls.
- Unable to reproduce the ductility as observed in experimental results despite the numerous ways of the application on the load –such as load control and indirect displacement control.

3. Cross-validation index buildings

3.1. Terraced house (T1*)

Table 3.1.1: Modelling notes

Component	Description
Analysis software and formulation	DIANA
Walls (in-plane)	Masonry modelled with shell elements using Total Strain Fixed Smeared Crack Model with Linear Tensile Softening, Elastic Compression and Constant Shear Reduction factor.
Walls (out-of-plane)	As above.
Spandrels/lintels and wall coupling	Spandrels modelled using the same approach as the walls.
Wall to wall connection (incl. flange effects)	Clamped connection. Flange effects are included explicitly.
Modelling of veneer walls (outer leaf)	Veneer walls has not been explicitly modelled since they do not cooperate in the lateral resistance of the building. Their mass has been considered and assigned to the walls they are connected to.
Wall ties	Not explicitly modelled.
Concrete diaphragm	Hollowcore slabs were simulated as shell elements.
Wall to diaphragm connection	Clamped connection.
Foundation	Modelled as rigid.

Table 3.1.2: Eigenvalue analysis notes

Eigenvalue analysis notes
<ul style="list-style-type: none">Performed with full elastic Young Modulus $E=4410$ MPa

Table 3.1.3: Nonlinear pushover analysis notes

Nonlinear pushover analysis notes
<ul style="list-style-type: none">Monotonic mass proportional pushover

Table 3.1.4: Nonlinear time history analysis notes

Nonlinear time history analysis notes
<ul style="list-style-type: none">1% damping assumed and modelled through Rayleigh damping factors.

Table 3.1.5: Model loading, materials and general comments

Loading	
Dead loads	Self-weight of the walls, hollowcore planks and roof structure.
Superimposed dead loads	Floors =2.4kPa Roof =0.5kPa
Live loads	Floors = 1.75kPa Roof =0
Load combination	DL + SDL + 0.24LL
Materials	Material properties including values and stress strain behaviour
Masonry	<p>According to Total Strain Smeared Crack Model:</p> <p>E=4410 MPa Young modulus $\nu=0.15$ Poisson coefficient $\rho=1900 \text{ kg/m}^3$ Unit mass $f_t=0.1 \text{ MPa}$ Tensile strength $G_t=50 \text{ N/m}$ Tensile fracture energy Exponential tension softening β variable Shear retention factor (reducing to zero with damage) $f_c=6.3 \text{ MPa}$ Compressive strength $G_c=12500 \text{ N/m}$ Compressive fracture energy Parabolic compressive softening</p>
Concrete	<p>Elastic material model $\rho =2400\text{kg/m}^3$ $E = 38\text{GPa}$ $\nu = 0.2$</p>
Timber/Plywood	<p>Elastic material model $\rho = 600 \text{ kg/m}^3$ $E = 6000\text{MPa}$ $\nu = 0.3$</p>
<u>Other key notes</u>	
<ol style="list-style-type: none"> 1) The gravity loads have been applied as uniformly distributed on the edges of the lateral walls. 2) Two model have been developed: a BASIC one, without the spandrels and a COMPLETE one, with spandrels included. Following results refer to the BASIC model. 3) The models do not include walls G5, G6, F5, F6 because they are disconnected at the level of the floors and they don't contribute to the lateral resistance of the building. 4) A sensitivity analysis has been carried out to investigate the effect of the connection of walls F1-F4 on the second floor and the effect of the inclusion of the spandrels. 5) The application of Record 3 involved an amplification of the response of the at the end of the acceleration time history with a substantial increment of the displacements at the top of the structure in X direction, for PGAs equal to 0.25g and 0.5g. 	

Table 3.1.6: Breakdown of loading and masses

Loading	DL [kPa]	SDL [kPa]	LL [kPa]	DL+SDL+0.24LL [kPa]	Area [m ²]
1 st Floor	3.25	2.4	1.75	6.07	41.5
2 nd Floor	3.25	2.4	1.75	6.07	41.5
Roof	0.27	0.5	0	0.77	56.8
Total model mass (including DL+SDL+0.24LL) = 87860 kg					
Masonry	Density [kg/m ³]		Thickness [m]	Total masonry mass [kg]	
Calcium silicate	1900		0.12 (TG1-2)	28666	
			0.1 (G1-G4)	2248	
Clay (vener)	1900		0.1	2248	

Table 3.1.7: Cut-section total z-forces (weight from gravity load at t=0) at different cut-plane heights

Cut-plane height (m)	Cut-section z-force (kN)
<Just above ground/base>	-872.75
<Just above L1 diaphragm>	-481.09

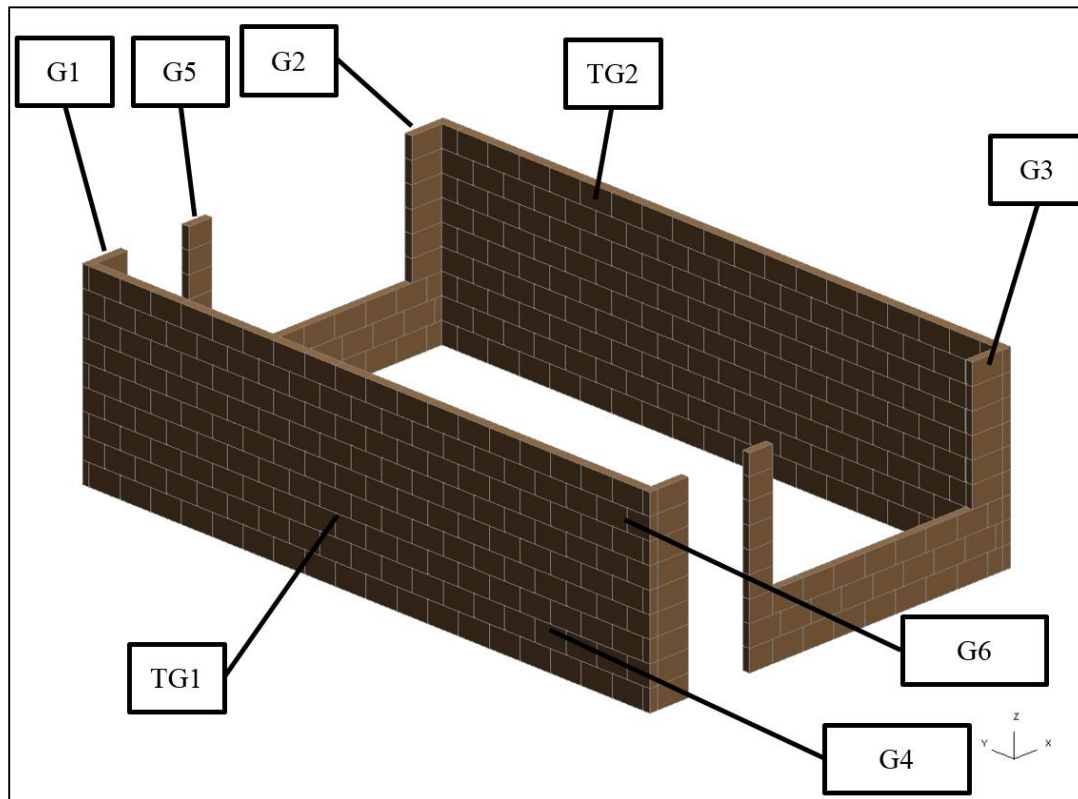


Figure 3.1.1: Pier labelling convention for T1* building (ground floor)

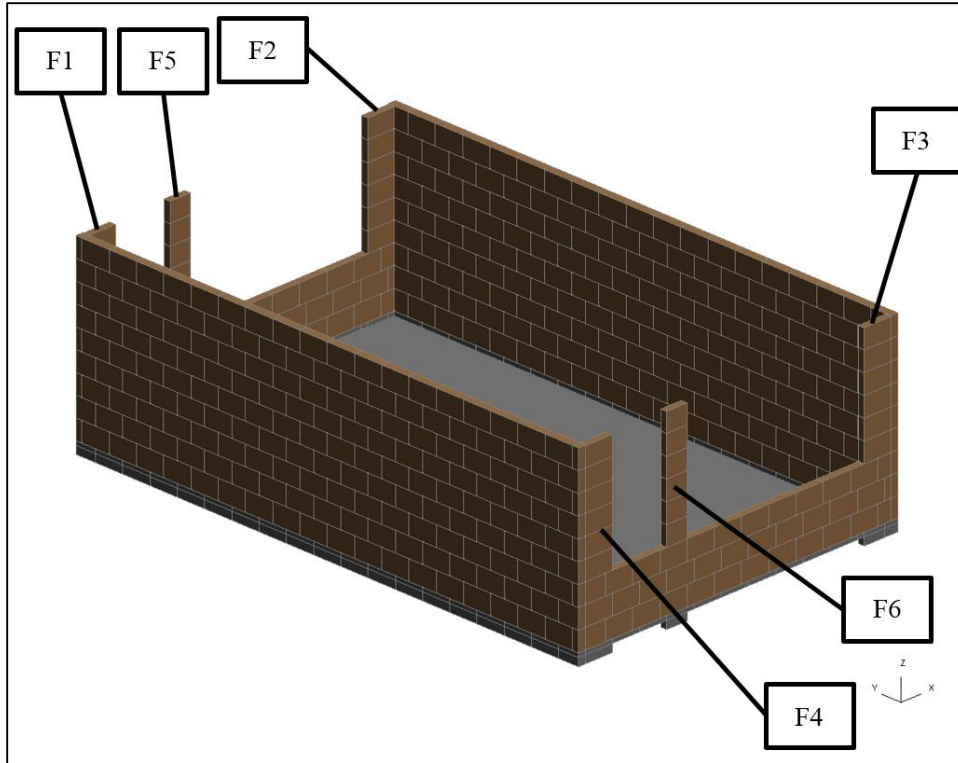


Figure 3.1.2: Pier labelling convention for T1* building (first floor)

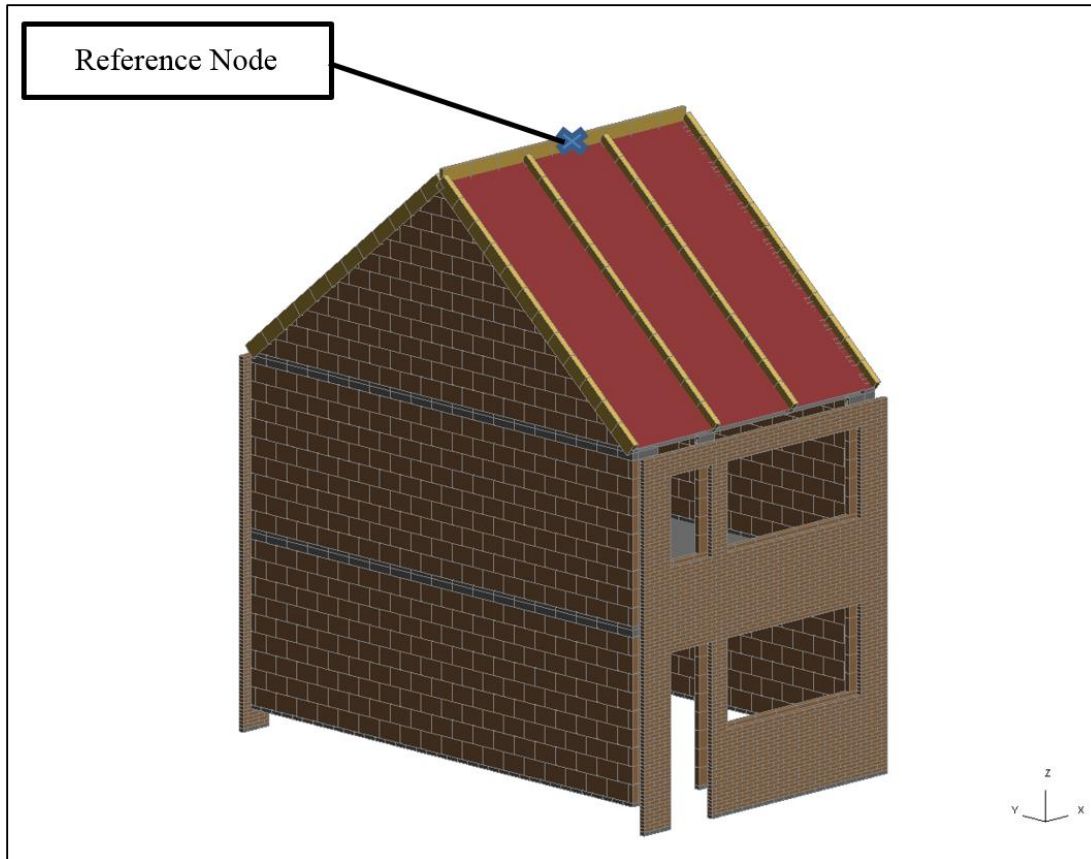


Figure 3.1.3: T1* model pushover reference node location

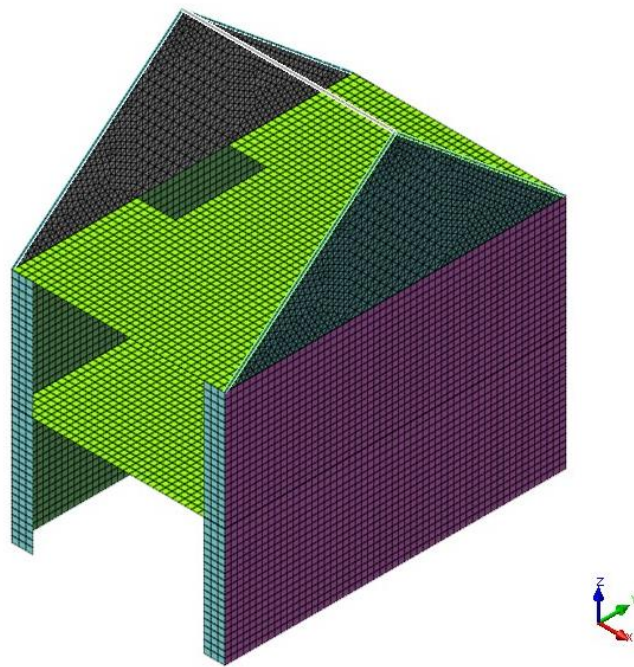


Figure 3.1.4: FE model for T1* model

3.1.1. Modal analysis

Table 3.1.8: Modal period, frequency, description, mass participation

Mode	Period (s)	Frequency (Hz)	Description of mode	Mass participation %	
				X	Y
1	0.635	1.575	1 st translation in X direction	80.72	≅0
2	0.350	2.853	Translation in X direction (roof)	6.04	≅0
3	0.199	5.031	2 nd translation in X direction	8.94	≅0
10	0.080	12.40	1 st translation in Y direction	≅0	29.24
11	0.079	12.65	2 nd translation in Y direction	≅0	25.03
13	0.067	14.91	Translation in Y direction (roof)	≅0	11.86

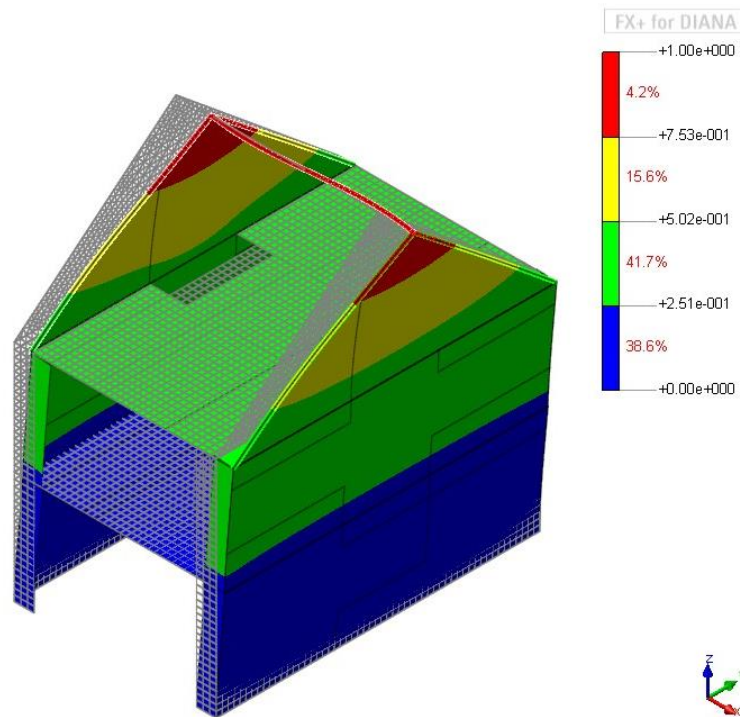


Figure 3.1.5: First lateral mode shape X direction.

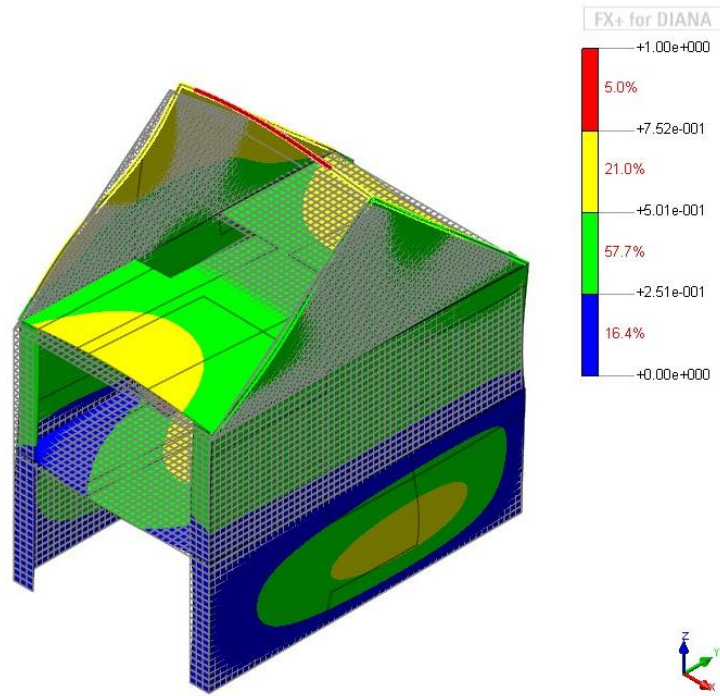


Figure 3.1.6: First lateral mode shape Y direction.

3.1.2. Pushover monotonic analysis

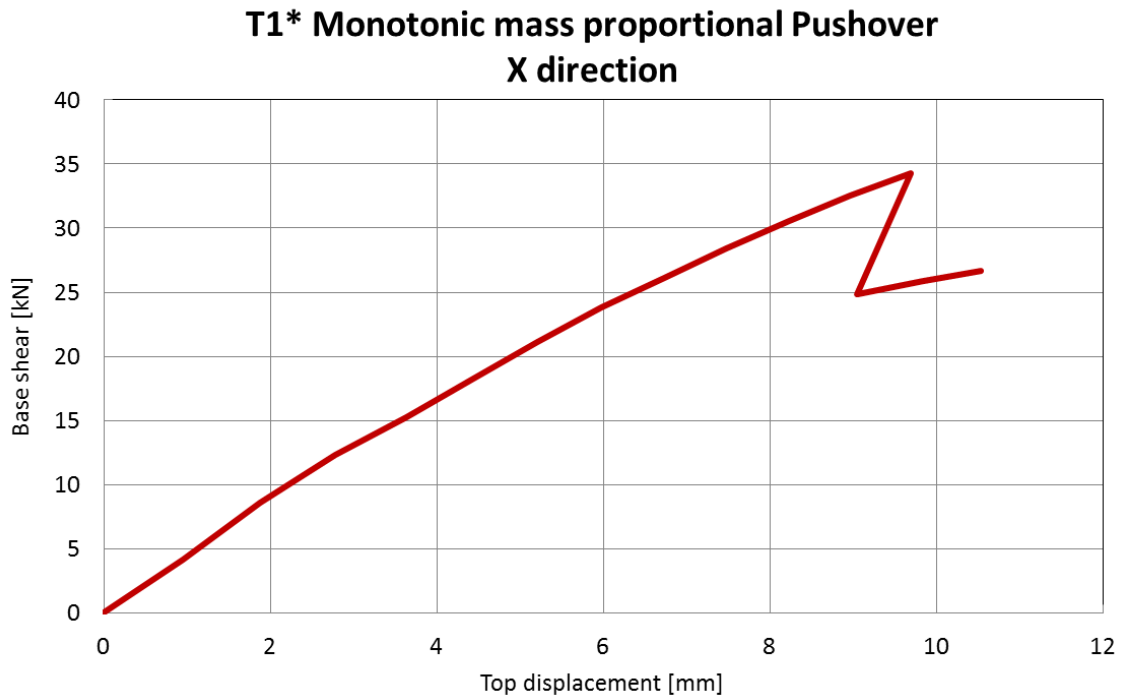


Figure 3.1.7: X direction base shear versus reference node displacement monotonic.

Table 3.1.9: Cut-planes pier forces at peak/plateau x-dir pushover base shear

Pier	X- dir pier force (kN) Cut-plane height ~1.65m		Pier	X-dir pier force (kN) Cut-plane height ~4.65m	
	Axial	Shear			Axial
G1	-39.15	9.85	F1	-9.23	2.79
G2	-9.88	0.95	F2	-3.28	1.15
G3	-32.52	6.37	F3	-5.37	0.41
G4	-32.27	9.81	F4	-10.38	3.30
G5	-	-	F5	-	-
G6	-	-	F6	-	-
TG1	-294.11	2.57	TG1	-172.30	3.64
TG2	-390.69	2.10	TG2	-207.31	4.69
Total	-798.62	31.65	Total	-407.78	15.98

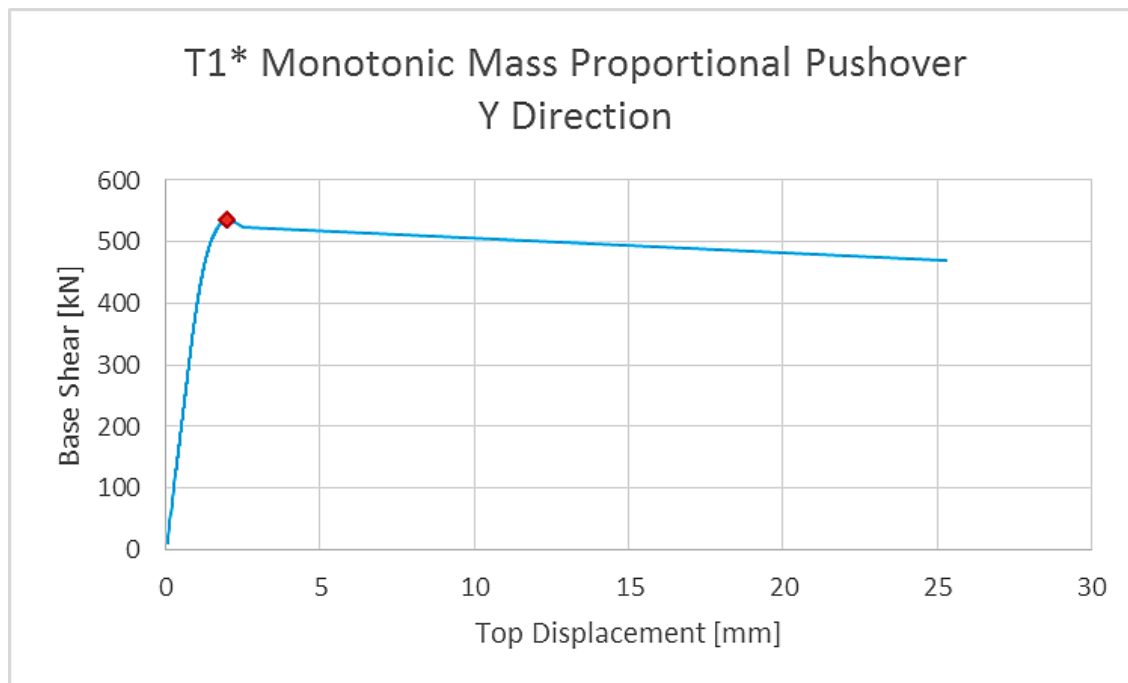


Figure 3.1.8: Y direction base shear versus reference node displacement monotonic (the point indicates the step where the axial and shear forces were calculated)

Table 3.1.10: Cut-planes pier forces at peak/plateau y-dir pushover base shear

Pier	Y- dir pier force (kN) Cut-plane height ~1.65m		Pier	Y-dir pier force (kN) Cut-plane height ~4.65m	
	Axial	Shear		Axial	Shear
G1	-36.80	0.48	F1	-6.81	0.02
G2	-37.15	0.47	F2	-6.99	0.03
G3	+0.74	0.07	F3	-1.36	0.03
G4	+2.17	0.08	F4	-1.30	0.03
G5	-	-	F5	-	-
G6	-	-	F6	-	-
TG1	-335.39	237.43	TG1	-182.18	121.97
TG2	-378.95	251.38	TG2	-203.30	128.52
Total	-785.39	489.91	Total	-401.95	250.60

3.1.3. Time history analysis

Table 3.1.11: Peak reference node displacement [mm] (3 records at each PGA level).

PGA	RECORD 3		RECORD 6		RECORD 7	
	X direction	Y direction	X direction	Y direction	X direction	Y direction
0.10g	59.62	0.47	26.83	0.97	27.3	0.81
0.25g	>248.65	2.9	73.62	2.51	61.1	1.95
0.50g	>281.65	7.5	128.83	5.22	121.75	6.39

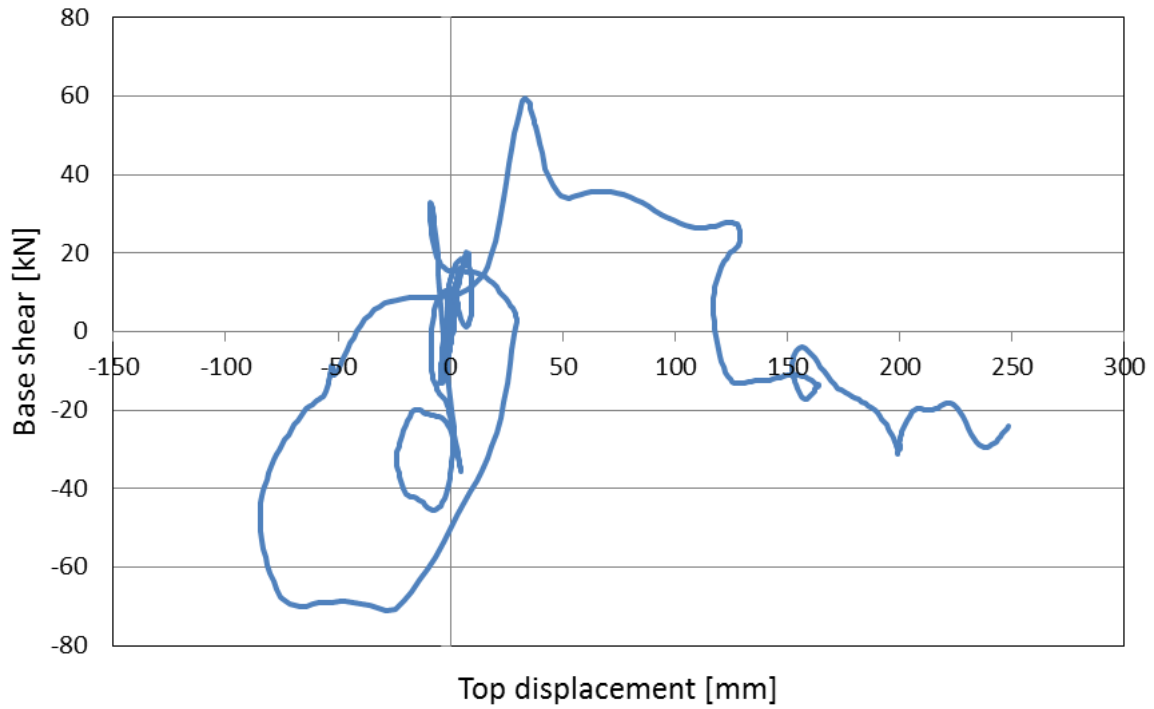


Figure 3.1.9: Base shear versus reference node displacement – 0.25g scaled PGA, record 3, X direction

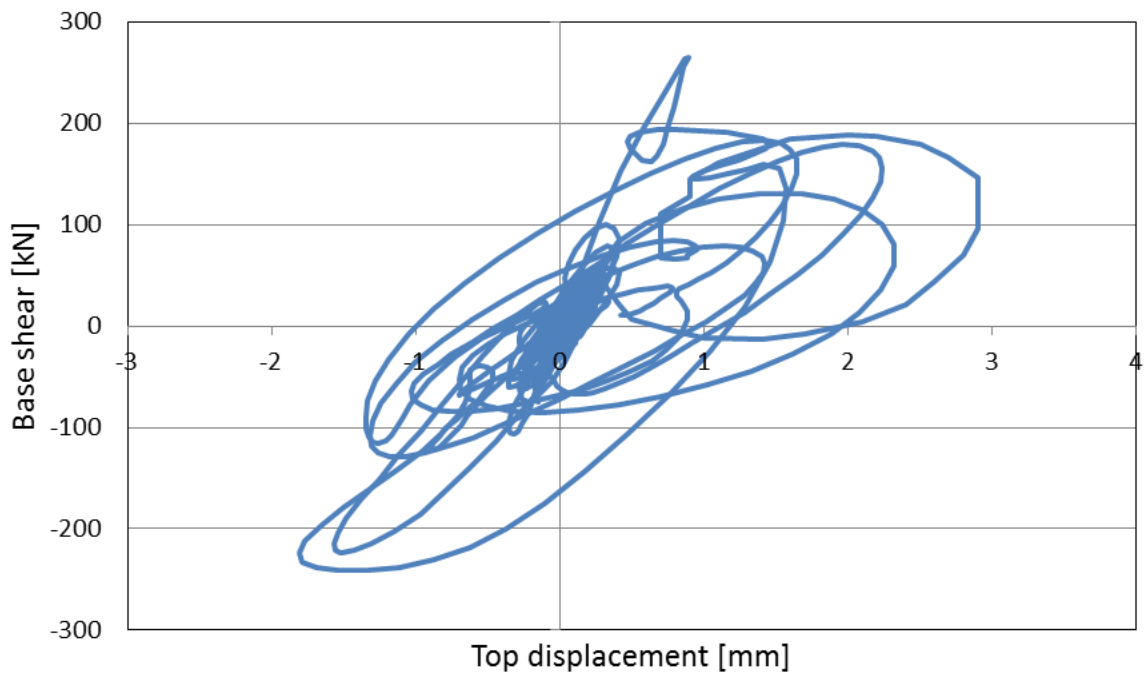


Figure 3.1.10: Base shear versus reference node displacement – 0.25g scaled PGA, record 3, Y direction

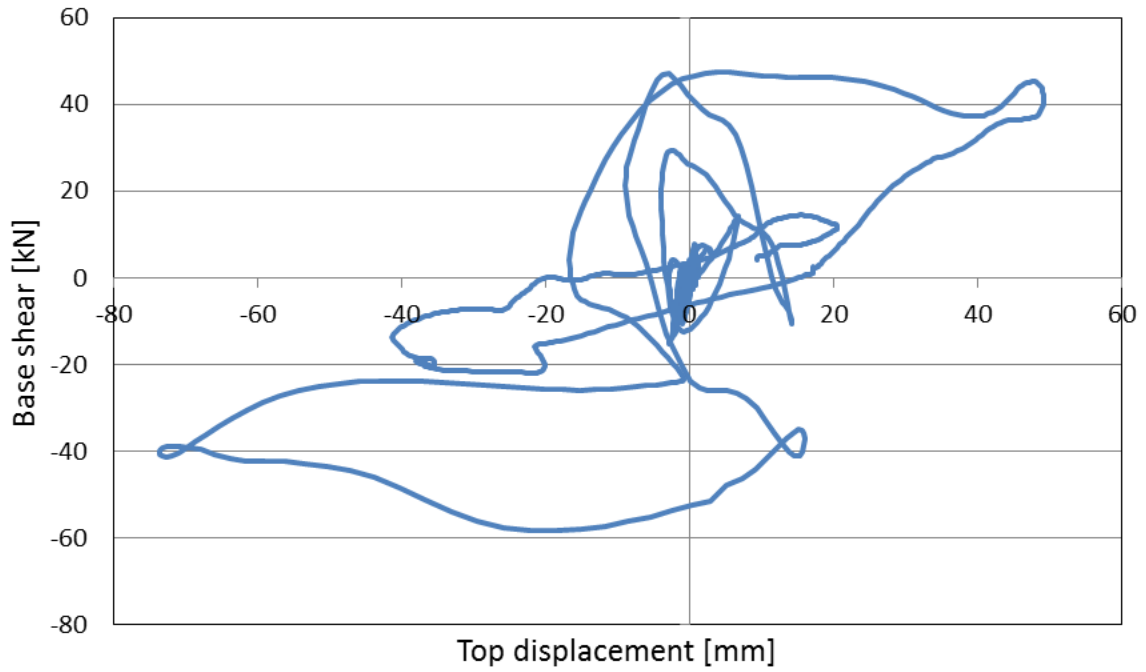


Figure 3.1.11: Base shear versus reference node displacement – 0.25g scaled PGA, record 6, X direction

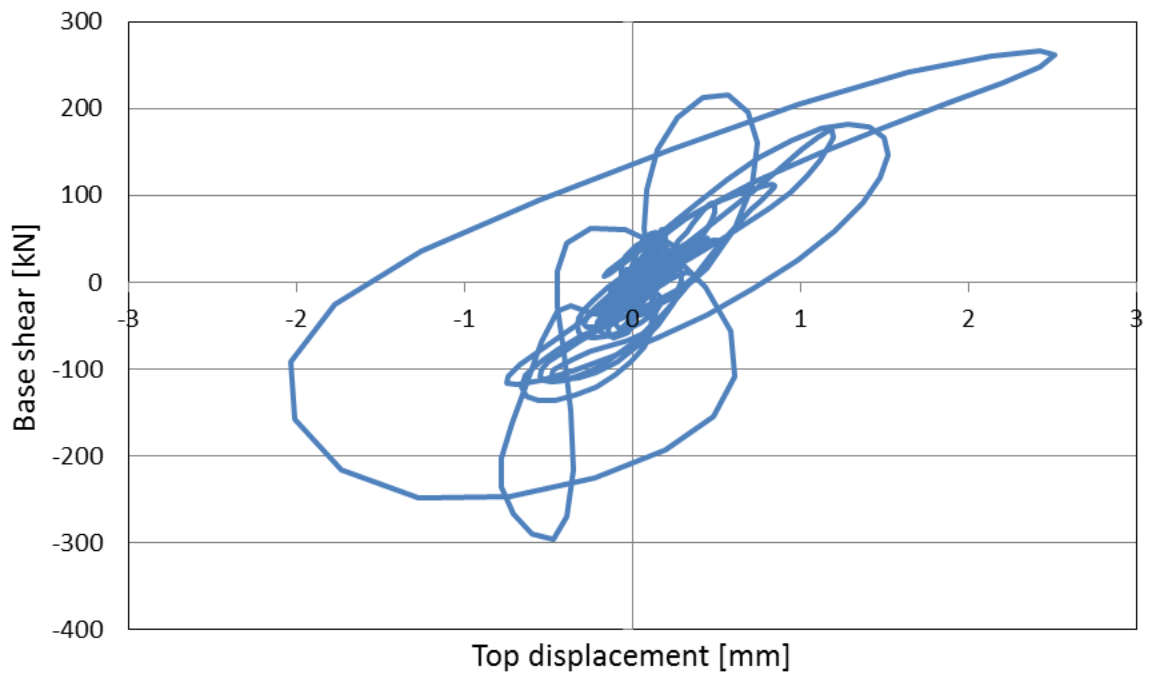


Figure 3.1.12: Base shear versus reference node displacement – 0.25g scaled PGA, record 6, Y direction

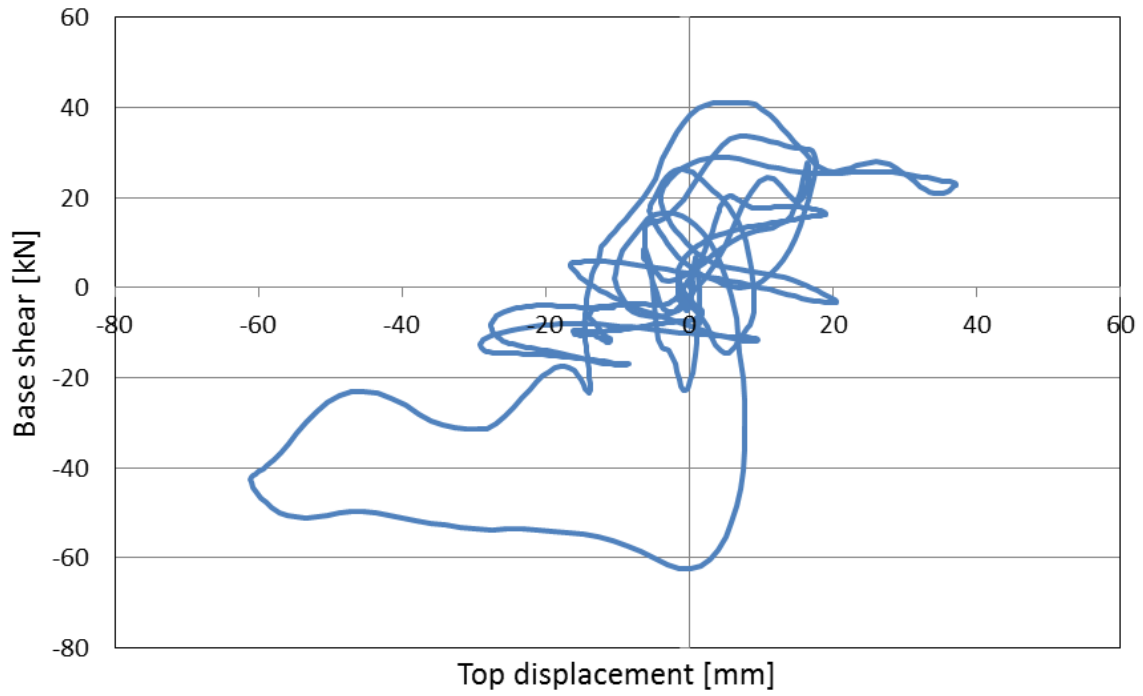


Figure 3.1.13: Base shear versus reference node displacement – 0.25g scaled PGA, record 7, X direction

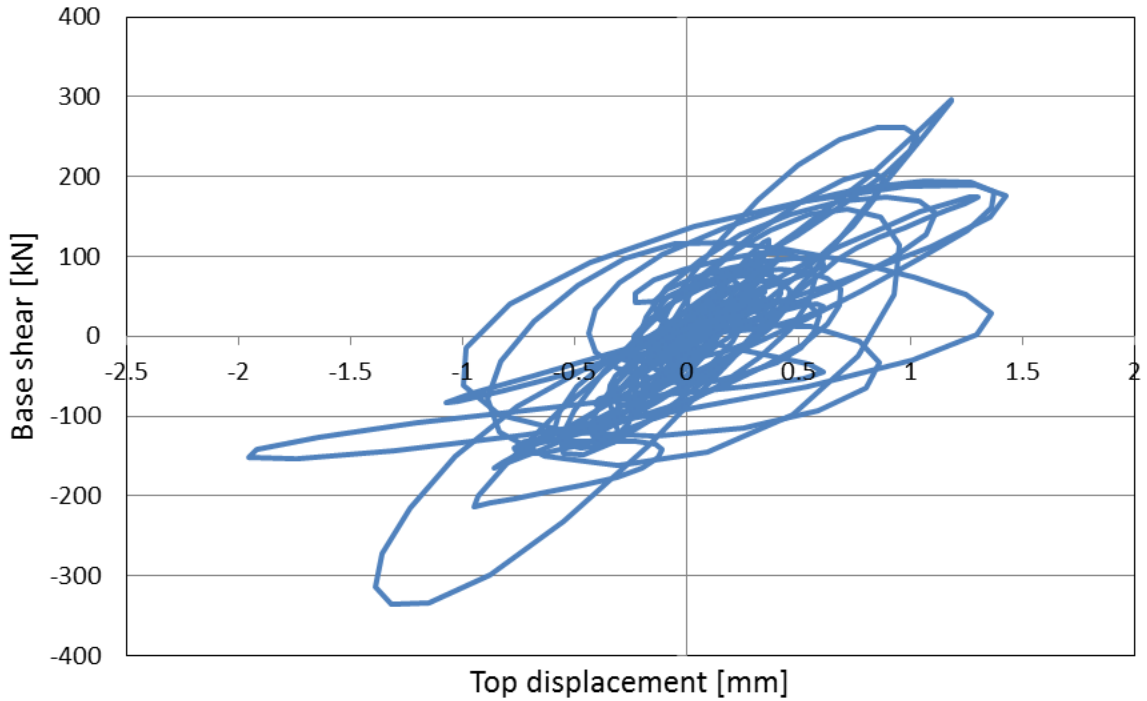


Figure 3.1.14: Base shear versus reference node displacement – 0.25g scaled PGA, record 7, Y direction

3.1.4. Discussion and sensitivity analyses

Effect of spandrels and connection of piers F1-F4 at the second floor (pushover analysis).

Developed model:

- BASIC_free: without spandrels and F1-F4 piers disconnected on top, at the level of the second floor.
- BASIC_clamp: without spandrels and F1-F4 piers clamped on top, at the level of the second floor.
- COMPLETE_clamp: with spandrels and F1-F4 piers clamped on top, at the level of the second floor.

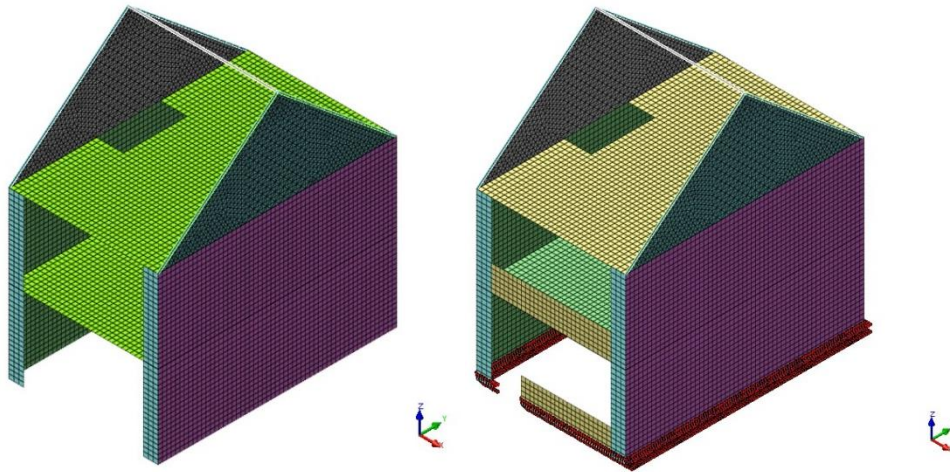


Figure 3.1.15: BASIC (right) and COMPLETE (left) finite element models.

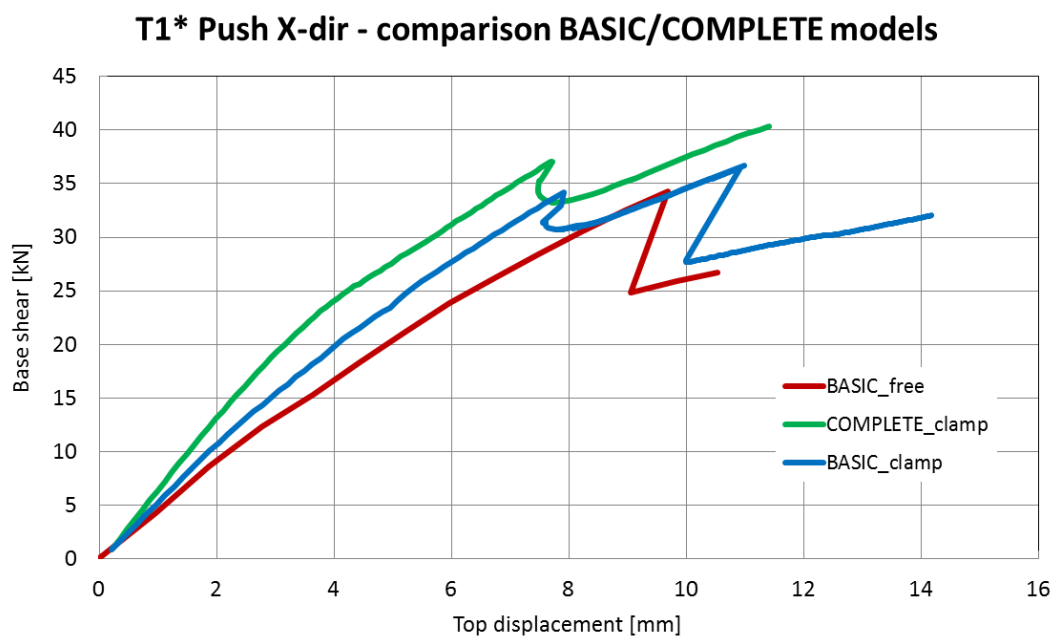


Figure 3.1.16: Pushover curves obtained in X direction for BASIC_free, BASIC_clamp and COMPLETE_clamp models.

As can be observed, the modeling of the top edge of piers F1-F4 as clamped leads to an increase in initial stiffness. The inclusion of the spandrels also involve an additional increase in stiffness.

The curves present one drop (free model) or two drops (clamped model): the first one is related to the disconnection of the upper edge of piers F1-F4 for models in which this connection is assumed as clamped at the beginning; the second one is related to the complete detachment of the vertical joints between the slender piers and the long orthogonal walls, that leads to a sudden drop in the capacity. It is interesting to observe that the stiffness of the BASIC_free model is almost equal to the stiffness observed in the BASIC_clamp model in the second ascending part of the curve (after the first drop).

Comments on obtained results

- Reasonable global response detected in both nonlinear static and dynamic analyses; the drops in the capacity curves are related to reasonable damage patterns developing in the structure;
- Difficulties in the determination of ductility (post-peak behaviour) in the pushover analyses, due to convergence issues.

3.2. Detached villa, timber floors (T3a)

Table 3.2.1: Modelling notes

Component	Description
Analysis software and formulation	DIANA
Walls (in-plane)	Masonry modelled with shell elements using Total Strain Fixed Smearred Crack Model with Linear Tensile Softening, Elastic Compression and Constant Shear Reduction factor.
Walls (out-of-plane)	As above.
Spandrels/lintels and wall coupling	Spandrels modelled using the same approach as the walls. Lintels modelled so that the elements remain elastic.
Wall to wall connection (incl. flange effects)	Clamped connection. Flange effects are included explicitly.
Wall ties	Represented by the above mentioned interface elements..
Timber diaphragm	The thickness of diaphragm is 61.7 mm (see other key notes)
Wall to diaphragm connection	Clamped Connection
Foundation	Modelled as rigid.

Table 3.2.2: Eigenvalue analysis notes

Eigenvalue analysis notes
•

Table 3.2.3: Nonlinear pushover analysis notes

Nonlinear pushover analysis notes
• Monotonic mass proportional pushover

Table 3.2.4: Nonlinear time history analysis notes

Nonlinear time history analysis notes
• 1% damping

Table 3.2.5: Model loading, materials and general comments

Loading	
Dead loads	Self-weight of the walls, diaphragms and roof structure.
Superimposed dead loads	Floor = 1 kPa Barn roof = 1 kPa Main roof = 0.5 kPa
Live loads	Floor = 1.75 kPa Barn roof = 1.75 kPa Main roof = 0 kPa
Load combination	DL + SDL + 0.24LL
Materials	
Masonry	E= 4410 MPa v = 0.15 $\rho = 1900 \text{ kg/m}^3$ Total crack fixed, elastic for compression $f_t = 0.1 \text{ MPa}$ $G_f = 0.005$
Steel	Elastic material model $\rho = 7850 \text{ kg/m}^3$ E = 300GPa v = 0.3
Timber/Plywood	Elastic material model $\rho = 600 \text{ kg/m}^3$ E = 6000 MPa v = 0.3 $G_{xy} = 64.3 \text{ MPa}$ $G_{xz} = G_{yz} = 600 \text{ MPa}$
Other key notes	
<p>1) Considering the contribution of wood beams, E along the beam direction is 259520 MPa</p> <p>2) Considering the contribution of roof frame, the thickness of roof is 61.7 mm instead of 25 mm</p> <p>3) Converting load to mass, the density of floor is 5430 kg/m^3, the density of roof is 1427 kg/m^3</p>	

Table 3.2.6: Breakdown of loading and masses

Loading	DL [kPa]	SDL [kPa]	LL [kPa]	DL+SDL+0.24LL [kPa]	Area [m ²]
Floor		1kPa	1.75 kPa		
Barn roof		1kPa	1.75 kPa		
Main roof		0.5 kPa	0		
Total model mass (including DL+SDL+0.24LL) = 85.77 tone					
Masonry	Density [kg/m ³]			Thickness [m]	Total masonry mass [kg]
Masonry	4410			0.22	

Table 3.2.7: Cut-section z-forces (weight from gravity load at t=0) at different cut-plane heights

Cut-plane height (m)	Cut-section z-force (kN)
<Just above ground/base>	682 kN
<Just above diaphragm>	222 kN
<Just above pier level plane>	369 kN
<Just above half wall>	460 kN

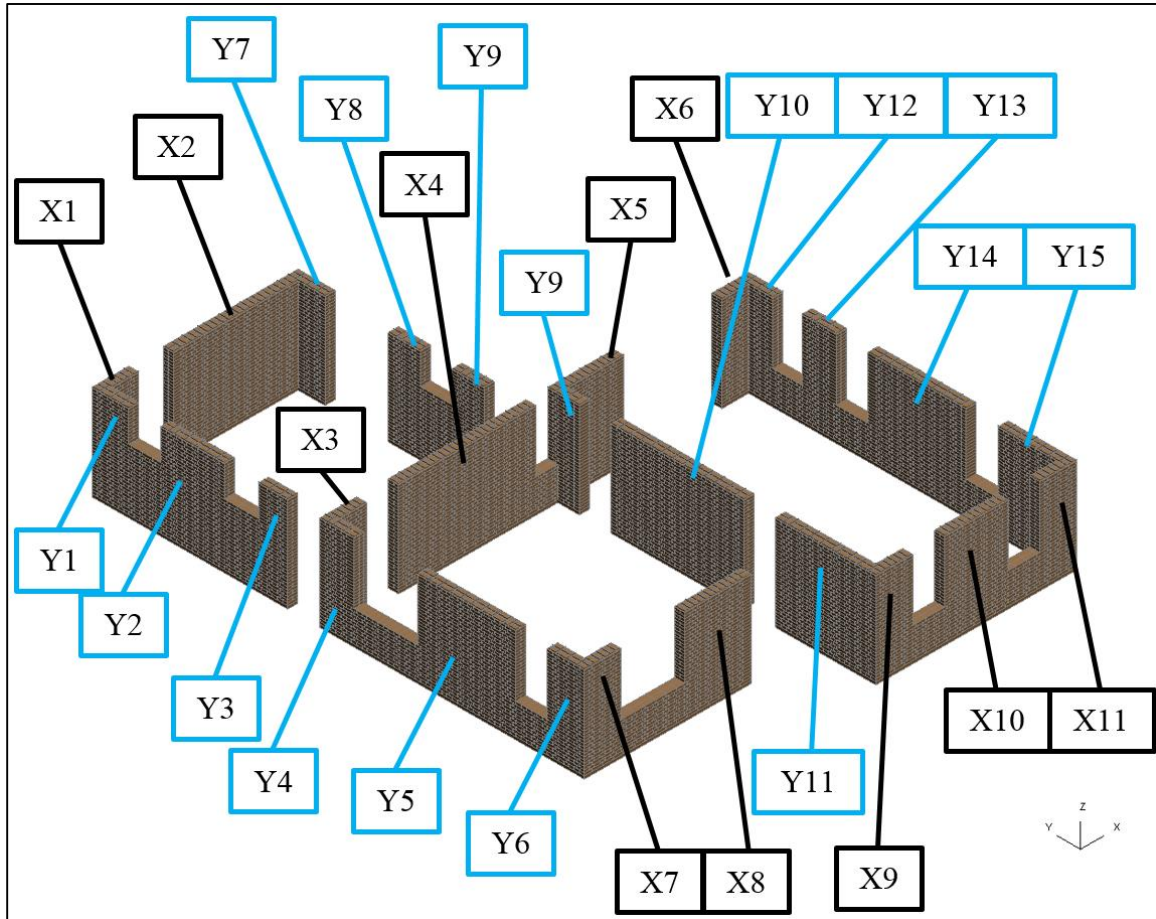


Figure 3.2.1: Pier labelling convention for T3a building

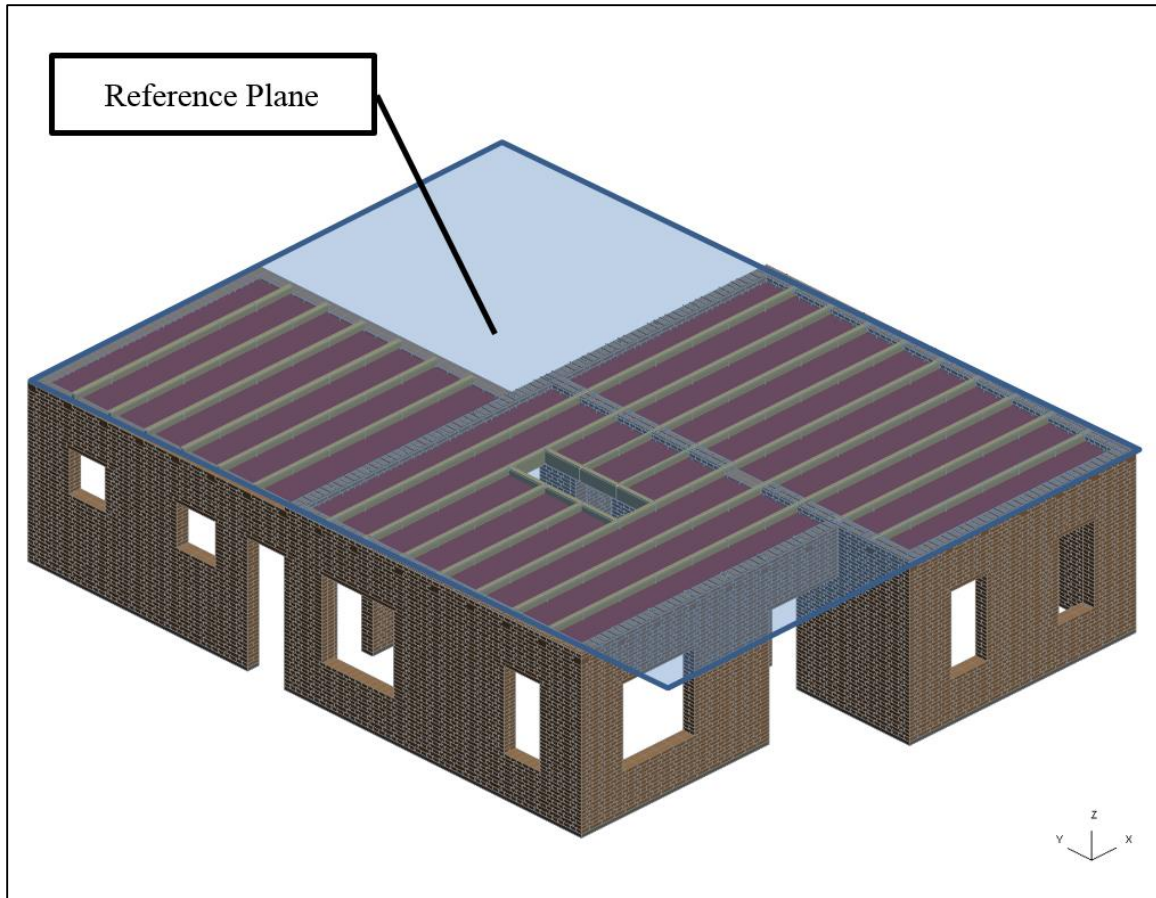


Figure 3.2.2: T3a model pushover reference plane location/height

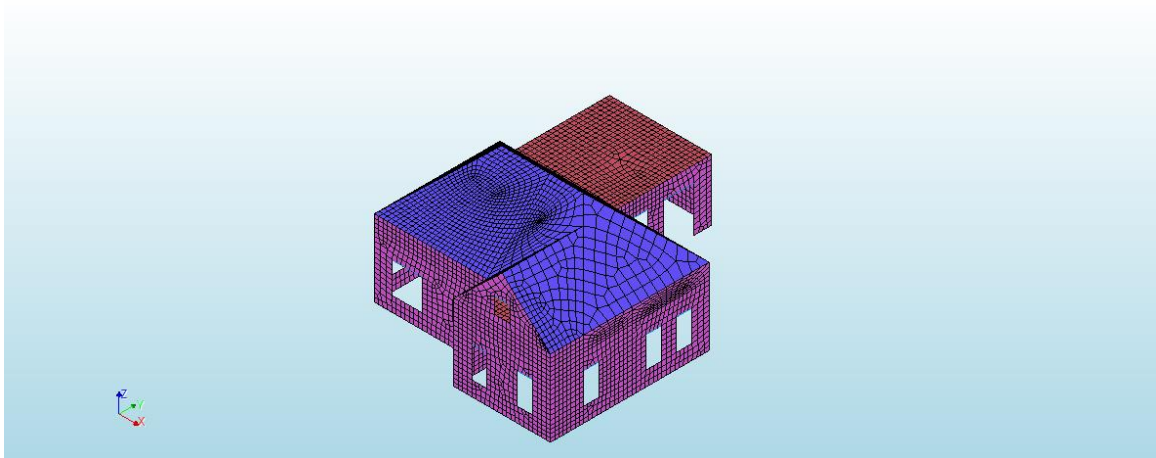


Figure 3.2.3: FE model for T3a model

3.2.1. Modal analysis

Table 3.2.8: Modal period, frequency, description, mass participation

Mode	Period (s)	Frequency (Hz)	Description of mode	Mass participation %	
				X	Y
16	0.094268477	10.608		43.468	0.39337
21	0.083759109	11.939		7.9498	0.1438
27	0.076365025	13.095		0.13937	5.9084
29	0.073099415	13.68		0.16745	15.863
30	0.071073205	14.07		0.58509	7.5251
33	0.065019506	15.38		0.055424	15.279
38	0.061709349	16.205		0.00593	4.0618

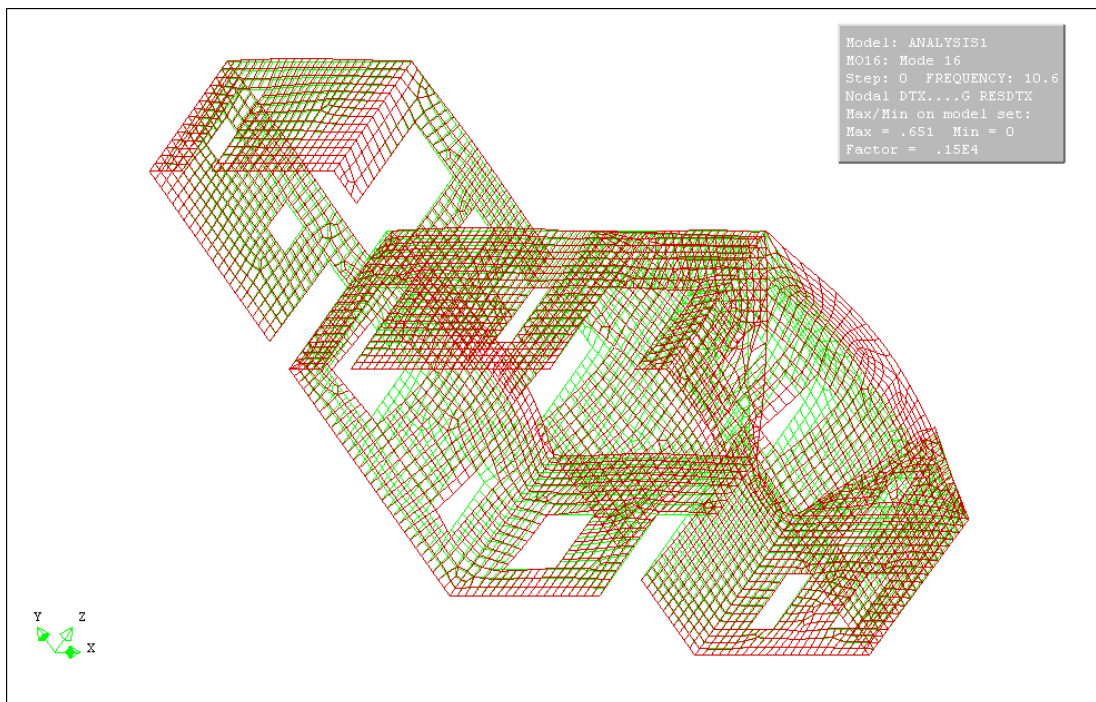


Figure 3.2.4: First lateral mode shape (X direction)

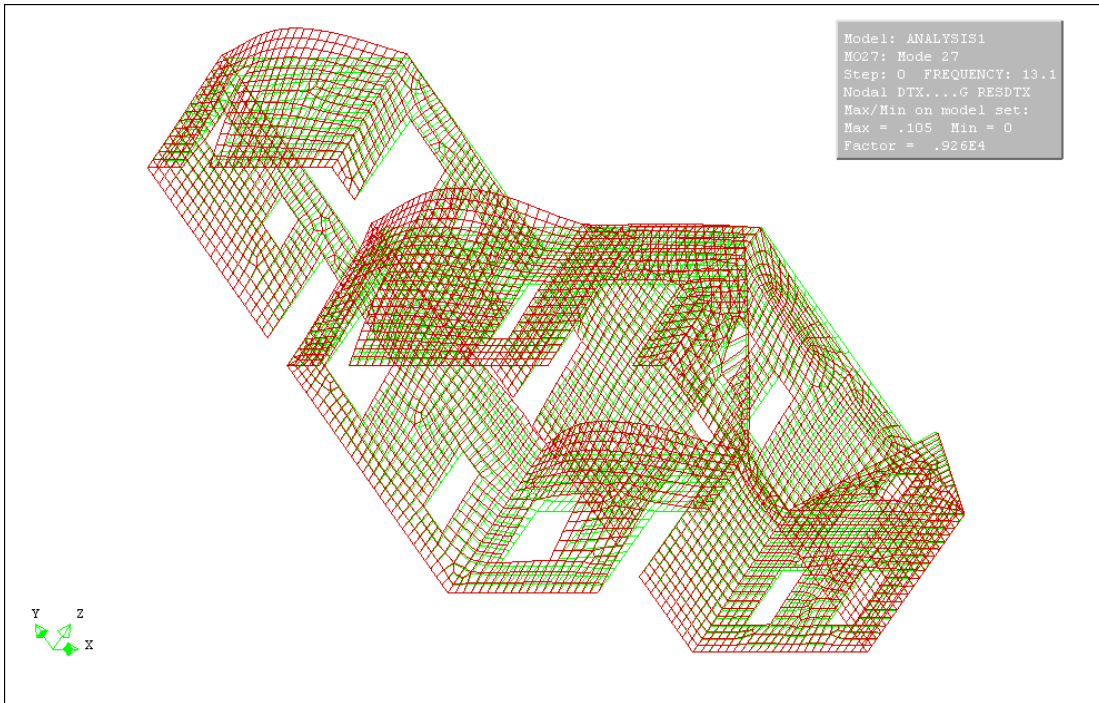


Figure 3.2.5: First lateral mode shape (Y direction)

3.2.2. Pushover analysis (monotonic and, if possible, cyclic)

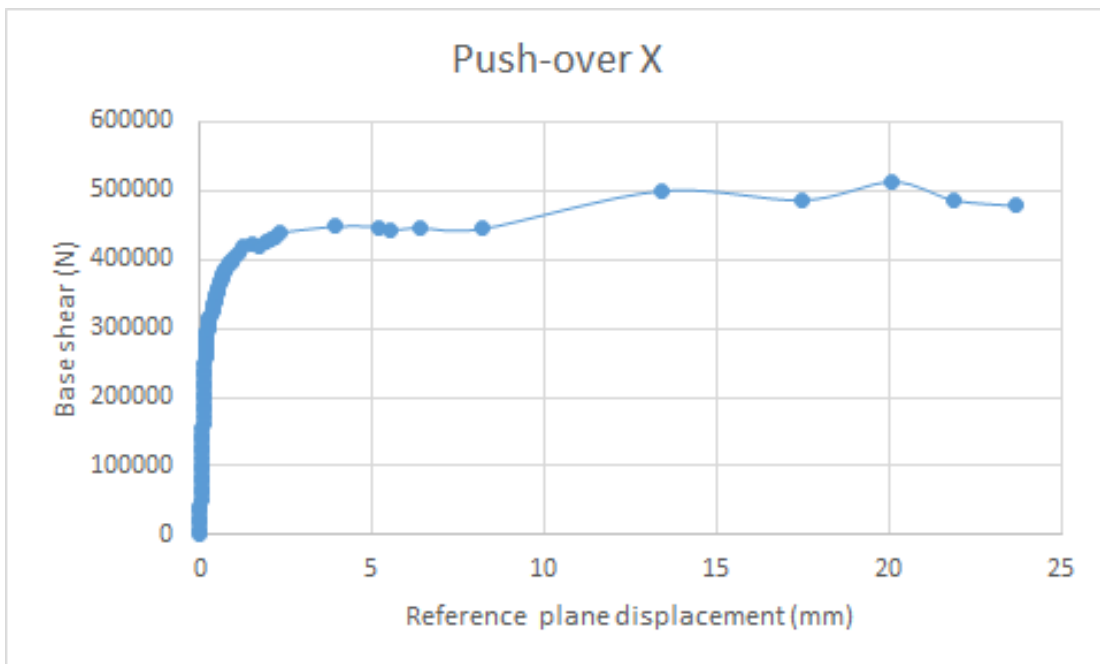


Figure 3.2.6: X direction base shear versus average reference height displacement

Table 3.2.9: Cut-plane pier forces at peak/plateau x-dir pushover base shear

Pier	X-dir pier force (kN) Cut-plane height ~1.4m	
	Axial	Shear
X1	5.4529	7.058
X2	22.899	33.48745
X3	6.746	6.557
X4	54.42422	87.0804
X5	78.5592	44.779
X6	34.711	24.4456
X7	12.249	6.756
X8	28.354	34.755
X9	30.0467	39.7755
X10	26.044	35.3731
X11	38.4026	7.02473
Y1	6.325	3.2852
Y2	13.3882	3.0486
Y3	5.2164	1.87656
Y4	1.6651	1.752
Y5	15.88073	5.2176
Y6	5.374	1.5185
Y7	9.398	1.3803
Y8	6.1517	1.2867
Y9	4.7212	1.58322
Y10	26.853	5.78196
Y11	20.767	4.3235706
Y12	1.7966	0.9872
Y13	7.485	1.4483
Y14	26.46	6.9167
Y15	15.384	2.53684
Y16	21.6365	5.8927
Total	526.39105	375.9277306

For the point (6.37mm, 445984.002 N), the first convergence point at the plateau.

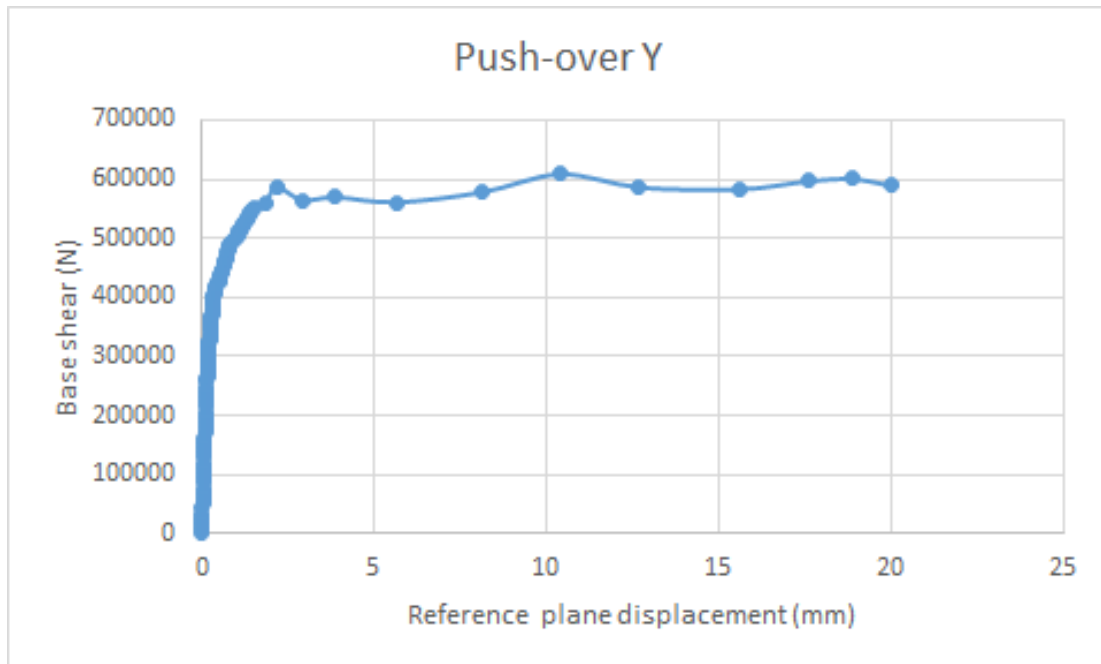


Figure 3.2.7: Y direction base shear versus average reference height displacement

Table 3.2.10: Cut-plane pier forces at peak/plateau y-dir pushover base shear

Pier	Y-dir pier force (kN) Cut-plane height ~1.4m	
	Axial	Shear
X1	2.9657	1.0531
X2	14.2999	6.8567
X3	9.91	2.2292
X4	17.789	10.18231
X5	12.9017	1.867
X6	13.7462	2.342
X7	4.498	2.762
X8	26.759	3.24202
X9	15.512078	9.45753
X10	7.138078	5.46273
X11	5.644	6.52
Y1	10.563	3.387
Y2	15.49719	25.712
Y3	9.29777	20.979
Y4	14.8242	4.1156
Y5	29.444	44.578
Y6	5.217	7.3284
Y7	17.431	12.871
Y8	7.6323	9.964
Y9	16.266	13.555

Y10	76.474	56.221
Y11	32.2974	28.3856
Y12	25.6742	11.476
Y13	9.9744	6.479
Y14	38.2366	66.68043
Y15	13.7362	15.274
Y16	42.2757	10.946995
Total	496.004616	389.927615

For the point (3.89 mm, 569712.5 N), the first convergence point at the plateau.

3.2.3. Time history analysis

Table 3.2.11: Peak average reference height displacement (3 records at each PGA level)

PGA	RECORD 3		RECORD 6		RECORD 7	
	X direction	Y direction	X direction	Y direction	X direction	Y direction
0.1g	0.15	0.14	0.17	0.14	0.136	0.18
0.25g	0.78	0.7	0.6	0.51	0.922	0.5
0.5g	6.9	4.1	4.2	3.6	6.08	5.8

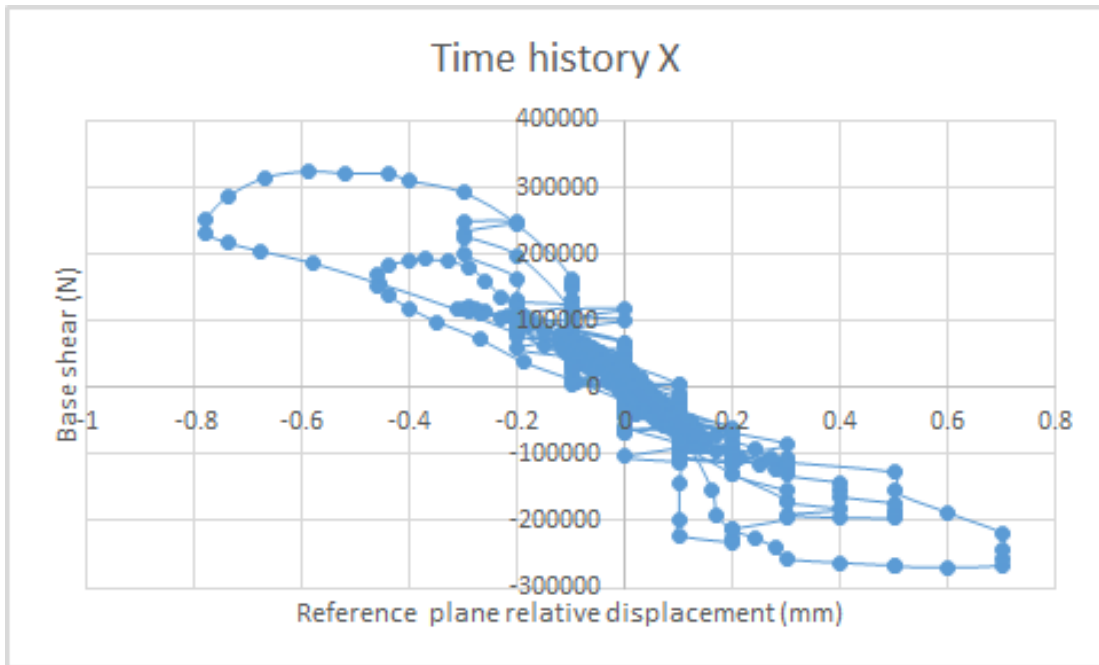


Figure 3.2.8: Base shear versus average reference height displacement – 0.25g scaled PGA, record 3, X direction

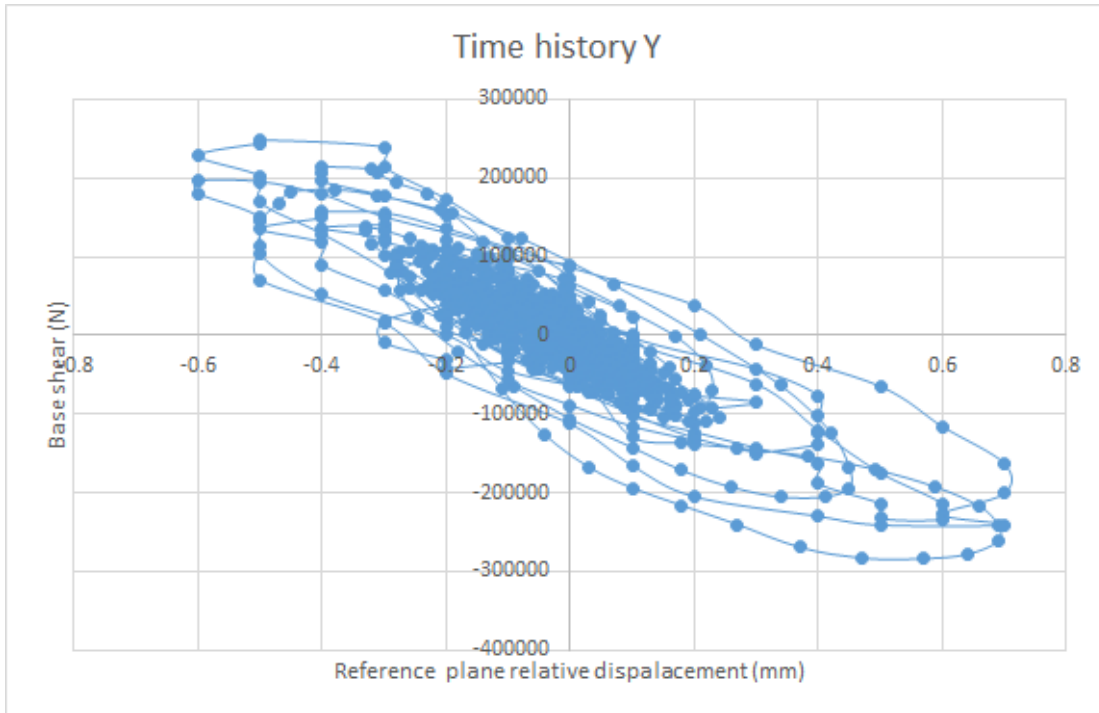


Figure 3.2.9: Base shear versus average reference height displacement – 0.25g scaled PGA, record 3, Y direction

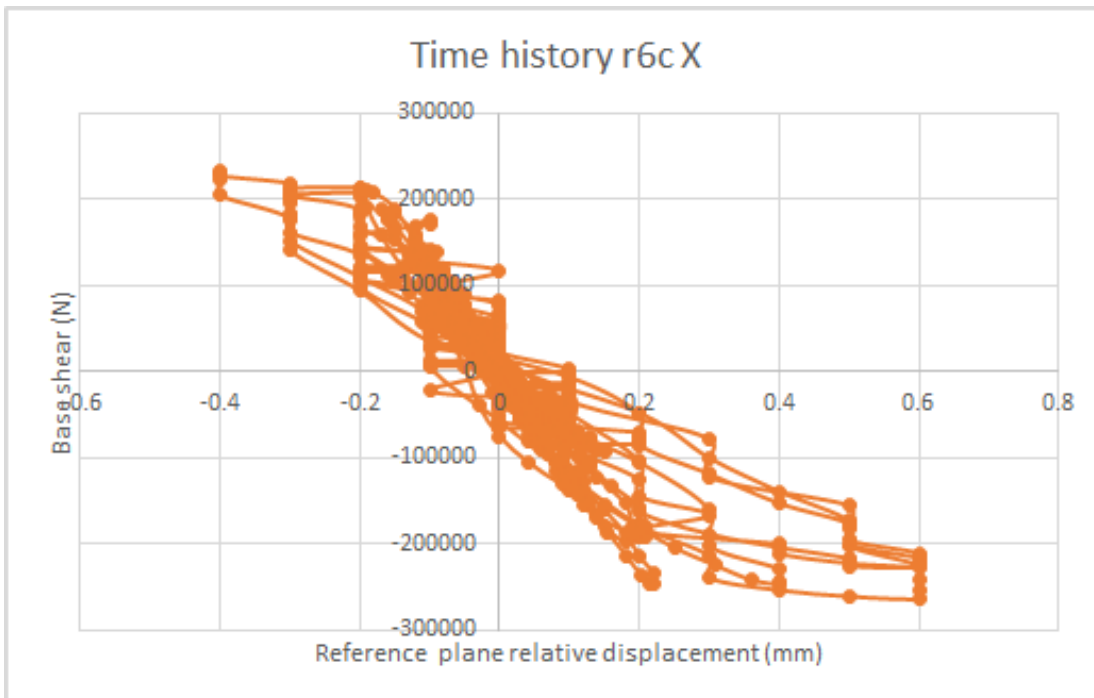


Figure 3.2.10: Base shear versus average reference height displacement – 0.25g scaled PGA, record 6, X direction

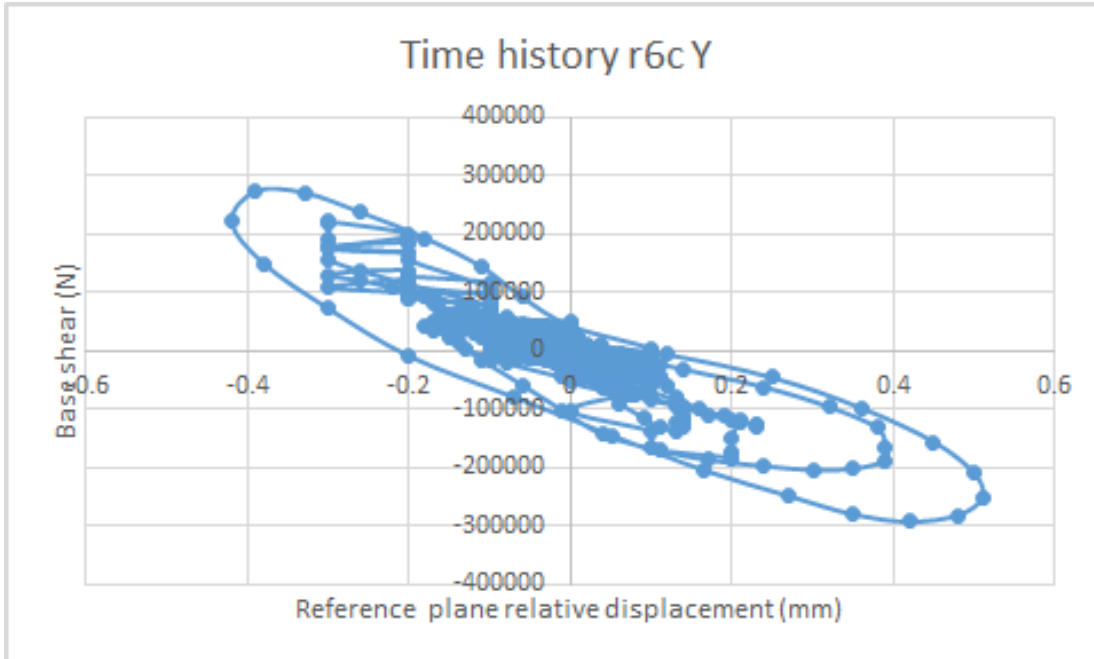


Figure 3.2.11: Base shear versus average reference height displacement – 0.25g scaled PGA, record 6, Y direction

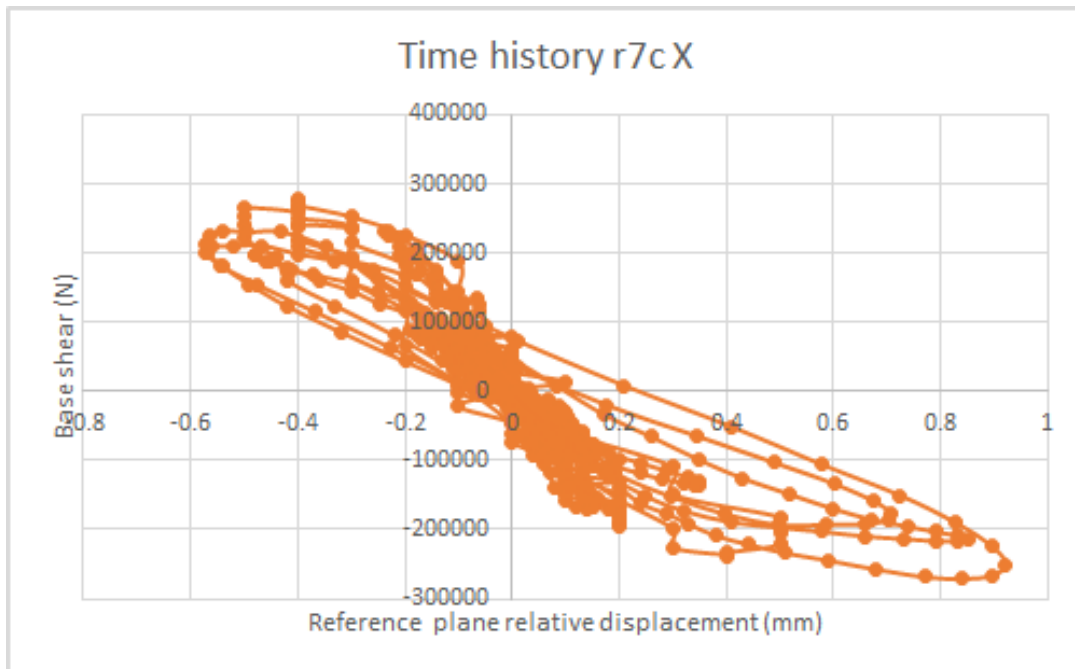


Figure 3.2.12: Base shear versus average reference height displacement – 0.25g scaled PGA, record 7, X direction

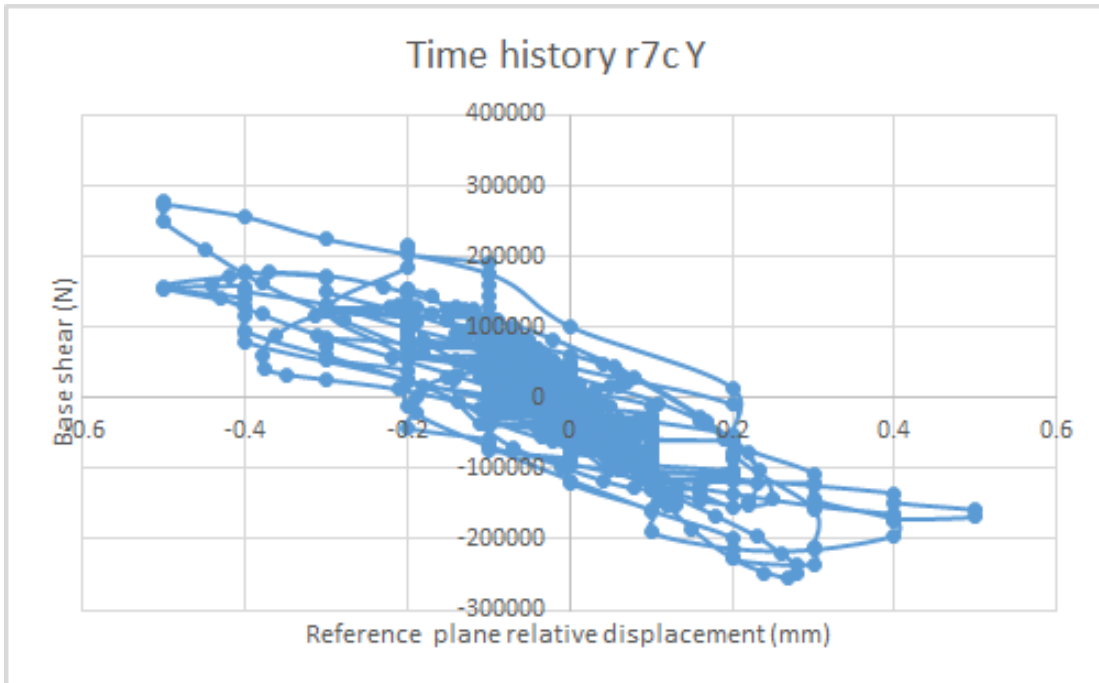
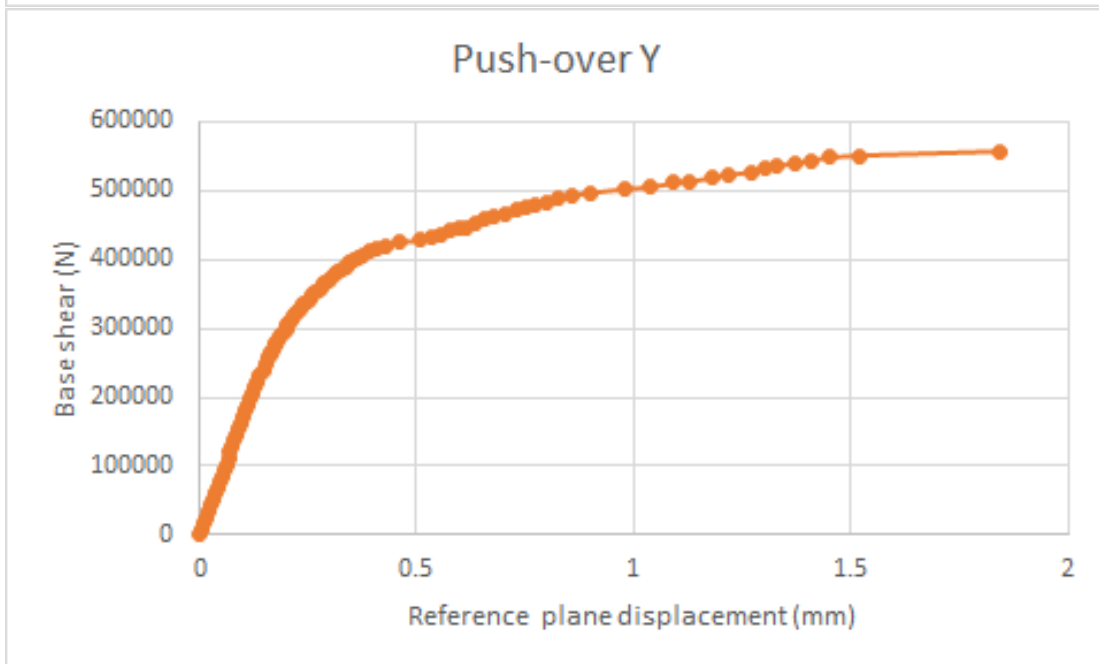
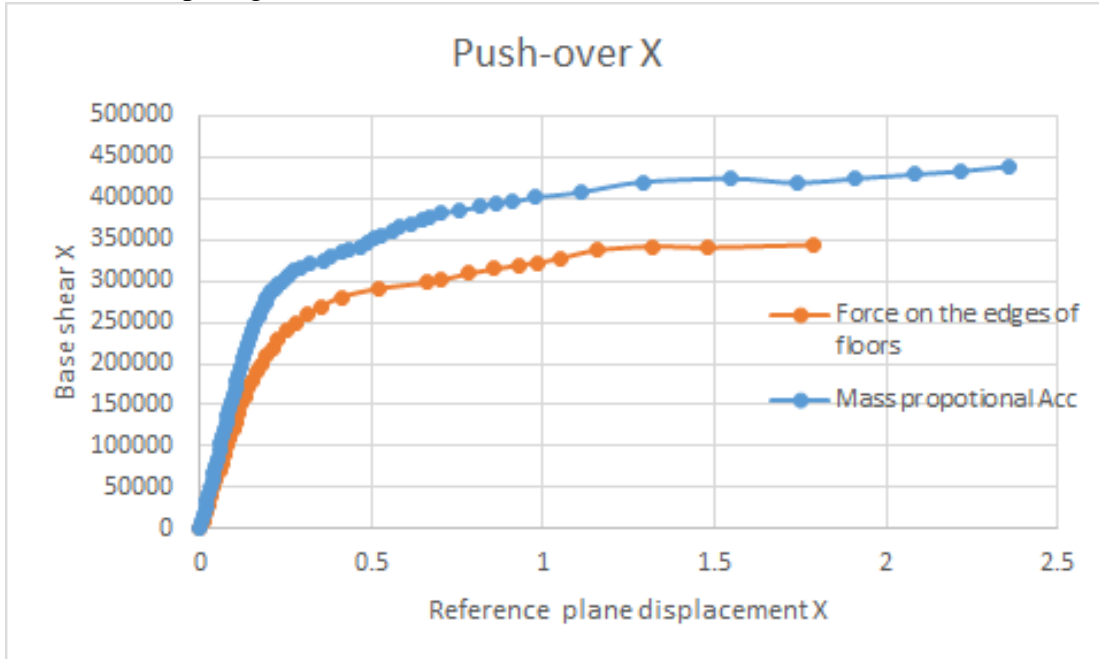


Figure 3.2.13: Base shear versus average reference height displacement – 0.25g scaled PGA, record 7, Y direction

3.2.4. Discussion and sensitivity analyses (if relevant)

<This is for teams to flexibly add contents deemed relevant to their modelling/analysis methods>

Results for comparing initial stiffness and different load method.



4. References

[1] Feenstra PH, Rots JG, Arnesen A, Teigen JG, Hoiseth KV. *A 3D constitutive model for concrete based on co-rotational concept*. In: Computational modelling of concrete structures. Proc. EURO-C 1998, Eds. R. de Borst et al., pp. 13-22, Balkema, Rotterdam, 1998.

[2] Rots JG. *Comparative study of crack models*. In: Finite Elements in Civil Engineering. Proc. Third DIANA World Conference 2002, Eds. Hendriks MAN & Rots JG, Balkema, Lisse, 2002, pp. 17-28.

[3] Mendes N, Lourenco PB. *Seismic assessment of masonry "Gaioleiro" buildings in Lisbon, Portugal*. Journal of Earthquake Engineering 14:80-101, 2010.

[4] Mendes N, Lourenco PB. *Seismic performance of ancient masonry buildings*. In: Proceedings of COMPDYN 2013, eds. Papadrakakis M. et al, Kos Island, Greece, 2013.